JOURNAL OF BIOLOGICAL REGULATORS & HOMEOSTATIC AGENTS
Volume 33, No. 4, July - August, 2020

CONTENTS

Editorials

T. C. Theoharides and P. Conti. Dexamethasone for COVID-19? Not so fast 1241

F. Agostini, M. Mangone, V. Santilli, M. Paoloni, A. Bernetti, R. Saggini and T. Paolucci. Idiopathic facial palsy: umbrella review of systematic reviews and meta-analyses 1245

Original articles

G. Sun, C. Zheng, Z. Deng, C. Huang and J. Huang. TRAF5 promotes the occurrence and development of colon cancer via the activation of PI3K/AKT/NF-**κB** signaling pathways 1257

G.-P. Ma, B.-Z. Yang, Y.-S. Zhang, B. Wang, X.-H. Wei, R.-F. Zhang, K.-H. Jia and J.-P. Gao. Protective effects of miRNA-589 on cerebral ischemia-reperfusion injury 1269

J.-X. Wang, Y.-L. Tao, Z. Wang and Q.-J. Mao. MiR-20a Promotes kidney injury in sepsis rats through autophagy pathway 1277

S.-H. Gui, Y.-M. Wang, C.-Y. Fan, L.-K. Han, T.-G. Wang, M.-Q. Di and J.-Q. Gu. MiR-424 Inhibits neuronal apoptosis in rats with cerebral infarction through regulating TGF-β1/Smad3 signaling pathway 1285

G.-H. Qiao, P. Zhu, L. Yue and S. Yue. MiR-125b Improves acute myocardial infarction in rats by regulating P38/Sirtl/P53 signaling pathway 1297

L-L. Bi, X-Q. Hua, W-H. Li, L. Wang, Y. Li and X-F. Jia. SNHG16 promotes cell proliferation and migration through sponging miR-132 in melanoma 1307

LL. Wang, JJ. Dong, BZ. An, J. Liang, KR. Cai, ZS. Jin, HS. Jin and JP. Hu. Has-miR-17 increases the malignancy of gastric lymphoma by HSP60/TNFR2 pathway 1317

D.-M. Wang, J.-J. Jin, L.-M. Tian and Z. Zhang. MiR-195 promotes myocardial fibrosis in MI rats via targeting TGF-β1/Smad 1325

Q-Q. Mao, J-J. Chen, W-J. Xu, X-G. Zhao, X. Sun and L. Zhong. miR-92a-3p promotes the proliferation and invasion of gastric cancer cells by targeting KLF2 1333

X.-M. Chen, Y.-X. Zhang, Y.-F. Bao and Y.-J. Xu. Correlation analysis between vitamin D receptor gene polymorphism (BsmI) and hallux valgus 1343

L-M. Zhang, Q-Y. Zhu, L. Chen, X-Q. Tang, Y-F. Zou, P. Lv, M-W. Liu and Y-F. Du. miR-382-3p Overexpression attenuates N-methyl-D-aspartate-induced HT22 cell apoptosis via the regulation of the RhoC/ROCK1 signaling pathway 1355

Q.-L. Dong, X.-H. Zhao, Q. Wang, L.-P. Zhang, X.-H. Yan, X.-M. Wang, Z.-J. Li and Y. Sun. Anti-aging gene Klotho ameliorates diabetic nephropathy in mice by inhibiting FGF2 signaling pathway 1369

L.A. de Oliveira, R.O. Soares, M. Buzzi, C.F.A.B. Mourão, T. Kawase and S.A.S. Kuckelhaus. Cell and platelet composition assays by flow cytometry: basis for new platelet-rich fibrin methodologies 1379

Letters to the Editor

P. Zhou, L. Zhang, Y-Q. Wang, B. Li, X-W. Chen, W-M. Lu and Z-L. Guo. Changes of D-Dimer levels in patients with lung cancer after treatment of acute venous thromboembolism 1391

FY. Yu, YM. Yin, ZM. Chen, N. Ren and RF. Li. Influence of blood flow of arteriovenous fistula on cardiac function of patients undergoing maintenance hemodialysis 1397

J-C. Zhang, Y-Y. Zheng, J-N. Tang, B. Qin, X-M. Yang, Q-Q. Guo, J-C. Guo, M-D. Cheng, Z-L. Zhang, F-H. Song, Z-Y. Liu, K. Wang, L-Z. Jiang, L. Fan, X-T. Yue, Y. Bai, X-Y. Dai, R-J. Zheng, S-S. Yin and J-Y. Zhang. Elevated fibrinogen to platelet is associated with increased all-cause mortality among patients undergoing primary percutaneous coronary intervention 1401

MM. Hou, XW. Mao, XB. Liu, YQ. Liu, XY. Bi and XJ. Hou. Novel c.971A>G mutation in the *HTRA1* gene in a Chinese family with CARASIL 1407

P. An, Q. Peng, T. Guo, P.-C. Xing, L.-D. Zhao and M.-J. Zhou. Potential influence of miR-192 on the efficacy of saxagliptin treatment in T2DM complicated with non-alcoholic fatty liver disease 1411

J. Li, HY. Yang, L. Wang, FF. Zhao, S. Yang and FB. Ning. MiR-133a Promoted cerebral ischemia/reperfusion injury by targeting brain-derived neurotrophic factor 1417

X-J. Ma, T-Y. Song, W-L Wang and Z-W. Zhang. Effect of microRNA-129-5p targeting High mobility group protein box1 on regulating inflammation in lipopolysaccharide-activated primary spinal microglia cells 1423

X. Yang, X. Yu, R.-H. Zhou and C. Liu. Serum miRNA-27b-3p is a biomarker of diabetic retinopathy 1431

YF. Gong, W. Han, Y. Cui, LY. Li, LY. Lu and CN. Ren. Therapeutic effect and underlying mechanism of Gonadotropin-releasing hormone in uterine fibroids 1437

XD. Rui, YQ. Sha, S. Wen, QY. Sun, JM. Hu, FF. Yan, LP. He and GH. Xie. Serum level of IL-10 and IL-10-1082G/A polymorphism are associated with the risk of ischemic stroke: A meta-analysis 1445

YX. He, K. Kang and GX. Jia. Effect of sarcopenia combined with platelet-rich plasma on transverse tibial bone transport in diabetic foot 1451

A. Goren, C.G. Wambier, J. McCoy, J. Shapiro, S. Vaño-Galván, S. Herrera and L.M. Glode. Clock genes may drive seasonal variation in SARS-CoV-2 infectivity: Are we due for a second wave of COVID-19 in the fall 1455

Y. Zhang, R.-Q. Du, L. Li, X.-Q. Hu and Q.-M. Li. Correlation between peripheral blood level of miRNA-29a and diabetic peripheral neuropathy 1459

F. Gao, N. Zhang, J.M. Wen, S.J. Li, S.G. Zhang, B.Y. Zhang, Y.L. Dai, R.N. He, Y.S. Huang and Q.Q. Yu. Establishment and potential mechanism of recurrent cystitis-induced overactive bladder-like model in female rats 1465

Y. Bai, LL. Lang, WT. Zhao, Q. Cao and R. Niu. Expression level of FGFR2 protein in patients with esophageal cancer and those with Barrett's esophagus-associated dysplasia 1471

DB. Xu, F. Lin, HJ. He and Y. Ying. Protective effects and underlying mechanism of sevoflurane pretreatment on cerebral ischemia-reperfusion injury in mice 1479

Q. Wang, F. Zhang, W. Cao, X-B. Wang, H-J. Wang and Q-T. Han. Predictive effect of strong ion gap on heart failure in patients with dilated cardiomyopathy 1487

N. Hameed, M.H. Abbasi, T. Akhtar and N. Sheikh. Hematotoxicity and testicular injury induced by Bisphenol A in *Rattus norvegicus* 1493

LL. Shi, WX. Peng, XZ. Hi, HL. Bi and J. Li. Coronary thrombosis as an etiology of woven coronary artery 1501

Y. Fu and XC. Jia. WTAP-mediated N6-methyladenosine modification on EGR3 in different types of epithelial ovarian cancer 1505

R-X. Ji, F. Ren, X-Q. Liu and X. Yuan. LncRNA FBXL19-AS1 promotes the development of gastric cancer by regulating miR-876-5p/HMGB3 axis 1513

Y. Jiang, R. Li, Y. Zhao, J. Liu, X. Zhu and L. Jin. Mechanism of MAPK/ERK1/2 signaling pathway and related proteins on receptor activity of rats with endometriosis 1519

L. Niu, X-F. Wang and X-R. Wang. Crocin suppresses cell proliferation and migration by regulating miR-577/NFIB in renal cell carcinoma 1523

YT. Zhang and GY. Yang. LncRNA SNHG17 acts as a ceRNA of miR-324-3p to contribute the progression of osteosarcoma 1529

Z-W. An, C. Chen, C-W. Wang, C. Zhu, F-Z. Chen, H-Z. Chen and W. Zheng. SNHG16 regulated cerebral ischemia/reperfusion injury via sponging miR-183 1535

L. Zhang, J-F. Guan and L. Qu. Reverse-view pharyngeal swab collection method 1541

A. Spacone, T. Paolucci, P. Prosperi, N. Giannandrea, L. Pezzi, R.G. Bellomo and R. Saggini. Possible phenotyping of apnoea obstructive sleep of female patients 1545

S. D'Agostino and M. Dolci. Antibiotic therapy in oral surgery: a cross sectional survey among Italian dentists 1549

E.M. Lori, A. Cozzi-Lepri, A. Tavelli, V. Mercurio, S.V. Ibba, S. Lo Caputo, F. Castelli, A. Castagna, A. Gori, G. Marchetti, C. Venditti, M. Clerici, A. D'Arminio Monforte and M. Biasin: for Icona Foundation Study Group. Evaluation of the effect of protective genetic variants on cART success in HIV-1-infected patients 1553

G. Barassi, A. Younes, P.A. Di Felice, A. Di Iulio, S. Guerri, L. Prosperi, A. Stamile and A. Di Iorio. Microcurrents in the treatment of chronic pain: biological, symptomatological and life quality effects 1561

P. Amori, G. Vitiello, A. Cancelli, K.M. Lomonosov, L. Antognoli, R. Sadoughifar, M. Goldust, M. Tirant, N. Van Thuong and T. Lotti. Treatment of genitourinary syndrome of menopause with a new radiofrequency device 1567

A. Pace, V. Rossetti, M. de Vincentiis, A. Greco, A. Colizza, G. Iannella, G. Gulotta, I.C. Visconti, P. Mastino and G. Magliulo. Diagnosis and grading of laryngopharyngeal reflux disease with narrow band imaging: preliminary study 1571

C. Bertoldi, P. Cortellini, S. Spinato and D. Zaffe. Clinical analysis on efficacy of root-surface conditioning by ethylenediaminetetraacetic acid on surgical treatment of gingival recessions with coronally advanced flap and enamel matrix derivative peptide: a retrospective study 1577

P.M. Marra, A. Itro, R. Santoro and A. Itro. Management of an anterior mandibular fracture in a 13-year-old patient 1585

F.M. Filannino, A. Pacifici, D. Carbone and L. Pacifici. Biological approach to minimally invasive, flapless, bone augmentation using innovative manual expanders 1589

D. Passali, G. Motta, F.M. Passali, M. Nunziata and G. Ciprandi. Oral quail egg homogenate in the treatment of allergic rhinitis: a first experience in clinical practice 1593

I. La Mantia, A. Varricchio, C. Andaloro and G. Ciprandi. Pidotimod in children with infectious mononucleosis: a preliminary randomized controlled study 1599

L. Signorini, F. De Leonardis, L. Santacroce, K. Haxhirexha, S. Topi, L. Fumarola, G. Dipalma, M. F. Coscia and F. Inchingolo. Probiotics may modulate the impact of aging on adults 1601

S. Cantore, A.D. Inchingolo, E. Xhajanka, V. Altini, I.R. Bordea, G. Dipalma and F. Inchingolo. Management of patients suffering from xerostomia with a combined mouthrinse containing sea salt, xylitol and lysozyme 1607

G. Mustafa, A. Aslam, M.Y. Tipu, S. Masood, U. Iqbal, A. Mahmood, M. Tayyab and I. Irshad. Efficacy evaluation of commercial vaccines against circulating filed isolates of avian influenza H9N2 and infectious bronchitis viruses in broiler chickens 1613

L. Signorini, A. D. Inchingolo, L. Santacroce, E. Xhajanka, V. Altini, I.R. Bordea, G. Dipalma, S. Cantore and F. Inchingolo. Efficacy of combined sea salt based oral rinse with xylitol in improving healing process and oral hygiene among diabetic population after oral surgery 1617

JOURNAL OF BIOLOGICAL REGULATORS & HOMEOSTATIC AGENTS Vol. 34, no. 4, 1241-1243 (2020)

EDITORIAL

Dexamethasone for COVID-19? Not so fast

T. C. Theoharides[1,2,3] and P. Conti[4]

[1]Laboratory of Molecular Immunopharmacology and Drug Discovery, Department of Immunology, Tufts University School of Medicine, Boston, USA; [2]School of Graduate Biomedical Sciences, Tufts University School of Medicine, Boston, USA; [3]Department of Internal Medicine, Tufts University School of Medicine and Tufts Medical Center, Boston, MA USA; [4]Postgraduate Medical School, University of Chieti, Chieti, Italy

Received June 17, 2020 - Accepted June 20, 2020

Recent announcements indicated, without sharing any distinct published set of results, that the corticosteroid dexamethasone may reduce mortality of severe COVID-19 patients only. The recent Coronavirus [severe acute respiratory syndrome (SARS)-CoV-2]-associated multiorgan disease, called COVID-19, has high morbidity and mortality due to autoimmune destruction of the lungs stemming from the release of a storm of pro-inflammatory cytokines. Defense against this Coronavirus requires activated T cells and specific antibodies. Instead, cytokines are responsible for the serious sequelae of COVID-19 that damage the lungs. Dexamethasone is a synthetic corticosteroid approved by the FDA in 1958 as a broad-spectrum immunosuppressor and it is about 30 times as active and with longer duration of action (2-3 days) than cortisone. Dexamethasone would limit the production of and damaging effect of the cytokines, but will also inhibit the protective function of T cells and block B cells from making antibodies, potentially leading to increased plasma viral load that will persist after a patient survives SARS. Moreover, dexamethasone would block macrophages from clearing secondary, nosocomial, infections. Hence, dexamethasone may be useful for the short-term in severe, intubated, COVID-19 patients, but could be dangerous during recovery since the virus will not only persist, but the body will be prevented from generating protective antibodies. Instead, a pulse of intravenous dexamethasone may be followed by administration of nebulized triamcinolone (6 times as active as cortisone) to concentrate in the lungs only. These corticosteroids could be given together with the natural flavonoid luteolin because of its antiviral and anti-inflammatory properties, especially its ability to inhibit mast cells, which are the main source of cytokines in the lungs. In the end, we should remember that "The good physician treats the disease; the great physician treats the patient who has the disease" [Sir William Osler's (1849-1919)].

Recent announcements indicated, without sharing any distinct published set of results, that use of the corticosteroid dexamethasone in a large trial in the UK apparently reduced mortality of only severe, intubated, COVID-19 patients by about 30% (1). It is obviously important to await the publication of the complete set of results, as well as the subsequent course of the patients enrolled.

The recent Coronavirus [severe acute respiratory syndrome (SARS)-CoV-2]-associated multiorgan disease, called COVID-19 (2), has high morbidity and mortality due to autoimmune destruction of the

Key words: COVID-19; dexamethasone; cytokines; mast cells

Corresponding Author:
Theoharis C. Theoharides, MS, MPhil, PhD, MD
Department of Immunology
Tufts University School of Medicine
136 Harrison Avenue, Suite 304
Boston, MA 02111, USA
Tel.: +1 617 636 6866 - Fax: +1 617 636 2456
e-mail: theoharis.theoharides@tufts.edu

0393-974X (2020)
Copyright © by BIOLIFE, s.a.s.
This publication and/or article is for individual use only and may not be further reproduced without written permission from the copyright holder.
Unauthorized reproduction may result in financial and other penalties
DISCLOSURE: ALL AUTHORS REPORT NO CONFLICTS OF INTEREST RELEVANT TO THIS ARTICLE.

lungs stemming from the release of a storm of pro-inflammatory cytokines (3). Defense against this Coronavirus requires activated T cells and specific antibodies (4, 5). Instead, cytokines are responsible for the serious sequelae of COVID-19 that damage the lungs (6).

Dexamethasone is a synthetic corticosteroid approved by the FDA in 1958 as a broad-spectrum immunosuppressor and it is about 30 times as active and with longer duration of action (2-3 days) than cortisone (7). Dexamethasone would limit the production and damaging effect of the cytokines (8), but will also inhibit the protective function of T cells and reduce the ability of B cells to synthesize antibodies (7). Moreover, dexamethasone would block macrophages and NK cells from clearing secondary, nosocomial, pathogens (9).

Clinical evidence does not support the use of corticosteroids in COVID-19 (10). Even worse, the use of corticosteroids has been associated with increased plasma viral load that will persist after a patient survives SARS (11). Hence, dexamethasone may be useful for the short-term in severe, intubated, COVID-19 patients, but could be outright dangerous during recovery since the virus will not only persist, but host defense mechanisms will be curtailed.

A safer approach would be to administer a pulse of intravenous dexamethasone, followed by nebulized triamcinolone (6 times as active as cortisone) to concentrate in the lungs. Once patients leave the hospital, they could be given anti-cytokines (12), such as the anti-IL-6 biologic tocilizumab (13), or inhibitors of other IL-1 family members (14).

A key source of pro-inflammatory cytokines are the mast cells (15) that release large amounts of IL-1β (16), IL-6 (17), and TNF (18). In this context, it would be important to inhibit mast cells in COVID-19 (19), with the natural flavonoid luteolin, which is safer than corticosteroids (20). Luteolin is a potent inhibitor of mast cells (21, 22), but also has anti-inflammatory (22, 23) and antiviral (19) properties.

Covid-19 is a multiorgan disease that requires not only addressing the causative agent, (SARS)-CoV-2, but care of the whole patient. As such, we should remember Sir William Osler's (1849-1919) statement that "The good physician treats the disease; the great physician treats the patient who has the disease" (24).

REFERENCES

1. Ledford H. Coronavirus breakthrough: dexamethasone is first drug shown to save lives [published online ahead of print, 2020 Jun 16]. Nature 2020;10.1038/d41586-020-01824-5.
2. Poon LLM, Peiris M. Emergence of a novel human coronavirus threatening human health. Nat Med 2020; 26(3):317-19.
3. Ye Q, Wang B, Mao J. The pathogenesis and treatment of the `Cytokine Storm' in COVID-19. J Infect 2020; 80(6):607-13.
4. Chen G, Wu D, Guo W et al. Clinical and immunological features of severe and moderate coronavirus disease 2019. J Clin Invest 2020; 130(5):2620-29.
5. Thevarajan I, Nguyen THO, Koutsakos M,et al. Breadth of concomitant immune responses prior to patient recovery: a case report of non-severe COVID-19. Nat Med 2020; Doi.org/10.1038/s41591-020-0819-2.
6. Conti P, Ronconi G, Caraffa A et al. Induction of pro-inflammatory cytokines (IL-1 and IL-6) and lung inflammation by Coronavirus-19 (COVI-19 or SARS-CoV-2): anti-inflammatory strategies. J Biol Regul Homeost Agents 2020; 34(2).
7. Giles AJ, Hutchinson MND, Sonnemann HM, et al. Dexamethasone-induced immunosuppression: mechanisms and implications for immunotherapy. J Immunother Cancer 2018; 6(1):51.
8. Chen H, Wang F, Zhang P, et al. Management of cytokine release syndrome related to CAR-T cell therapy. Front Med 2019; 13(5):610-17.
9. Cohn LA. The influence of corticosteroids on host defense mechanisms. J Vet Intern Med 1991; 5(2):95-104.
10. Russell CD, Millar JE, Baillie JK. Clinical evidence does not support corticosteroid treatment for 2019-nCoV lung injury. Lancet 2020; 395(10223):473-75.
11. Lee N, Allen Chan KC, Hui DS, et al. Effects of early corticosteroid treatment on plasma SARS-associated

Coronavirus RNA concentrations in adult patients. J Clin Virol 2004; 31(4):304-9.
12. Dinarello CA, Simon A, van der Meer JW. Treating inflammation by blocking interleukin-1 in a broad spectrum of diseases. Nat Rev Drug Discov 2012; 11(8):633-52.
13. Luo P, Liu Y, Qiu L, Liu X, Liu D, Li J. Tocilizumab treatment in COVID-19: A single center experience. J Med Virol 2020; 92(7):814-18.
14. Kritas SK, Ronconi G, Caraffa A, Gallenga CE, Ross R, Conti P. Mast cells contribute to coronavirus-induced inflammation: new anti-inflammatory strategy. J Biol Regul Homeost Agents 2020; 34(1).
15. Theoharides TC, Valent P, Akin C. Mast Cells, Mastocytosis, and Related Disorders. N Engl J Med 2015; 373(2):163-72.
16. Kandere-Grzybowska K, Letourneau R, Kempuraj D, et al. IL-1 induces vesicular secretion of IL-6 without degranulation from human mast cells. J Immunol 2003; 171(9):4830-36.
17. Taracanova A, Alevizos M, Karagkouni A, et al. SP and IL-33 together markedly enhance TNF synthesis and secretion from human mast cells mediated by the interaction of their receptors. Proc Natl Acad Sci U S A 2017; 114(20):E4002-E4009.
18. Taracanova A, Tsilioni I, Conti P, et al. Substance P and IL-33 administered together stimulate a marked secretion of IL-1β from human mast cells, inhibited by methoxyluteolin. Proc Natl Acad Sci U S A 2018; 115(40):E9381-E9390.
19. Theoharides TC. COVID-19, pulmonary mast cells, cytokine storms, and beneficial actions of luteolin. Biofactors. 2020; 46(3):306-8.
20. Conti P, Varvara G, Murmura G, et al. Comparison of beneficial actions of non-steroidal anti-inflammatory drugs to flavonoids. J Biol Regul Homeost Agents 2013; 27(1):1-7.
21. Seelinger G, Merfort I, Schempp CM. Anti-oxidant, anti-inflammatory and anti-allergic activities of luteolin. Planta Med 2008; 74(14):1667-77.
22. Weng Z, Patel AB, Panagiotidou S, Theoharides TC. The novel flavone tetramethoxyluteolin is a potent inhibitor of human mast cells. J Allergy Clin Immunol 2015; 135(4):1044-52.
23. Patel AB, Theoharides TC. Methoxyluteolin Inhibits Neuropeptide-stimulated Proinflammatory Mediator Release via mTOR Activation from Human Mast Cells. J Pharmacol Exp Ther 2017; 361(3):462-71.
24. Bondy P. What's so special about Osler? Yale J Biol Med 1980; 53:217-17.

EDITORIAL

Idiopathic facial palsy: umbrella review of systematic reviews and meta-analyses

F. Agostini[1], M. Mangone[1], V. Santilli[1], M. Paoloni[1], A. Bernetti[1], R. Saggini[2] and T. Paolucci[2]

[1]Department of Anatomical and Histological Sciences, Legal Medicine and Orthopedics, Sapienza University of Rome, Rome, Italy; [2]Department of Medical, Oral and Biotechnological Sciences, G. D'Annunzio University of Chieti-Pescara, Chieti, Italy

Received June 2, 2020 – Accepted July 22, 2020

Idiopathic facial palsy is the most common disease of the VII cranial nerve. There are many treatments to facilitate recovery from this condition: pharmacological, surgical, rehabilitative, but the effectiveness of some of these treatments, especially the latter, is still under discussion. The purpose of this umbrella review of systematic reviews is to analyse the literature in order to investigate the different rehabilitation interventions in patients suffering from idiopathic facial palsy. A scientific literature search was carried out from January 2009 until August 2019, using Mesh the terms "facial palsy", "Bell's Palsy", "idiopathic facial nerve palsy", combined with "rehabilitation" and "therapy". Initially all the systematic reviews and meta-analyses of the last 10 years concerning rehabilitation treatments for the recovery of injured functions in facial palsy were included. Given the heterogeneity of the studies in the literature, which do not differentiate the different causes of facial palsy, all the causes of idiopathic facial palsy were included in the review. The research resulted in 94 published systematic reviews but only 6 were considered in respect to the inclusion criteria. All studies agree on the lack of high-quality scientific work to be able to say that Bell's physiotherapy treatments for facial palsy are effective, in particular with regard to recovery times during the rehabilitation process. Future studies are needed, in order to highlight the therapeutic implications of the different rehabilitation methods, with standardized protocols, in patients suffering from facial palsy of different aetiology.

Idiopathic facial palsy is the most common disease of the VII cranial nerve (1). It is an inflammatory disease that affects the nerve, usually at the level of the stylomastoid foramen, for a variable segment of length. The aetiology is still unknown. The most accepted hypothesis remains the edema of the facial nerve, which is compressed causing ischemia and paresis, associated with an immunological or viral disorder (2). It is believed that infection with the Herpes Simplex virus is the most common cause, favoured by exposure to cold, hence the name "frigore", but also other viruses seem to be implicated in the onset of the disease (3). The onset of the disease is acute or evolves over days or hours, with retro-auricular pain. The deficit is peripheral and affects the upper and lower parts of the face equally, on one side only, often causing complete palsy. The affected side becomes relaxed and expressionless and the angle of the mouth is lowered. In severe cases, the eyelid rhyme is wide and the subject is unable to close his eye completely, going through complications such as irritation of the conjunctiva and drying of the cornea. During the squinting of the eyes there is an incomplete closure of the eyelid from the affected

Key words: idiopathic facial paralysis; Bell's palsy; rehabilitation; review

Corresponding Author:
Francesco Agostini, MD,
Department of Anatomical and Histological Sciences,
Legal Medicine and Orthopedics,
Sapienza University of Rome,
Piazzale Aldo Moro, 5, Rome, 00185, Italy
Tel.: +39 3404751090
e-mail: francescoagostini.ff@gmail.com

0393-974X (2020)
Copyright © by BIOLIFE, s.a.s.
This publication and/or article is for individual use only and may not be further reproduced without written permission from the copyright holder.
Unauthorized reproduction may result in financial and other penalties
DISCLOSURE: ALL AUTHORS REPORT NO CONFLICTS OF INTEREST RELEVANT TO THIS ARTICLE.

side and the automatic rotation of the eyeballs makes the sclera appear (Bell's sign). In kinetic tests, half of the face remains motionless (complete palsy) or moves conspicuously less than the other half (paresis). In showing the teeth, the commissure of lips is deformed towards the healthy side. Generally, the examination of sensitivity is normal, but sometimes the external auditory canal and a small area above the mastoid process can be painful on contact. The diagnosis of facial palsy is clinical. There are no specific diagnostic tests. Electromyography tests may be useful for prognosis. The prognosis is generally good, since almost 90% of cases spontaneously recover completely or very satisfactorily. The complications are characterized by a permanent deficit of mimic musculature, contractures, axonic confusion phenomena and synkinesis of the eyes and mouth (*crocodile tear syndrome*). There are many treatments to facilitate recovery from this condition: pharmacological (1), surgical (2), rehabilitative (3), but the effectiveness of some of these treatments is still under discussion. Drug therapy is mainly based on corticosteroids to reduce nerve edema, often associated with an antiviral, pain relievers, artificial tears, lubricating eye drops and ophthalmic cream, accompanied by bandages to protect the eye in case of incomplete closure. It is important to start therapy as early as possible in respect to the onset of palsy. In the case of permanent outcomes, botulinum toxin inoculations, blocking the release of acetylcholine at the neuromuscular junction to treat synkinesis and hyperkinesis (e.g. peri-ocular, peri-oral and cervical muscles) or, in worse cases, surgery can be used (4, 5). The usefulness of rehabilitation treatment is still controversial in the recovery of facial mimic functions and in the reduction of recovery times, as well as in the reduction of complications. The techniques commonly used today are manifold: proprioceptive neuro-muscular facilitation (6), mime therapy (7), facial neuromuscular re-education (8), biofeedback (9), electrostimulation (10) and exercises for facial expressiveness (11). To date, however, there are no studies that suggest which rehabilitation approach and rehabilitation protocols are unequivocally more effective than others. In addition to this, the evidence and recommendations present in the literature today are dated and have not always addressed all possible therapeutic strategies, even in relation to the innovations that have been made over the years. In recent years, rehabilitation professionals have had to choose from many systematic reviews in the literature that address the same topic, with a high variability in quality and aims, that made it difficult to administer the possible treatments. Recently, systematic reviews of other systematic reviews, relating to the same topic, were conducted, allowing the results to be compared in order to provide the necessary evidence (12). These systematic reviews, identified in the literature as umbrella reviews or summary of systematic reviews, are intended to summarize the evidence of more than one systematic review, including the combination of different interventions, different outcomes, different conditions, populations, or effects adverse. A working group formed by the Joanna Briggs Institute of the University of Adelaide (Australia) developed the methodological indications for the realization of an umbrella review including both quantitative and qualitative evidence (12). Taking this into consideration, the purpose of this umbrella review is to analyse the literature in order to investigate the different rehabilitation interventions on patients suffering from idiopathic facial palsy.

MATERIALS AND METHODS

Search strategy

A scientific literature search (PubMed, Google Scholar, PEDro and Cochrane) was carried out from January 2009 until August 2019, using Mesh terms and free-text terms as: "facial palsy", "Bell's Palsy", "idiopathic facial nerve palsy", combined with "rehabilitation" or "therapy", and "systematic reviews" or "meta-analyses". The search results were then combined with "Proprioceptive Neuro-muscular Facilitation", "Mime Therapy", "Facial Neuromuscular Re-education", "Biofeedback", "Electrostimulation" and "Exercises".

Inclusion/exclusion criteria

Initially all the systematic reviews and meta-analyses of the last 10 years concerning rehabilitation treatments for the recovery of injured functions in facial palsy were included. Given the heterogeneity of the studies in the literature, which

do not differentiate the different causes of facial palsy, all the causes of idiopathic facial palsy were included in the review. All studies published more than 10 years ago, not in English, which did not mention rehabilitation treatments, and which treated other types of peripheral facial palsy were excluded.

PICO

The population included had to have a diagnosis of peripheral facial palsy of any severity, and be over 15 years of age. The intervention was to be rehabilitative, compared to other pharmacological and non-pharmacological interventions. All instrumental physical therapy treatments (electrotherapy, thermotherapy, hydrotherapy, phototherapy, ultrasound therapy), manual (Neuromuscular Proprioceptive Facilitations, stretching) and specific exercises (Neuromuscular Facial Retraining, Mime Therapy, Mirror Therapy) and combinations of these were taken into consideration.

The primary outcome was to recover motor function, evaluated by scales, validated by the international scientific community [House-Brackmann Scale (13), Sunnybrook Facial Grading System (14), Facial Clinimetric Evaluation scale - FaCE (15)] or questionnaires [Facial Disability Index (16)]. The secondary outcome investigated the recovery time.

Data extraction

Three of the Authors conducted data extraction independently and the inconsistencies were overcome by the comparison of the data and the debate. The information

Table I. *Characteristics of the included studies*

Author	Type	Diagnosis	Topic	Results	Limits	AMSTAR
Teixeira et al.	Systematic review (12 RCT) and meta-analysis	- Bell's palsy - Idiopathic facial palsy	- Manual Therapy - Elettrostimol. - Exercise - Acupuncture	The study does not provide evidence regarding the benefits or risks of physiotherapy.	Lack of high-quality studies. Heterogeneity of interventions and controversial results. Conflict of interest not specified.	10/11
Fargher and Coulson	Systematic review (5 RCT) and meta-analysis	- Bell's palsy	Electrostimulation in the acute phase	No evidence in favor of electrostimulation.	No duplication of search and data extraction.	7/11
Ferreira et al.	Systematic review (2 RCTs)	- Idiopathic facial palsy	- Elettrostimolazione - Individual Exercise - Mime Therapy	Moderate efficacy in reducing paresis.	Reduced analysis sample. Unclear outcomes.	7/11
Holland et al.	Systematic review (13 mixed articles. 3 RCT on rehabilitation)	-Paralisi facciale periferica non specificata. - Bell's palsy	- Drugs - Hyperbaric Oxygen Therapy - Facial Re-Education (Mime Therapy and Exercise)	No evidence in favor of facial re-education.	Reduced and low-quality analysis sample. Extraction and analysis not performed by more than 1 researcher independently. Lack of inclusion criteria and detail on the search strategy.	5/11
Pereira et al.	Systematic review and meta-analysis (6 RCT)	- Bell's palsy 67% - Herpes Zoster: 13% Lyme disease: 1% Trauma: 1% Iatrogena: 1% Meningioma: 2% Facial neuronal apoptosis : 1%	Exercises	Increased facial mimic functions.	Inclusion criteria are unclear.	6/11
Baricich et al.	Systematic review (7 RCTs, 4 pilot studies, 1 preliminary study, 3 retrospective studies)	- Bell's palsy - Ramsay-Hunt Syndrome - Acustic neuroma - No specified Peripheral facial paralysis	- Electrostimulation - Mime therapy - Biofeedback - PNF - Neuromuscular Re-Education	Mime therapy can improve functional outcomes.	Missing list of excluded studies.	8/11

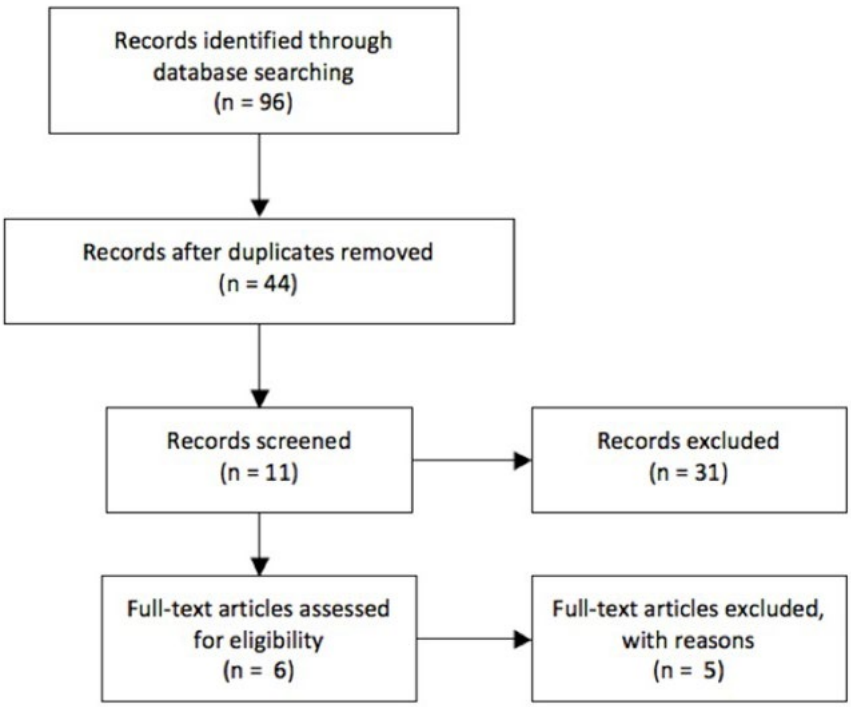

Fig. 1. *Flow chart*

obtained included: date of publication, research period, characteristics of the studies included and participants in the studies, interventions, objectives, results obtained and outcomes, and limitations.

Risk of bias assessment

All the systematic reviews and meta-analyses included in the study that met the inclusion criteria were assessed using the Assessment of Multiple Systematic Reviews (AMSTAR) as a quality assessment tool (17).

RESULTS

After the duplicates were removed, 44 articles were identified. Thirty-one articles were discarded after reading the abstracts because they did not meet the inclusion criteria. Eleven articles were selected for reading the full text. Five articles were discarded because they were narrative revisions. Six articles selected for the preparation of this umbrella review: 6 systematic reviews, including 3 meta-analyses (Flow chart – Fig. 1). The characteristics of the selected studies are summarized in Table I.

Teixeira et al. (2) published a Cochrane systematic review in 2012. Randomized controlled trials were selected that included rehabilitation interventions, with population of all ages and all severity of Bell's palsy. Twelve studies were selected: four studied the effect of electrostimulation; three of exercises; five combined or compared acupuncture physiotherapy treatments. GRADE was used in drafting the article. The primary outcome analysed was incomplete recovery six months after randomization. This study is of high quality (AMSTAR score of 10/11), but has some limitations due to the low quality of the trials analysed, the heterogeneity of the interventions, the controversy of the results and the lack of details regarding the method of data extraction used. They analysed the various rehabilitation interventions separately. Regarding electrostimulation, in three studies out of four, it did not bring any statistically significant improvement in the recovery of function,

and in one study, the control group, which did not receive electrostimulation, obtained better results than the group of study. Regarding the recovery time, two studies, of low quality and high risk of bias, obtained discordant results: one analysed the reduction of recovery times in the tympanic cord injuries, in the other, a large number of participants did not obtain results after three months. Only one study-analysed patients with chronic Bell's palsy diagnosed for at least 9 months. Limited by a small number of participants, the study reports an improvement in the House-Brackmann scale from grade V to grade III, but the authors of the review analysed how it was an improvement on the score but not necessarily a functional recovery. The facial exercises, analysed in three studies that used the Kabat method and conventional exercises, did not obtain statistically relevant results, however in one study, the recovery was faster in the group treated with the Kabat method for two weeks. In a subgroup analysis, participants with moderate palsy, treated with the Kabat method, shortened recovery time after 12 weeks compared to the control group treated with conventional exercises, while there was no difference in the subgroup with mild palsy. Facial exercises showed a better trend in chronic cases and in moderate/severe cases, but without a statistical significance. They conclude that there is no high-quality scientific evidence to support recovery or the risks of physiotherapy in Bell's palsy, but there are only low-quality articles in favour of the exercises, which suggest a reduction in recovery times and sequelae in acute cases. The effectiveness of patient-tailored exercises must be demonstrated with other randomised control trials (RCTs). There was no judgment regarding electrotherapy (2).

Fargher and Coulson (18), in a systematic review of 2017, analysed the effect of electrostimulation in the treatment of Bell's palsy. Five studies were included: four during recovery (acute phase); one in the chronic phase of facial palsy. The outcomes were: (i) the time required for complete recovery; (ii) the percentage of complete recovery out of the total study population; (iii) the improvement of facial functions; (iv) the percentage of complications that arose. This study is of medium quality (AMSTAR 7/11). The limits are the lack of an analysis of the risk of publication bias and the work carried out by the two authors not independently. They clearly report that electrostimulation did not effective in improving and/or shortening the recovery of facial functions in acute cases. The studies included in the review used different protocols for electrostimulation: three studies used similar electro-stimulated muscle contractions, but with different application frequency, from one to five times a week. Another study used continuous stimulation below the contraction threshold, placing the electrodes on the main branch of the facial nerve and not on the muscle bellies. Regarding recovery time, a single study divided the sample into two subgroups, with and without nerve degeneration, assessed by electromyography. In the subgroup without degeneration, there is no difference in recovery time. In the degenerative subgroup, the first movements appeared after fifty-three days, compared to the sixty-six of the control group, but the addition of (laser) radiation, as part of the intervention protocol, confuses the results. In the other studies, there is no significant difference in recovery times. The only study analysed on chronic facial palsy reports limited beneficial effects in the massive use of electrostimulation, but of low scientific quality. None of the studies included in the review report adverse effects such as reinforcement of synkinesias, but one study citing the potential risk of establishing this complication is cited (18).

Ferreira et al. (19), in their systematic review published in 2011, study the effectiveness of physiotherapy in recovering from idiopathic facial palsy. Only 2 RCTs were included in the review, which include facial neuromuscular re-education treatments, electrostimulation and Mime Therapy. The evaluation of the studies was carried out following the PEDro scale. This study (AMSTAR 7/11) is limited by the reduced number of RCTs analysed and by the non-explanation of the risks of publication bias. Authors affirm that the studies analysed demonstrate moderate efficacy in the treatment of facial neuromuscular re-education in association with the use of a mirror, in the acute and chronic phases respectively, but studies of better quality and greater sample size are needed to support their conclusions. Mime Therapy has also been shown to be effective in reducing facial asymmetry in

patients suffering from chronic idiopathic facial palsy, after three months of treatment, assessed with the Sunnybrook Facial Grading scale, and a reduction of 0.6 points on the House-Brackmann scale (19).

Holland and Bernstein (20) worked on a systematic review published in 2014. Their study investigated the effects of drug therapy and physiotherapy treatment for Bell's palsy in adults and adolescents. Three RCTs and two systematic reviews eligible for analysis were identified and were assessed through the GRADE. The outcomes were: (i) recovery of motor function; (ii) the presence of sequelae at 12 months; (iii) the recovery time; (iv) the presence of adverse effects. The treatments carried out were facial re-education exercises and Mime Therapy. This is not a high-quality study (AMSTAR 5/11), because of a lack of explanation of the inclusion criteria and a reduced sample of analysis. They analysed the effectiveness of facial rehabilitation treatments, such as Mime Therapy or facial exercises, compared to subjects on the waiting list for treatment, in patients suffering from unspecified chronic peripheral facial palsy and chronic Bell's palsy for at least nine months. The analysis of low-quality studies suggests that facial re-education may be more effective than receiving any treatment regarding the improvement of facial functions in three months but may not be effective in reducing the risk of incomplete recovery. Compared to conventional therapy, facial re-education treatments can shorten the time for starting and completing recovery, with a low level of evidence. In their article they report that it was not possible to recognize the effectiveness of physiotherapy in the treatment of Bell's palsy and idiopathic facial palsy, but they add in the comments that there is limited evidence in support of facial re-education for the improvement of facial functions and quality of life. The multidisciplinary environment allows optimal outcomes to be achieved thanks to the coordination between healthcare professionals in medicine, surgery, physiotherapy and psychotherapy (20).

Pereira et al. (21) carried out a systematic review with meta-analysis on facial exercise therapy for facial palsy, published in 2011. Of 132 studies found, only six met the inclusion criteria, and only one allowed meta-data analysis. The outcomes measures considered were: (i) facial symmetry; (ii) synkinesias; (iii) muscle rigidity; (iv) labial mobility; (v) physical and psychological aspects related to palsy. The treatments included re-education exercises combined with a mirror, neuromuscular rehabilitation exercises (Kabat), Mime Therapy, 30 minutes of autonomous exercises. With unclear inclusion criteria and a lack of risk assessment for publication bias, this study has an AMSTAR score of 6/11. They performed a meta-analysis, including a single study, on the effectiveness of Mime Therapy in the rehabilitation of facial palsy. The study participants were all patients with peripheral facial palsy for at least 9 months, who carried out rehabilitation treatments with Mime Therapy (one/week; 45 minutes per session) associated with exercises to be carried out independently, for a period of 3 months. The experimental group obtained better results than the control group, which did not carry out any type of treatment. The times and methods of application of the treatments were extremely heterogeneous: from once a month to five times a week, for a period ranging from two weeks up to diverse months. All treatments proved effective for the improvement of mimic functions, with a peak of improvement in the groups treated with Mime Therapy in cases of facial palsy for more than 9 months. The different methods of evaluation and description of the outcomes were the main limitations of this study, associated with the low number and low quality of the studies analysed. A single study reported no beneficial effects regarding synkinesias. The use of biofeedback with mirror and electromyography used in a single study of this review demonstrated a beneficial effect in the recovery of functions. The meta-analysis performed on the single study indicates that Mime Therapy is the most effective treatment for improving the outcomes of functionality, but only in patients suffering from chronic peripheral facial palsy (21).

Baricich et al. (22) published a systematic review in 2012 evaluating the effectiveness of rehabilitation treatments for peripheral facial palsy. The research was performed including all RCTs, control cases, cohort studies and case series over a period between 1990 and 2010. Fifteen studies were selected, assessed through the American Academy Evidence Classification of Neurology. The treatments carried out in the

included articles were: (i) electrostimulation; (ii) Mime Therapy; (iii) biofeedback; (iv) proprioceptive neuromuscular facilitation; (v) neuromuscular re-education. The review (AMSTAR 8/11), turns out to be a high-quality study. They analysed the various treatments used in the RCTs included in their review. Regarding electrostimulation, they did not obtain significant results. Two studies obtained favourable results in the treatment of chronic palsy, using two types of current: one below the muscle contraction threshold and another below the perceptible threshold. The results are favourable, but intensive treatment (6 hours/day, every day for 6 months) requires high patient compliance. Mime therapy has proved effective in the treatment of chronic peripheral facial palsy, maintaining the results obtained even one year after the treatment. The studies analysed, which included mirror biofeedback and electromyography, reported functional improvements without statistical significance, and in five out of six studies the groups were formed by facial palsy that arose at least five months earlier. One study included subjects with Bell's palsy that had occurred in the past month, who performed exercises associated with biofeedback with electromyography (EMG), achieving better results than the control group. Two studies investigated the effectiveness of the Kabat method performed in acute cases. The authors conclude by asserting that there is no unequivocal scientific evidence in favour of rehabilitation, but some benefits were recognized, in particular with Mime Therapy (level of effectiveness C), easy availability and low cost for patients (22).

The results obtained from the included articles are summarized in Table II. Table III represents a summary of the articles considered by the included studies.

Table II. *Results obtained from the included articles*

Author	Conclusion	Function improvement
Teixeira et al.	There is no high-quality scientific evidence to support benefits or risks in physiotherapy treatments for idiopathic facial paralysis. Low quality evidence exists in favor of tailor-made facial exercises to improve function, especially in cases of moderate and chronic severity. Low quality evidence that facial exercises reduce complications in the acute phase.	Electrostimulation vs control: in favor of control. Electrostimulation vs prednisone: favor electrostimulation Exercises towards waiting list: favor exercises Exercises vs conventional therapy: favor exercises
Fargher and Coulson	There is no scientific evidence to support electrostimulation during recovery from the acute phase of Bell's palsy. There is a low level of evidence in patients with chronic symptoms.	Electrostimulation HB: average difference: -0.38; 95% CI [-0.78,0.03]
Ferreira et al .	Based on moderate scientific evidence, facial neuromuscular reeducation can reduce asymmetric movements in the acute and chronic stages. 2 of the included studies reported adverse effects (clinical worsening, synkinesias) of electrostimulation.	Electrostimulation SB: experimental group 11 points more than control Mime Therapy: SB: +20.4 compared to the control HB: +0.6 compared to the control
Holland et al.	There is little evidence that facial re-education, such as Mime Therapy, can increase both the functionality and the quality of life of people with persistent facial paralysis.	Mime Therapy. FDI Score, 3 months later. From 56.8 to 73.5 = 16.7; p <0.02 FDI Social Score: 68.6 to 80.7 = 12.1 p <0.01 Exercises vs waiting list. SB; average difference 20.40; 95% CI [8.76, 32.04]. FDI: average difference 14.50, 95% CI [4.85, 24.15]
Pereira et al.	This systematic review suggests that Mime Therapy is effective for the outcome of functionality in facial paralysis.	Mime Therapy. FDI: standard average difference = 13.90; IC [4.31, 23.49]; p = 0.005
Baricich et al.	Level C of evidence regarding the effectiveness of physiotherapy in peripheral facial paralysis. Mime Therapy can be effective for improving functional outcomes.	PNF: improvement on the non-quantified HB scale (15 days from the onset of symptoms) Neuromuscular reeducation: 1 point improvement on the HB scale. Mime therapy: unspecified improvement of HB and SB after 12 months of treatment.

HB: House-Brackmann Grading System; SB: Sunnybrook Grading Scale; FDI: Facial Disability Index; PNF: Facilitazioni Neuromuscolari Propriocettive

Table III. *Summary of the articles considered by the included studies*

Study	Type of study	Teixeira et al, 2011	Fargher and Coulson, 2017	Ferreira et al, 2011	Holland and Bernstein, 2014	Pereira et al, 2011	Baricich et al, 2012
Alakram and Puckree, 2010	Preliminary study	X	X				X
Barbara et al, 2010	RCT	X				X	X
Barbara et al, 2003	Retrospective study						X
Beurskens, 2007	RCT	X					
Beurskens et al, 2006	RCT				X		
Beurskens and Heymans, 2003	RCT			X	X	X	X
Beurskens and Heymans, 2006	RCT						X
Cardoso et al, 2008	Systematic Review				X		
Dalla Toffola et al, 2005	Retrospective cases series review						X
de Almeida et al, 2009	Systematic Review				X		
Engström et al, 2008	RCT				X		
Farragher et al, 1987	RCT		X				
Flores et al, 1998	RCT	X					
Hyva¨rinen et al, 2008	Pilot case series						X
Kim et al, 2016	RCT		X				
Lee et al, 2013	RCT				X		
Lindsay et al, 2010	Retrospective cases series review						X
Lockhart et al, 2013	Systematic Review				X		
Manca et al, 1997	Pilot case series						X
Manikandan, 2007	RCT	X		X			X
Mosforth and Taverner, 1958	RCT	X	X				
Nakamura et al, 2003	RCT					X	X
Pan, 2004	RCT	X					
Qu, 2005	RCT	X					
Quant et al, 2009	Systematic Review				X		
Racic et al, 1997	RCT				X		
Ross et al, 1991	RCT					X	X
Salinas et al, 2013	Systematic Review				X	X	
Segal et al, 1995 (A)	RCT						X
Segal et al, 1995 (B)	Pilot case series						X
Sullivan et al, 2007	RCT				X		
Targan et al, 2000	Pilot case series						X
Teixeira et al, 2011	Systematic Review				X		
Wen and Zhang, 2004	RCT	X					
Wong et al, 2004	RCT	X					
Yang, 2001	RCT	X					
Zhang, 2005	RCT	X					

DISCUSSION

The scientific literature contains multiple studies, with a great variability of quality and objectives, relating to rehabilitation interventions concerning the most suitable treatment to be administered in this kind of patient. All studies agree on the lack of high-quality scientific work to be able to say that Bell's physiotherapy treatments for facial palsy are effective, in particular regarding recovery times during the rehabilitation process. Various methods have been analysed, but none has yet given appreciable results in order to make recommendations with strong scientific evidence in favour, while, on the other hand, it is possible to make recommendations that are not in favour.

Mime Therapy appears to be the most suitable rehabilitation treatment in chronic facial paralysis. Although there is still no high-quality scientific evidence to objectively verify its effectiveness, many studies agree that better results are obtained with this type of treatment, both regarding the improvement of mimic functions and for the reduction of recovery time. Mime Therapy includes self-massage, relaxation exercises, breathing exercises coordinated with facial movements, pronunciation of letters and words. The relatively short duration of this treatment (10 sessions in 4 weeks) supported by exercises to be carried out daily for 45 minutes independently, makes it a useful tool that is easy to access and apply by patients and therapists. In order to test this hypothesis, high-quality studies are needed.

Electrotherapy appears to be effective only in chronic patients, but with a low level of scientific evidence and requires extremely prolonged treatments (6 hours a day for 10 months). The effectiveness of electrostimulation, although easy to apply and available to patients, remains uncertain. The guidelines published by De Almeyda et al. (11) take sides against the use of electrotherapy in the acute phase of the disease, attributing a high risk of establishing synkinesias and muscle stiffness. The review by Fargher andCoulson (18) does not reveal any risk associated with electrostimulation taking into consideration the studies analyzed, but they also cite a previous study regarding the potential risk of negative outcomes. In the work of Texeira et al. (2), non-reassuring data are extrapolated regarding the use of this type of therapy; the authors refrain from giving their opinion on the matter by virtue of the conflicting results regarding recovery times, the results that show a greater improvement in the control group compared to the treatment group, the low quality of the studies carried out and the high risk of bias. At the same time, in patients with chronic facial weakness, electrostimulation seem to be effective in maintaining good muscle tone and trophism and in decreasing the risk of complications. The extreme heterogeneity of the rehabilitation protocols used during the development of the RCTs remains a fundamental problem to standardize and protocol the rehabilitation treatment. Electrostimulation applied for 30 minutes a day or for 6 continuous hours, different types of current used, exercises carried out independently at home or only with the presence of therapists, application times and duration of treatments extremely variable from study to study, makes it impossible to establish a unique protocol that can be used as a reference for rehabilitators.

The use of biofeedback as a support for rehabilitation seems to be an important factor in improving functions and reducing recovery times. Mirror therapy and EMG have proved extremely useful as accessory tools, helping the patient to perform coordinated movements and to separate movements. The multidisciplinary setting remains the ideal place to intervene on patients, allowing easy access to the EMG and the management of sequelae associated with the pathology.

In acute injuries, physiotherapy does not seem to play a fundamental role in recovery, with low scientific evidence in favour of rehabilitation with the Kabat method, applied as early as possible every day until the fifteenth day of illness. Given the lack of adequate scientific literature to formulate a standardized protocol, it cannot be assessed how much physiotherapy intervenes in the recovery of facial nerve palsies. The multidisciplinary management of the patient by professionals of medicine, surgery, nursing, physiotherapy and psychotherapy allows the improvement of the functional outcome and the quality of life of the patients.

Another important aspect not to be underestimated is the containment of synkinesias, an outcome that was not included in the writing of this article, but on which it is important to spend a few words. From the analysis of the literature, the rehabilitation strategies available to professionals in the sector seem not to be effective in reducing synkinesias. In literature there are few works of low quality, which show a poor efficacy of physiotherapy treatments on this complication .

Implication for future research and clinical practice

Today, it is extremely important to provide clear evidence and high-level recommendations, due to their clinical relevance. From the analysis of the literature, it is evident how difficult it is to compare different rehabilitative interventions (physiotherapy or instrumental physical therapy), which use different therapeutic protocols on patients with facial palsy, but with different aetiology and follow-ups. Future studies are needed, in order to highlight the therapeutic implications of the different rehabilitation methods, with standardized protocols, in patients suffering from facial palsy of different aetiology.

CONCLUSION

Although this is the first umbrella review on this topic, there are some limits to the study. The results are too heterogeneous to establish an effective rehabilitation protocol. The articles, analysed by the various systematic reviews included in this review, use extremely variable protocols for time of application and duration of treatments. Experimental work mostly of not very high-quality limits the possibility of drawing objective conclusions.

In most of the studies analysed, the causes of peripheral facial palsy are mixed. For this reason, a clear correlation between the causes, the time of onset of the disease and the effectiveness of the rehabilitation treatment cannot be declared.

Even if the individual authors, in the reviews analysed in respect to the use of electrostimulation, do not express a clear opinion, surely this rehabilitative approach must be further investigated. Certainly, Mime therapy should be preferred in the rehabilitation of patients with peripheral idiopathic paresis of the facial nerve. The physiatrist must have a clear clinical picture and apply the most suitable strategies for each patient, to obtain an estimate of the degree and recovery time of the injured functions. Further studies are needed in order to better quantify the effectiveness of the various rehabilitation interventions in patients with idiopathic facial palsy.

REFERENCES

1. Monini S, Lazzarino AI, Iacolucci C, Buffoni A, Barbara M. Epidemiology of Bell's palsy in an Italian Health District: incidence and case-control study. Acta Otorhinolaryngol Ital 2010; 30(4):198.
2. Teixeira LJ, Valbuza JS, Prado GF. Physical therapy for Bell's palsy (idiopathic facial palsy). Cochrane Database Syst Rev 2011; (12):CD006283.
3. Adour KK, Bell DN, Hilsinger RL Jr. Herpes simplex virus in idiopathic facial palsy (Bell palsy). JAMA 1975; 233:527-30.
4. Cooper L, Lui M, Nduka C. Botulinum toxin treatment for facial palsy: A systematic review. J Plast Reconstr Aesthet Surg 2017; 70(6):833-41.
5. Paolucci T, Cardarola A, Colonnelli P, et al. Give me a kiss! An integrative rehabilitative training program with motor imagery and mirror therapy for recovery of facial palsy. Eur J Phys Rehabil Med 2020; 56(1):58-67.
6. Maddali-Bongi S, Landi G, Galluccio F, et al. The rehabilitation of facial involvement in systemic sclerosis: efficacy of the combination of connective tissue massage, Kabat's technique and kinesitherapy: a randomized controlled trial. Rheumatol Int 2011; 31(7):895-901.
7. Hg Beurskens C, Al Burgers-Bots I, W Kroon D, Ab Oostendorp R. Literature review of evidence-based physiotherapy in patients with facial nerve paresis. J Jpn Phys Ther Assoc 2004; 7(1):35-39.
8. VanSwearingen, J. Facial rehabilitation: a neuromuscular reeducation, patient-centered approach. Facial Plast Surg 2008; 24:250-59.
9. Ross B, Nedzelski JM, McLean JA. Efficacy of feedback training in long-standing facial nerve paresis. Laryngoscope 1991; 101(7):744-50.
10. Targan RS, Alon G, Kay SL. Effect of long-term electrical stimulation on motor recovery and

improvement of clinical residuals in patients with unresolved facial nerve palsy. Otolaryngol Head Neck Surg 2000; 122:246Y52.

11. de Almeida JR, Guyatt GH, Sud S, et al. Bell Palsy Working Group, Canadian Society of Otolaryngology - Head and Neck Surgery and Canadian Neurological Sciences Federation. Management of Bell palsy: clinical practice guideline. CMAJ 2014; 186(12):917-22.
12. Aromataris E, Fernandez R, Godfrey C, Holly C, Kahlil H, Tungpunkom P. Methodology for JBI umbrella reviews. In: Joanna Briggs Institute reviewer's manual 2014. The Joanna Briggs Institute, Adelaide.
13. Sun M, Oh MC, Safaee MM, Kaur G, Parsa AT. Neuroanatomical correlation of the House-Brackmann grading system in the microsurgical treatment of vestibular schwannoma. Neurosurg Focus 2012; 33(3):E7.
14. Hu WL, Ross B, Nedzelski J. Reliability of the Sunnybrook Facial Grading System by novice users. J Otolaryngol 2001; 30:208-11.
15. Kahn JB, Gliklich RE, Boyev KP, Stewart MG, Metson RB, McKenna MJ. Validation of a patient-graded instrument for facial nerve palsy: the FaCE scale. Laryngoscope 2001; 111(3):387-98.
16. VanSwearingen JM, Brach JS. The Facial Disability Index: reliability and validity of a disability assessment instrument for disorders of the facial neuromuscular system. Phys Ther 1996; 76:1288-98.
17. Pieper D, Koensgen N, Breuing J, Ge L, Wegewitz U. How is AMSTAR applied by authors - a call for better reporting. BMC Med Res Methodol 2018; 18;18(1):56.
18. Fargher KA, Coulson SE. Effectiveness of electrical stimulation for rehabilitation of facial nerve palsy. Phys Ther Rev 2017; 22:169-76.
19. Ferreira M, Ribeiro S, Paula C, Duarte J. Idiopathic facial palsy and physical therapy: an intervention proposal following a review of practice. Phys Ther Rev 2011;16.237-43.
20. Holland NJ, Bernstein JM. Bell's palsy. BMJ Clin Evid 2014; 2014:1204
21. Pereira L, Obara K, Dias J, Menacho M, Lavado E, Cardoso J. Facial exercise therapy for facial palsy: systematic review and meta-analysis. Clin Rehab 2011; 25(7):649-58.
22. Baricich A, Cabrio C, Paggio R, Cisari C, Aluffi P. Peripheral facial nerve palsy: how effective is rehabilitation? Otol Neurotol 2012; 33(7):1118-26

TRAF5 promotes the occurrence and development of colon cancer via the activation of PI3K/AKT/NF-κB signaling pathways

G. Sun[1,2*], C. Zheng[3*], Z. Deng[2], C. Huang[4] and J. Huang[1]

[1]Department of Gastroenterology, The Second Affiliated Hospital of Guangxi Medical University, Nanning, P.R. China; [2]Department of Clinical Nutrition, The Third Affiliated Hospital of Guangxi Medical University, Nanning, P.R. China; [3]Department of Anatomy, Guangxi University of Chinese Medicine, Nanning, P.R. China; [4]Department of Oncology, The Third Affiliated Hospital of Guangxi Medical University, Nanning, P.R. China

Received November 28, 2019 – Accepted May 27, 2020

[*]These Authors contributed equally to this paper

This study aimed to investigate the expression and biological functions of TRAF5 in colon cancer at tissue and cellular levels. Forty-two patients with colon cancer were included in the present study. Tumor tissues and tumor-adjacent tissues were collected from all patients. Bioinformatics was used to analyze how TRAF5 was related to metastasis and prognosis of colon cancer. Quantitative real-time polymerase chain reaction was carried out to determine the expression of mRNA. SW620 and SW480 cells were used to study the inhibition and overexpression of TRAF5, respectively. CCK-8 assay was used to examine cell proliferation. Flow cytometry was employed to investigate cell phase and apoptosis. Transwell assay was used to study migration and invasion of cells. Western blotting was utilized to test how TRAF5 expression affected the activities of PI3K/AKT/NF-κB signaling pathways. Bioinformatics showed that the expression of TRAF5 in colon cancer tissues was correlated with metastasis and prognosis of the tumor. TRAF5 mRNA expression was up-regulated in colon cancer tissues, and related to recurrence and metastasis of the cancer. In vitro experiments showed that TRAF5 expression promoted proliferation, migration, and invasion of colon cancer cells, but reduced apoptosis of the cells. Moreover, TRAF5 might exert its biological functions by activating PI3K/AKT/NF-κB signaling pathways in colon cancer cells. In conclusion, TRAF5 expression in colon cancer tissues is up-regulated and correlated with prognosis, lymphatic metastasis and clinical staging. TRAF5 promotes the occurrence and development of colon cancer by activating PI3K/AKT/NF-κB signaling pathways, and acts as an oncogene.

Colon cancer is one of the most common digestive tract malignant tumors in the world, and its incidence is the third highest among all malignant tumors (1, 2). Epidemiological studies have shown that colon cancer is caused by various external and internal factors (3). External factors include exposure to carcinogens, environmental degradation, and unhealthy diet, and internal factors are mainly genetic, such as adenomatous polyposis coli (APC) protein inactivation and ras mutation (4). With the rapid development

Key words: *TRAF5, colon cancer, PI3K/AKT/NF-κB signaling pathway*

Corresponding Author:
Prof. Jie'an Huang,
Department of Gastroenterology,
The Second Affiliated Hospital of Guangxi Medical University,
No. 166 Daxuedong Road, Nanning 530007,
Guangxi Zhuang Autonomous Region, P.R. China
e-mail: jh23229@163.com

0393-974X (2020)
Copyright © by BIOLIFE, s.a.s.
This publication and/or article is for individual use only and may not be further reproduced without written permission from the copyright holder.
Unauthorized reproduction may result in financial and other penalties
DISCLOSURE: ALL AUTHORS REPORT NO CONFLICTS OF INTEREST RELEVANT TO THIS ARTICLE.

of Chinese economy and society, the incidence of colon cancer has been rising rapidly (5). The early clinical symptoms of colon cancer are hidden. When the patients are diagnosed, most of them are at the progression stage of the tumor, and distal metastasis greatly restricts the therapeutic effects of surgery and chemotherapy (6). Tumor recurrence and metastasis are the main causes of poor prognosis in colon cancer patients, however, there is still no effective means to inhibit the recurrence and metastasis (7). Studies show that tumor recurrence and metastasis involve many biological characteristics of tumor cells, such as epithelial mesenchymal transition, tumor angiogenesis, tumor stem cells, autophagy (8, 9). In addition, these processes are regulated by multiple genes and signaling pathways (8, 9). The molecular mechanisms of tumor recurrence and metastasis still remain to be further explored.

Tumor necrosis factor receptor-associated factor (TRAF) is an important adapter protein involved in intracellular signal transduction (10, 11). TRAF family of proteins may be linked to the members of TNFR and IL-1R/TLR families, and are involved in the activation of downstream signal transduction pathways such as NF-κB and JNK (12). Moreover, TRAF family of proteins have important regulatory roles on biological functions of normal and tumor cells such as proliferation, survival, apoptosis, and inflammatory responses (12). Six members of TRAF protein family (TRAF1-6) have been discovered with similar protein structures. It is reported that TRAF2, TRAF3, and TRAF6 are widely expressed in normal tissue cells, while the expression of TRAF1, TRAF4, and TRAF5 is tissue-specific (13, 14). One study shows that expression of TRAF proteins is disordered in a variety of tumors and closely related to the malignant phenotypes of tumor cells (15). For example, TRAF1 has been proven to be highly expressed in nasopharyngeal carcinoma (16), and TRAF3 participates in the regulation of apoptosis of bladder cancer cells (17). TRAF5 protein contains a meprin and TRAF homology (MATH) domain, a RING-type zinc finger, and two TRAF-type zinc fingers (18). On the one hand, TRAF5 binds with its receptor protein via TRAF domain at its carboxyl terminus; on the other hand, it mediates DNA-protein or protein-protein interactions and transfers internalized signals through zinc finger domain at its amino terminal (19). It is shown that TRAF5 participates in the signal transduction mediated by CD30 or LT-βR proteins, and is related to the regulation of NF-κB and JNK signaling pathways (20, 21). More importantly, TRAF5 is abnormally expressed in a variety of tumors and is closely related to the occurrence and development of tumors. At present, the expression and mechanisms of action of TRAF5 in colon cancer are not clear, and further studies are still needed. In the present study, we investigated the functions of TRAF5 in colon cancer using bioinformatics, cell biology and molecular biology.

MATERIALS AND METHODS

A total of 42 patients (31 males and 11 females; age range 32–67 years, mean 42.6 years) with colon cancer who underwent surgery at our hospital between January 2016 and January 2017 were included in the present study. Tumor tissues and tumor-adjacent tissues were collected from all patients. Patients who had undergone chemotherapy or radiotherapy before surgery, other types of tumors or basic chronic diseases, or long history of drug intake were excluded from the study. Clinical and pathological data of all patients were collected, including tumor size, TNM staging, tumor differentiation degree, lymphatic metastasis, and distal metastasis. All procedures were approved by the Ethics Committee of Guangxi Medical University. Written informed consents were obtained from all patients or their families.

Cell culture and transfection

Colon cancer SW480 and SW620 cells were cultured in DMEM medium supplemented with 10% fetal bovine serum (FBS), 100 IU/ml penicillin and 100 IU/ml streptomycin (all from Thermo Fisher Scientific, Waltham, MA, USA) under 37°C, 5% CO_2, and 70% humidity. The cells were passaged every three days, and cells in logarithmic growth phase were collected for experiments.

One day before transfection, SW620 or SW480 cells (2×10^5) were seeded onto 24-well plates, and cultured in antibiotic-free DMEM medium supplemented with 10% FBS until reaching 70% confluency. In the first vial, 1.5 μL TRAF5 small-interfering RNA (siRNA; 20 pmol/μL;

siRNA group) or TRAF5 plasmids (0.5 μg; TRAF5 group) (Hanbio Biotechnology Co., Ltd., Shanghai, China) was mixed with 50 μl Opti Mem medium (Thermo Fisher Scientific, Waltham, MA, USA). In the second vial, 1 μL Lipofectamine 3000 (Thermo Fisher Scientific, Waltham, MA, USA) was mixed with 50 μl Opti Mem medium. After standing still for 5 min, the two vials were combined before leaving at room temperature for 20 min. Then, the mixtures were added onto cells in respective groups before incubation under 5% CO_2 and 37°C. Six hours later, the medium was replaced with DMEM medium containing 10% FBS. After cultivation for 48 h under 5% CO_2 and 37°C, the cells were collected for further assays.

Bioinformatics

Chip No. GSE2509 was searched in GEODATASET database on PubMed website (http://www.pubmed.com). This chip was used to analyze differential expression of mRNA in colon cancer SW480 and SW620 cells. TRAF5 gene was inserted to confirm its expression in the two cell lines. In the meantime, we searched TRAF5 in Gepia database (http://gepia.cancer-pku.cn/) to analyze its expression in colon cancer and survival curve.

Quantitative real-time polymerase chain reaction (qRT-PCR)

Samples (100 mg colon cancer tissues) were ground into powder in liquid nitrogen and lysed using 1 ml TRIzol reagent following the manufacturer's manual (Thermo Fisher Scientific, Waltham, MA, USA). Then, total RNA was extracted using the phenol chloroform method. The concentration and quality of RNA was measured using ultraviolet spectrophotometry (Nanodrop ND2000, Thermo Scientific, Waltham, MA, USA). Then, cDNA was obtained by reverse transcription from 1 μg RNA and stored at -20°C. Reverse transcription of mRNA was performed using miScript II RT Kit (Qiagen, Hilden, Germany).

To detect mRNA expression, miScript SYBR® Green PCR Kit (Qiagen, Hilden, Germany) was used and GAPDH was used as internal reference. The reaction system (20 μl) was composed of 10 μl qRT-PCR-Mix, 0.5 μl upstream primer (5'-GGAGCACATGCGTTTGGTTT-3'), 0.5 μl downstream primer (5'-ATCCACCGCCTCTCTCTTCT-3'), 2 μl cDNA and 7 μl ddH_2O. PCR condition was: initial denaturation at 95°C for 10 min; 40 cycles of denaturation at 95°C for 1 min, elongation at 60°C for 30 s (iQ5; Bio-Rad, Hercules, CA, USA). The $2^{-\Delta\Delta Ct}$ method was used to calculate the relative expression of TRAF5 mRNA against internal reference. Each sample was tested in triplicate.

CCK-8 assay

Cells were seeded at a density of 2,000/well in 96-well plates. At 0, 24, 48 and 72 h, 20 μl CCK-8 (5 g/L; Beyotime, Shanghai, China) was added onto the cells. After incubation at 37°C for 2 h, the absorbance of each well was measured at 490 nm for plotting cell proliferation curves. Each group was tested in 3 replicate wells and the values were averaged.

Transwell assay

Matrigel was thawed at 4°C overnight and diluted with serum-free DMEM medium (dilution 1:2). The mixture (50 μl) was evenly smeared into the upper chamber (Merck Millipore, Billerica, MA, USA) and incubated at 37°C for 1 h. After solidification, 1×10^5 cells from each group were seeded into the upper chamber containing 200 μl serum-free DMEM medium. In addition, 500 μl DMEM medium supplemented with 10% FBS was added into the lower chamber. After cultivation under 37°C and 5% CO_2 for 24 h, the chamber was removed and the cells in the upper chamber were wiped off. After being fixed with 4% formaldehyde for 10 min, the membrane was stained using Giemsa method for microscopic observation of 5 random fields (200×). The number of Transwell cells was calculated for the evaluation of cell migration and invasion abilities. All procedures were carried out on ice with pipetting tips being precooled at 4°C.

Flow cytometry

At 24 h after transfection, cells (1×10^6) in each group were washed with pre-cooled phosphate-buffered saline twice and subjected to flow cytometry using Cell Cycle Assay Kit (BD Biosciences, Franklin Lakes, NJ, USA) following the manufacturer's manual to detect cell cycle. The data were analyzed using ModFit software (Verity Software House, Topsham, ME, USA).

At 24 h after transfection, cells (1×10^6) in each group was washed with pre-cooled phosphate-buffered saline twice and subjected to flow cytometry using ANXN V FITC Apoptosis DTEC Kit I (BD Biosciences, Franklin Lakes, NJ, USA) following the manufacturer's instructions. Cells with ANNEXIN V-positive values were early apoptotic

cells, those with PI-positive values were necrotic cells, and those with double positive values were late apoptotic cells.

Western blotting

Cells in each group were trypsinized and collected. Then, precooled Radio-Immunoprecipitation Assay (RIPA) lysis buffer (600 µl; 50 mM Tris-base, 1 mM EDTA, 150 mM NaCl, 0.1% sodium dodecyl sulfate, 1% TritonX-100, 1% sodium deoxycholate (Beyotime Institute of Biotechnology, Shanghai, China) was added to the samples. After lysis for 30 min on ice, the mixture was centrifuged at 12,000 rpm and 4°C for 10 min. The supernatant was used to determine protein concentration by bicinchoninic acid (BCA) protein concentration determination kit (RTP7102, Real-Times Biotechnology Co., Ltd., Beijing, China). Protein samples were then mixed with 5× sodium dodecyl sulfate loading buffer before denaturation in boiling water bath for 10 min. Afterwards, the samples (10 µl) were subjected to 10% sodium dodecyl sulfate-polyacrylamide gel electrophoresis. The resolved proteins were transferred to polyvinylidene difluoride membranes on ice (250 mA, 1 h) and blocked with 50 g/L skimmed milk at room temperature for 1 h. Then, the membranes were incubated with rabbit anti-human polyclonal TRAF5 (1:1,000; Abcam, Cambridge, UK), polyclonal p110α (1:1000; #4255; Cell Signaling Technology, Danvers, MA, USA), monoclonal P85 (1:1000; #4257; Cell Signaling Technology, Danvers, MA, USA), and monoclonal NF-κB (1:1000; AF1234; Beyotime, Shanghai, China) primary antibodies and mouse anti-human GAPDH primary antibody (1:4,000; Abcam, Cambridge, UK) at 4°C overnight. After extensive washing with phosphate-buffered saline with Tween 20 for 5 times of 5 min, the membranes were incubated with goat anti-rabbit (1:2,000) and goat anti-mouse (1:4,000) horseradish peroxidase-conjugated secondary antibodies (Abcam, Cambridge, UK), respectively, for 1 h at room temperature before washing with phosphate-buffered saline with Tween 20 for 5 times of 5 min. Then, the membrane was developed with enhanced chemiluminescence detection kit (Sigma-Aldrich, St. Louis, MO, USA) for imaging. Image lab v3.0 software (Bio-Rad, Hercules, CA, USA) was used to acquire and analyze imaging signals. The relative content of TRAF5 protein was expressed as TRAF5/GAPDH ratio.

Statistical analysis

The results were analyzed using SPSS 18.0 statistical software (IBM, Armonk, NY, USA). The data were expressed as means ± standard deviations. Data were tested for normality. Multigroup measurement data were analyzed using one-way ANOVA. In case of homogeneity of variance, Least Significant Difference and Student-Newman-Keuls methods were used; in case of heterogeneity of variance, Tamhane's T2 or Dunnett's T3 method was used. Comparison between two groups was carried out using Student's *t*-test. $P < 0.05$ indicated statistically significant differences.

RESULTS

TRAF5 mRNA expression in up-regulated in colon cancer tissues and may be closely related to the recurrence and metastasis of the cancer

To measure the expression of TRAF5, bioinformatics and qRT-PCR were used. GEO Datasets (GSE2509) analysis showed that expression of TRAF5 in SW620 cells was significantly higher than that in SW480 cells ($P < 0.01$) (Fig. 1A). In addition, Gepia database analysis showed that expression of TRAF5 in colon cancer tissues was significantly higher than that in tumor-adjacent tissues ($P < 0.01$) (Fig. 1B). Survival analysis results showed that overall survival of colon cancer patients with high expression of TRAF5 was not significantly different from that in patients with low expression of TRAF5 ($P = 0.06$), while disease-free survival of patients with high TRAF5 expression was significantly lower than that of patients with low TRAF5 expression ($P = 0.009$) (Fig. 1 C and D). qRT-PCR data showed that TRAF5 mRNA expression in colon cancer tissues was significantly higher than that in tumor-adjacent tissues ($P < 0.01$) (Fig. 1E). In addition, TRAF5 mRNA expression in colon cancer tissues from lymphatic metastasis group (N1) was significantly higher than that from the non-lymphatic metastasis group (N0) ($P < 0.05$) (Fig. 1F). TRAF5 mRNA expression in colon cancer tissues from patients at III/IV clinical stages was significantly higher than that from patients at I/II clinical stages ($P < 0.05$) (Fig. 1G). However, TRAF5 expressions in tumor cancer tissues from colon cancer patients with different degrees of differentiation were not significantly different from each other ($P > 0.05$) (Fig. 1H). The results suggest that TRAF5 mRNA

expression is up-regulated in colon cancer tissues and may be closely related to the recurrence and metastasis of the cancer.

TRAF5 expression promotes the proliferation of colon cancer cells

To test how TRAF5 affects the proliferation of colon cancer cells, interference and overexpression of TRAF5 were carried out. Western blotting data showed that TRAF5 protein expression in SW620 cells of siR-TRAF5 group was suppressed, while that in SW480 cells of TRAF5 overexpression group was up-regulated ($P < 0.01$) (Fig. 2 A and B). CCK-8 assay showed that the absorbance of SW620 cells in siR-TRAF5 group was significantly lower than that in siR-NC group at 24, 48 or 72 h ($P < 0.05$) (Fig. 2C). By contrast, the absorbance of SW480 cells in TRAF5 overexpression group was significantly higher than that in its relevant NC group at 24, 48 or 72 h ($P < 0.05$) (Fig. 2D). Flow cytometry showed that the percentage of SW620 cells in G1 phase from siR-TRAF5 group was significantly higher than that in siR-NC group ($P < 0.05$), while the percentage of the cells in S phase from siR-TRAF5 group was significantly lower than that in siR-NC group ($P < 0.05$) (Fig. 2E). However, the percentage of SW480 cells in G1 phase from TRAF5 overexpression group was significantly lower than that in its relevant NC group ($P < 0.05$), while the percentage of the cells in S phase from TRAF5 overexpression group was significantly higher than that in its relevant NC group ($P < 0.05$) (Fig. 2F). The results indicate that TRAF5 expression promotes the proliferation of colon cancer cells.

TRAF5 expression enhances the migration and invasion of colon cancer cells

To test examine the effect of TRAF5 expression on the migration and invasion abilities of colon cancer cells, Transwell assay was carried out. Migration and invasion data both showed that the number of SW620 cells in siR-TRAF5 group that crossed chamber membrane was significantly decreased compared with that in siR-NC group ($P < 0.05$), while the number of SW480 cells in TRAF5 overexpression group that crossed chamber membrane was significantly higher than that in its NC group ($P < 0.05$) (Fig. 3 A and B). These results suggest that TRAF5 expression enhances the migration and invasion of colon cancer cells.

TRAF5 expression reduces apoptosis of colon cancer cells

To study cell apoptosis, flow cytometry was used. The data showed that the apoptotic rate of SW620 cells in the siR-TRAF5 group was significantly higher than that in siR-NC group ($P < 0.05$), while the apoptotic rate of SW480 cells in TRAF5 overexpression group was significantly lower than that in its relevant NC group ($P < 0.05$) (Fig. 4). This result indicates that TRAF5 expression reduces apoptosis of colon cancer cells.

TRAF5 activates PI3K/AKT/NF-κB signaling pathways in colon cancer cells

To examine how TRAF5 expression affects PI3K/AKT/NF-κB signaling pathways, Western blotting was carried out. The data showed that expression of p110α, p85 and NF-κB proteins in SW620 cells of siR-TRAF5 group was significantly lower than that in siR-NC group ($P < 0.05$) (Fig. 5A). In addition, nucleic NF-κB expression of siR-TRAF5 group was significantly lower than that in siR-NC group ($P < 0.05$) (Fig. 5A). On the other hand, p110α protein level in SW480 cells of TRAF5 overexpression group was significantly higher than that in its NC group ($P < 0.05$), while the levels of p85 and NF-κB proteins in TRAF5 overexpression group were not significantly different from that in its NC group ($P > 0.05$) (Fig. 5B). By contrast, nucleic NF-κB protein expression in TRAF5 overexpression group was significantly higher than that in its NC group ($P < 0.05$) (Fig. 5B). These results suggest that TRAF5 activates PI3K/AKT/NF-κB signaling pathways in colon cancer cells.

DISCUSSION

Tumor recurrence and metastasis are the main reasons limiting clinical therapeutic effects in colon cancer patients (22). Studies show that the acquisition of high metastatic potential in colon cancer cells is a complex process involving a variety of factors, such as gene mutation, methylation, immunosuppression (23, 24). TRAF family proteins have been widely studied

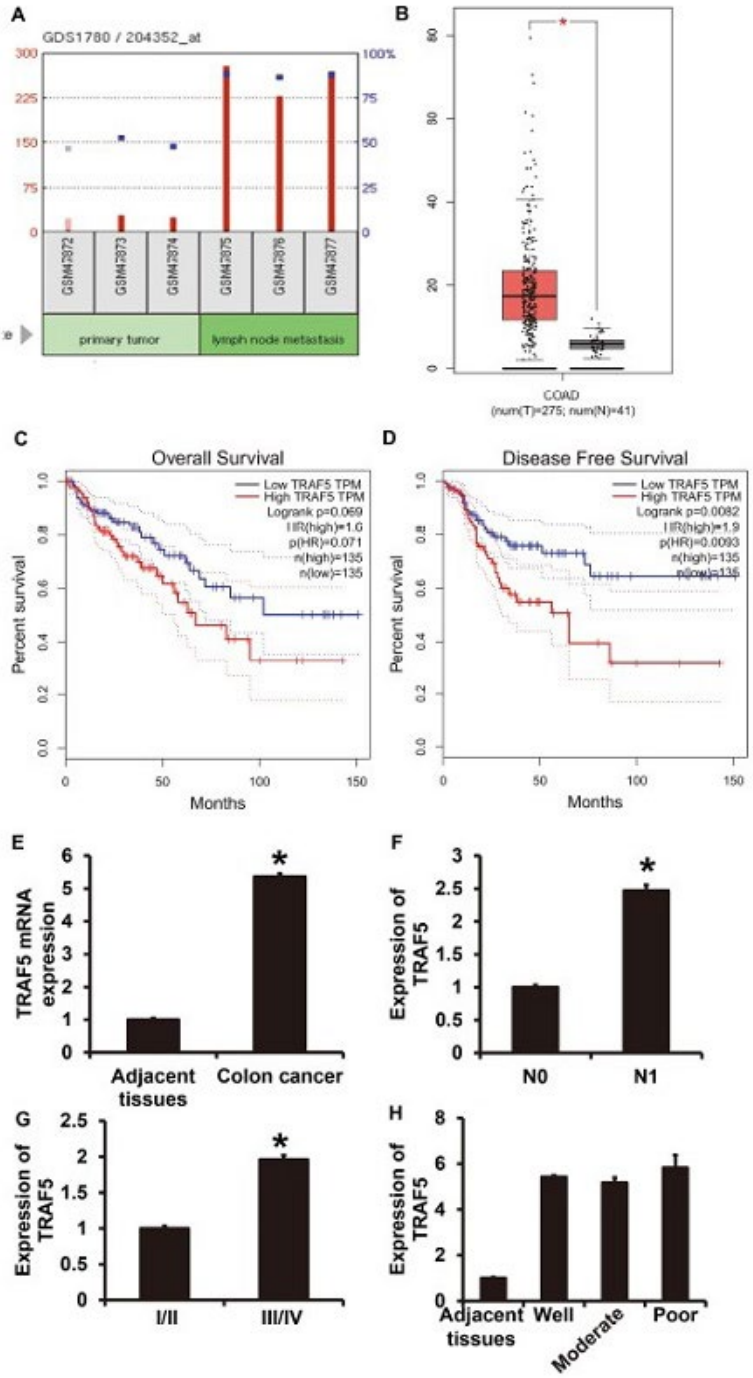

Fig. 1. *Expression of TRAF5 in colon cancer and its clinical relativity.* ***A****) Expression of TRAF5 in SW620 and SW480 cells as shown by GEO Datasets (GSE2509).* ***B****) Expression of TRAF5 in colon cancer tissues as shown by Gepia database analysis.* ***C****) Correlation between TRAF5 and overall survival of colon cancer patients.* ***D****) Correlation between TRAF5 and disease-free survival of colon cancer patients.* ***E****) Expression of TRAF5 mRNA in colon cancer and tumor-adjacent tissues. *P < 0.05 compared with tumor-adjacent tissues.* ***F****) Expression of TRAF5 mRNA in colon cancer tissues from patients without lymphatic metastasis (N0) and with lymphatic metastasis (N1). *P < 0.05 compared with N0 group.* ***G****) Expression of TRAF5 mRNA in colon cancer tissues from patients at TNM stages I/II and III/IV. *P < 0.05 compared with I/II group.* ***H****) Expression of TRAF5 mRNA in colon cancer tissues from patients with well, moderate and poor differentiation. TRAF5 mRNA levels were determined by quantitative real-time polymerase chain reaction.*

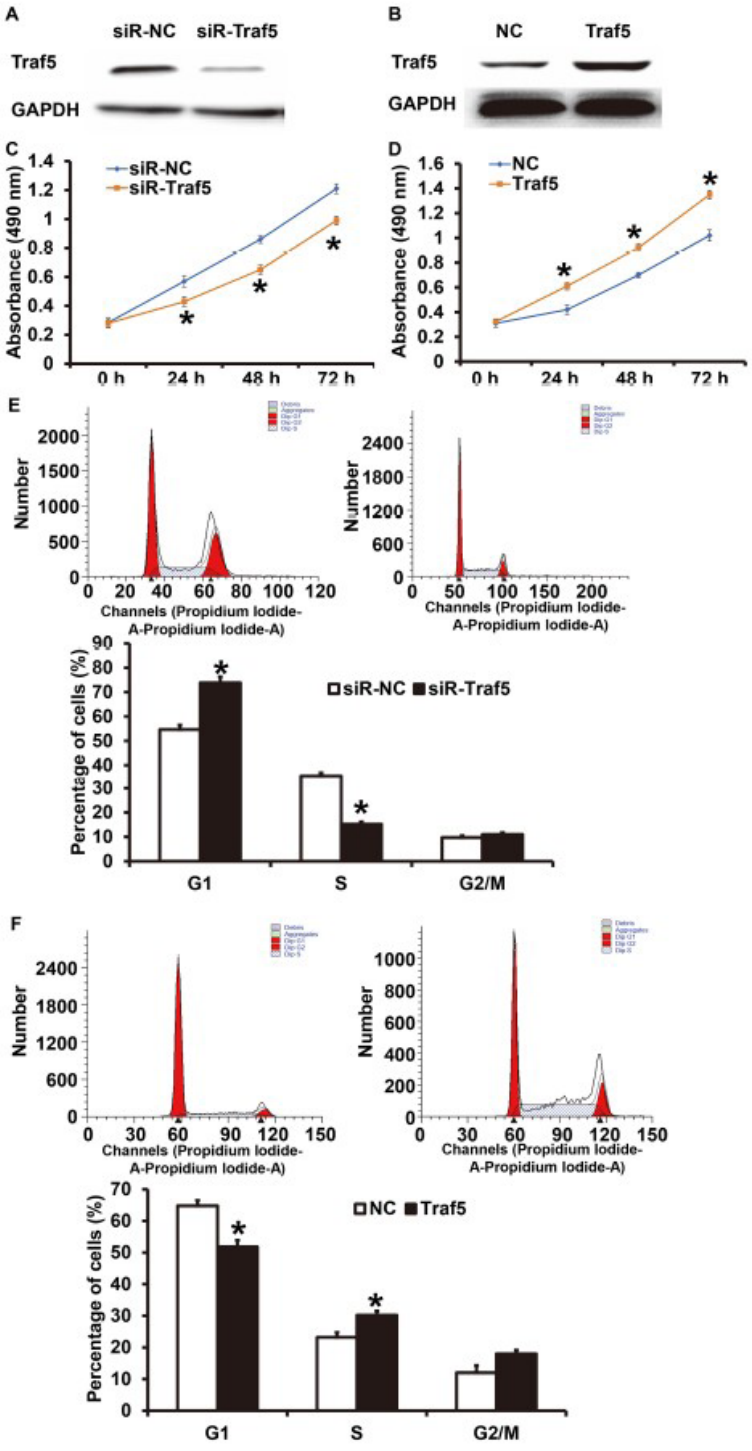

Fig. 2. *Effect of TRAF5 on the proliferation and cell cycle of colon cancer cells.* ***A-B****) TRAF5 protein expression in SW620 cells of (A) siR-TRAF5 group and (B) TRAF5 overexpression group was up-regulated.* ***C****) Effect of TRAF5 inhibition on the proliferation of SW620 cells. *P < 0.05 compared with siR-negative control (siR-NC) at indicated time points.* ***D****) Effect of TRAF5 overexpression on the proliferation of SW480 cells. *P < 0.05 compared with negative control (NC) at indicated time points.* ***E****) Effect of TRAF5 inhibition on the cell cycle of SW620 cells. *P < 0.05 compared with siR-NC at each phase.* ***F****) Effect of TRAF5 overexpression on the cell cycle of SW480 cells. *P < 0.05 compared with NC at each phase.*

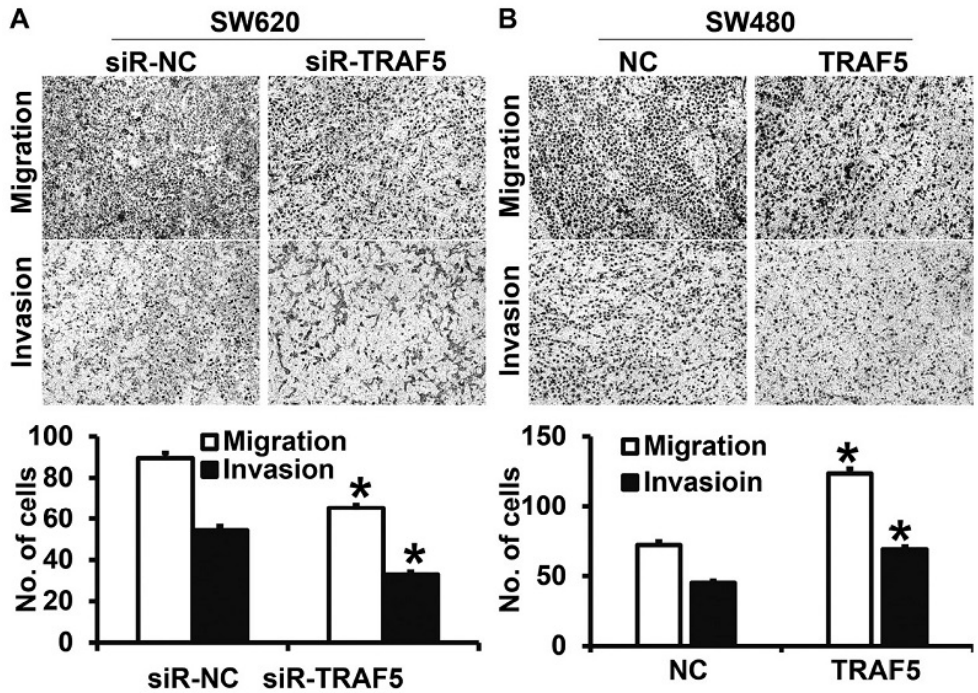

Fig. 3. *Effect of TRAF5 on the migration and invasion of colon cancer cells.* ***A)*** *Effect of TRAF5 inhibition on the migration and invasion of SW620 cells. *P < 0.05 compared with siR-NC for migration or invasion assays.* ***B)*** *Effect of TRAF5 overexpression on the migration and invasion of SW480 cells. *P < 0.05 compared with NC for migration or invasion assays.*

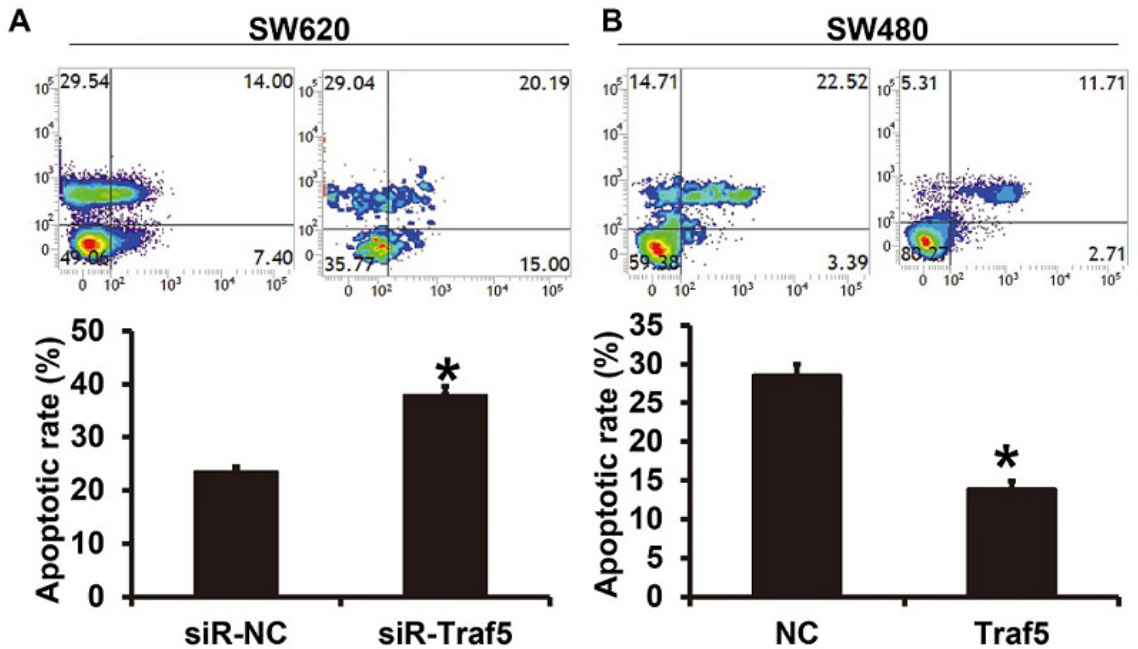

Fig. 4. *Effect of TRAF5 on the apoptosis of colon cancer.* ***A)*** *Effect of TRAF5 inhibition on the apoptosis of SW620 cells. *P < 0.05 compared with siR-NC.* ***B)*** *Effect of TRAF5 overexpression on the apoptosis of SW480 cells. *P < 0.05 compared with NC.*

in recent years because they act as joint proteins in signal transduction and play a role in regulating intracellular and extracellular signal transductions (25). It is reported that TRAF proteins play important roles in the occurrence and development of tumors, and participate in the regulation of the proliferation, apoptosis, metastasis and angiogenesis of tumor cells (26). For example, Wan et al. found that *Helicobacter pylori* induces up-regulation of TRAF1 protein, and promotes apoptosis resistance of infected cells, which may be related to the carcinogenicity of *Helicobacter pylori* (27). Zhou et al. discovered that TRAF4 is up-regulated in breast cancer and plays an oncogene function by mediating the activation of TGF-β signaling (28). However, the expression and function of TRAF proteins in colon cancer are unclear. In the present study, we found that the expression of TRAF5 protein in colon cancer SW620 cells with high invasive potential was significantly higher than that in colon cancer SW480 cells with low invasion potential according to bioinformatics. Further analysis showed that the disease-free survival of patients with high TRAF5 expression was lower than that of patients with low TRAF5 expression. Our qRT-PCR results

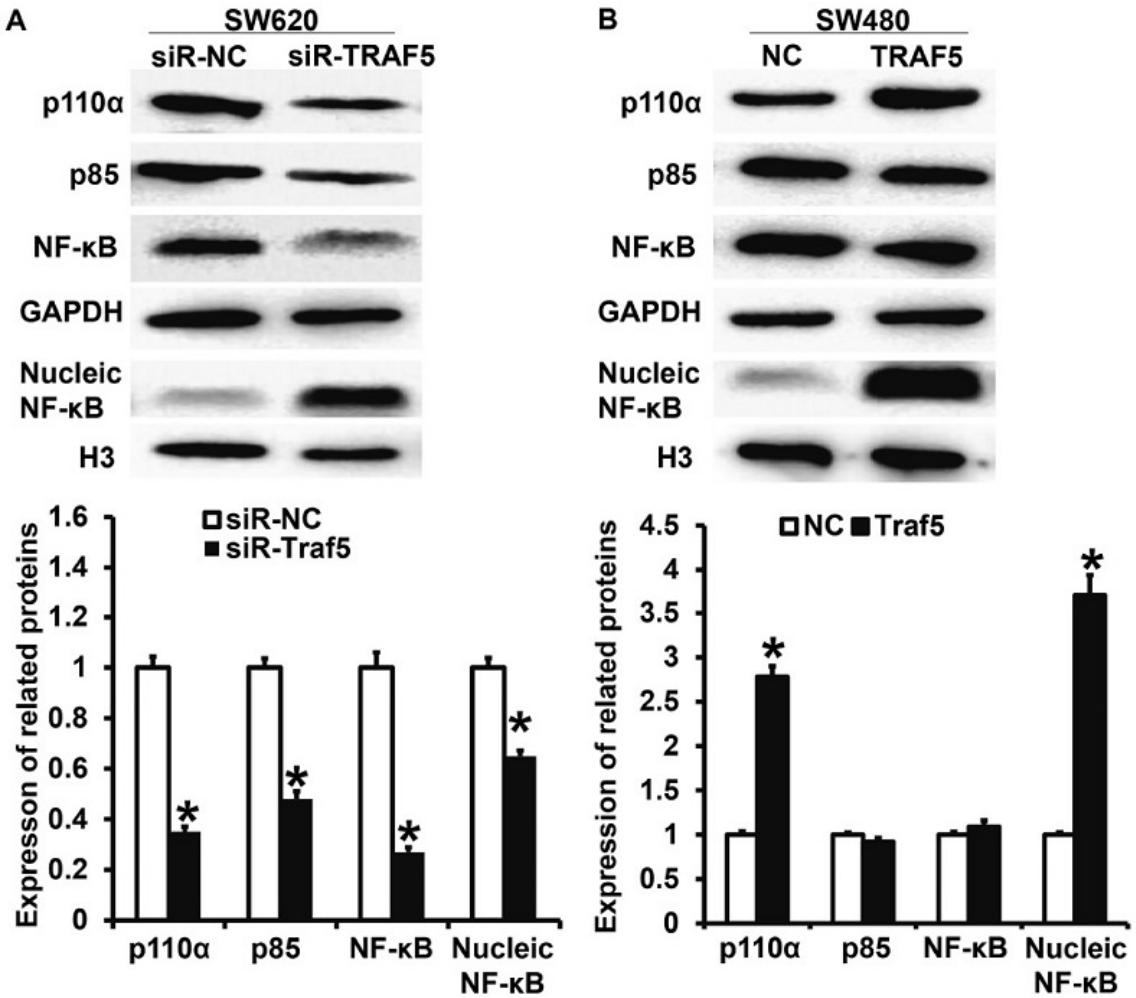

Fig. 5. *Effect of TRAF5 on the expression of proteins related to PI3K/AKT/NF-κB signaling pathways. **A**) Effect of TRAF5 inhibition on p110α, p85, NF-κB and nucleic NF-κB protein expression in SW620 cells. *P < 0.05 compared with siR-NC for each protein. **B**) Effect of TRAF5 overexpression on p110α, p85, NF-κB and nucleic NF-κB protein expression in SW480 cells. *P < 0.05 compared with NC for each protein.*

showed that TRAF5 mRNA expression in colon cancer tissues was higher than that in tumor-adjacent tissues, and positively correlated with lymphatic metastasis and TNM staging, suggesting that TRAF5 expression promoted the metastasis of colon cancer. In fact, literature regarding TRAF5 is scarce, and the function of TRAF5 differs among different tumors. For example, Chen et al. showed that TRAF5 is a downstream target gene of miR-26b, and the expression of TRAF5 induced by down-regulation of miR-26b can inhibit the metastasis of squamous cell carcinoma of the esophagus, suggesting that TRAF5 is a tumor-suppressor gene (29). By contrast, Li et al. discover that miR-26b inhibits the proliferation and metastasis of melanoma cells by down-regulation of TRAF5, suggesting that TRAF5 is an oncogene (30). Our study showed that the proliferation, migration and invasion of SW620 cells were down-regulated and the apoptosis was promoted after interfering TRAF5 expression. In addition, the proliferation, migration and invasion of SW480 cells were up-regulated after TRAF5 overexpression. These results indicated that TRAF5 played a role in colon cancer as an oncogene.

PI3K/AKT/NF-κB signaling pathway plays important roles in the proliferation, survival, and drug resistance of tumor cells (31). Studies show that TRAF family proteins have important interactions with PI3K/AKT/NF-κB signaling pathways. For example, Guo et al. discover that TRAF1 protein participates in the activation of NF-κB signaling pathway in Hodgkin lymphocytes (32). Lv et al. show that TRAF6/NF-κB signaling pathway is involved in miR-146a-mediated inflammation inhibition process (33). However, the regulatory relationship between the TRAF family and the PI3K/AKT signaling pathway is rarely reported. In the present study, we discovered that the expression of catalytic subunit p110α in PI3K/AKT signaling pathway was positively regulated by TRAF5, while the expression of regulatory subunit p85 and NF-κB was only down-regulated in SW620 cells with TRAF5 interference. Of note, Western blotting showed that TRAF5 promoted the nuclear entry of NF-κB. These results suggested that TRAF5 promoted the recurrence and metastasis of colon cancer by activating PI3K/AKT/NF-κB signaling pathways.

In conclusion, the present study demonstrates that TRAF5 expression is up-regulated in colon cancer, and closely related with the prognosis of patients. In addition, TRAF5 promotes the occurrence and development of colon cancer via the activation of PI3K/AKT/NF-κB signaling pathways.

ACKNOWLEDGEMENTS

We thank Xiangping Wang (The Third Affiliated Hospital of Guangxi Medical University) for help in sample collection, and Junlin Shi (Guangxi Medical University) for experimental technical assistance. Finally, we would like to thank Jianxiong Long (Guangxi Medical University) for help in data analysis.

REFERENCES

1. Di J, Zhuang M, Yang H, Jiang B, Wang Z, Su X. Clinical significance of circulating immune cells in left- and right-sided colon cancer. PeerJ 2017; 5:e4153.
2. Morris L, Beketaev I, Barrios R, Reardon P. Colon adenocarcinoma after jejunoileal bypass for morbid obesity. J Surg Case Rep 2017; 2017:rjx214.
3. Rai A, Kumar U, Raj V, et al. Novel 1,4-benzothazines obliterate COX-2 mediated JAK-2/STAT-3 signals with potential regulation of oxidative and metabolic stress during colorectal cancer. Pharmacol Res 2018; 132:188-203.
4. Yang L, He W, Yang Q, et al. Combination of primary tumor location and mismatch repair status guides adjuvant chemotherapy in stage II colon cancer. Oncotarget 2017; 8:991369149.
5. Sun ZQ, Chen C, Zhou QB, et al. Long non-coding RNA LINC00959 predicts colorectal cancer patient prognosis and inhibits tumor progression. Oncotarget 2017; 8:97052-60.
6. Zhou G, Peng K, Song Y, et al. CD177+ neutrophils suppress epithelial cell tumourigenesis in colitis-associated cancer and predict good prognosis in colorectal cancer. Carcinogenesis 2018; 39:272-82.
7. Ogutu FO, Mu TH, Sun H, Zhang M. Ultrasonic modified sweet potato pectin induces apoptosis like cell death in colon cancer (HT-29) cell line. Nutr Cancer 2018; 70:136-45.

8. Kabashima A, Kimura K, Sanefuji K, Maekawa S. Completely responsive multiple liver recurrence of colon cancer treated using chemotherapy with oral S-1 and oxaliplatin plus bevacizumab : A case report. Fukuoka Igaku Zasshi 2017; 108:8-13.
9. Dou H, Shen R, Tao J, et al. Curcumin suppresses the colon cancer proliferation by inhibiting Wnt/beta-Catenin pathways via miR-130a. Front Pharmacol 2017; 8:877.
10. Middleton AJ, Budhidarmo R, Das A, et al. The activity of TRAF RING homo- and heterodimers is regulated by zinc finger 1. Nat Commun 2017; 8:1788.
11. Qu F, Xiang Z, Zhou Y, Qin Y. A molluscan TNF receptor-associated factor 2 (TRAF2) was involved in host defense against immune challenges. Fish Shellfish Immunol 2017; 71:105-15.
12. Biswas R, Bagchi A. Inhibition of TRAF6-Ubc13 interaction in NFkB inflammatory pathway by analyzing the hotspot amino acid residues and protein-protein interactions using molecular docking simulations. Comput Biol Chem 2017; 70:116-24.
13. Cullell N, Muino E, Carrera C, Torres N, Krupinski J, Fernandez-Cadenas I. Role of TRAF3 in neurological and cardiovascular diseases: an overview of recent studies. Biomol Concepts 2017; 8:197-202.
14. Mao F, Li J, Zhang Y, Xiang Z, Zhang Y, Yu Z. Molecular cloning and functional analysis of tumor necrosis factor receptor-associated factor 6 (TRAF6) in Crossastrea gigas. Fish Shellfish Immunol 2017; 68:37-45.
15. Zhu LJ, Yang TC, Wu Q, et al. Tumor necrosis factor receptor-associated factor (TRAF) 6 inhibition mitigates the pro-inflammatory roles and proliferation of rheumatoid arthritis fibroblast-like synoviocytes. Cytokine 2017; 93:26-33.
16. Siegler G, Meyer B, Dawson C, et al. Expression of tumor necrosis factor receptor-associated factor 1 in nasopharyngeal carcinoma: possible upregulation by Epstein-Barr virus latent membrane protein 1. Int J Cancer 2004; 112:265-72.
17. Elmetwali T, Young LS, Palmer DH. CD40 ligand-induced carcinoma cell death: a balance between activation of TNFR-associated factor (TRAF) 3-dependent death signals and suppression of TRAF6-dependent survival signals. J Immunol 2010; 184:1111-20.
18. Gao L, Wang PX, Zhang Y, et al. Tumor necrosis factor receptor-associated factor 5 (Traf5) acts as an essential negative regulator of hepatic steatosis. J Hepatol 2016; 65:125-36.
19. Wang X, Yang J, Han L, et al. TRAF5-mediated Lys-63-linked polyubiquitination plays an essential role in positive regulation of RORgammat in promoting IL-17A expression. J Biol Chem 2015; 290:29086-94.
20. Horie R, Watanabe T, Ito K, et al. Cytoplasmic aggregation of TRAF2 and TRAF5 proteins in the Hodgkin-Reed-Sternberg cells. Am J Pathol 2002; 160:1647-54.
21. Horie R, Watanabe T, Morishita Y, et al. Ligand-independent signaling by overexpressed CD30 drives NF-kappaB activation in Hodgkin-Reed-Sternberg cells. Oncogene 2002; 21:2493-503.
22. Zheng H, Bae Y, Kasimir-Bauer S, et al. Therapeutic antibody targeting tumor- and osteoblastic niche-derived jagged1 sensitizes bone metastasis to chemotherapy. Cancer Cell 2017; 32:731-47.e736.
23. Frankl J, Eshghi N, Lundeen TF, Kuo PH. Artifactual hepatic metastasis on FDG PET/CT secondary to cryoablation for adrenal metastasis. Clin Nucl Med 2018; 43:e46-e47.
24. Kim CM, Son YJ, Kim S, Kim SY, Park HH. Molecular basis for unique specificity of human TRAF4 for platelets GPIbbeta and GPVI. Proc Natl Acad Sci U S A 2017; 114:11422-27.
25. Zhao J, Li H, Min L, et al. High expression of tumor necrosis factor receptor-associated factor 2 promotes tumor metastasis and is associated with unfavorable prognosis in gastric cancer. J Gastroenterol Hepatol 2018; 33:431-42.
26. Yamamoto H, Ryu J, Min E, et al. TRAF1 Is Critical for DMBA/Solar UVR-Induced Skin Carcinogenesis. J Invest Dermatol 2017; 137:1322-32.
27. Wan XK, Yuan SL, Tao HX, et al. The upregulation of TRAF1 induced by helicobacter pylori plays an antiapoptotic effect on the infected cells. Helicobacter 2016; 21:554-64.
28. Zhou F, Li F, Xie F, Zhang Z, Huang H, Zhang L. TRAF4 mediates activation of TGF-beta signaling and is a biomarker for oncogenesis in breast cancer. Sci China Life Sci 2014; 57:1172-76.
29. Chen Z, Zhao L, Zhao F, Yang G, Wang J. MicroRNA-26b regulates cancer proliferation migration and cell

cycle transition by suppressing TRAF5 in esophageal squamous cell carcinoma. Am J Transl Res 2016; 8:1957-70.

30. Li M, Long C, Yang G, Luo Y, Du H. MiR-26b inhibits melanoma cell proliferation and enhances apoptosis by suppressing TRAF5-mediated MAPK activation. Biochem Biophys Res Commun 2016; 471:361-67.
31. Wu J, Xue X, Zhang B, et al. The protective effects of paeonol against epirubicin-induced hepatotoxicity in 4T1-tumor bearing mice via inhibition of the PI3K/Akt/NF-kB pathway. Chem Biol Interact 2016; 244:1-8.
32. Guo F, Sun A, Wang W, He J, Hou J, Zhou P, Chen Z. TRAF1 is involved in the classical NF-kappaB activation and CD30-induced alternative activity in Hodgkin's lymphoma cells. Mol Immunol 2009; 46:2441-48.
33. Lv F, Huang Y, Lv W, Yang L, Li F, Fan J, Sun J. MicroRNA-146a ameliorates inflammation via TRAF6/NF-kappaB pathway in intervertebral disc cells. Med Sci Monit 2017; 23:659-64.

Protective effects of miRNA-589 on cerebral ischemia-reperfusion injury

G.-P. Ma[1*], B.-Z. Yang[2*], Y.-S. Zhang[1], B. Wang[1], X.-H. Wei[1], R.-F. Zhang[1], K.-H. Jia[1] and J.-P. Gao[1]

[1]Department of Neurology, The First Hospital of Tianshui, Tianshui, China; [2]Department of Special Needs Diagnosis and Treatment, The First Hospital of Tianshui, Tianshui, China

Received January 21, 2020 – Accepted May 28, 2020

[*]These Authors contributed equally to this work

To uncover the potential influence of microRNA-589 (miRNA-589) on cerebral ischemia-reperfusion injury (IRI) and the underlying mechanism, BV2 cells were stimulated by lipopolysaccharide (LPS) or conditioned medium (CM) of primary cortical neurons undergoing oxygen-glucose deprivation (OGD). Regulatory effects of miRNA-589 on the release of inflammatory factors in BV2 cells induced with LPS or CM of primary cortical neurons undergoing OGD were detected by quantitative real-time polymerase chain reaction (qRT-PCR) and enzyme-linked immunosorbent assay (ELISA). The interaction between miRNA-589 and TRAF6 was finally assessed by dual-luciferase reporter gene assay. MiRNA-589 was downregulated in BV2 cells induced with LPS or CM of primary cortical neurons undergoing OGD. Overexpression of miRNA-589 reduced the release of inflammatory factors in LPS or CM-induced BV2 cells. TRAF6 was verified to be the downstream gene of miRNA-589, and its level was negatively regulated by miRNA-589. MiRNA-589 is downregulated following cerebral IRI and alleviates inflammatory response through negatively regulating TRAF6.

Cerebral ischemia is one of the most common diseases of the central nervous system (1). The cerebral blood flow immediately drops after cerebral ischemia, leading to hypoxia and secondary brain damage. Timely ischemia reperfusion could effectively prevent severe neurological deficits and death, however, it may also aggravate neuronal damage (2). During the course of cerebral ischemia, abundant inflammatory cells are infiltrated and accumulated in the lesion parts. It is verified that inflammatory response is the leading cause of secondary damage at post-ischemia (3).

MicroRNAs (miRNAs) specifically recognize 3′-untranslated region (3′-UTR) of downstream mRNAs, thus directly degrading them or inhibiting their translation. They are of great significance in life activities (4, 5). A large number of miRNAs have been identified to be involved in the development of ischemic cerebrovascular diseases. Jeyaseelan et al (6) screened out 106 abnormally expressed miRNAs in rat with middle cerebral artery occlusion.

TRAF6 is a vital adaptor in intracellular signaling which directly or indirectly binds members in the TNF receptor superfamily and/or IL-1/Toll-like receptor superfamily. Through activating NF-κB, JNK/P38, PI3K/AKT and AP-1 pathways, TRAF6

Key words: MiRNA-589; cerebral IRI; BV2; TRAF6; inflammation

Corresponding Author:
Jianping Gao, BM,
Departments of Neurology, The First Hospital of Tianshui,
105 Jianshe Road, Qinzhou District,
Tianshui, Gansu, 741000, China
Tel.: +86 0938 8217779
e-mail: gaolian19830114@163.com

0393-974X (2020)
Copyright © by BIOLIFE, s.a.s.
This publication and/or article is for individual use only and may not be further reproduced without written permission from the copyright holder. Unauthorized reproduction may result in financial and other penalties
DISCLOSURE: ALL AUTHORS REPORT NO CONFLICTS OF INTEREST RELEVANT TO THIS ARTICLE.

participates in the regulation of cell behaviors, immune reaction, inflammatory response, oxidative stress, etc. (7, 8). In this paper, we explored the protective effect of miRNA-589 on cerebral IRI and the involvement of TRAF6.

MATERIALS AND METHODS

Cell culture and transfection

BV2 and HEK293 cells (American Type Culture Collection (ATCC) (Manassas, VA, USA)) were cultured in Dulbecco's modified eagle medium (DMEM) containing 10% fetal bovine serum (FBS) (HyClone, South Logan, UT, USA) in a 5%CO_2 incubator at 37°C. Cell passage was conducted using 0.5% trypsin at 80-90% confluence. Cells were inoculated in 6-well plates and transfected using Lipofectamine 2000 (Invitrogen, Carlsbad, CA, USA) at 60% confluence. Transfection plasmids were constructed by Ribobio Co., Ltd. (Guangzhou, China).

Collection of CM of primary cortical neurons undergoing OGD

Primary cortical neurons were cultured for 10 days, and the original medium was discarded. After phosphate buffered saline (PBS) washing for three times, OGD buffer was applied. Cells were maintained in a specific incubator with 95% N_2 and 5% CO_2 for 10 min. Subsequently, cells were transferred to a normal incubator. Three hours later, OGD buffer was replaced by Neurobasal medium. After overnight culture, CM was collected for functional experiments. Cells in the control group received the same procedures except for applying OGD buffer.

Enzyme-linked immunosorbent assay (ELISA)

Contents of inflammatory factors in cells were determined using ELISA kit [IL-6 ELISA kit was provided by Boster Biological Technology (Wuhan, China); others were provided by R&D, Minneapolis, MN, USA] following the procedures.

Quantitative real-time polymerase chain reaction (qRT-PCR)

TRIzol (Invitrogen, Carlsbad, CA, USA) was applied for isolating cellular RNA, which was quantified by Agilent BioAnalyzer 2100 (Agilent, Palo Alto, CA, USA). Complementary deoxyribose nucleic acids (cDNAs) were obtained using the miScript II RT and its mRNA level was determined using the miScript SYBR Green PCR kit (Qiagen, Hilden, German). GAPDH was used as the internal reference. The mRNA levels were calculated by $2^{-\Delta\Delta CT}$. Primer sequences were as follows: miRNA-589, forward: CGAGGTCAGCGTGATTTCATGG, reverse: TGTGTCCAAGTCCCAGCCAGAG; IL-1β, forward: CCTGCAGCTGGAGAGTGTGGAT, reverse: TGTGCTCTGCTTGTGAGGTGCT; IL-18, forward: ACGTGTTCCAGGACACAACA, reverse: GGCGCATGTGTGCTAATCAT; GAPDH, forward: AGCCTCGTCCCGTAGACAAAA, reverse: TGGCAACAATCTCCACTTTGC; COX-2, forward: CAGGCTGAACTTCGAAACA, reverse: GCTCACGAGGCCACTGATACCTA; IL-6, forward: GCAATGGCAATTCTGATTGTATG, reverse: AAGGACTCTGGCTTTGTCTTTCT; iNOS, forward: CAGGAGGAGAGAGATCCGATTTA, reverse: GCATTAGCATGGAAGCAAAGA; TNF-α, forward: CATCTTCTCAAAATTCGAGTGACAA, reverse: TGGGAGTAGACAAGGTACAACCC; TRAF6, forward: AAAGCGAGAGATTCTTTCCCTG, reverse: ACTGGGGACAATTCACTAGAGC.

Dual-luciferase reporter gene assay

HEK293 cells were inoculated in a 96-well plate with 5×10^3 cells per well. Cells were co-transfected with TRAF6-WT/TRAF6-MUT and miRNA-589 mimics/NC for 48 h. Relative luciferase activity was finally measured (Promega, Madison, WI, USA).

Statistical analysis

GraphPad software Version 6.0 (La Jolla, CA, USA) was used for data analysis. All data were expressed as mean ± SD (standard deviation). The paired two-tailed *t*-test was used for comparing differences between two groups. Comparison between multiple groups was carried out using One-way ANOVA test followed by Post Hoc Test (Least Significant Difference). $P<0.05$ considered as statistically significant.

RESULTS

Downregulated miRNA-589 and upregulated TRAF6 in BV2 cells induced with LPS or CM of primary neurons undergoing OGD

After 200 ng/mL LPS induction for 6 and 24 h, respectively, miRNA-589 was time-dependently

downregulated in BV2 cells (Fig. 1A), while TRAF6 level presented the opposite trend (Fig. 1C). Besides, miRNA-589 was downregulated in BV2 cells induced with CM of OGD-treated primary neurons (Fig. 1B), while TRAF6 was upregulated (Fig. 1D).

Overexpression of miRNA-589 reduced relative levels of inflammatory factors in LPS-induced BV2 cells

Transfection efficacy of miRNA-589 mimics was firstly verified in BV2 cells (Fig. 2A). QRT-PCR data revealed that mRNA levels of iNOS (Fig. 2B), COX-2 (Fig. 2C), TNF-α (Fig. 2D) and IL-6 (Fig. 2E) were remarkably upregulated in BV2 cells induced with 200 ng/mL LPS for 24 h. The increased trends were reversed by transfection of miRNA-589 mimics. Besides, ELISA results also indicated that overexpression of miRNA-589 reduced the elevated levels of TNF-α (Fig. 2F), IL-6 (Fig. 2G), IL-1β (Fig. 2H) and IL-18 (Fig. 2I) in LPS-induced BV2 cells.

Overexpression of miRNA-589 reduced relative levels of inflammatory factors in BV2 cells induced with CM of primary neurons undergoing OGD

Similarly, relative levels of inflammatory factors in BV2 cells induced with CM of primary neurons undergoing OGD were determined. Increased mRNA levels of iNOS (Fig. 3A), COX-2 (Fig. 3B), TNF-α (Fig. 3C) and IL-6 (Fig. 3D) were partially reversed by overexpression of miRNA-589. Meanwhile, ELISA results obtained the same trends on contents of TNF-α (Fig. 3E) and IL-6 (Fig. 3F).

TRAF6 was the direct target of miRNA-589

Potential binding sequences in the promoter regions of miRNA-589 and TRAF6 were predicted through bioinformatics (Fig. 4A). Decreased luciferase activity after co-transfection of TRAF6-WT and miRNA-589 mimics verified the binding between miRNA-589 and TRAF6 (Fig. 4B). It is shown that both mRNA

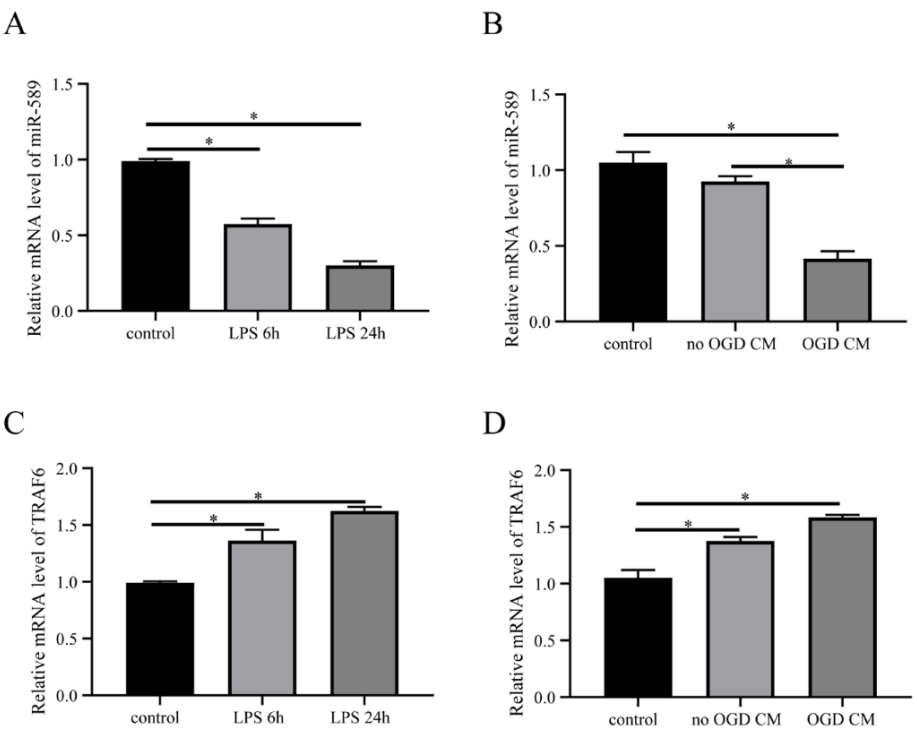

Fig. 1. *Downregulated miRNA-589 and upregulated TRAF6 in BV2 cells induced with LPS or CM of primary neurons undergoing OGD.* ***A****) MiRNA-589 level in BV2 cells treated with blank control, or 200 ng/ml LPS for 6 h and 24 h.* ***B****) MiRNA-589 level in BV2 cells treated with blank control, negative control of OGD or CM of primary neurons undergoing OGD.* ***C****) TRAF6 level in BV2 cells treated with blank control, or 200 ng/ml LPS for 6 h and 24 h.* ***D****) TRAF6 level in BV2 cells treated with blank control, or 200 ng/ml LPS for 6 h and 24 h.*

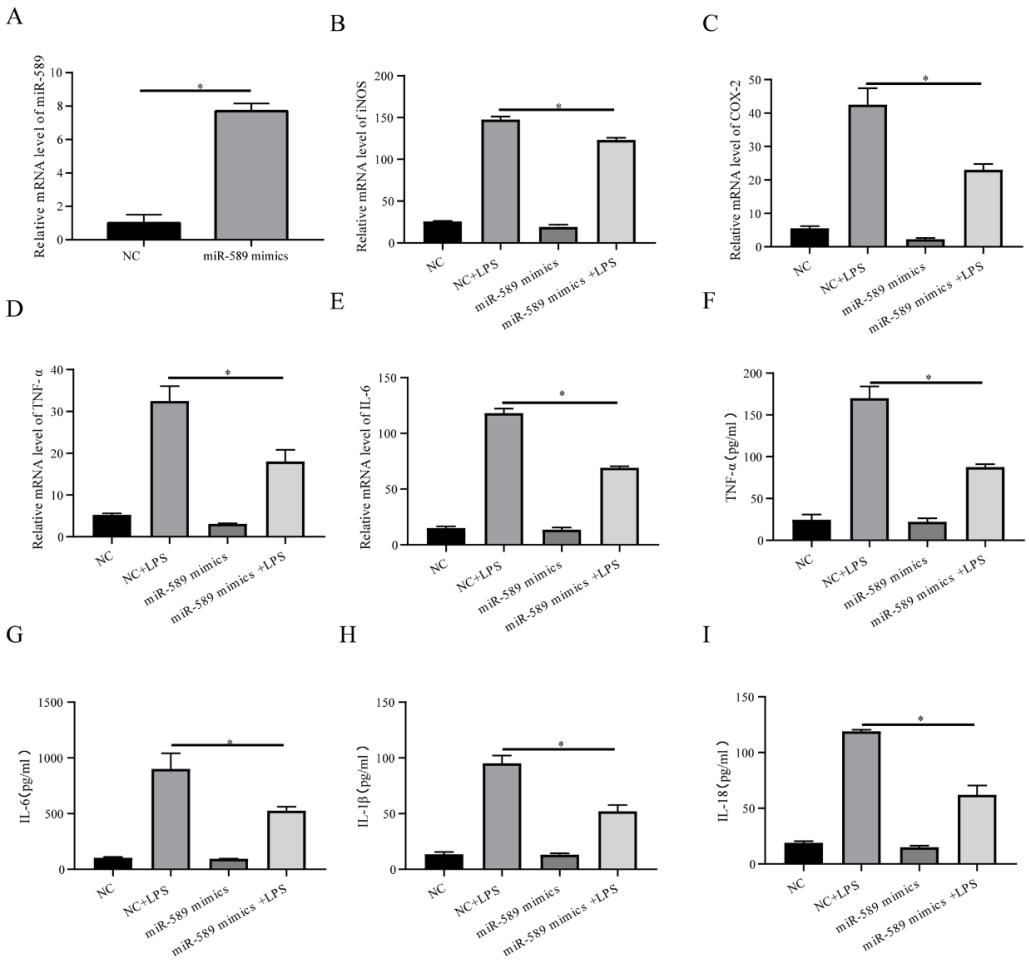

Fig. 2. *Overexpression of miRNA-589 reduced relative levels of inflammatory factors in LPS-induced BV2 cells.* ***A)*** *Transfection efficacy of miRNA-589 mimics in BV2 cells. B-E. QRT-PCR data revealed mRNA levels of iNOS (**B**), COX-2 (C), TNF-α (**D**) and IL-6 (**E**) in BV2 cells with 24-h LPS induction.* ***F-I)*** *ELISA results revealed contents of TNF-α (F), IL-6 (G), IL-1β (H) and IL-18 (I) in BV2 cells with 24-h LPS induction.*

and protein levels of TRAF6 were downregulated in BV2 cells overexpressing miRNA-589 (Fig. 4 C, E). Conversely, TRAF6 was upregulated after knockdown of miRNA-589 (Fig. 4 D, F).

DISCUSSION

Cerebral IRI is characterized as acute onset, high rate of recurrence and high mortality (9). Currently, it is believed that hypoxia, energy metabolism failure, ion balance disorder, free radical damage, excitatory amino acid toxicity, inflammatory damage and apoptosis are pathogenic factors for IRI (10). Inflammatory response at post-IRI is a key event in the aggravation of secondary damage. The release of abundant inflammatory factors deteriorates inflammatory cascade (11).

Microglia are a type of glial cells, which are macrophages colonized in the brain. They are the first and most important immune defense barrier in the central nervous system (CNS) (12). Microglia are vital in monitoring and defending potential damage from external stimuli on the brain (13). It is demonstrated that persistent activation of microglia at post-IRI releases abundant inflammatory factors. They cause irreversible damage to brain cells in the

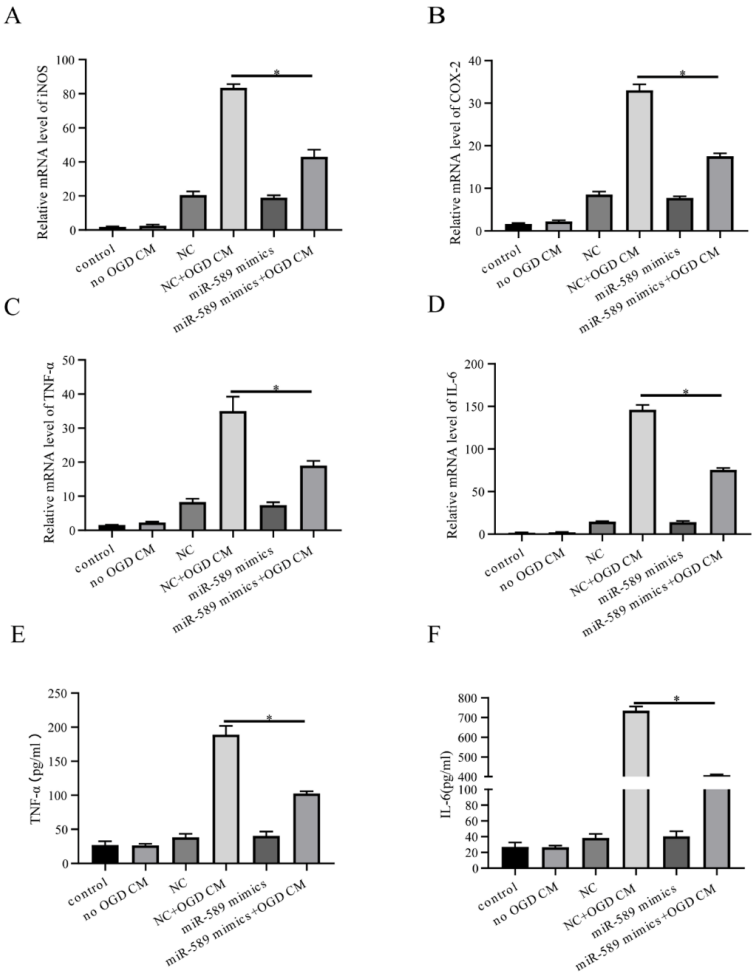

Fig. 3. *Overexpression of miRNA-589 reduced relative levels of inflammatory factors in BV2 cells induced with CM of primary neurons undergoing OGD.* ***A-D****) QRT-PCR data revealed mRNA levels of iNOS (A), COX-2 (B), TNF-α (C) and IL-6 (D) in BV2 cells induced with CM of primary neurons undergoing OGD.* ***E-F****) ELISA results revealed contents of TNF-α (E) and IL-6 (F) in BV2 cells induced with CM of primary neurons undergoing OGD.*

center of the lesion or ischemic penumbra. Seriously, the remote effect also leads to damage in normal brain tissues (14). Effective inhibition of microglia activation and toxicity could remarkably prevent the cascading amplification damage caused by the inflammatory response (15).

MiRNAs are non-coding RNAs that are highly conserved. They are extensively involved in biological processes (16). It is proven that miRNAs are closely related to cerebral ischemia.

Infiltration of inflammatory cells and release of inflammatory factors further deteriorate the disease course of cerebral IRI (17, 18). Interleukins are important cytokines inducing the interaction in leukocytes. A great number of interleukins is highly expressed after inflammation stimulation. It is reported that IL-1 is immediately upregulated in the cerebral ischemic area at the early phase, especially IL-1β. Production of adhesion factors is triggered by IL-1β and IL-6. Dysregulated IL-6 is a vital indicator assessing the severity of cerebral IRI (19). Structurally, IL-18 is similar to that of IL-1β. IL-18 is mainly expressed in microglia and macrophages. It is suggested that IL-18 may be critical during the late phase of inflammatory response following IRI. TNF-α is a pro-inflammatory factor with multi-

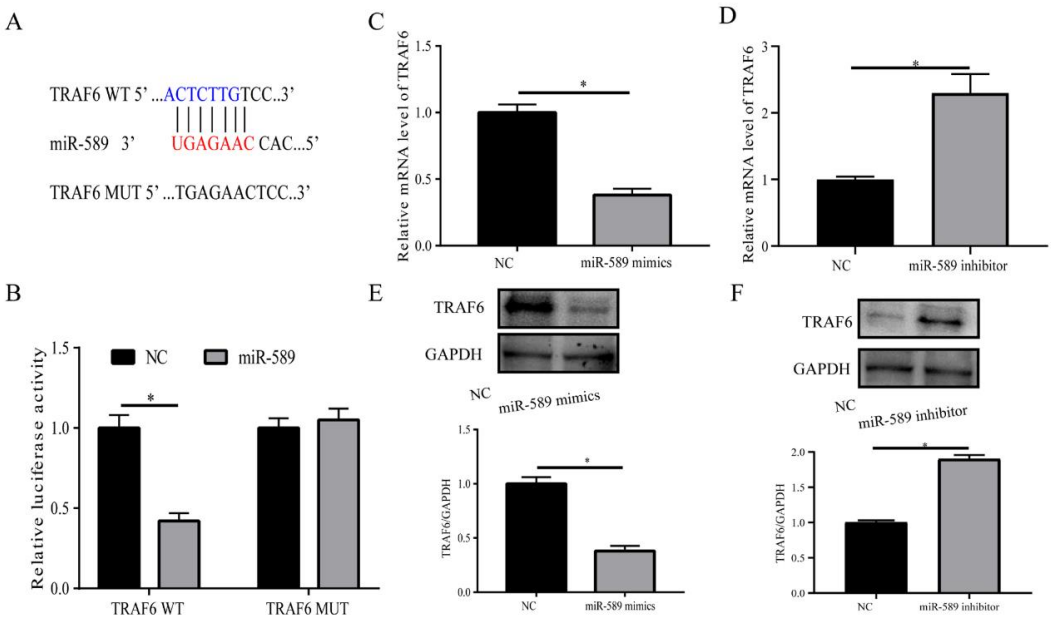

Fig. 4. *TRAF6 was the direct target of miRNA-589.* ***A)*** *Potential binding sequences in the promoter regions of miRNA-589 and TRAF6.* ***B)*** *Luciferase activity in HEK293 cells co-transfected with TRAF6-WT/TRAF6-MUT and miRNA-589 mimics/ NC for 48 h.* ***C)*** *The mRNA level of TRAF6 in BV2 cells transfected with NC or miRNA-589 mimics.* ***D)*** *The mRNA level of TRAF6 in BV2 cells transfected with NC or miRNA-589 inhibitor.* ***E)*** *The protein level of TRAF6 in BV2 cells transfected with NC or miRNA-589 mimics.* ***F)*** *The protein level of TRAF6 in BV2 cells transfected with NC or miRNA-589 inhibitor.*

effect pro-inflammatory and neurotoxic effects, which is the initiator of inflammatory response. He et al. (20) discovered that TNF-α is activated within 3 h following IRI in MCAO rats, and achieves the peak at 24 h.

In this paper, inflammation stimulation in microglia was conducted by LPS induction in BV2 cells. MiRNA-589 was time-dependently downregulated in LPS-induced BV2 cells. Overexpression of miRNA-589 reduced relative levels of inflammatory factors in LPS-induced BV2 cells, suggesting its protective effect against inflammation. In addition, cerebral IRI was constructed in BV2 cells through induction with CM of primary neurons undergoing OGD. Similarly, miRNA-589 was downregulated, and overexpression of miRNA-589 protected OGD-induced inflammatory response in BV2 cells. Hence, we believe that miRNA-589 was involved in cerebral IRI by regulating microglia inflammation.

Subsequently, potential binding sequences in the promoter regions of miRNA-589 and TRAF6 were predicted through bioinformatics. TRAF family contains seven members, namely TRAF1-TRAF7. TRAF6 is responsible for mediating bone metabolism, CD40, IL-1 and LPS signaling. It is capable of regulating natural and acquired immunity resulted by pathogen-associated molecular pattern, as well as inflammatory response (21). In this paper, dual-luciferase reporter gene assay verified the binding between miRNA-589 and TRAF6. In addition, TRAF6 level was negatively regulated by miRNA-589 in BV2 cells.

To sum up, miRNA-589 protected inflammatory response following cerebral IRI through negatively regulating TRAF6. We first investigated the role of miRNA-589 / TRAF6 axis in cerebral IRI. Our findings provide novel directions in clinical treatment of cerebral ischemic diseases in that miRNA-589 and TRAF6 may be promising therapeutic targets.

REFERENCES

1. Johnston SC, Mendis S, Mathers CD. Global variation in stroke burden and mortality: estimates from monitoring, surveillance, and modelling. Lancet Neurol 2009; 8:345-54.
2. Margaill I, Plotkine M, Lerouet D. Antioxidant strategies in the treatment of stroke. Free Radic Biol Med 2005; 39:429-43.
3. Lively S, Schlichter LC. Age-related comparisons of evolution of the inflammatory response after intracerebral hemorrhage in rats. Transl Stroke Res 2012; 3:132-46.
4. Hobert O. Gene regulation by transcription factors and microRNAs. Science 2008; 319:1785-86.
5. Ashraf SI, Kunes S. A trace of silence: memory and microRNA at the synapse. Curr Opin Neurobiol 2006; 16:535-39.
6. Jeyaseelan K, Lim KY, Armugam A. MicroRNA expression in the blood and brain of rats subjected to transient focal ischemia by middle cerebral artery occlusion. Stroke 2008; 39:959-66.
7. Arcipowski KM, Stunz LL, Bishop GA. TRAF6 is a critical regulator of LMP1 functions in vivo. Int Immunol 2014; 26:149-58.
8. Xie P. TRAF molecules in cell signaling and in human diseases. J Mol Signal 2013; 8:7.
9. Nour M, Scalzo F, Liebeskind DS. Ischemia-reperfusion injury in stroke. Interv Neurol 2013; 1:185-99.
10. Kogure K, Busto R, Schwartzman RJ, Scheinberg P. The dissociation of cerebral blood flow, metabolism, and function in the early stages of developing cerebral infarction. Ann Neurol 1980; 8:278-90.
11. Jin R, Yang G, Li G. Inflammatory mechanisms in ischemic stroke: role of inflammatory cells. J Leukoc Biol 2010; 87:779-89.
12. Savitz SI, Cox CJ. Concise Review: Cell therapies for stroke and traumatic brain injury: targeting microglia. Stem Cells 2016; 34:537-42.
13. Graeber MB, Streit WJ. Microglia: biology and pathology. Acta Neuropathol 2010; 119:89-105.
14. Nimmerjahn A, Kirchhoff F, Helmchen F. Resting microglial cells are highly dynamic surveillants of brain parenchyma in vivo. Science 2005; 308:1314-18.
15. Tremblay ME, Stevens B, Sierra A, Wake H, Bessis A, Nimmerjahn A. The role of microglia in the healthy brain. J Neurosci 2011; 31:16064-69.
16. Munari E, Marchionni L, Chitre A, et al. Clear cell papillary renal cell carcinoma: micro-RNA expression profiling and comparison with clear cell renal cell carcinoma and papillary renal cell carcinoma. Hum Pathol 2014; 45:1130-38.
17. Nilupul PM, Ma HK, Arakawa S, Howells DW, Markus R, Rowe CC, Donnan GA. Inflammation following stroke. J Clin Neurosci 2006; 13:1-8.
18. Chen B, Liao WQ, Xu N, et al. Adiponectin protects against cerebral ischemia-reperfusion injury through anti-inflammatory action. Brain Res 2009; 1273:129-37.
19. Kriz J, Lalancette-Hebert M. Inflammation, plasticity and real-time imaging after cerebral ischemia. Acta Neuropathol 2009; 117:497-509.
20. He ZJ, Huang ZT, Chen XT, Zou ZJ. Effects of matrix metalloproteinase 9 inhibition on the blood brain barrier and inflammation in rats following cardiopulmonary resuscitation. Chin Med J (Engl) 2009; 122:2346-51.
21. Wu H, Arron JR. TRAF6, a molecular bridge spanning adaptive immunity, innate immunity and osteoimmunology. Bioessays 2003; 25:1096-105.

MiR-20a Promotes kidney injury in sepsis rats through autophagy pathway

J.-X. Wang[1], Y.-L. Tao[2], Z. Wang[3] and Q.-J. Mao[4]

[1]Department of Critical Medicine, Sunshine Union Hospital, Shandong, China; [2]Department of Anesthesiology, Sunshine Union Hospital, Shandong, China; [3]Department of ECG Center, Sunshine Union Hospital, Shandong, China; [4]Department of Orthopedics Center, Sunshine Union Hospital, Shandong, China

Received March 21, 2020 – Accepted June 15, 2020

The aim of this work was to study the effects of micro ribonucleic acid (miR)-20a on acute kidney injury (AKI) in sepsis rats and its key molecular mechanism. Sprague-Dawley rats were randomly divided into healthy rat group (H group, n=3), sham group (S group, n=3), sepsis rat group (D group, n=3), sepsis rat + negative control transfection group (N group, n=3) and sepsis rat + miR-20a inhibitor transfection group (M group, n=3). At 6 h, 12 h and 24 h, serum creatinine (Scr) and blood urea nitrogen (BUN) were detected, the changes in miR-20a expression in kidney tissues were determined *via* reverse transcription-polymerase chain reaction (RT-PCR), the expression of autophagy marker protein microtubule-associated protein 1 light chain 3 (LC3) was measured *via* Western blotting, and the inflammatory cell infiltration in kidney tissues was detected using hematoxylin-eosin (HE) staining. There was no obvious change in each index in S group compared with H group. D group, N group and M group had higher levels of Scr, BUN and LC3 in kidney tissues than S group. The levels of Scr, BUN and LC3 in kidney tissues were lower in M group than those in N group. MiR-20a may cause AKI in sepsis rats *via* activating autophagy.

Sepsis refers to the infection-induced organ dysfunction threatening life, characterized by a high morbidity rate, high medical expenses and poor prognosis, so it has always attracted attention (1). According to statistics, sepsis is the major cause of death in critically ill patients in America, and there are about 250,000 deaths from sepsis every year (2). In infection, a large number of inflammatory factors are released to stimulate endothelial cells, and intravascular fluid extravasation is caused, thus leading to a series of pathophysiological processes, such as hemoconcentration, microthrombosis and hypoperfusion (5). The kidneys are "peripheral organs", and the blood supply to important organs, such as the brain and heart, will be guaranteed first in the body in the case of decline in blood pressure. Therefore, the kidneys are the most vulnerable to sepsis (4), and the mortality rate rises dramatically when acute kidney injury (AKI) occurs.

Micro ribonucleic acids (miRNAs) are small RNAs with 21-23 nucleotides in length widely expressed in human cells, which can regulate cell apoptosis, differentiation, proliferation, etc (5, 6). Studies have demonstrated that miR-20a can regulate cell apoptosis and proliferation *via* affecting autophagy (7, 8), and activated autophagy is closely related to the occurrence and development of AKI in sepsis (9, 10). However, whether miR-20a is involved in the

Key words: sepsis; acute kidney injury; miR-20a; autophagy; rats

Corresponding Author:
Qingjun Mao, MM
Department of Orthopedics Center,
Sunshine Union Hospital, No. 9000, Yingqian street,
high tech Zone, Weifang, Shandong, 261000, China
Tel.: +86 015098173609
e-mail: jiamoqing19900615@163.com

0393-974X (2020)
Copyright © by BIOLIFE, s.a.s.
This publication and/or article is for individual use only and may not be further reproduced without written permission from the copyright holder.
Unauthorized reproduction may result in financial and other penalties
DISCLOSURE: ALL AUTHORS REPORT NO CONFLICTS OF INTEREST RELEVANT TO THIS ARTICLE.

progression of AKI in sepsis has not yet been studied. In this study, therefore, the effect of miR-20a on the kidney function in sepsis and its possible mechanism were explored.

MATERIALS AND METHODS

Grouping of laboratory animals and establishment of sepsis model

This study was approved by the Animal Ethics Committee of Sunshine Union Hospital Animal Center. The healthy male Sprague-Dawley rats [aged 8 weeks old and weighing 180-200 g; Kay Biological Technology (Shanghai, China) Co., Ltd] were divided into healthy rat group (H group), sham group (S group), sepsis rat group (D group), sepsis rat + negative control transfection group (N group) and sepsis rat + miR-20a inhibitor transfection group (M group). At 12 h before the experiment, the rats were deprived of food, but not of water, and the sepsis model was established *via* cecal ligation and puncture (laparotomy, ligation of 1/3 cecum, fistulization and reduction) (11). After the operation, the rats had free access to food and water. In S group, only laparotomy was performed without any treatment. The concentration of both miR-20a and negative control was adjusted to 5 OD/300 μL. Then the normal saline containing 5 OD of miR-20a (M group) or negative control (N group) was injected *via* the caudal vein.

Detection of serum creatinine (Scr) and blood urea nitrogen (BUN)

Blood was drawn from the abdominal aorta, maintained at room temperature for 1 h and centrifuged at 1000 g and 4°C for 10 min. Then the upper-layer serum was collected and stored in a refrigerator at -20°C. Finally, the content of BUN and Scr was detected using a biochemical analyzer (Olympus, Tokyo, Japan).

Quantitative real-time polymerase chain reaction (qRT-PCR)

At 6 h, 12 h and 24 h after operation, the blood was drawn from the abdominal aorta in each group, and mRNA was extracted using the TRIzol method (Invitrogen, Carlsbad, CA, USA). The primer sequences were as

Table I. *Comparisons of levels of Scr and BUN at different time points in each group (n=3; ($\bar{x}$±s)*

Group	Scr (μmol/L)			BUN (mmol/L)		
	6 h	12 h	24 h	6 h	12 h	24 h
H	25.74±1.86	25.61±1.81	26.84±1.17	10.82±1.52	9.98±1.04	9.84±1.18
S	24.91±1.54[a]	26.19±1.94[a]	25.64±1.75[a]	10.18±1.17[a]	11.57±1.08[a]	0.97±0.99[a]
D	61.57±3.64[b]	105.67±6.34[c]	161.84±10.67[c]	35.87±3.19[b]	85.84±9.18[c]	124.87±10.87[c]
N	64.91±4.04[bd]	110.07±7.04[cd]	155.72±11.38[cd]	38.64±3.94[bd]	86.81±8.91[cd]	128.87±11.95[cd]
M	45.17±3.07[be]	80.87±5.91[be]	113.47±8.57[e]	29.67±3.08[be]	68.74±7.08[be]	91.84±8.81[bf]

[a]P>0.05, [b]P<0.05, [c]P<0.01 vs H group. [d]P>0.05, [e]P<0.05, [f]P<0.01 vs D group

Table II. *Comparison of expression of miR-20a in kidney tissues in each group (n=3, ($\bar{x}$±s)*

Group	MiR-20a		
	6 h	12 h	24 h
H	1±0.06	1±0.06	1±0.06
S	0.99±0.09[a]	1.14±0.09[a]	1.08±0.08[a]
D	1.09±0.11[a]	3.24±0.24 [c]	3.17±0.21[c]
N	1.18±1.01[a]	3.38±0.32[cd]	3.28±0.22[cd]
M	1.12±0.09[a]	1.84±0.11[be]	1.72±0.12[be]

[a]P>0.05, [b]P<0.05, [c]P<0.01 vs H group. [d]P>0.05, [e]P<0.05 vs D group

follows: miR-20a F: 5'-ATCCTTAGCCTTGCTCTACT-3', R: 5'-TAGGAATCGGAACGAGATGA-3'. U6 F: 5'-TCCGATCGTGAAGCGTTC-3', R: 5'-GTGCAGGTCCGAGGGGT-3'. glyceraldehyde 3-phosphate dehydrogenase (GAPDH) F: 5'-ACAAGCCTCAAGATCATCAGC-3', R: 5'-CACGCCACAGTTTCCCGGAG-3'. According to the instructions of the reverse transcription kit (TaKaRa, Tokyo, Japan), 1 μg of mRNA was reversely transcribed into complementary deoxyribose nucleic acid (cDNA). Then with cDNA as a template, primers and fluorescence mixture at an appropriate dose were added for fluorescence qPCR on the PCR instrument based on the instructions of the SYBR Green qPCR kit (TaKaRa, Tokyo, Japan). The reaction conditionsweare as follows: 95°C for 30 s, 95°C for 12 s and 60°C for 40 s, for a total of 45 cycles. With GAPDH as an internal reference, the relative expression of miR-20a was determined using $2^{-\Delta\Delta Ct}$ method.

Hematoxylin-eosin (H&E) staining

At 24 h after operation, the kidney tissues were taken after anesthesia in each group, and fixed in 4% paraformaldehyde fixative for 72 h, followed by dehydration and paraffin embedding. The tissues were sliced into 5 μm-thick sections, deparaffinized with xylene and eluted with alcohol at gradient concentrations, and then the alcohol was washed away with pure water. After deparaffinization, the sections were soaked and stained with hematoxylin, and then hematoxylin was washed away with clear water. After differentiation solution was added, the sections turned pale blue, and they were washed with running water until turning sky blue. The sections were soaked again in eosin solution, and then eosin was washed away with clear water. Then the sections were dried, dehydrated with alcohol and transparentized with xylene. Subsequently, the sections were added dropwise with resin, sealed with coverslips and baked dry, followed by observation of kidney tissues, especially inflammatory cell infiltration in renal tubules, under a light microscope (×200).

Western blotting

The total protein was extracted from kidney tissues, and its concentration was measured using the bicinchoninic acid (BCA) method (Beyotime, Shanghai, China). Then the protein was mixed with sodium dodecyl sulphate (SDS)-loading buffer prepared and boiled at 100°C for 5 min. An equal amount of protein was separated via 10% polyacrylamide gel electrophoresis (Applygen, Beijing, China), transferred onto a polyvinylidene fluoride (PVDF) membrane (Millipore, Billerica, MA, USA), sealed with 10% skim milk for 4 h and incubated with primary antibodies (Abcam, Cambridge, MA, USA) at 4°C overnight on a shaker. After the membrane was washed with tris-buffered saline with Tween®20 (TBST) for 3 times (15 min/time), the protein was incubated with corresponding secondary antibodies at room temperature for 1 h on the shaker. After the membrane was washed again with TBST for 3 times, electrochemiluminescence (ECL) solution was added for exposure and image development. Finally, the relative expressions of target proteins were analyzed using ImageJ software.

Detection of apoptosis of kidney tissues via TUNEL assay

At 24 h after operation, the rats were anesthetized in each group and the kidney tissues were harvested. According to the instructions of the TUNEL apoptosis assay kit (Sigma-Aldrich, St. Louis, MO, USA), the tissues were fixed, rinsed, infiltrated with 0.1% Triton X-100, and prepared into paraffin sections. Then the sealed sections were labeled with fluorescence developer, and TUNEL-positive cells were observed under a fluorescence microscope (×200). The rate of TUNEL-positive cells was calculated in 10 fields of view, indicating the apoptosis rate of kidney tissues.

Statistical analysis

Statistical Product and Service Solutions (SPSS) 20.0 software (IBM, Armonk, NY, USA) was used for analysis. The measurement data were expressed as mean ± standard deviation. Differences between two groups were analyzed by using Student's *t*-test. Comparison between multiple groups was made using One-way ANOVA test followed by Post Hoc Test (Least Significant Difference). $P<0.05$ suggested the statistically significant difference.

RESULTS

Comparisons of levels of Scr and BUN at different time points in each group

Compared with those in H group, the levels of Scr and BUN had no significant changes in S group ($P>0.05$), while they rose in group D and group N

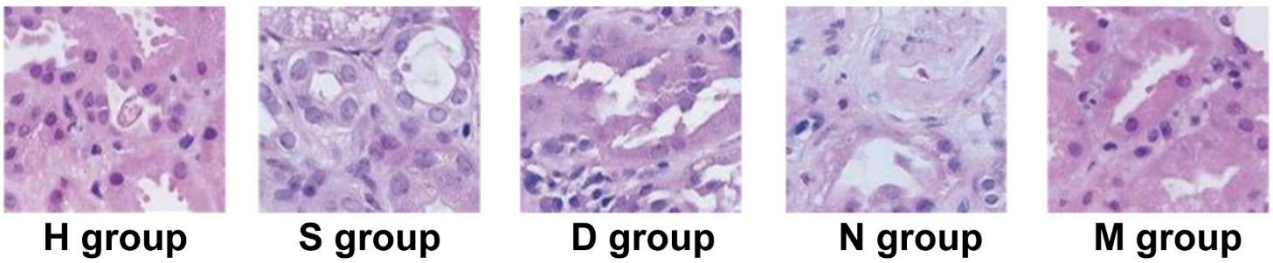

Fig. 1. *Changes in inflammatory cell infiltration in kidney tissues in each group (magnification: 200×).*

(P<0.05 or p<0.01). Moreover, compared with those in D group, the levels of Scr and BUN had no significant changes in N group (P>0.05), while they declined in M group (P<0.05 or P<0.01) (Table I).

Expression of miR-20a in kidney tissues in each group

Compared with that in H group, the expression of miR-20a in kidney tissues had no obvious change in S group (P>0.05), while it was increased in D group and N group (P<0.05 or P<0.01). Furthermore, compared with that in D group, the expression of miR-20a in kidney tissues had no obvious change in N group (P>0.05), while it was decreased in M group after 6 h (P<0.05) (Table II).

Changes in inflammatory cell infiltration in kidney tissues in each group

According to H&E staining, kidney tissues had normal morphology, orderly arrangement and uniform density in H group and S group. Kidney tissues had swelling, lower density and disorderly arrangement in D group, N group and M group. The tissue morphology was similar in N group to that in D group. In M group, the swelling was improved and the density was increased in kidney tissues compared with D group and N group (Fig. 1).

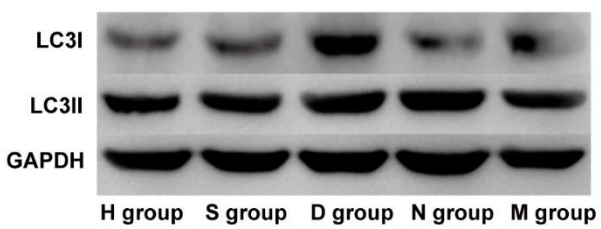

Fig. 2. *Expression of autophagy marker protein LC3 in each group*

Expressions of LC3 and Beclin1 in kidney tissues in each group

As shown in Fig. 2, compared with those in H group, the protein expressions of LC3I and LC3II had no marked changes in S group (P>0.05), while the protein expressions of LC3I and LC3II rose evidently in D group and N group (P<0.01). M group had lower protein expressions of LC3I and LC3II than D group (P<0.05) (Fig. 3).

Apoptosis of kidney tissues in each group

Compared with that in H group, no remarkable change in apoptosis was observed in S group (P>0.05), while enhanced apoptosis was found in D group, N group and M group (P<0.05). M group had weakened apoptosis of kidney tissues compared with D group and N group (P<0.05) (Figs. 4 and 5).

DISCUSSION

Sepsis is the excessive response of the body to infection, which can not only lead to dysfunction at the infection site, but also cause damage to the function of remote organs. It is reported that AKI occurs in 64.4% of sepsis patients, and the mortality rate in patients with AKI is 4 times that in patients without AKI (12, 13). Increasing progress has been made in the prevention and detection of sepsis-induced AKI, but it still remains an unavoidable complication. The specific mechanism of sepsis-induced AKI is still unclear. The inflammatory response is a self-protective response by which the immune system controls infection. According to previous studies, sepsis-induced AKI is the excessive uncontrolled inflammatory response caused by a large number of inflammatory cells and cytokines in essence (14).

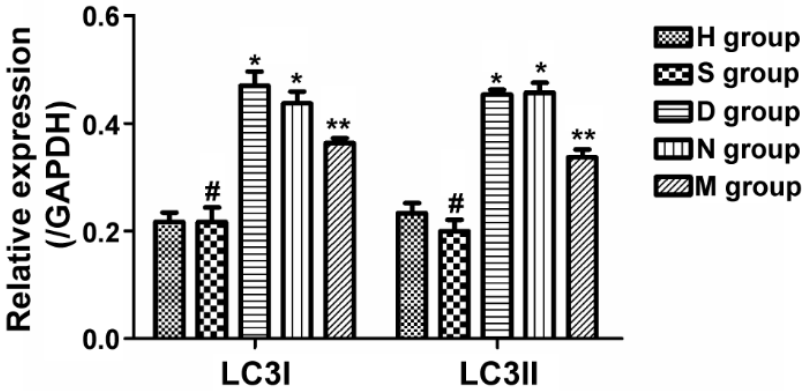

Fig. 3. *Ratio of gray value of LC3 to that of GAPDH in each group. # LC3I and LC3II expressions have no significant changes compared with H group (P>0.05). * LC3I and LC3II expressions rise significantly in D group and N group compared with those in H group (P<0.01). ** LC3I and LC3II expressions decline in M group compared with those in D group (P<0.05).*

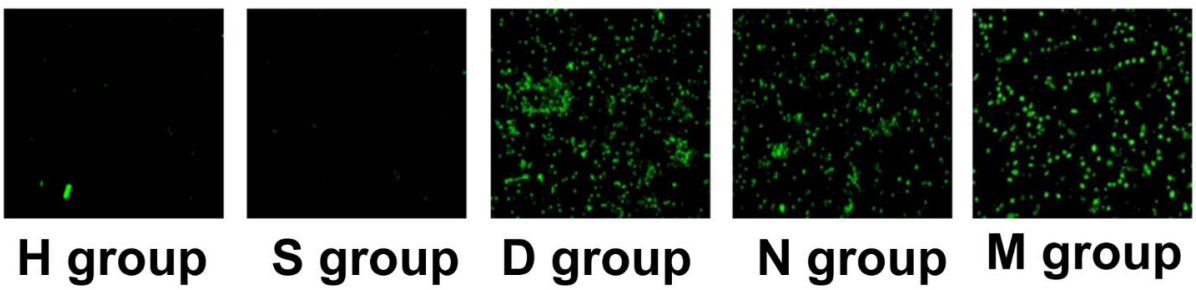

Fig. 4. *TUNEL staining of kidney tissues in each group (magnification: 200×).*

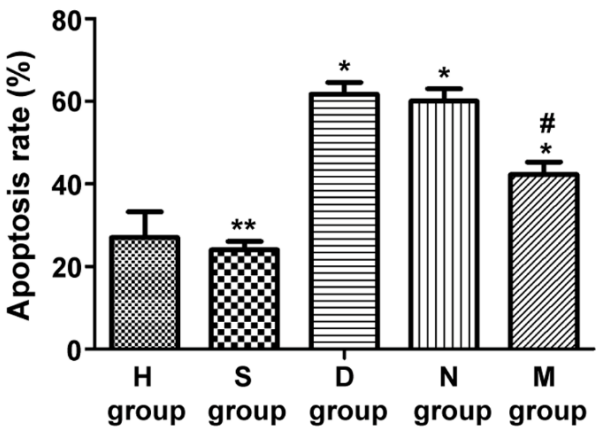

Fig. 5. *Comparison of apoptosis rate of kidney tissues in each group. ** There is no significant change in apoptosis compared with H group (P>0.05). * Enhanced apoptosis is found in D group, N group and M group compared with H group (P<0.05). # M group has weakened apoptosis of kidney tissues compared with D group and N group (P<0.05).*

Severe infection-induced AKI involves a variety of factors, such as hemodynamic disorders and inflammatory mediators, in which reactive oxygen species also increases, ultimately leading to renal hypoperfusion and injury (15). Therefore, studying the pathogenesis of AKI will not only help reduce the mortality rate, but also shorten the average length of stay and lower medical expenses.

MiRNAs are small-molecule single-stranded non-coding RNAs consisting of 19-22 nucleotides, which participate in the regulation of post-transcriptional gene expression. Substantial evidence suggests that miRNAs play key roles in various pathophysiological processes (6). MiR-20a is a typical member of the miR-17-92 gene cluster, one of the widely-studied families (5). It is reported that miR-20a is up-regulated in a variety of diseases and serves as an oncogene

in many cancers, such as lung, liver and anaplastic thyroid (16, 17). In the present study, it was found that at 12 h after the onset of sepsis, the levels of Scr and BUN declined in sepsis rats, and kidney tissues had improved swelling, increased density and relatively regular arrangement in M group. The above findings are similar to those in previous studies, and it can be seen that miR-20a may be an intervention target for the prevention of AKI in the future.

Autophagy is a volume degradation program in cells, which can regulate and keep the homeostasis of cells and tissues (18). The formation of autophagosomes is the major process of autophagy, and autophagosomes fuse with lysosomes to degrade the contents in autophagosomes. LC3B, a member of the LC3 family, is a homologous gene to ATG8 gene in mammalian cells, which is considered currently as an autophagy-related protein (19). Located on the surface of autophagic vesicle membranes, LC3 is involved in the formation of autophagosomes, and its expression is closely related to autophagic activity. When autophagy starts, LC3I binds to phosphatidylinositol on the autophagosome membrane *via* ubiquitination, thus forming LC3II (20). Therefore, the LC3II/LC3I level is directly proportional to the number of autophagic vesicles. In this experiment, the results showed that the LC3II/LC3I level rose in kidney tissues in sepsis-induced AKI, consistent with previous research results (21). After the miR-20a inhibitor was applied, the LC3II/LC3I level declined and the kidney function was improved.

In conclusion, miR-20a is involved in the occurrence and development of AKI in sepsis, which may play a role via activating autophagy. Monitoring the expression of miR-20a or using miR-20a as a therapeutic target may help early diagnosis of AKI in sepsis and reduce the morbidity rate of AKI.

REFERENCES

1. Singer M, Deutschman CS, Seymour CW, et al. The third international consensus definitions for sepsis and septic shock (Sepsis-3). JAMA 2016; 315:801-10.
2. Gaieski DF, Edwards JM, Kallan MJ, Carr BG. Benchmarking the incidence and mortality of severe sepsis in the United States. Crit Care Med 2013; 41:1167-74.
3. Hotchkiss RS, Levy JH, Levi M. Sepsis-induced disseminated intravascular coagulation, symmetrical peripheral gangrene, and amputations. Crit Care Med 2013; 41:e290-e291.
4. Kellum JA, Chawla LS, Keener C, et al. The effects of alternative resuscitation strategies on acute kidney injury in patients with septic shock. Am J Respir Crit Care Med 2016; 193:281-87.
5. Chekulaeva M, Filipowicz W. Mechanisms of miRNA-mediated post-transcriptional regulation in animal cells. Curr Opin Cell Biol 2009; 21:452-60.
6. Li JM, Zhang H, Zuo YJ. MicroRNA-218 alleviates sepsis inflammation by negatively regulating VOPP1 via JAK/STAT pathway. Eur Rev Med Pharmacol Sci 2018; 22:5620-26.
7. Liu L, He J, Wei X, et al. MicroRNA-20a-mediated loss of autophagy contributes to breast tumorigenesis by promoting genomic damage and instability. Oncogene 2017; 36:5874-84.
8. Guo L, Zhao J, Qu Y, et al. microRNA-20a Inhibits autophagic process by targeting ATG7 and ATG16L1 and favors mycobacterial survival in macrophage cells. Front Cell Infect Microbiol 2016; 6:134.
9. El-Rashid M, Ghimire K, Sanganeria B, Lu B, Rogers NM. CD47 limits autophagy to promote acute kidney injury. Faseb J 2019; 33:12735-49.
10. Bao H, Zhang Q, Liu X, et al. Lithium targeting of AMPK protects against cisplatin-induced acute kidney injury by enhancing autophagy in renal proximal tubular epithelial cells. Faseb J 2019; 33:14370-81.
11. Rittirsch D, Huber-Lang MS, Flierl MA, Ward PA. Immunodesign of experimental sepsis by cecal ligation and puncture. Nat Protoc 2009; 4:31-36.
12. Cruz MG, Dantas JG, Levi TM, et al. Septic versus non-septic acute kidney injury in critically ill patients: characteristics and clinical outcomes. Rev Bras Ter Intensiva 2014; 26:384-91.
13. Santos R, Carvalho A, Peres L, Ronco C, Macedo E. An epidemiologic overview of acute kidney injury in intensive care units. Rev Assoc Med Bras (1992) 2019; 65:1094-101.
14. Srisawat N, Kulvichit W, Mahamitra N, et al. The epidemiology and characteristics of acute kidney injury in the Southeast Asia intensive care unit: a prospective multicentre study. Nephrol Dial Transplant 2019; doi:

10.1093/ndt/gfz087.
15. Yeter H, Yildirim T, Eyupoglu D, et al. Mild to moderate proteinuria is a heralding sign for acute kidney injury and mortality for intensive care unit patients. Turk J Med Sci 2019; 49:543-50.
16. Marquez J, Fernandez-Pineiro I, Arauzo-Bravo MJ, et al. Targeting liver sinusoidal endothelial cells with miR-20a-loaded nanoparticles reduces murine colon cancer metastasis to the liver. Int J Cancer 2018; 143:709-19.
17. Yau TO, Wu CW, Tang CM, et al. MicroRNA-20a in human faeces as a non-invasive biomarker for colorectal cancer. Oncotarget 2016; 7:1559-68.
18. Mizushima N, Komatsu M. Autophagy: renovation of cells and tissues. Cell 2011; 147:728-41.
19. Zhang Y, Wang L, Meng L, Cao G, Wu Y. Sirtuin 6 overexpression relieves sepsis-induced acute kidney injury by promoting autophagy. Cell Cycle 2019; 18:425-36.
20. Chen S, Jiang YZ, Huang L, Zhou RJ, Yu KD, Liu Y, Shao ZM. The residual tumor autophagy marker LC3B serves as a prognostic marker in local advanced breast cancer after neoadjuvant chemotherapy. Clin Cancer Res 2013; 19:6853-62.
21. Wang Z, Choi ME. Autophagy in kidney health and disease. Antioxid Redox Signal 2014; 20:519-37.

MiR-424 Inhibits neuronal apoptosis in rats with cerebral infarction through regulating TGF-β1/Smad3 signaling pathway

S.-H. Gui, Y.-M. Wang, C.-Y. Fan, L.-K. Han, T.-G. Wang, M.-Q. Di and J.-Q. Gu

Department of Neurology, Affiliated Hospital of Jiangnan University/The Third People's Hospital of Wuxi, Wuxi, China

Received March 21, 2020 – Accepted June 17, 2020

It has been reported that micro ribonucleic acid (miR)-424 is an important molecule in cerebral ischemia. However, the precise mechanism of action and biological effects of miR-424 remain to be further explored. miR-424 mimic and miR-424 inhibitor were injected *via* the caudal vein in rats, and the effect of miR-424 expression on brain tissue damage induced by middle cerebral artery occlusion (MCAO) was detected. The miR-424 mimic-induced changes in genomic levels were detected via the gene chip assay, and the signaling pathways regulated by miR-424 and its potential targets were explored combined with target prediction. Then the effect of miR-424 mimic on apoptosis of PC12 cells induced by oxygen-glucose deprivation (OGD) was determined using Annexin V/PI assay. Finally, drosophila mothers against decapentaplegic protein 7 (Smad7) was overexpressed to further verify the mechanism of action of miR-424 mimic. Compared with that in the sham group, the expression of miR-424 in brain tissues significantly declined in the model group. The results of 2,3,5-triphenyltetrazolium chloride (TTC) staining and terminal deoxynucleotidyl transferase-mediated dUTP nick end labeling (TUNEL) assay revealed that the miR-424 mimic obviously reduced the cerebral infarction area and apoptosis level of brain tissues, while the miR-424 inhibitor obviously increased the cerebral infarction area and apoptosis level of brain tissues. It was found, using bioinformatics and KEGG enrichment analysis, that differentially expressed genes induced by miR-424 were significantly enriched in the transforming growth factor-β (TGF-β) signaling pathway. According to the results of reverse transcription-quantitative polymerase chain reaction (RT-qPCR) and Western blotting, the miR-424 mimic could evidently lower the expression of Smad7, thus activating the TGF-β1/Smad3 signaling pathway. Overexpression of Smad7 could weaken the protective effect of miR-424 mimic on ischemic-hypoxic cells. Increasing the expression of miR-424 can inhibit Smad7 to activate the TGF-β1/Smad3 signaling pathway, thereby exerting a protective effect against the brain tissue damage induced by MCAO.

Ischemic stroke refers to a disease in which the supply of oxygen and other nutrients fails to meet the metabolic demands of brain tissues due to the obstruction of blood supply in the brain in cerebrovascular diseases (1). Ischemic stroke has the highest mortality rate in patients aged over 60 years around the world (2), and it is also an important cause of disability in patients according to epidemiological studies (3). In ischemic stroke, the most important pathological change is cerebral ischemia-induced neuronal death, resulting in irreversible brain damage. Cerebral ischemia leads to a series of

Key words: miR-424; TGF-β1/Smad3 signaling pathway; cerebral infarction; neurons; apoptosis

Corresponding Author:
Junquan Gu, BM
Department of Neurology, Affiliated Hospital of Jiangnan University/
The Third People's Hospital of Wuxi,
585 Xinyuanbei Road, Liangxi District, Wuxi 214041, China
Tel./Fax: +86 015301516359
e-mail: gujusi19700216@163.com

0393-974X (2020)
Copyright © by BIOLIFE, s.a.s.
This publication and/or article is for individual use only and may not be further reproduced without written permission from the copyright holder.
Unauthorized reproduction may result in financial and other penalties
DISCLOSURE: ALL AUTHORS REPORT NO CONFLICTS OF INTEREST RELEVANT TO THIS ARTICLE.

complex pathophysiological processes, including the production of reactive oxygen species (4), calcium overload (5), inflammatory response (6) and apoptosis, which will cause irreversible brain tissue damage and loss of nerve function.

Micro ribonucleic acids (miRNAs) are a class of small molecule non-coding RNAs generally consisting of 19-22 nucleotide sequences, which inhibit the translation process of messenger RNAs (mRNAs) through binding to the mRNA 3'-untranslated region (3'UTR), thereby reducing the protein expression level. As important regulators, miRNAs play important roles in a variety of diseases. Moreover, there is increasing evidence that miRNAs occupy a pivotal position in ischemic stroke (7-9).

In the present study, the results of animal experiments showed that the expression of miR-424 significantly declined at 7 d after modeling of middle cerebral artery occlusion (MCAO). The miR-424 mimic could significantly improve the neurological function score, and reduce the cerebral infarction area and apoptosis rate of brain tissues in the model group. It was found *via* bioinformatics that the targets for miR-424 were obviously enriched in the transforming growth factor-β (TGF-β) signaling pathway, and the regulatory effect of miR-424 on apoptosis was related to the TGF-β1/Smad3 signaling pathway. In addition, *in vitro* experiments revealed that miR-424 could reduce the increase in the apoptosis rate of PC12 cells induced by oxygen-glucose deprivation (OGD) through regulating the expression of drosophila mothers against decapentaplegic protein 7 (Smad7). The research results not only further clarified the related mechanism of action of miR-424, but also further provided understanding of the related mechanism of neuronal apoptosis induced by cerebral ischemia.

MATERIALS AND METHODS

Establishment of rat model of cerebral infarction and experimental scheme

In this study, 48 male Sprague-Dawley rats weighing 250-300 g were divided into sham group, model group, miR-424 mimic group and miR-424 inhibitor group (miR-con group) using a random number table. All operations conformed to the standards in USA Care and Use of Laboratory Animals. This study was approved by the Ethics Committee of Jiangnan University Animal Center.

In this study, the rat model of cerebral infarction was established *via* MCAO using the suture according to the method in the literature. Briefly, firstly the rats were anesthetized with 10% chloral hydrate (3.5 mL/kg). An incision was made along the midline of the neck, and the muscles were bluntly separated to expose the common carotid artery (CCA), external carotid artery (ECA) and internal carotid artery (ICA). CCA was ligated loosely and tightly at about 5 mm and 3 mm away from the bifurcation, respectively, and a V-shaped incision was made between the two knots, from which the suture was inserted till 2 mm away from the bifurcation. Then the skin was sutured, and the rats were placed on a warm pad after operation until resuscitation. In the sham group, the operations were the same as above, except vascular ligation and insertion of suture. The miR-424 mimic was injected into rats in the miR-424 mimic group, while the miR-424 inhibitor was injected into rats in the miR-424 inhibitor group.

Detection of effect of miR-424 mimic on mRNA expression in MCAO rats via gene chip assay

Total RNA was extracted from brain tissues in the miR-424 mimic group and model group and quantified using the NanoDrop kit (Thermo Fisher, Waltham, MA, USA), and its integrity was evaluated using Bioanalyzer 2100 (Agilent, Santa Clara, CA, USA). In this study, 100 ng of total RNA was prepared into cRNA using the Affymetrix 3' IVT Express kit, followed by hybridization on an Affymetrix Primeview Human Array at 45°C for 16 h according to the manual of GeneChip 3' Array (Affymetrix, Santa Clara, CA, USA). In addition, the array was washed and stained on an Affymetrix FS-450 fluidic station and scanned on an Affymetrix GeneChip Scanner according to the manufacturer's instructions. Then the raw data of CEL file were imported into Partek Genomics Suite 6.6 software, and the probe set was normalized using the Robust Multiarray Average method. The significance of differentially expressed genes was determined using one-way analysis of variance, and the *p*-value was corrected using FDR.

Prediction of miR-424 target genes

The targets for miR-424 were predicted using the online

software TargetScan Human 5.1 (www.targetscan.org) and miRanda (http://www.microrna.org/) in silico.

Reverse transcription-quantitative polymerase chain reaction (RT-qPCR)

The differences in expressions of mRNA and miRNA in brain tissues were detected *via* RT and qPCR. 500 ng of RNA samples in RT were divided into three portions, the total RNA was diluted (10-fold) and 3 μL of total RNA was taken for PCR amplification. The amplification level of the target gene was verified *via* 5% agarose gel electrophoresis. The data were quantified and processed using LabWorks 4.0 image acquisition and analysis software. In this study, U6 was selected as an internal reference. The primers of miR-424 were purchased from ABM (Peterborough, Camb, Canada). To obtain reliable data, the experiment was repeated for 3 times in each group. In this study, the relative expression level of the target gene was analyzed using the $2^{-\Delta\Delta Ct}$ method. The primer sequences used are shown in Table I.

2,3,5-triphenyltetrazolium chloride (TTC) staining assay

After the neurological function scoring, the rats were sacrificed *via* cervical dislocation, and the brain tissues were collected to measure the cerebral infarction area. First, the brain was frozen in a at -20°C to make it hard to certain degree. Then the brain was cut into 2 mm-thick sections from the frontal lobe along the coronal plane, incubated in TTC dye containing 2% TTC (Sigma-Aldrich, St. Louis, MO, USA) at 37°C for 30 min and fixed with 4% paraformaldehyde overnight.

Terminal deoxynucleotidyl transferase-mediated dUTP nick end labeling (TUNEL) assay

In this study, the effect of miR-424 expression on brain cell apoptosis induced by cerebral ischemia in rats was detected using the TUNEL kit. The brain tissues of rats were sliced into 5 μm-thick frozen sections (Leica CM1950, Wetzlar, Germany) and stained using the TUNEL kit (Roche, Indianapolis, IN, USA) in strict accordance with the manufacturer's instructions. After successful staining, the sections were counterstained with 4',6-diamidino-2-phenylindole (DAPI) and sealed. Then the apoptotic cells were observed under a confocal microscope, and the green color indicated the nuclei of apoptotic cells.

Western blotting

An appropriate amount of radio immunoprecipitation assay (RIPA) lysis buffer was prepared, and the protease inhibitor phenylmethanesulfonyl fluoride (PMSF) (RIPA: PMSF = 100:1) (Beyotime, Shanghai, China) was added and mixed evenly. After the cells were digested with trypsin and lysed with lysis buffer, the lysate was collected and transferred into an Eppendorf (EP) tube, followed by centrifugation at 14,000 rpm and 4°C for 30 min using a refrigerated high-speed centrifuge. Then the protein supernatant was collected and subjected to heating bath at 95°C for 10 min for protein denaturation. The protein samples prepared were maintained at -80°C for later use, and the protein was quantified using the bicinchoninic acid (BCA) kit. After that, the sodium dodecyl sulphate-polyacrylamide gel electrophoresis (SDS-PAGE) gel was prepared, and

Table I. *Primer sequences in RT-qPCR*

Primer	Primer sequence (5'-3')
MiR-424	5'-AGCAGCAATTCATGTTTTGG-3'
	5'-GAACATGTCTGCGTATCTC-3'
U6	5'-CGCTTCGGCAGCACATATACTA-3'
	5'-CGCTTCACGAATTTGCGTGTCA-3'

the protein samples were loaded into the loading well for electrophoresis under the constant pressure of 80 V for 2.5 h. Then the protein was transferred onto a polyvinylidene fluoride (PVDF) membrane (Millipore, Billerica, MA, USA) using a semi-dry transfer method. The PVDF membrane was immersed in tris-buffered saline with Tween®20 (TBST) containing 5% skim milk powder and shaken slowly for 1 h on a shaking table for sealing. Then the protein was incubated with the primary antibody diluted with 5% skim milk powder, rinsed with TBST for 3 times (10 min/time), incubated again with the secondary antibody at room temperature for 2 h and rinsed again with TBST twice and with TBS once (10 min/time). Finally, the protein was detected using the electrochemiluminescence (ECL) reagent, followed by exposure in a darkroom. The relative expression of protein was analyzed using Image-Pro Plus v6 (Media Cybernetics, Silver Spring, MD, USA). The antibodies used included GAPDH (Abcam, Cambridge, MA, USA, ab181602), p-Smad3 (Abcam, Cambridge, MA, USA, ab63399), Smad3 (Abcam, Cambridge, MA, USA, ab157372) and Smad7 (Abcam, Cambridge, MA, USA, 99086).

Cell culture and OGD assay

The PC12 cells used in this study were purchased from the American Type Culture Collection (ATCC) (Manassas, VA, USA), and they were cultured in the Dulbecco's modified Eagle medium (DMEM) (Gibco, Rockville, MD, USA) containing 10% fetal bovine serum (FBS) (Gibco, Rockville, MD, USA) and 1% penicillin/streptomycin in an incubator with 5% CO_2 at 37°C. Before the experiment, all inoculated cells were cultured for 8 h and synchronized.

After transfection, the OGD-treated cells were added into the glucose-free DMEM and placed in an anoxic tank (37°C, 5% CO_2, 95% N_2) for 10 h, and the medium was replaced with the high-glucose DMEM containing 10% FBS, followed by culture for 24 h. Finally, flow cytometry was performed.

Cell transfection

The miR-424 mimic, negative control (NC)-mimic, NC-inhibitor and miR-424 inhibitor were purchased from Shanghai GenePharma Co., Ltd. (Shanghai, China), and transfected into PC12 cells using Lipofectamine 2000™ transfection reagent (Invitrogen, Carlsbad, CA, USA) in strict accordance with the manufacturer's instructions. After 4 h, the medium containing the transfection reagent was discarded. Then the transfected PC12 cells were further cultured in the fresh medium for 24 h, followed by OGD assay.

The Smad7 sequences were amplified *via* PCR and inserted into the Kpn I and BamH I sites of the pcDNA3.1 (+) vectors. The vectors were then transfected into PC12 cells using Lipofectamine 3000™ transfection reagent (Invitrogen, Carlsbad, CA, USA) in strict accordance with the instructions, with empty vectors as control. After 4 h, the medium containing the transfection reagent was discarded. Then the transfected PC12 cells were further cultured in the fresh medium for 24 h, followed by OGD assay.

Detection of apoptosis via flow cytometry

The changes in apoptosis after treatment were detected using the Annexin V/propidium iodide (PI) double-staining kit. 5×10^5 cells were digested with trypsin and rinsed twice with phosphate buffered saline (PBS) at 4°C. Then the centrifuged cells were resuspended in 500 μL of staining buffer and added with 5 μL of Annexin V-FITC and 5 μL of PI dye, followed by staining in a dark place at 37°C for 15 min. Finally, the cells were detected using the Guava flow cytometer (Millipore, Billerica, MA, USA).

Statistical analysis

All data were expressed as mean ± standard deviation. Statistical analysis was performed between two groups using unpaired Student's *t*-test and one-way analysis of variance. Statistical Product and Service Solutions (SPSS) 17.0 software (SPSS Inc., Chicago, IL, USA) was used for statistical analysis in this study. $P<0.05$ suggested the statistically significant difference.

RESULTS

MiR-424 significantly reduced MCAO-induced cerebral infarction area

In TTC staining, normal tissues were coloured bright red, while the infarction region was colored pale white (Fig. 1A). The brain tissues in sham group displayed the normal bright red color. The cerebral infarction area in brain tissues was significantly increased in the model

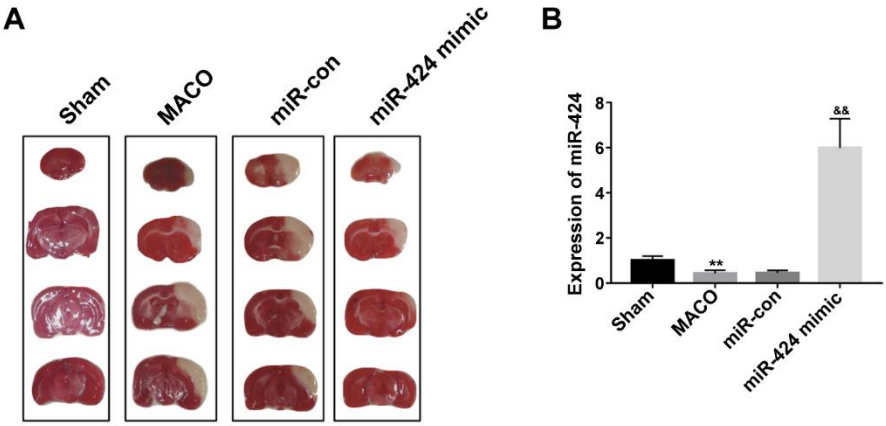

Fig. 1. *Effect of miR-424 expression on MCAO-induced cerebral infarction area.* ***A****) Difference in miR-424 expression in brain tissues in each group (n=7).* ***B****) Effect of miR-424 expression on MCAO-induced cerebral infarction area detected via TTC staining assay (n=5).* $^{**}P<0.01$ *vs sham group,* $^{\&\&}P<0.01$ *vs miR-con group. The cerebral infarction area is significantly increased in model group compared with that in sham group, while it is significantly decreased in miR-424 mimic group compared with that in miR-con group.*

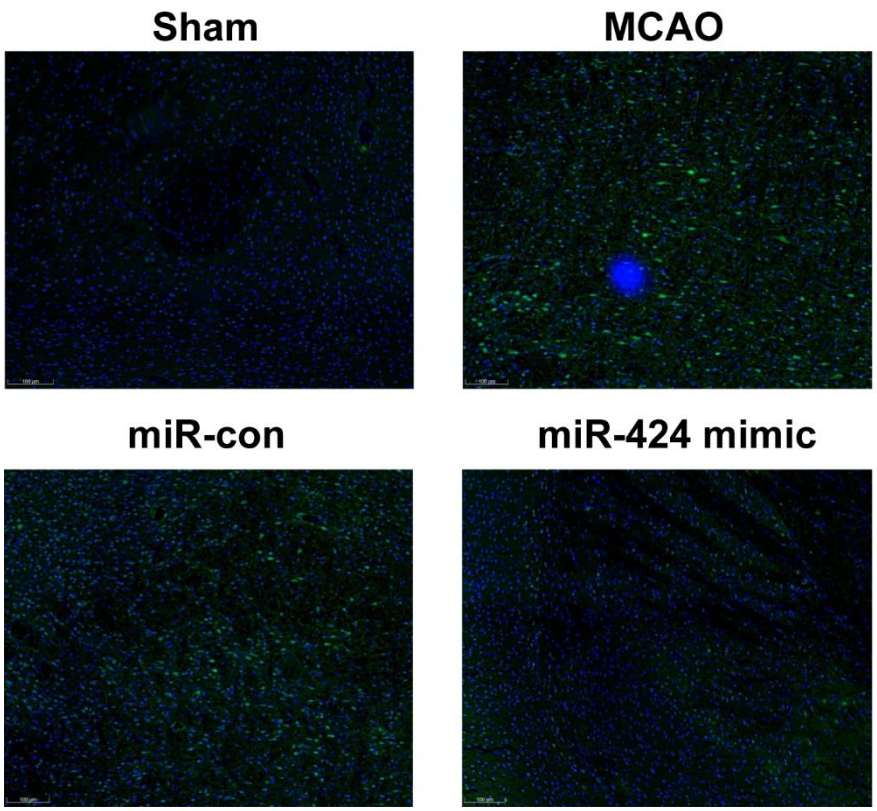

Fig. 2. *Effect of miR-424 expression on MCAO-induced apoptosis determined using TUNEL assay. (magnification: 200×). Blue fluorescence: DAPI-positive nuclei, green fluorescence: apoptotic cells. The number of apoptotic cells in brain tissues in miR-424 mimic group obviously declines.*

group compared with that in the sham group, while it was significantly decreased in the miR-424 mimic group compared with that in the miR-con group.

After the rat model was established, 50 nM of miR-424 mimic was given once daily to the miR-424 mimic group for 3 days. The results of RT-qPCR showed that the expression of miR-424 in brain tissues was significantly decreased in the model group compared with that in the sham group, while it was significantly increased in miR-424 mimic group compared with that in the miR-con group, showing a statistically significant difference ($P<0.05$) (Fig. 1B).

MiR-424 y reduced MCAO-induced apoptosis in brain tissues

As shown in Fig. 2, the number of apoptotic cells in brain tissues rose significantly in the model group compared with that in the sham group, while it obviously declined in the miR-424 mimic group compared with that in the miR-con group. The above results indicate that miR-424 mimic can signifcantly reduce MCAO-induced apoptosis in brain tissues.

Differentially expressed genes and target gene prediction

According to the gene chip screening results, there were significant differences in the mRNA expression profiles in brain tissues between the miR-424 mimic group and model group (Fig. 3A). It was found that 300 mRNAs had significant differences in brain tissues in the miR-424 mimic group compared with the model group (Fold change >1, $P<0.05$), among which 167 mRNAs were evidently up-regulated and 133 mRNAs were evidently down-regulated (Fig. 3B).

Based on prediction using bioinformatics, a total of 1,774 potential targets for miR-424 were obtained. Fifteen

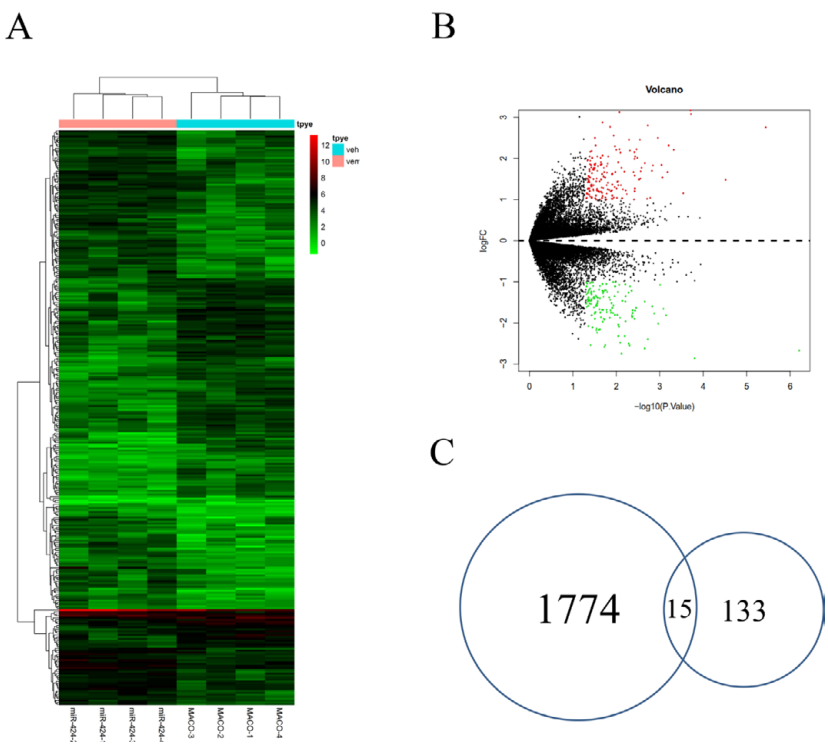

Fig. 3. *Differentially expressed genes and target gene prediction.* ***A)*** *Heat map of visualized analysis of differentially expressed mRNAs. MiR-424: miR-424 mimic group. Each row indicates one mRNA, red for a higher expression level and green for a lower expression level.* ***B)*** *Volcano plot of differentially expressed genes.* ***C)*** *Interaction between down-regulated differentially expressed mRNAs and potential targets for miR-424. There are significant differences in the mRNA expression profiles in brain tissues between miR-424 mimic group and model group. 300 differentially expressed mRNAs are obtained (Fold change >1, $P<0.05$), among which 167 mRNAs are up-regulated and 133 mRNAs are down-regulated. There are 15 interactions between potential targets for miR-424 and down-regulated mRNAs.*

interactions were obtained between 1,774 potential targets and 133 down-regulated differentially expressed mRNAs, among which the interaction of miR-424 with Smad7, CCNF, CHEK1 and WEE1 was confirmed (Fig. 3C).

Differentially expressed genes were significantly enriched in the TGF-β signaling pathway

Through KEGG enrichment analysis, 19 signaling pathways, in which differentially expressed genes were significantly enriched, were obtained, including apoptosis, cell cycle, PI3K-AKT signaling pathway and MAPK signaling pathway (Fig. 4). It can be seen that the TGF-β signaling pathway was the one most significantly enriched by differentially expressed genes. Interestingly, the direct target for miR-424, Smad7, was also located in this signaling pathway, which may be the reason for the fact that differentially expressed genes were significantly enriched in the TGF-β signaling pathway.

Effects of miR-424 expression on Smad7 and TGF-β1/Smad3 signaling pathways

To further verify the results of high-throughput gene chip assay, the effects of miR-424 mimic on Smad7 and TGF-β1/Smad3 signaling pathway were detected through Western blotting (Fig. 5A). The results manifested that model group had evidently lower p-Smad3/Smad3 protein expression but evidently higher Smad7 protein expression in brain tissues than sham group ($P<0.01$) (Fig. 5 B, C). MiR-424 mimic group had evidently higher p-Smad3/Smad3 protein expression but lower Smad7 protein expression in brain tissues than the model group, and there were statistically significant differences ($P<0.01$) (Fig. 5 B, C).

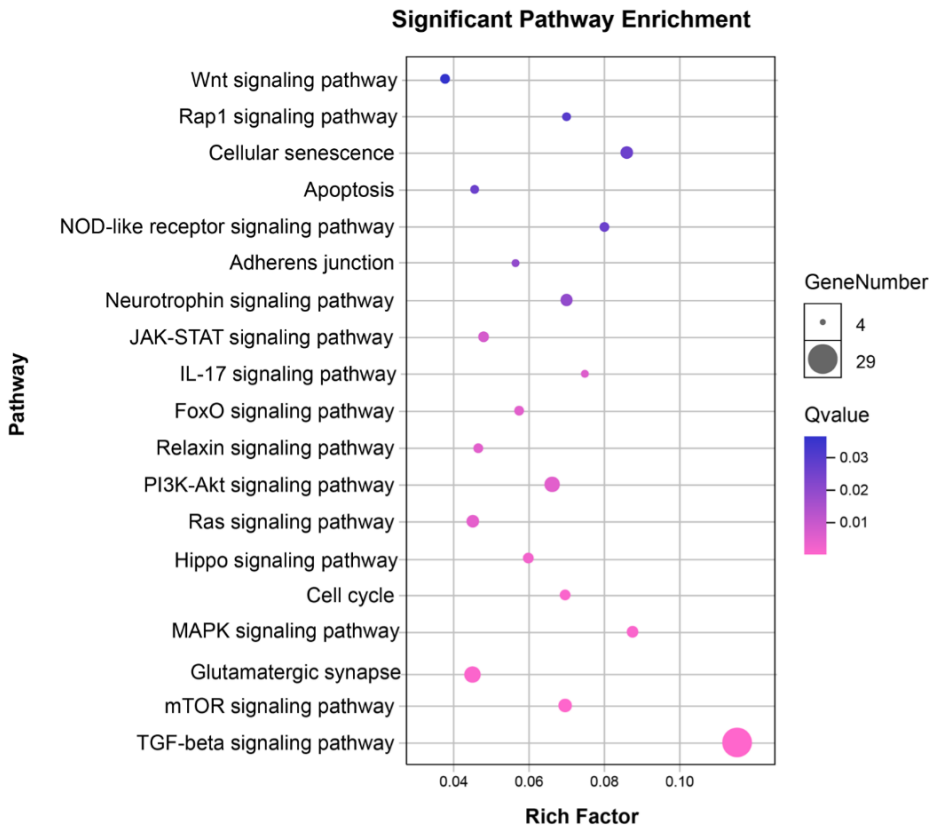

Fig. 4. *KEGG enrichment analysis of differentially expressed genes. Each row on the vertical axis indicates one KEGG signaling pathway. The larger the circle is, the more the genes are enriched in the signaling pathway. The pinker the color is, the larger the q value is. The larger the Rich Factor is, the higher the enrichment index is. According to KEGG enrichment analysis, differentially expressed genes in miR-424 mimic group are remarkably enriched in 19 signaling pathways, including apoptosis, cell cycle, PI3K-AKT signaling pathway, MAPK signaling pathway and TGF-β signaling pathway.*

Effect of miR-424 on apoptosis of PC12 cells induced by OGD

To explore the effect of miR-424 expression on PC12 cell apoptosis, flow cytometry and Annexin V/PI staining were performed (Fig. 6). The results of Annexin V/PI staining manifested that the apoptosis rate remarkably rose in the model group compared with that in the control group, while it remarkably declined in the miR-424 mimic group but remarkably rose in the NC-inhibitor group compared with that in the NC-mimic group.

Effect of miR-424 on OGD-induced apoptosis of PC12 cells through targeting Smad7

Compared with that of cells transfected with empty vectors, the apoptosis rate of cells transfected with miR-424 mimic and Smad7 was markedly increased (Fig. 7). The results indicate that overexpression of Smad7 can eliminate the protective effect of miR-424 mimic on ischemic-hypoxic cells, and further confirm that miR-424 inhibits Smad7 protein expression to activate the TGF-β1/Smad3 signaling pathway, thereby exerting a protective effect on ischemic-hypoxic brain tissues.

DISCUSSION

Ischemic stroke is an important cause of severe disability and death around the world, in which cerebral ischemia is the major determinant of brain damage in patients. Recently, the roles of miRNAs in the pathological process of cerebral ischemia have attracted widespread attention due to their potential as diagnostic factors, prognostic predictors and therapeutic targets for stroke.

MiR-424 is a member of the miR-15/miR-107 family, and is highly expressed in human brain tissues. There are increasingly more research

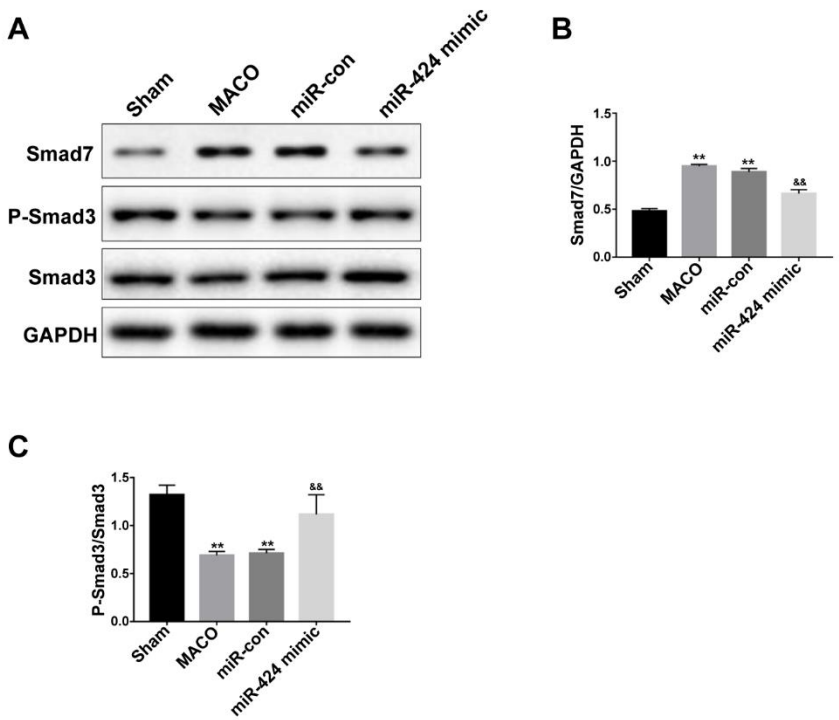

Fig. 5. *Effects of miR-424 expression on Smad7 and TGF-β1/Smad3 signaling pathways.* ***A, B****) Changes in key proteins in the TGF-β1/Smad3 signaling pathway in brain tissues in the 4 groups determined using Western blotting (n=5).* ***C****) Quantitative analysis of Western blotting results.* $^{**}P<0.01$ *vs sham group,* $^{\&\&}P<0.01$ *vs miR-con group. MiR-424 mimic evidently increases the p-Smad3/Smad3 protein expression but evidently decreases the Smad7 protein expression.*

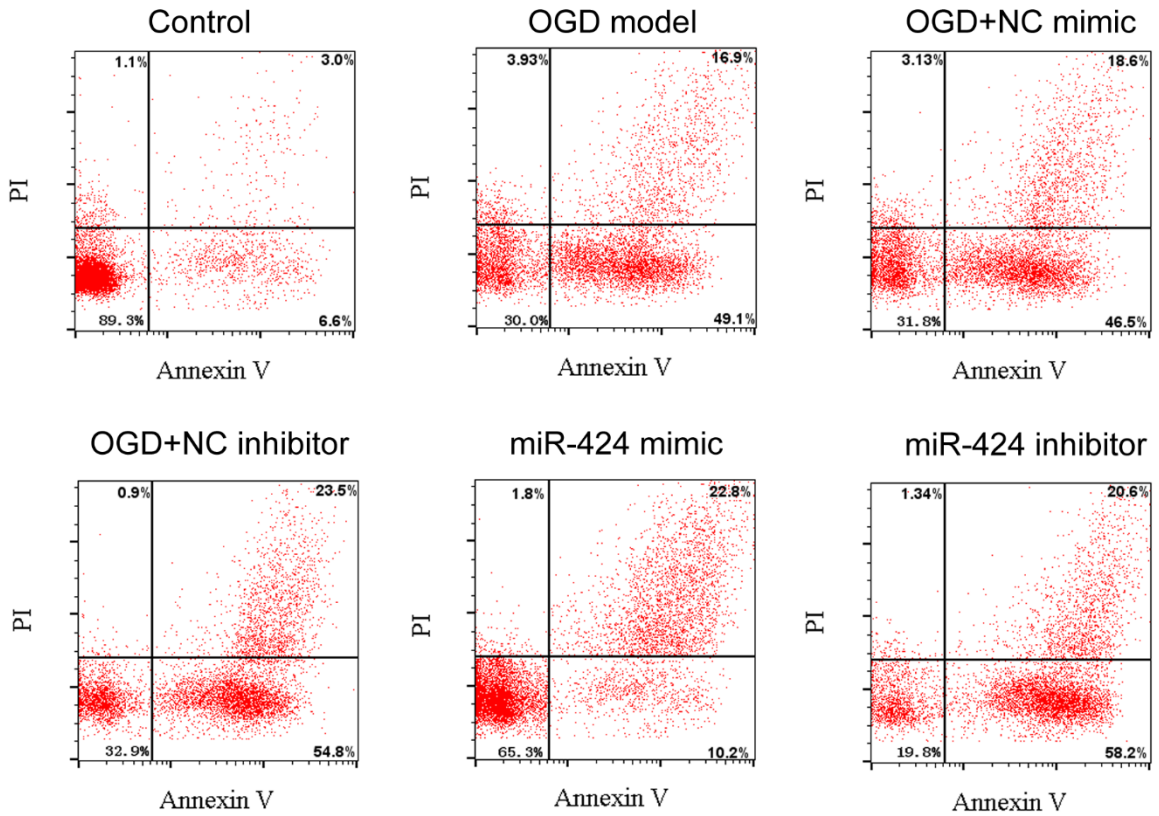

Fig. 6. *Effect of miR-424 on apoptosis of PC12 cells. Flow cytometry and Annexin V/PI staining are used to detect the effect of miR-424 expression on PC12 cell apoptosis (n=3). MiR-424 affects apoptosis induced by OGD in a dose-dependent manner. The OGD-induced apoptosis rate of PC12 cells declines in miR-424 mimic group, while it rises in miR-424 inhibitor group.*

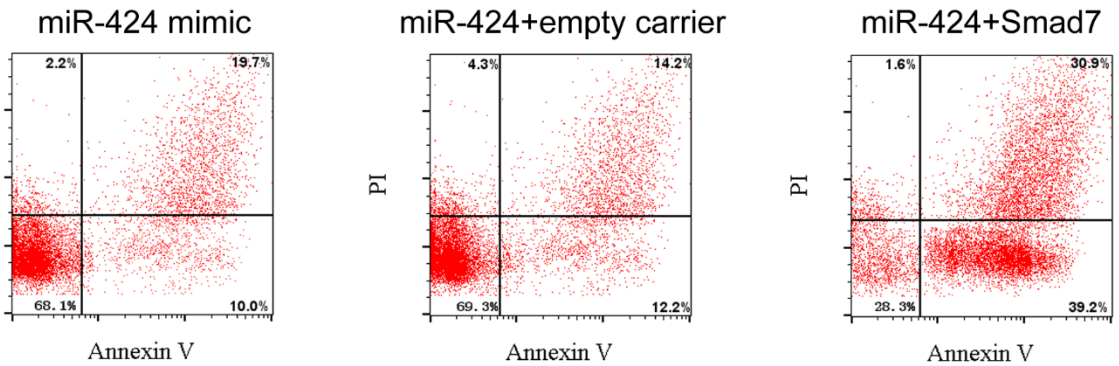

Fig. 7. *Effect of miR-424 on OGD-induced apoptosis of PC12 cells through targeting Smad7. Flow cytometry and Annexin V/PI staining are used to detect the role of Smad7 in the protective effect of miR-424 mimic on PC12 cells (n=3). Overexpression of Smad7 can eliminate the protective effect of miR-424 mimic on ischemic-hypoxic cells.*

results showing that miR-424 plays a key role in ischemic stroke. Firstly, studies have demonstrated that the expression level of miR-424 can be used in the diagnosis of ischemic stroke. For example, Li et al. (10) in their study found that the expression level of miR-424 in peripheral blood can be used to diagnose ischemic stroke and may affect the severity of acute stroke. Secondly, miR-424 may serve as a preventive target for disability after ischemic stroke in elderly patients. For example, Zhao et al. (11) pointed out that miR-424 can enhance the expression of H3K27me3 through the NFIA/DNMT1 signaling pathway, thereby preventing ischemia/reperfusion-induced astrocyte proliferation. In addition, miR-424 can be used as a target reducing neuronal apoptosis induced by cerebral ischemia during the pathological process of cerebral ischemia. Studies conducted by Liu et al. (12) and Cao et al. (13) showed that miR-424 can reduce cerebral ischemia-induced cell damage *via* inhibiting oxidative stress and regulating MKP-1. The important role of miR-424 in cerebral ischemia has been confirmed in a large number of studies, but its mechanism of action is rarely studied. In the present study, the mechanism of the protective effect of miR-424 against MCAO-induced brain damage was further explored.

In this study, it was first found *via* RT-qPCR that the expression of miR-424 in brain tissues in the model group at 7 days after cerebral ischemia was significantly lower than that in the sham group. The research results of Liu and Tabakman (12, 14), similar to the findings in the present study, manifested that the expression of miR-424 significantly declines in brain tissues of MCAO rats. Study results of Li et al. (11) point out that the expression level of miR-424 also obviously declines in peripheral immune cells of patients with ischemic stroke. Interestingly, the miR-424 expression level evidently rises in OGD-induced cell damage, indicating the differences between the *in vitro* model and the *in vivo* model.

The effects of miR-424 expression on MCAO-induced brain damage and apoptosis level of brain tissues were then determined *via* TTC staining and TUNEL assay. The results revealed that the miR-424 mimic remarkably reduced the infarction area and apoptosis of brain tissues, while the miR-424 inhibitor displayed the opposite effects, suggesting that the increased expression of miR-424 can markedly reduce MCAO-induced brain tissue damage. Currently, the protective effect of miR-424 on ischemic brain tissues has been reported in a large number of studies (10-13), proving the reliability of results in this study.

To further reveal the mechanism of the protective effect of miR-424 on ischemic brain tissues, differentially expressed genes were screened using gene chip assay, and the possible mechanism of action of miR-424 was explored through miRNA target prediction and functional enrichment analysis. It was found that miR-424-induced differentially expressed genes were significantly enriched in the TGF-β signaling pathway. Moreover, the results of Western blotting clarified that the miR-424 mimic could markedly activate the TGF-β1/Smad3 signaling pathway. The TGF-β signaling pathway is a key regulator of such biological processes as cell proliferation, migration, differentiation and apoptosis (15, 16), and its activation plays a protective role against ischemic injury, such as myocardial ischemia and cerebral ischemia. According to the research results of Yu et al. (17), the TGF-β1/Smad3 signaling pathway exerts a protective effect on ischemic brain tissues. Zhu et al. (15), through *in vitro* and *in vivo* experiments, pointed out that activating the TGF-β1/Smad3 signaling pathway in cerebral ischemia can inhibit the expression of pro-apoptosis protein, thereby suppressing neuronal apoptosis induced by cerebral ischemia.

The results revealed that miR-424 bound to the 3'UTR of Smad7 mRNA to reduce the mRNA and protein expressions of Smad7, thereby activating the TGF-β1/Smad3 signaling pathway. The research results of Hu et al. (18) indicate that miR-93-5p can activate the TGF-β1/Smad3 signaling pathway through targeting Smad7, thereby suppressing the drug resistance of prolactinoma and fibrosis. Monteleone et al. (19) studied and argued that, in patients with chronic inflammatory bowel disease and animal models, inhibiting the Smad7 activity can markedly enhance the p-smad3 protein expression and activate the TGF-β1/Smad3 signaling pathway.

In addition, the OGD assay found that the miR-424 mimic had a protective effect against OGD-induced apoptosis of PC12 cells, while overexpression of Smad7 could eliminate the protective effect of miR-424 mimic on ischemic-hypoxic cells, which further confirmed that miR-424 inhibits Smad7 protein expression to activate the TGF-β1/Smad3 signaling pathway, thereby exerting a protective effect on ischemic-hypoxic brain tissues.

In conclusion, increasing the expression of miR-424 can inhibit Smad7 to activate the TGF-β1/Smad3 signaling pathway, thereby exerting a protective effect against the brain tissue damage induced by MCAO.

REFERENCES

1. Frontera JA, Starling R, Cho SM, et al. Risk factors, mortality, and timing of ischemic and hemorrhagic stroke with left ventricular assist devices. J Heart Lung Transplant 2017; 36:673-83.
2. Sun H, Zou X, Liu L. Epidemiological factors of stroke: a survey of the current status in china. J Stroke 2013; 15:109-14.
3. Murray CJ, Vos T, Lozano R, et al. Disability-adjusted life years (DALYs) for 291 diseases and injuries in 21 regions, 1990-2010: a systematic analysis for the Global Burden of Disease Study 2010. Lancet 2012; 380:2197-223.
4. Zitnanova I, Siarnik P, Kollar B, et al. Oxidative stress markers and their dynamic changes in patients after acute ischemic stroke. Oxid Med Cell Longev 2016; 2016:9761697.
5. Hu J, Pang WS, Han J, Zhang K, Zhang JZ, Chen LD. Gualou Guizhi decoction reverses brain damage with cerebral ischemic stroke, multi-component directed multi-target to screen calcium-overload inhibitors using combination of molecular docking and protein-protein docking. J Enzyme Inhib Med Chem 2018; 33:115-25.
6. Kim JY, Park J, Chang JY, Kim SH, Lee JE. Inflammation after ischemic stroke: the role of leukocytes and glial Cells. Exp Neurobiol 2016; 25:241-51.
7. Liu DZ, Tian Y, Ander BP, et al. Brain and blood microRNA expression profiling of ischemic stroke, intracerebral hemorrhage, and kainate seizures. J Cereb Blood Flow Metab 2010; 30:92-101.
8. Selvamani A, Sathyan P, Miranda RC, Sohrabji F. An antagomir to microRNA Let7f promotes neuroprotection in an ischemic stroke model. Plos One 2012; 7:e32662.
9. Sun Y, Gui H, Li Q, Luo ZM, Zheng MJ, Duan JL, Liu X. MicroRNA-124 protects neurons against apoptosis in cerebral ischemic stroke. Cns Neurosci Ther 2013; 19:813-19.
10. Li G, Ma Q, Wang R, et al. Diagnostic and immunosuppressive potential of elevated Mir-424 levels in circulating immune cells of ischemic stroke patients. Aging Dis 2018; 9:172-81.
11. Zhao H, Li G, Wang R, et al. MiR-424 prevents astrogliosis after cerebral ischemia/reperfusion in elderly mice by enhancing repressive H3K27me3 via NFIA/DNMT1 signaling. Febs J 2019; 286:4926-36.
12. Liu P, Zhao H, Wang R, et al. MicroRNA-424 protects against focal cerebral ischemia and reperfusion injury in mice by suppressing oxidative stress. Stroke 2015; 46:513-519.
13. Cao YX, Wang ZQ, Kang JX, Liu K, Zhao CF, Guo YX, Jiao BH. miR-424 protects PC-12 cells from OGD-induced injury by negatively regulating MKP-1. Eur Rev Med Pharmacol Sci 2018; 22:1426-1436.
14. Tabakman R, Jiang H, Shahar I, Arien-Zakay H, Levine RA, Lazarovici P. Neuroprotection by NGF in the PC12 in vitro OGD model: involvement of mitogen-activated protein kinases and gene expression. Ann N Y Acad Sci 2005; 1053:84-96.
15. Zhu H, Gui Q, Hui X, et al. TGF-beta1/Smad3 signaling pathway suppresses cell apoptosis in cerebral ischemic stroke rats. Med Sci Monit 2017; 23:366-76.
16. Wang D, Zhang G, Chen X, et al. Sitagliptin ameliorates diabetic nephropathy by blocking TGF-beta1/Smad signaling pathway. Int J Mol Med 2018; 41:2784-92.
17. Yu Y, Li J, Zhou H, Xiong Y, Wen Y, Li H. Functional importance of the TGF-beta1/Smad3 signaling pathway in oxygen-glucose-deprived (OGD) microglia and rats with cerebral ischemia. Int J Biol Macromol 2018; 116:537-44.
18. Hu B, Mao Z, Du Q, et al. miR-93-5p targets Smad7 to regulate the transforming growth factor-beta1/Smad3 pathway and mediate fibrosis in drug-resistant prolactinoma. Brain Res Bull 2019; 149:21-31.

19. Monteleone G, Kumberova A, Croft NM, McKenzie C, Steer HW, MacDonald TT. Blocking Smad7 restores TGF-beta1 signaling in chronic inflammatory bowel disease. J Clin Invest 2001; 108:601-609.

MiR-125b Improves acute myocardial infarction in rats by regulating P38/Sirtl/P53 signaling pathway

G.-H. Qiao, P. Zhu, L. Yue and S. Yue

Department of Emergency Medicine, Luoyang Central Hospital Affiliated to Zhengzhou University, Luoyang, China

Received March 21, 2020 – Accepted June 18, 2020

The aim of this study was to investigate the differential expression of micro ribonucleic acid (miR)-125b in acute myocardial infarction (AMI) cases, and to explore the mechanism by which it affects cardiac function. Sprague-Dawley rats were used for AMI modeling, and the expression of miR-125b in the myocardial tissues of AMI rats was detected *via* fluorescence quantitative reverse transcription-polymerase chain reaction (qRT-PCR). Thereafter, the target genes of miR-125b were collected and uploaded to WenGestalt for gene ontology (GO) and pathway enrichment analyses. *In-vitro* experiments were then applied to determine the p38-sirtuin 1 (Sirt1)-p53 expression change and cardiomyocyte apoptosis under down-regulation of miR-125b. Next, the interaction between miR-125b and its target genes was verified by luciferase reporter gene assay. The expression of miR-125b in the cardiac tissues was decreased in theAMI group compared with that in the Sham group ($p<0.05$). The luciferase reporter gene assay confirmed that p38 was the target gene of miR-125b. Furthermore, the down-regulated expression of miR-125b in H9C2 cells up-regulated the protein expressions of p38 and phosphorylated p38, thus activating the Sirt1-p53 signaling pathway. Moreover, the down-regulation of miR-125b expression in H9C2 cells gave rise to the elevated apoptosis rate, and the down-regulated expression of miR-125b induced cardiomyocyte apoptosis through activating the p38-Sirt1-p53 signaling pathway.

Acute myocardial infarction (AMI), a cardiovascular disease characterized by rapid progression, can cause inadequate blood supply to the heart in a short time, so it is one of the most serious diseases leading to death of the elderly at present (1). It severely impairs the cardiac function if not diagnosed and treated timely after onset. Moreover, AMI is extremely prone to being complicated with ventricular septal rupture, with a mortality rate as high as 90% (2). Heart failure after myocardial infarction plays an important role in pathology, and the decrease in ventricular wall thickness and heart failure triggered by cardiomyocyte degeneration inevitably occur during AMI. The apoptosis-induced loss of cardiomyocytes is a leading cause of heart failure after myocardial infarction (3). Currently, there are numerous therapeutic methods for AMI in clinical use, but none of them is absolutely secure and 100% curative due to individual differences (4). Hence, the development of new methods for AMI and the exploration of its mechanism are conducted extensively.

Key words: cardiomyocyte; apoptosis; miR-25b; p38

Corresponding Author:
G.-H. Qiao, BM.
Department of Emergency Medicine,
Luoyang Central Hospital Affiliated to Zhengzhou University,
288 Zhongzhou Middle Road, Xigong District, Luoyang,
Henan, 471000 China
Tel.: +86015896611352
e-mail: guohuang19740311@163.com

0393-974X (2020)
Copyright © by BIOLIFE, s.a.s.
This publication and/or article is for individual use only and may not be further reproduced without written permission from the copyright holder.
Unauthorized reproduction may result in financial and other penalties
DISCLOSURE: ALL AUTHORS REPORT NO CONFLICTS OF INTEREST RELEVANT TO THIS ARTICLE.

Increasingly more micro ribonucleic acids (miRNAs) have been discovered and studied by scientific researchers during the exploitation of novel sensitive, high-efficient and highly specific biomarkers. miRNAs are small single-stranded non-coding RNAs, about 22 nt in length, which can pair with the 3'-untranslated region (UTR) of messenger RNAs (mRNAs) and regulate gene expressions at the transcriptional and post-transcriptional levels by means of mRNA degradation or protein translational repression (5). It is estimated that miRNAs regulate more than one-third of encoding genes in humans (6). The specific regulatory mechanism of miRNAs in mRNAs has not yet been completely clarified, but miRNAs can silence specific targets through a certain mechanism, thereby modulating gene expression in cells and tissues. The widespread miRNAs are closely associated with the complicated changes in cardiomyocytes, and they are increasingly considered as vital regulators of cardiac functions and diseases (7-9). The early diagnosis of AMI depends on biomarkers with high sensitivity and specificity, and approximately 20 kinds of miRNAs including miR-123, miR-208 and miR-214 have been found to be related to the occurrence and development of AMI to date (5). Studies have reported that abnormal miR-125b level is correlated with the increased incidence rate of human AMI (10, 11). It was revealed through the rat model of AMI in this research that miR-125b was differentially expressed in AMI rats, and the mechanism by which miR-125b affects AMI was further investigated.

Sirtuin (Sirt) proteins belong to an ancient and evolutionarily conserved family of nicotinamide adenine dinucleotide, which possess the activity of deacetylase or transribosylase (12, 13). Moreover, Sirt proteins are involved in such processes such as injury repair, gene expression, heat control and anti-aging (14-16). 1-7 Sirt proteins (Sirt1-Sirt7) have been observed in mammals, and are located at different sites. For example, Sirt1 is mainly located in the nucleus and cytoplasm (12, 13). The activity of Sirt is primarily related to post-translational modification and the expression and enzymatic ability of various proteins including regulators. According to previous studies, Sirt1 participates in cardiac protection, and Hariharan et al. (17) reported that Sirt1 can mediate glucose starvation-induced autophagy *via* deacetylation of FOXO in cardiomyocytes. In addition, Sirt1 overexpression protects the heart from ischemia/reperfusion injury by inhibiting cell apoptosis (18). In the present study, therefore, the differential expression profiles of miRNAs in the cardiac tissues of AMI rats were observed using sequencing techniques. It was assumed that miR-125b triggers the changes in proliferation and apoptosis activity of cardiomyocytes through regulating the p38/Sirt1 activity. Moreover, the differential expression of miR-125b was testified to further elaborate the influence of miR-125b on AMI, and its action mechanism was explored, so as to provide more adequate theoretical bases proving that miR-125b is a marker and target of AMI.

MATERIALS AND METHODS

Sprague-Dawley (SD) rats were purchased from Nanjing Better Biotechnology Co., Ltd., and myocardium cell lines (H9C2) were bought from the cell bank of Chinese Academy of Sciences (Shanghai, China). This study was approved by the Animal Ethics Committee of Zhengzhou University Animal Center.

Preparation of rat model of AMI

A total of 20 male SD rats weighing about 250 g were randomly divided into AMI group and Sham group, in which the rat model of AMI was established by ligating the left anterior descending coronary artery (19). Then the rats were anesthetized by isoflurane, and the chest was shaved and cleaned using alcohol. Next, the thoracic cavity was cut open through a left parasternal incision, and the heart was exposed from the left third and fourth intercostal spaces. Subsequently, the pericardium was opened, and the coronary artery was ligated by sutures. In the Sham group, the thoracic cavity was sutured after opening, without ligation of the coronary artery. All the rats underwent euthanasia at 6 h after treatments, so as to obtain the cardiac tissues.

Sequencing analysis of miRNAs

Three rats were selected from both AMI group and Sham group for miRNA sequencing by KangChen Bio-Tech (Shanghai, China). In short, siRNAs were first isolated and purified from total RNAs, which was then conjugated with 5'-linker and purified, followed by

conjugation with 3'-linker and purification. Next, the siRNAs were synthesized into first-strand and second-strand complementary deoxyribose nucleic acids (cDNAs), and then Illumina Genome Analyzer IIx sequencing analysis was performed. FC>2.0 and $p<0.05$ suggested that the miRNAs were differentially expressed.

Prediction and analysis of target genes

The intersection of target genes of miR-125b predicted by TargetScan, miRPathDB and miRDB was uploaded to WebGestalt (20) for Genome Ontology (GO) and pathway enrichment analyses. Later, the miRNA-target interaction network was visualized by means of Cytoscape 3.7.1 (21).

Cell culture and transfection

Normal human cardiomyocytes (H9C2) were cultured with RPMI-1640 medium (Nanjing BioChannel Biotechnology Co., Ltd., Nanjing, China) supplemented with 10% FBS and 1% Pen/Strep solution in an incubator with 5% CO_2 at 37°C. Then H9C2 cells were paved in a 24-well plate and transfected with 100 nM miR-125b siRNA (miR-125b group) and negative control (NC) (Control group) according to the instructions of miRNA transfection reagent; 24 h later, the cells and supernatant were collected for subsequent analyses.

Quantitative reverse transcription-polymerase chain reaction (qRT-PCR)

The total RNAs were extracted from the cardiac tissues and cardiomyocytes using TRIzol reagent (Invitrogen, Carlsbad, CA, USA) and quantified using NanoDrop ND-2000. Later, the total RNAs were synthesized into cDNAs of miR-125b and genes using reverse transcriptase *as per* the kit instructions, and the levels of miR-125b and genes were determined by SYBR Green PCR kits on a 7500-Fast real-time PCR system (Applied Biosystems, Foster City, CA, USA). Finally, the relative expression levels of miR-125b and genes were calculated through $2^{-\Delta\Delta Ct}$ method, with U6 as an internal reference of miRNA and glyceraldehyde-3-phosphate dehydrogenase (GAPDH) as an internal reference of genes. The primer sequences for qRT-PCR are shown in Table I.

Western blotting analysis

RIPA lysis buffer was applied to extract proteins from the cardiac tissues and cardiomyocytes, and the protein concentration was measured via the bicinchoninic acid (BCA) method (Pierce, Rockford, IL, USA) and maintained uniform for all samples, followed by gel electrophoresis (10% SDS-PAGE, 60 μg/lane). After that, the proteins on the gel were transferred onto a PVDF membrane, sealed in Tris-buffered saline-Tween 20 (TBST) (Tris-buffered saline + 0.1% Tween 20) containing 5% skim milk powder for 1 h and incubated with primary antibodies (Abcam, Cambridge, MA, USA) at 4°C overnight. The next day, the membrane was washed for 3-5 times and then incubated with secondary antibodies at room temperature for 1 h, followed by washing with TBST and color development.

Terminal deoxynucleotidyl transferase (TdT)-mediated dUTP nick end labeling (TUNEL) assay

The cardiomyocytes were fixed with formaldehyde, washed with PBS for 3 times and permeabilized using 1% Tritonx-100 at room temperature, followed by reaction with TdT solution, color development and mounting with 4',6-diamidino-2-phenylindole (DAPI). Finally, the cardiomyocytes were observed under a microscope, and the $TUNEL^+$ cells were counted.

Table I. *Primer sequences for qPCR*

Index	Forward primer sequence (5'-3')	Reverse primer sequence (5'-3')
GAPDH	GGAGCGAGATCCCTCCAAAAT	GGCTGTTGTCATACTTCTCATGG
U6	CTCGCTTCGGCAGCACA	AACGCTTCACGAATTTGCGT
MiR-125b	TCCCTGAGACCCTAACTTGTGA	TGGTGTCGTGGAGTCG
Interleukin-1 beta (IL-1β)	GCAACTGTTCCTGAACTCAACT	ATCTTTTGGGGTCCGTCAACT
IL-6	TAGTCCTTCCTACCCCAATTTCC	TTGGTCCTTAGCCACTCCTTC
Tumor necrosis factor-alpha (TNF-α)	GACGTGGAACTGGCAGAAGAG	TTGGTGGTTTGTGAGTGTGAG

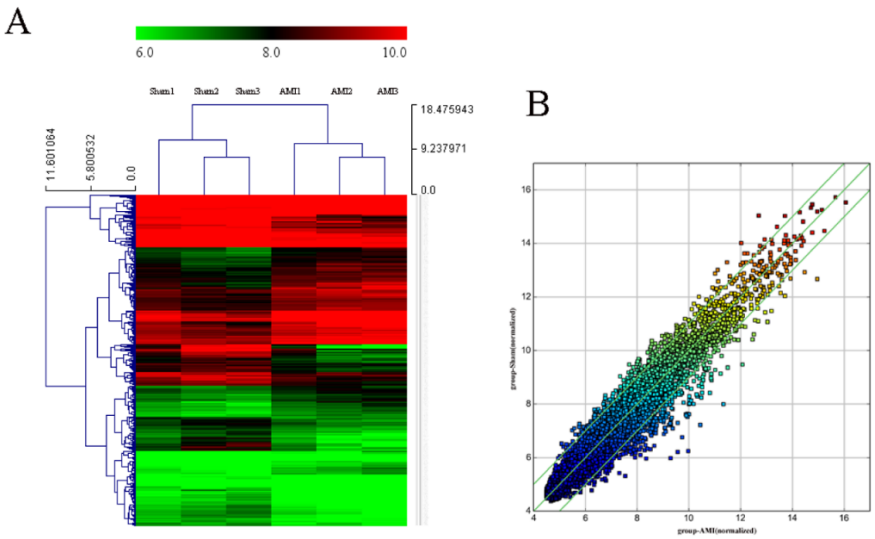

Fig. 1. *Differentially expressed miRNAs in AMI rats.* ***A****) Heat map of differentially expressed miRNAs in AMI rats.* ***B****) Scatter plot of differentially expressed miRNAs in AMI, where dots stood for miRNAs, and light green lines for fold changes. The dots above the topmost line and below the bottom line denoted the miRNAs with a fold change of difference between AMI group and Sham group exceeding 2.0.*

Dual-luciferase reporter assay system

The wild-type (WT) and mutant (MUT) sequences in the 3'-UTR of p38 were inserted into pGL3-CMV vectors (Promega, Madison, WI, USA) to investigate the relationship between miR-125b and p38 expressions. Then H9C2 cells were co-transfected with pGL3-p38-3'-UTR and miR-125b mimic or miR-NC using Lipofectamine 2000 (Invitrogen, Carlsbad, CA, USA). After 48 h, the cells were harvested to detect the luciferase activity according to the manuals of the kit (Promega, Madison, WI, USA).

Statistical analysis

Statistical Product and Service Solutions (SPSS) 22.0 software (IBM, Armonk, NY, USA) was employed for statistical analysis. The numerical variables were expressed as mean ± standard deviation, independent-samples *t*-test was used for comparison between two groups, and $p<0.05$ suggested that the difference was statistically significant.

RESULTS

MiR-125b expression was up-regulated in AMI rats

It was found through miRNA sequencing analysis that the expression of miR-125b was decreased in the AMI group compared with that in the Sham group ($p<0.05$) (Fig. 1). Then the expression of miR-125b was verified by means of qRT-PCR, and it was shown that the AMI group exhibited a reduced miR-125b expression in comparison with the Sham group ($p<0.05$) (Fig. 2).

Predicted target genes of miR-125b

According to the intersection of potential target genes from miRDB, miRPathDB and TargetScan, a total of 218 possible target genes of miR-125b were obtained. Moreover, Cytoscap 3.7.1 (20) was utilized to visualize the miR-125b-target interaction network (Fig. 3).

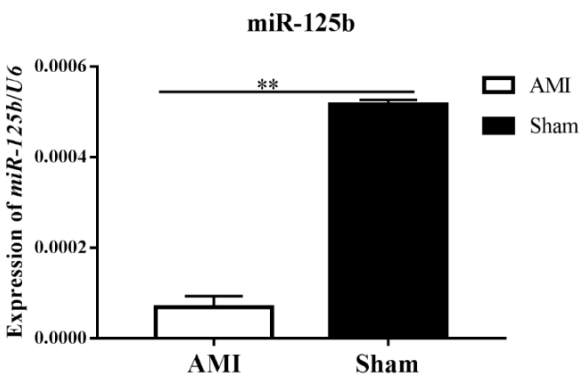

Fig. 2. *Decreased expression of miR-125b in AMI rats shown in qRT-PCR. Note: The expression of miR-125b was decreased in AMI group compared with that in Sham group (**p<0.01).*

GO and pathway enrichment analyses on target genes of miR-125b

The target gene sets of miR-125b were uploaded to WebGestalt online tool for enrichment analysis. 218 target genes were successfully enriched, and a series of target genes involved in event procedures covering abundant categories and pathways were acquired (Fig. 4). The pathways obtained via enrichment are shown in Table II.

Expression of inflammatory factors in cardiac tissues was raised in AMI rats

In order to identify the inflammation level in AMI rats, the mRNA levels of IL-1β, IL-6 and TNF-α in the cardiac tissues were measured. The results of qRT-PCR indicated that the mRNA levels of IL-1β, IL-6 and TNF-α in the cardiac tissues were elevated remarkably in AMI group compared with those in Sham group, suggesting a

Table II. *Pathway enriched for target genes of miR-125b*

Gene Set	Description	Ratio	*p*-value
mmu00514	Other types of O-glycan biosynthesis	11.84	0.0019434
mmu04010	MAPK signaling pathway	2.9533	0.0019582
mmu00512	Mucin type O-glycan biosynthesis	9.303	0.0039331
mmu00600	Sphingolipid metabolism	5.4267	0.017605
mmu00510	N-Glycan biosynthesis	5.316	0.018599
mmu05206	MicroRNAs in cancer	3.0573	0.023705
mmu04659	Th17 cell differentiation	3.405	0.029784
mmu04722	Neurotrophin signaling pathway	2.8703	0.050606
mmu05152	Tuberculosis	2.439	0.05416
mmu04142	Lysosome	2.8009	0.054472

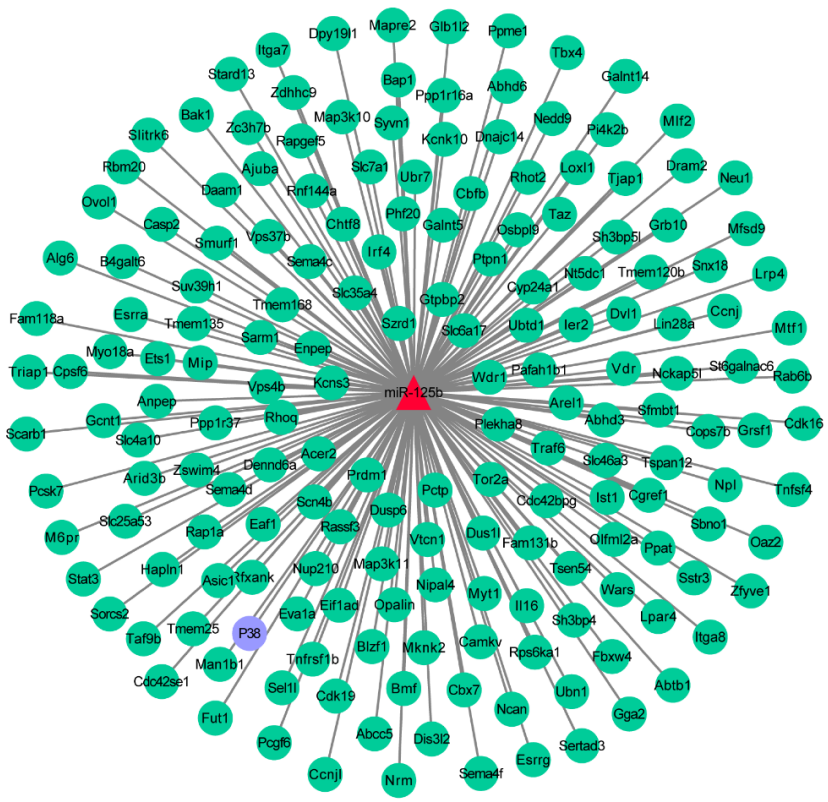

Fig. 3. *MiR-125b-target interaction network. The nodes stood for genes or miRNA, the lines for associations, and the red triangle for miR-125b. The circular nodes represented target genes, among which the light blue node represented p38.*

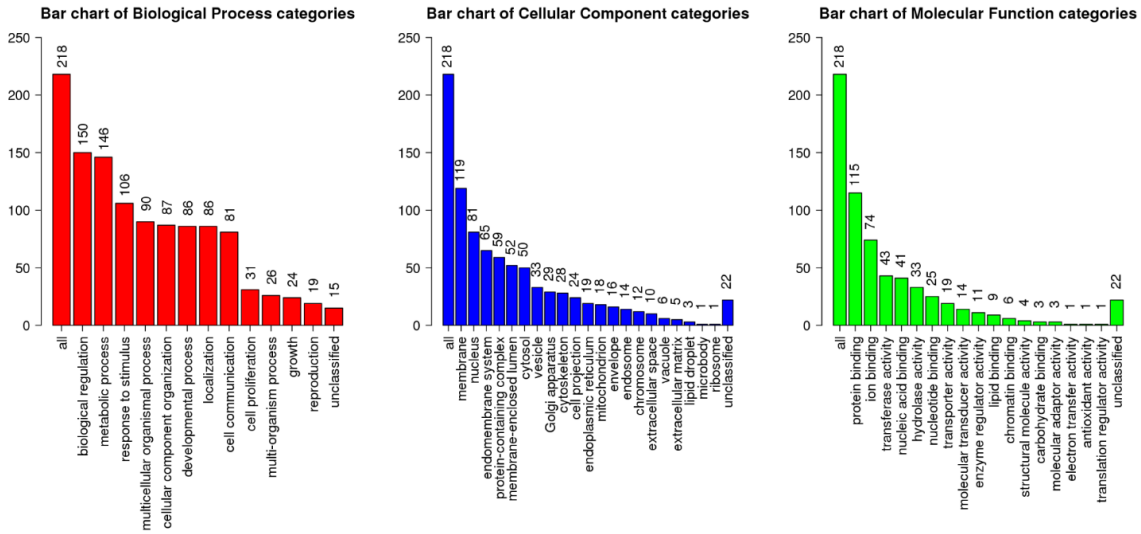

Fig. 4. *Detailed information of GO enrichment for target genes of miR-125b. Note: Biological Process (BP): enrichment of biological processes; Cellular Component (CC): enrichment of cellular components; Molecular Function (MF): enrichment of molecular function.*

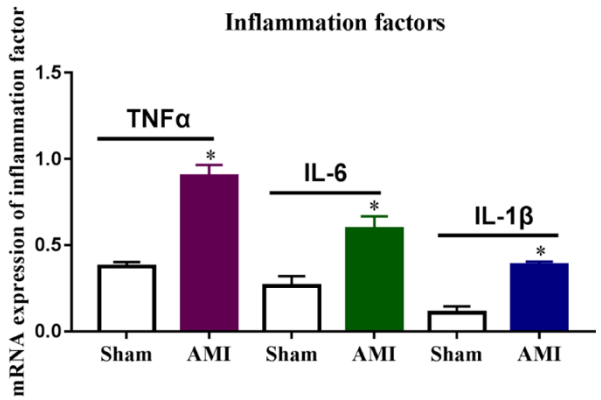

Fig. 5. *Expression of representative inflammatory factors in the cardiac tissues of AMI rat. Note: Sham group vs AMI group, with a statistically significant difference in expression (*p<0.05).*

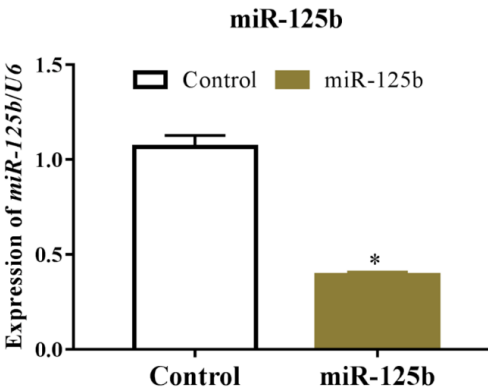

Fig. 6. *Expressions of miR-125b after transfection. Note: MiR-125b group exhibited an obviously lower expression level of miR-125b than Control group (*p<0.05).*

certain degree of inflammatory responses in AMI rats (Fig. 5).

Knockdown of miR-125b activated the p38 signaling pathway

The changes in miR-125b content in the cardiomyocytes were detected after transfection with miR-125b siRNA (miR-125b group), so as to determine the action mechanism of miR-125b. It was manifested that miR-125b group exhibited an obviously lower expression of miR-125b than Control group ($p<0.05$) (Fig. 6). The expressions of p38, phosphorylated p38 (p-p38) and p53 were higher, while Sirt1 expression was lower after miR-125b knockdown in the miR-125b group than those in the Control group ($p<0.05$) (Fig. 7).

Knockdown of miR-125b induced cardiomyocyte apoptosis

To identify the impact of miR-125b on apoptosis, the number of TUNEL+ cardiomyocytes after transfection with miR-125b siRNA was determined through TUNEL assay. It was shown that the miR-125b group had an increased number of TUNEL+ cells in comparison with the Control group ($p<0.05$) (Fig. 8).

MiR-125b directly bound to p38 to inhibit its activity

Subsequently, for the purpose of further exploring the mechanism of miR-125b in AMI, the luciferase

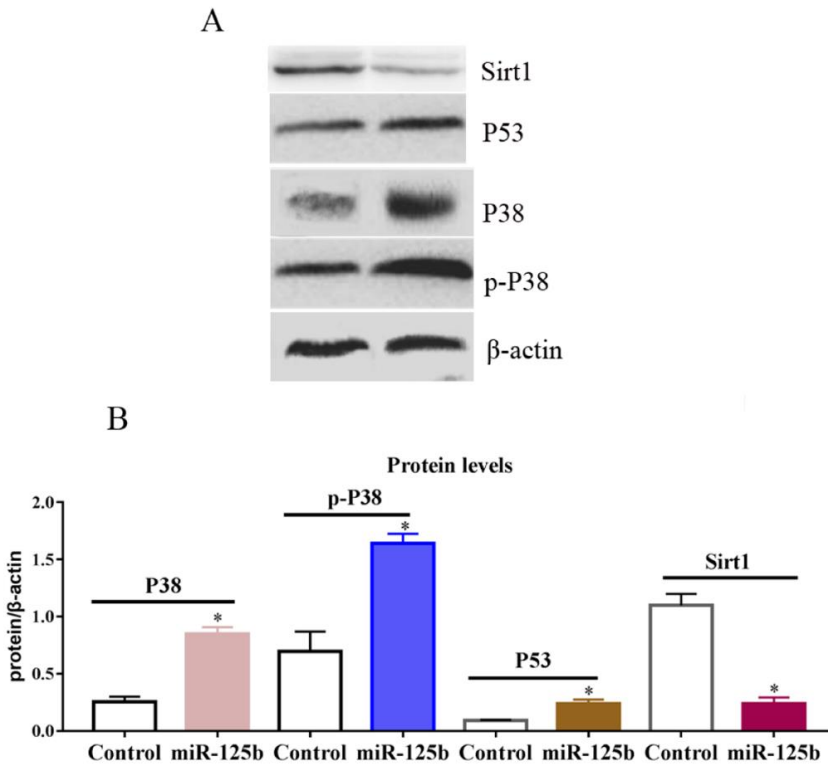

Fig. 7. *Expression levels of related proteins detected via Western blotting.* ***A****) Electrophoresis results of related proteins (Left: Control; right: miR-125b).* ***B****) Quantification results of related proteins. Note: There were differences in changes in protein levels of p38, p-p38, p53 and Sirt1 between the Control group and miR-125b group (*p<0.05).*

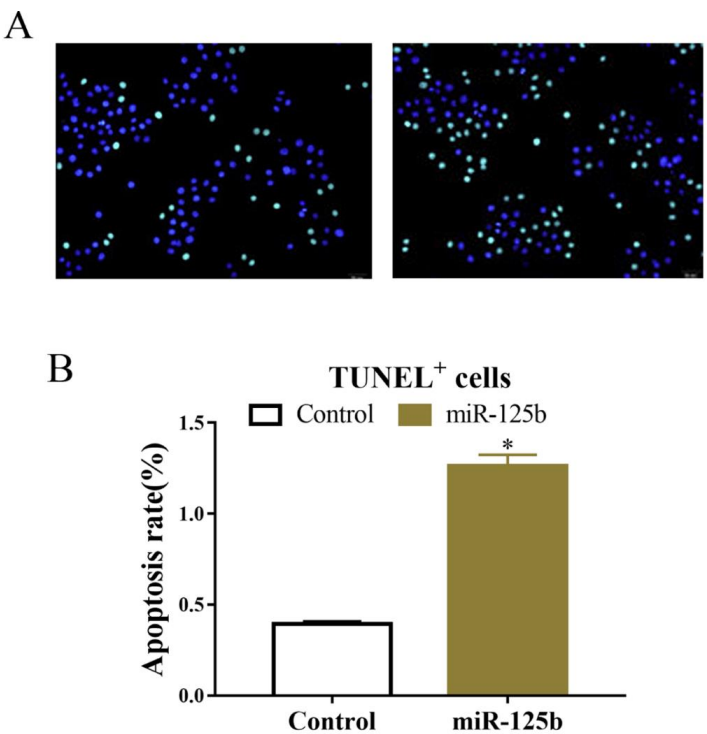

Fig. 8. *Impact of miR-125b on apoptosis of cardiomyocytes H9C2.* ***A****) Fluorescence staining of apoptotic cells (Left: Control; right: miR-125b), (magnification: 400×).* ***B****) Count of apoptotic cells (*p<0.05).*

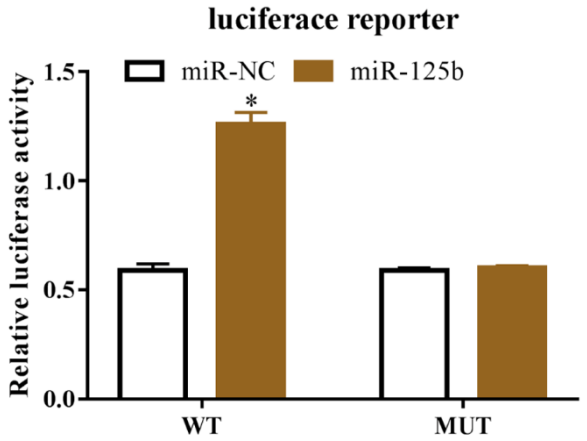

Fig. 9. *MiR-125b repressed the activation of the p38-Sirt1-p53 signaling pathway by directly binding to p38. Note: Luciferase activity of reporter genes carrying WT or MUT p38 after the cardiomyocytes were transfected with miR-NC and miR-125b (*p<0.05).*

reporter gene assay was applied to detect the interaction between p38 and miR-125b in cardiomyocytes, and TargetScan was utilized to predict their binding sites. Based on the results, it was found that the luciferase activity of reporter plasmids carrying WT p38 in cardiomyocytes was enhanced in miR-125b group (p<0.05), but no apparent changes were observed in the reporter gene system of MUT p38 (Fig. 9). All these results imply that miR-125b represses the activation of the p38-Sirt1-p53 signaling pathway by directly binding to p38.

DISCUSSION

Starting with animal experiments, the differentially expressed miRNAs in AMI rats were firstly obtained by means of sequencing technique in this research. Then the BPs and pathways involving the target genes of miR-125b were analyzed using enrichment analyses, and it was indicated that there were abundant categories in the BPs, in which the target genes of miR-125b were involved. A growing number of studies have investigated the roles of miRNAs in various diseases. As a class of small non-coding RNAs, miRNAs are highly conserved in the process of biological evolution, which do not encode proteins but can exert regulatory effects by binding to corresponding sites in the 3'-UTR of target genes involved in many crucial BPs. Such binding will lead to the degradation or expression suppression of target genes (22, 23). Currently, miRNAs are increasingly becoming a hot spot in the field of cardiovascular research. They not only play vital roles in the development of the cardiovascular system, but also participate in diverse pathophysiological processes of the heart, including myocardial hypertrophy, local ischemia and arrhythmia, according to previous studies (24-26). Moreover, miRNA expression changes in patients with congenital heart disease, physiological or pathological cardiac hypertrophy and heart failure (27), illustrating that miRNA may have biological effects in AMI. It has been reported in previous studies that miR-125b regulates SFRP5 expression to promote the growth and activation of cardiac fibroblasts (28) and represses cardiomyocyte apoptosis to protect the cardiomyocytes from AMI invasion (29). Although there are constantly increasing data from human and rodent research, the interaction between miRNAs and their mRNA targets is complex, so the action mechanism of miRNAs remains controversial (30, 31) and needs to be further explored. In contrast, the BPs involving the target genes of miR-125b were analyzed more comprehensively, and it was indicated that miR-125b participates in the regulatory processes of cell proliferation and apoptosis from the aspects of GO and pathway. Moreover, it was predicted that p38 serves as a target gene of miR-25b. It was also observed in this research that miR-125b expression changed in the cardiac tissues of AMI rats and exerted its regulatory effect by targeting p38. However, there were still some deficiencies in this research despite fairly adequate prediction and verification. For instance, there was insufficient experimental validation *in vivo*, and the mechanism needs to be investigated continuously. In addition, it is necessary to conduct in-depth studies on the *in-vivo* effects of miR-125b through clinical data in the future due to species differences between rats and human.

Sirts are NAD-dependent class III histone deacetylases that are highly conserved (32). Among them, Sirt1 can stimulate the interaction between and deacetylation of varying transcription factors and regulators, thus modulating the expression of

downstream genes. Clinically, Sirt1 is associated with many diseases (33-36). A growing number of studies have confirmed that Sirt1 plays an essential role in cardiac protection in the case of various cardiovascular diseases through complicated signaling networks (e.g. autophagy (17) and apoptosis (37). It also extensively protects cardiac tissues from injury (38-40). In the present experiment, the expressions of p38 and p-p38 were activated, Sirt1 expression was inhibited, and apoptotic cells were increased after miR-125b was knocked down. Additionally, it was confirmed through dual-luciferase reporter gene assay that miR-25b directly interacted with p38, suggesting that miR-125b controls the cardiomyocyte apoptosis in AMI by regulating the p38-Sirt1-p53 signaling pathway and repressing Sirt1 expression.

In summary, the expression profiles of differentially expressed miRNAs in the case of AMI were screened in this research, and more miRNAs with diagnostic significance in AMI are expected to be explored. Furthermore, it was clarified that miR-125b was differentially expressed in the cardiac tissues of AMI rats, laying a foundation for its subsequent functions in AMI, as well as theoretical and scientific bases for the treatment of AMI patients with miR-125b. The possibility of miR-125b acting as a potential therapeutic target of AMI, as well as for some other related diseases has been proposed, enriching and expanding the roles of miR-125b in diseases. Furthermore, the mechanism of p38-Sirt1-p35 in AMI was preliminarily clarified in this research, which is conducive to further deepening the understanding of the action mechanism of the signaling pathway.

REFERENCES

1. Benjamin EJ, Virani SS, Callaway CW, et al. Heart Disease and Stroke Statistics-2018 Update: A Report From the American Heart Association. Circulation 2018; 137:e67-e492.
2. Munuswamy K, Alpert MA, Parker BM, Madigan NP, Miller DP. Ventricular septal rupture after acute myocardial infarction: diagnosis by two-dimensional echocardiography. South Med J 1983; 76:87-89.
3. Abbate A, Narula J. Role of apoptosis in adverse ventricular remodeling. Heart Fail Clin 2012; 8:79-86.
4. Ko SQ, Valsdottir LR, Strom JB, et al. Meta-Analysis of Bleeding Risk Prediction Scores in Patients After Percutaneous Coronary Intervention on Dual Antiplatelet Therapy. Am J Cardiol 2018; 122:1843-52.
5. Nabialek E, Wanha W, Kula D, et al. Circulating microRNAs (miR-423-5p, miR-208a and miR-1) in acute myocardial infarction and stable coronary heart disease. Minerva Cardioangiol 2013; 61:627-37.
6. Szabo L, Morey R, Palpant NJ, et al. Statistically based splicing detection reveals neural enrichment and tissue-specific induction of circular RNA during human fetal development. Genome Biol 2015; 16:126.
7. van Rooij E, Marshall WS, Olson EN. Toward microRNA-based therapeutics for heart disease: the sense in antisense. Circ Res 2008; 103:919-28.
8. Catalucci D, Gallo P, Condorelli G. MicroRNAs in cardiovascular biology and heart disease. Circ Cardiovasc Genet 2009; 2:402-408.
9. van Rooij E. The art of microRNA research. Circ Res 2011; 108:219-34.
10. Huang S, Chen M, Li L, et al. Circulating MicroRNAs and the occurrence of acute myocardial infarction in Chinese populations. Circ Cardiovasc Genet 2014; 7:189-98.
11. Wang X, Ha T, Zou J, et al. MicroRNA-125b protects against myocardial ischaemia/reperfusion injury via targeting p53-mediated apoptotic signalling and TRAF6. Cardiovasc Res 2014; 102:385-95.
12. Yamamoto H, Schoonjans K, Auwerx J. Sirtuin functions in health and disease. Mol Endocrinol 2007; 21:1745-55.
13. Yu J, Auwerx J. The role of sirtuins in the control of metabolic homeostasis. Ann N Y Acad Sci 2009; 1173 Suppl 1:E10-E19.
14. Anastasiou D, Krek W. SIRT1: linking adaptive cellular responses to aging-associated changes in organismal physiology. Physiology (Bethesda) 2006; 21:404-10.
15. Liu L, Liu C, Zhang Q, et al. SIRT1-mediated transcriptional regulation of SOX2 is important for self-renewal of liver cancer stem cells. Hepatology 2016; 64:814-27.
16. Liu B, Ghosh S, Yang X, et al. Resveratrol rescues

SIRT1-dependent adult stem cell decline and alleviates progeroid features in laminopathy-based progeria. Cell Metab 2012; 16:738-50.
17. Hariharan N, Maejima Y, Nakae J, Paik J, Depinho RA, Sadoshima J. Deacetylation of FoxO by Sirt1 Plays an Essential Role in Mediating Starvation-Induced Autophagy in Cardiac Myocytes. Circ Res 2010; 107:1470-82.
18. Hsu CP, Zhai P, Yamamoto T, et al. Silent information regulator 1 protects the heart from ischemia/reperfusion. Circulation 2010; 122:2170-82.
19. Cao M, Yu C, Yao Z, Gao X, Wu S. Atractylodesin III maintains mitochondrial function and inhibits caspase-3 activity to reverse apoptosis of cardiomyocytes in AMI rats. Int J Clin Exp Pathol 2019; 12:198-204.
20. Zhang B, Kirov S, Snoddy J. WebGestalt: an integrated system for exploring gene sets in various biological contexts. Nucleic Acids Res 2005; 33:W741-W748.
21. Shannon P, Markiel A, Ozier O, et al. Cytoscape: a software environment for integrated models of biomolecular interaction networks. Genome Res 2003; 13:2498-504.
22. Wang B, Bu X, Sun H, Liu Y. MicroRNA-98 promotes cell proliferation and invasion of glioblastoma via targeting HMGA2. J Neurosurg Sci 2019; doi: 10.23736/S0390-5616.19.04792-1.
23. Wu Q, Zhong H, Jiao L, et al. MiR-124-3p inhibits the migration and invasion of Gastric cancer by targeting ITGB3. Pathol Res Pract 2019:152762.
24. van Rooij E, Sutherland LB, Qi X, Richardson JA, Hill J, Olson EN. Control of stress-dependent cardiac growth and gene expression by a microRNA. Science 2007; 316:575-79.
25. Cai B, Pan Z, Lu Y. The roles of microRNAs in heart diseases: a novel important regulator. Curr Med Chem 2010; 17:407-11.
26. Shi JY. Microscopical quantification of Chinese drugs. Zhong Yao Tong Bao 1985; 10:11-13.
27. Thum T, Galuppo P, Wolf C, et al. MicroRNAs in the human heart: a clue to fetal gene reprogramming in heart failure. Circulation 2007; 116:258-67.
28. Bie ZD, Sun LY, Geng CL, et al. MiR-125b regulates SFRP5 expression to promote growth and activation of cardiac fibroblasts. Cell Biol Int 2016; 40:1224-34.
29. Bayoumi AS, Park KM, Wang Y, et al. A carvedilol-responsive microRNA, miR-125b-5p protects the heart from acute myocardial infarction by repressing pro-apoptotic bak1 and klf13 in cardiomyocytes. J Mol Cell Cardiol 2018; 114:72-82.
30. Filipowicz W, Bhattacharyya SN, Sonenberg N. Mechanisms of post-transcriptional regulation by microRNAs: are the answers in sight? Nat Rev Genet 2008; 9:102-14.
31. Oliveto S, Mancino M, Manfrini N, Biffo S. Role of microRNAs in translation regulation and cancer. World J Biol Chem 2017; 8:45-56.
32. Imai S, Armstrong CM, Kaeberlein M, Guarente L. Transcriptional silencing and longevity protein Sir2 is an NAD-dependent histone deacetylase. Nature 2000; 403:795-800.
33. Finkel T, Deng CX, Mostoslavsky R. Recent progress in the biology and physiology of sirtuins. Nature 2009; 460:587-91.
34. Haigis MC, Sinclair DA. Mammalian sirtuins: biological insights and disease relevance. Annu Rev Pathol 2010; 5:253-95.
35. Horio Y, Hayashi T, Kuno A, Kunimoto R. Cellular and molecular effects of sirtuins in health and disease. Clin Sci (Lond) 2011; 121:191-203.
36. Houtkooper RH, Pirinen E, Auwerx J. Sirtuins as regulators of metabolism and healthspan. Nat Rev Mol Cell Biol 2012; 13:225-38.
37. Zheng W, Lu YB, Liang ST, et al. SIRT1 mediates the protective function of Nkx2.5 during stress in cardiomyocytes. Basic Res Cardiol 2013; 108:364.
38. Sundaresan NR, Pillai VB, Gupta MP. Emerging roles of SIRT1 deacetylase in regulating cardiomyocyte survival and hypertrophy. J Mol Cell Cardiol 2011; 51:614-18.
39. Tanno M, Kuno A, Horio Y, Miura T. Emerging beneficial roles of sirtuins in heart failure. Basic Res Cardiol 2012; 107:273.
40. Yamamoto T, Sadoshima J. Protection of the heart against ischemia/reperfusion by silent information regulator 1. Trends Cardiovasc Med 2011; 21:27-32.

SNHG16 promotes cell proliferation and migration through sponging miR-132 in melanoma

L-L. Bi[1*], X-Q. Hua[2*], W-H. Li[3], L. Wang[4], Y. Li[5] and X-F. Jia[6]

[1]Department of Dermatology, Yeda Hospital of Yantai, Yantai. China; [2]Department of Clinical Laboratory, Jinan Zhangqiu District Hospital of TCM, Jinan, China; [3]No 2 Department of Oncology, Qingdao Central Hospital, Qingdao University, Qingdao, China; [4]Department of Radiotherapy, Jinan Zhangqiu District Hospital of TCM, Jinan, China; [5]Department of Interventional Angiology, the People's Hospital of Zhangqiu Area, Jinan, China; [6]Department of Oncology, Jining No.1 People's Hospital, Affiliated Jining No. 1 People's Hospital of Jining Medical University, Jining Medical University, Jining, China

Received March 3, 2020 – Accepted June 23, 2020

[*]These Authors contributed equally to this work

Melanoma, which originates from the transformation of normal melanocytes, is one of the three main types of skin cancer. We aimed to explore the functions of SNHG16 and miR-132 in melanoma. CCK-8, Transwell assays were used to measure the viability and migration, respectively. Spearman's correlation analysis was performed to analyze the relationship between the expression of SNHG16, miR-132 and LAPTM4B in melanoma tissues. SNHG16 was overexpressed, and miR-132 was low expressed in melanoma tissues and cell lines. Moreover, overexpression of SNHG16 was associated with poor prognosis of melanoma patients. The expression of SNHG16 had a negative connection with the expression of miR-132, and it had a positive relationship with the expression of LAPTM4B in melanoma tissues. Knockdown of SNHG16 or overexpression of miR-132 inhibited SK-MEL-2 cell proliferation and migration. In addition, we confirmed that SNHG16 directly binding to miR-132 promotes the expression of LAPTM4B, facilitating the tumorigenesis of melanoma. SNHG16 promotes the expression of LAPTM4B by sponging miR-132, thereby acting as an oncogene in melanoma. This study demonstrated that the lncRNA-miRNA-mRNA signal cascade existed in melanoma, which may help elucidate the tumorigenesis and development mechanism of melanoma.

Melanoma is a highly aggressive malignant tumor that originates from the transformation of normal melanocytes (1). Melanoma, one of the three main types of skin cancer, is the most difficult to cure because of its high degree of malignancy and few treatment options (2). Previous studies have shown that the inflammatory microenvironment and genetic factors play key roles in the occurrence of melanoma (3, 4), however, the molecular mechanism of melanoma development is unclear.

Long non-coding RNAs (lncRNAs) are non-coding RNAs with more than 200 nucleotides, which regulate gene expression through multiple regulatory mechanisms (5, 6). Increasing evidence has shown that lncRNAs are involved in several biological processes including cancer proliferation,

Key words: SNHG16; miR-132; LAPTM4B; melanoma

Corresponding Author:
Dr Xuefeng Jia,
Department of Oncology,
Jining No.1 People's Hospital,
6 Jiankang Road, Rencheng District,
Jining 272011, China
e-mail: pukouhao30454@163.com

0393-974X (2020)
Copyright © by BIOLIFE, s.a.s.
This publication and/or article is for individual use only and may not be further reproduced without written permission from the copyright holder.
Unauthorized reproduction may result in financial and other penalties
DISCLOSURE: ALL AUTHORS REPORT NO CONFLICTS OF INTEREST RELEVANT TO THIS ARTICLE.

metastasis and physiology (7). LncRNA has been extensively researched due to tissue specificity and abnormal expression in cancers (8). For example, SNHG16 promoted cell proliferation an invasion of lung adenocarcinoma via sponging let-7a (9). SNHG16 enhanced diffuse large B-cell lymphoma cell proliferation and inhibited cell apoptosis via miR-497-5p/PIM1 axis (10). Moreover, silencing of SNHG16 suppressed the aggressiveness of gastric cancer via upregulating microRNA-628 (11).

MicroRNAs (miRNAs) are a class of endogenous short non-coding RNAs, about 22 nucleotides in length (12, 13). MiRNAs usually complement the 3'-untranslated region (UTR) of the target mRNAs, resulting in mRNA degradation or translation inhibition (14, 15). Substantial evidence revealed that miRNAs play key functions in various cellular processes that include cell differentiation, adhesion, development and angiogenesis (12, 16).

MATERIALS AND METHODS

Cell culture and transfection

Human melanoma cell lines SK-MEL-2, A375 were bought from the American Type Culture Collection (Manassas, VA, USA), while an epidermal melanocyte HEMa-LP was obtained from Thermo Fisher Scientific (Shanghai, China). All the cells were cultured in DMEM medium with 10% FBS at 37°C in a humidified of 5% CO2.

A short hairpin RNA (shRNA) against human lncRNA SNHG16 was ligated into the U6/GFP/Neo plasmid (GenePharma, China) to become sh-CCAT1. The full-length SNHG16 sequence is constructed in pEX-2 and is called pEX-SNHG16. In this study, miR-143 mimics and their NCs were synthesized and transfected into SK-MEL-2 cells (GenePharma). Cell transfection was performed using Lipofectamine 3000 reagent (Thermo Fisher Scientific, USA) according to the manufacturer's instructions. Stably transfected cells were selected by medium containing G418 (Sigma-Aldrich, USA). After about 4 weeks, G418-resistant SK-MEL-2 cells were established and collected for subsequent experiments.

Patients and tissue specimens

From January 2015 to December 2018, the melanoma and corresponding normal tissue specimens were obtained from 46 melanoma patients who underwent surgery at the Jining No.1 People's Hospital. None of the patients had been treated with preoperative neoadjuvant chemotherapy. All patients provided written informed consent to participate in the protocol, which was approved by the Hospital Ethics Committee before specimen collection.

Transwell assay

The migratory ability was assessed using Transwell chambers (BD Biosciences). After 48 hours of incubation, the transfected cells were collected, centrifuged, and resuspended in DMEM without FBS. The cell concentration was adjusted to 1 × 105 cells/mL. A total of 200 μL of the cell suspension was added to the upper chamber, while the bottom chamber was covered with 500 μL of DMEM supplemented with 10% FBS. The chamber was then kept at 37°C and 5% CO2 for 24 h, and then the cells were fixed with 4% paraformaldehyde and stained with 0.5% crystal violet. Thereafter, images of migrating cells were captured under an inverted microscope (Olympus Corporation, Tokyo, Japan). The number of migrating cells in each group of five random fields was determined, and the mean and standard deviation (SD) were calculated to describe the migrating capability.

Cell count kit-8 assay for cell proliferation

CCK-8 assay kit (Dojindo Molecular Technologies, Kumamoto, Japan) was used to detect cell proliferation according to the manufacturer's protocol. Briefly, 10 μL of CCK-8 solution was added to each well, and the transfected cells were incubated at 37°C for a further 2 h. The absorbance was measured on a microplate reader (Bio-Rad Laboratories, Hercules, CA, USA) at a wavelength of 450 nm.

Total mRNA extraction and qRT-PCR analysis

Total RNA was isolated from tissue samples or cells using the TRIzol reagent (Invitrogen; Thermo Fisher Scientific), and then reverse transcribed into complementary DNA (cDNA) using a miScript reverse transcription kit (Qiagen GmbH, Hilden, Germany). The expression of miR-132 was detected by qPCR using a miScript SYBR Green PCR kit (Qiagen GmbH, Hilden, Germany), and standardized to U6 small nuclear RNA. To quantify the expression of SNHG16, cDNA synthesis was performed using a PrimeScript RT kit, followed by qPCR using SYBR Premix Ex Taq (Takara Biotechnology, Dalian, China).

The expression levels of SNHG16 were normalized to GAPDH. The expression of SNHG16 and miR-132 were calculated using the ΔΔCT ($2^{-\Delta\Delta Ct}$) method, and normalized with GAPDH. Each experiment was repeated three times independently.

Luciferase reporter assay

A DNA fragment was synthesized and cloned into a pmirGLO vector (Promega Corporation, Madison, Wisconsin, USA). For reporter gene assays, cells were seeded in 24-well plates and then co-transfected with miR-132 or NC and wild type or mutant reporter plasmids. After transfection for 48 h, luciferase activity was measured using a dual luciferase reporter gene assay system (Promega Corporation), standardized determination of Renilla luciferase activity.

Statistical analysis

Statistical analysis was performed using SPSS software (version 17.0) and GraphPad Prism (version 7.0). Quantitative data are expressed as mean ± SD. The Student's *t*-test was used to analyze the difference between the mean of the two samples. The correlation between SNHG16 mRNA level and miR-132 expression level was analyzed by Spearman's rank correlation test. $P < 0.05$ indicated that statistical tests were considered significant.

RESULTS

SNHG16 observed to be overexpressed in melanoma implied a worse prognosis of NPC patients

The expression of SNHG16 in 46 pairs of melanoma tissues and adjacent tissues were evaluated by RT-qPCR. As expected, SNHG16 was upregulated in melanoma tissues compared with the adjacent tissues ($P<0.05$) (Fig. 1A). We also found that higher expression of SNHG16 suggested poor survival for melanoma patients ($P<0.05$) (Fig. 1B). All the data suggested that overexpression of SNHG16 may be critical for the progression of melanoma. Moreover, the expression of SNHG16 was higher in melanoma cells SK-MEL-2 and A375 than HEMA-LP (Fig. 1C). All the results indicated that lncRNA SNHG16 was up-regulated in melanoma tissues and cell lines, but the roles of lncRNA SNHG16 in melanoma remains unclear. Since SNHG16 was significantly overexpressed in SK-MEL-2 cells, SK-MEL-2 cells were chosen as the for further research.

SNHG16 promoted the proliferation and migration of SK-MEL-2 cells

Since SNHG16 was highly expressed in SK-MEL-2 cells, SK-MEL-2 cells were selected for

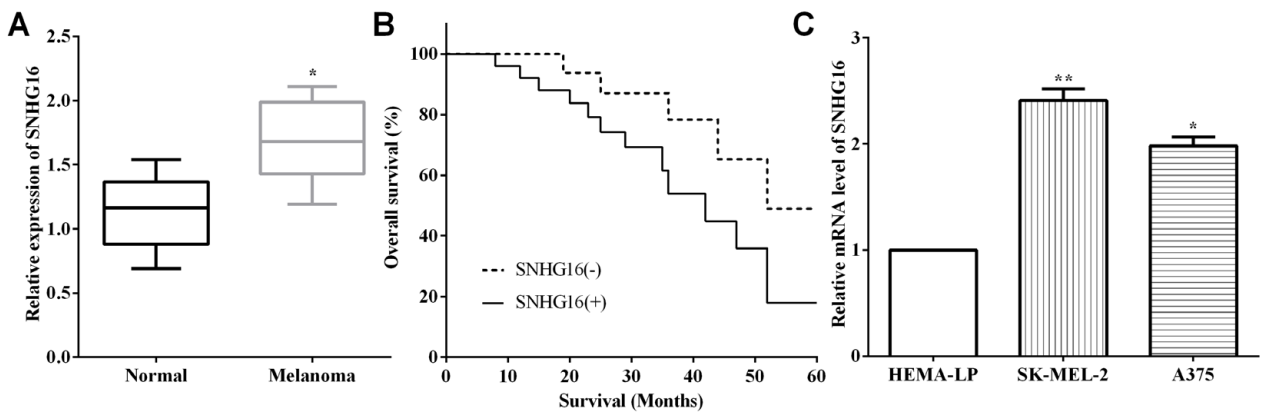

Fig. 1. *SNHG16 was observed to be overexpressed in melanoma implied a worse prognosis in NPC patients.* ***A)*** *SNHG16 was upregulated in melanoma tissues.* ***B)*** *High expression of SNHG16 suggested poor survival of melanoma patients.* ***C)*** *The expression of SNHG16 was higher in melanoma cells SK-MEL-2 and A375 than HEMA-LP.*

SNHG16 knockdown assay. RT-qPCR was used to detect the expression level of lncRNA SNHG16 in SK-MEL-2 cells transfected with sh-SNHG16 or sh-NC. Compared with sh-NC, the expression of SNHG16 in sh-SNHG16 transfected cells was significantly reduced ($P < 0.01$) (Fig. 2A). CCK8 and Transwell assay were applied to measure cell viability and migration of SK-MEL-2 cells. CCK-8 assay demonstrated that knockdown of SNHG16 inhibited SK-MEL-2 cell viability compared with the control group ($P < 0.05$) (Fig. 2B). Similarly, through Transwell assay, we discovered that, compared to the sh-NC, knockdown of SNHG16 remarkable suppressed the migration of SK-MEL-2 cells ($P < 0.05$) (Fig. 2C). Taken together, knockdown of SNHG16 inhibited the viability and migration in SK-MEL-2 cells.

lncRNA SNHG16 sponge miR-132 in SK-MEL-2 cells

StarBase (http://www.starbase.com) was employed to perform the bioinformatics analysis and the results showed that SNHG16 contained a potential target sequence of miR-132 (Fig. 3A). After that, the expression was evaluated of miR-132 and SNHG16 in melanoma tissues, and the RT-qPCR results demonstrated that the expression of SNHG16 was negatively correlated with miR-132 in melanoma tissues ($P<0.05$) (Fig. 3B). To confirm that SNHG16 directly targeted miR-132, the potential binding sequences were mutated and then a dual luciferase reporter assay was carried out. The results indicated that the luciferase activity of wild type SNHG16 was reduced by miR-132 mimic ($P<0.05$), but the luciferase activity of mutant SNHG16 exerted no significant effect ($P<0.05$) (Fig. 3C). In addition, the expression of miR-132 was upregulated by knocking down of SNHG16 ($P<0.05$), whereas overexpression of SNHG16 downregulated the expression of miR-132 in SK-MEL-2 cells ($P<0.05$) (Fig. 3D). The

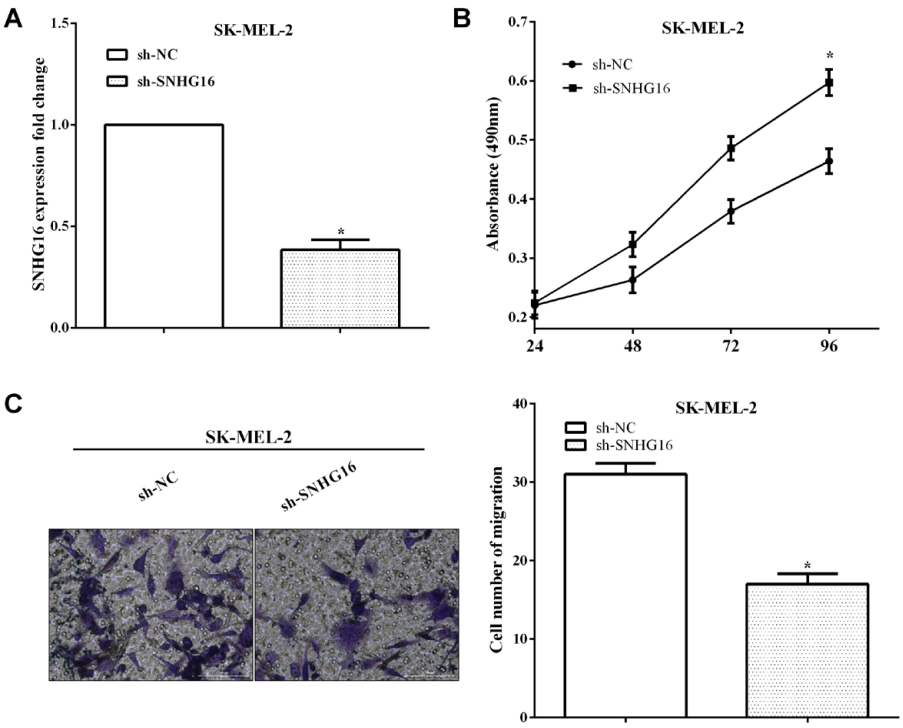

Fig. 2. *SNHG16 promoted the proliferation and migration of SK-MEL-2 cells.* ***A****) The expression of SNHG16 in sh-SNHG16 transfected cells was significantly reduced.* ***B****) CCK-8 assay demonstrated that knockdown of SNHG16 inhibited cell viability compared with the control group.* ***C****) Knockdown of SNHG16 remarkable suppressed the migration of SK-MEL-2 cells.*

results revealed that miR-132 was a downstream target of SNHG16 and its expression may be negatively regulated by SNHG16.

Low expression of miR-132 facilitated the progression of melanoma

The expression of miR-132 in tissue samples and cell lines were assessed using RT-qPCR. As expected, miR-132 was low expressed in melanoma tissues compared with the non-tumor tissues ($P<0.05$) (Fig. 4A). Moreover, the expression of miR-132 was also lower in melanoma cell lines SK-MEL-2 ($P<0.01$) and A375 ($P<0.05$) than HEMA-LP cells (Fig. 4B). To explore how miR-132 affected the progression of melanoma, we constructed SK-MEL-2 cells that overexpressed miR-132 ($P<0.05$) (Fig. 4C). The CCK-8 assay was conducted to calculate cell proliferation, and the results showed that overexpression of miR-132 suppressed the proliferation of SK-MEL-2 cells ($P<0.05$) (Fig. 4D). Transwell assay was performed to measure the cell migratory ability. We observed that overexpressed miR-132 impaired the migration of SK-MEL-2 cells ($P<0.05$) (Fig. 4E). All results indicated that miR-132 has a significant inhibitory effect on the growth and migration of SK-MEL-2 cells.

MiR-132 directly binding to LAPTM4B

To explore the downstream molecular targets of miR-132, a bioinformatics analysis was performed on TargetScan (http://www.targetscan.org), and this indicated that miR-132 and LAPTM4B had potential binding site. To confirm that miR-132 directly targeted LAPTM4B, double luciferase activity assay was performed (Fig.5A). miR-132 mimic reduced the luciferase activity of wild type LAPTM4B ($P<0.05$), but exerted no effect on the luciferase activity of mutant LAPTM4B ($P>0.05$) (Fig. 5B), indicating that miR-132 directly targeted

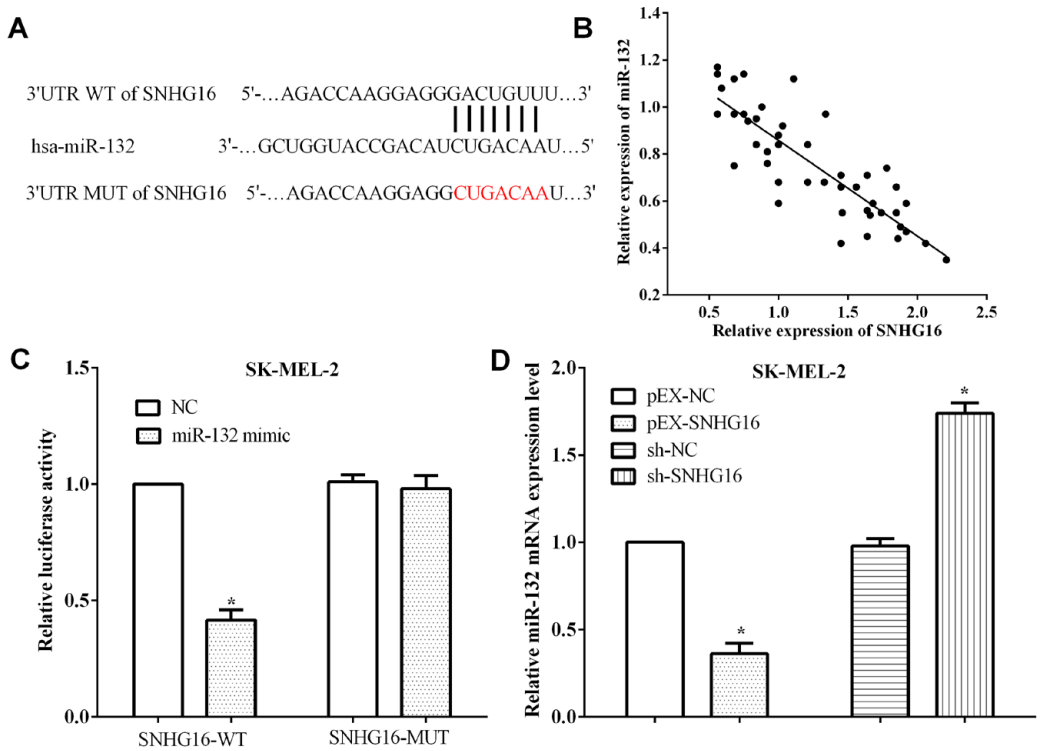

Fig. 3. *LncRNA SNHG16 sponge miR-132 in SK-MEL-2 cells. **A**) SNHG16 contained a potential target sequence of miR-132. **B**) The expression of SNHG16 was negatively correlated with miR-132 in melanoma tissues. **C**) The luciferase activity of wild type SNHG16 was reduced by miR-132 mimic, but the luciferase activity of mutant SNHG16 exerted no significant effect. **D**) The expression of miR-132 was upregulated by knocking down SNHG16, whereas overexpression of SNHG16 downregulated the expression of miR-132 in SK-MEL-2 cells.*

LAPTM4B. The expression of LAPTM4B was calculated using RT-qPCR, and it was downregulated in miR-132 mimic-transfected cells compared to the NC group (P<0.05) (Fig. 5C). The expression of LAPTM4B was calculated in tissues, and LAPTM4B was overexpressed in melanoma tissues compared with normal tissues (P<0.05) (Fig. 5D). Since the expression of LAPTM4B was upregulated in melanoma, the relationship of miR-132 and LAPTM4B in melanoma was hypothesised. As expected, the expression of miR-132 had a negative correlation with the expression of LAPTM4B in melanoma tissues (P<0.05) (Fig. 5E). LAPTM4B was also overexpressed in melanoma cells SK-MEL-2 (P<0.05) and A375 (P<0.05) *vs* HEMA-LP cells (Fig. 5F).

SNHG16 promoted the proliferation and migration of SK-MEL-2 cells via miR-132/LAPTM4B axis

To detect whether SNHG16 mediated the proliferation and migration of SK-MEL-2 cells via miR-132/LAPTM4B axis, miR-132 mimic were transfected into SNHG16 overexpressed SK-MEL-2 cells (P<0.05) (Fig. 6A). CCK8 assay revealed that

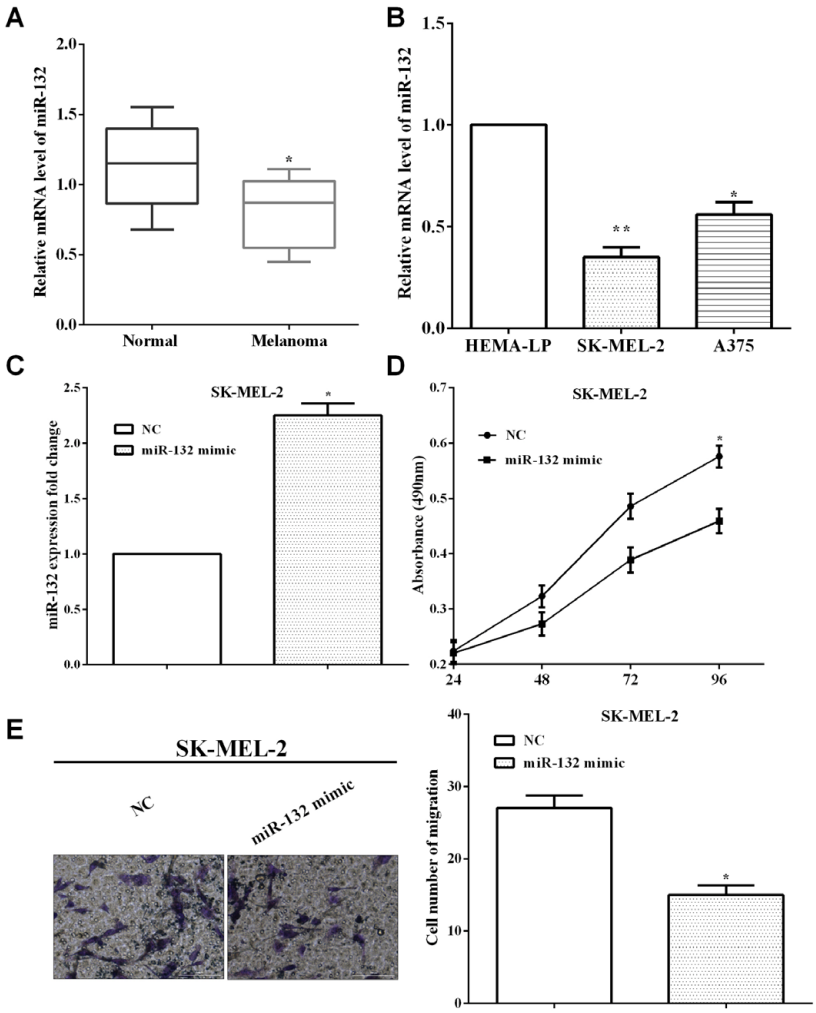

Fig. 4. *The low expression of miR-132 facilitated the progression of melanoma.* ***A****) miR-132 was low expressed in melanoma tissues compared with the non-tumor tissues.* ***B****) The expression of miR-132 was lower in melanoma cell lines than normal cells.* ***C****) miR-132 mimic was used to overexpress miR-132 in SK-MEL-2 cells.* ***D****) Overexpression of miR-132 suppressed the proliferation of SK-MEL-2 cells.* ***E****) miR-132 has a significant inhibitory effect on migration of SK-MEL-2 cells.*

miR-132 mimic reduced the proliferation of SK-MEL-2 cells (P<0.05), whereas upregulation of SNHG16 impaired the inhibition of miR-132 on cell proliferation (P<0.05) (Fig. 6B). Transwell assay demonstrated that transfection of miR-132 mimic suppressed the functions of SNHG16 in promoting cell migration (P<0.05) (Fig. 6C). The expression of LAPTM4B was also evaluated after knocking down SNHG16 in SK-MEL-2 cells (P<0.05) (Fig. 6D). Also, the expression of LAPTM4B had a positive correlation with the expression of SNHG16 in melanoma tissues (P<0.05) (Fig. 6F). All the findings indicated that SNHG16 promoted the proliferation and migration of SK-MEL-2 cells via miR-132/LAPTM4B axis.

DISCUSSION

In our study, we discovered that SNHG16 and LAPTM4B were overexpressed, while miR-132 was

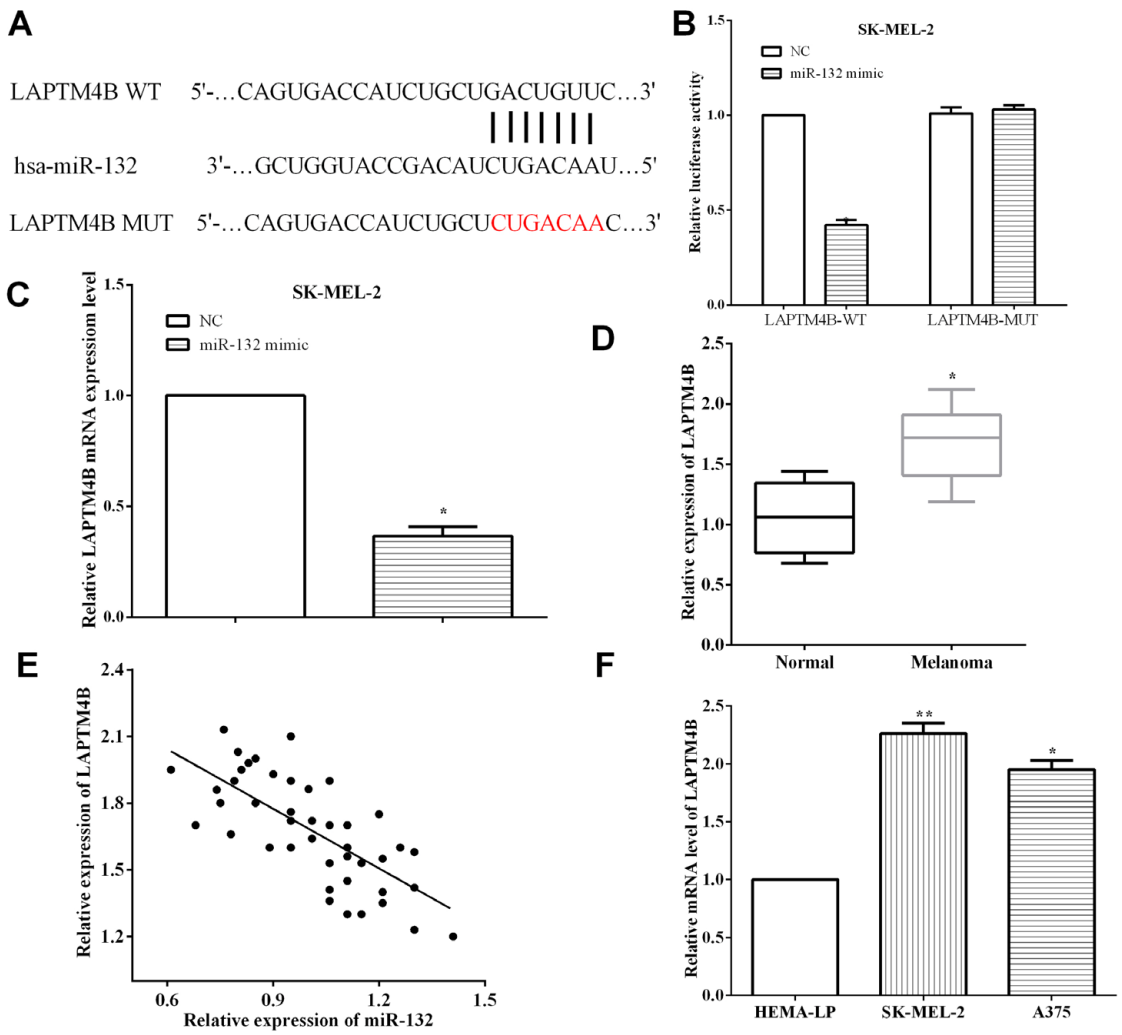

Fig. 5. *LAPTM4B directly binding to miR-132.* ***A****) TargetScan predicted that miR-132 and LAPTM4B had potential binding site.* ***B****) miR-132 mimic reduced the luciferase activity of wild type LAPTM4B, but exerted no effect on the luciferase activity of mutant LAPTM4B.* ***C****) The expression of LAPTM4B was downregulated in miR-132 mimic-transfected cells compared to the NC group.* ***D****) LAPTM4B was overexpressed in melanoma tissues compared with normal tissues.* ***E****) The miR-132 expression had negatively correlated with the expression of LAPTM4B in melanoma tissues.* ***F****) LAPTM4B was also overexpressed in melanoma cells SK-MEL-2 and A375 versus HEMA-LP cells.*

low expressed in melanoma. SNHG16 and LAPTM4B enhanced the proliferation and migration of SK-MEL-2 cells, whereas miR-132 exerted the opposite effect.

LncRNAs exist extensively in cell nucleus and cytoplasm, through regulated gene expression at transcription and post-transcription levels through gene silencing, thereby regulating the occurrence and development of cancer (17). LncRNA SNHG16 promoted the progression of osteosarcoma and enhances cisplatin resistance by sponging miR-16 (18). SNHG16 promoted glioma tumorigenicity by enhanced the colon formation, migration and invasion through activating PI3K/AKT pathway (19). SNHG16 accelerated cell proliferation, migration and invasion by regulating miR-186 expression in hepatocellular carcinoma (20). Consistent with previous studies, we found that SNHG16 was overexpressed in melanoma tissues and cells, and overexpression of SNHG16

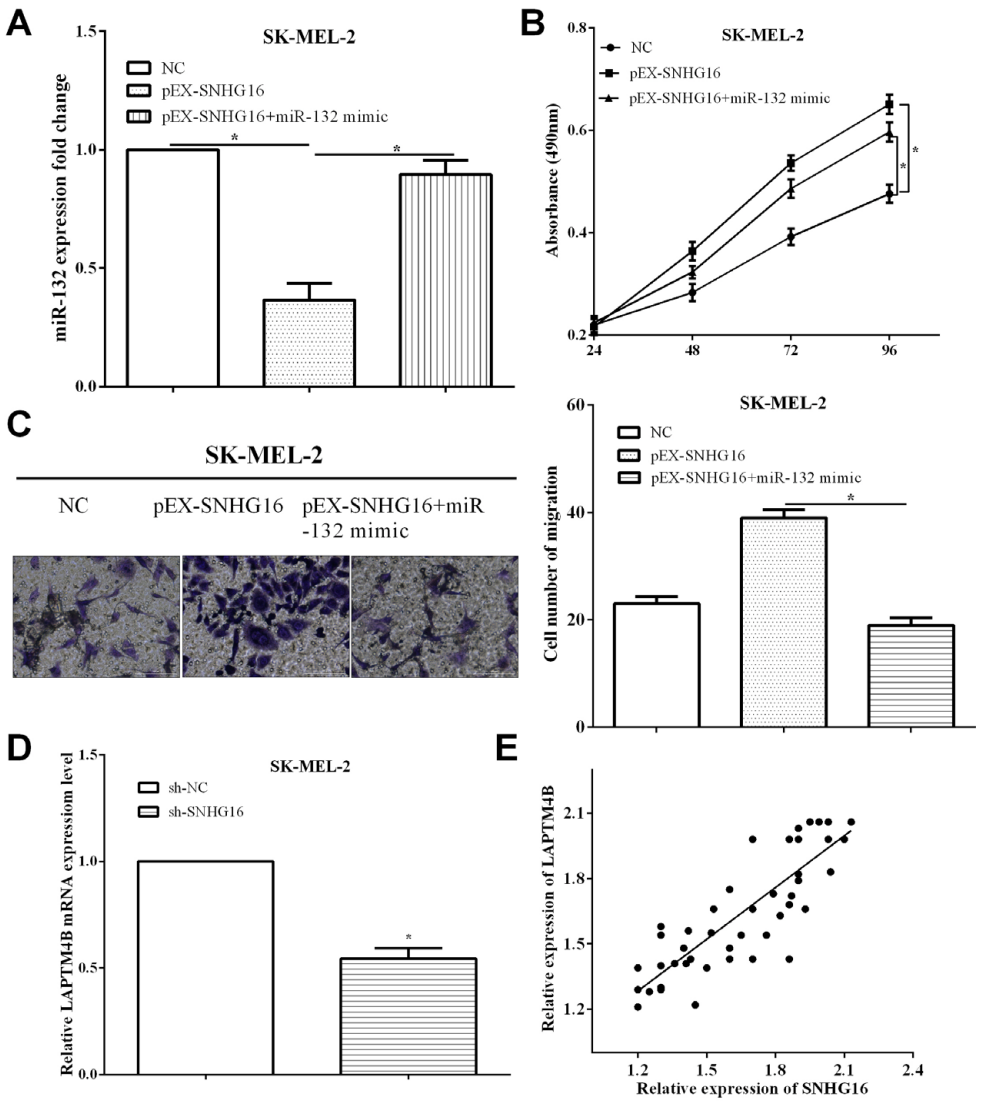

Fig. 6. *SNHG16 promoted the proliferation and migration of SK-MEL-2 cells via miR-132 and LAPTM4B.* ***A****) miR-132 mimic were transfected into SNHG16 overexpressed SK-MEL-2 cells.* ***B****) miR-132 mimic reduced the proliferation of SK-MEL-2 cells, whereas upregulation of SNHG16 impaired the inhibition of miR-132 on cell proliferation.* ***C****) Transfection of miR-132 mimic suppressed the functions of SNHG16 in promoting cell migration.* ***D****) The expression of LAPTM4B was also evaluated after knockdown SNHG16 in SK-MEL-2 cells.* ***E****) The expression of LAPTM4B had a positive correlation with the expression of SNHG16 in melanoma tissues.*

predicted a worst outcome. Knockdown of SNHG16 suppressed melanoma cell proliferation and migration. We first demonstrated that SNHG16 promoted the malignant phenotype of cancer melanoma cells, suggesting that SNHG16 can be used as a potential therapeutic target.

Recently, it has been reported that lncRNA can act as an miRNA sponge, which regulates tumor progression through sponging miRNA. SNHG16 enhanced cell proliferation, invasion and tumorigenesis via sponging miR-195 in hepatocellular carcinoma (21). Similarly, SNHG16 accelerated cell proliferation and colony formation, and promoted apoptosis in retinoblastoma (22). In the present study, we first proposed that SNHG16 sponge miR-132 in SK-MEL-2 cells. The expression of SNHG16 has a negative connection with miR-132 in melanoma tissues, and it was confirmed by using luciferase reporter assay. In addition, overexpression of SNHG16 reduced the expression of miR-132, while interference of SNHG16 increased the expression of miR-132 in melanoma cells. MiR-132 inhibited transcription of ribosomal proteins to promote protective Th1 immunity and was essential for T-cell activation and protective immunity against pathogens (23). Moreover, miR-132 suppressed cell proliferation, invasion and migration in pituitary tumor (24). miR-132 was low expressed in melanoma tissue specimens and cells, therefore we used miR-132 mimic to overexpress the expression of miR-132 in SK-MEL-2 cells. miR-132 mimic impaired the proliferation and migration of SK-MEL-2 cell. In addition, miR-132 partially reversed functions of SNHG16 on cell proliferation and migration. In this study, we verified the regulatory relationship between SNHG16 and miR-132, and determined that miR-132 is a tumor suppressor in melanoma.

LAPTM4B facilitates tumor growth and induces autophagy in hepatocellular carcinoma (25). LAPTM4B acted as a novel diagnostic and prognostic marker for lung adenocarcinoma and head and neck squamous cell carcinoma (26, 27). Also, LAPTM4B promoted cell proliferation, migration, invasion, and assisted drug resistance in breast cancer (28). Intriguingly, TargetScan was performed to search for the downstream target gene of miR-132, and we selected LAPTM4B as the target gene of miR-132. Also, miR-132 directly targets LAPTM4B in breast cancer cells (29). Consistent with that, we found that miR-132 mimic inhibited the expression of LAPTM4B, and this was confirmed by reducing the luciferase activity of wild type LAPTM4B. Moreover, the expression of miR-132 was negatively correlatived with LAPTM4B in melanoma tissues. In addition, the expression of SNHG16 and LAPTM4B had positive connection in melanoma tissues. Knockdown of SNHG16 also reduced the expression of LAPTM4B in SK-MEL-2 cells. Hence, SNHG16 could function as a competitive endogenous RNA (ceRNA) for miR-132 in melanoma to regulate the expression of LAPTM4B, thereby accelerating the growth and metastasis.

In conclusion, our study verified that SNHG16 promoted the proliferation and migration via miR-132/LAPTM4B axis in SK-MEL-2 cells. SNHG16 can mediate the expression of LAPTM4B to regulate the biological behaviors of melanoma cells by acting as a ceRNA of miR-132. This study indicated for the first time the functions of the SNHG16/miR-132/LAPTM4B axis in melanoma, thereby providing therapeutic targets for melanoma diagnosis and treatment.

REFERENCES

1. Haass NK, Smalley KS, Herlyn M. The role of altered cell-cell communication in melanoma progression. J Mol Histol 2004; 35:309-18.
2. Atkinson V. Recent advances in malignant melanoma. Intern Med J 2017; 47:1114-21.
3. Bald T, Quast T, Landsberg J, et al. Ultraviolet-radiation-induced inflammation promotes angiotropism and metastasis in melanoma. Nature 2014; 507:109-13.
4. Fu S, Wu H, Zhang H, Lian CG, Lu Q. DNA methylation/hydroxymethylation in melanoma. Oncotarget 2017; 8:78163-73.
5. Iyer MK, Niknafs YS, Malik R, et al. The landscape of long noncoding RNAs in the human transcriptome. Nat Genet 2015; 47:199-208.
6. Wapinski O, Chang HY. Long noncoding RNAs and human disease. Trends Cell Biol 2011; 21:354-61.
7. Prensner JR, Chinnaiyan AM. The emergence of lncRNAs in cancer biology. Cancer Discov 2011;

1:391-407.
8. Yang G, Lu X, Yuan L. LncRNA: a link between RNA and cancer. Biochim Biophys Acta 2014; 1839:1097-109.
9. Guo Y, Zhen H, Chen W, Sun Y, Li K, Feng E. Long non-coding RNA SNHG16 promotes cell proliferation and invasion in lung adenocarcinoma via sponging let-7a-5p. Minerva Chir 2019; 74:509-11.
10. Zhu Q, Li Y, Guo Y, et al. Long non-coding RNA SNHG16 promotes proliferation and inhibits apoptosis of diffuse large B-cell lymphoma cells by targeting miR-497-5p/PIM1 axis. 2019; 23:7395-405.
11. Pang W, Zhai M, Wang Y, Li Z. Long noncoding RNA SNHG16 silencing inhibits the aggressiveness of gastric cancer via upregulation of microRNA-628-3p and consequent decrease of NRP1. Cancer Manag Res 2019; 11:7263-77.
12. Jonas S, Izaurralde E. Towards a molecular understanding of microRNA-mediated gene silencing. Nat Rev Genet 2015; 16:421-33.
13. Matoulkova E, Michalova E, Vojtesek B, Hrstka R. The role of the 3' untranslated region in post-transcriptional regulation of protein expression in mammalian cells. RNA Biol 2012; 9:563-76.
14. Krol J, Loedige I, Filipowicz W. The widespread regulation of microRNA biogenesis, function and decay. Nat Rev Genet 2010; 11:597-610.
15. Sandberg R, Neilson JR, Sarma A, Sharp PA, Burge CB. Proliferating cells express mRNAs with shortened 3' untranslated regions and fewer microRNA target sites. Science 2008; 320:1643-7.
16. Farazi TA, Spitzer JI, Morozov P, Tuschl T. miRNAs in human cancer. J Pathol 2011; 223:102-15.
17. Peng WX, Koirala P, Mo YY. LncRNA-mediated regulation of cell signaling in cancer. Oncogene 2017; 36:5661-67.
18. Liu Y, Gu S, Li H, Wang J, Wei C, Liu Q. SNHG16 promotes osteosarcoma progression and enhances cisplatin resistance by sponging miR-16 to upregulate ATG4B expression. Biochem Biophys Res Commun 2019; 518:127-33.
19. Zhou XY, Liu H, Ding ZB, Xi HP, Wang GW. lncRNA SNHG16 promotes glioma tumorigenicity through miR-373/EGFR axis by activating PI3K/AKT pathway. Genomics 2020; 112:1021-29.
20. Chen H, Li M, Huang P. LncRNA SNHG16 promotes hepatocellular carcinoma proliferation, migration and invasion by regulating miR-186 expression. J Cancer 2019; 10:3571-81.
21. Xie X, Xu X, Sun C, Yu Z. Long intergenic noncoding RNA SNHG16 interacts with miR-195 to promote proliferation, invasion and tumorigenesis in hepatocellular carcinoma. Exp Cell Res 2019; 383:111501.
22. Xu C, Hu C, Wang Y, Liu S. Long noncoding RNA SNHG16 promotes human retinoblastoma progression via sponging miR-140-5p. Biomed Pharmacother 2019; 117:109153.
23. Hewitson JP, Shah KM, Brown N, Grevitt P, Hain S, Newling K, Sharp TV. miR-132 suppresses transcription of ribosomal proteins to promote protective Th1 immunity. EMBO Rep 2019; 20(4):e46620.
24. Renjie W, Haiqian L. MiR-132, miR-15a and miR-16 synergistically inhibit pituitary tumor cell proliferation, invasion and migration by targeting Sox5. Cancer Lett 2015; 356:568-78.
25. Wang F, Wu H, Zhang S, et al. LAPTM4B facilitates tumor growth and induces autophagy in hepatocellular carcinoma. Cancer Manag Res 2019; 11:2485-97.
26. Wang L, Meng Y, Zhang QY. LAPTM4B is a novel diagnostic and prognostic marker for lung adenocarcinoma and associated with mutant EGFR. BMC Cancer 2019; 19:293.
27. Kotowski U, Kadletz L, Schneider S, Oberndorfer F, Schnoell J, Gurnhofer E, Kenner L. Overexpression of LAPTM4B-35 is a negative prognostic factor in head and neck squamous cell carcinoma. Sci Rep 2019; 9:18866.
28. Wang L, Meng Y, Xu JJ, Zhang QY. The Transcription Factor AP4 Promotes Oncogenic Phenotypes and Cisplatin Resistance by Regulating LAPTM4B Expression. Mol Cancer Res 2018; 16:857-68.
29. Li S, Xu JJ, Zhang QY. MicroRNA-132-3p inhibits tumor malignant progression by regulating lysosomal-associated protein transmembrane 4 beta in breast cancer. Cancer Sci 2019; 110:3098-109.

Has-miR-17 increases the malignancy of gastric lymphoma by HSP60/TNFR2 pathway

LL. Wang[1], JJ. Dong[2], BZ. An[3], J. Liang[4], KR. Cai[2], ZS. Jin[5], HS. Jin[2] and JP. Hu[2]

[1]Department of Library, Mudanjiang Medical University, Mudanjiang, China; [2]Department of Histology and Embryology, Mudanjiang Medical University, Mudanjiang, China; [3]Department of Anatomy, Mudanjiang Medical University, Mudanjiang, China; [4]Stem Cell Institute, Mudanjiang Medical University, Mudanjiang, China; [5]Department of Pathology, Mudanjiang Medical University, Mudanjiang, China

Received February 3, 2020 – Accepted June 29, 2020

The purpose of this study was to investigate the expression and mechanism of miR-17 in gastric lymphoma. miR-17mimics, miR-17 inhibitors and negative controls were transfected into human gastric lymphoma cell line cyp6d. The proliferation, invasion and apoptosis of cyp6d cells were detected by CCK-8, Transwell and TUNEL methods, respectively. The expression and clinicopathological features of miR-17 in gastric lymphoma were analyzed by real-time quantitative PCR. The target gene of miR-17 was predicted by targetscan 7.2, and the expression of miR-17 related protein was detected by Western blot. The results showed that the expression of miR-17 in gastric lymphoma was significantly higher than that in normal tissues ($P < 0.05$), which was closely related to lymph node metastasis, tumor size and distant metastasis ($P < 0.05$). The high expression of miR-17 significantly promoted the proliferation and invasion of cyp6d cells and inhibited apoptosis ($P < 0.05$). The high expression of miR-17 can regulate the expression of HSP60 and TNFR2. It has been found that miR-17 can promote the development of gastric lymphoma by regulating HSP60/TNFR2 pathway, which is a potential molecular target for the diagnosis and treatment of gastric lymphoma.

Primary gastric lymphoma (PGL) is a type of tumor originating from the lymph tissue in the submucosa of the stomach, which may be associated with involvement of perigastric and abdominal lymph nodes (1). Extranodal lymphoma (ENL) is the most common lymphoma, most of which are NHL (including gastric lymph node) accounting for 30-50% (2, 3). In recent years, the incidence of PGL has been increasing (4). Common causes include immunosuppression, inflammatory bowel disease, HIV infection, chronic diarrhea, *Helicobacter pylori* infection. Primary gastrointestinal lymphoma is most common in the stomach, followed by rectum, colon and small intestine, with the lowest incidence of esophagus. Primary gastric lymphoma is a common extranodal lymphoma with complex pathology, occult disease and no specific clinical manifestations. At present, it is difficult carry out accurate early diagnosis, and it is easy to miss diagnosis and misdiagnose. Therefore, it is of important to find new molecular targeted drugs or new therapeutic targets to effectively treat PGL.

Key words: miR-17; HSP60; TNFR2; gastric lymphoma

Corresponding Author:
Dr Jiangping Hu,
Department of Histology and Embryology,
Mudanjiang Medical University,
No.3 Tongxiang Road,
Mudanjiang 157011, China
e-mail: jiangpinghu157@yeah.net

0393-974X (2020)
Copyright © by BIOLIFE, s.a.s.
This publication and/or article is for individual use only and may not be further reproduced without written permission from the copyright holder.
Unauthorized reproduction may result in financial and other penalties
DISCLOSURE: ALL AUTHORS REPORT NO CONFLICTS OF INTEREST RELEVANT TO THIS ARTICLE.

miRNA is a kind of endogenous noncoding RNA composed of 20-24 nucleotides, and its properties are relatively stable. miRNA can promote its targeted mRNA degradation and interfere with the translation process to play miRNA regulatory role in gene expression (5, 6). Exosomes are vesicles, secreted by many living cells of animals, which can contain a large number of proteins, DNA, RNA, miRNA and other components, and transmit them to surrounding or distant cells, mediating a series of biological reactions. Exosomes can not only promote the excretion of metabolic waste, but also mediate the exchange of materials and information between cells, in which exosomes from tumor cells participate in tumor invasion and metastasis and other pathological processes. In recent years, it has been found that miRNAs play an important role in the process of cell aging, including miRNA-15, 17, 29, 34, 217 and 885 (7, 8). miR-17, located on human chromosome 13, is a member of miR-17-92 gene family. It is highly expressed in cervical cancer, cholangiocarcinoma, esophageal cancer and other tissues or in patients' serum. It may be a kind of oncogene, involved in the occurrence and development of tumor (9, 10). miR-17 plays an important role in almost all cell processes, such as cell proliferation and differentiation, and can inhibit cell aging (11). Some studies have shown that miR-17 can induce gastric cancer cell proliferation and inhibit its apoptosis through p21p, 53inp1 and other pathways (12). However, the role of miR-17 in PGL is not clear, especially in large B-cell lymphoma (DLBCL).

Therefore, the purpose of this study was to investigate the expression and clinicopathological characteristics of miR-17 in gastric lymphoma, to predict the target gene of miR-17, to explore the regulatory effect of miR-17 on HSP60/TNFR2 signaling pathway, and to explore the inhibitory effect of miR-17 on proliferation and apoptosis of human gastric lymphoma cells.

MATERIALS AND METHODS

Specimens and cells

In this study, 52 patients with PGL diagnosed at the Affiliated Hongqi Hospital of Mudanjiang Medical University between January 1, 2016 and June 31, 2019 were taken as the research subjects. All the patients were confirmed by endoscopy or surgical pathological biopsy, all of which were treated initially and met Dawson's standards: (i) there was no or little enlargement in superficial lymph nodes of the whole body, but pathology could not confirm lymphoma; (ii) the classification and count of white blood cells in peripheral blood were normal; (iii) chest X-ray or chest CT confirmed no posterior sternum or mediastinal lymph node enlargement; (iv) lesions were confined to the gastrointestinal tract and lymph nodes in the drainage area; (v) the liver and spleen were not large. Clinical data were collected including age, clinical manifestations, pathological types, lymph node metastasis and distant metastasis. The study was approved by the Ethics Committee of the Affiliated Hongqi Hospital of Mudanjiang Medical University, and all the patients signed an informed consent to participate in the study.

Three lymphoma cell line CYP6D were purchased from American Type Culture Collection (ATCC, Manassas, VA, USA), and were cultured in MEM-EBSS: Minimum Essential Medium (MEM Eagles with Earle's Balanced Salts) plus 10% fetal bovine serum (FBS, Thermo Fisher Scientific, USA), 2 mmol/L L-glutamine (Thermo Fisher Scientific, USA) and 100 units/mL penicillin/ streptomycin (Thermo Fisher Scientific, USA), at 37°C in 5% CO2.

RNA extraction and quantitative real-time polymerase chain reaction (qRT-PCR)

Total RNA was extracted with TRIzol reagent (Invitrogen, USA) and RNA reverse transcription was performed with PrimeScript® RT reagent Kit with gDNA Eraser (Takara Bio, CN). QRT-PCR was carried out using the SYBR® Premix Ex Taq II (Takara Bio, CN). The standard internal reference was glyceraldehyde-3-phosphate dehydrogenase (GAPDH). The primers of miR-17 for qRT-PCR was F: 5'- GTGCAGGGTCCGAGGT-3', R: 5'-GAGTTCAAAGTGCTTACAGTGC-3', and GAPDH-F: 5'- CGGAGTCAACGGATTTGGTCGTAT-3', R: 5'-AGCCTTCTCCATGGTGGTGAAGAC-3'. The primer in this study was a compound from Applied Biosystems company. The content of miR-17 in PGL tissues was measured.

Transfection and groups

Logarithmic growth cells were divided into three groups: miR-17 mimic group (Mimic), miR-17 inhibitor group (Inhibitor), and blank control group (Control).

The cells in Mimic, Inhibitor, and Control groups were transfected by related Lipofectamine 3000 (Thermo Fisher Scientific, USA). CYP6D Cells were collected 24 h after transfection and subjected to subsequent experiments.

CCK-8 assay

Cells were incubated in 96-well plates at a density of 5 × 104 / ml for 0, 24, 48, 72 and 96 h, respectively, and then 10 ml CCK-8 (MSK, CN) was added. Then, the plates were incubated at 37°C for 4 h. The absorbance at 450 nm was measured with a microplate reader (Thermo Fisher Scientific, USA).

Transwell assay

Migration tests were performed using a 24-well Boyden cavity and an uncoated filter with an aperture of 8 mm. Cells were collected from a petri dish and washed twice with PBS. Cells were suspended in serum-free medium and 3 × 104 cells were seeded in the insertion chamber. The cells were cultured in a basal chamber (0.6 mL mems medium containing 10% FBS) at 37°C (5% CO_2) for 24 h. Cells were stained with 4,6-diamino-2-phenylindole and counted under a vertical microscope.

Apoptosis assay

In the 6-well cyp6d cell culture plate, 10 μg/ml brustasol was added and placed in the dark for 10 min, the cells were fixed and stained, and then washed with PBS. Under inverted fluorescence microscope, the apoptotic cells had obvious morphological changes in the nucleus, which could be identified by nuclear densification or staining fragment densification.

Bioinformatics to predict the interaction of miR-17 with protein and Western blot analysis

Targetscan7.2(http://www.targetscan.org/vert_72/) was used to predict synergistic proteins of CYP6D, consult the literature, and select preselected targets for HSP60, IL8, TNFR2 and PPP3R1. Western blot was used to detect the content of three experimental group-related proteins. Protein samples were extracted with Ripa buffer. The protein samples were denatured and separated by 10% twelve alkyl sulfate polyacrylamide gel electrophoresis. The separated protein was transferred to PVDF membrane. These membranes were incubated overnight with the primary antibody at 4°C, and then incubated with the corresponding secondary antibody at room temperature for 1 h. Finally, we use bimyosin to calculate the protein concentration.

Statistical analysis

GraphPad Prism 7.0.5 software was used to make statistical analysis after data processing. The comparison between the three groups used the F test for precise comparison, ** means P value < 0.05.

RESULTS

miR-17 expression in PGL specimens

The expression levels of miR-17 in 52 pairs of PGL tissues and adjacent normal tissues were measured by qRT-PCR. The results showed that miR-17 expression was upregulated in PGL samples relative to adjacent normal mucosal tissues (Fig. 1) and the highest content was found in gastric lymphoma tissues with diffuse large B cells (Table I). In addition, its expression level was closely related to tumor size, distant metastasis and lymph node metastasis (P<0.05) (Table II).

The expression of miR-17 mRNA

As shown in Fig. 2, the miR-17 expression in the Control group was compared with the Mimic group, the expression of miR-17 in the Mimic group was significantly increased (p<0.05) and compared

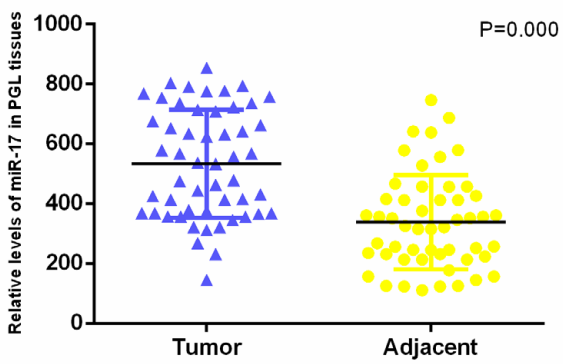

Fig. 1. *miR-17 is upregulated in primary gastric lymphoma specimens. The relative expression of miR-17 determined by qRT-PCR in 52 paired primary gastric lymphoma tissues and adjacent normal tissues.*

Table I. *Pathological types of 52 primary gastric lymphoma patients*

Pathological Type	Cases	Percentage (%)
Diffuse large B-cell lymphoma	35	67.3
MALT lymphoma	8	15.4
Burkitt lymphoma	3	5.8
Plasmablastic lymphoma	3	5.8
ALK negative lymphoma	3	5.8

Table II. *Correlation between miR-17 expression in primary gastric lymphoma and clinical characteristics*

Variables		miR-17 high expression		miR-17 low expression		*P*
	Total	N=36	Percentage	N=16	Percentage	
Age	52					
<50 years	35	18	51.4%	17	48.6%	0.768
≥50 years	17	8	47.1%	9	52.9%	
Tumor Size						
0-2cm	15	8	53.3%	7	46.7%	0.043
2-5cm	20	15	75.0%	5	25.0%	
>5cm	17	13	76.5%	4	23.5%	
Stomachache						
Yes	37	29	78.4%	9	24.3%	0.546
No	15	8	53.3%	7	46.7%	
Fever						
Yes	11	4	36.4%	7	63.6%	0.813
No	41	32	78.0%	9	22.0%	
Metastasis						
Yes	28	19	67.9%	9	32.1%	0.023
No	24	17	70.8%	7	29.2%	
Lymph Metastasis						
N0	19	13	68.4%	6	31.6%	0.032
N1/N2/N3	33	23	69.7%	10	30.3%	

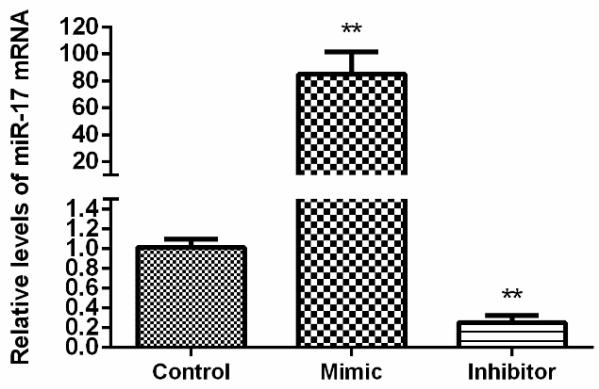

Fig. 2. *The expression of miR-17 in different groups.*

with the NC group, the expression of miR-17 in the Inhibitor group was significantly decreased ($p<0.05$). The results showed that the transfection was successful.

Proliferation and invasion of CYP6D cells

Compared with Control group, miR-17 inhibitor could inhibit the proliferation of CYP6D cells, while miR-17 mimic could promote the proliferation of CYP6D cells (Fig. 3A). Transwell results showed that miR-17 mimic could promote the invasiveness of CYP6D cell, while miR-17 inhibitor could reduce

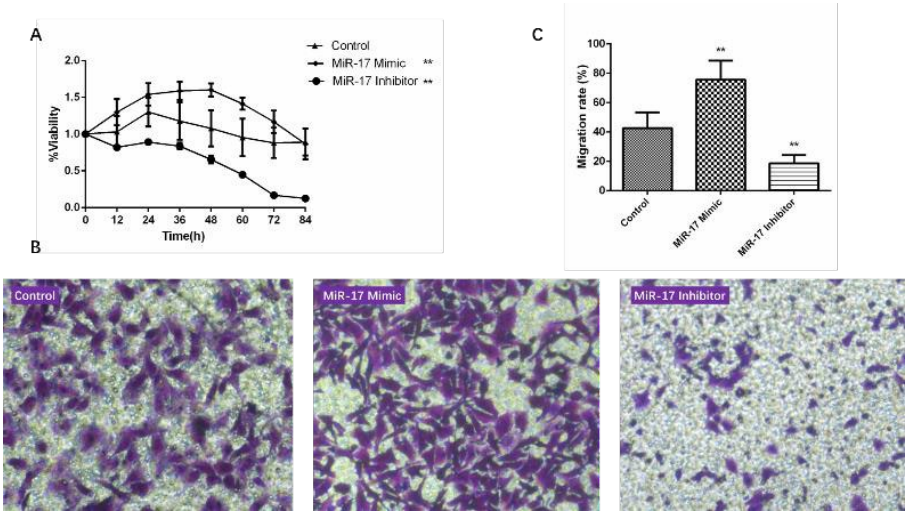

Fig. 3. *Results of cell proliferation assay and transwell assay in Control groups, miR-17 mimic and miR-17 inhibitor.* ***A)*** *Proliferation of different groups of CYP6D cells;* ***B*** *and* ***C****) Invasion ability of different groups of CYP6D cells.*

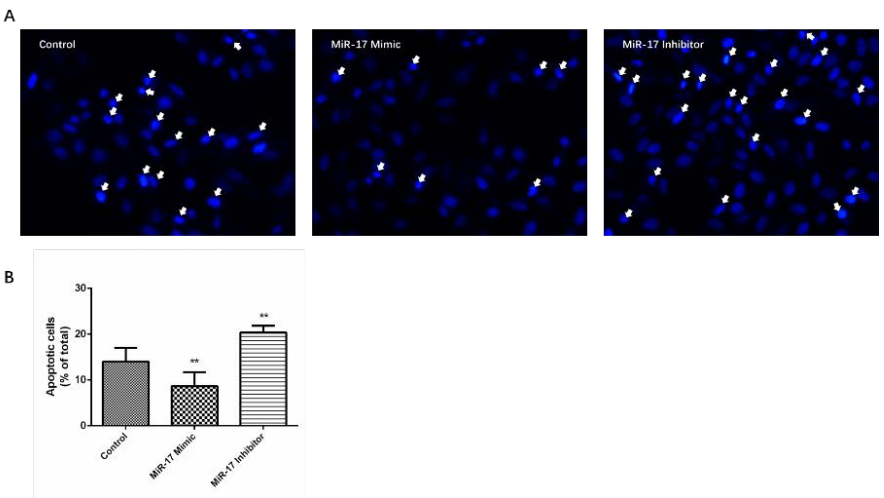

Fig. 4. *Results of apoptosis assay in control group, miR-17 mimic group and miR-17 inhibitor group.*

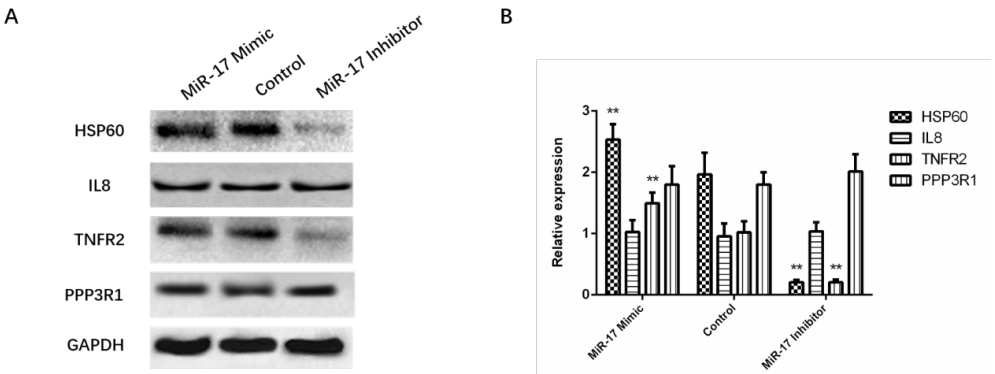

Fig. 5. *Different expression of HSP60, IL8, TNFR2 and PPP3R1 protein in control group, miR-17 mimic group and miR-17 inhibitor group.*

the invasiveness of CYP6D cell by 50-60% (Fig. 3 B and 3C).

Effect of miR-17 on apoptosis of CYP6D cells

Fluorescence apoptosis experiments showed that miR-17 inhibitor could significantly inhibit the apoptosis of CYP6D cells, while miR-17 mimic could increase the apoptosis of CYP6D cells. (Fig. 4 A and 4B).

MiR-17 affects CYP6D cells through the miR-17 HSP60/TNFR2 pathway

The result of Targetscan 7.2 prediction showed that a lot of proteins that may be related to miR-17 that could interact with each other. After referring to the relevant literature, four candidate proteins were finally selected HSP60, IL8, TNFR2 and PPP3R1 for Western blot. The Western blot analysis results showed that the content of HSP60 and TNFR2 increased with the increase of miR-17, but were not related to the expression of IL8, while the expression of PPP3R1 did not change significantly with different groups (Fig. 5A and 5B).

DISCUSSION

Although the incidence rate of PGL is relatively low, the incidence rate of PGL has increased significantly in recent years. The pathological type is mainly B cell origin, clinical symptoms are not specific, and colonoscopy is more frequent, and the results from biopsy are relatively difficult to make a diagnosis often leading to misdiagnosis (15-20). PGL is common in middle-aged and elderly men, mainly in the body and antrum of the stomach, with abdominal pain, distention, anorexia and wasting as the main clinical symptoms (18). The main pathological type is DLBCL which accounts for 30-40% of NHL and is one of the most common malignant tumors in the lymphatic system (21). The biological characteristics, gene mutation and immunophenotype of DLBCL are diverse, and the pathogenesis of DLBCL is not clear (22). miR-17 in this study belongs to the miR-17-92 gene cluster, which is a highly conserved gene cluster that encodes seven miRNAs, including miR-17-5p, miR-17-3p, miR-18a, miR-19a, miR-20a, miR-19b-1 and miR-92-1, with two side homologous of miR-106a-363 and miR-106b-25 gene cluster (23). MiR-17-92 gene cluster is one of the most studied miRNA clusters, and some studies found that it plays a very important role in the growth and development of the body, immune regulation, cardiovascular disease and aging process. MiR-17-92 gene cluster also plays a regulatory role in many tumors, including B-cell lymphoma, acute granulocytic leukemia, retinoblastoma, pancreatic cancer, and breast cancer (24-26).

Through TargetScan database analysis, the present study found that miR-17 could bind to HSP60 and TNFR2. It was further confirmed by Western blot that miR-17 was the upstream target of HSP60 and TNFR2 and regulated the expression of HSP60 and TNFR2. HSP is a highly conserved protein produced in cells under stress. HSP60 is an important member of the HSPs family, which belongs to the molecular chaperone family. Its expression level is closely related to the occurrence and development of tumor (2). HSP60 is expressed in all grades of gastric lymphoma, and with the increase of malignancy, the expression of HSP60 is also increased, indicating that there is a positive correlation between HSP60 expression and the development of gastric lymphoma. Moreover, the expression of HSP60 in different grades of gastric lymphoma was significantly different, and the expression increased gradually with the grades, which indicated that HSP60 overexpression may not only participate in the proliferation of tumor cells, but also have a certain protective effect on tumor cells. (27, 28). TNF-α was produced by tumors and tumor microenvironment and was originally thought to be a protein responsible for the death of tumor cells, hence its name. Some studies have shown that low expression of TRAF2 can significantly inhibit the growth, migration and invasion of AGS gastric cancer cells. The expression of TRAF2 is increased in gastric cancer, which is related to the prognosis of gastric cancer. However, subsequent studies have found that TNF-α plays a two-sided role in tumor development as well as an important role in tumor immunosuppressive microenvironment, among which TNFR2 can enhance the role of TCR activated cells (29, 30).

Our experiments showed that miR-17 could regulate the proliferation, invasion and apoptosis of CYP6D

cells through HSP60 and TNFR2. The dysregulation of miR-17 expression may be one of the mechanisms promoting the development of DLBCL.

In conclusion, this study showed that miR-17 promoted the proliferation and inhibited apoptosis of lymphoma cells. The mechanism may be related to HSP60/TNFR2 pathway. Our study shows that miR-17 can be a potential target for the diagnosis and treatment of PGL. However, there are still some drawbacks in the study, such as the small number of cases and the incomplete prediction of genes. In the future, more in-depth research on oncogene and immune cell infiltration will be carried out in combination with modern medical databases such as bioinformatics.

ACKNOWLEDGEMENT

This work was supported by Heilongjiang Provincial Department of Education Overseas Scholars Project (1153h16).

REFERENCES

1. Juárez-Salcedo LM, Sokol L, Chavez JC, Dalia S. Primary gastric lymphoma, epidemiology, clinical diagnosis, and treatment. Cancer Control 2018; 25(1): 1073274818778256.
2. Katsura M, Nishina H, Shigemori Y, Nakanishi T. Extranodal lymphoma originating in the gluteal muscle with adjacent bone involvement and mimicking a soft tissue sarcoma. Int J Surg Case Rep 2015; 7c:161-64.
3. Peña C, Russo M, Martinez V, Cabrera ME. Extranodal lymphomas in the public health system in Chile: Analysis of 1251 patients from the National Adult Cancer Program. Hematol Oncol 2019; 37(1):47-53.
4. Wang YG, Zhao LY, Liu CQ, et al. Clinical characteristics and prognostic factors of primary gastric lymphoma: A retrospective study with 165 cases. Medicine (Baltimore) 2016; 95(31):e4250.
5. Acuna SM, Floeter-Winter LM, Muxel SM. MicroRNAs: biological regulators in pathogen-host interactions. Cells 2020; 9(1).
6. Guo D, Ding M, Song X, et al. Regulatory roles of differentially expressed MicroRNAs in metabolic processes in negative lens-induced myopia guinea pigs. BMC Genomics, 2020; 21(1):13.
7. Bai X, Hua S, Zhang J, Xu S. The MicroRNA family both in normal development and in different diseases: the miR-17-92 Cluster. Biomed Res Int 2019; 2019:9450240.
8. Dyson G, Farran B, Bolton S, et al. The extrema of circulating miR-17 are identified as biomarkers for aggressive prostate cancer. Am J Cancer Res 2018; 8(10):2088-95.
9. Gruszka R, Zakrzewska M. The Oncogenic Relevance of miR-17-92 cluster and its paralogous miR-106b-25 and miR-106a-363 clusters in brain tumors. Int J Mol Sci 2018; 19(3).
10. Gong R, Lv X, Liu F. MiRNA-17 encoded by the miR-17-92 cluster increases the potential for steatosis in hepatoma cells by targeting CYP7A1. Cell Mol Biol Lett 2018; 23:16.
11. Wu D, Zhang H, Ji F, Ding W. MicroRNA-17 promotes osteosarcoma cells proliferation and migration and inhibits apoptosis by regulating SASH1 expression. Pathol Res Pract 2019; 215(1):115-20.
12. Cui X, Zhou T, Jiang D, et al. Clinical manifestations and endoscopic presentations of gastric lymphoma: a multicenter seven year retrospective survey. Rev Esp Enferm Dig 2017; 109(8):566-71.
13. Fitch DD, Wilson JA. Primary gastrointestinal lymphoma. South Med J 1985; 78(8):909-13.
14. Huang J, Zhong M, Tang Y, Lu J, Li X, Li G. Clinical features of 50 cases of primary gastric lymphoma. Zhong Nan Da Xue Xue Bao Yi Xue Ban 2012; 37(10):997-1002.
15. Ge Z, Liu Z, Hu X. Anatomic distribution, clinical features, and survival data of 87 cases primary gastrointestinal lymphoma. World J Surg Oncol 2016; 14:85.
16. Hossain F S, Koak Y, Khan F H. Primary gastric Hodgkin's lymphoma. World J Surg Oncol 2007; 5:119.
17. Nakai S, Masaki T, Shintani T, et al. Diffuse large B-cell primary gastric lymphoma treated successfully with the CD20 monoclonal antibody (rituximab): a case with severe liver dysfunction due to liver cirrhosis and hepatocellular carcinoma. Oncol Rep 2005; 13(6):1065-68.
18. Tth I, Nagy Z, Barna T, Szucs G. [Changes in the

treatment strategy of primary gastric lymphoma]. Magy Seb 2007; 60(2):79-86.
19. Yang HJ, Lim SH, Lee C, et al. Management of suspicious mucosa-associated lymphoid tissue lymphoma in gastric biopsy specimens obtained during screening endoscopy. J Korean Med Sci 2016; 31(7):1075-81.
20. Zieliska-Pajak E, Liszka L, Pajak J, Goka D, Lampe P, Pilch-Kowalczyk J, Mrowiec S. Two cases of lymphoepithelial cyst of the pancreas: first - a cyst coexisting with a primary gastric lymphoma, second - incidentally found pancreatic cyst. Z Gastroenterol 2008; 46(10):1188-93.
21. Schmitz R, Wright GW, Huang DW, et al. Genetics and Pathogenesis of Diffuse Large B-Cell Lymphoma. N Engl J Med 2018; 378(15):1396-407.
22. Dong H, Wang Q, Zhang G, et al. OSdlbcl: An online consensus survival analysis web server based on gene expression profiles of diffuse large B-cell lymphoma. Cancer Med 2020; 9(5):1790-97
23. Xin H, Katakowski M, Wang F, et al. MicroRNA cluster miR-17-92 cluster in exosomes enhance neuroplasticity and functional recovery after stroke in rats. Stroke 2017; 48(3):747-53.
24. Baumjohann D. Diverse functions of miR-17-92 cluster microRNAs in T helper cells. Cancer Lett 2018; 423:147-52.
25. Kuo G, Wu CY, Yang HY. MiR-17-92 cluster and immunity. J Formos Med Assoc 2019; 118(1 Pt 1):2-6.
26. Luo XQ, Shao JB, Xie RD, et al. Micro RNA-19a interferes with IL-10 expression in peripheral dendritic cells of patients with nasal polyposis. Oncotarget 2017; 8(30):48915-21.
27. Kumar S, O'Malley J, Chaudhary AK, Inigo JR, Yadav N, Kumar R, Chandra D. Hsp60 and IL-8 axis promotes apoptosis resistance in cancer. Br J Cancer 2019; 121(11):934-43.
28. Vocka M, Langer D, Fryba V, et al. Novel serum markers HSP60, CHI3L1, and IGFBP-2 in metastatic colorectal cancer. Oncol Lett 2019; 18(6):6284-92.
29. Al-Hatamleh MAI, E A R ENS, Boer JC, et al. Synergistic effects of nanomedicine targeting TNFR2 and DNA demethylation inhibitor-an opportunity for cancer treatment. Cells 2019; 9(1).
30. Wang X, Cheng D, Hu G, et al. Tumor Necrosis Factor (TNF) receptor expression determines keratinocyte fate upon stimulation with TNF-Like weak inducer of apoptosis. Mediators Inflamm 2019; 2019:2945083.

MiR-195 promotes myocardial fibrosis in MI rats via targeting TGF-β1/Smad

D.-M. Wang[1,2,3], J.-J. Jin[1,2], L.-M. Tian[4] and Z. Zhang[1,2,5]

[1]The First School of Clinical Medicine, Lanzhou University, Lanzhou, Gansu, China; [2]Department of Heart Center, The First Hospital of Lanzhou University, Lanzhou, Gansu, China, [3]Department of Cardiology, Zhang Ye People's Hospital Affiliated To Hexi University, Gansu, China; [4]Clinical Medical College, Hexi University, Gansu, China; [5]Department of Heart Center, Gansu Clinical Medical Research Center for Cardiovascular Diseases, Lanzhou, Gansu, China

Received April 5, 2020 – Accepted June 29, 2020

The aim of this study was to investigate the effect of micro ribonucleic acid (miR)-195 on myocardial infarction (MI) in rats via regulating the transforming growth factor-β1 (TGF-β1)/Smad signaling pathway. A total of 36 Sprague-Dawley rats were randomly divided into a normal group (n=12), a model group (n=12) and an miR-195 antagomir group (n=12). In the normal group, the heart was exposed only, and normal saline was intraperitoneally injected after operation. In the model group, the acute MI model was established. In the miR-195 antagomir group, the acute MI model was also established, and miR-195 antagomir was intraperitoneally injected. The samples were collected at 2 weeks after surgery. Then cardiac function was detected via echocardiography, and the morphology of heart tissues was observed via hematoxylin and eosin (H&E) staining. Moreover, the expression of Collagen I was determined using immunohistochemistry, the protein expressions of TGF-β1, Smad3 and Smad7 were detected using Western blotting, and the expression of miR-195 was detected via quantitative polymerase chain reaction (qPCR). It was found by echocardiography that, compared with those in the normal group, left ventricular ejection fraction (LVEF) and left ventricular fractional shortening (LVFS) significantly declined, while left ventricular end-diastolic diameter (LVDd) and left ventricular end-systolic diameter (LVDs) significantly rose in the other two groups (P<0.05). In comparison with the model group, the miR-195 antagomir group had significantly increased LVEF and LVFS, and significantly decreased LVDd and LVDs (P<0.05). The immunohistochemistry results showed that the mean optical density of tissues with positively expressed Collagen I was obviously higher in the other two groups than that in the normal group (P<0.05), while it was obviously lower in the miR-195 antagomir group than that in the model group (P<0.05). According to the results of Western blotting, the protein expressions of TGF-β1 and Smad3 were evidently increased, while the protein expression of Smad7 was evidently decreased in the other two groups compared with those in the normal group (P<0.05). The opposite results were found in the miR-195 antagomir group compared with those in the model group (P<0.05). The results of qPCR manifested that the expression of miR-195 was markedly higher in the other two groups than that in the normal group (P<0.05), while it was markedly lower in the miR-195 antagomir group than in the model group (P<0.05). Moreover, it was observed using H&E staining that the myocardial fibers in the normal group had normal arrangement and intact structure, without obvious morphological abnormalities. In the model group, the myocardial fibers were arranged disorderly, and there were massive proliferating fibrous tissues, with a high degree of fibrosis. In themiR-195 antagomir group, the myocardial fibers

Corresponding Author:
Zheng Zhang, MD
No. 1, Donggang West Road,
Lanzhou, Gansu 730000, China
Fax/Tel: +86 9318619797
e-mail: zhangccu@yeah.net

0393-974X (2020)
Copyright © by BIOLIFE, s.a.s.
This publication and/or article is for individual use only and may not be further reproduced without written permission from the copyright holder.
Unauthorized reproduction may result in financial and other penalties
DISCLOSURE: ALL AUTHORS REPORT NO CONFLICTS OF INTEREST RELEVANT TO THIS ARTICLE.

were damaged and arranged less disorderly, and proliferation and fibrosis could be seen in some fibrous tissues, but to a lesser extent than the model group. In conclusion, miR-195 promotes myocardial fibrosis in MI rats via up-regulating the TGF-β1/Smad signaling pathway.

Key words: myocardial infarction; TGF-β1/Smad signaling pathway; miR-195; fibrosis

Myocardial infarction (MI) is a common critical disease of the cardiovascular system, which can cause sudden death of patients in severe cases, making it a major threat to human health (1, 2). According to the literature, MI frequently occurs in people aged 40-60 years, and is one of the important causes of cardiac dysfunction (such as heart failure) and even death in this age group (3, 4). However, with the changes in lifestyle and the accelerated pace of life, the incidence rate of MI is becoming increasingly higher due to bad living habits, and even shows a younger trend. In recent years, MI has occured in a large number of young people, therefore, its prevention and treatment are the focus of current clinical research.

There are a series of complex pathological responses after MI, including myocardial fibrosis, myocardial apoptosis, inflammation and oxidative stress response, among which myocardial fibrosis exerts an important effect on myocardial remodeling and myocardial function recovery after MI (5, 6). As one of the important signal transduction pathways, the transforming growth factor-β1 (TGF-β1)/Smad pathway is closely related to myocardial fibrosis. Following activation, the TGF-β1/Smad signaling pathway plays a crucial regulatory role in tissue proliferation and fibrosis.

Micro ribonucleic acid (miR)-195 is an important member of the miRNA family, which can exert a vital regulatory effect, especially on cell proliferation, apoptosis, inflammation and fibrosis, *via* regulating the activation of multiple downstream signaling pathways and the expression of multiple effector molecules (7, 8). Therefore, this study aims to explore the effect of miR-195 on MI rats through regulating the TGF-β1/Smad signaling pathway.

MATERIALS AND METHODS

Laboratory animals and grouping

Thirty-six female Sprague-Dawley rats weighing (200±10) g were randomly divided into a normal group (n=12), a model group (n=12) and an miR-195 antagomir group (n=12). The rats were fed with pure water and sufficient feed every day under a 12/12 h light/dark cycle in the laboratory animal center. This study met the requirements of the Animal Ethics Committee of Lanzhou University Animal Center.

Modeling and treatment in each group

After successful anesthesia *via* intraperitoneal injection of 2.5% pentobarbital sodium (30 mg/kg), the rats were fixed on an operating table and depilated, followed by skin preparation and aseptic towel draping. Thereafter, the rats were connected to an electrocardiograph monitor, and a tracheal cannula was inserted between the 3rd and 4th cartilaginous rings and connected to a ventilator (tidal volume: 7 mL/kg, expiratory/inspiratory ratio: 1:1). Then a longitudinal incision (about 3 cm long) was made near the left sternum, and the skin, muscles and fascia were cut in order. The 3rd and 4th ribs were cut off, and the thoracic cavity was fully expanded to expose the heart. Next, the pericardium was carefully cut off with ophthalmic forceps, and the 0-gauge silk thread was inserted between the left auricle and the arterial cone. The electrocardiogram manifestations were observed, and the typical ischemic electrocardiogram manifestations indicated the successful establishment of acute MI model. Later, the wound was sutured layer by layer, and the air in the thoracic cavity was removed. After resuscitation, the ventilator was withdrawn, and the rats were kept warm and fed in separate cages.

In the normal group, the rats were fed with normal feed and pure water every day. In the model group, after the acute MI model was successfully established using the above method, the rats were fed with normal feed and pure water every day and intraperitoneally injected with normal saline once a day. In the miR-195 antagomir group, the acute MI model was also established using the above method, and then 3 μM of miR-195 antagomir (Boster, Wuhan, China) was intraperitoneally injected using a microsyringe once

a day. All rats were sacrificed at 14 days after surgery to obtain samples.

Detection of cardiac function

Before the rats were sacrificed, the cardiac function was detected *via* echocardiography, as follows: After successful anesthesia *via* intraperitoneal injection of 2.5% pentobarbital sodium (30 mg/kg), the rats were fixed on the operating table and connected to the electrocardiograph monitor. Then left ventricular ejection fraction (LVEF), left ventricular fractional shortening (LVFS), left ventricular end-diastolic diameter (LVDd) and left ventricular end-systolic diameter (LVDs) were measured.

Sampling

After anesthesia, the abdominal cavity was cut open to expose the abdominal aorta, from which the blood was drawn and stored for later use. Six rats in each group were fixed with paraformaldehyde. After stiffening of limbs, the heart tissues were taken and fixed in paraformaldehyde for 48 h. Furthermore, the heart tissues were directly taken from the remaining 6 rats in each group, placed in an Eppendorf (EP) tube and stored in an ultra-low temperature refrigerator.

Hematoxylin-eosin (HE) staining

The paraffin-embedded tissues were sliced into 5-μm-thick sections, flattened in warm water at 42°C, removed, baked and prepared into paraffin sections. Then the sections were soaked and routinely deparaffinized in xylene solution and alcohol with gradient concentrations. According to the instructions of the H&E staining kit (Solarbio, Beijing, China), the sections were sealed and stained.

Immunohistochemistry

The paraffin-embedded tissues were sliced into 5-μm-thick sections, flattened in warm water at 42°C, fished up, baked and prepared into paraffin sections. Then the sections were soaked and routinely deparaffinized in xylene solution and alcohol with gradient concentrations, placed in citric acid buffer, and heated in a microwave for 3 times (3 min/time, braised for 5 min each time) for complete antigen retrieval. After the sections were washed, the endogenous peroxidase blocker was added dropwise for 10-min reaction. Then the sections were washed again and sealed with goat serum for 20 min. Following the removal of the goat serum, the anti-Collagen I primary antibody (1:200, Abcam, Cambridge, MA, USA) was added for incubation at 4°C overnight. On the next day, the sections were washed, reacted with the secondary antibody for 10 min, fully washed and reacted with streptavidin-peroxidase solution for 10 min, followed by color development with diaminobenzidine (DAB) (Solarbio, Beijing, China). Finally, the nuclei were counterstained with hematoxylin, and the sections were sealed and observed.

Western blotting

The cryopreserved heart tissues were lysed with lysis buffer, subjected to ice bath for 1 h and centrifuged at 14,000 g for 10 min. The protein was quantified using bicinchoninic acid (BCA) method (Beyotime, Shanghai, China). Next, the absorbance of protein was detected using a microplate reader and the standard curve was plotted, based on which the protein concentration was calculated. After protein denaturation, the protein in tissue specimens was separated *via* sodium dodecyl sulphate-polyacrylamide gel electrophoresis (SDS-PAGE), and the position of the Marker protein was observed. The electrophoresis was terminated when the Marker protein reached the bottom of the glass plate in a straight line. Then the protein was transferred onto a polyvinylidene fluoride (PVDF) membrane (Millipore, Billerica, MA, USA), sealed with the sealing buffer for 1.5 h and incubated with the anti-TGF-β1 (1:1000, Abcam, Cambridge, MA, USA), anti-Smad3 (1:1000, Abcam, Cambridge, MA, USA) and anti-Smad7 (1:1000 Abcam, Cambridge, MA, USA) primary and secondary antibodies (1:1000). After the membrane was washed, the image was fully developed using the chemiluminescent reagent for 1 min in the dark.

QPCR

The total RNA was extracted from heart tissues using the RNA extraction reagent, and reversely transcribed into complementary deoxyribose nucleic acid (cDNA) using the reverse transcription kit. The qPCR system (20 μL) was designed and carried out under the following conditions: reaction at 53°C for 5 min, pre-denaturation at 95°C for 10 min, denaturation at 95°C for 10 s, annealing at 62°C for 30 s, a total of 35 cycles. The ΔCt value was calculated first, and then the difference in the expression of target gene was calculated. The primer sequences are shown in Table I.

Statistical analysis

Statistical Product and Service Solutions (SPSS) 20.0 software (IBM, Armonk, NY, USA) was used for analysis. *t*-test was used for the data in line with normal distribution and homogeneity of variance, corrected *t*-test for the data in line with normal distribution and heterogeneity of variance, and non-parametric test for the data not in line with normal distribution and homogeneity of variance. Rank sum test was adopted for ranked data, and *chi*-squared test for enumeration data.

RESULTS

Cardiac function

It was found that LVEF and LVFS significantly declined, while LVDd and LVDs significantly rose in the other two groups compared with those in the normal group, displaying statistically significant differences ($P<0.05$). Compared with the model group, the miR-195 antagomir group had significantly increased LVEF and LVFS, and significantly decreased LVDd and LVDs, displaying statistically significant differences ($P<0.05$) (Fig. 1).

Immunohistochemistry results

Positively expressed Collagen I were dark brown, and it was lower in the normal group but higher in the other two groups (Fig. 2A). According to the statistical results (Fig. 2B), the mean optical density of positively expressed Collagen I was obviously higher in the other two groups than that in the normal group ($P<0.05$), while it was obviously lower in the

Table I. *Primer sequences*

Gene	Primer sequence
MiR-195	F: 5'-TTTAGGCATTGAGGACCTGC-3'
	R: 5'-AATTGCGGCCCTAAGGCGCA-3'
GAPDH	F: 5'-ACGGCAAGTTCAACGGCACAG-3'
	R: 5'-GAAGACGCCAGTAGACTCCACGAC-3'

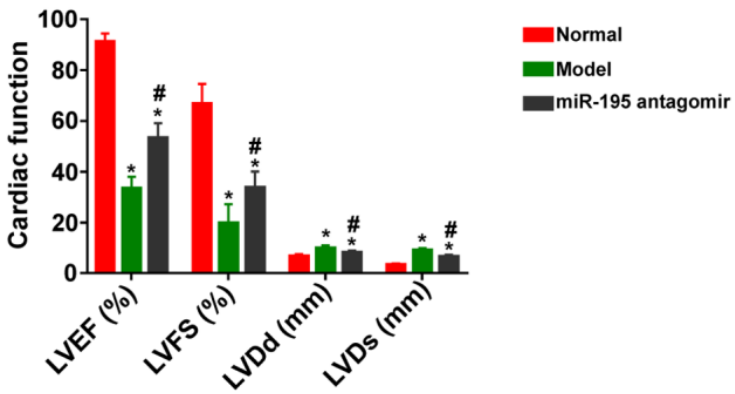

Fig. 1. *Cardiac function.* $^{*}P<0.05$ *vs normal group,* $^{\#}P<0.05$ *vs model group.*

miR-195 antagomir group than that in the model group (P<0.05). The differences were all statistically significant.

Western blotting results

The protein expressions of TGF-β1 and Smad3 were evidently increased, while the protein expression of Smad7 was evidently decreased in the other two groups compared with those in the normal group, with statistically significant differences (P<0.05). The opposite results were found in the miR-195 antagomir group compared with those in the model group, and there were also statistically significant differences (P<0.05) (Fig. 3).

QPCR results

As shown in Fig. 4, the expression of miR-195 was markedly higher in the other two groups than that in the normal group (P<0.05), while it was markedly lower in the miR-195 antagomir group than

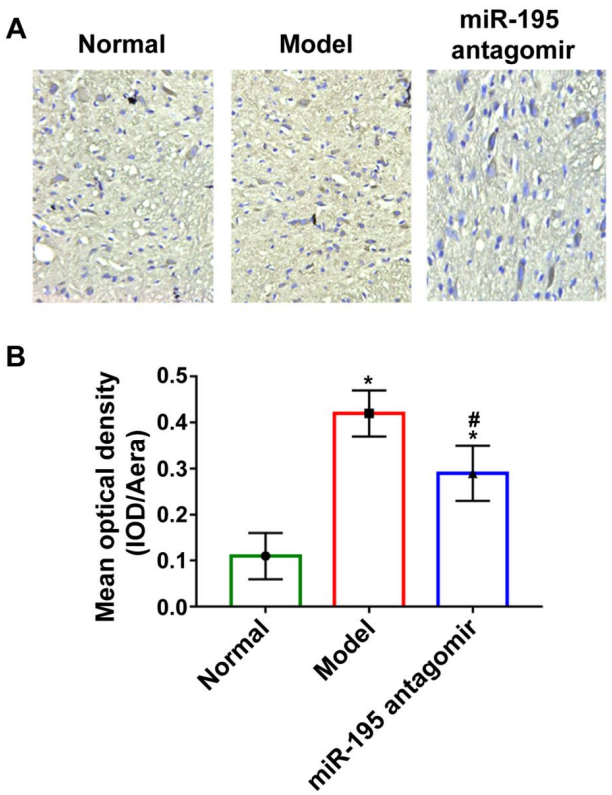

Fig. 2. *Immunohistochemistry results.*
A) *Immunohistochemistry results (magnification: 400×).* ***B)*** *Mean optical density of positive expression. *P<0.05 vs normal group, #P<0.05 vs model group.*

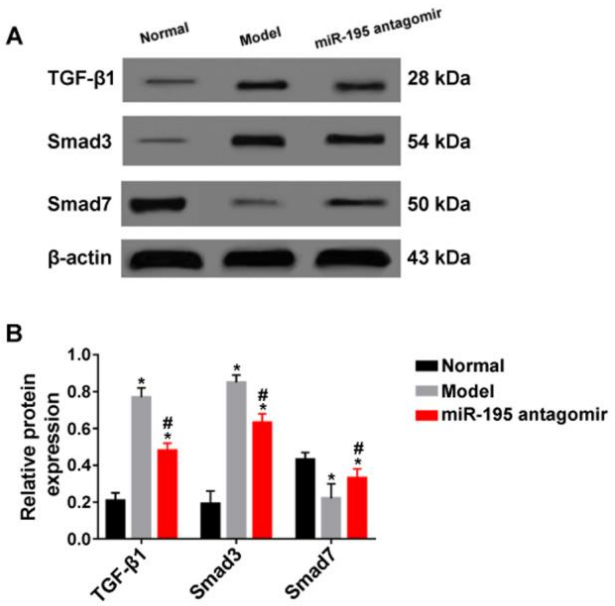

Fig. 3. A) *Western blotting results.* ***B)*** *Relative protein expression in each group. *P<0.05 vs normal group, #P<0.05 v. model group.*

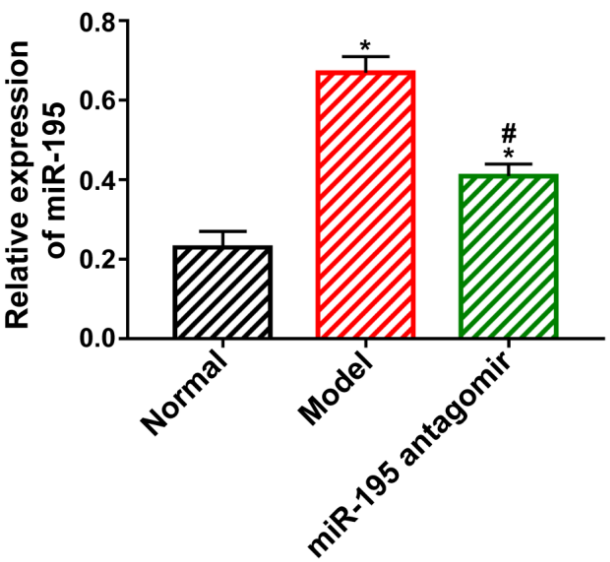

Fig. 4. *Expression of miR-195 detected via qPCR. Note: *P<0.05 vs normal group, #P<0.05 vs model group.*

in the model group (P<0.05). The differences were statistically significant.

HE staining results

The myocardial fibers in the normal group had normal arrangement and intact structure, without obvious morphological abnormalities. In the model

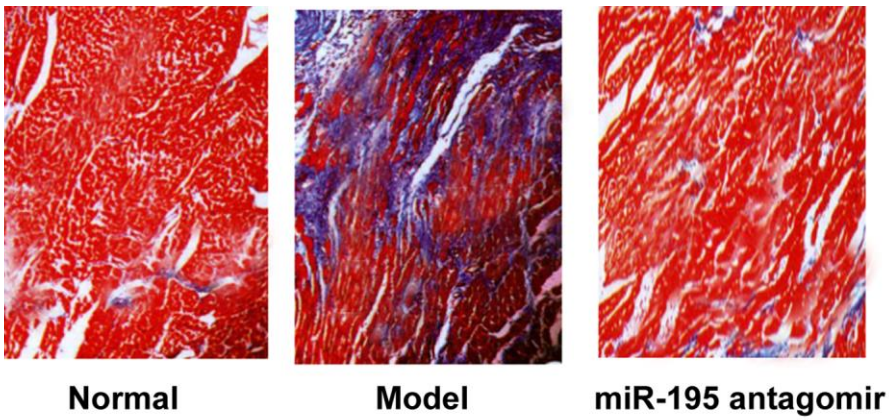

Fig. 5. *HE staining results. (magnification: 400×)*

group, the myocardial fibers were arranged disorderly, and there were massive proliferating fibrous tissues, with a high degree of fibrosis. In miR-195 antagomir group, the myocardial fibers were damaged and arranged less disorderly, and proliferation and fibrosis could be seen in some fibrous tissues, but to a lesser extent than the model group (Fig. 5).

DISCUSSION

MI often leads to cardiac dysfunction and even sudden death, so it has become a major threat to human health (9, 10). In particular, with the increase in the incidence rate and the younger trend of patients in recent years, MI has attracted increasingly more attention of clinicians and researchers, and has become a research hot spot around the world. Therefore, it is extremely important to study the pathogenesis of MI and the pathological response process after onset. It is currently believed that the pathological response after MI is complex, including inflammation, oxidative stress and apoptosis. Through interactions and corresponding effects, these responses exert vital regulatory effects in ventricular remodeling and cardiac function after MI (11). Excessive myocardial fibrosis caused by various factors is an important pathological response after MI. According to many studies (12, 13), multiple signaling pathways and effector molecules, especially Collagen I and TGF-β1/Smad signaling pathway that play important roles, are involved in scar hyperplasia and fibrosis after MI. As a critical effector protein of myocardial fibrosis, Collagen I is an important player during myocardial scarring and excessive fibrosis, as well as an important component of fibrous tissues. It has been found (14, 15) that due to the massive accumulation of Collagen I at the injury site, tissue morphological abnormality, structural disorders and dysfunction can be further caused in MI, ultimately resulting in poor ventricular remodeling, and affecting myocardial function recovery and ventricular remodeling. In addition, the TGF-β1/Smad signaling pathway is one of the crucial signaling pathways in the body, regulating scar hyperplasia and fibrosis through exerting an important regulatory effect on the expression of multiple downstream proteins (16-18). Under the action of injury factors, inflammatory factors and cytokines after injury, TGF-β1, the key molecule in the TGF-β1/Smad signaling pathway, can be highly expressed to activate this pathway, thus further activating Smad3 and Smad7 to trigger Smad3 high expression and Smad7 low expression. Smad3 can up-regulate the expression of Collagen I to promote fibroplasia, while Smad7 can inhibit the expression of Collagen I to suppress fibroplasia. There is a dynamic balance between Smad3 and Smad7 under physiological conditions, and they jointly keep the stability of fibrosis (19, 20). In this study, it was observed that Collagen I, TGF-β1 and Smad3 were highly expressed, while Smad7 was lowly expressed in the heart tissues of MI rats. Such

findings demonstrate that the TGF-β1/Smad signaling pathway is activated, and excessive fibrosis occurs in myocardial tissues, which may be one of the important causes of cardiac dysfunction in MI rats.

MiR-195 is one of the critical members of the miRNA family, which plays an important regulatory role in such pathophysiological reactions as cell proliferation and apoptosis. It has been confirmed that miR-195 can exert important pathophysiological effects *via* regulating downstream signaling pathways after injury, including regulating inflammation, apoptosis and fibrosis. In this study, it was found that miR-195 was highly expressed in the heart tissues of MI rats. After the expression of miR-195 was reduced by the inhibitor, the expressions of Collagen I, TGF-β1 and Smad3 declined, while that of Smad7 rose, which suggests that miR-195 has an important regulatory effect on the TGF-β1/Smad signaling pathway. After MI, the TGF-β1/Smad signaling pathway was up-regulated due to the high expression of miR-195, thereby raising the expressions of Collagen I, TGF-β1 and Smad3, and lowering the expression of Smad7. After miR-195 was inhibited, the TGF-β1/Smad signaling pathway was immediately suppressed, which may be one of the reasons for the improved cardiac function in miR-195 antagomir group. In conclusion, miR-195 promotes myocardial fibrosis in MI rats *via* up-regulating the TGF-β1/Smad signaling pathway.

REFERENCES

1. Holmes MV, Millwood IY, Kartsonaki C, et al. Lipids, Lipoproteins, and Metabolites and Risk of Myocardial Infarction and Stroke. J Am Coll Cardiol 2018; 71:620-32.
2. Park CS, Choi EK, Han KD, et al. Association between adult height, myocardial infarction, heart failure, stroke and death: a Korean nationwide population-based study. Int J Epidemiol 2018; 47:289-98.
3. Sabin P, Koshy AG, Gupta PN, Sanjai PV, Sivaprasad K, Velappan P, Vellikat VR. Predictors of no- reflow during primary angioplasty for acute myocardial infarction, from Medical College Hospital, Trivandrum. Indian Heart J 2017; 69 Suppl 1:S34-S45.
4. Dreyer RP, Dharmarajan K, Hsieh AF, Welsh J, Qin L, Krumholz HM. Sex differences in trajectories of risk after rehospitalization for heart failure, acute myocardial infarction, or pneumonia. Circ Cardiovasc Qual Outcomes 2017; 10:e003271.
5. Vereckei A, Katona G, Szelenyi Z, Takacs E, Maurovich-Horvat P, Becker D. ECG stress test induced atrial ischemia in a patient with old inferior myocardial infarction due to a distal coronary artery lesion. J Geriatr Cardiol 2017; 14:73-77.
6. El-Gohary OA, Allam MM. Effect of vitamin D on isoprenaline-induced myocardial infarction in rats: possible role of peroxisome proliferator-activated receptor-gamma. Can J Physiol Pharmacol 2017; 95:641-646.
7. Sahu SK, Kumar M, Chakraborty S, et al. MicroRNA 26a (miR-26a)/KLF4 and CREB-C/EBPbeta regulate innate immune signaling, the polarization of macrophages and the trafficking of Mycobacterium tuberculosis to lysosomes during infection. Plos Pathog 2017; 13:e1006410.
8. Lu J, Song G, Tang Q, et al. MiR-26a inhibits stem cell-like phenotype and tumor growth of osteosarcoma by targeting Jagged1. Oncogene 2017; 36:231-41.
9. Phan K, Phan S, Khuong JN, Yan TD. Intra-aortic balloon pump therapy for acute myocardial infarction: Trial sequential analysis. Int J Cardiol 2016; 202:520-521.
10. Heusch G, Gersh BJ. The pathophysiology of acute myocardial infarction and strategies of protection beyond reperfusion: a continual challenge. Eur Heart J 2017; 38:774-84.
11. O'Donoghue ML, Glaser R, Cavender MA, et al. Effect of Losmapimod on Cardiovascular Outcomes in Patients Hospitalized With Acute Myocardial Infarction: A Randomized Clinical Trial. JAMA 2016; 315:1591-99.
12. Zhang Y, Li C, Meng H, et al. BYD Ameliorates Oxidative Stress-Induced Myocardial Apoptosis in Heart Failure Post-Acute Myocardial Infarction via the P38 MAPK-CRYAB Signaling Pathway. Front Physiol 2018; 9:505.
13. Chen H, Xu Y, Wang J, Zhao W, Ruan H. Baicalin ameliorates isoproterenol-induced acute myocardial infarction through iNOS, inflammation and oxidative stress in rat. Int J Clin Exp Pathol 2015; 8:10139-47.
14. Yu Y, Yin G, Bao S, Guo Z. Kinetic alterations of

collagen and elastic fibres and their association with cardiac function in acute myocardial infarction. Mol Med Rep 2018; 17:3519-3526.
15. Park SH, Uzawa T, Hattori F, Ogino S, Morimoto N, Tsuneda S, Ito Y. "All-in-one" in vitro selection of collagen-binding vascular endothelial growth factor. Biomaterials 2018; 161:270-78.
16. Hu Z, Qin F, Gao S, Zhen Y, Huang D, Dong L. Paeoniflorin exerts protective effect on radiation-induced hepatic fibrosis in rats via TGF-beta1/Smads signaling pathway. Am J Transl Res 2018; 10:1012-21.
17. Huang Z, Li S, Fan W, Ma Q. Transforming growth factor beta1 promotes invasion of human JEG-3 trophoblast cells via TGF-beta/Smad3 signaling pathway. Oncotarget 2017; 8:33560-70.
18. Guan Y, Tan Y, Liu W, et al. NF-E2-Related Factor 2 Suppresses Intestinal Fibrosis by Inhibiting Reactive Oxygen Species-Dependent TGF-beta1/SMADs Pathway. Dig Dis Sci 2018; 63:366-80.
19. Liu T, Xu L, Wang C, et al. Alleviation of hepatic fibrosis and autophagy via inhibition of transforming growth factor-beta1/Smads pathway through shikonin. J Gastroenterol Hepatol 2019; 34:263-76.
20. Ji Q, Liu X, Han Z, et al. Resveratrol suppresses epithelial-to-mesenchymal transition in colorectal cancer through TGF-beta1/Smads signaling pathway mediated Snail/E-cadherin expression. Bmc Cancer 2015; 15:97.

miR-92a-3p promotes the proliferation and invasion of gastric cancer cells by targeting KLF2

Q-Q. Mao, J-J. Chen, W-J. Xu, X-G. Zhao, X. Sun and L. Zhong

Department of Gastroenterology, North Hospital of Huashan Hospital Affiliated to Fudan University, Shanghai, China

Received April 4, 2020 – Accepted June 30, 2020

MicroRNAs (miRNAs) have pivotal roles in the initiation and progression of gastric cancer (GC), and miR-92a-3p has been proved to act as an oncogene in multiple malignancies. However, the molecular mechanisms by which miR-92a-3p contributes to GC remain unclear. The differentially expressed miRNAs were screened by GEO dataset, and the association of miR-92a-3p expression with clinicopathological characteristics and prognosis in patients with GC was analyzed by TCGA dataset. The target genes of miR-92a-3p were identified by bioinformatic analysis, and their interaction was confirmed by luciferase reporter assay. MTT, EdU and Transwell assays were conducted to determine the role of miR-92a-3p in GC cells. As a result, it was found that the expression levels of miR-92a-3p were increased in GC tissues and were associated with tumor size, lymph node infiltration and distant metastasis, acting as an independent prognostic factor of poor survival in patients with GC. Restored expression of miR-92a-3p facilitated cell proliferation, DNA synthesis and cell invasion, but its inhibitor reversed these effects. KLF2 was further identified as a direct target of miR-92a-3p, indicating a negative correlation with miR-92a-3p expression and harboring a favorable prognosis in GC. In addition, KLF2 repressed cell proliferation and invasion and attenuated the tumor-promoting effects of miR-92a-3p in GC cells. Altogether, our findings demonstrated that miR-92a-3p promoted the proliferation and invasion of GC cells by targeting KLF2.

Gastric cancer (GC) ranks the fourth most common malignancy and the third leading cause of cancer-related deaths in China (1). In spite of the widespread application of gastroscopy in detection of GC, the advanced cases have a poor prognosis due to its multiple metastases (2). Previous studies showed that dysregulation of coding RNAs or noncoding RNAs (ncRNAs) is associated with the prognosis of GC (3, 4). Therefore, identification of new biomarkers for detection of GC is urgently needed.

MicroRNAs (miRNAs) as small ncRNAs have been implicated in post-transcriptional regulation of their target genes in GC (5). Previous studies showed that miR-92a-3p is upregulated and predicts a poor prognosis in patients with breast cancer (BC) (6), and exosomal miR-92a-3p is related to pathological stage in colorectal cancer (CRC) (7). In addition, miR-92a-3p facilitates tamoxifen resistance in BC and cell invasion in esophageal carcinoma by targeting PTEN (8), but downregulation of miR-92a-3p represses cell proliferation in acute megakaryoblastic leukemia (9) and glioma (10). Moreover, cancer-associated fibroblasts secreted exosomal miR-92a-3p favoring the metastasis and chemotherapy resistance in CRC

Key words: miR-92a-3p; proliferation; invasion; KLF2; gastric cancer

Corresponding Author:
Dr Liang Zhong,
Department of Gastroenterology, North Hospital of Huashan Hospital Affiliated to Fudan University, Jingpohu Road 518, Baoshan District, Shanghai 201907, China
Tel.: +86 021 66894835
e-mail: lang_zhong2019@163.com

0393-974X (2020)
Copyright © by BIOLIFE, s.a.s.
This publication and/or article is for individual use only and may not be further reproduced without written permission from the copyright holder.
Unauthorized reproduction may result in financial and other penalties
DISCLOSURE: ALL AUTHORS REPORT NO CONFLICTS OF INTEREST RELEVANT TO THIS ARTICLE.

(11) and promotes liposarcoma cell proliferation and metastasis (12), but chronic myeloid leukemia-derived exosomal miR-92a-3p alleviates the adipogenesis of adipose derived mesenchymal stem cells (13).

MiR-92a-3p is also regulated by lncRNA MT1JP and inhibits FBXW7 expression in GC (14). In the present study, increased expression of miR-92a-3p was associated with tumor size, lymph node infiltration and distant metastasis, acting as an independent prognostic factor of poor survival in patients with GC. MiR-92a-3p enhanced cell proliferation, DNA synthesis and cell invasion in GC by targeting Kruppel-like factor 2 (KLF2) and might offer a promising therapeutic target for GC.

MATERIALS AND METHODS

Clinical data

The clinical data for 383 cases of GC samples, 42 normal tissues and prognostic information as well as miR-92a-3p and KLF2 expression levels were downloaded from The Cancer Genome Atlas (TCGA) dataset (https://genome-cancer.ucsc.edu). GC tissues of 7 cases were stored at -80°C in our laboratory. All patients gave informed and signed consent to participate in our study. Our studies were approved by the Ethics Committee of our hospital.

Identification of the target of miR-92a-3p

The target of miR-92a-3p was identified by using the prediction tool TargetScanHuman7.1 (http://www.targetscan.org/vert_71/) according to the cumulative weighted text score.

Cell culture

Human Gastric Mucosal Epithelial Cell Line GES 1 and GC cell lines (BGC-823, SGC-7901, MGC-803, AGS and MKN-45) were purchased from the Chinese Academy of Sciences Cell Bank, and were cultured in Dulbecco's Modified Eagle medium supplemented with 10% heat-inactivated fetal bovine serum in a humidified atmosphere containing 5% CO2 at 37°C.

Quantitative real-time PCR (qRT-PCR)

RNA was isolated from GC cells using Trizol reagent (Invitrogen). One Step SYBR® PrimeScript™ PLUS RT-PCR Kit (TaKaRa, Beijing, China) was used to detect the expression of KLF2. TaqMan® MicroRNA Reverse Transcription Kit and TaqMan Universal Master Mix II (Thermo Fisher Scientific, Runcorn, UK) were used to detect miR-92a-3p expression. The primer sequences were as follows: KLF2, F:5'- CTACACCAAGAGTTCGCATCTG -3', R: 5'- CCGTGTGCTTTCGGTAGTG -3'; miR-92a-3p, F:5'- UAUUGCACUGUCCCGGCCUGU -3', R: 5'- CTCAACTGGTGT CGTGGAGTCGGCAATTCAGTTGAGACAGGCCG -3'; GAPDH, F:5'- CTGGGC TACACTGAGCACC -3', R: 5'- AAGTGGTCGTTGAGGGCAATG -3'; U6, F:5'- CAGCACATATACTAAAATTGGAACG -3', R: 5'- ACGAATTTGCGTGTCATCC-3'. U6 or GAPDH was used as an internal parameter. The $2^{-\Delta\Delta CT}$ equation was used to quantify the data in triplicate.

Western blot analysis

BGC-823 and MKN-45 cell lines were harvested and extracted using lysis buffer. Cell extracts were boiled in loading buffer and equal amount of cell extracts were separated on 15% SDS-PAGE gels. Separated protein bands were transferred onto polyvinylidene fluoride membranes. The primary antibody against KLF2 (ab139699, Rabbit polyclonal antibody, Abcam, Cambridge, MA, USA) and GAPDH (ab181602, Rabbit monoclonal antibody, Abcam, Cambridge, MA, USA) were diluted at a ratio of 1:1000 according to the manufacturer's instructions, and incubated overnight at 4°C. The specific details were as previously reported (4).

Luciferase reporter assay

BGC-823 and MKN-45 cell lines were seeded into 96-well plates and were co-transfected with a mixture of 60 ng of luciferase, 6 ng of pRL-CMV-KLF2 3'UTR luciferase reporter, and miR-92a-3p mimic or inhibitor. After 48 h of incubation, the luciferase activities were measured with a dual-luciferase reporter assay (Promega, Madison, WI, USA).

Plasmid, siRNA and miR-92a-3p mimic and inhibitor

Plasmid-mediated KLF2, siRNA targeting KLF2 (si-KLF2: GCAAGACCTACACCAAGAG), and its negative control (pcDNA3.1: GCATCCACACAAACGAGAG), miR-92a-3p mimic, inhibitor and the control vectors were purchased from Genepharma (Shanghai, PR, China). BGC-823 and MKN-45 cell lines were planted in 6-well plates

24 h prior to si-KLF2, pcDNA3.1, miR-92a-3p mimic or inhibitor transfection with 50-70% confluence, and then were transfected with Lipofectamine 2000 (Invitrogen, Carlsbad, CA, USA) according to the manufacturer's instructions.

MTT, EdU and Transwell assays were conducted as previously reported (4).

Statistical analysis

Statistical analyses were carried out by SPSS 20.0 (IBM, SPSS, Chicago, IL, USA) and GraphPad Prism. Student's *t*-test, *Chi*-squared test or Analysis of Variance (ANOVA) was used to assess the statistical significance for comparisons of two groups. Overall survival curves were analyzed with the Kaplan-Meier method and log-rank test. Univariate and multivariate analyses were conducted by a Cox proportional hazard regression model. $P < 0.05$ was considered statistically significant.

RESULTS

Increased expression of miR-92a-3p was associated with poor survival in patients with GC

A microarray chip (GSE101502) was used to screen differentially expressed miRNAs between GC and normal tissues. With the criteria of *P* value

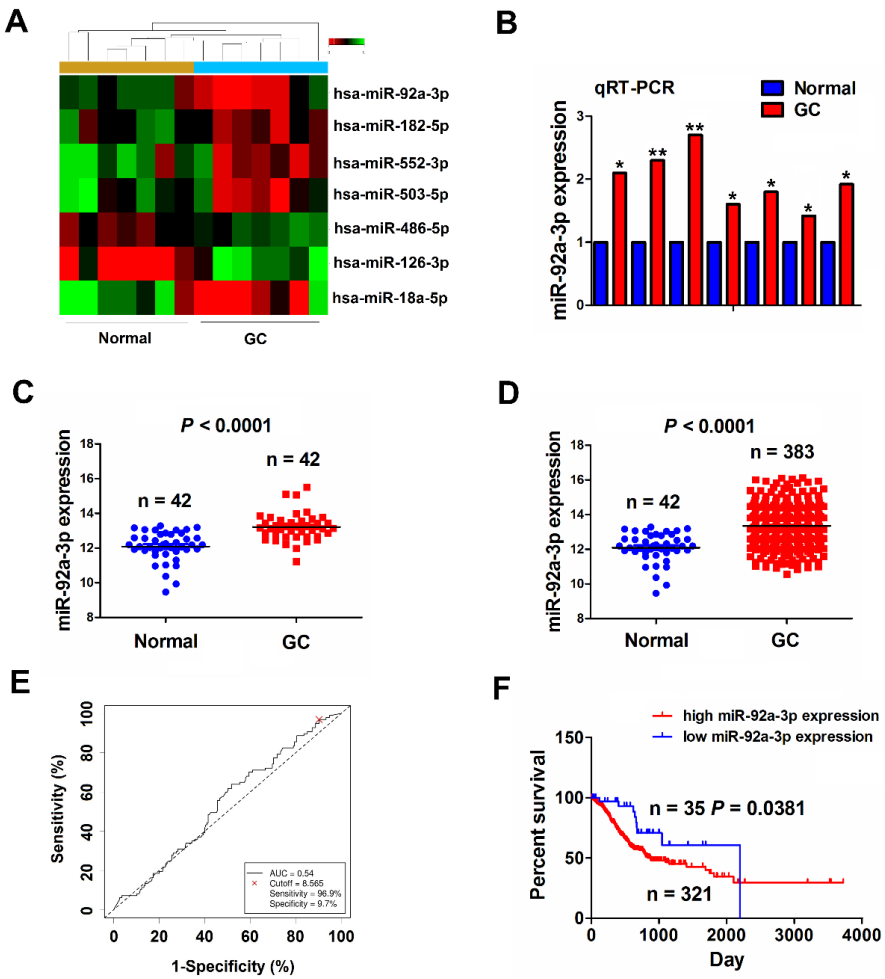

Fig. 1. *High expression of miR-92a-3p was associated with poor survival in patients with GC. **A)** GEO analysis of the differentially expression miRNAs between GC and normal tissues. **B)** qRT-PCR analysis of the expression levels of miR-92a-3p in 7 paired GC tissues. **C, D)** TCGA analysis of the expression levels of miR-92a-3p in pair-matched and unpaired GC tissues. **E)** The cutoff, AUC and sensitivity of miR-92a-3p were obtained according to the miR-92a-3p, survival time and status. **F)** Kaplan-Meier analysis of the association of high or low miR-92a-3p expression with overall survival in patients with GC. * P < 0.05; ** P < 0.01.*

< 0.001 and FC > 2.0, 5 upregulated miRNAs and 2 downregulated miRNAs were identified in GC samples, of which miR-92a-3p harbored a significantly increased expression in GC tissues (FC = 3.46, P = 0.0002; Fig. 1A). The expression of miR-92a-3p was detected in GC tissues by qRT-PCR analysis, which indicated that miR-92a-3p expression was increased in GC tissue samples as compared with the normal tissues ($P < 0.05$; Fig. 1B). This result was further confirmed in TCGA cohort in paired (n = 42, $P <$ 0.0001; Fig. 1C) and unpaired GC samples (n = 383, $P < 0.0001$; Fig. 1D).

According to miR-92a-3p expression levels, survival time and status, a cutoff value (8.565) of miR-92a-3p was obtained in GC (Fig. 1E). As shown in Table I, high expression of miR-92a-3p was

Table I. *The association of miR-92a-3p expression with clinicopathological characteristics of GC patients.*

Variables	Cases (n)	miR-92a-3p		*P* value
		High	Low	
Total	356	321	35	
Age (years)				
≥60	228	205	23	
<60	128	116	12	0.829
Gender				
Male	217	196	21	
Female	139	125	14	0.903
Pathological stage				
I/II	170	153	17	
III/IV	186	168	18	0.919
T stage				
T1/T2	92	76	16	
T3/T4	264	245	19	0.005
N stage				
Negative	115	96	19	
Positive	241	225	16	0.003
M stage				
Negative	263	242	21	
Positive	93	79	14	0.049

Table II. *Cox regression analysis of miR-92a-3p expression as a survival predictor.*

Variables	Univariate Cox regression analysis		Multivariate Cox regression analysis	
	RR (95% CI)	*P* value	RR (95% CI)	*P* value
Age (years)				
<60 *vs* ≥60	1.757 (1.111 to 2.779)	0.016	1.969 (1.241 to 3.124)	0.004
Gender				
Male *vs* Female	1.257 (0.820 to 1.928)	0.293	NA	NA
Pathological stage				
III/IV*vs* I/II	1.852 (1.212 to 2.813)	0.004	1.771 (1.109 to 2.829)	0.017
T stage				
T3+T4 *vs* T1+T2	1.755 (1.037 to 2.973)	0.036	1.284 (0.781 to 2.297)	0.399
N staging				
Positive *vs* Negative	1.457 (0.929 to 2.284)	0.101	NA	NA
M stage				
Positive *vs* Negative	1.642 (0.915 to 2.949)	0.097	NA	NA
miR-92a-3p expression				
High *vs* Low	3.042 (0.963 to 9.611)	0.038	3.130 (0.985 to 9.945)	0.046

NA: not analyzed

associated with tumor size (P = 0.005), lymph node infiltration (P = 0.003) and distant metastasis (P = 0.049) in patients with GC. Kaplan-Meier analysis demonstrated that the patients with high miR-92a-3p expression harbored a poorer survival as compared with those with low miR-92a-3p expression (P = 0.0381; Fig. 1F). Univariate and multivariate analysis uncovered that high expression of miR-92a-3p as well as pathological stage was an independent prognostic factor of poor survival in GC patients (P = 0.046; Table II).

miR-92a-3p promoted the proliferation and invasion of GC cells

We detected the expression of miR-92a-3p in multiple GC cell lines and found that it had a lower expression in BGC-823 cell line but a higher expression in MKN-45 cell line as compared with the normal control GES1 (P < 0.01, Fig. 2A). Thus, the overexpression efficiency of miR-92a-3p mimic or inhibitory efficiency of miR-92a-3p inhibitor was respectively confirmed in BGC-823 or MKN-45 cells by qRT-PCR analysis (Fig. 2B). As a result, we

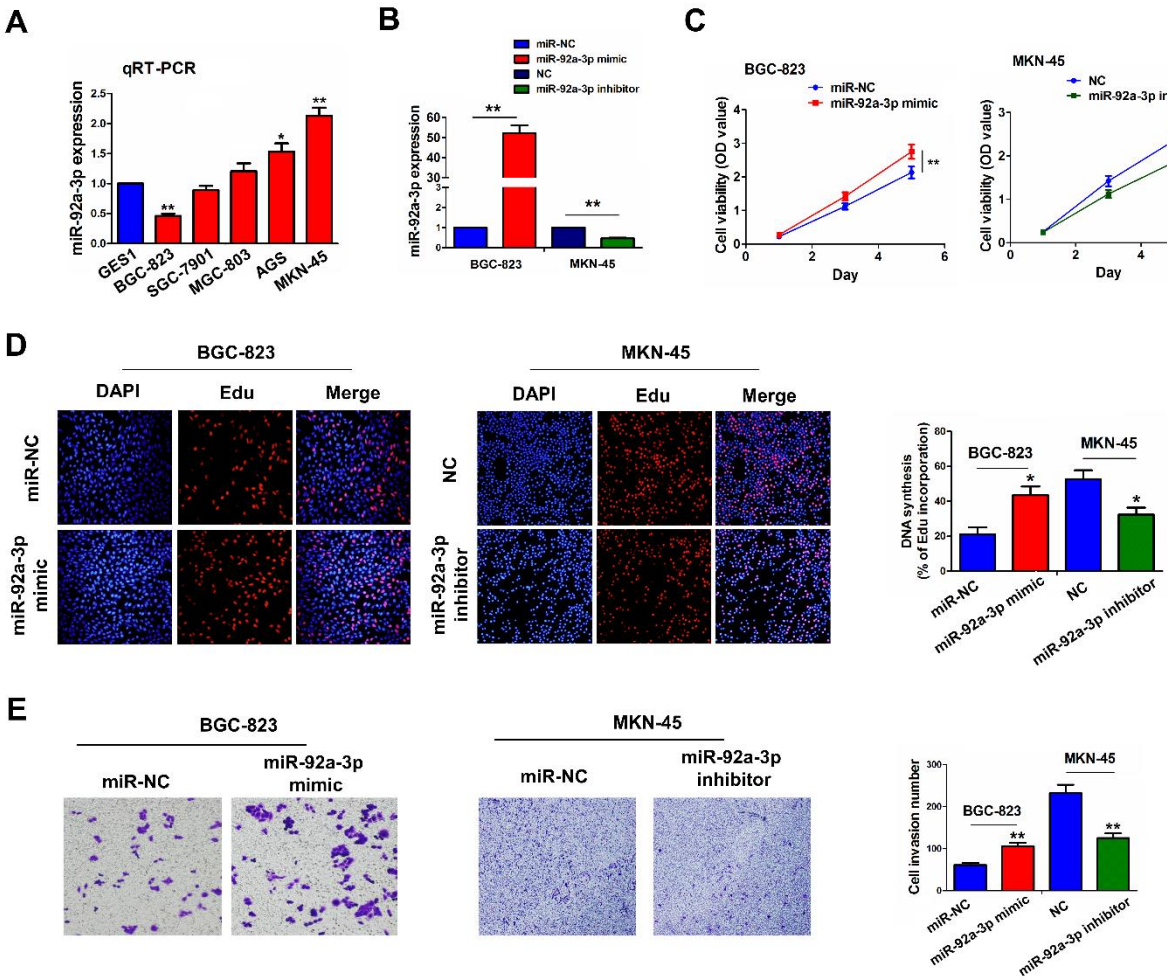

Fig. 2. *MiR-92a-3p promoted the proliferation and invasion of GC cells.* ***A****) qRT-PCR analysis of the expression levels of miR-92a-3p in multiple GC cell lines.* ***B****) qRT-PCR analysis of the transfection efficiency of miR-92a-3p mimic or inhibitor in BGC-823 or MKN-45 cell line.* ***C****) MTT analysis of the effects of miR-92a-3p mimic or inhibitor on cell viability in BGC-823 or MKN-45 cell line.* ***D****) EdU analysis of the effects of miR-92a-3p mimic or inhibitor on DNA synthesis in BGC-823 or MKN-45 cell line.* ***E****) Transwell analysis of the effects of miR-92a-3p mimic or inhibitor on cell invasion in BGC-823 or MKN-45 cell line. * P < 0.05; ** P < 0.01.*

found that overexpression of miR-92a-3p promoted cell viability (Fig. 2C), DNA synthesis (Fig. 2D) and invasive potential (Fig. 2E) in BGC-823 cells, but miR-92a-3p inhibitor reversed these effects (Fig. 2C-E).

KLF2 was a direct target of miR-92a-3p in GC cells

It was predicted that KLF2 might be a target of miR-92a-3p by using TargetScanHuman7.1 and the binding sites between miR-92a-3p and WT or Mut KLF2 3'UTR were indicated in Fig. 3A. Pearson correlation analysis demonstrated that miR-92a-3p had a negative correlation with KLF2 expression in GC tissues (r = -0.4531, $P < 0.0001$; Fig. 3B). To confirm whether miR-92a-3p could bind with KLF2, we co-transfected miR-92a-3p mimic and WT (Mut) KLF2 3'UTR into BGC-823 cells or miR-92a-3p inhibitor and WT (Mut) KLF2 3'UTR into MKN-45 cells and found that, miR-92a-3p reduced the luciferase activities of WT KLF2 3'UTR in BGC-823 cell line, while miR-92a-3p inhibitor increased its luciferase activities in MKN-45 cell line (Fig. 3C). However, miR-92a-3p mimic or inhibitor had no effects on those of Mut KLF2 3'UTR as compared with the control group (Fig. 3C). qRT-PCR and Western blot analysis showed that miR-92a-3p mimic decreased the expression of KLF2 in BGC-823 cell line, while its inhibitor increased its expression in MKN-45 cell line (Fig. 3D, E).

Decreased expression of KLF2 was associated with poor survival in patients with GC

We then estimated the genetic or epigenetic alterations of KLF2 expression in GC (n=384), and found that KLF2 had no obvious alterations at the genetic and methylation levels (Fig. 4A), indicating that KLF2 was indeed negatively modified by post-

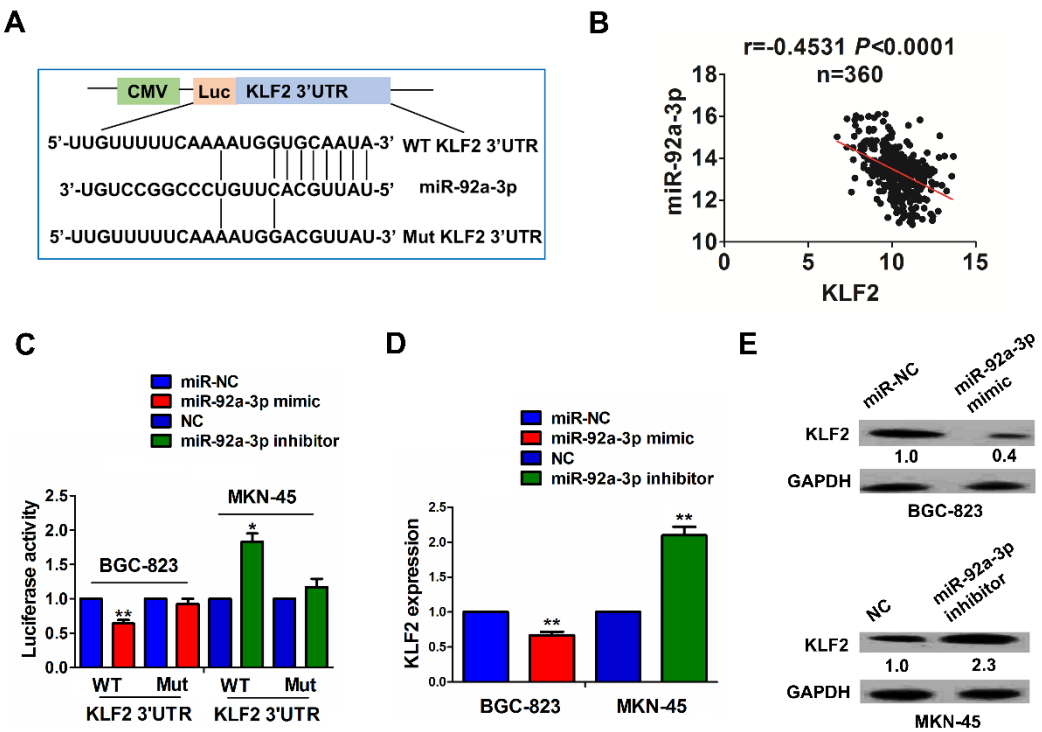

Fig. 3. *KLF2 was a direct target of miR-92a-3p in GC cells.* ***A****) The binding sites between miR-92a-3p and WT or Mut KLF2 3'UTR.* ***B****) TCGA analysis of the correlation of miR-92a-3p with KLF2 expression in GC tissues.* ***C****) Luciferase activities of WT or Mut KLF2 3'UTR after treatment with miR-92a-3p mimic or inhibitor in BGC-823 or MKN-45 cell line.* ***D, E****) qRT-PCR and Western blot analysis of the effects of miR-92a-3p mimic or inhibitor on KLF2 expression in BGC-823 or MKN-45 cell line. * $P < 0.05$; ** $P < 0.01$.*

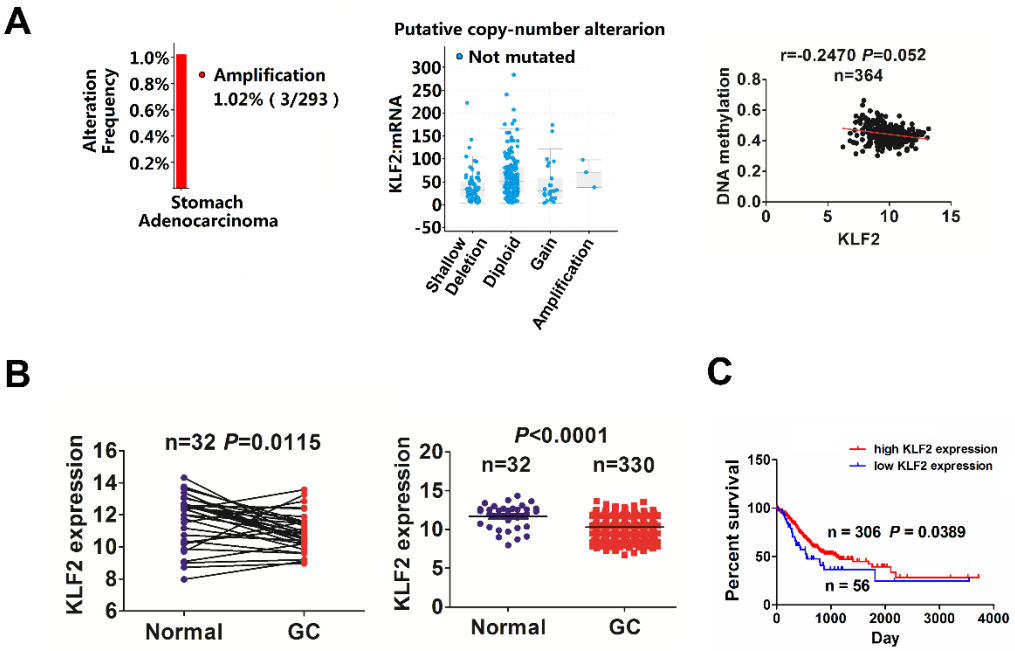

Fig. 4. *Low expression of KLF2 was associated with poor survival in patients with GC.* ***A)*** *TCGA analysis of the association of KLF2 with genetic mutation, copy number and DNA methylation in GC samples.* ***B)*** *TCGA analysis of the expression levels of KLF2 in pair-matched and unpaired GC tissues.* ***C)*** *Kaplan-Meier analysis of the association of high or low KLF2 expression with overall survival in patients with GC.*

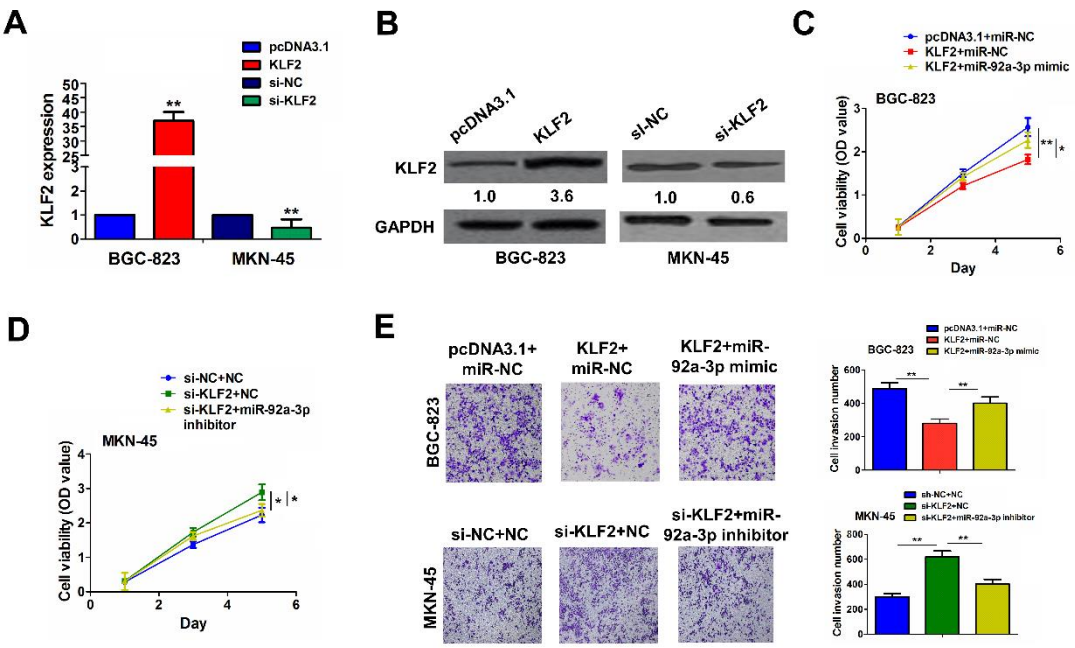

Fig. 5. *KLF2 reversed the tumor-promoting effects of miR-92a-3p in GC cells.* ***A, B)*** *qRT-PCR and Western blot analysis of the transfection efficiency of KLF2 in in BGC-823 cells or si-KLF2 in MKN-45 cells.* ***C, D)*** *MTT analysis of the cell viability after co-transfection with miR-92a-3p mimic and KLF2 in BGC-823 cells or miR-92a-3p inhibitor and si-KLF2 in MKN-45 cells.* ***E)*** *Transwell analysis of the cell invasion after co-transfection with miR-92a-3p mimic and KLF2 in BGC-823 cells or miR-92a-3p inhibitor and si-KLF2 in MKN-45 cells. * $P < 0.05$; ** $P < 0.01$.*

transcriptional regulation of miR-92a-3p in GC.

TCGA cohort showed that, KLF2 expression was downregulated in paired (n = 32, P = 0.0115) and unpaired GC samples (n = 330, P < 0.0001; Fig. 4B). Low expression of KLF2 was associated with tumor size (P = 0.007) and distant metastasis (P = 0.015) in patients with GC. Kaplan-Meier analysis demonstrated that the patients with low KLF2 expression harbored a poorer survival as compared with those with high KLF2 expression (P = 0.0389; Fig. 4C). Univariate and multivariate analysis unveiled that low expression of KLF2 as well as pathological stage was an independent prognostic factor of poor survival in GC patients (P = 0.022).

KLF2 reversed the tumor-promoting effects of miR-92a-3p in GC cells

The overexpression efficiency of KLF2 or silencing efficiency of si-KLF2 was respectively determined in BGC-823 or MKN-45 cells by qRT-PCR and Western blot analysis (Fig. 5A, B). We then found that overexpression of KLF2 inhibited cell viability, invasive potential and reversed the tumor-promoting effect in BGC-823 cells, but knockdown of KLF2 had the opposite effects in MKN-45 cells (Fig. 5C-E).

DISCUSSION

Accumulating data have shown that miR-92a-3p as an oncogenic miRNA is upregulated in a variety of cancers (6-8) and is linked to a worse prognosis in BC patients (6). It was reported that miR-92a-3p expression regulated by lncRNA MT1JP is increased in GC (14, however, the prognostic value of miR-92a-3p in GC remains undocumented. Herein, we identified that miR-92a-3p exerted a differentially-expressed in GC and upregulation of miR-92a-3p was associated with tumor size, lymph node infiltration and distant metastasis in patients with GC. Further analysis indicated that miR-92a-3p was an independent prognostic factor of poor survival in patients with GC. Our study suggested that miR-92a-3p might be a potential biomarker of GC.

Some studies have demonstrated that miR-92a-3p acts as an oncogenic factor in multiple cancers (11-13). We herein estimated the function of miR-92a-3p in GC cells and found that miR-92a-3p accelerated cell proliferation, DNA synthesis and invasion, but its inhibitor reversed these effects. Our results indicated that miR-92a-3p might be an oncogenic factor in GC cells.

The regulatory mechanisms revealed that miR-92a-3p functions predominantly by inhibiting its multiple target genes. For example, miR-92a-3p prompts the proliferation and invasion of esophageal squamous cell cancer by targeting PTEN (8), and enhances glioma and glioma stem-like cell growth by targeting CDH1/β-Catenin and Notch-1/Akt signaling pathways (10). KLF2 has been reported to be downregulated in CRC (15), hepatocellular carcinoma (HCC) (16), prostate cancer (17) and GC (18) and suppresses the proliferation and invasion in these cancer cells (15-18), however, individual study indicated KLF2 as a proliferation-promoting factor in HCC by upregulating c-myc (19). We herein identified KLF2 as a direct target of miR-92a-3p and it was unaffected by the genomic mutation, copy number and DNA methylation in GC samples. KLF2 was downregulated and displayed a negative correlation with miR-92a-3p expression in GC. High expression of KLF2 was associated with tumor size and distant metastasis, acting as an independent prognostic factor of poor survival in GC patients. Moreover, KLF2 repressed the proliferation and invasion and attenuated the tumor-promoting effects of miR-92a-3p in GC cells.

In conclusion, our findings demonstrated that miR-92a-3p expression was elevated in GC tissues and acted as an independent prognostic factor of poor survival in GC patients. We also found that miR-92a-3p facilitated the proliferation and invasion of GC cells by targeting KLF2 and might provide a potential therapeutic target for GC.

ACKNOWLEDGEMENT

This work was supported by the project from Shanghai Health and Family Planning Commission (NO. 201640310).

REFERENCES

1. Chen W, Zheng R, Zhang S, et al. Cancer incidence and mortality in China, 2013. Cancer Lett 2017; 401:63-71.
2. Kao YC, Fang WL, Wang RF, et al. Clinicopathological

differences in signet ring cell adenocarcinoma between early and advanced gastric cancer. Gastric Cancer 2019; 22:255-63.
3. Wang L, Chunyan Q, Zhou Y, He Q, Ma Y, Ga Y, Wang X. BCAR4 increase cisplatin resistance and predicted poor survival in gastric cancer patients. Eur Rev Med Pharmacol Sci 2017; 21:4064-70.
4. Huang Y, Zhang J, Hou L, et al. LncRNA AK023391 promotes tumorigenesis and invasion of gastric cancer through activation of the PI3K/Akt signaling pathway. J Exp Clin Cancer Res 2017; 36(1):194.
5. Zhang J, Jin M, Chen X, Zhang R, Huang Y, Liu H, Zhu J. Loss of PPM1F expression predicts tumour recurrence and is negatively regulated by miR-590-3p in gastric cancer. Cell Prolif 2018; 51:e12444.
6. Cun J, Yang Q. Bioinformatics-based interaction analysis of miR-92a-3p and key genes in tamoxifen-resistant breast cancer cells. Biomed Pharmacother 2018; 107:117-28.
7. Fu F, Jiang W, Zhou L, Chen Z. Circulating Exosomal miR-17-5p and miR-92a-3p Predict Pathologic Stage and Grade of Colorectal Cancer. Transl Oncol 2018; 11:221-32.
8. Li X, Guo S, Min L, Guo Q, Zhang S. miR-92a-3p promotes the proliferation, migration and invasion of esophageal squamous cell cancer by regulating PTEN. Int J Mol Med 2019; 44:973-81.
9. Sharifi M, Salehi R. Blockage of miR-92a-3p with locked nucleic acid induces apoptosis and prevents cell proliferation in human acute megakaryoblastic leukemia. Cancer Gene Ther 2016; 23:29-35.
10. Song H, Zhang Y, Liu N, Zhao S, Kong Y, Yuan L. miR-92a-3p Exerts Various Effects in Glioma and Glioma Stem-Like Cells Specifically Targeting CDH1/β-Catenin and Notch-1/Akt Signaling Pathways. Int J Mol Sci 2016; 17.pii: E1799.
11. Hu JL, Wang W, Lan XL, et al. CAFs secreted exosomes promote metastasis and chemotherapy resistance by enhancing cell stemness and epithelial-mesenchymal transition in colorectal cancer. Mol Cancer 2019; 18:91.
12. Casadei L, Calore F, Creighton CJ, et al. Exosome-derived miR-25-3p and miR-92a-3p stimulate liposarcoma progression. Cancer Res 2017; 77:3846-56.
13. Wan Z, Chen X, Gao X, et al. Chronic myeloid leukemia-derived exosomes attenuate adipogenesis of adipose derived mesenchymal stem cells via transporting miR-92a-3p. J Cell Physiol 2019; 234:21274-83.
14. Zhang G, Li S, Lu J, et al. LncRNA MT1JP functions as a ceRNA in regulating FBXW7 through competitively binding to miR-92a-3p in gastric cancer. Mol Cancer 2018; 17:87.
15. Lu L, Huang W, Hu W, et al. Kruppel-like factor 2 mediated anti-proliferative and anti-metastasis effects of simvastatin in p53 mutant colon cancer. Biochem Biophys Res Commun 2019; 511:772-79.
16. Lin J, Tan H, Nie Y, et al. Krüppel-like factor 2 inhibits hepatocarcinogenesis through negative regulation of the Hedgehog pathway. Cancer Sci 2019; 110:1220-31.
17. Wang B, Liu M, Song Y, Li C, Zhang S, Ma L. KLF2 Inhibits the Migration and Invasion of Prostate Cancer Cells by Downregulating MMP2. Am J Mens Health 2019; 13:1557988318816907.
18. Mao QQ, Chen JJ, Dong L, Zhong L, Sun X. Krüppel-like factor 2 suppresses growth and invasion of gastric cancer cells in vitro and in vivo. J Biol Regul Homeost Agents 2016; 30:703-12.
19. Zou K, Lu X, Ye K, Wang C, You T, Chen J. Krüppel-like factor 2 promotes cell proliferation in hepatocellular carcinoma through up-regulation of c-myc. Cancer Biol Ther 2016; 17:20-26.

Correlation analysis between vitamin D receptor gene polymorphism (BsmI) and hallux valgus

X.-M. Chen*, Y.-X. Zhang*, Y.-F. Bao and Y.-J. Xu

Department of Foot and Ankle Surgery, Wuxi 9th Affiliated Hospital of Soochow University, Wuxi 9th People's Hospital, Wuxi, China

Received April 4, 2020 – Accepted July 10, 2020

*These authors contributed equally to this work

Hallux valgus is a common foot deformity disease caused by various extrinsic and intrinsic factors, and systemic conditions, but the etiopathogenesis and pathogenesis of this deformity are still unknown. Hallux valgus affects 10-20% of Chinese adults. Although considered highly heritable, the candidate gene is unclear. We conducted the first candidate gene study of hallux valgus to identify the biological mechanism. Between June 2015 and July 2018, the records and radiographs of 80 patients diagnosed with hallux valgus and 80 controls who were treated were analyzed. In order to compare the differences in severity associated with this deformity, the charts of 80 patients were divided into 3 groups from the angle of hallux valgus. Clinical and basic studies were also statistically compared by PCR and data analysis. Patients and controls had significant differences in age and gender, however, there were no significant differences in age and gender among the light, moderate and severe groups. Post-operative groups resulted in significant improvements in all of the measured radiographic parameters compared with pre-operative groups. BsmI seemed to show a specific variation, and may serve as a useful bio-marker for the disease (OR = 5.88, 95% CI 1.54-22.35, P <0.001). In this paper, the article which proved the VDR polymorphisms (BsmI) playing an important role in hallux valgus were studied to understand and manage the hallux valgus more scientifically.

Hallux valgus (HV) is characterized by lateral deflection of the big toe, resulting in subluxation of the first meta toe joint, callus formation, capsule formation, and bursitis of the thumb toe on the bony process (1). Marked deformation worsens health-related quality of life in 23% of people aged 18 to 65 years (2). The recent increase in this common foot deformity is considered to be largely due to gender, footwear, body mass index (BMI), first metatarsal length and osteoarthritis (3, 4). However, consensus regarding genetic variations has yet to be established, as the etiology of HV is thought to be multifactorial.

Vitamin D receptor (VDR) protein is an endocrine member of the nuclear receptor superfamily and can be used as a transcription factor. Activated VDR binds to 1,25-dihydroxyvitamin D3 and interacts with vitamin D response elements in the vitamin D target gene promoter, regulating biological processes such as bone metabolism, cell proliferation, and immune response (5, 6). The 1,25-dihydroxy

Key words: hallux valgus; VDR gene; polymorphism; SNP; bio-marker

Corresponding Author:
Yajun Xu, BM
Department of Foot and Ankle Surgery,
Wuxi 9th Affiliated Hospital of Soochow University,
Wuxi 9th People's Hospital, 999 Liangxi Road,
Binhu District, Wuxi, Jiangsu, 214062, China
Tel.: +86 013812250377
e-mail: yajiu484369399@126.com

0393-974X (2020)
Copyright © by BIOLIFE, s.a.s.
This publication and/or article is for individual use only and may not be further reproduced without written permission from the copyright holder.
Unauthorized reproduction may result in financial and other penalties
DISCLOSURE: ALL AUTHORS REPORT NO CONFLICTS OF INTEREST RELEVANT TO THIS ARTICLE.

vitamin D3 receptor is located on chromosome 12q13.11, has a size of 75 kb, and has more than 470 single nucleotide polymorphisms (SNP). One of the main researched SNPs is BsmI (G>A). The VDR gene polymorphisms may affect the stability and expression of VDR mRNA, and has long been assumed to have a genetic predisposition for HV. 60.4% of 634 female college students suffering from HV were significantly positively associated with history of HV in family members (7). In the study of Neri et al., the Authors concluded that HV in men is usually hereditary and transmitted by mothers, with earlier onset and higher severity than women (8). In the Framing-ham Heart Study, HV was found to be highly heritable in 429 Caucasian families of European descent (1,370 participants) (9). In a study on healthy twins in Korea, Lee et al. believed that genetics had a greater impact on HV, and for the first time, heritability of HV was found to be 0.51 (10). To date, the only Genome-Wide Association study (GWAS) concerning HV found that the most significantly associated SNP in men was rs9675316 and in women was rs7996797 (11). Vitamin D receptor (VDR) is found in a variety of tissues, including chondrocytes, bone, and soft tissue. However, previous studies have shown that VDR gene polymorphisms are related to bone metabolism and soft tissue hyperplasia. However, to our knowledge, no study has yet estimated the candidate gene association of such foot disorders.

Identifying the genetic factors associated with HV can help to further understand its biological mechanism as well as aiding clinicians and researchers to screen high-risk populations and prevent or slow down functional decline. Therefore, the associations of HV with VDR polymorphism (BsmI) were analyzed to estimate the on-set and development of HV.

MATERIALS AND METHODS

We retrospectively analyzed the clinical records and radiographs of all patients who underwent symptomatic HV surgery from June 2015 to July 2018. After failure of conservative treatment, 85 patients with moderate to severe HV were treated with proximal osteotomy. Each patient's medical history was reviewed to determine the symptoms and severity. The main symptom of most patients was unbearable pain. Five patients were lost to follow-up. At the most recent follow-up, data for 70 women and 10 men were available for evaluation. The average age at the time of surgery was 61.1 years (32-81); the follow-up was for 3 months, and did not include patients with inflammation, infections or trauma. The control group consisted of 80 normal healthy people, all of whom had no HV deformity. Prior to the study, each participant gave written informed consent. The Ethics Committee of Wuxi 9th Affiliated Hospital of Soochow University approved the protocol.

Anthropometric measurement

X-rays before and 3 months after surgery were available for all patients. A line was drawn along the center of the anatomical axis of the first, second, and proximal phalanges as described previously (12, 13). The angle defined by the angle between the longitudinal axis of the first meta bone and the proximal phalanx of the thumb toe represents HVA (valgus valgus angle), usually 10–15°. The angle determined by the intersection of the longitudinal axis of the first and second meta bones is IMA. This value is usually 7-9°. The angle between the effective joint surface of the first proximal phalanx and the longitudinal axis of the first proximal phalanx represents DASA (distal joint angle), usually 8°. The angle between the effective joint surface and the longitudinal axis of the first meta bone represents PASA (proximal angle), usually < 10° (Fig. 1)

Immunohistochemical analysis

Specimens including soft tissues were used for histological and immunochemical studies (Fig. 2). The samples were immersed in formalin (4%; pH 7.4) for 24 h. Samples up to 1.5 cm thick were embedded in paraffin. The block was cut into 5 μm thick slices on a standard microtome. Sections were attached to polylysine-coated glass slides. Subsequently, the slides were immersed in continuous ethanol and immersed in 3% H_2O_2 for 30 min to inhibit all endogenous peroxidase activity. Immunohistochemical studies of polyclonal anti-human and rabbit VDR antigens (Abcam plc., Cambridge, MA, USA) were performed in a room-temperature humidity cabinet. Subsequently, the secondary biotinylated antibody and peroxidase complex were applied for 30 min each,

respectively. Finally, 0.07% diaminobenzidine (DAB) and 0.03% hydrogen peroxide were mixed until the sections were light brown. Different cells had different staining intensities, which is apparently due to the localization of the antigen near the cell membrane. However, it was easy to separate stained and unstained cells (14).

Genotyping

Genomic DNA was isolated from whole blood according to standard procedures and processed within 1 h. Analysis of VDR polymorphic sites (rs1544410) was performed using specific oligonucleotide primers (Fig. 3). PCR amplification was performed in an automatic thermal cycler. Polymorphic sites were amplified using specially designed primers for the first 5'-CTGTGGTGTGTGGACGCTGA-3' and the last 5'-GCCCCTCTTTGGACCTCATT-3' (Table I). The PCR reaction was performed under the conditions of a total volume of 50 μL, containing 0.1-0.5 mg of genomic DNA, 8 mm dNTP, 2-3 mm $MgCl_2$, and 2 U Taq-DNA polymerase, and then denatured at 94°C for 45 s, annealed at 56°C for 45 s, and extended at 72°C 45s. Finally, it was extended at 72°C for 5 min. Then, 6 ml of the amplified product was digested with BsmI restriction enzyme (New England Biolabs Inc., MA, USA) (65°C, 15 min). All digestion products were loaded using 1.5% agarose gel electrophoresis and ethidium bromide respectively, and electrophoresed at 100 V for 30 min, and then observed by UV transmission. The protocol details were reported previously (15, 16). A 100 bp DNA ladder (Keygentec Inc., Nanjing, China) was used to estimate the size of the fragment. The genotype was identified according to the presence or absence of the BsmI site as follows: BB = 358 bp (GG); Bb = 358 bp and 193 bp (GA); bb = 193 bp and 165 bp lengths (AA) respectively; b was the mutation allele (Fig. 3).

Evaluation procedure

Visual analogue score (VAS) was recorded before (admission day) and post-operation (3-month follow-up). VAS includes a horizontal line with a length of 100 mm (100 points): no pain (0-4 points); mild pain (less than 30 points); moderate pain (40-60 points); severe pain (70-100 points) (17). All patients were interviewed and scored according to the American Orthopedic Foot and Ankle Association (AOFAS) score before (admission day) and post-surgery (at 3-month follow-up) (18). VAS scale and AOFAS scores (3 years before surgery) were collected by patient recalls, with radiograph and related measurement data to illustrate progress of disorders.

Statistical analysis

Hardy-Weinberg balanced SNP was tested in the patient group and the control group. χ^2 test was used to compare the laboratory data of patients and control group. Differences between two groups were analyzed by using the Student's *t*-test. Comparison between multiple groups was made using One-way ANOVA test followed by Post Hoc Test (Least Significant Difference). Multiple logistic regression analysis was used to assess whether each polymorphism was independently associated with HV and to adjust for potential confounding effects of important clinical variables. The odds ratio (OR) and 95% confidence interval (CI) were calculated. Receiver operating characteristic curve (ROC) analysis was used to determine whether BsmI polymorphism could distinguish HV subjects from control group. Statistical significance was defined at the 5% ($p \leq 0.05$) level. Statistical Product and Service Solutions (SPSS) software s used for all analysis (SPSS, version 16.0, SPSS Inc., Chicago, IL, USA).

RESULTS

Fig. 1 shows the X-ray of the left metatarsal bone of HV patients in this study; (A) HV angle (HVA), (B) distal joint angle (DASA), (B) proximal joint angle (PASA) (D) Intermediate angle (IMA).

Fig. 2 illustrates immunohistochemical analysis of bunion tissue staining of vitamin D receptor (VDR) (Fig. 2). The bunion is composed of soft, fibrous tissue, and nuclear receptors are positive (Fig. 2A). The bunion demonstrated a trend towards increased staining for VDR (Fig. 2B). However, in the control group there were few positive cells as negative controls (Fig. 2C). These cells do not secrete much VDR. Moreover, soft tissue overlying the bunion without loading secondary antibody was also found to be negative (Fig. 2D), indicating that staining was reliable and unbiased.

Fig. 3 shows the VDR polymorphism genotypes analyzed by PCR-RFLP and then isolated on a 1.5%

agarose gel; Lane 1: molecular weight size marker (100 bp DNA ladder). Lanes 2-4 restriction BsmI enzyme digestion: lane 2 = BB (358 bp fragment, GG), lane 3 = Bb (358 bp and 193 bp fragments, GA), lane4 = bb (193 bp and 165 bp fragments, AA), respectively.

The VDR single nucleotide frequencies selected by patients and controls are shown in Table II. The distribution of the selected SNPs in the control group and HV patients was consistent with the expected distribution of Hardy-Weinberg equilibrium (P>0.05), indicating that the selection of the analysis

Table I. *PCR-RFLP premiers and conditions for VDR gene polymorphism.*

Gene	Role	Polymorphism analyzed	rs Number	Primer	Tm (℃)	RE
VDR	Vitamin D receptor	Bsm I (G/A)	1544410	5'-AGCTGGCCCTGGCACTGCTCTGCTCT-3' 5'-ATGGAAACACCTTGCTTCTTCTCCCTC-3'	65	BsmI

VDR: Vitamin D receptor gene; RE: restriction endonuclease

Table II. *Frequencies of selected VDR SNPs in the study population.*

Group	Total no.	Genotype (% distribution)			Allele frequency (% distribution)	HWE	
		Bsm I BB	*Bsm I* Bb	*Bsm I* bb	Allele B	χ^2	P[a]
Patients	80	13(16)	29(36)	38(48)	55(34)	3.09	0.08
Controls	80	55(69)	20(25)	5(6)	130(81)	2.58	0.11

[a] *P ≤0.05 (not consistent with HWE)*

Table III. *Demographic and clinical data, Mean±SD.*

		Age	Female n(%)	N
	Patients	61.06±11.32	70(87.5)	80
	Controls	40.51±16.72	54(67.5)	80
HVA of Patients	Mild (15-20 degrees)	60.22±9.85	7(77.8)	9
	Moderate (21-39 degrees)	60.98±12.03	53(91.4)	58
	Severev (40 degrees)	62.08±9.50	10(76.9)	13
	P[a]	0.00**	0.00**	-
	P[b]	0.553	0.234	-

*** Statistically significant differences at P≤0.01. [a] Pearson's chi-squared test was used between patients and controls. [b] t-test was used among three groups (mild, moderate, severe). HVA: hallux valgus angle*

Table IV. *Individual genotype and allele χ^2 value, p value, odds ratio, 95% confidence interval for VDR Bsm I*

Gene Polymorphism	Genotype & Allele	Frequency of Genotypes and Alleles (% distribution)		Logistic Regression			
		Patients N=80	Controls N=80	χ^2	P[a]	OR[a]	95% CI
VDR BsmI	BB	13(16)	55(69)	43.34	0.00**	0.14	0.05-0.39
	Bb	29(36)	20(25)			0.17	0.05-0.65
	bb	38(48)	5(6)			5.88	1.54-22.35
	B	55(34)	130(81)	55.21	0.00**	0.10	0.05-0.20
	b	105(66)	30(19)			9.62	4.99-18.54

*** Statistically significant differences at P < 0.01. [a] Values adjusted for age using logistic regression*

group was correct. Subject characteristics including demographic and clinical data are presented in Table III. There were significant differences between patients and controls for age and gender (female). The age of patients with HV was higher than that of controls (61.06±11.32 and 40.51±16.72, respectively, P<0.01). A large component of the excess risk factors are associated with HV in women (P<0.01).

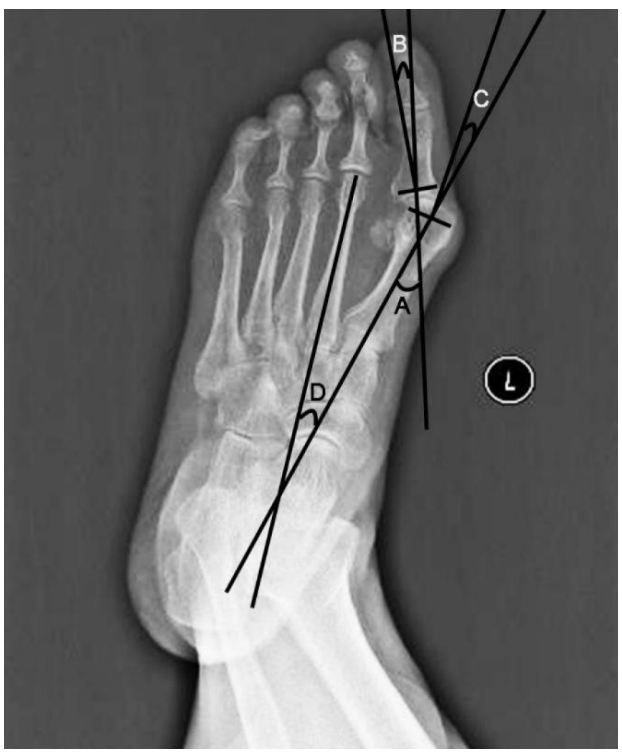

Fig. 1. *Preoperative X-ray shows the angle of measurement. **A)** HVA (hallux valgus angle). **B)** DASA (distal articular set angle). **C)** PASA (proximal articular set angle). **D)** IMA (intermetatarsal angle).*

Together, these findings revealed that middle-aged and elderly females may be susceptible to HV. When we classified the patient data according to HV angles, we find there were no significant differences among the mild, moderate and severe groups regarding age and gender.

Individual genotype and allele χ^2 value, *p*-value, odds ratio, 95% confidence interval were calculated for both groups separately (Table IV). The frequency of mutation genotype of VDR (bb gene) was significantly higher in HV cases than the controls. Nearly half of the HV cases carried the mutation genotype bb compared to 6% of the controls (OR = 5.88, 95 % CI 1.54-22.35). Thirty-six percent (36%) of the cases carried the mutation genotype Bb compared to that in 25% of the controls (OR = 0.17, 95%CI 0.05-0.65). The BB genotype seems to be protective for HV with a marked significant difference between the cases (13/80, 16%) and the controls (55/80, 69%) (OR = 0.14, 95% CI 0.05-0.39). The frequency of B allele in the cases was 34% (55/160) and in the controls 81% (130/160) (P <0.001). The value of OR was 0.10 (95% CI 0.05-0.20). However, the bb genotype illustrated a risk role (OR = 5.88, 95% CI 1.54-22.35, P <0.001). The frequency of b allele in the cases was 66% (105/160) and in the controls 19% (30/160) (P=0.002). The value of OR was 9.62 (95% CI 4.99-18.54). This locus seems to show a specific variation, and it may serve as a useful bio-marker for the disease.

We further performed ROC analysis to determine serotypes as a biomarker to distinguish HV subjects from controls. We found that the genotype at the

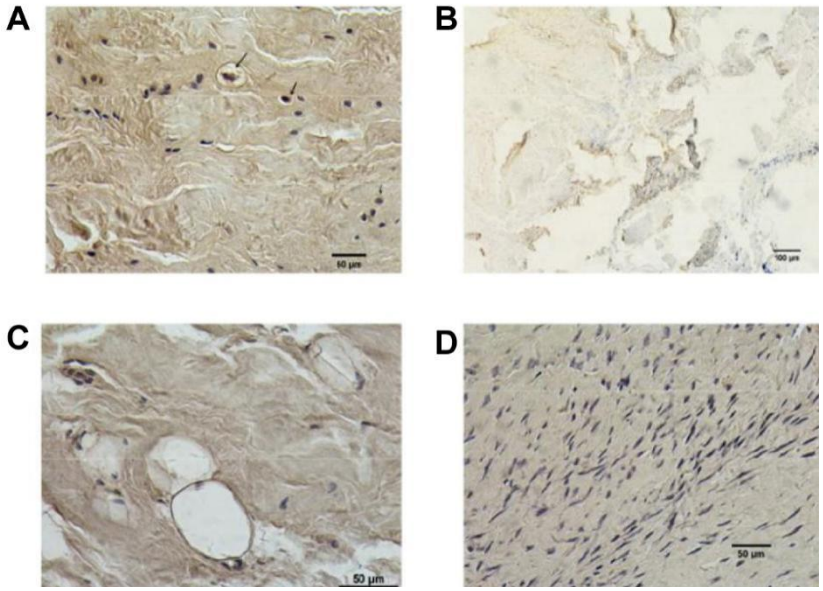

Fig. 2. *Photomicrograph of immunohistochemical staining of vitamin D receptor (VDR).* ***A****) Nuclear receptors are positive (VDR antibody, DAB stain; original magnification, 400x).* ***B****) Soft tissue overlying the bunion is positive (VDR antibody, DAB stain; original magnification, 200x).* ***C****) VDR is negative in the soft tissue of the control group (VDR antibody, DAB stain; original magnification, 400x).* ***D****) Soft tissue overlying the bunion without second antibody (VDR antibody, DAB stain; original magnification, 400x).*

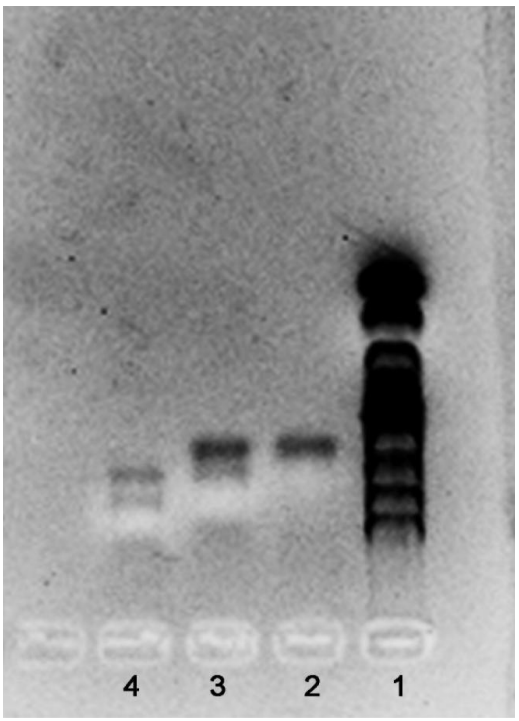

Fig. 3. *1.5% agarose gel electrophoresis of the allele-specific PCR products. Lane 1: Molecular weight marker (100 bp DNA ladder). Lanes 2-4 restriction BsmI enzyme digestion: lane 2 = BB (358 bp fragment), lane 3 = Bb (358 bp, 193 bp fragments), lane4 = bb (193 bp and 165 bp fragments), respectively.*

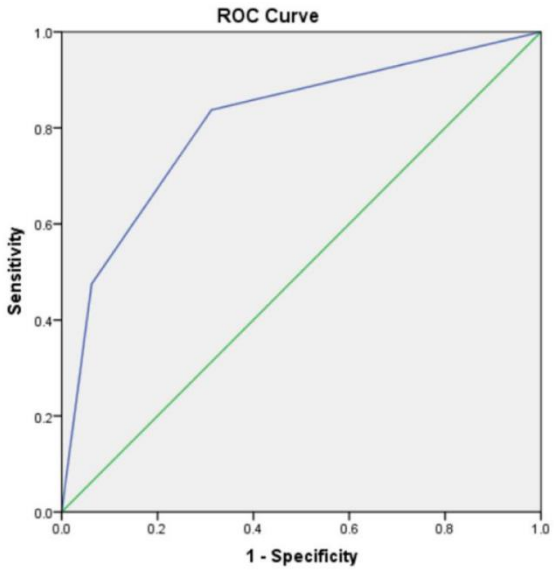

Fig. 4. *ROC analysis of genotype differentiation between HV and control group. AUC=0.811, P <0.01.*

critical point of Bb (Ff) distinguished HV subjects from control groups (area under curve=0.811, P<0.01, sensitivity=83.8% and specificity=31.3%) (Fig. 4).

Post-operative groups resulted in significant improvements in all of the measured radiographic parameters compared with pre-operative groups (Fig. 5). It seems that the effect of surgery on the three SNPs groups was almost consistently positive. The pre-operative HVA was lower in the BB group than that in Bb+bb groups (19.2 degrees *vs* 25.6+29.3 degrees, P<0.001) (Fig. 5A). The pre-operative DASA, PASA and IMA in the BB group were higher than those in Bb+bb groups (13.3 degrees *vs* 10.50+8.96 degrees and 19.2 degrees *vs* 9.80+11.60 degrees, P<0.001) (Fig. 5 B-D). Angles of patients with b allele in pre-operative groups were more severe than those with B allele in the post-operative groups (P<0.001). However, angles were not significantly different among the three genotype groups post-operatively. Post-operative groups resulted in significant improvements in VAS scale and AOFAS scores compared with pre-operative groups (P<0.01). The post-operative VAS scale was lower than that in pre-operative groups (P<0.01), while the post-operative AOFAS scores were higher than that in post-operative groups (P<0.01) (Fig. 5 E, F). Graphical illustration for pain *via* VAS scale and AOFAS scores demonstrated steady and significant improvement at each follow-up.

Moreover, progress of HV (pre-operative) for three gene polymorphisms are illustrated in Fig. 6. Duration of HV pre-operative development influenced VAS scale and AOFAS scores. Subjects with bb genotype showed lower VAS scale and AOFAS scores compared to other groups. During the first post-operative year, subjects with bb

genotype had lower scores (VAS scale 3.49-2.85, AOFAS scores 56.3-52.8), while in the pre-operative 3rd year, VAS scale and AOFAS scores of BB polymorphism carriers were slightly higher compared to other groups.

DISCUSSION

To our knowledge, these findings establish for the first time that vitamin D receptor gene polymorphism (BsmI) has a potentially protective effect on HV. To clarify the effect of BsmI on HV, we performed several molecular-biological and epidemiological experiments, and detected that the VDR polymorphism plays an important role in the onset and development of HV. Our results show that the BsmI gene polymorphisms may be formed as a potential marker for prediction of HV onset and development.

Bunions are composed of soft, fibrous tissue. Our immunohistochemical analysis of bunion tissue staining of vitamin D receptor showed that nuclear receptors are positive. The bunions demonstrated a trend towards increased staining for VDR, while the negative control group did not secrete much VDR. This illustrated that vitamin D receptor gene was highly expressed in the soft tissue and fibrous tissue of bunion**.** There were significant differences between patients and controls regarding age and gender, suggesting that females aged approximately 61 years may be susceptible to HV. We calculated individual odds ratio, 95% confidence interval for patients and controls and found that the B allele seems to be protective for HV while the b allele

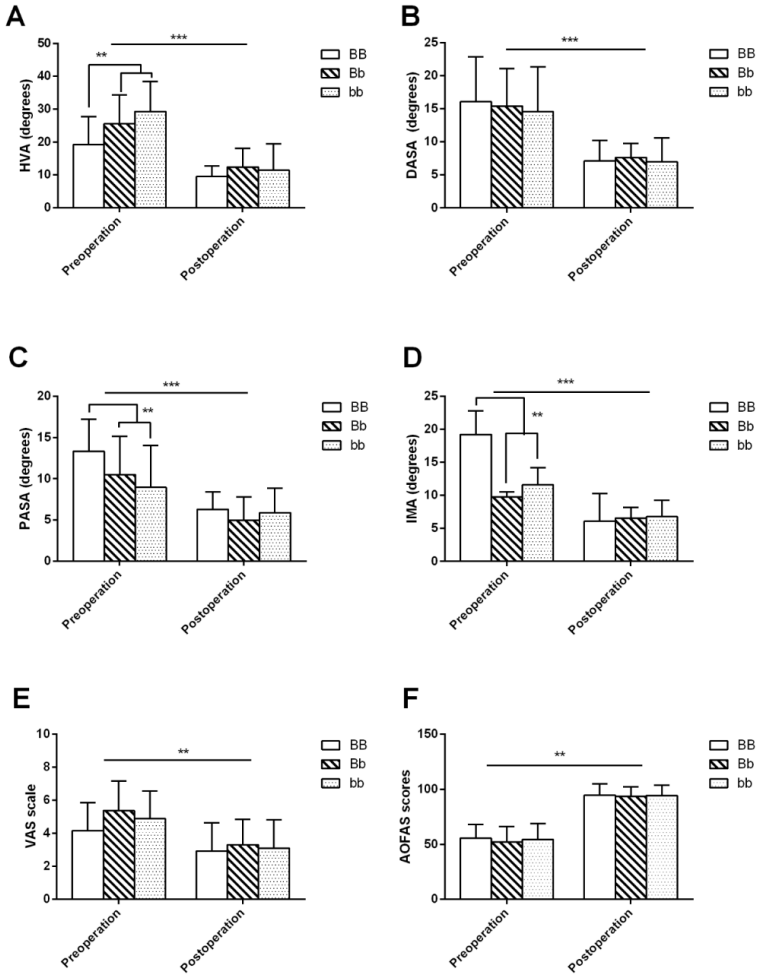

Fig. 5. *Pre-operative and post-operative radiographic parameters, VAS scale and AOFAS scores for VDR polymorphisms. ** P < 0.01. ***P < 0.001.*

illustrated a risk role. It indicated that b allele may serve as a useful bio-marker for HV. ROC analysis was then carried out and proved that b allele was a potential bio-marker to predict onset and development of HV. The BsmI polymorphism cannot affect post-operative results and can achieve similar efficacy, but VAS scale and AOFAS scores of bb genotype carriers were slightly lower compared to other groups, which showed that development of bb carriers was faster and more serious.

Our immunohistochemical analyses are consistent with Norlin et al. (19) who demonstrated that fibroblasts have an active vitamin D3 metabolizing system. Vitamin D hormone activity is mainly due to the hydroxylated metabolites of vitamin D3,1-α, 25-dihydroxyvitamin D3. Vitamin D receptor is an intracellular hormone receptor that specifically binds and mediates 1,25 (OH) $_2D_3$. Our findings on the risk of HV in middle-aged and older women are consistent with those of Katsui et al. (20) and Uritani et al. (21), who found females at the mean age of 60 years have more probability to suffer HV. Many females suffered HV for a long time, due to wearing unsuitable fashionable shoes, and went to the clinic for unbearable pain and deformation (22). A similar observation in Korea has been documented for the relative importance of genetics on HV (10). Our study not only found that genetic factors play an important role in determining HV deformity, but showed that BsmI polymorphism of VDR may be a potential bio-

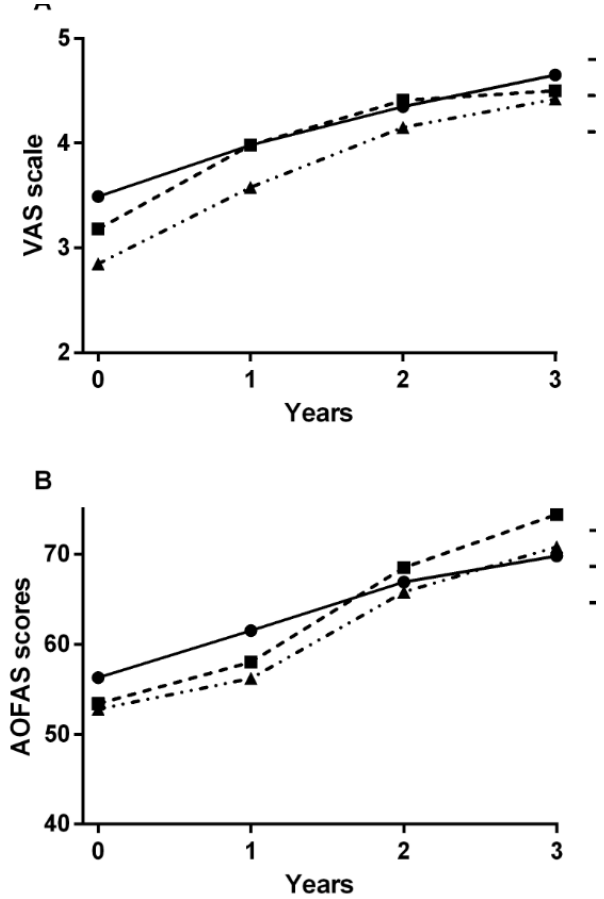

Fig. 6. *VAS scale, AOFAS scores and progress of HV (pre-operative) for three gene polymorphisms.*

marker of HV. Although considered highly heritable, the candidate genes are unclear. Only several case reports have reported genetic mutation associated with HV, such as HOXA13, hENT3 (23, 24). Recently, a genome-wide meta-analysis reported genetic mutations associated with HV in white and African Americans, identifying genetic variants of HV and underlying pathophysiological mechanisms (11). The authors found that HV was gender-specific, and had a strong genetic predisposition. In our research, we also found HV were gender-specific. However, unlike Hsu et al. (11), we observed that HV was associated with VDR BsmI polymorphism and b allele may be a risk role. On the one hand, they make a meta-analyze in Caucasian and African Americans without stringent P-value cut-off while we made clinical research in a Chinese cohort, which is a different ethnic and research type. On the other hand, more HV populations and more genetic research may be helpful. It is generally believed that we can use VAS scale and AOFAS score to assess patients' pre-operative and post-operative conditions of HV (17, 18). Our findings support the interpretation that post-operative groups resulted in significant improvements in all of the measured radiographic parameters compared with pre-operative groups. Since no one reported association between polymorphisms and efficacy of HV osteotomy, we first found that BsmI genotypes cannot affect post-operative results and achieve the similar efficacy.

We demonstrate for the first time that VDR polymorphism (BsmI) is associated with onset and development of HV, and b allele can be a potential bio-marker to predict HV. The major strength of this study was that we analyzed polymorphisms statistically with stringent P-value cut-off, which may help clinicians and researchers to screen for high-risk individuals and choose an innovative therapeutic option to prevent or slow down the progression of HV.

However, additional data and a larger multicenter study are necessary to shed more light on this issue and eliminate possible single center bias. Further research is needed to determine the exact mechanisms responsible for the associations between genetic polymorphisms and HV.

These data together prove that VDR polymorphisms play an important role in the occurrence and development of HV. Middle-aged and elderly females may be at more risk of suffering HV. The BB genotype seems to be protective for HV while the bb genotype illustrated a risk role. Post-operative groups resulted in significant improvements in all of the measured radiographic parameters compared with pre-operative groups, but three genotype groups cannot affect post-operative results and can achieve similar efficacy.

In conclusion, according to VAS scale and AOFAS scores, progress of bb polymorphism carriers was faster and the condition was more serious compared to BB carriers. The BsmI gene polymorphisms of VDR may thus be used as a potential bio-marker for prediction of HV onset and development. Moreover,

early diagnosis of HV in middle-aged and elderly females plays a very important role in preventing and slowing down the progress of disease. The study of a greater HV cohort and more candidate genes may provide further insight into the etiology of the disease.

REFERENCES

1. Geng X, Wang C, Ma X, et al. Mobility of the first metatarsal-cuneiform joint in patients with and without hallux valgus: in vivo three-dimensional analysis using computerized tomography scan. J Orthop Surg Res 2015; 10:140.
2. Nix S, Smith M, Vicenzino B. Prevalence of hallux valgus in the general population: a systematic review and meta-analysis. J Foot Ankle Res 2010; 3:21.
3. Hurn SE, Vicenzino BT, Smith MD. Non-surgical treatment of hallux valgus: a current practice survey of Australian podiatrists. J Foot Ankle Res 2016; 9:16.
4. Chen JY, Lee MJ, Rikhraj K, et al. Effect of obesity on outcome of hallux valgus surgery. Foot Ankle Int 2015; 36:1078-83.
5. Szymczak I, Pawliczak R. The active metabolite of vitamin D3 as a potential immunomodulator. Scand J Immunol 2016; 83:83-91.
6. van der Meijden K, Bakker AD, van Essen HW, Heijboer AC, Schulten EA, Lips P, Bravenboer N. Mechanical loading and the synthesis of 1,25(OH)2D in primary human osteoblasts. J Steroid Biochem Mol Biol 2016; 156:32-39.
7. Okuda H, Juman S, Ueda A, Miki T, Shima M. Factors related to prevalence of hallux valgus in female university students: a cross-sectional study. J Epidemiol 2014; 24:200-208.
8. Nery C, Coughlin MJ, Baumfeld D, Ballerini FJ, Kobata S. Hallux valgus in males--part 2: radiographic assessment of surgical treatment. Foot Ankle Int 2013; 34:636-44.
9. Ramagopalan SV, Heger A, Berlanga AJ, et al. A ChIP-seq defined genome-wide map of vitamin D receptor binding: associations with disease and evolution. Genome Res 2010; 20:1352-60.
10. Lee CH, Lee S, Kang H, et al. Genetic influences on hallux valgus in Koreans: the healthy twin study. Twin Res Hum Genet 2014; 17:121-26.
11. Hsu YH, Liu Y, Hannan MT, et al. Genome-wide association meta-analyses to identify common genetic variants associated with hallux valgus in Caucasian and African Americans. J Med Genet 2015; 52:762-69.
12. Scharer BM, DeVries JG. Comparison of chevron and distal oblique osteotomy for bunion correction. J Foot Ankle Surg 2016; 55:738-42.
13. Brogan K, Lindisfarne E, Akehurst H, Farook U, Shrier W, Palmer S. Minimally invasive and open distal chevron osteotomy for mild to moderate hallux valgus. Foot Ankle Int 2016; 37:1197-204.
14. Lim YY, Kim SY, Kim HM, Li KS, Kim MN, Park KC, Kim BJ. Potential relationship between the canonical Wnt signalling pathway and expression of the vitamin D receptor in alopecia. Clin Exp Dermatol 2014; 39:368-75.
15. Colombini A, Brayda-Bruno M, Lombardi G, et al. FokI polymorphism in the vitamin D receptor gene (VDR) and its association with lumbar spine pathologies in the Italian population: a case-control study. Plos One 2014; 9:e97027.
16. Ozel L, Ata P, Ozel MS, et al. Risk factors for osteoporosis after renal transplantation and effect of vitamin D receptor Bsm I polymorphism. Transplant Proc 2011; 43:858-62.
17. Mahadevan D, Lines S, Hepple S, Winson I, Harries W. Extended plantar limb (modified) chevron osteotomy versus scarf osteotomy for hallux valgus correction: A randomised controlled trial. Foot Ankle Surg 2016; 22:109-13.
18. Kovacs D, Eszlari N, Petschner P, et al. Interleukin-6 promoter polymorphism interacts with pain and life stress influencing depression phenotypes. J Neural Transm (Vienna) 2016; 123:541-48.
19. Norlin M, Lundqvist J, Ellfolk M, Hellstrom PM, Gustafsson J, Wikvall K. Drug-mediated gene regulation of vitamin D3 metabolism in primary human dermal fibroblasts. Basic Clin Pharmacol Toxicol 2017; 120:59-63.
20. Katsui R, Samoto N, Taniguchi A, Akahane M, Isomoto S, Sugimoto K, Tanaka Y. Relationship between displacement and degenerative changes of the sesamoids in hallux valgus. Foot Ankle Int 2016; 37:1303-9.
21. Uritani D, Fukumoto T, Matsumoto D, Shima M. Associations between toe grip strength and hallux

valgus, toe curl ability, and foot arch height in Japanese adults aged 20 to 79 years: a cross-sectional study. J Foot Ankle Res 2015; 8:18.

22. Formosa C, Gatt A, Chockalingam N. The importance of clinical biomechanical assessment of foot deformity and joint mobility in people living with type-2 diabetes within a primary care setting. Prim Care Diabetes 2013; 7:45-50.
23. Molho-Pessach V, Lerer I, Abeliovich D, et al. The H syndrome is caused by mutations in the nucleoside transporter hENT3. Am J Hum Genet 2008; 83:529-34.
24. Parker L, Mangwani J, Wakeling E, Singh D. Hallux valgus interphalangeus and a novel mutation in HOXA13. Part of the broadening spectrum of hand-foot-genital syndrome. Foot Ankle Surg 2011; 17:e28-e30.

miR-382-3p Overexpression attenuates N-methyl-D-aspartate-induced HT22 cell apoptosis via the regulation of the RhoC/ROCK1 signaling pathway

L-M. Zhang[1,2*], Q-Y. Zhu[1*], L. Chen[2], X-Q. Tang[3], Y-F. Zou[3], P. Lv[3], M-W. Liu[3] and Y-F. Du[2]

[1]Institute of Primate Translational Medicine, Kunming University of Science and Technology, Wuhua District, Kunming, China; [2]Department of Neurology, the First Affiliated Hospital of Kunming Medical University, Wuhua District, Kunming, China; [3]Department of Emergency Medicine, the First Affiliated Hospital of Kunming Medical University, Kunming, China

Received April 24, 2020 – Accepted July 13, 2020

[*]These Authors contributed equally to this work

miR-382-3p can regulate apoptosis through multiple pathways, but the mechanism remains unknown. In this experiment, we explored whether miR-382-3p can modulate the N-methyL-D-aspartate (NMDA)-induced HT22 cell apoptosis by regulating the RhoC/ROCK1 signaling pathway. An excitatory neurotoxicity model of HT22 cells was induced *in vitro* with 2 mmol/L NMDA. The cells were divided into normal control, NMDA-induced, NMDA + miR-382-3p mimic, and NMDA + miR-382-3p inhibitor groups. The 3-(4,5)-dimethylthiahiazo (-z-y1)-3,5-di-phenytetrazoliumromide (MTT) method, Real-time PCR, Western blot, and flow cytometry were performed to investigate the mechanisms. The results found that NMDA can increase the oxidative stress of HT22 cells in a dose-dependent manner, downregulate the expression of miR-382-3p, upregulate the expression of mRNA and protein abundance of ROCK1 and RhoC, increase the expression levels of proapoptotic proteins Bax, Caspase-3, and Caspase-9, increase the apoptosis of HT22 cells, and reduce the activity and survival rate of HT22 cells. Compared with the NMDA-induced group, the miR-382-3p mimic-transfected HT22 cells increased the expression of miR-382-3p, reduced the expression of the mRNA and protein abundance of ROCK1 and RhoC, inhibited the expression of proapoptotic proteins Bax, Caspase-3, and Caspase-9, reduced the apoptosis of HT22 cells, and increased the activity and survival rate of HT22 cells. The results suggest that increasing the expression of miR-382-3p can inhibit the activity of the RhoC/ROCK1 signaling pathway, reduce the expression of proapoptotic proteins, reduce the oxidative stress and apoptosis of HT22 cells, and increase the activity and survival rate of HT22 cells.

Epilepsy (EP), a neuropsychiatric disease that is emphatically prevented and treated in the current world, is a chronic central nervous system dysfunction syndrome caused by the abnormal discharge of brain neurons (1, 2). The long-term and frequent seizure of EP restricts the physical, mental, and intellectual health of patients (1, 2). Epileptic seizure is an overexcitation of neurons and accumulation of excessive free radicals. Studies have shown that epileptic seizure can cause oxidative damage and apoptosis and reduced

Key words: miR-382-3p; N-methyl-D-aspartate; HT22 cells; ROCK1

Corresponding Author:
Dr Ming-wei Liu,
Department of Emergency Medicine,
the First Affiliated Hospital of Kunming Medical University,
245 Xichang Road, Wuhua District,
Kunming, 650032, China
e-mail: lmw2004210@163.com

0393-974X (2020)
Copyright © by BIOLIFE, s.a.s.
This publication and/or article is for individual use only and may not be further reproduced without written permission from the copyright holder.
Unauthorized reproduction may result in financial and other penalties
DISCLOSURE: ALL AUTHORS REPORT NO CONFLICTS OF INTEREST RELEVANT TO THIS ARTICLE.

antioxidant capacity in the brain (3). The increased susceptibility of the brain to oxidative damage further demonstrates the importance of oxidative stress and apoptosis in the pathophysiology of EP (4, 5). Numerous oxygen free radicals are generated during the onset of EP. The delayed removal of these radicals can lead to a high level of oxidative reaction and disturb the energy metabolism of local nerve cells. As a result, a suitable environment can be created for nerve cell apoptosis, and the apoptosis of neurons can be aggravated. Studies have shown that neuronal apoptosis in the hippocampus, amygdala, cerebral cortex, thalamus, cerebellum, and other parts remarkably increase after epileptic seizures. Particularly, the apoptotic cells in the hippocampal CA3 and the CA1 regions have the largest number in 24 h and last for more than three weeks (4).

Glutamate, the most abundant excitatory neurotransmitter in the brain, is closely related to the pathogenesis of EP. Studies have found that the release of glutamate can lead to the apoptosis of neurons (6). The release of presynaptic glutamic acid triggers the activation of the postsynaptic NMDA receptor, thereby leading to a large influx of calcium ions and triggering the cascade of apoptosis (7). Studies have shown that the usage of the antagonists of NMDA receptor can significantly inhibit the neuronal apoptosis induced by EP and has neuroprotective effects (8, 9).

The Rho subfamily proteins play various biological functions through a series of downstream effector molecules. The Rho-associated coiled coil-containing protein kinase (ROCK) 1 is one of the most important downstream effector molecules. RhoA and its downstream effector ROCK can control and regulate the dynamics of the cytoskeleton. Moreover, ROCK1 is an important signal transduction system and molecular switch in organisms due to its involvement in life activities, such as cell contraction, movement, proliferation, apoptosis, and gene expression (10). In nerve cells, RhoA/ROCK is closely related to nerve cell migration, dendritic development, and axon extension. RhoA activation can induce growth cone collapse, prevent axon elongation, and cause the apoptosis of neurons and glial cells (11). Therefore, the RhoA/ROCK pathway plays an important role in the occurrence and development of EP. Studies have shown that the expression of RhoA protein in rats is increased by ischemia–reperfusion to promote ROCK1 protein expression, neural axis growth and neural function repair; increase the neuronal apoptosis; aggravate neurological damage; inhibit the RhoA expression; and reduce the ROCK1 protein expression and neuronal apoptosis (12).

miRNAs consist of a class of small noncoding RNAs that control the expression of the complementary target messenger RNAs (13). In vertebrates, miRNAs are significantly more expressed in the brain than in other organs. miRNAs, which are expressed during the embryonic and developmental maturity stages, are involved in various physiological and pathological processes that determine the fate of cells, providing clues for the further study of their roles in the development of the nervous system and in various diseases (13). miRNAs are conserved in evolution and can bind to the target gene at the 3′-UTR to inhibit the translation or degradation of the target gene (14). According to studies, miRNAs are involved in cell proliferation, differentiation, and apoptosis and are closely related to the occurrence and development of diseases, such as EP and cerebral infarction. Other studies found that overexpression of the miR-29 family inhibited the OGD/R-induced elevation of ROS and reduction of MMP in HT-22 cells (15), downregulation of miR-212-5p promoted ferroptotic cell death partially by targeting prostaglandin-endoperoxide synthase-2 (Ptgs2) in HT-22 and Neuro-2a cell lines (16). Moreover, miRNAs have important roles in EP, Parkinson's disease, and cerebral infarction (13-17).

miR-382-5p is highly expressed in tissues and cell lines with breast cancer. *In- vitro* and *in-vivo* experiments have found that miR-382-5p can inhibit breast cancer cell apoptosis by regulating the RERG/Ras/ERK signaling axis and promote the vitality, survival rate, migration, invasion and tumorigenesis, and metastasis of breast cancer cells (18). miR-382 can inhibit the metastasis of ovarian cancer cells by regulating ROCK (19) and regulate the occurrence and development of gliomas by regulating the expression of the cancer-promoting SETD8 (20). In the present study, the TargetScan prediction has suggested that ROCK1 may be a regulatory target of mir-382-

3p. Therefore, the possible inhibitions of the Rho/ROCK1 signal transduction pathway, the expression of proapoptotc proteins, the oxidative stress of EP, and the NMDA-induced HT22 cell apoptosis *in vitro* were investigated. Such inhibitions are conducive in controlling or reducing the incidence of EP by promoting the expression of miR-382-3p.

MATERIALS AND METHODS

Cell culture

Human neuroma cell line HT22 was provided by the Medical Experiment Department of the Guangzhou General Hospital of Guangzhou Military Region. The HT22 cells were collected from the cell bank, quickly thawed, transferred to a centrifuge tube on a clean bench, added with an appropriate amount of freshly prepared medium, and centrifuged. The sediment was collected. Then, the HT22 cells were added with fresh medium and cultured in DMEM culture medium containing 10% fetal calf serum, 100 U/mL penicillin, and 100 μg/mL streptomycin. The cells were routinely placed in a humidification incubator at 37°C containing 5% CO_2 and 95% air. The logarithmic growth phase cells were used in experiments. To observe the effects of NMDA on HT22 cell activity, apoptosis, and survival rate, as previously described (21, 22), we added different concentrations of NMDA (0.5, 1, 2, 3, and 5 mmol/L) to the 24 h cell culture. Subsequently, various related indicators were measured.

Cell transfection

An appropriate amount of HT22 cells in the logarithmic growth phase was collected and inoculated into a 6-well plate. When the cells adhered to the wall overnight and grew to 60%, miR-382-3p mimic, miR-382-3p inhibitor, mimic control, and inhibitor control were transfected into the HT22 cells following the instructions on the Lipofectamine 2000 transfection reagent. The transfection concentration was 50 nmol/L. After 6 h transfection, the medium was replaced with fresh medium and cultured for 24 h. The cells were collected for PT-PCR and Western blot detection.

Detection of cell proliferation using the MTT assay

The cells in logarithmic growth phase were inoculated into a 96-well plate at a volume of 100 μL cells/well and cell density of 5×10^7/L. The cells were cultured in a 5% CO_2 incubator to make them adhere to the wall. Before dosing the next day, the old medium was removed, and five duplicate wells were set for each group. In the experimental group, different concentrations of NMDA (0.5, 1, 2, 3, and 5 mmol/L), mir-382-3p mimic, or mir-382-3p inhibitor were added to each well at 100 L. In the blank group, no cell was observed, and only the medium was added, whereas in the control group, only the same medium was added. After dosing, the cells were cultured into 96-well plates for 24 h, added with 20 μL MTT solution (5 g/L), and cultured for 4 h. Then, the supernatant was discarded. DMSO (150 μL) was added to each well. The wells were shaken to dissolve the crystals. Finally, the cell absorbance (A) was detected at the wavelength of 490 nm.

Detection of cell viability with CCK-8 assay

The cells in logarithmic growth phase were inoculated into a 96-well plate at a volume of 100 μL cells/well and cell density of 5×10^7/L. The cells were cultured in a 5% CO_2 incubator to make the cells adhere to the wall. Before dosing the next day, the old medium was removed, and five duplicate wells were set for each group. In the experimental group, different concentrations of NMDA (0.5, 1, 2, 3, and 5 mmol/L), mir-382-3p mimic, or mir-382-3p inhibitor were added to each well at 100 L. In the blank group, no cells were observed, and only the medium was added, whereas in the control group, only the same medium was added. After dosing, the cells were cultured into 96-well plates for 24 h, added with 20 μL CKK-8 solution (5 g/L), and cultured at 37°C for 1 h. Then, the culture was terminated. The blank hole was set as zero. The OD value of each hole was detected at the wavelength of 450 nm after 3 min of oscillation on the microplate reader. The cell activity was recorded and calculated.

Detection of cell apoptosis

HT22 cells were inoculated into 6-well culture plates. Different concentrations of NMDA (0.5, 1, 2, 3, and 5 mmol/L), miR-382-3p mimic, or miR-382-3p inhibitor were added. The cells were collected, washed thrice with PBS, centrifuged at 1200 r/min for 5 min, and added with 200 μL 1×Binding buffer to resuspend the cells. Then, the cells were added with 5 μL Annexin V–EGFP and mixed well and with 5 μL Propidium iodide (PI) and mixed well. The reaction was conducted at room temperature and kept in the dark for 15 min. Cell apoptosis was detected

by flow cytometry. The excitation (Ex) and the emission (Em) wavelengths were 488 and 530 nm, respectively. The green fluorescence of Annexin V–EGFP was detected using the FITC channel, whereas the red fluorescence of PI was detected using the PI channel.

Detection of intracellular ROS levels

DCFH-DA was diluted in serum-free DMEM/F12 medium to a final concentration of 10 μmol/L. After the cell culture was completed, the culture solution was discarded, and each well was added with 100 μL diluted DCFH-DA and incubated in a CO_2 incubator at 37°C for 20 min. The cells were washed thrice with serum-free DMEM/F12 medium to remove DCFH-DA that had not entered the cells while being careful not to aspirate the cells. The detection was performed using flow cytometry, and the Ex and Em were 488 and 525 nm, respectively. The fluorescence intensities before and after drug treatment were detected.

Detection of SOD activity and MDA content

The cells of each group were homogenized and lysed on ice. The supernatant was collected by centrifugation. The SOD viability test was performed, and the MDA content was measured using the relevant kits.

ATP content test

HT22 cells were inoculated into 6-well culture plates. After the intervention treatment in accordance with the experimental grouping, the operation was performed strictly following the instructions of the ATP content test kit. The absorbance value of each well was detected using an UV spectrophotometer. The ATP content was recorded and calculated.

Mitochondrial membrane potential (MMP) analysis

The HT22 cells were inoculated into 6-well culture plates. The cells were collected after intervention treatment in accordance with the experimental grouping, washed thrice with PBS, added with Rhodamine 123 to a final concentration of 2 μmol/L, incubated at 37°C in the dark for 30 min, and centrifuged at 1200 r/min for 5 min. The supernatant was discarded. The cells were washed thrice with PBS and resuspended by adding 200 μL PBS. MMP was detected using a flow cytometer at an Ex and maximum Em of 507 and 529 nm, respectively.

Protein extraction and Western blot

The HT22 cells were inoculated into 6-well culture plates. The cells were collected in accordance with the experimental group treatment. The cells were washed thrice with PBS and lysed by adding RIPA lysis buffer containing protease and phosphatase inhibitors. Protein content determination and sample preparation were performed in accordance with the BCA kit. The samples were subjected to SDS–PAGE run at 70 V for 30 min and then at 140 V for 50 min. After electrophoresis, the protein was transferred to the NC membrane by semiwet transfer with 18 V and 350 mA for 20 min. The NC membrane was blocked with 5% PBS milk powder for 30 min and washed thrice with PBST buffer for 5 min each time. The membrane was cut and incubated in the primary antibody at 4°C overnight (β-actin was diluted at a ratio of 1:1000, whereas RhoC, ROCK1, Bax, caspase-3, Bcl-2, and caspase-9 were diluted at a ratio of 1:500) (Abcam, UK). Then, the primary antibody was collected. The NC membrane was washed thrice with PBST buffer and incubated in the secondary antibody. A secondary goat antirabbit IgG-horseradish peroxidase (HRP) antibody (1:2000) or goat antimouse IgG-HRP antibody (1:2000) was obtained from Santa Cruz Biotechnology (Santa Cruz, CA, USA) and diluted in 5% (w/v) dry nonfat milk in TBST for 1 h at room temperature. Equal protein loading of the samples was confirmed by β-actin. All Western blots were quantified using densitometry.

Real-time Quantitative PCR

After the cell treatment was completed, the cells were collected by centrifugation at 2000 g/min and washed with PBS. The total RNA was extracted with the TRIzol® Reagent method by using the PrimeScript TM RT reagent kit. mRNA was reverse-transcribed into cDNA by using the M-MLV reverse transcriptase. Then, real-time quantitative PCR was used to detect the expression of RhoC and ROCK1 mRNA in the cells. The reaction system was as follows: 10 μL SYBR Premix Ex TaqTM II, 2 μL PCR primer, 2 μL DNA template, 6 μL DEPC water, and total reaction system of 20 μL. Three replicate wells were established for each sample, and the reaction system was placed on the PCR Amplifier. The conditions for amplification were as follows: predenaturation at 94°C for 30 s; 35 cycles of reaction at 94°C for 10 s and at 60°C for 30 s; and cooling to 4°C. The TaqMan MicroRNA Assays Kit (Applied Biosystems, Foster City, CA, USA) were used, and the miR-382-3p

expression level was calculated using the $2^{-\Delta\Delta Ct}$ method to detect the level of miR-382-3p. The reaction conditions were as follows: predenaturation at 95°C for 30 s, 40 cycles of reaction at 95°C for 5 s, and annealing at 60°C for 30 s. The primers used in this study are shown in Table I. The gene U6 was used as internal reference for the miR-223-3p, whereas β-actin was used as the internal reference for RhoC and ROCK1 mRNA expression. After the reaction, the cycle threshold (Ct) of each gene was calculated and compared with the internal reference gene U6 or β-actin to determine the expression levels of target genes.

Double luciferase reporter assay

The target gene prediction software miR-Base (http://www.mirbase.org/), TargetScan (http://www.TargetScan.org/), and PicTar (http://pictar.mdc-berlin.de/) were used for prediction. The target gene of miR-382-3p may be ROCK1. The wild-type (wt) ROCK1 and mutant (mut) ROCK1 luciferase gene vectors were constructed using the previous method. The two plasmids were transfected into HT22 cells with mir-382-3p mimics, mir-382-3p inhibitor, mimics control, and inhibitor control, which were labeled as Wt + miR-382-3p mimics, Mut + miR-382-3p, Wt + negative control, and Mut + negative control, respectively. After incubation at 37°C for 48 h in a 5% CO2 incubator, the cell dual luciferase activity was detected using the dual luciferase reporter gene kit. RT-PCR and Western blot were used to detect ROCK1 levels in HT22 cells after miR-382-3p overexpression. The ratio of the luminous intensity of sea cucumber luciferase to that of firefly luciferase reflected the binding activity of miR-382-3p to ROCK1.

Statistical analysis

The experimental data were expressed as mean ± standard error of mean. Statistical analysis was performed using SPSS 20.0. One-way ANOVA was used for to compare groups with homoscedasticity. The LSD method was used to compare groups with variance heterogeneity. Dunnett's T3 method was used for multiple comparison.

RESULTS

NMDA attenuated HT22 cell activity and proliferation

The effects of NMDA on HT22 cell viability, survival rate, and cell apoptosis were observed. HT22 cells were incubated with various concentrations of NMDA (0.5, 1, 2, 3, and 5 mmol/L) for 24 h. The HT22 cell viability and proliferation inhibition rate were measured using the CCK-8 and the MTT assays, respectively. NMDA decreased the viability (Fig. 1A) and increased the proliferation inhibition rate (Fig. 1B) of HT22 cells in a concentration-dependent manner. NMDA concentrations as low as 20 mmol/L effectively decreased the HT22 cell viability and proliferation inhibition rate (Fig. 1 A, B).

NMDA increased the HT22 cell oxidative stress and induced the HT22 cell mitochondrial dysfunction

The HT22 cells were incubated with various concentrations of NMDA (0.5, 1, 2, 3, and 5 mmol/L) for 24 h to investigate the effect of NMDA on the HT22 cell oxidative stress. The SOD activity and the levels of ROS and MDA were determined. The ROS and the MDA levels were significantly increased (Fig. 1 D, E), and the SOD activity was markedly decreased (Fig. 1C) after NMDA administration for 24 h in a concentration-dependent manner. NMDA concentrations as low as 20 mmol/L effectively increased the HT22 cell oxidative stress (Fig. 1 C, E). The HT22 cells were incubated with various concentrations of NMDA (0.5, 1, 2, 3, and 5 mmol/L) for 24 h to investigate further the effect of NMDA on the HT22 cell mitochondrial dysfunction. The levels of the mitochondrial membrane potential and the ATP were measured. NMDA decreased the HT22 cell mitochondrial membrane potential and ATP levels (Fig. 1 F, G). NMDA concentrations as low as 2 mmol/L effectively decreased the HT22 cell mitochondrial membrane potential and the ATP levels (Fig. 1 F, G).

NMDA attenuated the activities of miR-382-3p and increased the activity of RhoC/ROCK1 signaling pathway in HT22 cells

The HT22 cells were incubated with various concentrations of NMDA (0.5, 1, 2, 3, and 5 mmol/L) for 24 h to analyze the effect of NMDA on the miR-382-3p and the activity of RhoC/ROCK1 signaling pathway in HT22 cells. miR-382-3p, RhoC, and ROCK1 gene expression levels were measured using RT-PCR. The protein expression levels of RhoC and ROCK1 were measured by Western blot analysis. NMDA attenuated

miR-382-3p expression (Fig. 2A) and increased RhoC and ROCK1 gene and protein expression levels in HT22 cells in a concentration-dependent manner (Fig. 2 B–E). NMDA concentrations as low as 20 mmol/L effectively increased the activity of the RhoC/ROCK1 signaling pathway and attenuated the miR-382-3p signaling pathways in HT22 cells (Fig. 2 A–E).

NMDA increased Bax, caspase-3, and caspase-9 expression levels and suppressed Bcl-2 expression level in HT22 cells

The HT22 cells were incubated with various concentrations of NMDA (0.5, 1, 2, 3, and 5 mmol/L) for 24 h to evaluate the effect of NMDA on the Bax, caspase-3, Bcl-2, and caspase-9 expression levels in

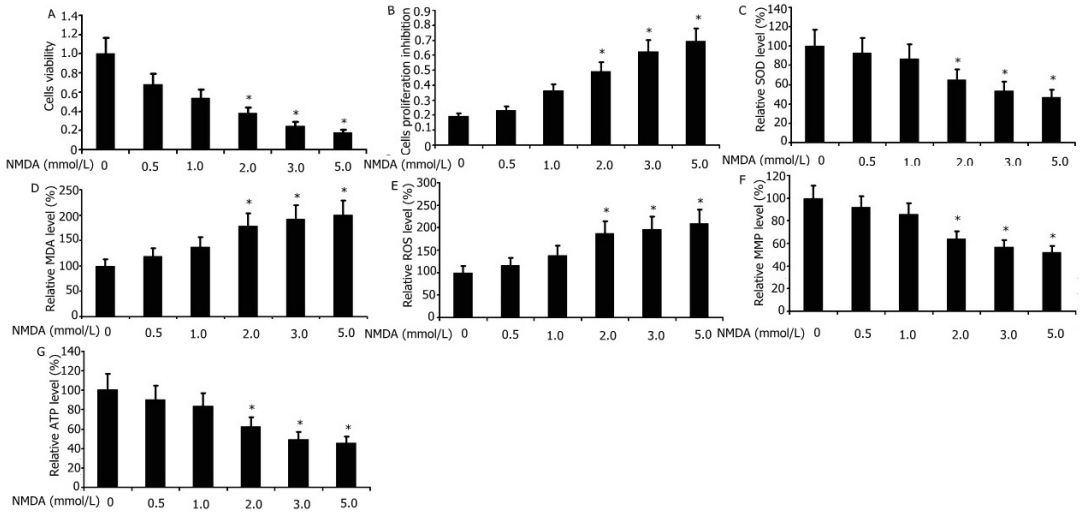

Fig. 1. *Effect of NMDA on HT22 cell activity, proliferation inhibition rate, oxidative stress, and mitochondrial function. The HT22 cells were incubated with various concentrations of NMDA (0.5, 1, 2, 3, and 5 mmol/L) for 24 h. The HT22 cell viability and proliferation inhibition rate were measured using the CCK-8 and the MTT assays, respectively. The SOD activity, levels of MDA and ROS, and mitochondrial function were determined. The data from three independent experiments were presented as mean ± SEM. *P < 0.05 vs the control group. #P < 0.05 vs the NMDA (1 mmol/L) group. P > 0.05 the NMDA (3 mmol/L) group vs the NMDA (5 mmol/L) group.*

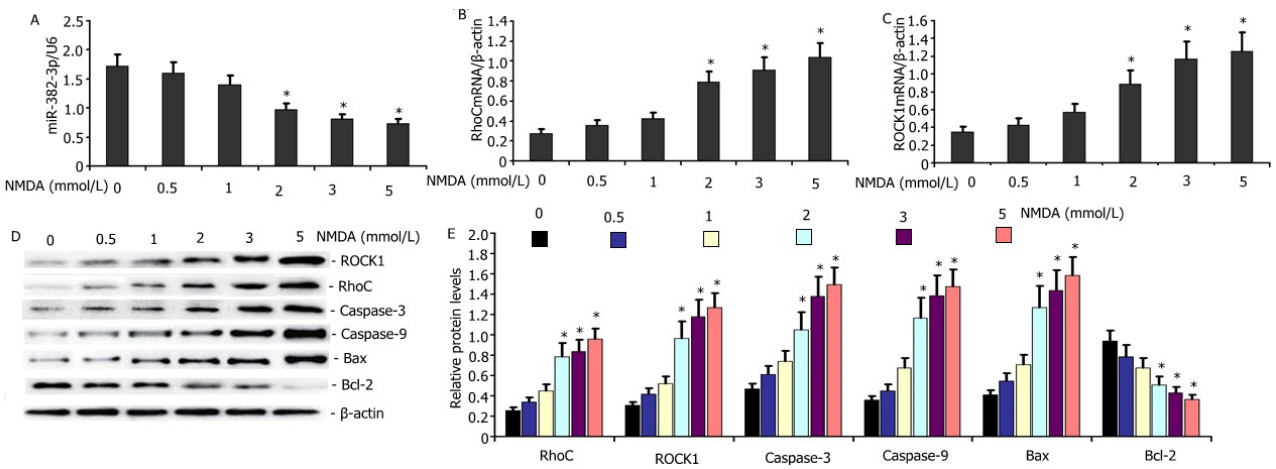

Fig. 2. *Effect of NMDA on the activities of miR-382-3p and RhoC/ROCK1 signaling pathway and the expression of apoptotic protein in HT22 cells. After the incubation of HT22 cells with various concentrations of NMDA (0.5, 1, 2, 3, and 5 mmol/L) for 24 h, miR-382-3p, RhoC and ROCK1 gene expression levels were measured using RT-PCR. RhoC, ROCK1, Bax, Caspase-3, Caspase-9, and Bcl-2 expressions were measured by Western blot. The data from three independent experiments were presented as mean ± SEM. *P < 0.05 vs the control group. #P < 0.05 vs the NMDA (1 mmol/L) group. P > 0.05 the NMDA (3 mmol/L) group vs the NMDA (5 mmol/L) group.*

HT22 cells. The expression levels of Bax, caspase-3, Bcl-2, and caspase-9 proteins were measured by Western blot analysis. NMDA increased Bax, caspase-3, and caspase-9 expression levels and attenuated Bcl-2 expression level in a concentration-dependent manner (Fig. 2 D, E). The NMDA concentrations as low as 2 mmol/L effectively increased Bax, caspase-3, and caspase-9 expression and attenuated Bcl-2 expression in HT22 cells (Fig. 2 D, E).

miR-382-3p overexpression increased NMDA-induced HT22 cell activity and proliferation

The effects of miR-382-3p on NMDA-induced HT22 cell activity and proliferation were observed. The HT22 cells were transfected with miR-382-3p mimic and miR-382-3p inhibitor for 48 h in the presence of 2 mmol/L NMDA. The HT22 cell viability and proliferation were measured using the CCK-8 and the MTT assays, respectively. miR-382-3p overexpression increased the viability and reduced the proliferation inhibition rate of NMDA-induced HT22 cells (Fig. 3 A, B). On this basis, the increase in miR-382-3p expression can enhance NMDA-induced HT22 cell activity and proliferation.

miR-382-3p overexpression decreased NMDA-induced HT22 cell oxidative stress and improved NMDA-induced HT22 mitochondrial dysfunction

The effects of miR-382-3p on NMDA-induced HT22 cell oxidative stress and mitochondrial dysfunction were investigated. The HT22 cells were transfected with miR-382-3p mimic and miR-382-3p inhibitor for 48 h in the presence of 2 mmol/L NMDA. The SOD activity and the levels of ROS and MDA were determined, and the levels of mitochondrial membrane potential and ATP were measured. miR-382-3p overexpression increased SOD activity and reduced the levels of ROS and MDA in NMDA-induced HT22 cells (Fig. 3 C–E). Moreover, the miR-382-3p overexpression enhanced the levels of mitochondrial membrane potential and ATP (Fig. 3 F, G). On this basis, the increase in miR-382-3p expression can improve HT22 cell SOD activity and mitochondrial dysfunction.

miR-382-3p overexpression attenuated NMDA-induced HT22 cell apoptosis

The effect of NMDA on HT22 cell apoptosis was observed. The HT22 cells were incubated with various concentrations of NMDA (0.5, 1, 2, 3, and 5 mmol/L) for 24 h. HT22 cell apoptosis was measured using flow cytometry. NMDA increased the HT22 cell apoptosis in a concentration-dependent manner (Fig. 4 A–E and 4K). NMDA concentrations as low as 20 mmol/L effectively increased HT22 cell apoptosis (Fig. 4 A–F and K). The effect of miR-382-3p on NMDA-induced HT22 cell apoptosis was evaluated. The HT22 cells were transfected with miR-382-3p mimic and miR-382-3p inhibitor for 48 h in the presence of 2 mmol/L NMDA. The HT22 cell apoptosis was measured using flow cytometry. miR-382-3p overexpression by miR-382-3p mimic resulted in decreased NMDA-induced HT22 cell apoptosis (Fig. 4 G–J and L). On this basis, the increase in miR-382-3p expression can attenuate NMDA-induced HT22 cell apoptosis.

miR-382-3p overexpression blocked the activities of RhoC/ROCK1 signaling pathway in HT22 cells

The effect of miR-382-3p on the activities of RhoC/ROCK1 signaling pathway in HT22 cells were further analyzed. The HT22 cells were transfected with miR-382-3p mimic and miR-382-3p inhibitor in the presence of 2 mmol/L NMDA for 48 h. miR-382-3p expression was measured using RT-PCR. RhoC and ROCK1 protein expressions were measured using Western blot. The miR-382-3p overexpression by miR-382-3p mimic resulted in decreased NMDA-induced RhoC and ROCK1 protein expression (Fig. 5 A, B) and increased miR-382-3p expression (Fig. 5C) in HT22 cells. Results suggested that the increase in miR-382-3p expression can inhibit the activities of NMDA-induced RhoC/ROCK1 signaling pathway in HT22 cells, and the miR-382-3p mimic and the miR-382-3p inhibitor successfully transfected NMDA-induced HT22 cells.

miR-382-3p overexpression decreased Bax, caspase-3, and caspase-9 expressions and enhanced Bcl-2 expression in HT22 cells

The effects of miR-382-3p on the Bax, caspase-3, Bcl-2, and caspase-9 expressions in HT22 cells were investigated. The HT22 cells were transfected with miR-382-3p mimic and miR-382-3p inhibitor in the presence of 2 mmol/L NMDA for 48 h. The expression

Table I. *Primer sequences for RT-PCR analysis.*

Gene	Primer	Product
miR-382-3p	F-5'-CTGCAATCATTCACGGACAAC-3'	178
	R-5'-GTGTCGTCGAGTCGGCAATTC-3'	
U6	F-5'-CTCGCTTCGGCAGCACA-3'	241
	R-5'-AACGCTTCACGAATTTGCGT-3'	
ROCK1	F-5'-AAAGCCTTACTGTCGATTGCC-3'	159
	R-5'-AGGGTAATGCAACTTCCACTG-3'	
RhoC	F-5'-CAGGATGAT GGGCACGTT G-3'	173
	R-5'-GAAGACCTGCCTCCTCATCG 3′	
β-actin	F-5′-ACGGGAAATCGTGAT-3'	154
	R-5'- GAACTTTGGGGGATGCTCGC-3'	

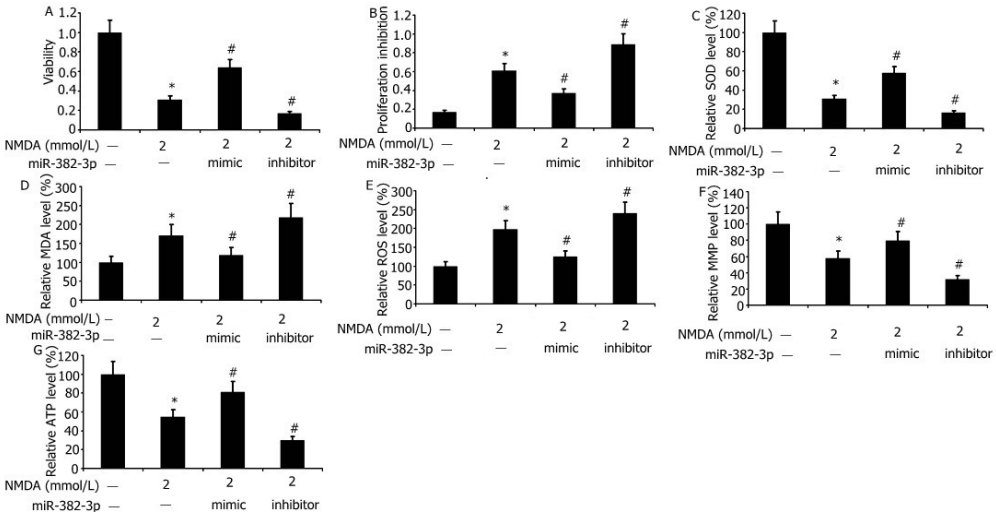

Fig. 3. *Effect of miR-382-3p on NMDA-induced HT22 cell activity, proliferation, oxidative stress, and mitochondrial function. The HT22 cells were transfected with miR-382-3p mimic and miR-382-3p inhibitor for 48 h in the presence of 2 mmol/L NMDA. HT22 cell viability and proliferation were measured using the CCK-8 and the MTT assays, respectively. The SOD activity, levels of MDA and ROS, and mitochondrial function were determined. Data from three independent experiments were presented as mean ± SEM. *P < 0.05 vs the control group. #P < 0.05 vs the NMDA-induced HT22 cells.*

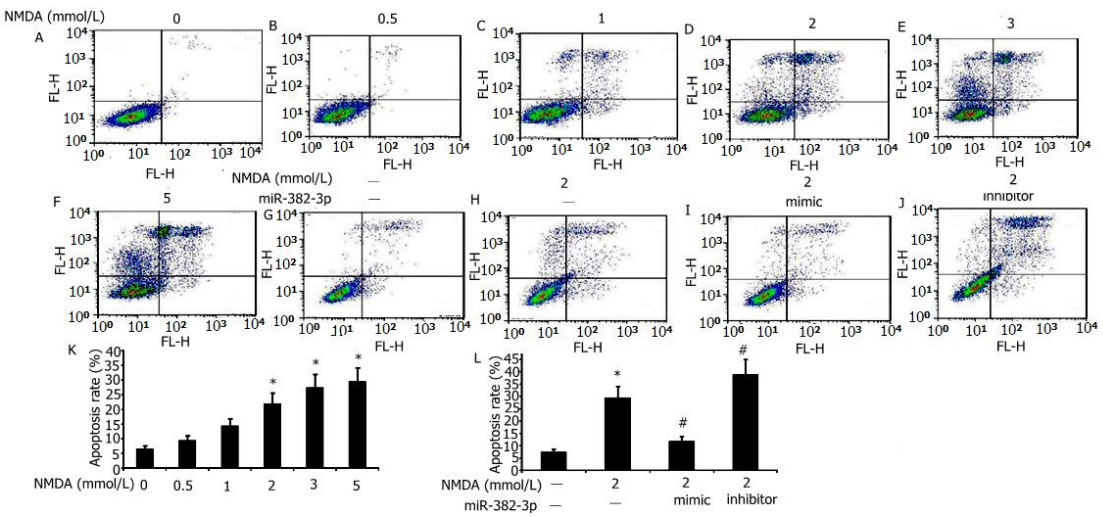

Fig. 4. *Effect of miR-382-3p on NMDA-induced HT22 cell apoptosis. The HT22 cells were incubated with various concentrations of NMDA (0.5, 1, 2, 3, and 5 mmol/L) for 24 h and transfected with miR-382-3p mimic and miR-382-3p inhibitor in the presence of 2 mmol/L NMDA for 48 h. The HT22 cell apoptosis was measured using flow cytometry. Data from three independent experiments were presented as mean ± SEM. *P < 0.05 vs the control group. #P < 0.05 vs the NMDA-induced HT22 cells.*

levels of Bax, caspase-3, Bcl-2, and caspase-9 were measured using Western blot analysis. The miR-382-3p overexpression by miR-382-3p mimic resulted in decreased Bax, caspase-3, and caspase-9 protein expressions and increased Bcl-2 protein expression in HT22 cells (Fig. 5 A, B). On this basis, the increase in miR-382-3p expression can inhibit the expression of proapoptotic proteins and increase the expression of antiapoptotic proteins in NMDA-induced HT22 cells.

ROCK1 was directly targeting miR-382-3p

The TargetScan database was used for predicting the likely targets of miR-382-3p and determine how miR-382-3p mediates NMDA-induced HT22 cell apoptosis. ROCK1 is an important regulator of NMDA-induced HT22 cell apoptosis. ROCK1 mRNA and protein levels were dramatically decreased after miR-382-3p overexpression (Fig. 6 A–C).The wild-type and mutant ROCK1 were constructed for dual luciferase reporter assay (Fig. 6 D, E) to validate the interaction between miR-382-3p and ROCK1. As hypothesized, miR-382-3p became bound to the wild-type ROCK1 rather than to the mutants (Fig. 6E).

Correlation between ROCK1 and miR-382-3p

The correlation between ROCK1 and miR-382-3p expression in NMDA-induced HT22 cells was also analyzed. Linear correlation was determined to evaluate the correlation between mRNA and protein expression of ROCK1 and miR-382-3p expression. Results showed that a negative correlation existed between ROCK1 protein and miR-382-3p as well as between ROCK1mRNA and miR-382-3p in NMDA-induced HT22 cells.

DISCUSSION

NMDA is an excitatory amino acid that can act on the NMDAR of postsynaptic neurons, activate receptor-gated calcium channels, and cause intracellular calcium overload. A large amount of Ca^{2+} influx can lead to acute intracellular edema and secondary cytotoxicity. The secondary cytotoxicity is a product of the release of intracellular Ca^{2+} caused by the influx of Ca^{2+} and activation of the metabolic glutamate receptor when NMDA is activated. Ca^{2+} can combine with CaM to form the Ca^{2+}–CaM complex to

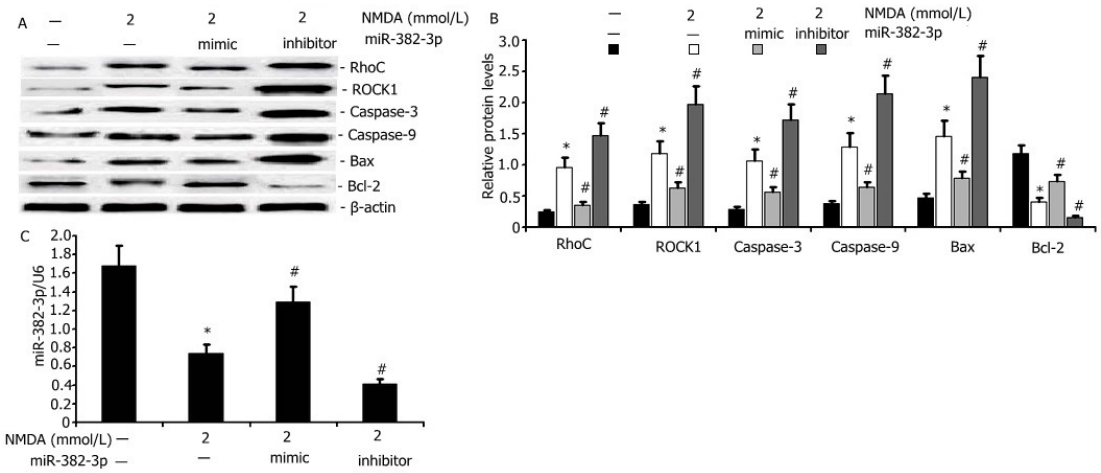

Fig. 5. *Effect of miR-382-3p on the activities of miR-382-3p and RhoC/ROCK1 signaling pathway, and apoptotic protein expression in HT22 cells. The HT22 cells were transfected with miR-382-3p mimic and miR-382-3p inhibitor in the presence of 2 mmol/L NMDA for 48 h. The RhoC, ROCK1, Bax, caspase-3, Bcl2 and caspase-9 protein expression levels were measured using Western blot, and miR-382-3p expression was measured using RT-PCR. Data from three independent experiments are presented as mean ± SEM. *P < 0.05 vs the control group. #P < 0.05 vs the NMDA-induced HT22 cells.*

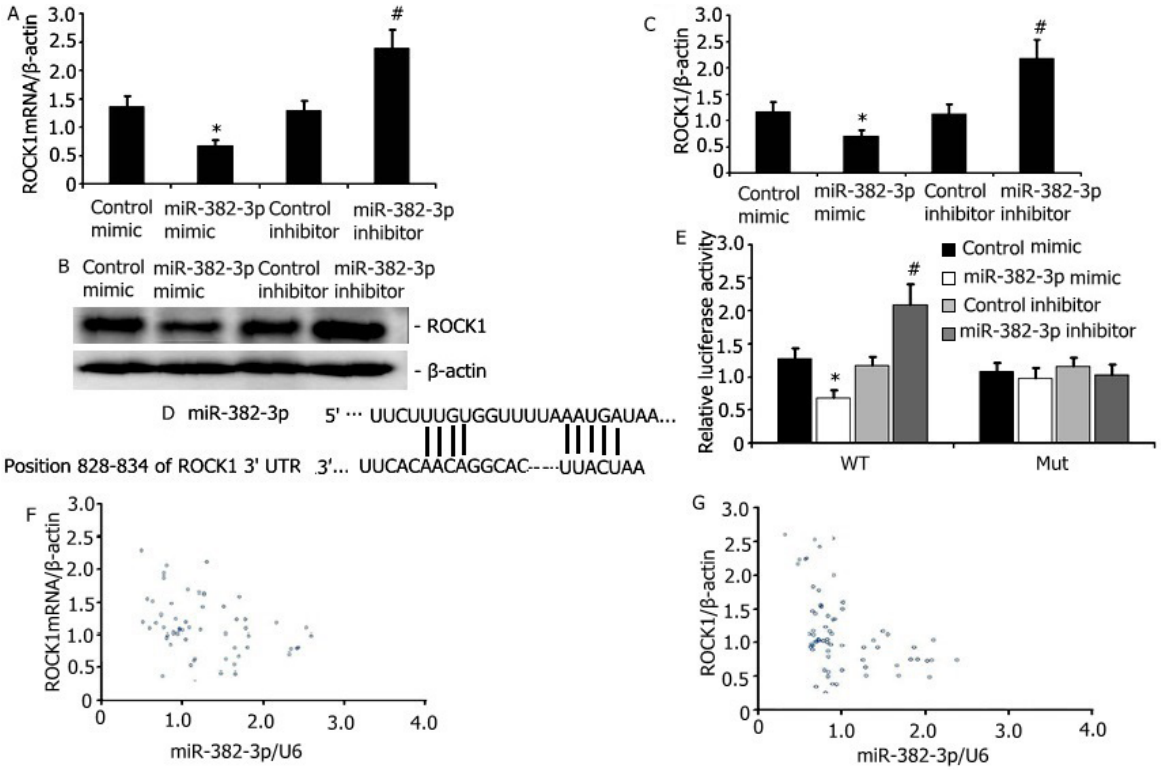

Fig. 6. *ROCK1 is a downstream target of miR-382-3p and correlation between ROCK1 and miR-382-3p in NMDA-induced HT22 cells.* ***A****) The mRNA levels of ROCK1 were decreased in NMDA-induced HT22 cells after miR-382-3p overexpression (P < 0.05). The levels of ROCK1 mRNA expression were enhanced after miR-382-3p downregulation (P < 0.05).* ***B–C****) ROCK1 protein expression was decreased in NMDA-induced HT22 cells with miR-382-3p overexpression relative to the empty vector control (P < 0.05). ROCK1 protein expression was significantly increased in cells with miR-382-3p downregulation.* ***D****) miR-382-3p was bound to the 3′-UTR regions of ROCK1. Binding was interrupted in mutant ROCK1.* ***E****) Dual luciferase reporter assay indicated that miR-382-3p mimic was bound to the 3′-UTR region of wild-type ROCK1 rather than to ROCK1 mutants (P < 0.05).* ***F****) Negative correlation between ROCK1 protein and miR-382-3p.* ***G****) Negative correlation between ROCK1mRNA and miR-382-3p.*

increase nerve excitability, leading to the occurrence of EP by regulating the action of enzymes, such as kinase II (23, 24). Prolonged epileptic seizures and epileptic persistent states can cause different degrees of brain damage, with hippocampal neuron damage being the most prominent (25, 26). This damage can promote the occurrence and development of EP and cause the impairment of cognitive function (27). In this experiment, an in vitro glutamate model of NMDA-induced HT22 cell injury was established to simulate a postepileptic cell apoptosis model. The apoptosis mechanism of hippocampal neurons after epileptic seizure or epileptic state was also studied. In this experiment, decreased activity of HT22 cells and proliferation rate and increased cell apoptosis were observed when HT22 cells were cultured for 48 h.

The complex factors involved in EP include ion channels, glial cells, synaptic transmission, and other changes in the character of neurons. Oxidative stress, apoptosis, and other factors can also lead to changes in the characteristics of neurons and abnormal discharge of neurons, thereby leading to EP (28, 29). During EP attack, a large number of oxygen free radicals are not removed in time, thereby leading to oxidation reaction at a high level and causing damage to neurons, ultimately aggravating the nerve cell damage or inducing EP (28). In this experiment, NMDA increased ROS and MDA generated in HT22 cells, decreased the activity of SOD, and increased oxidative stress in HT22 cells were observed. As a

result, the mitochondrial function was impaired, and apoptosis was increased in HT22 cells.

Apoptosis is a kind of programmed death. Bax, bcl-2, caspase-3, and caspase-9 are all apoptosis-regulating genes. Caspase-3 activates related signaling pathways by cleaving downstream effector molecules, thereby leading to apoptosis. As an anti/proapoptotic gene, bcl-2/Bax can be used as an upstream regulatory gene of caspase-3 and caspase-9. The overexpression of Bax can activate downstream caspase-3 and caspase-9 proteases and mediate cell survival or death, and bcl-2 can form a dimer with Bax to inhibit Bax activity (29, 30). In this experiment, HT22 cells were cultured with NMDA for 48 h. Results showed increased Bax, caspase-3, and caspase-9 expressions and decreased bcl-2 expression in HT22 cells. Moreover, increased HT22 cell apoptosis and nerve damage were observed.

Studies have found that the inhibition of the RhoA/ROCK pathway activity can significantly reduce apoptosis (31). The activated RhoA/ROCK pathway can promote the synthesis of proapoptotic proteins. RhoA activates p53, upregulates the proapoptotic gene Bax in the Bcl-2 gene family, and mediates mitochondrial apoptosis (31). RhoA can also promote the synthesis of the proapoptotic neurotrophin receptor p75 (p75 neurotrophin receptor, p75NTR) and the occurrence of the apoptotic cascade induced by p75NTR (32). Studies have also found that the expression of active RhoA can activate p38 and induce the death of neuronal cells that are sensitive to the antiapoptotic protein bcl-2 (33). The ROCK levels in a rat model of retinal excitatory toxicity induced by NMDA increase before neuronal death (34). The inhibition of ROCK activity by fasudil can significantly improve the survival rate of neurons (34). Treatment with the ROCK inhibitor Y-27632 can significantly reduce ROCK activity and protect hippocampal neurons from kainic acid-induced toxic damage (35). In the current study, treatment with the NMDA increased the expression of RhoA, abundance of ROCK mRNA and protein, Bax, caspase-3, and caspase-9, decreased the bcl-2 expression, and increased the apoptosis in HT22 cells. However, treatment with the miR-382-3p mimic increased the expression of miR-382-3p, inhibited the expression of RhoA and ROCK mRNA and protein in HT 22 cells, reduced the expression of Bax, caspase-3 and caspase-9 in HT22 cells, increased expression of bcl-2, and reduced apoptosis in HT22 cells. On this basis, inhibiting the activity of the RhoA/ROCK pathway can reduce the expression of antiapoptotic proteins, increase the expression of antiapoptotic proteins, and reduce NMDA-induced apoptosis.

According to various reports, miR-382 is dysregulated in many types of tumor cells, and plays an important role in the occurrence and development of tumors (36, 37). The expression level of mir-382-5p is negatively correlated with the recurrence rate of osteosarcoma, which can directly target the Y-box-binding protein 1 to regulate the apoptosis of tumor cells and the formation and metastasis of osteosarcoma (37). Recent studies have found that silencing MATAT1 can increase the expression of miR-382-3p, decrease the expression of resistin, increase the levels of NO and p-Akt/Akt, inhibit the generation of IL-6, sICAM-1, sVCAM-1, ET-1, and p-IRS/ISR-1 in insulin-antagonized mouse models, reduce the inflammatory reaction and oxidative stress of insulin antagonist mice, and improve the insulin antagonist (38). Further research has found that directly targeting CX43t can regulate the TLR4/MyD88/NF-κB signaling pathway, inhibit IL-1β-induced chondrocyte inflammation, and reduce chondrocyte apoptosis (39). On this basis, miR-382-3p can regulate apoptosis through multiple pathways, but the specific mechanism is still unclear. In the current study, with the increase in NMDA dose, gradually decreased miR-382-3p expression, gradually increased RhoA expression, abundance of ROCK mRNA and protein, and Bax, caspase-3, and caspase-9 expressions; gradually decreased bcl-2 expression; increased apoptosis; and aggravated nerve injury were observed in NMDA-induced HT22 cells. At the same time, increasing the expression of miR-382-3p by transfecting with miR-382-3p mimic can reduce the expression of RhoA, abundance of ROCK mRNA and protein, and Bax, caspase-3, and caspase-9 expressions; increase the expression of bcl-2; reduce apoptosis; and reduce nerve damage in HT22 cells. On this basis, miR-382-3p may regulate NMDA-induced HT22 cell apoptosis by regulating the activity of the RhoA/ROCK pathway.

Studies have shown that Mir-382-3p can target and regulate the expression of ROCK1(19). In the present experiment, miR-382-3p and ROCK1 could regulate NMDA-induced apoptosis in HT22 cells. ROCK1 is target-regulated by miR-382-3p using the TargetScan database software to clarify the relationship between miR-382-3p and ROCK1. Increasing the expression of miR-382-3p can increase the expression of ROCK1 mRNA and protein. By contrast, downregulating the expression of miR-382-3p can reduce the expression of ROCK1 mRNA and protein. Double luciferase reporter assays suggested that ROCK1 was a regulatory target of miR-382-3p. On the basis of this test, ROCK1 was a regulatory target of miR-382-3p and miR-382-3p can regulate NMDA-induced HT22 cell apoptosis by regulating the activity of the RhoA/ROCK pathway. The correlation between miR-382-3p and ROCK1 in regulating NMDA-induced apoptosis in HT22 cells was further investigated. miR-382-3p was negatively correlated with ROCK1 mRNAs and protein expression.

In summary, NMDA increases the oxidative stress, causes mitochondrial dysfunction, and increases apoptosis in HT22 cells. Moreover, increasing the expression of miR-382-3p can inhibit the activity of the RhoC/ROCK1 signaling pathway, inhibit the expression of proapoptotic proteins, reduce the oxidative stress and apoptosis of HT22 cells, and increase the activity and survival rate of HT22 cells induced by NMDA. ROCK1 is a regulatory target of miR-382-3p, and the miR-382-3p is negatively correlated with ROCK1 mRNAs and protein expression. The regulation of miR-382-3p on HT22 may involve inflammation, autophagy, pyrolysis, and so on. Its mechanism needs to be further studied.

ACKNOWLEDGEMENTS

This research was supported by the National Natural Science Foundation of China (81760243), Yunnan Basic Research Project(2018FB115), and the Yunnan Health Training Project of High-Level Talents Project (H-2018058).

All experiments were approved by the Ethics Committee of Kunming Medical University (Kunming, China) and performed according to The Guidelines of the Animal Care Committee of Kunming Medical University

REFERENCES

1. Melin E, Nanobashvili A, Avdic U, et al. Disease modification by combinatorial single vector gene therapy: a preclinical translational study in epilepsy. Mol Ther Methods Clin Dev 2019; 15:179-93.
2. Pansani AP, Cysneiros RM, Colugnati DB, et al. Long-term monotherapy treatment with vitamin E reduces oxidative stress, but not seizure frequency in rats submitted to the pilocarpine model of epilepsy. Epilepsy Behav 2018; 88:301-307.
3. Wu ZS, Huang WL, Gong SJ . Effect of adenovirus-mediated overexpression of PTEN on brain oxidative damage and neuroinflammation in a rat kindling model of epilepsy. Chin Med J (Engl) 2019; 132:2628-35.
4. Prakash C, Mishra M, Kumar P, Kumar V, Sharma D. Dehydroepiandrosterone alleviates oxidative stress and apoptosis in iron-induced epilepsy via activation of Nrf2/ARE signal pathway. Brain Res Bull 2019; 153:181-90.
5. Yu JT, Liu Y, Dong P, et al. Up-regulation of antioxidative proteins TRX1, TXNL1 and TXNRD1 in the cortex of PTZ kindling seizure model mice. PLoS One 2019; 14:e0210670.
6. Inquimbert P, Moll M, Latremoliere A, et al. NMDA receptor activation underlies the loss of spinal dorsal horn neurons and the transition to persistent pain after peripheral nerve injury. Cell Rep 2018; 23 (9):2678-89.
7. Szychowski KA, Wnuk A, Rzemieniec J, Kajta M, Leszczyńska T, Wójtowicz AK. triclosan-evoked neurotoxicity involves NMDAR subunits with the specific role of GluN2A in caspase-3-dependent apoptosis. Mol Neurobiol 2019; 56:1-12.
8. Wu C, Wang J, Guo X, Zhang Y. Ketamine exacerbates cortical neuroapoptosis under hyperoxic conditions by upregulating expression of the N-methyl-D-aspartate receptor subunit NR1 in the developing rat brain. BMC Anesthesiol 2018; 18:52.
9. Jiang S, Li X, Jin W, Duan X, et al. Ketamine-induced neurotoxicity blocked by N-Methyl-d-aspartate is mediated through activation of PKC/ERK pathway in developing hippocampal neurons. Neurosci Lett 2018;

673:122-31.
10. Zhang Q, Hu C, Huang J, et al. ROCK1 induces dopaminergic nerve cell apoptosis via the activation of Drp1-mediated aberrant mitochondrial fission in Parkinson's disease. Exp Mol Med 2019; 51(10):116.
11. Zhang C, Lu C, Wang Z, Feng G, et al. Antimony enhances c-Myc stability in prostate cancer via activating CtBP2-ROCK1 signaling pathway. Ecotoxicol Environ Saf 2018; 164:61-68.
12. Knipe RS, Probst CK, Lagares D, et al. The Rho kinase isoforms ROCK1 and ROCK2 each contribute to the development of experimental pulmonary fibrosis. Am J Respir Cell Mol Biol 2018; 58(4):471-81
13. Martinez B, Peplow PV. MicroRNAs in blood and cerebrospinal fluid as diagnostic biomarkers of multiple sclerosis and to monitor disease progression. Neural Regen Res 2020; 15 (4):606-19.
14. Goh SY, Chao YX, Dheen ST, Tan EK, Tay SS. Role of MicroRNAs in Parkinson's Disease.Int J Mol Sci 2019; 20(22):E5649
15. Wei R, Zhang R, Li H, et al. MiR-29 Targets PUMA to suppress oxygen and glucose deprivation/reperfusion (OGD/R)-induced cell death in hippocampal neurons. Curr Neurovasc Res 2018; 15:47-54.
16. Xiao X, Jiang Y, Liang W, et al. miR-212-5p attenuates ferroptotic neuronal death after traumatic brain injury by targeting Ptgs2. Mol Brain 2019; 12(1):78
17. Costard LS, Neubert V, Venø MT, et al. Electrical stimulation of the ventral hippocampal commissure delays experimental epilepsy and is associated with altered microRNA expression. Brain Stimul 2019; 12(6):1390-401.
18. Ho JY, Hsu RJ, Liu MJ, et al. MicroRNA-382-5p aggravates breast cancer progression by regulating the RERG/Ras/ERK signaling axis. Oncotarget 2017; 8:22443-59.
19. Liu Y, Wang Y, Fu X, Lu Z. Long non-coding RNA NEAT1 promoted ovarian cancer cells' metastasis through regulation of miR-382-3p/ROCK1 axial. Cancer Sci 2018; 109:2188-98.
20. Ma Z. Downregulation of SETD8 by miR-382 is involved in glioma progression. Pathol Res Pract 2018; 214 (3):356-60.
21. Zheng S, Eacker SM, Hong SJ, Gronostajski RM, Dawson TM, Dawson VL. NMDA-induced neuronal survival is mediated through nuclear factor I-A in mice. J Clin Invest 2010; 120:2446-56.
22. Valera E, Sánchez-Martín FJ, Ferrer-Montiel AV, Messeguer A, Merino JM. NMDA-induced neuroprotection in hippocampal neurons is mediated through the protein kinase A and CREB (cAMP-response element-binding protein) pathway. Neurochem Int. 2008; 53(5):148-54.
23. Zhu J, Lee KY, Jong TT, Tsai NP. C2-lacking isoform of Nedd4-2 regulates excitatory synaptic strength through GluA1 ubiquitination-independent mechanisms. J Neurochem 2019; 151 (3):289-300.
24. Furness AM, Pal R, Michealis EK, Lunte CE, Lunte SM. Neurochemical investigation of multiple locally induced seizures using microdialysis sampling: Epilepsy effects on glutamate release. Brain Res 2019; 1722:146360.
25. Mao XY, Zhou HH, Li X, Liu ZQ. Huperzine A Alleviates oxidative glutamate toxicity in hippocampal HT22 cells via activating BDNF/TrkB-Dependent PI3K/Akt/mTOR signaling pathway. Cell Mol Neurobiol 2016; 36:915-25.
26. Dai H, Wang P, Mao H, Mao X, Tan S, Chen Z. Dynorphin activation of kappa opioid receptor protects against epilepsy and seizure-induced brain injury via PI3K/Akt/Nrf2/HO-1 pathway. Cell Cycle 2019; 18:226-37.
27. Pearson JN, Rowley S, Liang LP, White AM, Day BJ, Patel M. Reactive oxygen species mediate cognitive deficits in experimental temporal lobe epilepsy. Neurobiol Dis 2015; 82:289-97.
28. Rowley S, Patel M. Mitochondrial involvement and oxidative stress in temporal lobe epilepsy. Free Radic Biol Med 2013; 62:121-31.
29. Prakash C, Mishra M, Kumar P, Kumar V, Sharma D. Dehydroepiandrosterone alleviates oxidative stress and apoptosis in iron-induced epilepsy via activation of Nrf2/ARE signal pathway. Brain Res Bull 2019; 153:181-90.
30. Guo XQ, Cao YL, Hao F, Yan ZR, Wang ML, Liu XW. Tangeretin alters neuronal apoptosis and ameliorates the severity of seizures in experimental epilepsy-induced rats by modulating apoptotic protein expressions, regulating matrix metalloproteinases, and activating the PI3K/Akt cell survival pathway. Adv Med Sci 2017; 62 (2):246-53.
31. Wang J, Li H, Yao Y, et al. β-Elemene Enhances GAP-43 Expression and Neurite Outgrowth by Inhibiting

RhoA Kinase Activation in Rats with Spinal Cord Injury. Neuroscience 2018; 383:12-21.
32. Wang YT, Lu XM, Zhu F, et al. Ameliorative effects of p75NTR-ED-Fc on axonal regeneration and functional recovery in spinal cord-injured Rats. Mol Neurobiol 2015; 52 (3):1821-34.
33. Namachivayam K, MohanKumar K, Arbach D, et al. All-trans retinoic acid induces TGF-β2 in intestinal epithelial cells via RhoA- and p38α MAPK-mediated activation of the transcription factor ATF2. PLoS One 2015; 10(7):e0134003.
34. Kitaoka Y, Kitaoka Y, Kumai T, et al. Involvement of RhoA and possible neuroprotective effect of fasudil, a Rho kinase inhibitor, in NMDA-induced neurotoxicity in the rat retina. Brain Res 2004; 1018(1):111-18.
35. Swanger SA, Mattheyses AL, Gentry EG, Herskowitz JH. ROCK1 and ROCK2 inhibition alters dendritic spine morphology in hippocampal neurons. Cell Logist 2015; (4):e1133266
36. Liu D, Zhong L, Yuan Z, et al. miR-382-5p modulates the ATRA-induced differentiation of acute promyelocytic leukemia by targeting tumor suppressor PTEN. Cell Signal 2019; 54:1-9
37. Xu M, Jin H, Xu CX, et al. miR-382 inhibits osteosarcoma metastasis and relapse by targeting Y box-binding protein 1. Mol Ther 2015; 23(1):89-98.
38. Liu SX, Zheng F, Xie KL, Xie MR, Jiang LJ, Cai Y. Exercise reduces insulin resistance in type 2 diabetes mellitus via mediating the lncRNA MALAT1/ MicroRNA-382-3p/Resistin Axis. Mol Ther Nucleic Acids 2019; 18:34-44.
39. Lei J, Fu Y, Zhuang Y, Zhang K, Lu D. miR-382-3p suppressed IL-1β induced inflammatory response of chondrocytes via the TLR4/MyD88/NF-κB signaling pathway by directly targeting CX43. J Cell Physiol 2019; 234:23160-68.

Anti-aging gene Klotho ameliorates diabetic nephropathy in mice by inhibiting FGF2 signaling pathway

Q.-L. Dong, X.-H. Zhao, Q. Wang, L.-P. Zhang, X.-H. Yan, X.-M. Wang, Z.-J. Li and Y. Sun

Kidney Disease and Dialysis Center, Shaanxi Provincial People's Hospital, Xi'an, China

Received May 16, 2020 – Accepted July 14, 2020

The aim of this study was to observe the expression of Klotho in renal tissues of mice with diabetic nephropathy (DN), and to further explore the effect of Klotho on DN in mice and its mechanism. The 10-week-old mice in this experiment were divided into three groups: heterozygous db/+ mouse group (db/+ group, n=20), homozygous db/db mouse group (db/db group, n=20) and homozygous db/db mice + Klotho group (db/db + Klotho group, n=20). Firstly, Western blotting and immunohistochemical staining were applied to detect the protein expression of Klotho in the renal tissues of diabetic and non-diabetic mice of different ages. Finally, the protein expressions of fibroblast growth factor 2 (FGF2) and E-cadherin in the renal tissues of mice in each group were examined by Western blotting. The protein expression level of Klotho in the renal tissues of mice aged 10 and 16 weeks in the db/db group was remarkably lower than that in yhedb/+ group. In addition, it was found that db/db + Klotho group exhibited a prominently lower degree of interstitial fibrosis and content of Collagen I and Collagen III in the renal tissues than db/db group. Furthermore, it was revealed that the overexpression of Klotho could significantly repress the protein expression level of FGF2 but elevate that of E-cadherin in the renal tissues of DN mice. Klotho protein may ameliorate the renal injury and fibrosis in diabetic mice by inhibiting FGF2, so it is expected to become a targeted drug for DN.

Diabetes mellitus is a common type of hyperglycemia-induced metabolic disorder, and persistent hyperglycemia in the body can trigger various complications in the heart, kidney, nerve and retina (1, 2). As one of the most common microvascular complications of diabetes mellitus, diabetic nephropathy (DN) has become the leading cause of end-stage renal disease in many countries (3). DN is characterized by the accumulation of extracellular matrix (ECM) proteins and the activation of myofibroblast and tubulointerstitial fibrosis, which ultimately results in chronic renal failure (4). The pathogenesis of DN is extremely complex, and involves the abnormal activation or inhibition of multiple signaling pathways, therefore further clarifying the molecular mechanisms of the occurrence and development of DN is of important significance for improving the prognosis of patients with diabetes mellitus in the future.

Klotho, initially regarded as an anti-aging gene, is capable of encoding single-channel transmembrane proteins and serves as a co-receptor of fibroblast growth factors (FGFs) (5). It is widely expressed in a variety of organs in the human body and exhibits the highest expression level in renal tissues. Klotho protein can also be secreted into the cerebrospinal fluid, blood and urine through the ectodomain shedding mediated by membrane-anchored proteases. The secretory Klotho

Key words: Klotho, diabetic nephropathy, renal fibrosis, FGF2

Corresponding Author:
Yan Sun, MM,
Kidney Disease and Dialysis Center,
Shaanxi Provincial People's Hospital,
256 Youyi West Road, Beilin District,
Xi'an, 710068, Shaanxi, China
Tel.: +86 02985251331
e-mail: yanzi7591@163.com

0393-974X (2020)
Copyright © by BIOLIFE, s.a.s.
This publication and/or article is for individual use only and may not be further reproduced without written permission from the copyright holder.
Unauthorized reproduction may result in financial and other penalties
DISCLOSURE: ALL AUTHORS REPORT NO CONFLICTS OF INTEREST RELEVANT TO THIS ARTICLE.

protein acts as an enzyme or hormone by means of internal secretion (6, 7). Klotho deficiency in rodents can induce progeria, mainly featured with ectopic soft-tissue calcification (8). Moreover, it can lead to vascular calcification in mice with chronic renal diseases (9). However, little is known about the role and potential mechanism of Klotho in DN at present.

In this research, the expression of Klotho in the renal tissues of healthy and DN mice was detected. Subsequently, the effects of exogenous Klotho on renal injury and fibrosis in DN mice were observed. Furthermore, the potential mechanism of Klotho in resisting DN was investigated, to provide references for clinical treatment of DN in the future.

MATERIALS AND METHODS

Animal grouping and model establishment

A total of 20 male heterozygous db/+ mice and 40 male homozygous db/db mice aged 10 weeks were divided into heterozygous db/+ mouse group (db/+ group, n=20), homozygous db/db mouse group (db/db group, n=20) and homozygous db/db mice + Klotho group (db/db + Klotho group, n=20) using a random number table. The rats in db/db + Klotho group were intraperitoneally injected with Klotho protein (0.02 mg/kg/d) (10), while those in db/+ group and db/db group were intraperitoneally injected with an equivalent volume of normal saline for 6 consecutive weeks. Finally, the blood was collected from the orbital vein, and renal specimens were obtained at the same time. This study was approved by the Animal Ethics Committee of Shaanxi Provincial People's Hospital Animal Center.

Hematoxylin and eosin (H&E) staining

The kidneys obtained from each group of mice were placed in 10% formalin overnight, then dehydrated and embedded in paraffin blocks. Subsequently, all the renal tissues were sliced to 5 μm-thick sections, fixed on glass slides and baked dry, followed by staining. According to the instructions, the sections were sequentially soaked in xylene, gradient ethanol and hematoxylin, and mounted in resin. After air drying, the sections were observed and photographed under a light microscope. Finally, the morphology of the renal cells, tubules and interstitium was observed.

Detection of expressions of related proteins in renal tissues via immunohistochemical staining

First of all, the renal tissue sections of the mice were deparaffinized in an incubator at 60°C for 30 min and then subjected to antigen retrieval via high-pressure citrate buffer method. Next, the renal tissues were covered with 3% hydrogen peroxide for 20 min of incubation and sealed in 8% goat serum for 30 min. Later, the renal tissues were completely covered with primary antibodies against Klotho, Collagen I and Collagen III (diluted with phosphate buffered saline (PBS) at 1:200) added in drops and incubated at 4°C overnight. The next day, the tissue sections were rewarmed, added dropwise with secondary antibody B solution and incubated at room temperature for 30 min, followed by flushing, addition with diaminobenzidine (DAB) developer working solution (Solarbio, Beijing, China) in drops and color development under a light microscope for a strictly controlled time period. After that, the tissue sections in each group were counterstained with hematoxylin, dehydrated in gradient ethanol and mounted. Finally, non-repeating regions of 10 randomly selected renal tissue sections were photographed under the light microscope (200×).

Detection of blood creatinine and urea nitrogen

Blood samples collected from the orbital vein were centrifuged at 3,000 rpm and 4°C in a centrifuge for 5 min. Then the supernatant was taken to determine the levels of creatinine and urea nitrogen in the blood samples using a fully-automatic biochemical analyzer.

Detection of expression of pro-inflammatory cytokines via reverse transcription-polymerase chain reaction (RT-PCR)

The total ribonucleic acids (RNAs) were extracted from fresh frozen renal tissues of mice by means of a TRIzol™ kit (Invitrogen, Carlsbad, CA, USA). The concentration and purity of the extracted RNAs in each group of samples were then tested by a spectrophotometer. After that, 2 μg of RNAs from each sample were reversely transcribed into complementary deoxyribonucleic acids (cDNAs). Subsequently, RT-PCR was performed for the cDNAs in a system containing 2.5 μL of 10× Buffer, 1 μL of cDNAs, 0.5 μL of forward primer (20 μmol/L), 0.5 μL of reverse primer (20 μmol/L), 10 μL of LightCycler® 480 SYBR Green I Master (2×) and 5.5 μL of ddH_2O. The RT-PCR

amplification system was the same for all the samples, and the gene primers applied are shown in Table I.

Masson's trichrome staining

Paraffin-embedded renal tissue sections were deparaffinized and dehydrated, followed by chromate treatment or elimination of mercury salt precipitation. Subsequently, the sections were washed with tap water and distilled water in sequence, and the cell nuclei were stained with Regaud hematoxylin staining solution or Weigert hematoxylin staining solution for 5-10 min. Next, the sections were washed in water and stained with Masson's ponceau acid fuchsin liquid for 5-10 min. After soaking in 2% glacial acetic acid solution, the sections were differentiated in 1% phosphomolybdic acid solution for 3-5 min. Finally, the sections were cleared in 95% alcohol, absolute alcohol and xylene and then mounted in neutral balsam.

Observation of glomerular mesangium through transmission electron microscopy

The fresh renal tissues were first cut into cubes (1 mm × 1 mm × 1 mm) and quickly fixed in fixative for transmission electron microscopy for 2 h. Post-fixation, the renal tissues were fixed in 1% osmic acid: 0.1 M phosphate buffer (PB) (pH7.4) at room temperature (20°C) for 2 h. Later, the tissues were rinsed with 0.1 M PB (pH7.4) for 15 min × 3 times. After repeated dehydration and permeation, the tissues were embedded in paraffin and cut into sections, followed by uranium-lead double staining (15 min in 2% ethanol solution saturated with uranyl acetate and 15 min in lead citrate) and drying at room temperature overnight. Finally, the sections were observed under a transmission electron microscope, and images were collected.

Western blotting

Frozen renal tissues of the mice in each group were taken out from the -80°C cryo-container, preliminarily cut into pieces and fully ground in a grinder. After ultrasonication, the lysis buffer was centrifuged, and the supernatant was aspirated and subpackaged into Eppendorf (EP) tubes. Later, the protein concentration was determined through bicinchoninic acid (BCA) method (Pierce, Rockford, IL, USA) and ultraviolet spectrophotometric assay, and the volume of all the sample proteins were maintained constant with an equal concentration. Next, the proteins were subpackaged and preserved in the refrigerator at -80°C. Then the total protein was extracted and subjected to sodium dodecyl sulphate-polyacrylamide gel electrophoresis (SDS-PAGE). After that, the proteins in the gel were transferred onto a polyvinylidene fluoride (PVDF) membrane (Millipore, Billerica, MA, USA) and incubated with primary antibodies at 4°C overnight and then with goat anti-rabbit secondary antibodies in the dark for 1 h. Finally, the protein bands were scanned and quantified using an Odyssey membrane scanner (Odyssey, Torrance, CA, USA).

Statistical analysis

All the data were analyzed using Statistical Product and Service Solutions (SPSS) 22.0 software (IBM, Armonk, NY, USA), the measurement data were presented as

Table I. *Primer sequences of indexes for RT-PCR*

Target gene		Primer sequence
GAPDH	Forward	5'-GACATGCCGCCTGGAGAAACCC-3'
	Reverse	5'-AGCCCAGGATGCCCTTTAGTCCA-3'
Interleukin-1 beta (IL-1β)	Forward	5'-CAGCTGATAGTCGTGATGTCGTAG-3'
	Reverse	5'-ACGTGTGATGACTGTGTACGTGTA-3'
IL-6	Forward	5'-ACGTAGCTAGCTGTGTAGTCGTAG-3'
	Reverse	5'-ATGTAGCTAGTCGATCGTAGAGAA-3'
Tumor necrosis factor-alpha (TNF-α)	Forward	5'-ACGTAGCTAGTCGTAGGAGAAAC-3'
	Reverse	5'-ACGTAGCTAGCTGTGTAGTCGTAG-3'

mean ± standard deviation, and *t*-test was performed for comparison of data between two groups. P<0.05 suggested that the difference was statistically significant.

RESULTS

Expression of Klotho in renal tissues of DN mice

The results of Western blotting (Fig. 1A) manifested that the mice aged 10 and 16 weeks in db/db group had a remarkably decreased expression level of Klotho in the renal tissues compared with those aged 16 weeks in db/+ group (P<0.05). It was further confirmed by the results of immunohistochemical staining that the protein expression level of Klotho in the renal tissues of db/db mice at the age of 16 weeks was notably lower than that in db/+ mice of the same age (Fig. 1B).

Effects of Klotho on renal functions of each group of mice

The levels of blood creatinine and urea nitrogen declined markedly in db/db + Klotho group in comparison with those in db/db group (P<0.05), suggesting that Klotho has potential nephroprotective effects (Fig. 2).

Effects of Klotho on DN mice

The H&E staining results (Fig. 3) indicated that in contrast with those in db/+ group, apparent abnormal pathological changes, such as cellular edema, necrosis, disorder arrangement and basement membrane injury, occurred in the renal tissues in the db/db group. However, such pathological damage to the renal tissues was evident only in the db/db + Klotho group compared with that in db/db group.

According to the results of transmission electron microscopy (Fig. 4), db/db group exhibited a distinctly larger area of glomerular mesangium than db/+ group (P<0.05), while exogenous supplementation of Klotho could prominently inhibit the widening of the glomerular mesangium in db/db + Klotho group (P<0.05).

Based on the RT-PCR results (Fig. 5), the expression levels of pro-inflammatory cytokines IL-1β, IL-6 and TNF-α in the renal tissues were elevated clearly in db/db group in comparison with those in db/+ group (P<0.05), while they were lowered remarkably after the exogenous supplementation of Klotho in db/db + Klotho group (P<0.05).

Renal fibrosis is one of the crucial pathological

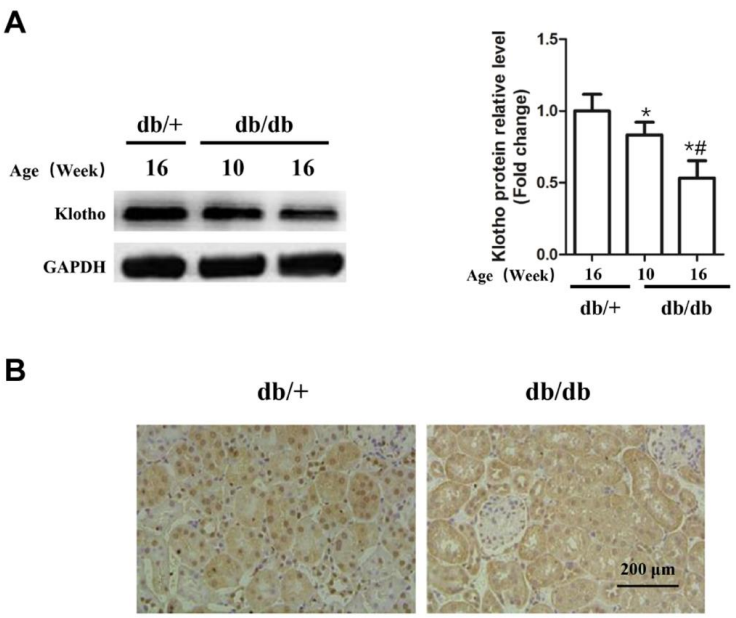

Fig. 1. *Expression of Klotho in renal tissues of DN mice. **A)** Western blotting **B)** immunohistochemical staining (magnification: 400×) db/+: control group, db/db: diabetic nephropathy group. *P<0.05 vs db/+ group, #P<0.05 vs db/db group (10 w).*

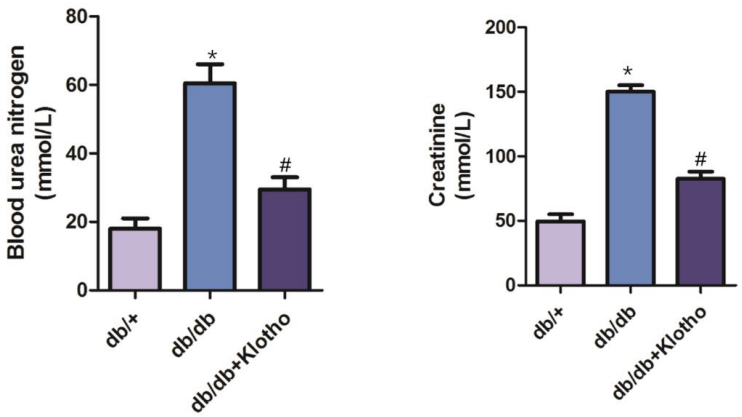

Fig. 2. *Effects of Klotho on renal functions of DN mice. db/+: control group, db/db: diabetic nephropathy group, db/db + Klotho: diabetic nephropathy + Klotho group. *P<0.05 vs db/+ group, #P<0.05 vs db/db group.*

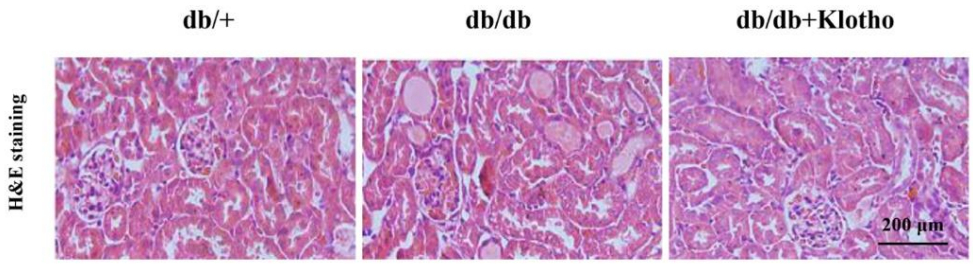

Fig. 3. *Effects of Klotho on pathological damage to renal tissues of DN mice. (magnification: 400×) db/+: control group, db/db: diabetic nephropathy group, db/db + Klotho: diabetic nephropathy + Klotho group*

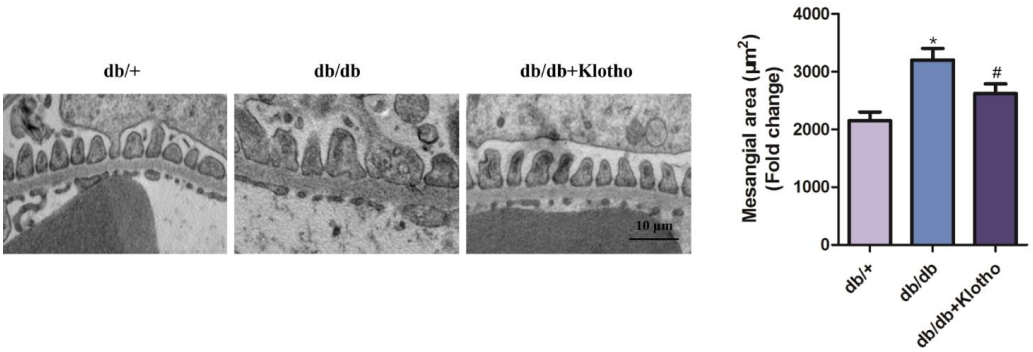

Fig. 4. *Effect of Klotho on glomerular mesangium of DN mice. db/+: control group, db/db: diabetic nephropathy group, db/db + Klotho: diabetic nephropathy + Klotho group. *P<0.05 vs db/+ group, #P<0.05 vs db/db group*

changes of DN. Hence, the status of renal fibrosis in each group of mice was examined, and it was found that the severity of interstitial fibrosis and the content of Collagen I and Collagen III in the renal tissues was evidently lower in db/db + Klotho group than those in db/db group (P<0.05) (Fig. 6).

The protein expression of FGF2 was enhanced notably, while that of E-cadherin was repressed obviously in the renal tissues in the db/db group in contrast with those in db/+ group (*P*<0.05)

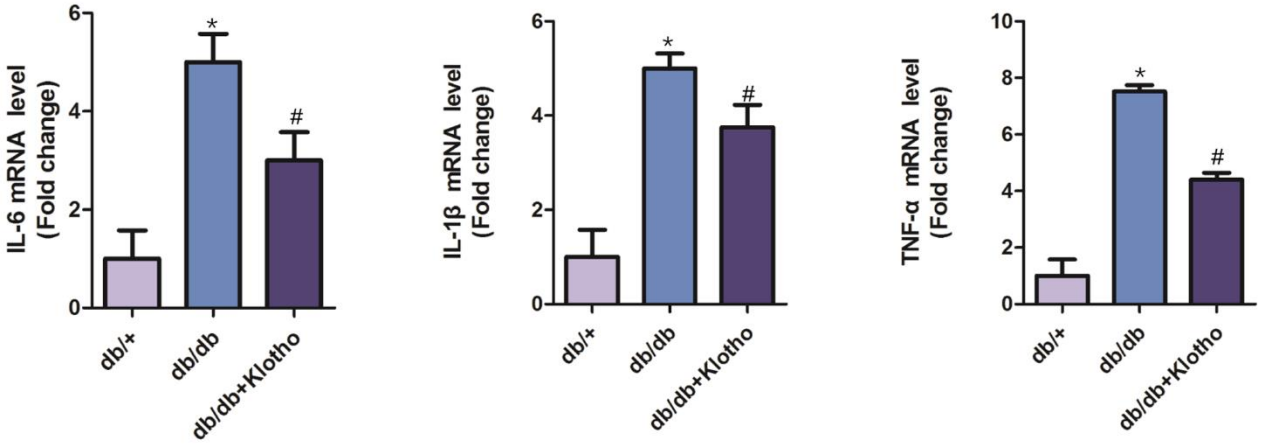

Fig. 5. *Effects of Klotho on expressions of pro-inflammatory cytokines in renal tissues of DN mice. db/+: control group, db/db: diabetic nephropathy group, db/db + Klotho: diabetic nephropathy + Klotho group. *P<0.05 vs db/+ group, #P<0.05 vs db/db group.*

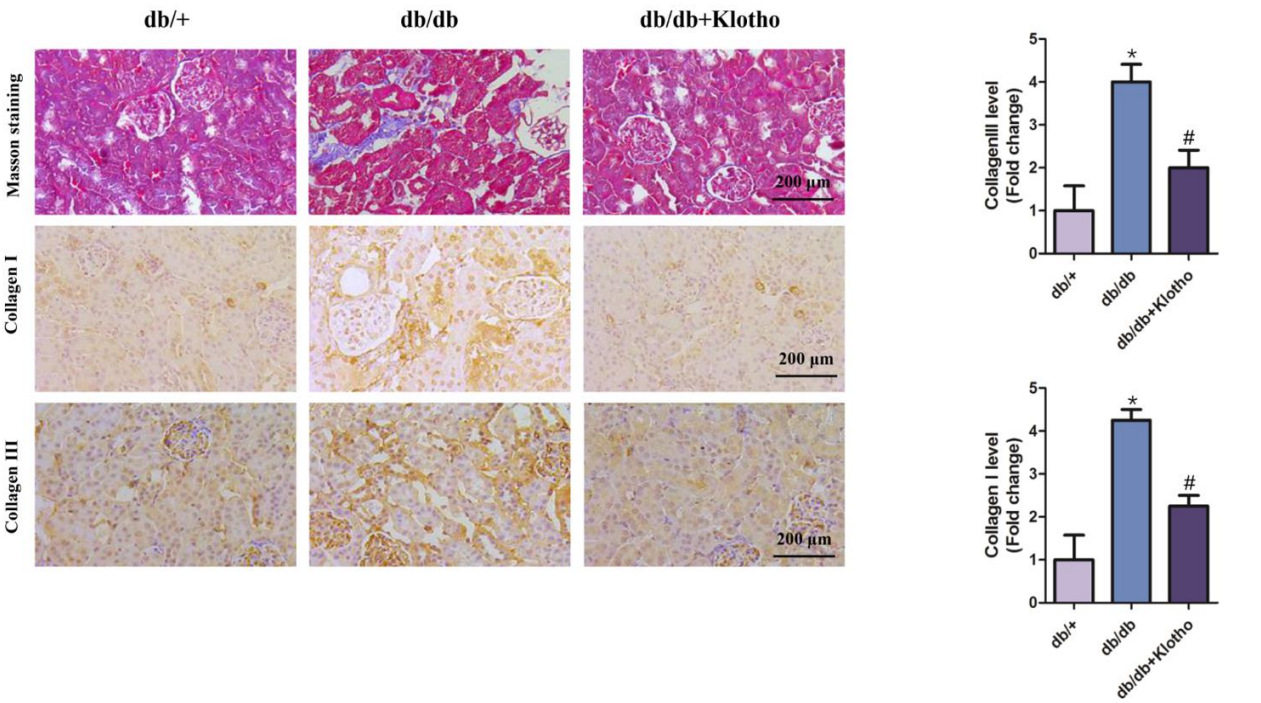

Fig. 6. *Effect of Klotho on fibrosis of renal tissues of DN mice. (magnification: 400×) db/+: control group, db/db: diabetic nephropathy group, db/db + Klotho: diabetic nephropathy + Klotho group. *P<0.05 vs db/+ group, #P<0.05 vs db/db group.*

(Fig. 7). With the exogenous supplementation of Klotho, however, the protein expression of FGF2 was inhibited distinctly, while that of E-cadherin was raised significantly in db/db + Klotho group compared with db/db group (P<0.05).

DISCUSSION

DN is not only a progressive renal disease secondary to diabetes mellitus, but is also one of the most common microvascular complications in

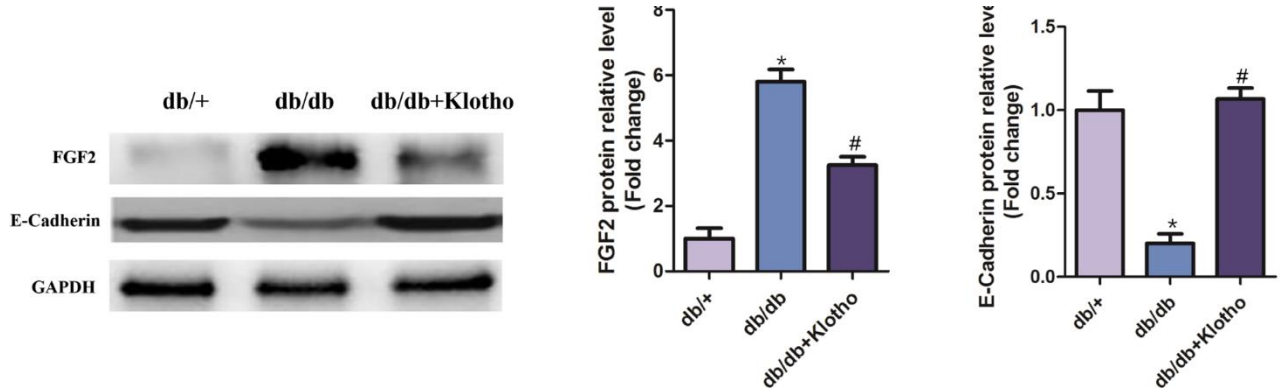

Fig. 7. *Impacts of Klotho on protein expressions of FGF2 and E-cadherin in renal tissues of DN mice. db/+: control group, db/db: diabetic nephropathy group, db/db + Klotho: diabetic nephropathy + Klotho group. * P<0.05 vs db/+ group, #P<0.05 vs db/db group.*

diabetic patients (11). Studies have illustrated that DN is an important cause of renal insufficiency, renal fibrosis and end-stage renal disease. According to statistics, 30-50% of the populations receiving renal replacement therapy in the world are DN patients treated with renal dialysis (12). It is well known that DN results from the combined action of various factors, such as genetic susceptibility, glucose metabolic disorders, changes in renal hemodynamics, oxidative stress and abnormalities of cytokines (13). The changes in renal function and structure are the major pathological characteristics of DN, including proteinuria, increase in renal glomeruli and renal tubules, thickening of glomerular basement membrane, renal interstitial fibrosis and podocyte damage (14). The severity of renal fibrosis is taken as a key indicator for the deterioration of renal function, and it is also an essential reason for the high mortality rate of DN, whose mechanism mainly involves the accumulation of ECM proteins (e.g. collagen and fibronectin) and epithelial-mesenchymal transition (15). Currently, microalbuminuria is considered the gold standard of DN diagnosis. DN patients can manifest microalbuminuria in the early stage and, as the disease progresses, obvious proteinuria and impaired renal function can be detected, and the glomerular filtration rate decreases gradually, finally resulting in end-stage renal disease (16). Therefore, deeply exploring the key molecular targets involved in the occurrence and development of DN is of important significance for the clinical targeted therapy for DN in the future.

As an anti-aging gene, Klotho is capable of encoding single-channel transmembrane proteins. The extracellular domain of Klotho protein is lysed by membrane-anchored proteases on the cell surface and then released into the blood, urine and cerebrospinal fluid. Klotho protein possesses diverse functions, including regulating multiple ion channels and oxidative stress (17). A previous study demonstrated that Klotho protein is closely associated with the development and progression of numerous diseases, such as atherosclerosis, heart failure, hypertension, acute renal injury, chronic renal disease, diabetes mellitus and cancer (18). Under physiological conditions, Klotho protein is highly expressed in the kidneys, but its expression is suppressed prominently in several animal models of renal injury and patients with chronic renal failure. For example, the treatment with calcineurin inhibitor can reduce the mRNA and protein expression levels of Klotho in the renal tissues of mice in in a dose- and time-dependent manner. The expression of Klotho has correlations with the activity of renin-angiotensin system, tubulointerstitial fibrosis and oxidative stress markers (19, 20). In the case of Klotho deficiency, the kidneys are more vulnerable to tacrolimus-induced injury, which may be strongly related to the aggravation of tacrolimus-induced oxidative

stress (21). Klotho participates in the transduction of a variety of signaling pathways in cells, including the PKC, FGF23, FGF2, cAMP, TGF-β, p53/p21, Wnt and PDLIM2/NF-κB p65 signaling pathways (22, 23). FGF23, a member of the FGF family, is unique in its property as a hormone that originates from skeleton but can regulate renal functions, while the majority of the FGF family members modulate various cell functions at local levels (24). It has been reported that FGF2, another member of the FGF family, is implicated in the occurrence and development of renal interstitial fibrosis, the mechanism of which is probably associated with the inhibition of FGF2 on E-cadherin. In this study, it was revealed that the DN mice had obviously increased protein expression level of FGF2 but notably decreased expression level of E-cadherin in the renal tissues. Nevertheless, the overexpression of Klotho could prominently repress the protein expression level of FGF2 and up-regulate that of E-cadherin in the kidneys of DN mice. Meanwhile, the injury and fibrosis of the renal tissues were alleviated distinctly, suggesting that Klotho may exert its nephroprotective effects by regulating the protein expression level of FGF2/E-cadherin. However, the specific action targets for Klotho need to be explored via in-depth studies.

In summary, it was verified in this research for the first time that Klotho expression is lowered in DN, while the exogenous Klotho may resist renal fibrosis by means of inhibiting the protein expression of FGF2 and activating the expression of E-cadherin.

ACKNOWLEDGEMENTS

Shaanxi Science and Technology Research and Development Project Fund (2017SF-263); Key Research Project in Shaanxi Province (2018SF-168).

REFERENCES

1. Harris MI, Eastman RC. Early detection of undiagnosed diabetes mellitus: a US perspective. Diabetes Metab Res Rev 2000; 16:230-36.
2. Ohishi M. Hypertension with diabetes mellitus: physiology and pathology. Hypertens Res 2018; 41:389-93.
3. GBD 2015 Eastern Mediterranean Region Diabetes and Chronic Kidney Disease Collaborators. Diabetes mellitus and chronic kidney disease in the Eastern Mediterranean Region: findings from the Global Burden of Disease 2015 study. Int J Public Health 2018; 63:177-86.
4. Ding C, Yang Z, Wang S, Sun F, Zhan S. The associations of metabolic syndrome with incident hypertension, type 2 diabetes mellitus and chronic kidney disease: a cohort study. Endocrine 2018; 60:282-91.
5. Urakawa I, Yamazaki Y, Shimada T, et al. Klotho converts canonical FGF receptor into a specific receptor for FGF23. Nature 2006; 444:770-74.
6. Li SA, Watanabe M, Yamada H, Nagai A, Kinuta M, Takei K. Immunohistochemical localization of Klotho protein in brain, kidney, and reproductive organs of mice. Cell Struct Funct 2004; 29:91-99.
7. Erben RG, Andrukhova O. FGF23-Klotho signaling axis in the kidney. Bone 2017; 100:62-68.
8. Lim K, Lu TS, Molostvov G, Lee C, Lam FT, Zehnder D, Hsiao LL. Vascular Klotho deficiency potentiates the development of human artery calcification and mediates resistance to fibroblast growth factor 23. Circulation 2012; 125:2243-55.
9. Hu MC, Shi M, Zhang J, Quinones H, Griffith C, Kuro-o M, Moe OW. Klotho deficiency causes vascular calcification in chronic kidney disease. J Am Soc Nephrol 2011; 22:124-36.
10. Sugiura H, Yoshida T, Mitobe M, Yoshida S, Shiohira S, Nitta K, Tsuchiya K. Klotho reduces apoptosis in experimental ischaemic acute kidney injury via HSP-70. Nephrol Dial Transplant 2010; 25:60-68.
11. Wu R, Liu X, Yin J, et al. IL-6 receptor blockade ameliorates diabetic nephropathy via inhibiting inflammasome in mice. Metabolism 2018; 83:18-24.
12. Kim Y, Lim JH, Kim MY, et al. The adiponectin receptor agonist adiporon ameliorates diabetic nephropathy in a model of type 2 diabetes. J Am Soc Nephrol 2018; 29:1108-27.
13. Zhang XG, Zhang YQ, Cheng QP, Cao Y, Sun JM, Lv XF. The impact of insulin pump therapy to oxidative stress in patients with diabetic nephropathy. Eur J Med Res 2018; 23:7.

14. Shima K, Hirota M, Fukuda M, Tanaka A. Determination of urinary lysozyme for potential detection of tubular dysfunction in diabetic nephropathy. Clin Chem 1986; 32:1818-1822.
15. Zhu L, Han J, Yuan R, Xue L, Pang W. Berberine ameliorates diabetic nephropathy by inhibiting TLR4/NF-kappaB pathway. Biol Res 2018; 51:9.
16. Wang D, Zhang G, Chen X, et al. Sitagliptin ameliorates diabetic nephropathy by blocking TGF-beta1/Smad signaling pathway. Int J Mol Med 2018; 41:2784-92.
17. Lee S, Choi J, Mohanty J, et al. Structures of beta-klotho reveal a 'zip code'-like mechanism for endocrine FGF signalling. Nature 2018; 553:501-5.
18. Luo K, Lim SW, Quan Y, et al. Role of Klotho in chronic calcineurin inhibitor nephropathy. Oxid Med Cell Longev 2019; 2019:1825018.
19. Han DH, Piao SG, Song JH, et al. Effect of sirolimus on calcineurin inhibitor-induced nephrotoxicity using renal expression of KLOTHO, an antiaging gene. Transplantation 2010; 90:135-41.
20. Raeisi S, Ghorbanihaghjo A, Argani H, et al. Effects of angiotensin ii receptor blockade on soluble Klotho and oxidative stress in calcineurin inhibitor nephrotoxicity in rats. Iran J Kidney Dis 2016; 10:358-63.
21. Lim SW, Jin L, Luo K, Jin J, Shin YJ, Hong SY, Yang CW. Klotho enhances FoxO3-mediated manganese superoxide dismutase expression by negatively regulating PI3K/AKT pathway during tacrolimus-induced oxidative stress. Cell Death Dis 2017; 8:e2972.
22. Ji B, Wei H, Ding Y, et al. Protective potential of Klotho protein on diabetic retinopathy: evidence from clinical and in vitro studies. J Diabetes Investig 2020; 11:162-69.
23. Cong LH, Du SY, Wu YN, et al. Upregulation of Klotho potentially inhibits pulmonary vascular remodeling by blocking the activation of the Wnt signaling pathway in rats with PM2.5-induced pulmonary arterial hypertension. J Cell Biochem 2018; 119:5581-97.
24. Kuro-o M. Overview of the FGF23-Klotho axis. Pediatr Nephrol 2010; 25:583-90.

Cell and platelet composition assays by flow cytometry: basis for new platelet-rich fibrin methodologies

L.A. de Oliveira[1,2*], R.O. Soares[1], M. Buzzi[2], C.F.A.B. Mourão[3], T. Kawase[4] and S.A.S. Kuckelhaus[1]

[1]Nucleus of Research in Applied Morphology and Immunology, Faculty of Medicine, University of Brasilia, Brasília, Brazil; [2]Innovacorium Inc., Gainesville, USA; [3]Department of Oral Surgery, Federal Fluminense University, Niterói, Brazil; [4]Division of Oral Bioengineering, Institute of Medicine and Dentistry, Niigata University, Niigata, Japan

Received May 15, 2020 – Accepted July 10, 2020

Platelet-rich plasma (PRP) and platelet-rich fibrin (PRF) are selective blood fractions obtained by centrifugation. They act locally on inflammation and immunity as adjuvant homeostatic modulators during tissue regeneration. In recent years, many methods for achieving these blood concentrates have emerged, whose parameters of time and force of centrifugation presented themselves as critical, conflicting, and poorly understood points. Thus, the present study aimed to evaluate the effect of different centrifugal experimental parameters on the concentration of cells and platelets in samples of anticoagulated blood. Blood samples were centrifuged by forces of 200, 400 and 800 x g for 5, 10 and 15 minutes of centrifugation times to obtain three fractions: a) platelet-poor plasma (PPP), b) leukocyte-rich plasma (L- PRP) and c) red blood cell sediment (RBC). The leukocyte and platelet content of each centrifuged fraction was measured by automated flow cytometry associated with the peroxidase reaction for differential leukocyte count. The application of 200 x g generated a more significant dispersive content of leukocytes and platelets in the supernatant fraction of PPP when compared to the other two strength ranges. However, it presented the highest concentration of platelets in the sediment (P <0.05 ANOVA), representing a loss of total mass during processing. The 400 and 800 x g forces showed leukocytes and platelets condensed in the L-PRP fraction and lower levels in the sediment, demonstrating the greater effectiveness of buoyancy in the resuspension of these sedimented elements. Our experimental data showed that the concentration and organization of leukocytes and platelets in the centrifuged blood matrices are very sensitive to variations in g force and centrifugation time, thus generating products with different biological composition and characteristics, and with specific potential therapeutic effects. The present study did not focus on comparing authoring methods, but on presenting the impact of methodological variations on the biological nature of centrifuged blood matrices. Further in vivo studies are needed to assess the specific clinical effect of each methodological change.

In blood clotting, the fibrin network, platelets/exosomes, microparticles and leukocytes are directly responsible for the early stages of tissue repair, and factors such as fibrin matrix of higher density, leukocytes and platelet concentration and erythrocyte segregation are fundamental (1). In the tissue repair process, blood elements that act on cell signalling and adhesion are especially derived from

Keywords: centrifugation; g-force; platelets; leukocytes; platelet rich-fibrin

Corresponding Author:
Leonel Alves de Oliveira, DDS, MSc, PhD.
Department of Morphology,
Faculty of Medicine, University of Brasilia, Brasilia,
Federal District, Brazil 70910-000
Tel.: +55 61 981755505
e-mail: profleonel2@gmail.com

0393-974X (2020)
Copyright © by BIOLIFE, s.a.s.
This publication and/or article is for individual use only and may not be further reproduced without written permission from the copyright holder.
Unauthorized reproduction may result in financial and other penalties
DISCLOSURE: ALL AUTHORS REPORT NO CONFLICTS OF INTEREST RELEVANT TO THIS ARTICLE.

platelets, leukocytes and blood plasma. These include glycoproteins, immunoglobulins, cytokines, growth factors and circulating microparticles that act in modulating the angiogenic and reparative response in injured sites (2-3).

The principle of obtaining a blood matrix rich in platelets and leukocytes is selective blood separation with differential centrifugation according to their relative corpuscular densities of its figurative elements (4). Thus, in the context of regenerative medicine, platelet-rich plasma (PRP) emerged for autologous non-transfusion therapies (5). This therapy using blood concentrate had its apex with the studies of Marx (6) and Anitua (7) and became quite popular during the 1990s and 2000s (8). The methodological principle for obtaining PRP was based on double centrifugation to ensure a small fraction of leukocyte-free plasma and intact platelets for subsequent chemical activation. Its use in the coagulation cascade lacked standardization and even xenogenic agents, such as bovine thrombin, that were used in its processing (9-12), leading to controversial or ineffective results as an adjuvant in tissue repair (13-14).

Choukroun et al. (15) devised a simplified, additive-free methodology for obtaining platelet-rich fibrin (PRF), and later Dohan Ehrenfest (16) characterized by the leukocytes and platelet composition, ultrastructural morphology, mechanical resistance and platelet growth factors. These studies provided the science of clinical use blood concentrates with extensive and enlightening scientific production (1, 17, 18). Ghanaati et al. (19) proposed a low-speed centrifugation concept (LSCC) for enriched cell composition and presented the new method named 'advanced platelet-rich fibrin' (A-PRF™) (20).

Generally, the PRF is a red blood cell (RBC) free clot with supraphysiological blood platelet concentrations by proportional volume, obtained without anticoagulants in a closed sterile system and by a single low-speed centrifugation process (20); its clinical use should be exclusively autologous.

Current literature shows that several g-forces have been used in clinical and laboratory trials without showing their real influence on the biological composition of blood concentrates, PRP and PRF (21-23). Miron et al. (24) presented research that contributed to a better understanding of the effects of g-force on the cellular composition of PRF matrices evaluating only the A-PRF ™ (200 x g/8 min) and intraspin L-PRF ™ (400 x g/12 min) protocols.

Considering platelet concentration correlates with the therapeutic potential of the autologous blood concentrates, the present study aimed to observe the effects of diverse experimental ranges of g-forces and spin time on cell/platelet concentration in experimental anticoagulated blood fractions as a basis for PRF methodologies development.

MATERIALS AND METHODS

Individuals and ethical aspects

The participants were 5 healthy adult volunteers, non-smokers and free from any systemic disease (2 females, 3 males, age range: 25-49 years), who consented to donate 40 mL of blood for the study. All ethical standards for scientific research with humans were strictly adhered to, in accordance with Law 6.638/79 and in accordance with the Declaration of Helsinki (World Medical Association Recommendation 2013). The study was approved by the Research Ethics Committee of the Medical School of the University of Brasilia under number 055468/2015.

Plasma samples to cell count

In order to collect blood plasma samples, 10 tubes (4 mL) of anticoagulant-containing polystyrene (EDTA) (Greiner Bio-One, Brazil) were used. Blood collection was performed with tubes containing anticoagulant to enable cell counting by automated hemocytometer. Thus, blood plasma fractions after the experimental centrifugations was characterized as platelet poor plasma (PPP) and platelet rich leukocyte plasma (L-PRP).

Volunteers' blood was collected by peripheral venipuncture in one of the antecubital fossa veins and was immediately transferred to a fixed-angle rotor centrifuge Fibrinfuge25 (Montserrat, Brazil) (Fig. 1a). Blood plasma specimens were obtained by differential centrifugation with 200, 400 and 800 x g-forces at time intervals (Δt) of 5, 10 or 15 min, and

at room temperature. Then, 3 aliquots (1 mL) from distinct regions (Fig. 1b) of each tube were extracted by aspiration immediately after centrifugation to avoid stationary sedimentation using automatic pipette (Gilson, France) - Top of supernatant or platelet poor plasma (PPP): 1; Lower part of the supernatant or platelet rich plasma (PRP) + buffy coat zone was denominated (L-PRP): 2; Red blood cells sediment (RBC): 3 – were collected and transferred to additive-free plastic cryovials (Eppendorf, USA).

Sequential pipetting methodology

In order to investigate cell concentration after centrifugation using different experimental parameters, a sequential pipetting methodology was made by the same operator. Each 1 mL of the blood fraction was then analyzed by hemocytometry.

Cell and platelet quantification

Hemocytometry was performed using the automatic hematology counter coupled to the peroxidase reaction staining method for leukocyte differentiation ADVIA 2120 Hematology System (Siemens, Germany). As control, red blood cells, leukocytes and platelets were quantified in aliquots of whole blood before centrifugation.

Statistical analysis

The results were evaluated using Bartlett's test for equal variances and the Kolmogorov–Smirnov test for normal distribution before comparative analysis. The analyses were performed by the ANOVA test, followed by the Student–Newman-Keuls method or Kruskal–Wallis test, followed by Dunn's method to compare multiple unrelated samples of normally or non-normally distributed data, respectively. The Prism 8.0 software package (GraphPad, USA) was employed for statistical tests and graphical presentation of the data and differences with a two-tailed value of $p < 0.05$ were considered statistically significant.

RESULTS

Concentration of leukocytes and platelets

Cell count included total erythrocyte, total

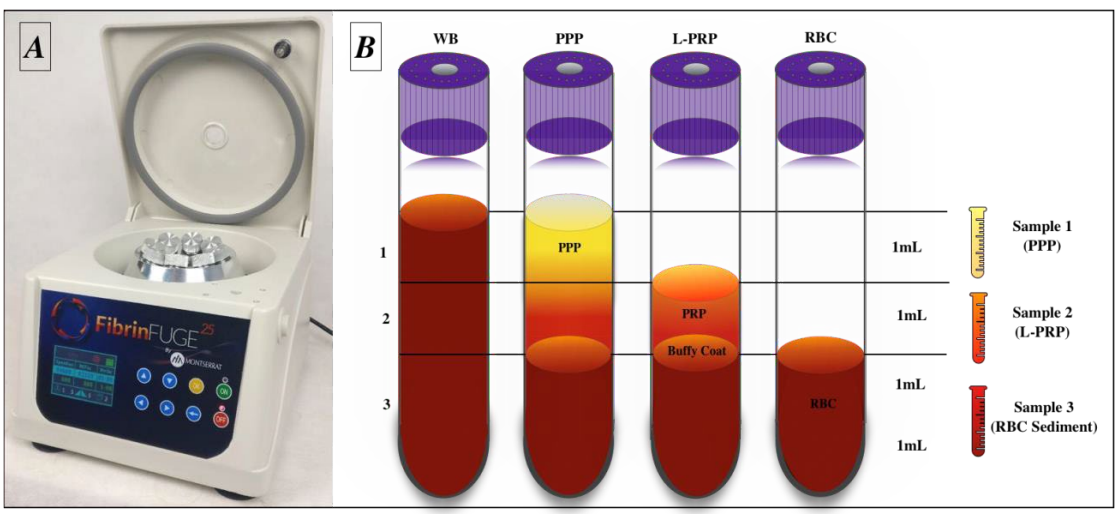

Fig. 1. ***A)*** *FibrinFUGE[25] centrifuge device;* ***B)*** *Illustrative diagram of the blood regions after centrifugation containing (1): PPP, (2): L-PRP, and (3): RBC sediment fractions elected for leukocyte and platelet quantitation. The L-PRP fraction corresponds to the added buffy coat and PRP. WB: whole blood; PPP: platelet-poor plasma; L-PRP: leukocyte platelet-rich plasma; RBC: red blood cells.*

and differential leukocyte and platelet in whole blood, RBC sediment, and two supernatant fractions - PPP and L-PRP - obtained by elected experimental centrifugations in which whole blood (WB) count served as the baseline for comparing the hematological. Fig. 2 (1-4) shows the whole blood cytogram which represents the baseline for comparative counts. All PPP experimental fractions (A1, A2 and A3) show platelet concentrations below physiological levels. PPP at 200 x g (A1) shows higher platelet concentration in these groups. L-PRP zones show higher platelet and leukocyte concentration highlighting (B1). B3 presented higher concentration than B2 (B1> B3> B2). RBC sediment showed the presence of leukocytes and platelets in C1 and C2 with lower concentration in C3.

Centrifugation at 200 x g

The 200 x g was sufficient to generate supraphysiological concentrations of platelet in supernatant fractions (PPP and L-PRP). However, RBC sediment evaluation showed that a significant part of the platelets (21-61%) were sedimented with the erythrocytes, and this represented functional loss (Fig. 3B). PPP concentrations were below the physiological levels observed in WB. The data demonstrated inverse proportionality between time and platelet concentration, i.e., 5, 10 and 15 min showed significant reduction in concentrations ($p = 0.002$, ANOVA). L-PRP concentrations were increased to levels higher than WB in all Δts. Fig. 3C, shows that leukocyte was present in the sediment, indicating that the lower the Δt, the higher the concentration ($p = 0.013$ ANOVA). Leukocyte low levels ($<0.02 \times 10^3$cell/µl) were found in PPP in all Δts, whereas in L-PRP, average leukocyte levels were found close to the physiological values of WB. Fig. 3D shows that granulocyte concentrations between

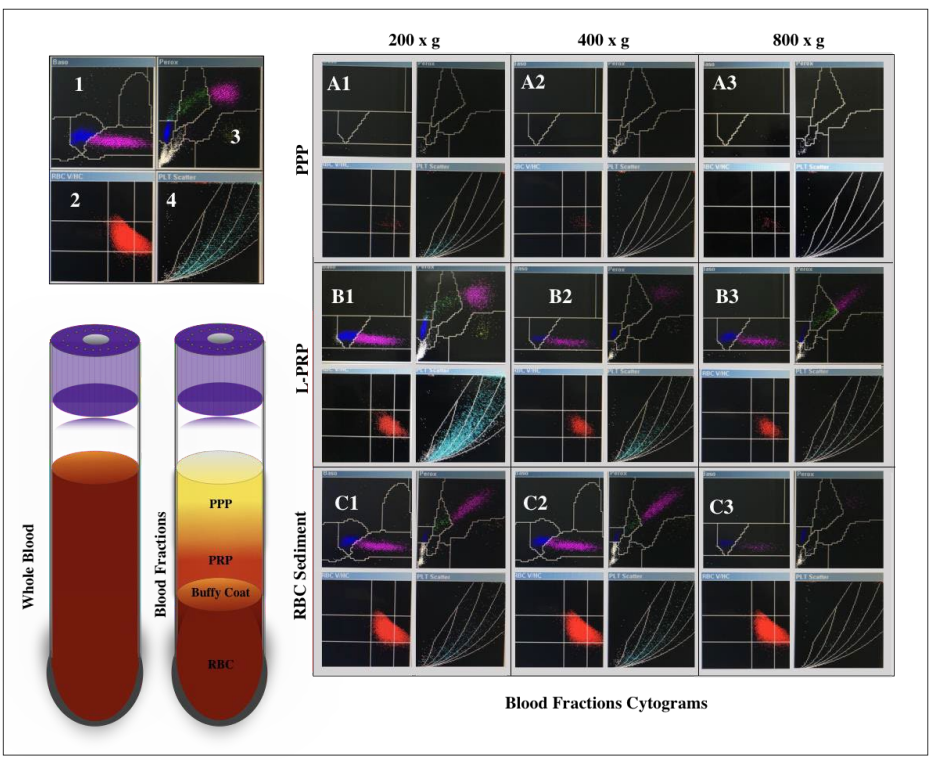

Fig. 2. *Cytogram by flow cytometry. Whole blood baseline, blood fractions (PPP, L-PRP and RBC Sediment) only (Δt) 10 min at g-forces of 200, 400 and 800 x g. Note reduced cell concentration in all PPP fractions and leukocytes in RBC sediment. (L-PRP = PRP + Buffy Coat). (1): Granulocytes and mononuclear cells; (2): RBC; (3): Differential leukocyte count; (4): Platelet Scattering.*

the sediment and the L-PRP fraction were similar. Although the density of the granulocytes was close to that of the erythrocytes, most of them remained in the supernatant fraction, especially in L-PRP. Significantly higher concentration of monocytes was observed in PPP and L-PRP at 5 min condition ($p = 0.02$ ANOVA) (Fig. 3E). Fig. 3F, shows that lymphocyte content in the sediment in the PPP concentrations were drastically reduced, whereas in L-PRP the levels were higher particularly at 5 and 10 min Δts conditions.

The 200 x g/5min centrifugation generated erythrocyte concentrations equivalent to that of whole blood, as well as a significant reduction in supernatant fractions. This centrifugation condition was efficient to settle red blood cells. The concentration of the L-PRP platelet supernatant (328.67±19.86 x 10^3 cell/µl) correspond an increase of 46.5% in relation to the concentration in whole blood (WB) (224.00±7.94 x 10^3 cell/µl). Platelet concentration of PPP (0.02±0.00 x 10^6 cell/µl) was observed to be 24.5% below the physiological levels found in the WB. Total leukocyte count in RBC sediment (4,95±0.91 x 10^3 cell/µl) revealed that about 67.7% of leukocytes were kept in the sediment, demonstrating that the 5 min time interval was not sufficient to favor leukocyte diffusion into the sediment - lower density particle thrust to the supernatant fraction or limiting meniscus. The differential leukocyte counts showed a high L-PRP lymphocyte concentration (4.64±0.64 x 10^3 cell/µl), whereas granulocyte concentration (1.19±0.37 x 10^3 cell/µl) was proportionally lower to physiological levels (26.6%). A percentage of 73.4% of total granulocytes was found in the sediment. This demonstrates that proximity of corpuscular density between erythrocytes (1.095g/dL) and granulocytes (1.085g/dL) favored granulocyte sedimentation with centrifugation of 200 x g/5min.

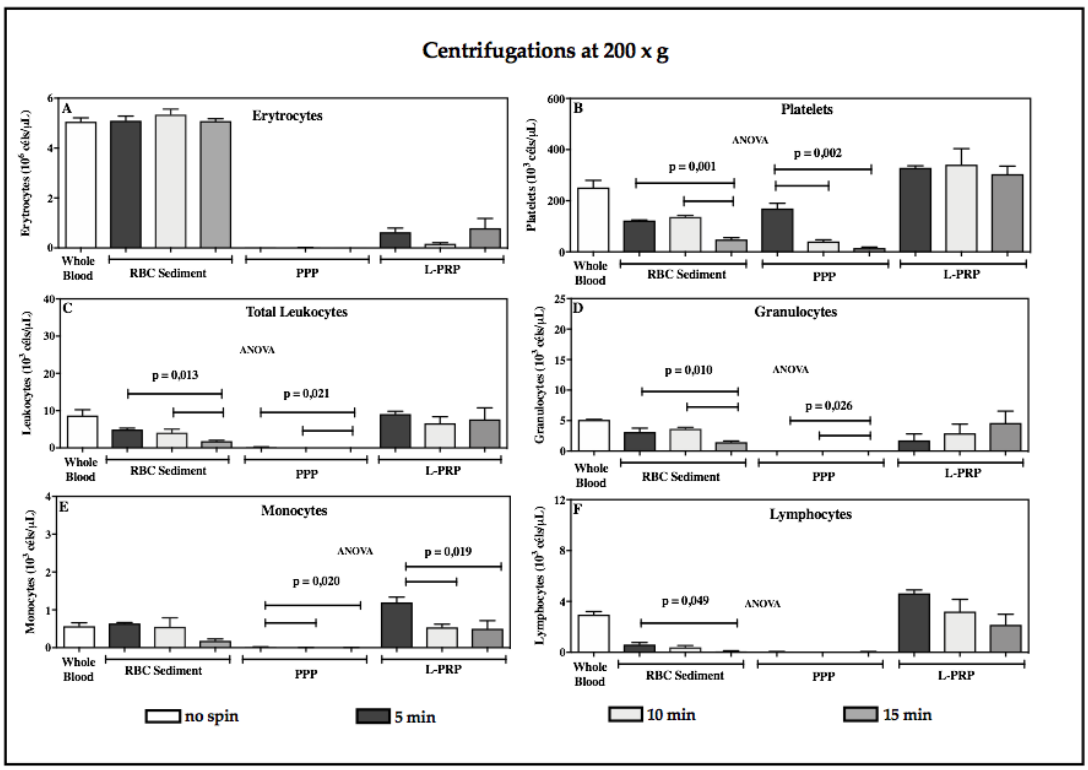

Fig. 3. *Hematological indexes (erythrocytes, platelets, total leukocytes, granulocytes, monocytes and lymphocytes) in whole blood, in the RBC sediment and in the supernatant fractions of PPP and L-PRP, (n = 5) where (p <0.05 ANOVA) represented significant difference between time intervals (Δt) 5, 10 and 15 min at RCF 200 x g.*

The 200 x g/10 min centrifugation revealed some similarities with the findings 200 x g/5 min, except for the 81.84% reduction in platelet concentrations in PPP (40.67±16.50 x 10^3 cell/µl) and the elevation in lymphocyte concentration in L-PRP (3.20±2.39 x 10^3 cell/µl) being 15.9% above that observed in WB (2.76±0,26 x 10^3 cell/µl). Monocytes presented slightly higher concentrations (5.76% (1.19±0.37 x 10^3 cell/µl) than in WB and the presence of granulocytes in L-PRP showed a perceptible reduction of 64.93% when compared to the centrifugation of 200 x g/5min (26.6%).

The 200 x g/15 min centrifugation showed an increase in leukocyte concentration in L-PRP (7.65±0.37 x 10^3 cell/µl) but completely sedimented in the buffy coat zone. Platelet concentration (304.00±76.62 x 10^3 cell/µl) was equivalent with 5 and 10 min. In the PPP fraction, a significant reduction in the platelet and leukocyte concentration was observed. The assays with 200 x g/5 (3.66±0.54 x 10^3 cell/µl) and 10 (3.13±1.56 x 10^3 cell/µl) min showed higher concentrations of granulocytes in the sediment and lower with 15 min (4.60±4.73 x 10^3 cell/µl).

Centrifugation at 400 x g

Centrifugation at 400 x g/5 min resulted in a high leukocyte concentration in the sediment which corresponded to 67.75% (4.87±2.66 x 10^3 cell/µl) of the total leukocytes in the sample. The platelet concentration presented levels compared to those obtained in the g-force centrifugations of 200 x g. The monocyte concentration increased by 128.84% (1.49±1.57 x 10^3 cell/µl) when compared to the WB.

Centrifugation at 400 x g/10 min kept the total leukocyte content in supernatant fractions near to the physiological levels of WB. Neutrophils (0.76±0.64 x 10^3 cell/µl) and lymphocytes showed the highest concentrations in this condition, 78.27% and 114.51%, respectively. Platelet concentration in the sediment represented 42% of the total in WB. This demonstrated that this parameter causes a reduction in the final platelet concentration in the supernatant portions PPP and L-PRP, where its gain was only 38.24%.

Centrifugation at 400 x g/15 min resulted in platelet concentrations that were inversely proportional to the centrifugation time. The concentration of total leukocytes was below (2.26±0.91 x 10^3 cell/µl) the values of WB. Thus, such configuration was not useful to enrich the supernatant with leukocytes and platelets.

With concentration of hematological indexes under the effect of g-force of 400 x g at 5, 10 and 15 min, the erythrocytes levels in the sediment showed higher levels than those found in WB, indicating higher sedimentation force when compared to all times in the g-force of 200 x g (Fig. 4A). Supernatant fraction of PPP showed low levels, which also indicated the sedimentation efficiency in this RCF range. L-PRP fraction at 5 min Δt, on the other hand, showed the highest erythrocyte concentration among the 3 Δts compared to 400 x g. The presence of platelets in the sediment was verified, with higher concentration in Δt of 5 min, representing slightly more than 1/3 of the WB concentration (Fig. 4B). As Δt increased, platelet concentration decreased. This behavior was also reproduced in the supernatant fractions. However, in PPP the concentrations were greatly reduced when compared to 200 x g, with a significant difference as a function of time ($p = 0.049$ ANOVA). In L-PRP, platelet concentrations reproduced a pattern similar to that observed in 200 x g with a slight increase. The total leukocyte count exhibited higher sediment concentrations than at 5 and 10 min (Fig. 4C). In PPP, the presence of leukocytes was greatly reduced, and in L-PRP, despite the significant concentration at 10 min Δt ($p = 0.49$ ANOVA), the levels were still below the physiological concentration of WB. The granulocyte count showed that about 50% remained in the sediment (Fig. 4D). The fraction of PPP presented low concentration, it being higher in L-PRP. The monocyte count showed higher concentration lower relative sediment concentrations compared to total leukocytes and granulocytes (Fig. 4E). In L-PRP the concentration observed at Δt 5 min was above 100% of physiological WB values. The lymphocyte counts showed lower sediment concentrations and high L-PRP levels, and the most prominent subgroup was at Δt 10 min with concentration equivalent to the WB (Fig. 4F).

Centrifugation at 800 x g

With centrifugation at 800 x g/5 min, L-PRP fraction showed an increase over 100% in all the hematological indices (platelets 114%; total

leukocytes 136.66%; granulocytes 119.62%; lymphocytes 103.62%, monocytes 127%). This centrifugation condition was efficient to separate blood elements allowing a greater harvesting of cells and platelet when compared to the conditions with 200 and 400 xg in same Δt.

Centrifugation at 800 x g/10 min exhibited elevated hematologic indexes in the supernatant fraction of L-PRP (platelets 171.12%; total leukocytes 264.43%; granulocytes 214.22%; lymphocytes 205.43%, monocytes 346.15%). The PPP supernatant fraction was very scarce where only the 0.5% platelet concentration stood out. With this configuration the leukocyte and platelet population was more compacted in the buffy coat zone.

Centrifugation at 800 x g/15 min gave leukocytes and platelet indexes in the supernatant fractions close to those observed at 800 x g/10 min and 800 x g/5 min.

Erythrocyte counts demonstrated total sedimentation in all Δt subgroups (Fig. 5 A-F). The L-PRP fraction exhibited very low levels, especially at Δt 15 min. Fig. 5B shows a significant reduction in platelet concentration in the sediment and in PPP (p = 0.001 ANOVA). L-PRP fraction showed the highest concentrations in leukocyte population and was predominantly condensed in this fraction, especially under the condition of Δt 10 min (Fig. 5C). Granulocyte count (Fig. 5D) exhibited similar patterns to total leukocytes, however, remnant concentrations were observed in the sediment,

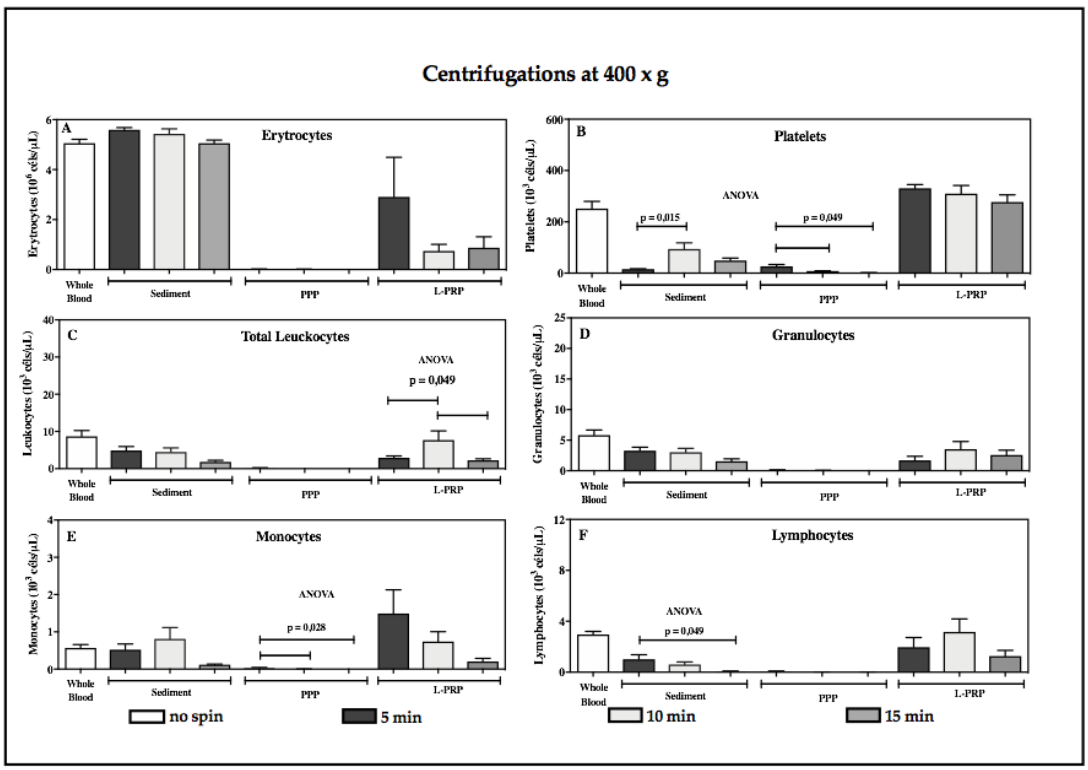

Fig. 4. *Hematological indexes (erythrocytes, platelets, total leukocytes, granulocytes, monocytes and lymphocytes) in whole blood, in the RBC sediment and in the supernatant fractions of PPP and L-PRP, (n = 5) where (p <0.05 ANOVA) represented significant difference between time intervals (Δt) 5, 10 and 15 minutes at RCF 400 x g.*

lower than those observed in the other g-forces, but significant enough to demonstrate that the perpendicular g-force applied to the fixed-rotor angle (25º) of the tube favored the thrust of granulocytes to the upper fractions by buoyance residual force. The monocytes were predominately separated in L-PRP with levels above 100% at Δt 10 min (Fig. 5E). Lymphocytes showed no counts in the sediment, but in PPP and L-PRP fractions they reached the supraphysiological levels (Fig. 5F).

DISCUSSION

The present study verified the influences of g-forces and time of centrifugation on the leukocyte and platelet composition in anticoagulated blood samples. The experiments carried out showed that the choice of the g-force used to obtain blood concentrates has a high impact on this content of the centrifuged fractions due to the system of mechanical forces integrating the angular movement.

Archibald et al. (25) demonstrated that centrifugation is an artificial gravitational microsystem generated by angular motion where particles settle as a function of their shape, volume and density. The g-force is an inertial force resultant of sedimentation, friction and thrust forces in this system (25). Fraser et al. (26), assessing chylomicron sedimentation, demonstrated that g-force is an interactive mechanism between frictional sedimentation (Fs) and buoyancy (Fb) mechanical forces where the corpuscular density of each particle is crucial to promote a stratification.

Several studies (25-27) demonstrated the fundamentals of density gradient centrifugation that are reproduced in blood fractionation. In this way,

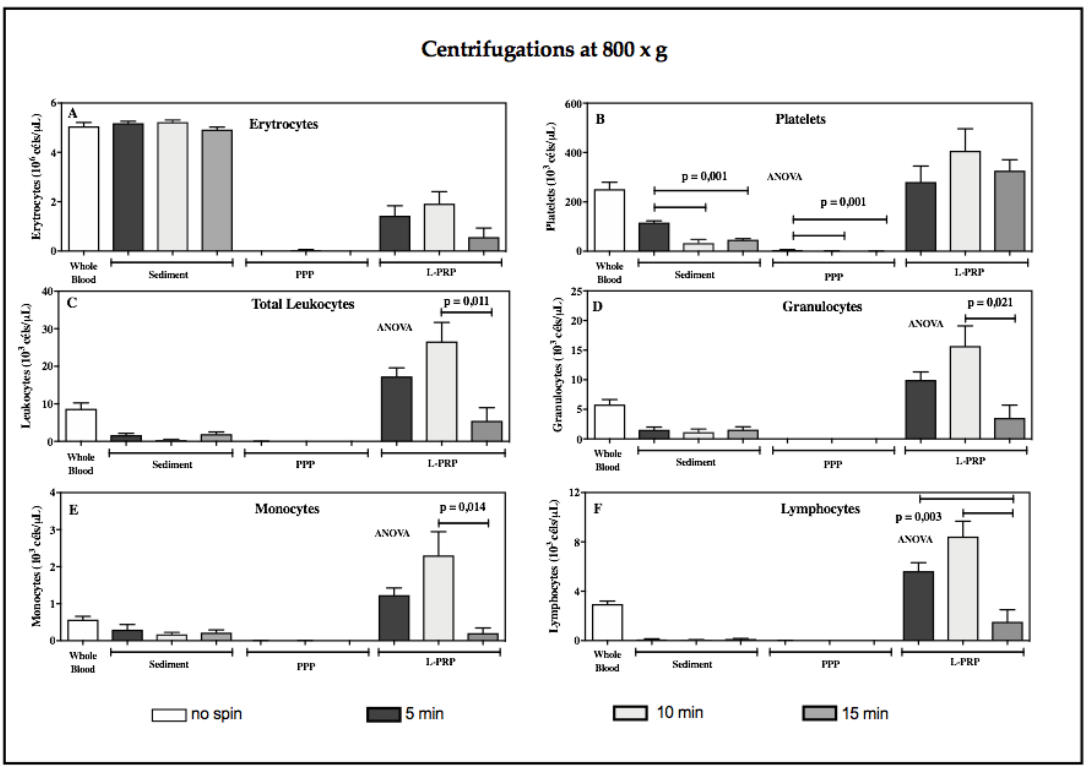

Fig. 5. *Hematological indexes (erythrocytes, platelets, total leukocytes, granulocytes, monocytes and lymphocytes) in whole blood, in the RBC sediment and in the supernatant fractions of PPP and L-PRP, (n = 5) where (p <0.05 ANOVA) represented significant difference between time intervals (Δt) 5, 10 and 15 minutes at RCF 800 x g.*

the system of forces acting on the centrifugation of the blood generates sedimentation and thrust, causing lower density particles to be suspended in the opposite direction to sedimentation. Thus, for selective blood separation to obtain therapeutic blood concentrate, differential centrifugation is able to fractionate the figurative elements of this multiphase colloidal fluid according to their relative corpuscular densities (28).

In recent years, studies have been developed with the purpose of understanding and standardizing centrifugation methods aiming to a better efficacy in obtaining fibrin matrices for autologous therapeutic purposes (19, 21, 29-31). In these studies, elements such as cell concentration have gained prominence, since they may influence the concentration of exosomes and growth factors (32). However, indistinct forces provided by indiscriminate methodological variations have also been frequent, but without presenting a specific technical approach to their influence on morphological, biochemical and functional aspects of blood concentrates (33). Different methods for obtaining L-PRF matrices have shown diversity in nomenclature and parameters without any evidence of plausible clinical or therapeutic advantage, as their comparisons are limited to *in vitro* analyses (34). This motivated us to observe the effects of experimental g-forces and time ranges on cell/platelet concentration in different parametric variations. Thus, we observed the cellular concentration under the parametric effect, not limiting the observation to pre-established methodologies, as has been recurrent in some comparative studies (4, 24, 35). In the same way that matrices with increased platelet concentration can generate more significant cellular interaction with the adjacent tissue, fibrin matrices without cells or platelets can configure specific therapeutic strategies, such as drug system delivery or protecting dressings, with minus metabolic interference from growth factors.

In the present study, cells and platelets were quantified, with red blood cells allowing comparison with whole blood and sediment data after centrifugation. These data showed the efficiency of centrifugation in erythrocyte sedimentation, even in the smallest g-forces and times ranges used by the proximity of experimental concentrations to those observed in whole blood (WB). The observed erythrocyte concentration in PPP were close to zero under all experimental conditions. However, the lower the g-forces and time, the higher the L-PRP concentrations.

Platelet count represented a relevant point of this study. Since platelet corpuscular density is approximately 1.040 g/mL, its location in a selective fractionation by low speed centrifugation occupied an intermediate region between mononuclear leukocytes (1.065 g/mL) and blood plasma (1.020g/dL), in the buffy coat zone with more dispersive concentration in supernatant fraction. Miron et al. (24) showed more cell and platelet concentrates in terminal serum and buffy coat zones with low speed centrifugation. This same group show higher leukocytes concentration in buffy coat and adjacent sediment with 400 x g (22). Despite methodological differences, these data are similar to the results of the present study, however, we presented a directly proportional correlation between g-force and buffy coat leukocyte concentration.

Although blood concentrates are known as platelet-rich, the experimental observations of the present study showed that platelet concentrations in the supernatant fractions rarely exceeded 2-fold higher in relation to the physiological concentration of the whole blood used as a control. The highest concentrations were observed in L-PRP fractions under all experimental conditions. However, only the 200 x g presented the highest platelet concentrations in the PPP.

When composing the total platelet concentration of the supernatant by the sum of the PPP + L-PRP fractions, only in the 200 and 800 x g platelet supraphysiological concentrations were observed. The study by Varela et al. (23) performed automated platelet analysis using 400 x g and observed average concentrations with only 15% gain compared to whole blood in correspondent PPP zone.

Total leukocyte counts under experimental conditions of 200 and 400 x g at different Δts did not exhibit supraphysiological concentrations in PPP and L-PRP. At 800 x g the total leukocyte concentrations in L-PRP came to represent 2-fold higher of the whole blood values, confirmed by the significant reduction in sediment, a fact that did not occur under other experimental conditions.

Such observations are associated with the sedimentation potential that is directly proportional to the RCF. This was demonstrated by the decreasing leukocyte concentrations in PPP as RCF was increased. However, 800 x g showed data demonstrating that increased RCF increased the concentration of the leukocyte fraction only in the L-PRP, significantly decreasing it in the sediment, i.e., increased erythrocyte sedimentation and concomitant thrust; This range of RCF promoted the highest concentration of total leukocytes among all experimental conditions observed, especially with Δt of 10 min.

In the observations of differential leukocyte counts, granulocyte concentrations in the sediment showed that their relative density, 1.080 g/mL, was crucial for reducing their concentration in the supernatant, PPP and L-PRP fractions; both sediment and L-PRP showed concentrations below whole blood. In 800 x g, the highest concentration of granulocytes in L-PRP was also observed.

The high relative concentration of mononuclear cells strengthened the concept of selective fractionation as a function of corpuscular density. The significant presence of mononuclear cells was evidenced, especially the lymphocytes, that were the main leukocytes found in the supernatant fractions. The study by Varela et al. (23) and Miron et al. (24) corroborated the findings of this experiment.

The present study verified the influences of g-forces and time of centrifugations on the leukocyte and platelet composition in anticoagulated blood samples. The experiments carried out allowed the observation of cellular and platelet concentrations at supraphysiological levels in the various experimental conditions. The lower g-force ranges (200 x g) were more promising in relation to the platelet composition and dispersive accommodation in the total supernatant content. The higher experimental g-force (800 x g) elevated buffy coat zone total leukocytes by the combined action of the sedimentation and buoyance effect during centrifugation. The low concentration of granulocytes in the sediment in this experimental range means that g-force acting obliquely on the blood content produces an antagonist sedimentation effect bringing a selective separation as a function of the relative density of the blood elements. The longer centrifugation time the higher leukocytes and platelet concentration was found in the L-PRP fraction.

The established experimental conditions allowed the verification of their influences on the cellular and platelet organization and concentration in the blood fractions. High centrifugation forces tended to concentrate the leukocyte/platelet content in the buffy coat zone while smaller forces tended to concentrate mononuclear leukocytes and platelets more dispersive in the supernatant content. Because it is an *in vitro* investigation, this study was limited to presenting the characteristics of the cellular composition obtained under the different parametric conditions. Specific therapeutic conditions may require matrices with higher or lower levels of cells/platelets. Thus, *in vivo* studies are indispensable for verifying the therapeutic efficacy of each methodological variation and thus consolidating itself as an effective and reproducible non-transfusion therapy in the field of tissue regeneration.

REFERENCES

1. Dohan DM, Choukroun J, Diss A, Dohan SL, Dohan AJJ, Mouhyi J, Gogly B. Platelet-rich fibrin (PRF): A second-generation platelet concentrate. Part III: Leucocyte activation: A new feature for platelet concentrates? Oral Surg Oral Med Oral Pathol Oral Radiol Endod 2006; 101:e51-5. doi: 10.1016/j.tripleo.2005.07.010. PMID: 16504851.
2. Niewland R, Sturk A. Platelet-Derived Microparticles. In: Platelets, 2nd ed.; Michelson, A.D.; editor. Platelets. Second. Burlington: Elsevier; 2007; p. 403-14.
3. Dulmovits BM, Herman IM. Microvascular remodeling and wound healing: A role for pericytes. Int J Biochem Cell Biol 2012; 44:1800-12. Doi: 10.1016/j.biocel.2012.06.031. PMID: 22750474.
4. El Bagdadi K, Kubesch A, Yu X, et al. Reduction of relative centrifugal forces increases growth factor release within solid platelet-rich-fibrin (PRF)-based matrices: a proof of concept of LSCC (low speed centrifugation concept). Eur J Trauma Emerg Surg 2019; 45:467-79. doi: 10.1007/s00068-017-0785-7. PMID: 28324162.
5. Dohan Ehrenfest DM, Andia I, Zumstein MA, Zhang C-Q, Pinto NR, Bielecki T. Classification of platelet concentrates (Platelet-Rich Plasma-PRP, Platelet-

Rich Fibrin-PRF) for topical and infiltrative use in orthopedic and sports medicine: current consensus, clinical implications and perspectives. Muscles Ligaments Tendons J 2014; 4:3-9. PMID: 24932440.

6. Marx RE. Platelet-rich plasma (PRP): what is PRP and what is not PRP? Implant Dent 2001; 10:225-28. doi: 10.1097/00008505-200110000-00002. PMID: 11813662.
7. Anitua E. Plasma rich in growth factors: preliminary results of use in the preparation of future sites for implants. Int J Oral Maxillofac Implants 1999; 14:529-35. PMID: 10453668.
8. Smets F, Croisier J-L, Forthomme B, Crielaard J-M, Kaux, J-F. Applications cliniques du plasma riche en plaquettes (PRP) dans les lésions tendineuses: revue de la littérature. Sci Sports 2012; 27:141-53. doi: 10.1016/j.scispo.2011.12.007
9. Dohan DM, Choukroun J. PRP, cPRP, PRF, PRG, PRGF, FC … How to find your way in the jungle of platelet concentrates? Oral Surg Oral Med Oral Pathol Oral Radiol Endod 2007; 103:305-6. doi: 10.1016/j.tripleo.2006.10.009
10. Dohan Ehrenfest DM, Rasmusson L, Albrektsson T. Classification of platelet concentrates: from pure platelet-rich plasma (P-PRP) to leucocyte- and platelet-rich fibrin (L-PRF). Trends Biotechnol 2009; 27:158-67. doi: 10.1016/j.tibtech.2008.11.009. PMID: 19187989.
11. Casati MZ, de Vasconcelos Gurgel BC, Gonçalves PF, Pimentel SP, da Rocha Nogueira Filho G, Nociti Jr FH, Sallum EA. Platelet-rich plasma does not improve bone regeneration around peri-implant bone defects—A pilot study in dogs. Int J Oral Maxillofac Surg 2007; 36:132-36. doi: 10.1016/j.ijom.2006.06.004. PMID: 16890407.
12. Papalia R, Vasta S, Zampogna B, Tecame A, Maffulli N, Denaro V. Platelet-rich plasma injections and surgery: short-term outcomes and long-term prognosis. Oper Tech Orthop 2012; 22:71-77. doi: 10.1053/j.oto.2012.01.001
13. Herberg S, Kondrikova G, Periyasamy-Thandavan S, et al. Inkjet-based biopatterning of SDF-1?? augments BMP-2-induced repair of critical size calvarial bone defects in mice. Bone 2014; 67:95-103. doi: 10.1016/j.bone.2014.07.007. PMID: 25016095.
14. Pallua N, Wolter T, Markowicz M. Platelet-rich plasma in burns. Burns 2010; 36:4-8. doi: 10.1016/j.burns.2009.05.002. PMID: 19541423.
15. Choukroun J, Adda F, Schoeffloer C, Vervelle A. Une opportunité en paro implantologie, le PRF. Implantodontie 2001; 42:55-62.
16. Dohan Ehrenfest DM. How to optimize the preparation of leukocyte- and platelet-rich fibrin (L-PRF, Choukroun's technique) clots and membranes: Introducing the PRF Box. Oral Surg Oral Med Oral Pathol Oral Radiol Endod 2010; 110:275-78. doi: 10.1016/j.tripleo.2010.05.048. PMID: 20727495.
17. Choukroun J, Diss A, Simonpieri A, et al. Platelet-rich fibrin (PRF): A second-generation platelet concentrate. Part IV: Clinical effects on tissue healing. Oral Surg Oral Med Oral Pathol Oral Radiol Endod 2006; 101:e56-e60. doi: 10.1016/j.tripleo.2005.07.011. PMID: 16504852.
18. Dohan DM, Choukroun J, Diss A, Dohan SL, Dohan AJJ, Mouhyi J, Gogly B. Platelet-rich fibrin (PRF): A second-generation platelet concentrate. Part I: Technological concepts and evolution. Oral Surg Oral Med Oral Pathol Oral Radiol Endod 2006; e37-e44. doi: 10.1016/j.tripleo.2005.07.008. PMID: 16504849.
19. Ghanaati S, Booms P, Orlowska A, et al. Advanced platelet-rich fibrin: a new concept for cell-based tissue engineering by means of inflammatory cells. J Oral Implantol 2014; 40:679–689. doi: 10.1563/aaid-joi-D-14-00138. PMID: 24945603.
20. Kawase T, Tanaka T. An updated proposal for terminology and classification of platelet-rich fibrin. Regen Ther 2017; 7:80-81. doi: 10.1016/j.reth.2017.10.002. PMID: 30271855.
21. Kubesch A, Barbeck M, Al-Maawi S, et al. A low-speed centrifugation concept leads to cell accumulation and vascularization of solid platelet-rich fibrin: an experimental study in vivo. Platelets 2018; 30:329-40. doi: 10.1080/09537104.2018.1445835. PMID: 29509050.
22. Miron R, Choukroun JGS, Ghanaati S. Controversies related to scientific report describing g forces from studies on platelet rich fibrin: necessity for standardization of relative centrifugal force values. Int J Growth Factors Stem Cells Dent 2018; 1:80-89. doi: 10.4103/GFSC.GFSC_23_18.

23. Varela HA, Souza JCM, Nascimento RM, et al. Injectable platelet rich fibrin: cell content, morphological, and protein characterization. Clin Oral Investig 2019; 23:1309-18. doi: 10.1007/s00784-018-2555-2. PMID: 30003342.
24. Miron RJ, Xu H, Chai J, et al. Comparison of platelet-rich fibrin (PRF) produced using 3 commercially available centrifuges at both high (~ 700 g) and low (~ 200 g) relative centrifugation forces. Clin Oral Investig 2020; 24:1171-82. doi: 10.1007/s00784-019-02981-2. PMID: 31321574.
25. Archibald WJ. The process of diffusion in a centrifugal field of force. Phys Rev 1938; 53:746-52. doi: 10.1103/PhysRev.53.746.
26. Fraser R. Size and lipid composition of chylomicrons of different Svedberg units of flotation. J Lipid Res 1970; 11:60-65. PMID: 5411985.
27. Buckner D, Eisel R, Perry S. Blood Cell separation in the dog by continuous flow centrifugation. Blood 1968; 31:653-72. doi: 10.1182/blood.V31.5.653.653. PMID: 5646306.
28. Rosenberg R, Gertler R, Friederichs J, et al. Comparison of two density gradient centrifugation systems for the enrichment of disseminated tumor cells in blood. Cytometry 2002; 49:150-58. doi: 10.1002/cyto.10161. PMID: 12454978.
29. Dohan Ehrenfest DM, Pinto NR, Pereda A, et al. The impact of the centrifuge characteristics and centrifugation protocols on the cells, growth factors, and fibrin architecture of a leukocyte- and platelet-rich fibrin (L-PRF) clot and membrane. Platelets 2018; 29:171-84. doi: 10.1080/09537104.2017.1293812. PMID: 28437133.
30. Fujioka-Kobayashi M, Miron RJ, Hernandez M, Kandalam U, Zhang Y, Choukroun J. Optimized platelet rich fibrin with the low speed concept: growth factor release, biocompatibility and cellular response. J Periodontol 2017; 88:112-21. doi: 10.1902/jop.2016.160443. PMID: 27587367.
31. Kobayashi E, Flückiger L, Fujioka-Kobayashi M, et al. Comparative release of growth factors from PRP, PRF, and advanced-PRF. Clin Oral Invest 2016; 20:2353-60. doi: 10.1007/s00784-016-1719-1. PMID: 26809431.
32. Dohan Ehrenfest DM, Del Corso M, Diss A, Mouhyi J, Charrier J-B. Three-Dimensional architecture and cell composition of a Choukroun's platelet-rich fibrin clot and membrane. J Periodontol 2010; 81:546-55. doi: 10.1902/jop.2009.090531. PMID: 20373539.
33. Miron RJ, Pinto NR, Quirynen M, Ghanaati S. Standardization of Relative Centrifugal Forces (RCF) in studies related to platelet rich fibrin. J Periodontol 2019; 90:817-20. doi: 10.1002/JPER.18-0553. PMID: 30730050.
34. Kawase T, Tanaka T. An updated proposal for terminology and classification of platelet-rich fibrin. Regen Ther 2017; 7:80-81. doi: 10.1016/j.reth.2017.10.002. PMID: 30271855.
35. Choukroun J, Ghanaati S. Reduction of relative centrifugation force within PRF- (Platelet-Rich-Fibrin) concentrates advances patients' own inflammatory cells and platelets: First introduction of the Low Speed Centrifugation Concept. Eur J Trauma Emerg Surg 2018; 44:87-95. doi: 10.1007/s00068-017-0767-9. PMID: 28283682.

LETTER TO THE EDITOR

Changes of D-Dimer levels in patients with lung cancer after treatment of acute venous thromboembolism

P. Zhou[1*], L. Zhang[2*], Y-Q. Wang[3], B. Li[1], X-W. Chen[1], W-M. Lu[1] and Z-L. Guo[1]

[1]Department of Thoracic Surgery, Hebei Hengshui People's Hospital, Hengshui, Hebei, China; [2]Third Department of Thoracic Surgery, Hebei Provincial Thoracic Hospital, Shijiazhuang, Hebei, China; [3]Department of General Medicine, Hebei Hengshui People's Hospital, Hengshui, Hebei, China

Received February 25, 2020 – Accepted June 1, 2020

[*]These authors contributed equally to this work

To the Editor,

Correlation between venous thrombosis (VT) and cancer has been confirmed since 1865 when Armand Trousseau, a French physician, self-diagnosed pancreatic cancer through migratory venous thromboses (1). In general, it is estimated that approximately 25% of patients with first diagnosis of VT will finally receive a diagnosis of cancer. Cancer patients have 4-7-fold increased risk of VT compared to the general population or cancer-free patients. Over the past ten years, the reported incidence of cancer-associated VT has increased due to improvement in the methods of detecting and reporting the venous thrombotic events, however, its incidence varies widely among studies, depending on patient population, cancer type and stage, the method used to detect thrombotic events, start and duration of follow-up. Overall, ovarian, pancreas, brain and lung cancer are shown to be associated with the highest risks of VT events.

The pathological mechanisms responsible for VT in lung cancer patients remain poorly understood. The etiology is likely to be multifactorial, depending on the clinic setting. Nowadays, it is believed that membrane particles shed by tumor cells, which probably contain high level of tissue factors and membrane lipids, propagate the coagulation response. In addition, risk of VT varies depending on the type of lung cancer and the treatment for cancer. Previous studies have demonstrated that adenocarcinomas induces the highest risk (2). Furthermore, VT is a well-known complication of combined chemotherapy (3).

Generally, lung cancer patients with VT have rapidly deteriorating disease course and increased mortality compared to patients without. It is recommended that these patients should receive anticoagulant treatment as early as possible which can improve survival and quality of life via preventing pulmonary embolism events (4). Therefore, it is important to identify such patients and monitor the effect of anticoagulant treatment.

MATERIALS AND METHODS

Patients and study design

Two hundred and fifty-four patients diagnosed with lung cancer were initially screened in the Hebei Hengshui People's Hospital. The enrollment criteria included: i) small cell lung cancer or non-small lung cancer diagnosed

Key words: lung cancer; D-Dimer; venous thrombosis; anticoagulant treatment; clinical outcome

Corresponding Author:
Dr Zhanling Guo,
Department of Thoracic Surgery,
Hebei Hengshui People's Hospital, No. 180, Renmin East Road,
Hengshui 053000, Hebei, China
Tel.: +86 18831879806
e-mail: guozhanling0318@126.com

0393-974X (2020)
Copyright © by BIOLIFE, s.a.s.
This publication and/or article is for individual use only and may not be further reproduced without written permission from the copyright holder.
Unauthorized reproduction may result in financial and other penalties
DISCLOSURE: ALL AUTHORS REPORT NO CONFLICTS OF INTEREST RELEVANT TO THIS ARTICLE.

by an experienced pathologist; ii) over 18 years of age; iii) a score of Karnofsky performance status (KPS) ≥ 70; iv) finished at least two cycles of chemotherapy with an intact record of efficacy; v) intact medical record of follow-up in the thoracic department. The exclusion criteria included: i) severe disease include myocardial ischemia or infarction, liver or kidney failure, sepsis ii) uncontrolled hypertension or hyperglycemia; iii) indication for anticoagulant treatment for a disease other than low-molecular-weight heparin (LMWH); iv) more than two cycles of chemotherapy; v) KPS < 70; and vi) incomplete records; vii) bleeding risk. Patients who withdrew consent or dropped out were also excluded. Finally, 52 patients were excluded. Deep VT was diagnosed based on the evidence of one or more filling defects at compression venography, ultrasonography, CT venography, or MR venography involving the popliteal or more proximal veins. Patients with VT all received LMWH with an optimal duration of 6 months. The LMWH Dalteparin was administered subcutaneously, at a dose of 200 IU/kg per day for the first month and reduced to 150 IU/kg per day for the remaining 5 months. Human studies were approved by the Ethics Committee in Hebei Hengshui People's Hospital.

Platelet count and measurement of serum D-Dimer

Platelets were counted using Beckman Coulter LH780 Coulter Hematology Analyzer (Beckman Coulter, Inc., Brea, CA, USA). The D-Dimer level was determined before and 6, 12, and 24 hours following administration of LMWH, using ELISA assay. A cut-off level of 500 ng/ml was used to categorize patients into all level groups. All patients were followed-up regularly for 24 months unless death occurred earlier than 24 months.

Statistical analysis

All continuous variables are presented as the means ± standard deviation (S.D). Student's paired or unpaired two-tailed t-test was used for comparison between two groups. Nonparametric data was analyzed by Chi-squared test. SPSS 13.0 was used to plot Kaplan-Meier survival curves. All statistical tests were 2-sided and a P value smaller than 0.05 was considered significant.

RESULTS

Patients

Among the 254 patients, 52 were excluded due to consent withdrawal, indication for anticoagulant treatment for a disease other than LMWH, bleeding risk, or drop-out. Of the remaining 202 patients, 106 were diagnosed with deep VT and received anticoagulant treatment with LMWH (Fig. 1, study

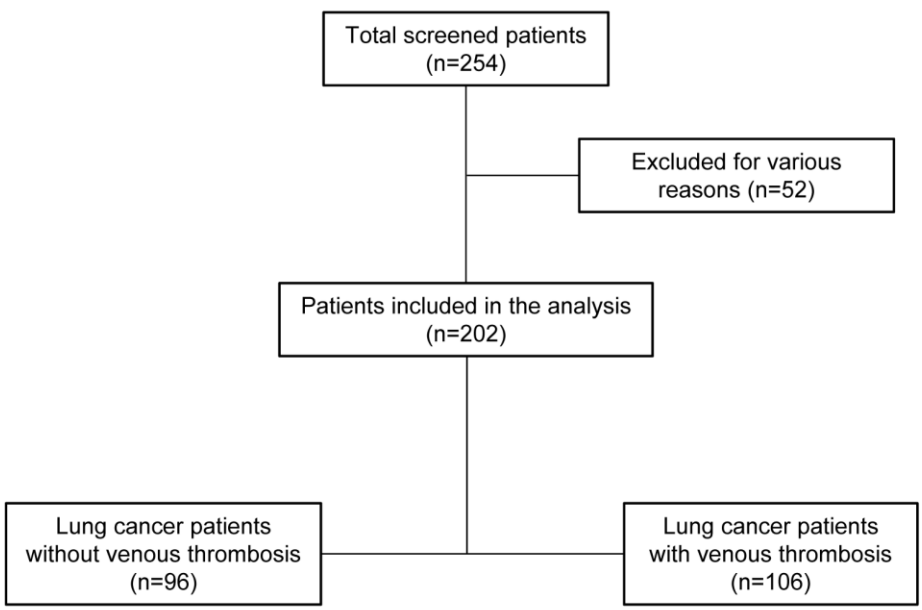

Fig. 1. *Study Design. Patients were excluded for the following reasons: consent withdrawal; Indication for anticoagulant treatment for a disease other than low-molecular-weight heparin (LMWH); bleeding risk; and drop-out.*

design). Characteristics of all enrolled 202 patients are shown in Table I. In particular, there were 25 more patients with VT who had an advanced cancer stage (Table I).

Platelet and serum D-Dimer levels

As mentioned above, of 202 patients, 106 lung cancer patients were diagnosed with deep VT and 96 were thrombosis free. The platelet and serum D-Dimer levels in these two groups were then compared. As indicated in Fig. 2A, there was no difference in the platelet level between patients with thrombosis and patients without. As expected, the thrombosis group has a significantly higher level of D-Dimers than the thrombosis-free group ($P<0.001$, Fig. 2B). In addition, anticoagulant treatment with LMWH led to persistent decrease of D-Dimers within 24 hours (Fig. 3).

Correlation between serum D-Dimer levels and survival

Since D-Dimer has a high sensitivity for diagnosis of thrombosis, in the present study, it was used as a mean of predictive for the lung cancer prognosis. We categorized the 202 patients into two groups based on their serum D-Dimer (the cut-off was 500ng/ml). There were 100 patients in the low-level group and 102 in the high-level group. Then the correlation between the survival and serum D-Dimer level was assessed. As indicated in Fig. 4, the results showed a significant correlation between serum D-Dimer and survival.

DISCUSSION

Over the years, it has been confirmed that patients diagnosed with lung cancer are at highest risk of developing VT. In several prospective studies, the 1-year cumulative occurrence of VT is reported to be around 3% (5). However, in retrospective studies, the reported incidence of VT in patients with lung cancer varies from 3% to as high as 14%. The variation in retrospective studies might be attributed to difference in population, cancer types, stage of cancers and treatment. The prevalence of VT in our patient population is over 50%. There are a few reasons that might be responsible for this abnormally high incidence of VT in our patient group. Firstly, the patients had a relatively long history of lung cancer. Secondly, all of them had received at least two cycles of chemotherapy which could lead to increased risk of VT. Thirdly, the major cancer type in our patients was adenocarcinoma which is associated with the

Table I. *General data of the study population.*

	VTE Group (n=106)	CON Group (n=96)	P value
Age (year)	63±13	62±14	0.751
Sex			
Male	67	60	
Female	39	36	
Lung Cancer Types			
NSCLC	74	69	
SCLC	32	27	
Tumor Staging			
I＋II	9	24	
III＋IV	97	72	<0.001

VTE: Venous Thromboembolism; NSCLC: non-small cell lung cancers; SCLC: small cell lung cancers. CON: Control

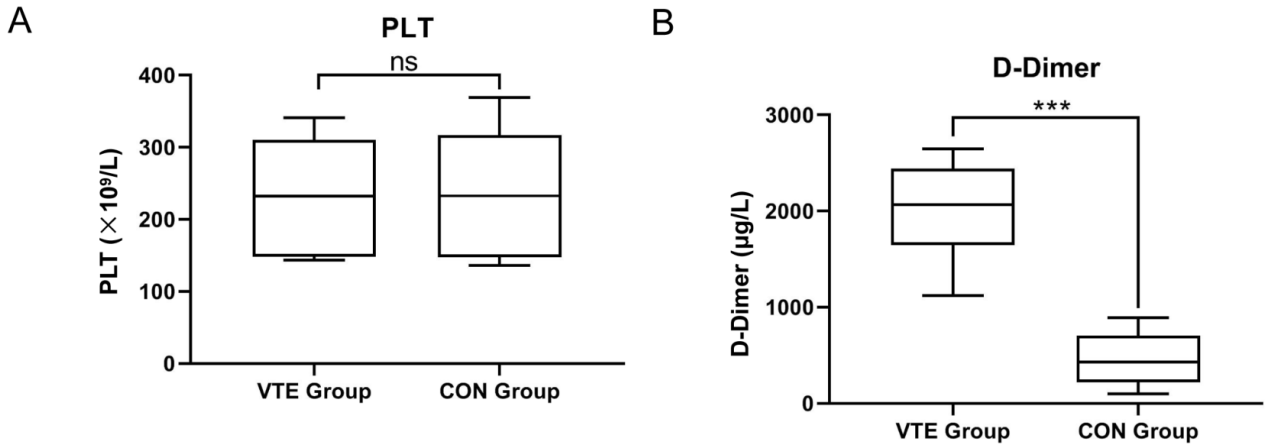

Fig. 2. *Comparison of PLT (platelet) and D-Dimer levels between lung cancer patients with VTE and those lung cancer patients without VTE (CON group). A. Quantification of platelets in peripheral blood. B. Serum D-Dimmer level. Data was shown as mean ± S.D, ns, no statistical significance, ***p<0.001.*

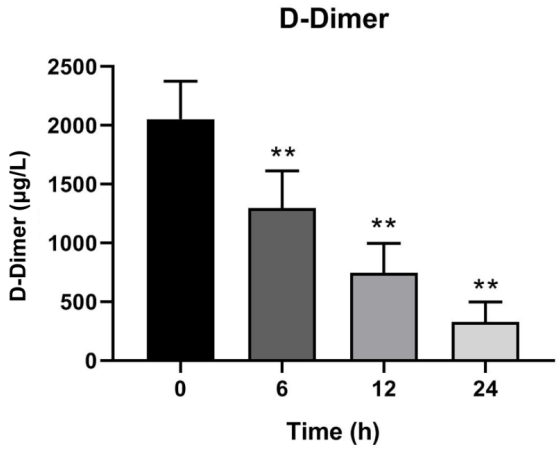

Fig. 3. *Comparisons of D-Dimer levels in lung cancer patients with VTE before and after LMWH treatment. Data was shown as mean ± S.D, **p<0.01.*

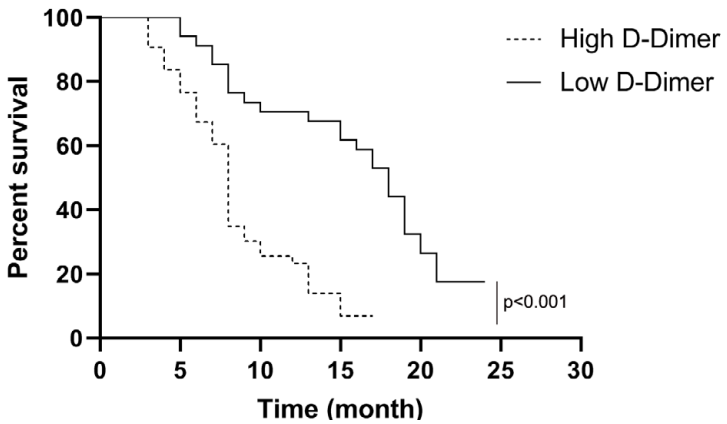

Fig. 4. *Comparison of lung cancer patient survival with high levels of D-Dimer and low levels of D-Dimer. The cut-off level of 500 ng/ml was used to distinguish between high and low results.*

highest risk of VT. Nevertheless, the results indicate that VT could be more common than was previously believed.

Plasma levels of D-dimer, a highly sensitive predictor for thromboembolism event, are elevated in patients with malignant tumors and it has been reported to be predictive for a worse prognosis (6). Our results showed that all lung cancer patients with VT had a high serum level of D-Dimer which decreased in response to anticoagulant treatment. In addition, as expected, high serum D-Dimer was correlated with poor clinical outcomes.

It has been reported that high coagulant activity in patients diagnosed with lung cancer is also associated with increased platelet count. For example, a study by Pedersen and Milman showed that increased platelet counts were observed in 32% of patients with lung cancer (7). However, in terms of the prevalence of VT, suggesting elevated platelets is not a risk factor predisposing to VT in lung cancer patients. In the present study, we compared the platelet counts between patients with and without VT. Consistent with previous study, we found no significant difference in platelet counts between these two groups.

ACKNOWLEDGEMENTS

This study was supported by the Hebei Science and Technology Support Program (15277782D).

REFERENCES

1. Buller HR, van Doormaal FF, van Sluis GL, Kamphuisen PW. Cancer and thrombosis: from molecular mechanisms to clinical presentations. J Thromb Haemost 2007; 5(Suppl 1):246-54.
2. Blom JW, Osanto S, Rosendaal FR. The risk of a venous thrombotic event in lung cancer patients: higher risk for adenocarcinoma than squamous cell carcinoma. J Thromb Haemost 2004; 2:1760-65.
3. Crivellari G, Monfardini S, Stragliotto S, Marino D, Aversa SM. Increasing chemotherapy in small-cell lung cancer: from dose intensity and density to megadoses. Oncologist 2007; 12:79-89.
4. Rossel A, Robert-Ebadi H, Combescure C, et al. Anticoagulant therapy for acute venous thrombo-embolism in cancer patients: A systematic review and network meta-analysis. PLoS One 2019; 14:e0213940.
5. Chew HK, Davies AM, Wun T, Harvey D, Zhou H, White RH. The incidence of venous thromboembolism among patients with primary lung cancer. J Thromb Haemost 2008; 6:601-8.
6. Stender MT, Larsen AC, Sall M, Thorlacius-Ussing O. D-Dimer predicts prognosis and non-resectability in patients with pancreatic cancer: a prospective cohort study. Blood Coagul Fibrinolysis 2016; 27:597-601.
7. Pedersen LM, Milman N. Prognostic significance of thrombocytosis in patients with primary lung cancer. Eur Respir J 1996; 9:1826-30.

LETTER TO THE EDITOR

Influence of blood flow of arteriovenous fistula on cardiac function of patients undergoing maintenance hemodialysis

FY. Yu[1*], YM. Yin[2*], ZM. Chen[1], N. Ren[3] and RF. Li[4]

[1]Department of Nephrology Ward, Binzhou Medical University Hospital, Shandong, China; [2]Hemodialysis Room, Shandong Dongying People's Hospital, Shandong, China; [3]Department of Dermatology, Binzhou Medical University Hospital, Shandong, China; [4]Hemodialysis Room, Binzhou Medical University Hospital, Shandong, China

Received February 6, 2020 – Accepted June 3, 2020

[*]These Authors contributed equally to this study

To the Editor,

Hemodialysis patients usually need long-term treatment; therefore, to maintain long-term dialysis and prolong the life of patients, good vascular access is a necessary condition (1, 2). Arteriovenous fistula (AVF) has become a routine vascular access for hemodialysis, and has the advantages of convenient operation, sufficient blood flow, high patency rate and few complications (3-5). However, the diameter of the AVF is closely related to the patency of the patient's vascular access and dialysis-related complications. The high blood flow in AVF increases the burden on the heart, which can lead to heart failure. The low blood flow in AVF can lead to form thrombus formation and block the mouth of orificium fistulae repeatedly, which can lead to the life-threatening dysfunction of internal fistula (6). Therefore, it is of great significance for the prognosis of patients to choose the appropriate internal fistula blood flow to meet the needs of hemodialysis and reduce the risk of cardiovascular disease. In this study, the changes of cardiac output, cardiac index and ejection fraction in patients with chronic renal failure were observed by color Doppler ultrasound before and after surgery with the aim to explore the influence of the blood flow of AVF on cardiac function.

MATERIALS AND METHODS

One hundred and twenty patients (76 males and 44 females aged 37-72 years, average 42.46±5.22) with chronic renal failure who underwent maintenance hemodialysis with AVF (end-to-end and end-to-side of forearm anastomosed) from August 2017 to October 2018 were selected as the study subjects. All the selected patients received medical history evaluation, physical examination and laboratory examination; there were 15 cases of diabetic nephropathy, 20 cases of lupus nephritis, 24 cases of chronic glomerulonephritis, 28 cases of obstructive nephropathy, and 33 cases of hypertensive nephropathy; the disease course was 1~17 years (average 4.27 years). The duration of hemodialysis was 11~87 months (average (35.72±17.90) months), and hemodialysis was performed at least twice a week, for a minimum of three months. Patients

Key words: arteriovenous fistula; hemodialysis; blood flow; cardiac function

Corresponding Author:
Dr Rufen Li,
Hemodialysis Room,
Binzhou Medical University Hospital,
No.661 Huanghe II Road,
Shandong, 256603, China
e-mail: lirufenou@163.com

0393-974X (2020)
Copyright © by BIOLIFE, s.a.s.
This publication and/or article is for individual use only and may not be further reproduced without written permission from the copyright holder.
Unauthorized reproduction may result in financial and other penalties
DISCLOSURE: ALL AUTHORS REPORT NO CONFLICTS OF INTEREST RELEVANT TO THIS ARTICLE.

who had severe chronic obstructive pulmonary disease, pulmonary embolism, primary pulmonary hypertension, unstable angina pectoris, recent myocardial infarction (< one month), history of heart valve operation, severe mitral valve, aortic valve or pulmonary valve regurgitation and/or stenosis, underwent hemodialysis because of non-renal diseases, or failed to complete follow-up were excluded (2, 3). The study was approved by the medical ethics committee of the hospital, and informed consent was obtained from all patients.

MATERIALS AND METHODS

One month after anastomosis of AVF, the AVF blood flow was measured by color Doppler ultrasound, and according to the measurement value the patients were divided into three groups: low flow group (37 cases, ≤ 400 mL/min), medium flow group (44 cases, 400~600 mL/min) and high flow group (39 cases, ≥ 600 mL/min). The patients were followed-up for one year after discharge. Conventional heparin anticoagulation was used in dialysis, and carbonate dialysis was performed two or three times a week. In order to maintain the hemoglobin level between 100g/L and 130g/L, the anemia patients were treated with transfusion correction or erythropoietin.

The occurrence of high-risk events and internal fistula dysfunction during dialysis was observed, and the cardiac function indexes of the three groups of patients were detected. According to the New York Heart Association classification of cardiac function, the occurrence above level III or hospitalization due to cardiovascular complications was considered a high-risk event (7). According to the characteristics of internal fistula murmur, tremor and pulsation, the blood flow in the vascular pathway of the patients was evaluated. If there was slight tremor and vascular murmur in the inner side of the fistula, it was considered that the internal fistula was unobstructed; otherwise it was considered that the internal fistula lost function. During the study, the cardiac index (CI), cardiac output (CO) and ejection fraction (EF) were measured before dialysis (one month after AVF anastomosis) and one year after dialysis.

Statistical analysis

The data were statistically processed by SPSS 22.0, and the measurement data were expressed by mean ± standard deviation. The inter-group comparison was tested by analysis of variance. The comparison between any two groups was performed using LSD *t*-test. Enumeration data were processed by *Chi*-squared test. Linear correlation analysis was used in the relationship between variables. $P<0.05$ was used for statistical significance.

RESULTS

Comparison of cardiac function indexes between three groups

There was no significant difference in CI, CO and EF between the three groups before dialysis ($P>0.05$), but were significantly higher after dialysis ($P<0.05$), and the indexes in the high flow group were higher than those in the low flow group and medium flow group ($P<0.05$, Table I).

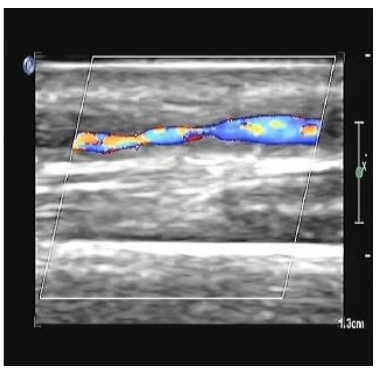

Fig. 1. *Complication of cephalic vein stenosis of a patients with AVF*

Fig. 2. *Complication of angiomatous dilatation of cephalic vein of a patient with AVF*

Table I. *Comparison of heart function indexes in three groups*

Group		Low flow group	Medium flow group	High flow group	F/P value
CO (L/min)	Before dialysis	4.41±0.57	4.22±0.40	4.35±0.53	1.319/0.268
	After dialysis	4.57±0.58	4.82±0.35	5.98±0.63	50.819/0.000
CI (L·min-1·m-2)	Before dialysis	2.66±0.34	2.75±0.43	2.72±0.50	1.627/0.218
	After dialysis	2.73±0.38	3.41±0.48	3.77±0.34	35.278/0.000
EF (%)	Before dialysis	53.28±3.26	53.37±5.82	54.41±6.07	0.401/0.668
	After dialysis	53.83±4.41	56.70±3.81	59.02±6.56	7.613/0.001

Table II. *Comparison of heart function indexes in three groups*

Group	Low flow group	Medium flow group	High flow group	χ^2	P
Incidence of internal fistula dysfunction	11(29.72)	4(9.09)	3(7.69)	9.137	0.010
Incidence of high-risk events	5(13.51)	8(18.18)	16(41.03)	9.201	0.010

Comparison of clinical observation indexes between the three groups

There was a significant difference in the incidence of internal fistula dysfunction between the three groups (P<0.05). The incidence of the low flow group was higher than that of the medium flow group and high flow group (P<0.05). There was a significant difference in the incidence of high-risk events between the three groups (P<0.05); the incidence of high-risk events in the high flow group was higher than that of the medium flow group and low flow group (P<0.05, Table II).

Typical cases of cephalic vein complications are shown in Figs. 1 and 2.

DISCUSSION

Hemodialysis is a process of removing metabolic waste, maintaining electrolyte and acid-base balance, and eliminating excessive water in the body. A well-functioning vascular pathway is an important guarantee for the life of hemodialysis patients. To improve the survival rate of patients, the minimum standard of kidney disease of the American National Kidney Foundation suggests that an internal fistula be established in the patient's own arteriovenous vein for hemodialysis (8). One study (9) has shown that repeated puncture was easy to damage blood vessels in the use of internal fistula, which will make them hard, narrow and fibrotic and affect blood flow, and the blood flow of vascular access will further affect the cardiac function the of dialysis patient; therefore, it is of great significance to detect the blood flow of internal fistula regularly.

In this study, after dialysis, the levels of CI, CO and EF in the three groups were higher than those before dialysis, and the increase of the indexes in the high flow group was more significant than that in the low flow group and medium flow group (P < 0.05). This might be related to the increase of the returned blood volume, end diastolic diameter and volume of the heart after the establishment of AVF in these patients. The larger the AVF blood flow, the greater the changes of CI, CO and EF, and the greater the

impact on the cardiac function. In addition, in this study, the lower the blood flow of AVF, the lower the risk of high-risk events and the higher the risk of internal fistula dysfunction; the higher the blood flow of arteriovenous fistula, the lower the risk of internal fistula dysfunction in hemodialysis patients, and the higher the risk of high-risk events, which is consistent with the relevant research results (10-12). The possible mechanism was low blood flow led to form early embolism, and to the loss of internal fistula function and could not fully achieve the dialysis effect, and the high blood flow would increase the cardiac output, which could lead to high-risk events such as congestive heart failure.

In conclusion, it is appropriate to control the blood flow of AVF at 400-600 ml/min, which can ensure a good effect of dialysis and low incidence of cardiovascular adverse events. It is worth clinical promotion and in future studies, the scope of observation can be further expanded.

REFERENCES

1. Aragoncillo I, Abad S, Caldés S, et al. Adding access blood flow surveillance reduces thrombosis and improves arteriovenous fistula patency: a randomized controlled trial. J Vasc Access 2017; 18(4):325-58.
2. Yazin M, GuyA, Tullett K, Krishnan H, Jones RG, Inston NG. Patterns of blood flow as a predictor of maturation of arteriovenous fistula for haemodia lysis. J Vasc Access 2014; 15(3):169-74.
3. Karkar A, Chaballout A, Ibrahim MH, Abdelrahman M, Al Shubaili M. Improving arteriovenous fistula rate: effect on hemodialysis quality. Hemodial Int 2014; 18(2):516-21.
4. Coentrão L, Turmel-Rodrigues L. Monitoring dialysis arteriovenous fistulae: it's in our hands. J Vasc Access 2013; 14(3):209-15.
5. Demir D, Ceviker K, Aydin MS, Sahinalp S. Complications of arteriovenous fistula with polytetraflouroethylen grafts in hemodialysis patients. Niger J Clin Pract 2015; 18(1):120-23.
6. Kamyar MM, Modaghegh MHS, Kazemzadeh G. Limb complaints after autogenous arteriovenous fistula creation in chronic hemodialysis patients. Semin Vasc Surg 2016; 29(4):172-77.
7. Miller-Davis C, Marden S, Leidy NK. The New York Heart Association Classes and functional status: what are we really measuring? Heart Lung 2006; 35(4) : 217-24.
8. Sun X, He Y, Ma Y, He H, Zhang L, de Seabra Rodrigues Dias IR, Liu Y. A single-center retrospective analysis of the efficacy of a new balloon catheter in autogenous arteriovenous fistula dysfunction resistant to conventional balloon angioplasty. Ann Vasc Surg 2018; 48(6):79-88.
9. Kamijo Y, Kanda E, Horiuchi H, et al. Continuous monitoring of blood pressure by analyzing the blood flow sound of arteriovenous fistula in hemodialysis patients. Clin Exp Nephrol 2017; 22(3):677-83.
10. Chin AI, Tong K, Mcvicar JP. Successful hemodialysis arteriovenous fistula creation in a patient with continuous-flow left ventricular assist device support. Am J Kidney Dis 2017; 69(2):314-16.
11. Rao N, Worthley M, Disney P, Faull R. Dramatic improvement in decompensated right heart failure due to severe tricuspid regurgitation following ligation of arteriovenous fistula in a renal transplant recipient. Semin Dial 2014; 27(2):24-26.
12. Cheng Y, Zhang F, Zhu J, et al. Influence of blood pressure variability on the life of arteriovenous fistulae in maintenance hemodialysis patients. Clin Hemorheol Microcirc 2016; 62(2):129-37.

JOURNAL OF BIOLOGICAL REGULATORS & HOMEOSTATIC AGENTS Vol. 34, no. 4, 1401-1405 (2020)

LETTER TO THE EDITOR

Elevated fibrinogen to platelet is associated with increased all-cause mortality among patients undergoing primary percutaneous coronary intervention

J-C. Zhang[1,2*], Y-Y. Zheng[1,2*], J-N. Tang[1,2], B. Qin[3], X-M. Yang[4], Q-Q. Guo[1,2], J-C. Guo[1,2], M-D. Cheng[1,2], Z-L. Zhang[1,2], F-H. Song[1,2], Z-Y. Liu[1,2], K. Wang[1,2], L-Z. Jiang[1,2], L. Fan[1,2], X-T. Yue[1,2], Y. Bai[1,2], X-Y. Dai[1,2], R-J. Zheng[1,2], S-S. Yin[5] and J-Y. Zhang[1,2]

[1]Department of Cardiology, First Affiliated Hospital of Zhengzhou University, China; [2]Key Laboratory of Cardiac Injury and Repair of Henan Province, China; [3]Translational Medical Center, First Affiliated Hospital of Zhengzhou University, China; [4]Department of Cardiology, The First Affiliated Hospital and College of Clinical Medicine of Henan University of Science and Technology, Luoyang, China; [5]Institute of Medicine, University of Zhengzhou, Henan Province, China

Received March 6, 2020 – Accepted June 3, 2020

[*]These Authors contributed equally to this work

To the Editor,

Percutaneous coronary intervention (PCI) has been demonstrated to reduce symptoms in patients with coronary artery disease (CAD), however, there are still potential risks of cardiac death at the early stage and gradually increased risk of all-cause mortality in the long-term after PCI (1, 2). Thus, risk stratification in patients treated with PCI can be important to guide management decisions and to further reduce mortality in these patients.

In recent years, the role of inflammatory response and activation of the coagulation and fibrinolysis system in the pathogenesis and prognosis of CAD has gained wide attention (3). Recent studies have shown that elevated fibrinogen is associated with short-term adverse events after PCI (4). Additionally, platelet level is considered to be the main mediator of homeostasis and thrombin generation, and plays a vital role in the inflammatory process (5). Wakatsuki et al. suggested that fibrinogen-to-platelet ratio (FPR) as an inflammatory and coagulative index is more valuable than the plasma fibrinogen level in terms of prediction of the prognosis of gastric cancer patients (6). Consequently, the present study was performed to investigate the correlation between FPR and long-term adverse events in patients undergoing PCI.

MATERIALS AND METHODS

Study design and population

Retrospective data from patients with CAD who underwent PCI from January 2013 to December 2017 were obtained from the database of the First Affiliated Hospital of Zhengzhou University. The study was approved by the ethics committee of the First Affiliated Hospital of Zhengzhou University and all subjects gave informed, signed consent to participate in the study. The study was registered with ChiCTR.org (ID: ChiCTR-TRC-1800019699).

Patients eligible for CAD including stable angina, unstable angina and myocardial infarction, who were

Key words: cardiovascular diseases; percutaneous coronary intervention; fibrinogen-to-platelet ratio; mortality

Corresponding Author:
Dr Jinying Zhang,
Department of Cardiology, The First Affiliated Hospital of Zhengzhou University, Zhengzhou, Henan 450052, China
Tel.: +86 13503830283
e-mail: jyzhang@zzu.edu.cn

0393-974X (2020)
Copyright © by BIOLIFE, s.a.s.
This publication and/or article is for individual use only and may not be further reproduced without written permission from the copyright holder. Unauthorized reproduction may result in financial and other penalties
DISCLOSURE: ALL AUTHORS REPORT NO CONFLICTS OF INTEREST RELEVANT TO THIS ARTICLE.

undergoing coronary angiography with at least one stenosis ≥50% and receiving at least one stent via implantation were included. The exclusion criteria were: severe congenital heart disease; rheumatic heart disease; severe heart failure; pulmonary heart disease; serious dysfunction of the liver or kidney; or unavailable to fibrinogen or platelet count results. Ultimately, a total number of 3,352 patients qualified for the present study. The fibrinogen levels and platelet counts before coronary angiography were retrospectively recorded for the included patients. The FPR was calculated by dividing the platelet count (10^9/L) by the fibrinogen level (mg/dl).

The primary endpoint was long-term mortality, including all-cause mortality (ACM) and cardiac mortality (CM). The secondary endpoint was the composite of major adverse cardiac events (MACEs) and the composite of major adverse cardiac and cerebrovascular events (MACCEs). MACEs were defined as cardiac death, heart failure, bleeding events and readmission. MACCEs were defined as MACEs combined with stroke. In this study, all of the patients were followed-up for at least 2 years, and the mean value was 37.59±22.24 months. Clinical follow-up was performed through patient visits and telephone interviews.

Statistical analysis

SPSS version 22.0 (SPSS Inc., Chicago, Illinois, United States) was utilized to analyze all data. Continuous variables were presented as the mean ± standard deviation and compared using t-tests. Categorical variables were presented as frequencies and percentages, and were compared using the chi-square test. Receiver operating characteristic (ROC) curves were utilized to determine the cut-off value of the FPR. The Kaplan-Meier method and the log-rank test were performed to estimate the cumulative incidences of long-term outcomes according to the FPR (<1.46 and ≥1.46). Multivariate Cox proportional hazards regression models were conducted to evaluate the independent predictive value of the FPR with regard to long-term outcomes. All *P*-values < 0.05 were assumed to be significant.

RESULTS

Baseline characteristics

A total of 3,352 patients with CAD after PCI were enrolled. According to the ROC curve, the optimal cut-off value of FPR for all-cause mortality was 1.46. Based on the cut-off value, patients were divided into two groups: low FPR group (FPR<1.46) and high FPR group (FPR≥1.46). As shown in Table I, there was significant difference for several variables between the two groups, such as hypertension, alcohol intake, uric acid (UC), high-density lipoprotein (HDL-C), low-density lipoprotein cholesterol (LDL-C), total cholesterol (TC) and triglyceride (TG) (all *P*<0.05).

Clinical outcomes

During the follow-up period, the incidence of ACM (4.8% *vs* 2.6%, *P*=0.001) and CM (3.1% *vs* 1.6%, *P*=0.004) was significantly higher in in the high FPR group compared with the low FPR group. For MACEs (12.2% *vs* 10.7%, *P*=0.176) and MACCEs (15.2% *vs* 14.4%, *P*=0.517), there was no significant difference between the two groups (Table I).

Multivariate Cox regression analyses were conducted to evaluate the prognostic value of FPR after adjusting for confounders, including gender, age, diabetes, smoking, alcohol intake, blood urea nitrogen (BUN), TC, TG, LDL-C and HDL-C. As shown in Tables II and III, patients with a higher FPR (FPR≥1.46) have a higher risk of long-term ACM (HR=1.512, 95% CI: 1.018-2.246, *P*=0.041), compared with the lower FPR group. However, there is no statistical significance regarding the risk of long-term CM in post-PCI patients (HR=1.498, 95% CI: 0.901-2.490, *P*=0.119). Kaplan-Meier survival curve also suggested that the cumulative incidence of ACM in the high FPR group was significantly higher than that in the low FPR group (*P*=0.001) (Fig. 1).

DISCUSSION

The aim of this study is to identify a novel and easily calculable prognostic index combining inflammation and coagulation system for patients underwent PCI to predict long term adverse events. In this study, we found that elevated FPR was associated with long-term mortality among post-PCI patients.

As an acute phase protein, fibrinogen is able to facilitate platelet aggregation by binding the glycoprotein IIb/IIIa receptor onto the platelet surface

Table I. *Baseline characteristics*

Variables	FPR<1.46 (n=1515)	FPR≥1.46 (n=1837)	χ^2/t	*P* value
Gender (male), n (%)	984 (65.0)	1323 (72.0)	19.377	<0.001
Age, years	61.93±10.49	64.44±10.49	-6.895	<0.001
Hypertension, n (%)	857 (56.6)	995 (54.2)	1.940	0.164
Diabetes, n (%)	319 (21.1)	468 (25.5)	9.029	0.003
Smoking, n (%)	420 (27.7)	596 (32.4)	8.762	0.003
Alcohol intake, n (%)	242 (16.0)	300 (16.3)	0.078	0.780
BUN, mmol/L	5.53±3.21	5.87±5.22	-2.316	0.021
UA, mmol/L	297.04±84.52	299.88±87.01	-0.943	0.346
TC (mmol/L)	3.99±1.03	3.84±1.01	4.155	<0.001
TG (mmol/L)	1.74±1.21	1.59±1.02	3.700	<0.001
HDL-C (mmol/L)	1.06±0.27	1.02±0.30	3.559	<0.001
LDL-C (mmol/L)	2.47±0.87	2.34±0.81	4.270	<0.001
ACM n (%)	40 (2.6)	88 (4.8)	10.451	0.001
CM, n (%)	24 (1.6)	57 (3.1)	8.121	0.004
MACE , n (%)	162 (10.7)	224 (12.2)	1.835	0.176
MACCE, n (%)	218 (14.4)	279 (15.2)	0.419	0.517

BUN: blood urea nitrogen; HDL-C: high-density lipoprotein; LDL-C: low-density lipoprotein cholesterol; TC: total cholesterol; TG: triglyceride; UA: uric acid; ACM: all-cause mortality; CM: cardiac mortality; MACEs: major adverse cardiovascular events; MACCEs: major adverse cardiac and cerebrovascular events.

Table II. *Multivariate Cox regression analysis results for ACM*

Variables	*B*	*SE*	*Wald*	*P* value	*HR (95%CI)*
Gender (female)	-0.268	0.237	1.276	0.259	0.765 (0.481, 1.217)
Age (years)	0.070	0.010	48.832	<0.001	1.072 (1.051, 1.093)
Smoking	-0.061	0.266	0.053	0.817	0.940 (0.558, 1.584)
Alcohol intake	0.314	0.300	1.098	0.295	1.369 (0.761, 2.465)
Diabetes	0.456	0.199	5.276	0.022	1.578 (1.069, 2.330)
TC	0.242	0.181	1.788	0.181	1.273 (0.894, 1.814)
TG	-0.025	0.110	0.054	0.817	0.975 (0.787, 1.208)
HDL-C	-0.613	0.419	2.140	0.144	0.542 (0.238, 1.232)
LDL-C	-0.225	0.199	1.281	0.258	0.798 (0.541, 1.179)
BUN	0.028	0.008	12.710	<0.001	1.029 (1.013, 1.045)
FPR≥1.46	0.413	0.202	4.186	0.041	1.512 (1.018, 2.246)

BUN: blood urea nitrogen; HDL-C: high-density lipoprotein; LDL-C: low-density lipoprotein cholesterol; TC: total cholesterol; TG: triglyceride; FPR: fibrinogen-to-platelet ratio; ACM: all-cause motility.

Table III. *Multivariate Cox regression analysis results for CM*

Variables	*B*	*SE*	*Wald*	*P* value	*HR (95%CI)*
Gender (female)	-0.573	0.327	3.068	0.080	0.564 (0.297, 1.070)
Age (years)	0.065	0.013	26.493	<0.001	1.067 (1.041, 1.093)
Smoking	0.246	0.306	0.646	0.421	1.279 (0.702, 2.330)
Alcohol intake	-0.129	0.367	0.123	0.725	0.879 (0.428, 1.806)
Diabetes	0.491	0.252	3.794	0.051	1.634 (0.997, 2.679)
TC	-0.078	0.354	0.048	0.826	0.925 (0.463, 1.851)
TG	0.007	0.158	0.002	0.966	1.007 (0.738, 1.373)
HDL-C	-0.860	0.598	2.069	0.150	0.423 (0.131, 1.366)
LDL-C	0.128	0.369	0.120	0.729	1.136 (0.551, 2.341)
BUN	0.025	0.010	5.589	0.018	1.025 (1.004, 1.046)
FPR≥1.46	0.404	0.259	2.430	0.119	1.498 (0.901, 2.490)

BUN: blood urea nitrogen; HDL-C: high-density lipoprotein; LDL-C: low-density lipoprotein cholesterol; TC: total cholesterol; TG: triglyceride; FPR: fibrinogen-to-platelet ratio; CM: cardiac motility.

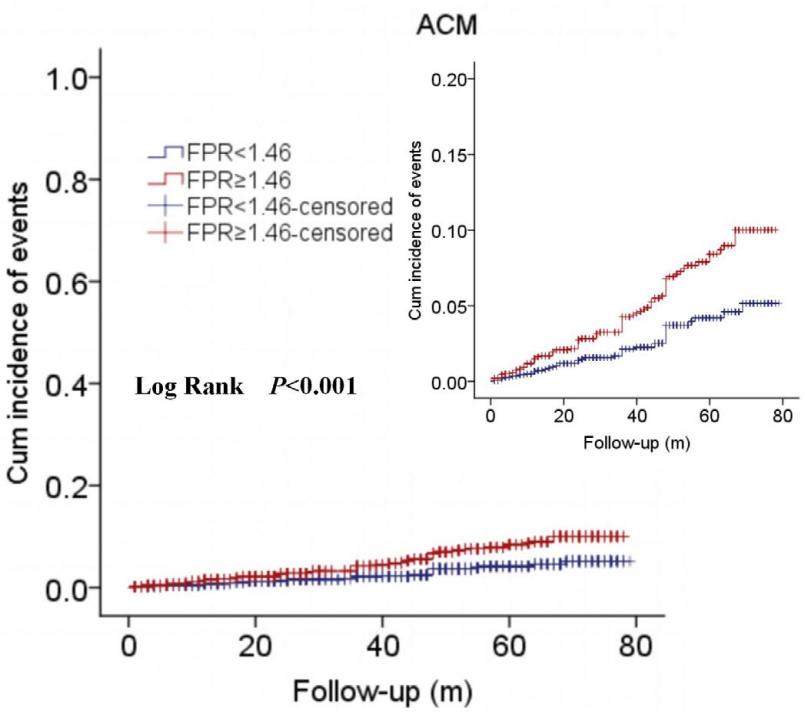

Fig. 1. *Cumulative Kaplan-Meier estimates of the time to the first adjudicated occurrence of all-cause mortality*

and increase the reactivity of platelets, augmenting their degranulation in response to adenosine diphosphate (7). The effects of fibrinogen on platelet function may be relevant to clinical conditions in which hyper-aggregability of platelets is associated with hyper-fibrinogenemia and thrombosis (8). The aggregation of platelets plays a vital role in the pathophysiological process of thrombosis formation, eventually leading to myocardial infarction (9). Hence, we assume that, as a novel prognostic index combining fibrinogen and platelet, FPR may reflect platelet-fibrin aggregates states and are associated with adverse events in patients with CAD or after PCI.

Disorder of inflammation and coagulation system was considered to be implicated in the pathogenesis of CAD. Previous studies suggested that inflammation-related biomarkers, such as C-reactive protein (CRP), are associated with the prognosis in patients undergoing PCI (10). Tousoulis et al. showed that fibrinogen and its products fibrin play a key role in the inflammatory process and participate in the formation of the lipid core of the atherosclerotic lesion by binding LDL and lipids (8). Moreover, recent study demonstrated that platelet is released from the spleen after myocardial infarction, facilitating myocardial accumulation of platelets and leucocytes and promoting post-infarct inflammation (11). Thus, Tang et al. had developed one therapeutic platform on the basis of the accumulation mechanism of platelets to treat ischemia/reperfusion (12). As a compliance indicator for combining fibrinogen and platelets, we suppose that FPR may reflect the inflammatory state in patients with CAD.

In conclusion, this study demonstrated that, as a novel combination index of inflammation and coagulation system, elevated FPR was associated with long-term mortality among patients undergoing primary PCI.

ACKNOWLEDGEMENTS

This work was supported Nature Science Foundation of China (No. 81800267, 81870328, 81760043), Henan Medical Science and Technology Joint Building Program (No.2018020002, 2018020094).

REFERENCES

1. Cutlip DE, Fischman DL. Mortality after percutaneous coronary intervention: narrowing the knowledge gap. Circ Cardiovasc Interv 2018; 11(7):e7008.
2. Spoon DB, Psaltis PJ, Singh M, et al. Trends in cause of death after percutaneous coronary intervention. Circulation 2014; 129(12):1286-94.
3. Gorog DA. Prognostic value of plasma fibrinolysis activation markers in cardiovascular disease. J Am Coll Cardiol 2010; 55(24):2701-09.
4. Ang L, Behnamfar O, Palakodeti S, et al. Elevated baseline serum fibrinogen: effect on 2-year major adverse cardiovascular events following percutaneous coronary intervention. J Am Heart Assoc 2017; 6(11):e006580.
5. Semple JW, Italiano JJ, Freedman J. Platelets and the immune continuum. Nat Rev Immunol 2011; 11(4):264-74.
6. Wakatsuki K, Matsumoto S, Migita K, et al. Prognostic value of the fibrinogen-to-platelet ratio as an inflammatory and coagulative index in patients with gastric cancer. Surg Today 2019; 49(4):334-42.
7. Schneider DJ, Taatjes DJ, Howard DB, Sobel BE. Increased reactivity of platelets induced by fibrinogen independent of its binding to the IIb-IIIa surface glycoprotein: a potential contributor to cardiovascular risk. J Am Coll Cardiol 1999; 33(1):261-66.
8. Tousoulis D, Papageorgiou N, Androulakis E, Briasoulis A, Antoniades C, Stefanadis C. Fibrinogen and cardiovascular disease: genetics and biomarkers. Blood Rev 2011; 25(6):239-45.
9. Maple-Brown LJ, Cunningham J, Nandi N, Hodge A, O'Dea K. Fibrinogen and associated risk factors in a high-risk population: urban Indigenous Australians, the DRUID Study. Cardiovasc Diabetol 2010; 9(1):69.
10. Bisoendial RJ, Boekholdt SM, Vergeer M, Stroes ES, Kastelein JJ. C-reactive protein is a mediator of cardiovascular disease. Eur Heart J 2010; 31(17):2087-91.
11. Gao XM, Moore XL, Liu Y, et al. Splenic release of platelets contributes to increased circulating platelet size and inflammation after myocardial infarction. Clin Sci 2016; 130(13):1089-104.
12. Tang J, Su T, Huang K, et al. Targeted repair of heart injury by stem cells fused with platelet nanovesicles. Nat Biomed Eng 2018; 2:17-26

LETTER TO THE EDITOR

Novel c.971A>G mutation in the *HTRA1* gene in a Chinese family with CARASIL

MM. Hou*, XW. Mao*, XB. Liu, YQ. Liu, XY. Bi and XJ. Hou

Department of Neurology, Shanghai Changhai Hospital affiliated to Second Military Medical University, People's Republic of China

Received November 13, 2019 – Accepted June 10, 2020

*These authors contributed equally to this article

To the Editor,

Cerebral autosomal recessive arteriopathy with subcortical infarcts and leukoencephalopathy (CARASIL) is a hereditary cerebral small-vessel arteriosus characterized by young-adult onset dementia, alopecia, and spinal deformity (1). A growing body of evidence suggests that CARASIL is caused by homozygous or heterozygous mutations in the high-temperature requirement A serine peptidase 1 (*HTRA1*) gene (2; 3). *HTRA1* is composed of nine exons that encode a serine protease containing 480 residues and four functional domains. Exons 3–6 encode the main protease domain that can inhibit signaling from transforming growth factor (TGF)-β family members (4). To date, several pathogenic mutations of *HTRA1* have been identified, including c.883G>A (5), c.517G>A (6), c. 1091T>C (7), and c.961G>A (8). In the present study, we evaluated the clinical and genetic characteristics of a Chinese family with CARASIL. In addition, we reported a novel missense mutation in the *HTRA1* gene. This study protocol was approved by the medical ethics committee of Changhai hospital, Shanghai, China. All patients and their family members provided written informed consent.

Case report

A 36-year-old Chinese man presented to the Department of Neurology with impaired control of his upper and lower limbs on one side of his body. His parents were first cousins (father is 71 years old and mother is 70 years old). He has a brother (49 years old) and two sisters, one of whom is 46 years old and the other died at the age of eight for unknown reasons. The pedigree chart of this family is shown in Fig. 1. Neither the parents nor siblings of the patient reported any significant medical problems. Magnetic resonance imaging (MRI) scans of his siblings' brains are displayed in Figs. 2A (brother) and 2B (sister). The scans showed no obvious abnormalities in the cranium. In detail, bilateral hemispheres were symmetrical, gray matter contrast was normal, and no local signal abnormalities were observed. The proband had fine scalp hair from childhood which significantly worsened from age 23. From age 31, he suffered from dizziness and cervicobrachialgia. Subsequently, he suffered a stroke at the age of 37.

Neurological examination revealed that he had hemiparesis in the left side, an active tendon reflex in the lower limb tendon, and a Babinski sign in the left side. The patient reported slight memory

Key words: cerebral autosomal recessive arteriopathy with subcortical infarcts and leukoencephalopathy; HTRA1; gene mutation; Chinese family

Corresponding Author:
Dr Xiaojun Hou,
Department of Neurology, Shanghai Changhai Hospital affiliated to Second Military Medical University,
No. 168 Changhai Road, Yangpu district,
Shanghai, 200433, People's Republic of China
Tel./Fax: +86 31161939
e-mail: 13311931663@163.com

0393-974X (2020)
Copyright © by BIOLIFE, s.a.s.
This publication and/or article is for individual use only and may not be further reproduced without written permission from the copyright holder.
Unauthorized reproduction may result in financial and other penalties
DISCLOSURE: ALL AUTHORS REPORT NO CONFLICTS OF INTEREST RELEVANT TO THIS ARTICLE.

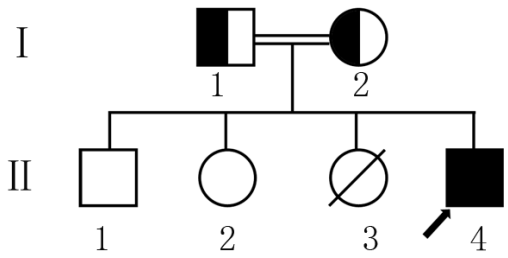

Fig. 1. *The pedigree chart of the family with cerebral autosomal recessive arteriopathy with subcortical infarcts and leukoencephalopathy (CARASIL). Roman numerals indicate generations and Arabic numbers indicate individuals. Arrow represents the proband, solid symbol indicates patients, half-filled symbol represent the carrier of mutated genes, squares represent men, circles refer to women, oblique represents deceased sister (died at the age of 8 of unknown causes).*

loss and was tested using the Montreal Cognitive Assessment (MoCA) test. His MoCA score was 26, and the results revealed that he was slightly impaired in visuospatial skill, calculation, and memory. Laboratory tests showed that electrocardiograms, electroencephalography, hemograms, and biochemical analysis were within normal parameters. Brain MRI scans showed an acute cerebral infarction in the right ventricle that appeared hyperintense with diffusion weighted imaging (DWI) (Fig. 2C). T2-weighted images revealed hyperintense diffuse leukoaraiosis. Scattered multiple lacunar infarcts and encephalomalacia foci were observed in the periventricular white matter and centrum semiovale (Fig. 2D). Susceptibility-weighted image showed several microhemorrhages in lobes and the brainstem (Fig. 2 E, F). Moreover, degenerative disc disease was observed on spinal MRI scans (Fig. 2 G, H).

Blood samples of the proband and his parents were collected and genomic DNA was extracted from peripheral leukocytes using a DNA extraction kit. Second-generation sequencing was performed to analyze the total exons, and Sanger sequencing was conducted to obtain base sequence of suspicious mutations. A homozygous missense mutation at nucleotide 971, corresponding to codon 324 (c.971A>G, p.N324S), within exon 4 in the *HTRA1* gene of the patient was identified (Fig. 3A). This mutation caused an amino acid change from asparagine to serine. Both his parents were found to have a heterozygous c.971A>G mutation. This

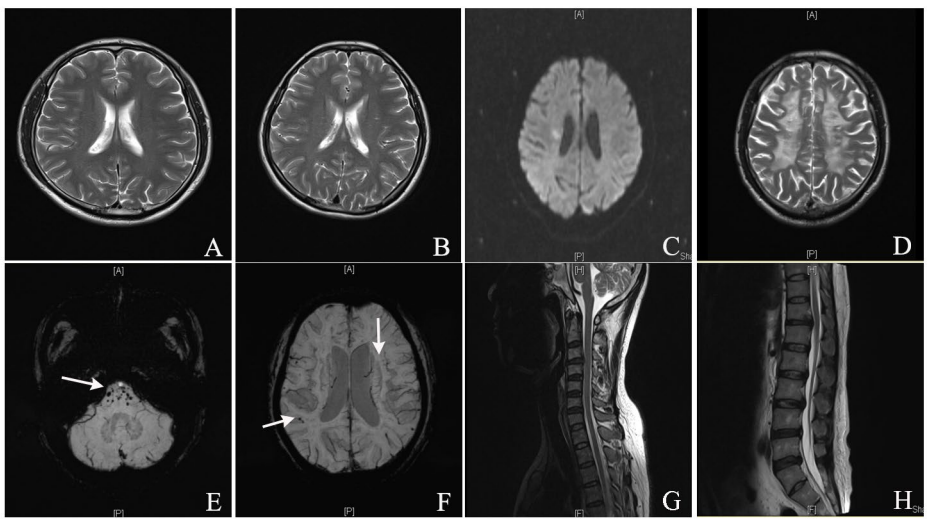

Fig. 2. *MRI scans.* ***A)*** *Older brother.* ***B)*** *Older sister. The brain MRI was normal, bilateral hemispheres were symmetrical, gray matter contrast was normal, and no local signal abnormalities were observed.* ***C)*** *Proband DWI showed a signal near the right ventricle suggesting acute cerebral infarction.* ***D)*** *T2-weighted images showed diffuse leukoaraiosis in the periventricular white matter and centrum semiovale.* ***E-F)*** *Susceptibility-weighted image showed several microbleeds in branstem (arrow) (E) and lobes (arrow) (F).* ***G-H)*** *Sagittal view of cervical (G) and dorsolumbar (H) spine demonstrated degenerative disc disease.*

mutation was not discovered in the 1000 Genomes database, the National Heart, Lung, and Blood Institute (NHLBI) Exome Sequencing Project, the Exome Aggregation Consortium (ExAC) database, or the Human Gene Mutation Database (HGMD). Silico analysis showed that the mutation was highly conserved among vertebrates (Fig. 3B). Additionally, the frequency of this variation was rare in the general population (met the PM2 rule). Furthermore, the c.971A>G mutation of *HTRA1* was predicted to be pathogenic by SIFT, PolyPhen_2, and MutationTaster. Unfortunately, blood samples from the patient's siblings were not available.

DISCUSSION

Using clinical and molecular genetic testing of the patient, we discovered a novel missense mutation (c.971A>G) associated with the pathogenesis of CARASIL. The missense mutation in the protease domain of the *HTRA1* gene (p.N324S) was inherited from his parents. The homological analysis of *HTRA1* verified that this mutation occurred in the protease domain of trypsin-like serine, a highly conserved region crucial for the protease activity of HtrA1 (Fig. 3B). Additionally, *HTRA1* is essential for skeletal development (6), which may explain the disc degeneration in the proband.

CARASIL is a rare genetic disease characterized by mutations in the *HTRA1* gene located on chromosome 10q. There are only three articles reporting *HTRA1* mutations in Chinese families with CARASIL. Wang and colleagues identified a homozygous mutation in exon 6 of *HTRA1* (c. 1091T>C, p.L364P) (7). Cai et al. discovered a homozygous frameshift mutation in exon 1 of *HTRA1* (c.161_162insAG) (9). Finally, a homozygous mutation in exon 4 (c.854 C>T) was previously reported by Chen et al. (10). Mutations in *HTRA1* result in the loss of proteolytic enzyme activity which leads to an increase in TGF-β signaling, resulting in the degeneration of smooth muscle cells into small cerebral blood vessels and lymphangiopathy. In the present study, we observed a novel homozygous mutation (c.971A>G) in exon 4 of *HTRA1* gene, which resulted in the substitution of asparagine to serine (p.N324S). This mutation might also affect the activity of proteolytic enzyme and have a vital role in the pathogenesis of CARASIL.

A

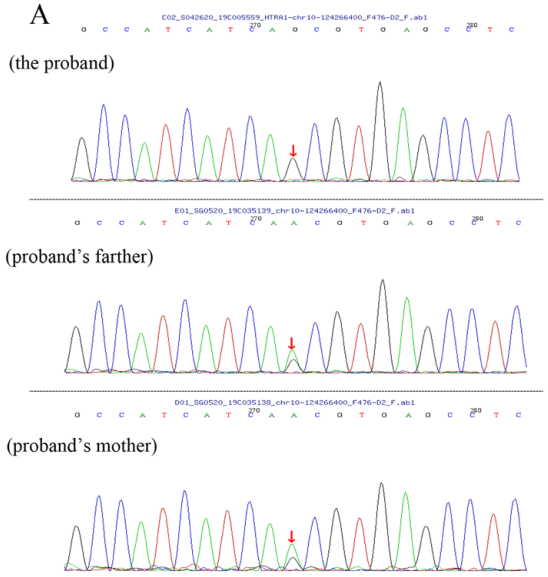

B

Species	Gene	Amino acid
		324
Homo sapiens	HTRA1	T D A I I N Y G N S G
Mus musculus	HTRA1	T D A I I N Y G N S G
Pan troglodytes	HTRA1	T D A I I N Y G N S G
Felis catus	HTRA1	T D A I I N Y G N S G
Bos tauru	HTRA1	T D A I I N Y G N S G
Loxodonta africana	HTRA1	T D A I I N Y G N S G
Ovis aries	HTRA1	T D A I I N Y G N S G
Canis lupus familiaris	HTRA1	T D A I I N Y G N S G
Mutation in this case	HTRA1	S

Fig. 3. *Genetic sequencing of the family with CARASIL.* ***A****) The proband had a novel homozygous mutation (c.971A>G) in exon 4 of the HTRA1 gene. His father and mother had heterozygous A/G mutations.* ***B****) The mutation at position 324 causes a substitution of asparagine to serine (shaded in gray).*

CARASIL is a recessive hereditary disease, and there is no effective treatment for CARASIL patients. By comprehensively studying *HTRA1* mutations, we provide new insights into the diagnosis and treatment of patients with CARASIL. Consistent with our findings, other mutations were also identified in exon 4 of the *HTRA1* gene, suggesting that this exon may be a hot spot for variation (11). The novel c.971A>G mutation adds to the variety of mutations associated with CARASIL, and may facilitate clinical diagnosis and genetic consultation of CARASIL. However, the mechanism through which this mutation influences CARASIL remains unknown; therefore, further research is required to validate the function of this mutation.

In summary, a novel mutation in the *HTRA1* gene (c.971A>G) was detected in a Chinese CARASIL pedigree resulting in the substitution of asparagine to serine and was associated with the pathogenesis of CARASIL. This finding will provide new perspectives for genetically diagnosed CARASIL research.

ACKNOWLEDGEMENTS

The authors thank the Chinese family for their cooperation in this study.

This work was supported by major project of Shanghai Science and Technology Commission(subproject) Program No. 11411950300.

REFERENCES

1. Uemura M, Nozaki H, Koyama A, et al. HTRA1 mutations identified in symptomatic carriers have the property of interfering the trimer-dependent activation cascade. Front Neurol 2019; 10:693.
2. Kono Y, Nishioka K, Li Y, et al. Heterozygous HTRA1 mutations with mimicking symptoms of CARASIL in two families. Clin Neurol Neurosurg 2018; 172:174-76.
3. Ito J, Nozaki H, Toyoshima Y, et al. Histopathologic features of an autopsied patient with cerebral small vessel disease and a heterozygous HTRA1 mutation. Neuropathology 2018; doi: 10.1111/neup.12473.
4. Fasano A, Formichi P, Taglia I, et al. HTRA1 expression profile and activity on TGF-β signaling in HTRA1 mutation carriers. J Cell Physiol 2020; doi: 10.1002/jcp.29609.
5. Mendioroz M, Fernández-Cadenas I, Río-Espinola A, et al. A missense HTRA1 mutation expands CARASIL syndrome to the Caucasian population. Neurology 2010; 75:2033-5
6. Khaleeli Z, Jaunmuktane Z, Beaufort N, et al. A novel HTRA1 exon 2 mutation causes loss of protease activity in a Pakistani CARASIL patient. J Neurol 2015; 262:1369-72
7. Wang X, Li C, Guo H, Cao B. A novel mutation in the HTRA1 gene identified in Chinese CARASIL pedigree. CNS Neurosci Ther 2012; 18:867-9
8. Silvia B, Chiara DP, Gian Nicola G, et al. Two novel HTRA1 mutations in a European CARASIL patient. Neurology 2014; 82:898-900
9. Cai B, Zeng J, Lin Y, et al. A frameshift mutation in HTRA1 expands CARASIL syndrome and peripheral small arterial disease to the Chinese population. Neurol Sci 2015; 36:1387-91
10. Chen Y, He Z, Meng S, Li L, Yang H, Zhang X. A novel mutation of the high-temperature requirement A serine peptidase 1 (HTRA1) gene in a Chinese family with cerebral autosomal recessive arteriopathy with subcortical infarcts and leukoencephalopathy (CARASIL). J Int Med Res 2013; 41:1445-55
11. Nozaki H, Nishizawa M, Onodera O. Features of cerebral autosomal recessive arteriopathy with subcortical infarcts and leukoencephalopathy. Stroke 2014; 45:3447-53

JOURNAL OF BIOLOGICAL REGULATORS & HOMEOSTATIC AGENTS Vol. 34, no. 4, 1411-1415 (2020)

LETTER TO THE EDITOR

Potential influence of miR-192 on the efficacy of saxagliptin treatment in T2DM complicated with non-alcoholic fatty liver disease

P. An[1*], Q. Peng[2*], T. Guo[3], P.-C. Xing[1], L.-D. Zhao[1] and M.-J. Zhou[1]

[1]Department of Emergency and Critical Care Medicine, Shanghai Sixth People's Hospital East, Shanghai, China; [2]Department of Laboratory Medicine, Maternal and Child Health of Qujing Yunnan Province China; [3]Department of Internal Medicine, Shanghai the People's Hospital of Putuo District, Shanghai, China

Received March 8, 2020 – Accepted June 12, 2020

[*]These Authors contributed equally to this work

To the Editor,

Non-alcoholic fatty liver disease (NAFLD) is pathologically classified into simple fatty liver (SFL), nonalcoholic steatohepatitis (NASH), fatty liver fibrosis and fatty cirrhosis. The incidence of NAFLD has increased in recent years, and 25-45% of the global population is affected. In particular, the incidence of NAFLD is up to 70-90% in people with obesity, diabetes or metabolic syndromes. Unfortunately, there is a lack of effective therapeutic strategies of NAFLD-associated cirrhosis, and liver transplantation is the final choice (1); therefore, it is necessary to clarify the pathogenesis of NAFLD and to seek therapeutic targets.

One relevant study illustrated that miR-34a is more upregulated in serum and liver tissues of NAFLD patients than those in healthy controls (2). Furthermore, it has been identified that miR-122 is capable of diagnosing NAFLD and determining its pathological stage (3). MiR-192 locates on human chromosome 11, which is widely distributed in human colon, liver and kidneys (4). MiR-192 is abnormally expressed in serum of patients with NAFLD (5) and diabetic pancreatic ductal adenocarcinoma (6), serving as a potential hallmark.

Gangadharan et al. (7) demonstrated that saxagliptin protects kidney damage by inhibiting inflammatory response and oxidative stress. Zhuge et al. (8) showed that linagliptin stimulates the transformation from M1 macrophages to M2 in adipose and liver tissues of high-fat fed mice, thus reducing inflammation and insulin resistance. Saxagliptin also regulates macrophage polarization (9). In this trial, patients with diabetes complicated with NAFLD were treated with saxagliptin for 6 months, and the influence of miR-192 on the therapeutic efficacy of saxagliptin in NAFLD was observed.

MATERIALS AND METHODS

A total of 150 type 2 diabetic mellitus (T2DM) patients complicated with NAFLD treated in our hospital between July 2016 and December 2018 were included in this study. T2DM was diagnosed based on the following criteria (10): FPG ≥ 1,260 mg/L, 2 h postprandial plasma

Key words: MiR-192; NAFLD; diabetes; saxagliptin

Corresponding Author:
Minjie Zhou, DM
Department of Emergency and Critical Care Medicine,
Shanghai Sixth People's Hospital East,
No. 222 West Three Road around Lake,
Nanhui New City Town, Pudong District, Shanghai, 201306, China
Tel.: +86 018817307584
e-mail: minjiean19890611@163.com

0393-974X (2020)
Copyright © by BIOLIFE, s.a.s.
This publication and/or article is for individual use only and may not be further reproduced without written permission from the copyright holder.
Unauthorized reproduction may result in financial and other penalties
DISCLOSURE: ALL AUTHORS REPORT NO CONFLICTS OF INTEREST RELEVANT TO THIS ARTICLE.

glucose≥ 200 g/L, HbA1c ≥ 6.5%, symptoms of high blood sugar or hyperglycemic crisis or casual plasma glucose ≥ 200 g/L. Inclusion criteria for NAFLD (11) were: patients with no history of drinking or alcohol use < 140 g/week (<70 g/week for women), no viral hepatitis or drug-induced liver disease that could cause fatty liver, and histological changes of fatty liver disease or diffuse fatty liver performances in liver imaging that could not be explained by other reasons. Patients with severe heart and liver failure, fatty liver due to alcohol or other clear causes, or malignancies, or those who were allergic to saxagliptin were excluded. This study was approved by the Ethic Committee of Shanghai Sixth People's Hospital East, and all subjects signed the informed consent.

The patients included orally took saxagliptin (5 mg, qd, Bristol-Myers Squibb, J20110029, New York, NY, USA) for 6 months. 2 mL of venous blood was collected from each patient before and after saxagliptin treatment and were centrifuged at 3,000 r/min, and serum samples were stored at -80°C.

Quantitative real-time polymerase chain reaction (qRT-PCR)

Serum miRNAs were extracted using the miRNeasy Mini Kit (Qiagen, Hilden, Germany), which were reversely transcribed using the Taqman microRNA reverse Transcription Kit (Thermo Fisher, Waltham, MA, USA). QRT-PCR was performed using the 2×SYBR Green PCR Master Mix. U6 was the internal reference. Primer sequences were listed below: MiR-192, F: 5′-GGCCGAATGATTGCTGAGGAAATCATGG and R: 5′-TTACAGCGGCCATGGCAAGTCACTAAAG-3′, and U6, F: 5′-CTCGCTTCGGCAGCACATATACT-3′ and R: 5′-ACGCTTCACGAATTTGCGTGTC-3′.

Observational indicators

The relative levels of fasting plasma glucose (FPG), 2h postprandial plasma glucose (2hPPG), glycosylated hemoglobin (HbA1c), alanine aminotransferase (ALT), aspartate aminotransferase (AST), gamma-glutamyltransferase (GGT), total cholesterol (TC) and triglyceride (TG) before and after 6-month saxagliptin treatment were determined. Therapeutic efficacy of NAFLD was assessed according to symptoms and laboratory indexes after treatment: (i) Complete response: Clinical symptoms were alleviated or had disappeared. B-ultrasound showed that the signs of fatty liver were remarkably reduced. Liver function returned to normal, and the blood lipid was decreased by more than 30%. (ii) Partial response: Clinical symptoms were alleviated. Signs of fatty liver were reduced in B-ultrasound examination, and liver function was improved. Blood lipid was decreased by more than 10%. (iii) No response: Symptoms remained unchangeable. Overall response rate = the proportion of patients with a partial response to therapy + the proportion of patients with a complete response to therapy.

Statistical analysis

Statistical Product and Service Solutions (SPSS) 20.0 (IBM, Armonk, NY, USA) was used for all statistical analysis. Measurement data were expressed as mean ± SD (standard deviation), and enumeration data were expressed as percentage (%). The *t*-test and *chi*-squared test were performed for analyzing differences between groups. $P<0.05$ indicated the statistically significant difference.

RESULTS

Baseline characteristics of subjects

The serum level of miR-192 was detected in the 150 included subjects, and the median level was 4.87±1.27. Based on this level, patients were assigned into miR-192 high-level (n=89) or low-level groups (n=61), respectively. Through analyzing their baseline characteristics, no significant differences in age, sex and BMI were found between the two groups (Table I).

Serum levels of FPG, 2hPPG and HbA1c before and after saxagliptin treatment

Before saxagliptin treatment, no significant differences in the serum levels of FPG, 2hPPG and HbA1c were found between two groups ($P>0.05$). After 6-month saxagliptin treatment, the levels were remarkably reduced in both groups, especially in the miR-192 high-level group ($P<0.05$) (Table II). It is suggested that saxagliptin treatment alleviates hyperglycemia, especially in those expressing a high level of miR-192.

Liver function and blood lipid indexes before and after saxagliptin treatment

The potential influences of miR-192 on the

therapeutic efficacy of saxagliptin in liver function and blood lipid were analyzed. No significant differences in the serum levels of ALT, AST, GGT, TC and TG were observed before saxagliptin treatment between the two groups (P>0.05). After 6-month saxagliptin treatment, their levels were remarkably reduced in both groups, especially in the miR-192 high-level group (P<0.05) (Table III). It is indicated that highly expressed miR-192 is favorable to saxagliptin treatment in improving liver function and blood lipid.

Therapeutic efficacy of NAFLD

Based on symptoms and laboratory examinations, 150 subjects following 6-month saxagliptin treatment were classified into three groups, namely complete

Table I. *Baseline characteristics of subjects*

Variable	High level of miR-192 (n=89)	Low level of miR-192 (n=61)	t/χ^2	P
age	54.3±7.88	56.13±8.23	1.372	0.172
Sex (male/female)	47/42	35/26	0.305	0.619
BMI (kg/m^2)	21.98±3.67	22.34±3.96	0.571	0.569

BMI: Body mass index

Table II. *Serum levels of FPG, 2hPPG and HbA1c before and after treatment*

Variable	High level of miR-192 (n=89)		Low level of miR-192 (n=61)	
	Before treatment	After treatment	Before treatment	After treatment
FPG (mmol/L)	10.21±2.36	5.62±1.63*	10.03±2.05	6.98±2.39*#
2hPPG (mmol/L)	14.22±2.69	8.22±2.34*	14.37±2.81	9.82±2.69*#
HbAlc (%)	8.56±1.62	6.12±1.02*	8.49±1.57	6.20±1.13*

**P<0.05: Comparison before and after treatment in the same group, and #P<0.05 Comparison between the two groups after treatment. FPG: Fasting plasma glucose; 2hPPG: 2-hour postprandial plasma glucose; HbA1c: glycated hemoglobin.*

Table III. *Liver function and blood lipid indexes before and after saxagliptin treatment*

Variable	High level of miR-192 (n=89)		Low level of miR-192 (n=61)	
	Before treatment	After treatment	Before treatment	After treatment
ALT (U/L)	36.77±7.39	16.95±5.44*	36.35±7.13	26.37±9.28*#
AST (U/L)	29.53±5.31	20.87±5.69*	28.78±5.27	25.96±6.32*#
GGT (U/L)	58.63±29.55	28.69±11.65*	57.29±28.62	36.25±15.36*#
TC (mmol/L)	5.36±1.52	3.82±1.19*	5.32±1.48	4.25±1.35*#
TG (mmol/L)	3.56±0.59	1.12±0.23*	3.69±0.62	2.26±0.44*#

**P<0.05: Comparison before and after treatment in the same group, and #P<0.05: Comparison between the two groups after treatment. ALT: Alanine aminotransferase, AST: Aspartate aminotransferase, GGT: γ-glutamyl transpeptidase, TC: total cholesterol and TG: Triglyceride*

Table IV. *Therapeutic efficacy of NAFLD*

Curative effect	High level of miR-192 (n=89)	Low level of miR-192 (n=61)	χ^2	P
Effectiveness (n%)	42 (47.20%)	14 (22.95%)	9.09	0.003
Validation (n%)	35 (39.33%)	11 (18.03%)	7.718	0.007
Invalidation (n%)	12 (13.48%)	36 (59.02%)	34.49	<0.001
Overall response rate (n%)	77 (86.52%)	25 (40.98%)		

response group, partial response group and no response group. The data revealed that the overall response rate of NAFLD was 68%, which was 86.52% in miR-192 high-level group and 40.98% in low-level group (Table IV). The complete response and partial response rates were higher in the miR-192 high-level group, suggesting that miR-192 contributes to enhancing the therapeutic efficacy of saxagliptin in patients with diabetes complicated with NAFLD.

DISCUSSION

Saxagliptin is a dipeptidyl peptidase (DPP-4) inhibitor used for T2DM treatment. It is a new type of oral hypoglycemic agent based on enterotropin. Through inhibiting the role of DPP-4 enzymes in hydrolysis of enterotrypsin, saxagliptin stimulates insulin secretion and β cell regeneration. A recent study has shown that DPP-4 enzymes affect lipid metabolism by inactivating GLP-1 and neuropeptide Y, and they regulate energy balance. DPP-4 activity in blood and its expression in the liver are closely related to liver steatosis and NAFLD progression. Clinical evidence has demonstrated the protective effect of DPP-4 inhibitors on diabetes complicated with NAFLD by regulating insulin resistance, oxidative stress, and inflammatory response. Sitagliptin is proven to reduce liver enzymes and improve balloon degeneration of liver cells. DPP-4 inhibitors not only control blood glucose, but also improve blood lipid and liver function (12), which were consistent with our findings.

This trial explored the influence of differentially expressed miR-192 on saxagliptin sensitivity in T2DM patients complicated with NAFLD. The results demonstrated that patients with highly expressed miR-192 had higher benefit with saxagliptin treatment. It is believed that miR-192 can be utilized as a sensitive hallmark in T2DM complicated with NAFLD, and patients with diabetes complicated with NAFLD expressing a high level of miR-192 are more sensitive to saxagliptin treatment.

ACKNOWLEDGEMENTS

We wish to thank Dr. P. An (Peng An) (Department of Emergency and Critical Care Medicine, Shanghai Sixth People's Hospital East, Shanghai 201306, China) for his great contribution into the research funding support and also the concept of the whole study.

REFERENCES

1. Loomba R, Sanyal AJ. The global NAFLD epidemic. Nat Rev Gastroenterol Hepatol 2013; 10:686-90.
2. Salvoza NC, Klinzing DC, Gopez-Cervantes J, Baclig MO. Association of circulating serum miR-34a and miR-122 with dyslipidemia among patients with non-alcoholic fatty liver disease. Plos One 2016; 11:e153497.
3. Yamada H, Ohashi K, Suzuki K, et al. Longitudinal study of circulating miR-122 in a rat model of non-alcoholic fatty liver disease. Clin Chim Acta 2015; 446:267-71.

4. Ge Y, Yan X, Jin Y, et al. MiRNA-192 [corrected] and miRNA-204 directly suppress lncRNA HOTTIP and interrupt GLS1-Mediated glutaminolysis in hepatocellular carcinoma. Plos Genet 2015; 11:e1005726.
5. Liu CH, Ampuero J, Gil-Gomez A, et al. miRNAs in patients with non-alcoholic fatty liver disease: A systematic review and meta-analysis. J Hepatol 2018; 69:1335-48.
6. Skrha P, Horinek A, Pazourkova E, Hajer J, Fric P, Skrha J, Andel M. Serum microRNA-196 and microRNA-200 in pancreatic ductal adenocarcinoma of patients with diabetes mellitus. Pancreatology 2016; 16:839-43.
7. Gangadharan KM, Gross S, Zaky A, Pollock C, Panchapakesan U. Saxagliptin reduces renal tubulointerstitial inflammation, hypertrophy and fibrosis in diabetes. Nephrology (Carlton) 2016; 21:423-31.
8. Zhuge F, Ni Y, Nagashimada M, et al. DPP-4 Inhibition by linagliptin attenuates obesity-related inflammation and insulin resistance by regulating M1/M2 macrophage polarization. Diabetes 2016; 65:2966-79.
9. Shirakawa J, Fujii H, Ohnuma K, et al. Diet-induced adipose tissue inflammation and liver steatosis are prevented by DPP-4 inhibition in diabetic mice. Diabetes 2011; 60:1246-57.
10. Malmstrom H, Walldius G, Carlsson S, et al. Elevations of metabolic risk factors 20 years or more before diagnosis of type 2 diabetes: Experience from the AMORIS study. Diabetes Obes Metab 2018; 20:1419-26.
11. Zeng MD, Fan JG, Lu LG, Li YM, Chen CW, Wang BY, Mao YM. Guidelines for the diagnosis and treatment of nonalcoholic fatty liver diseases. J Dig Dis 2008; 9:108-12.
12. Zheng T, Chen B, Yang L, Hu X, Zhang X, Liu H, Qin L. Association of plasma dipeptidyl peptidase-4 activity with non-alcoholic fatty liver disease in nondiabetic Chinese population. Metabolism 2017; 73:125-34.

LETTER TO THE EDITOR

MiR-133a Promoted cerebral ischemia/reperfusion injury by targeting brain-derived neurotrophic factor

J. Li[1*], HY. Yang[1*], L. Wang[2], FF. Zhao[1], S. Yang[1] and FB. Ning[1]

[1]Department of Neurology, Taian City Central Hospital, Taian, China; [2]Department of Interventional Radiology, Taian City Central Hospital, Taian, China

Received March 6, 2020 – Accepted June 17, 2020

[*]These Authors contributed equally to this work

To the Editor,

Cerebral ischemia-reperfusion (CIR) injury is a pathological process, in which neurological damage caused by ischemia and hypoxia is further aggravated after a short-term recovery of blood perfusion (1). Reperfusion therapy has made great progress, but the therapeutic effects are still unsatisfactory, so reducing reperfusion injury after cerebral infarction is an important research topic (2, 3). The expression of miR-133a is still unclear, thus, the aim of this study is to investigate the role of miR-133a in cerebral ischemia-reperfusion induced injury using an OGD/R model.

MicroRNAs (miRNAs) are small non-coding RNAs that target the 3'-untranslated region of mRNA, and are key mediators of post-transcriptional gene silencing (4). There is increasing evidence that miRNAs play key roles in cerebral ischemia. Previous studies have reported that miR-133a enhanced cell proliferation and autophagy via regulating FOXP3 in gastric cancer (5). In fact, upregulation of miR-133a promoted cell viability and inhibited OGDR-induced apoptosis by targeting BDNF (6). In the current work, an OGDR model was constructed in HCN-2 cells, to focus on cell proliferation and apoptosis of cerebral ischemia injury.

Brain derived neurotrophic factor (BDNF) encodes a member of the nerve growth factor family of proteins, which can promote neuronal differentiation and neural tissue regeneration in MSCs (7). BDNF improved glucose metabolism after cerebral ischemic stress in mice. In this study, we found that miR-133a promoted cell proliferation and inhibited cell apoptosis via BDNF in OGD/R treated HCN-2 cells.

MATERIALS AND METHODS

Cell culture and transfection

Human HCN-2 cells from the Cell Bank of the Chinese Academy of Sciences (Shanghai, China) were purchased for this study. The HCN-2 cells were calculated in Dulbecco's Modified Eagle Medium (DMEM; Gibco, Grand Island, NY, USA) supplement with 10% fetal bovine serum (FBS; Gibco, Grand Island, NY, USA) in an incubator at 37°C with 5% CO2.

The miR-133a mimic, inhibitor and small interfering RNA (siRNA) of BDNF were obtained from GenePharma (Shanghai, China). Transient transfection of plasmids, miR-133a mimic, inhibitors or BDNF siRNA were transfected in HCN-2 cells using Lipofectamine 2000 (Life Technologies) following the manufacturer's recommended protocol.

Key words: miR-133; BDNF; cerebral ischemia/reperfusion injury; oxygen glucose deprivation/reoxygenation

Corresponding Author:
Dr Fangbo Ning,
Department of Neurology,
Taian City Central Hospital,
No 29 Longtan Road,
Taian 271000, China
e-mail: feigaoou93338@163.com

0393-974X (2020)
Copyright © by BIOLIFE, s.a.s.
This publication and/or article is for individual use only and may not be further reproduced without written permission from the copyright holder.
Unauthorized reproduction may result in financial and other penalties
DISCLOSURE: ALL AUTHORS REPORT NO CONFLICTS OF INTEREST RELEVANT TO THIS ARTICLE.

Establishment of cerebral ischemia-reperfusion (OGDR) Model

To build an OGD model, HCN-2 cells were cultured in a glucose-free Hanks' balanced salt solution (Invitrogen, Carlsbad, CA, USA) under hypoxic conditions (1% O2/94% N 2/5% CO2) at 37°C for 4 h. The cells were then placed in a glucose medium with 10% FBS, and cultured under normoxic conditions (95% air/5% CO_2) for 48 h for reperfusion. HCN-2 cells cultured under normoxic conditions were used as controls.

Real time-quantitative polymerase chain reaction (RT-qPCR)

The total RNA of HCN-2 cells was extracted using the TRIzol reagent (Invitrogen, Carlsbad, CA, USA). The synthesis of complementary deoxyribose nucleic acid (cDNA) was performed using PrimeScript RT Master Mix (TaKaRa, Dalian, China). Real Time-Quantitative Polymerase Chain Reaction (RT-qPCR) was performed using the SYBR PrimeScript miRNA RT-PCR Kit (TaKaRa, Dalian, China) on an ABI 7500 Fast system (Applied Biosystems, Foster City, CA, USA). The internal control of miR-133a or BDNF were U6 or glyceraldehyde 3-phosphate dehydrogenase (GAPDH).

MTT (3-(4,5-dimethylthiazol-2-yl)-2,5-diphenyltetrazolium bromide) assay

Cell viability was assessed using MTT assay (Sigma-Aldrich, St. Louis, MO, USA). HCN-2 cells were incubated in 96-well plates at a density of 4×103 cells for 48 h. Next, the cells were incubated in serum-free medium containing 20 μL MTT. After incubating for 4 h at 37°C, the supernatant was removed. Thereafter, the cells were dissolved in 100 μL of dimethyl sulfoxide, and the absorbance was read at 490 nm on a microplate spectrophotometer (Thermo Labsystems, Vantaa, Finland).

Dual-luciferase reporter assay

The wild or mutant BDNF and miR-133a mimic were co-transfected into HCN-2 cells for Luciferase reporter gene detection. The relative firefly luciferase activity was normalized to Renilla luciferase activity. The experiment was repeated at least three times. Finally, the Luciferase activity was measured by a Dual-Luciferase assay system (Promega, Madison, WI, USA).

Western blot analysis

The radioimmunoprecipitation assay (RIPA) lysis buffer (Beyotime, Shanghai, China) was used to lyse cells to obtain protein samples. Proteins were then separated by 10% sodium dodecyl sulphate-polyacrylamide gel electrophoresis (SDS-PAGE). The proteins were then transferred onto a polyvinylidene difluoride (PVDF) membrane (Millipore, Billerica, MA, USA) for 2 h at room temperature. After blocking with 5% skim milk, the membrane was incubated with primary antibodies overnight at 4°C. The membrane was incubated with horseradish peroxidase (HRP)-conjugated secondary antibody at room temperature for 2 h. Finally, the electrochemiluminescence (ECL) (Pierce, Waltham, MA, USA) was used to visualize the protein.

Statistical analysis

All data are expressed as mean ±standard deviation (SD), repeated at least three times in each group. The date was analyzed using the Statistical Product and Service Solutions (SPSS) 19.0 (SPSS Inc., Chicago, IL, USA) or GraphPad Prism 6 (La Jolla, CA, USA). Comparisons between groups were performed using One-way analysis of variance (ANOVA) test followed by Post-Hoc Test (Least Significant Difference). A significant difference was defined as $p<0.05$.

RESULTS

Expression of MiR-133a was increased in the OGDR model

The expression of miR-133a was tested in OGDR cells and normal HCN-2 cells. The results showed that, compared with the control group, the expression of miR-133a in HCN-2 cells treated with OGDR was significantly up-regulated ($p <0.01$, Fig. 1A), indicating that cerebral ischemia/reperfusion can enhance the expression of miR-133a. Next, miR-133a mimics or inhibitors were transfected into HCN-2 cells cultured under OGDR conditions. Compared with the OGDR group, miR-133a mimics can promote its expression, while miR-133a inhibitors can reduce its expression in HCN-2 cells ($p <0.01$, Fig. 1B), suggesting that the expression of miR-133a was successfully regulated artificially.

MiR-133a regulated the viability and apoptosis in HCN-2 cells

The MTT assay was used to examine the effect of

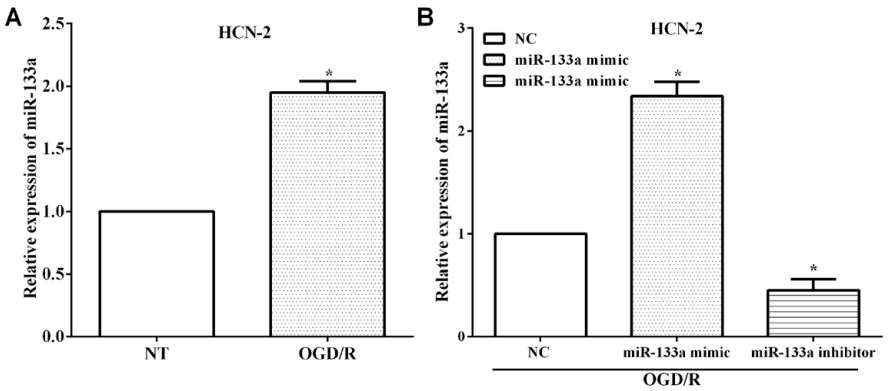

Fig. 1. *Expression of MiR-133a was Increased in the OGDR model.* ***A****) The expression of miR-133a in HCN-2 cells treated with OGDR was significantly up-regulated.* ***B****) MiR-133a mimics or inhibitors were transfected into HCN-2 cells cultured under OGDR conditions.*

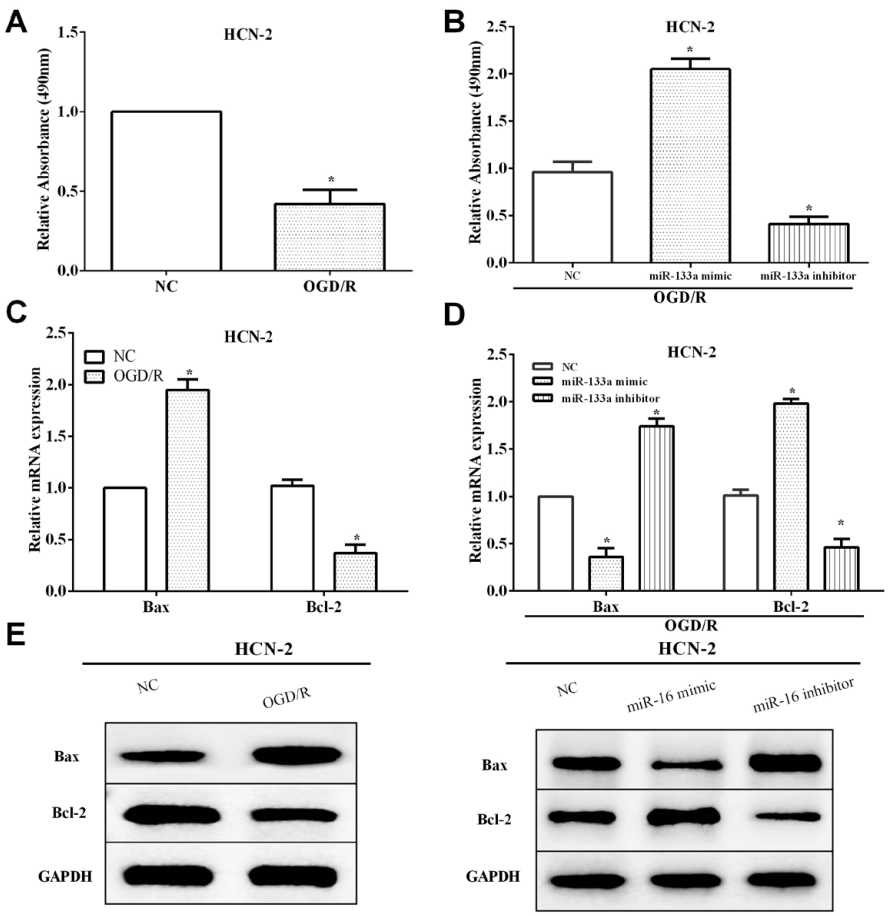

Fig. 2. *MiR-133a regulated cell viability and apoptosis in HCN-2 cells.* ***A****) OGDR significantly inhibited the viability of HCN-2 cells.* ***B****) MiR-133a mimics promoted HCN-2 cell proliferation under hypoxic conditions. MiR-133a inhibitors inhibited cell proliferation in HCN-2 cells under hypoxic conditions.* ***C****) Treated with OGDR increased the mRNA level of Bax and decreased Bcl-2 mRNA.* ***D****) Altering miR-133a significantly regulated the expression of Bax and Bcl-2.* ***E****) The protein expression of Bax and Bcl-2 were calculated after treated with OGDR.* ***F****) The protein levels of Bax and Bcl-2 were measured after overexpressing or knocking down miR-133a.*

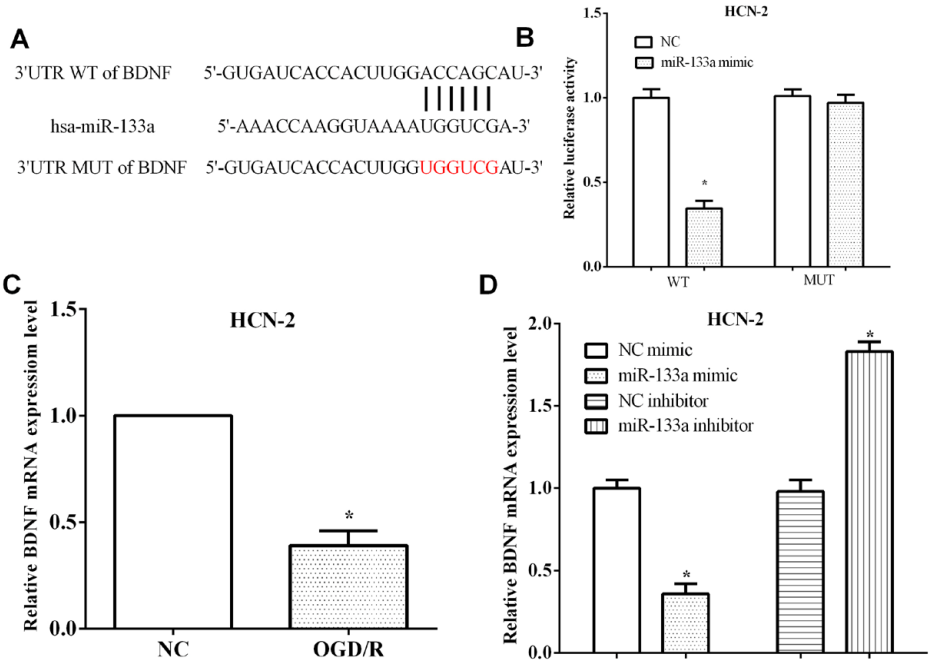

Fig. 3. *BDNF was a direct target gene of MiR-133a.* ***A****) MiR-133a has a potential binding site with 3'-UTR of BDNF.* ***B****) MiR-133a mimics significantly inhibited the luciferase activity of wild-type BDNF.* ***C****) MiR-133a mimics further reduced BDNF expression in HCN-2 cells treated with OGDR.* ***D****) MiR-133a inhibitors enhanced BDNF expression levels.*

miR-133a on cell viability. The results showed that OGDR significantly inhibited the viability of HCN-2 cells ($p < 0.05$, Fig. 2A). Moreover, compared to the OGDR group, miR-133a mimics promoted the proliferation under hypoxic conditions of HCN-2 cell ($p < 0.01$, Fig. 2B). In contrast, miR-133a inhibitors inhibited the proliferation in HCN-2 cells under hypoxic conditions ($p < 0.05$, Fig. 2B). Therefore, it is believed that miR-133a is thought to reverse the effects of OGDR and prolong cell survival time.

Next, the apoptosis regulated by miR-133a after cerebral ischemic injury was studied, therefore RT-qPCR and Western blot were used to detect the expression of apoptosis-related genes Bax and Bcl-2 in HCN-2 cells. First, OGDR treatment increased Bax expression and decreased Bcl-2 expression ($p < 0.05$, Fig. 2C). Compared with the OGDR group, the up-regulation of miR-133a significantly reduced Bax expression and promoted the expression of the survival gene Bcl-2 ($p < 0.05$, Fig. 2D). The protein expression of Bax and Bcl-2 were calculated after being treated with OGDR ($p < 0.05$, Fig. 2E). Compared with OGDR treatment, inhibition of MiR-133a could promote Bax expression and inhibit Bcl-2 expression ($p < 0.05$, Fig. 2F). Based on these results, under OGDR conditions, overexpression of miR-133a promoted the viability of HCN-2 cells and inhibited apoptosis.

BDNF was a direct target gene of MiR-133a

In addition, the molecular mechanism of miR-133a inhibiting OGDR was studied. Through TargetScan, we found that miR-133a has a potential binding site with 3'-UTR of BDNF (Fig. 3A). To confirm the interaction between miR-133a and BDNF, a dual luciferase reporter assay was performed in HCN-2. The results showed that the up-regulation of miR-133a significantly inhibited the luciferase activity of wild-type BDNF, but had no effect on mutant BDNF ($p < 0.05$, Fig. 3B), proving that miR-133a directly targets BDNF.

Moreover, compared with the group without OGDR, the expression of BDNF was significantly reduced under OGDR conditions ($p < 0.05$, Fig. 3C). Interestingly, miR-133a mimics further reduced

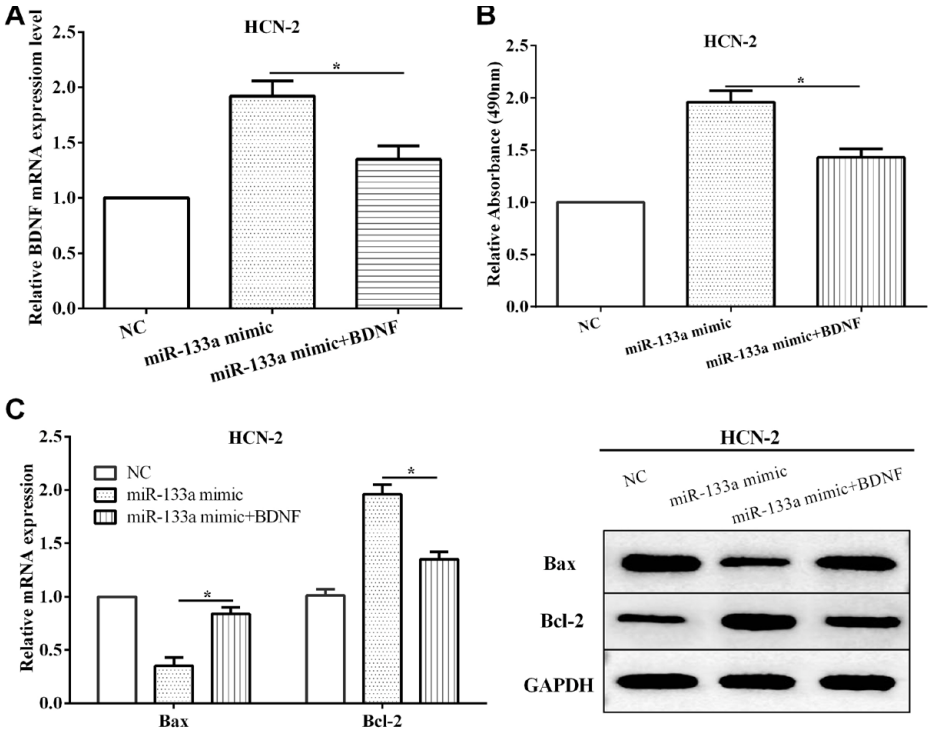

Fig. 4. *MiR-26 regulated cerebral ischemia injury by targeting BDNF. A) Overexpression of BDNF could reverse the miR-133a mimic's reduction of BDNF expression. B) Under OGDR conditions, the BDNF plasmid prevented miR-133a from promoting the proliferation of HCN-2 cells. C) Overexpression of BDNF also reversed the inhibitory effect of miR-133a on apoptosis.*

BDNF expression in HCN-2 cells treated with OGDR. However, miR-133a inhibitors enhanced BDNF expression levels ($p < 0.05$, Fig. 3D). Therefore, miR-133a can further inhibit the expression of BDNF to regulate cerebral ischemic injury.

MiR-26 regulated cerebral ischemia injury by targeting BDNF

Finally, miR-133a mimic and BDNF overexpression plasmid were co-transfected into HCN-2 cells under OGDR conditions to further examine their interactions in cerebral ischemic injury. The results of RT-qPCR analysis showed that the BDNF overexpression plasmid could reverse the miR-133a mimic's reduction of BDNF expression ($p < 0.05$, Fig. 4A). More importantly, under OGDR conditions, the BDNF plasmid prevented miR-133a from promoting the proliferation of HCN-2 cells ($p < 0.05$, Fig. 4B). Similarly, overexpression of BDNF also reversed the inhibitory effect of miR-133a on apoptosis ($p < 0.05$, Fig. 4C). Therefore, miR-133a is thought to promote HCN-2 cell viability and inhibit apoptosis by targeting BDNF under OGDR conditions.

DISCUSSION

In this study, miR-133a was found to be markedly overexpressed in HCN-2 cells treated with OGDR compared to the control group, indicating that cerebral ischemia/reperfusion may promote the expression level of miR-133a. MTT assay showed that miR-133a was considered to reverse the effects of OGDR and prolong cell survival. Apoptosis is an important biological process of cerebral ischemic injury and an important type of cell death. Bax and Bcl-2 are proteins related to apoptosis: Bcl-2 inhibits apoptosis, and Bax promotes apoptosis. Here, overexpression of miR-133a was found to inhibit cell apoptosis induced by OGDR treatment.

BDNF was predicted to be a target of miR-

133a, with a binding site on its mRNA 3'-UTR by TargetScan. Dual-Luciferase reporter assay was performed to confirm the interaction between miR-133a and BDNF. Interestingly, miR-133a further regulated the expression of BDNF in HCN-2 cells treated with OGDR. Finally, the decreased expression of BDNF induced by miR-133a mimics was recovered by BDNF overexpression plasmid. More importantly, BDNF overexpression plasmid prevented the acceleration of miR-133a on the proliferation of HCN-2 cells under OGDR conditions. It is well known that BDNF is considered as one of the strategies for treating cognitive-related diseases (8, 9). Even so, there are still some shortcomings in current research, such as the lack of animal experiments. Therefore, we will further explore the role of miR-133a and BDNF in cerebral ischemic injury *in vivo*. Our findings will help us develop new uses for miR-133a as a therapeutic target for cerebral ischemic injury.

In brief, this study mainly elucidated that miR-133a negatively regulates cerebral ischemic injury by targeting BDNF to promote cell viability and inhibit apoptosis.

REFERENCES

1. Diaz-Canestro C, Merlini M, Bonetti NR, et al. Sirtuin 5 as a novel target to blunt blood-brain barrier damage induced by cerebral ischemia/reperfusion injury. Int J Cardiol 2018; 260:148-55.
2. Wang X, An F, Wang S, An Z, Wang S. Orientin attenuates cerebral ischemia/reperfusion injury in rat model through the AQP-4 and TLR4/NF-kappaB/TNF-alpha signaling pathway. J Stroke Cerebrovasc Dis 2017; 26:2199-214.
3. Wang W, Xu J. Curcumin attenuates cerebral ischemia-reperfusion injury through regulating mitophagy and preserving mitochondrial function. Curr Neurovasc Res 2020; doi: 10.2174/1567202617666200225122620.
4. Bartel DP. MicroRNAs: target recognition and regulatory functions. Cell 2009; 136:215-33.
5. Li JP, Zhang HM, Liu MJ, et al. miR-133a-3p/FOXP3 axis regulates cell proliferation and autophagy in gastric cancer. J Cell Biochem 2020; 121:3392-405.
6. Guo XL, Liang H, Sun Y, Wang CB. MicroRNA-26a regulates cerebral ischemia injury through targeting PTEN. Eur Rev Med Pharmacol Sci 2019; 23:7033-41.
7. Shi W, Huang CJ, Xu XD, et al. Transplantation of RADA16-BDNF peptide scaffold with human umbilical cord mesenchymal stem cells forced with CXCR4 and activated astrocytes for repair of traumatic brain injury. Acta Biomater 2016; 45:247-61.
8. Lu B, Nagappan G, Lu Y. BDNF and synaptic plasticity, cognitive function, and dysfunction. Handb Exp Pharmacol 2014; 220:223-50.
9. Xu J, Kurup P, Azkona G, et al. Down-regulation of BDNF in cell and animal models increases striatal-enriched protein tyrosine phosphatase 61 (STEP61) levels. J Neurochem 2016; 136:285-94.

LETTER TO THE EDITOR

Effect of microRNA-129-5p targeting High mobility group protein box1 on regulating inflammation in lipopolysaccharide-activated primary spinal microglia cells

X-J. Ma[1], T-Y. Song[1*], W-L Wang[2] and Z-W. Zhang[3]

[1]Department of Anesthesiology, The First Hospital of Shijiazhuang, Shijiazhuang, China; [2]Department of Gynaecology, Maternal and Child Health Care Hospital of Shijiazhuang, Shijiazhuang, China; [3]Department of Anesthesiology, The Bethune International Peace Hospital of P.L.A., Shijiazhuang, China

Received March 30, 2020 – Accepted June 23, 2020

To the Editor,

Neuropathic pain usually originates from tissue damage or dysfunction in the central nervous system or the peripheral nervous system, which occurs following medical situations such as viral infection, trauma, nervous system diseases, etc. Activation of microglia and neuroinflammation plays a pivotal role in the process of neuropathic pain. Inflammation occurs at the site of damaged nerves and initiates a cascade of inflammatory responses, resulting in release of proinflammatory cytokines and other chemical constituents of inflammation. The resultant neuroinflammatory environment can activate glia cells which play a role in nociception. On the other hand, the activated microglia could proliferate and generate pro-inflammatory responses that further exacerbate neuropathic pain (1). Lipopolysaccharide (LPS)-activated microglia was previously used as an *in vitro* model to study the neuroinflammation and microglia activation in neuropathic pain (2).

High mobility group protein box1 (HMGB1) is an important inflammatory mediator in various diseases related to inflammation, and anti-HMGB1 treatment by antagonists or specific pharmacological agents was found to be beneficial in many experimental models of inflammatory diseases (3). Emerging evidence suggested an association of HMGB1 with the pathology of neuropathic pain progression (4). Preclinical experiments showed that administration of HMGB1 induced neuropathic pain-like behaviors in rodents, while HMGB1 antibodies played a protective effect in animal models of neuropathic pain (5).

MATERIALS AND METHODS

HEK-293T cells were purchased from CCTCC (Wuhan, China) and maintained in DMEM containing 10% FBS and 1% penicillin/streptomycin (all purchased from Gibco, Carlsbad, CA. USA). Rat primary spinal microglia cells were isolated following a protocol described previously (6), with some modifications. In brief, the spinal cord from region T1 to T12 was dissected from adult Sprague Dawley (SD) rats and placed in ice-cold Hanks balanced salt solution (HBSS). After all meninges were peeled away, the tissues were cut into small pieces and digested in HBSS containing 0.2 g/L EDTA and 2.5 g/L trypsin at 37°C for 30 min. Then the media was discarded and replaced with primary microglia culture media (DMEM-GlutaMAX-I media with 15% FBS and 1% penicillin/streptomycin, Gibco). The tissue sections were triturated thrice using a 1 ml pipette and the cells were collected, resuspended in culture media and then filtered using cell strainers (40 μm,

Key words: neuropathic pain; high mobility group protein box1 (HMGB1); miR-129-5p; inflammation; microglia

Corresponding Author:
Dr Tieying Song,
Department of Anesthesiology, The First Hospital of Shijiazhuang,
No.36 Fanxi Road, Chang'an District,
Shijiazhuang 050000, China
Tel.: +86 13303110200
e-mail: tysong1234@163.com

0393-974X (2020)
Copyright © by BIOLIFE, s.a.s.
This publication and/or article is for individual use only and may not be further reproduced without written permission from the copyright holder.
Unauthorized reproduction may result in financial and other penalties
DISCLOSURE: ALL AUTHORS REPORT NO CONFLICTS OF INTEREST RELEVANT TO THIS ARTICLE.

BD Biosciences, Franklin Lakes, NJ, USA). Cells were counted using a hemocytometer and plated on 12-well plates (at 1×10^5 cells/well).

Luciferase assay

The wildtype or mutated 3' UTR of HMGB1 was sub-cloned into pGL3 Basic vector (Promega, Madison, WI, USA) (termed as WT-HMGB1 and MUT-HMGB1 respectively) (Fig. 1A). These luciferase reporter plasmids along with miR-129-5p mimics or inhibitors were transfected into HEK293 cells by Lipofectamine 2000 reagent (Invitrogen, Waltham, MA USA). Briefly, 1 µg plasmid and 20 pmol miRNA were diluted in 100 µl serum-free DMEM. 1 µl Lipofectamine 2000 was diluted in 100 µl serum-free DMEM and placed at room temperature for 5 min. Then the plasmid, miRNA and Lipofectamine dilutions were mixed and incubated at room temperature for 20 min to form transfection compound. The culture medium in the wells was replaced by serum-free DMEM medium and the transfection compound was added. Luciferase activity was measured at 48 h after transfection using a dual-luciferase assay kit (Promega). Renilla luciferase reporter plasmids (Promega) were co-transfected to normalize transfection efficiency.

Cell transfection and LPS stimulation

For LPS stimulation alone, the culture media of primary spinal microglia cells was replaced by DMEM. LPS (Sigma, St. Louis, MO) was diluted with DMEM and added into the wells of LPS treatment groups at a final dose of 5 µg/ml, whereas the Control group received equal volume of DMEM. Cells were harvested at indicated timepoints. The mRNA levels of miR-129-5p and HMGB1 was measured.

For transfection and LPS stimulation, rat primary spinal microglia cells were transfected with mimics or inhibitors of miR-129-5p, or HMGB1 shRNA by Lipofectamine 2000. The miR-129-5p sequence obtained from the database was (miRNA base): 5'-GTCGTATCCAGTGCAGGGTC-CGAGGTATTCGCACTGGATACGACGCAAGC-3'. Mimics and inhibitors of miR-129-5p their negative control

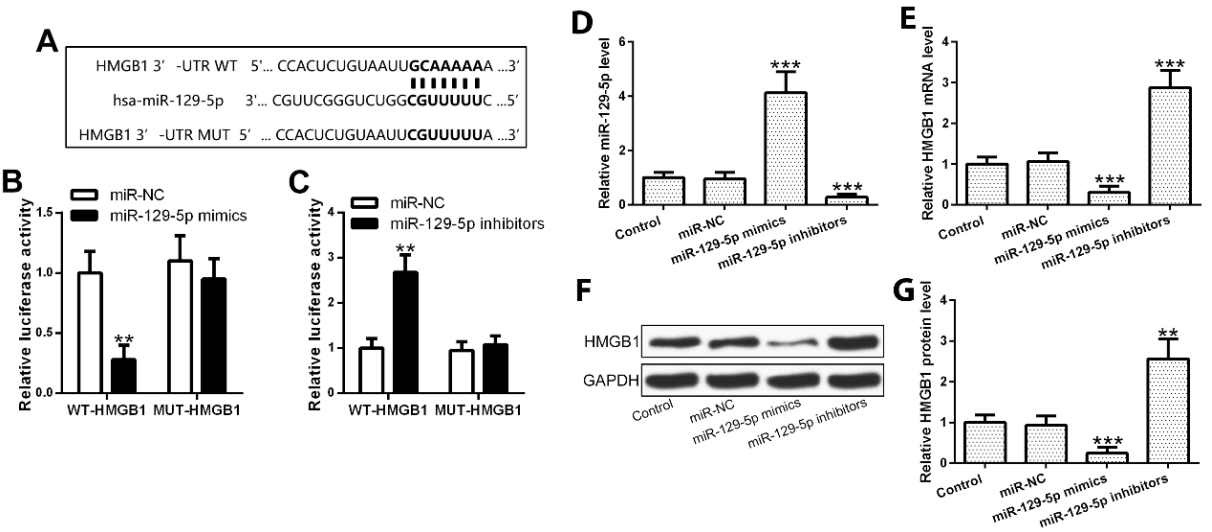

Fig. 1. *miR-129-5p directly targets HMGB1 and regulates HMGB1 expression in rat spinal microglia cells.* ***A****) The suspected binding of miR-129-5p with the wild-type 3'-UTR region of HMGB1 mRNA is shown. A mutated 3'-UTR of HMGB1 is also shown.* ***B****) WT-HMGB1 or MUT-HMGB1 was co-transfected into HEK-293T cells with miR-129-5p mimics or their corresponding negative controls. After 48 h of incubation, relative luciferase activities were measured.* ***C****) WT-HMGB1 or MUT-HMGB1 was co-transfected into HEK-293T cells with miR-129-5p inhibitors or their corresponding negative controls. After 48 h of incubation, relative luciferase activities were measured.* ***D****) The expression of miR-129-5p in rat spinal microglia cells subjected to miR-129-5p mimics or miR-129-5p inhibitors transfection for 24 h.* ***E****) RT-PCR was used to measure the mRNA expression of HMGB1 in rat spinal microglia cells subjected to miR-129-5p mimics or miR-129-5p inhibitors transfection for 24 h.* ***F****) Western blotting was used to measure the protein expression of HMGB1 in rat spinal microglia cells subjected to miR-129-5p mimics or miR-129-5p inhibitors transfection for 24 h and relative expression was normalized to control group (H). Data are presented as mean ± SD.* $^{**}p < 0.01$, $^{***}p < 0.001$.

were synthesized by the Shanghai GenePharma Co, Ltd (Shanghai, China) using GenBank (ID: 24520) information as reference. HMGB1 shRNA was synthesized by Sango Biotech (Shanghai, China) with following sequence: sense 5'- CGC GTC GTA ACA AAG CGC GGC TAT CCA AGG ATT AGC GCG CGC TTT GTT ACC TTT TTT CCAC-3', anti-sense 5'-TCG AGT TGG AAA AAA GTA ACC AAA GCG CGC AAT CTC TTG AAT TAG CCG CGC TTT GTT ACGA-3'. Briefly, 20 pmol miRNA and 1 µl Lipofectamine 2000 was diluted in 100 µl serum-free DMEM, respectively, and placed at room temperature for 5 min. Then the miRNA and Lipofectamine dilutions were mixed and incubated at room temperature for 20 min to form transfection compound. The culture medium in the wells was replaced by serum-free DMEM medium and the transfection compound was added and incubated for 24 h. After that, the medium was replaced with DMEM containing LPS (final dose of 5 µg/ml) and incubated for another 24 h. To observe the microglial morphology, images of microglia were captured using a high-resolution digital camera equipped with a computer (Olympus, Tokyo, Japan). Then cells were harvested and subjected to the following experiments.

Quantitative RT-PCR

RNA from treated cells was purified by TRIzol reagent (Invitrogen). For miR-129-5p, cDNA was synthesized by an iScript cDNA synthesis kit (Bio-Rad) and the qRT-PCR assays were performed using a miRNA qPCR detection kit (Tiangen, Beijing). For mRNA, qRT-PCR was performed using a SYBR Green PCR Master Mix kit (Applied Biosystems, Waltham, MA, USA) in ABI 7500 PCR system (Life Tech, Pleasanton, CA, USA). Each sample was tested in three wells.

Western blot

After treatment, protein was extracted using RIPA lysis buffer. Western blot was carried out using a standard procedure. Briefly, extracted protein samples (40 µg) were separated on SDS/PAGE gels and transferred onto a PVDF (Millipore) membrane, and blocked with 5% skimmed milk for 2 h at room temperature. Then, the membrane was incubated with primary antibodies anti-HMGB1 (#3935S, 1:800, Cell Signaling Technology, Danvers, MA, USA) and anti-GAPDH (#AF5718, 1:800, Santa Cruz) at 4°C overnight. Subsequently, the membrane was incubated with HRP-conjugated second antibody (1:1000, Cell Signaling Technology) for 2 h at room temperature. An ECL reagent (Signaling Technology) was used to visualize the immune bonds.

Measurement of cell viability

After transfection and LPS stimulation as described above, cell viability was measured using CCK-8 method (Boster, Wuhan, China). Culture media was collected and concentrations of lactate dehydrogenase (LDH) were detected by LDH cytotoxicity assay kits (Biotime, Shanghai, China) following the manufacturer's protocol.

Measurement of NO and Prostaglandin E2 (PGE2)

After transfection and LPS stimulation as described above, cell culture media were collected. NO was measured by Griess reagent system (Promega). PGE2 concentrations were detected by an ELISA kit (Jiangcheng Bioengineering, Nanjing, China).

Measurement of cytokines

After cell transfection and LPS stimulation, the supernatant of cells was collected. The levels of interleukin (IL)-6, IL-1β, tumor necrosis factor (TNF)-α and IL-10 were detected using commercial ELISA kits (R&D Systems, Minneapolis, MN, USA).

Statistical analysis

Data were presented as mean ± SD. Student's *t*-test or one-way ANOVA followed by post hoc Bonferroni test was used to assess the differences among groups. Significance: $P < 0.05$.

RESULTS

MiR-129-5p directly targets HMGB1

WT-HMGB1 luciferase activity was significantly reduced by miR-129-5p mimics and significantly increased by miR-129-5p inhibitors (Fig. 1 B, C). On the other hand, neither miR-129-5p mimics nor inhibitors significantly influenced the MUT-HMGB1 luciferase activity (Fig. 1 B, C), indicating that miR-129-5p directly targeted HMGB1 on the 3'-UTR.

MiR-129-5p regulates HMGB1 in rat spinal microglia cells

MiR-129-5p mRNA was significantly increased by miR-129-5p mimics and significantly reduced by

miR-129-5p inhibitors (Fig. 1D), which confirmed the effectiveness of mimics or inhibitor transfection. Meanwhile, the mRNA expression and protein level of HMGB1 in rat spinal microglia cells were significantly decreased by miR-129-5p mimics transfection and significantly increased by miR-129-5p inhibitor transfection (Fig. 1 E-G).

MiR-129-5p regulates HMGB1 in LPS stimulated rat spinal microglia cells

MiR-129-5p mRNA expression was significantly reduced after 6 h-LPS treatment, and further reduced after 12 h- and 24 h-LPS treatment (Fig. 2A). On the contrary, the mRNA level of HMGB1 significantly increased after 6 h-LPS treatment, and further increased after 12 h- and 24 h-LPS treatment (Fig. 2B). Compared with the control group, cells subjected to LPS, LPS + miR control or LPS + miR-129-5p inhibitor treatment had significantly lower miR-129-5p level (Fig. 2C). Compared with that in LPS treatment group, miR-129-5p level was significantly higher in cells treated with LPS + miR-

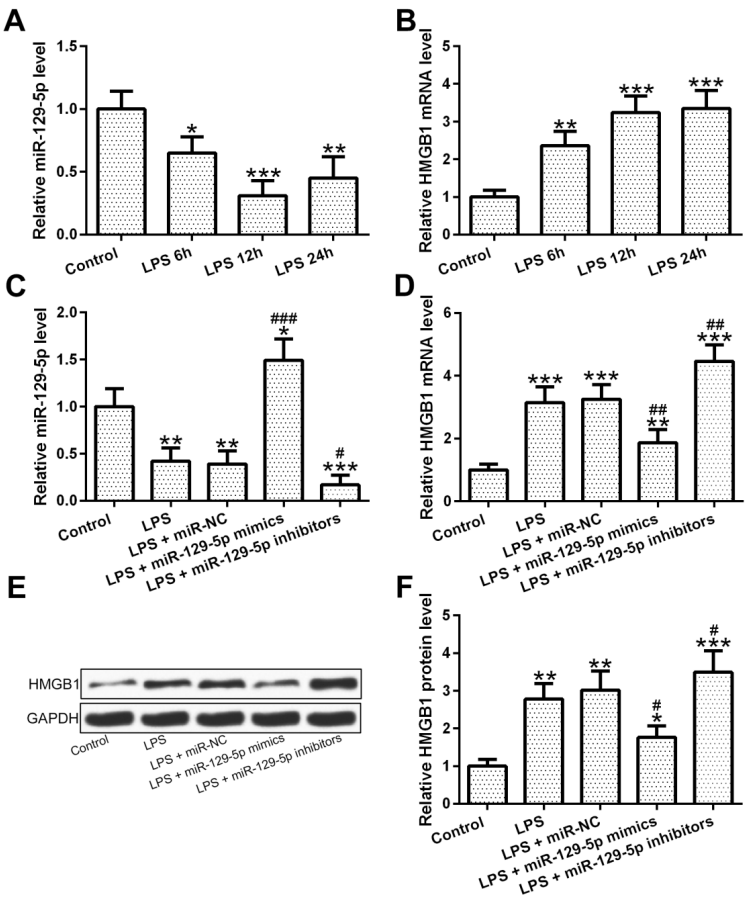

Fig. 2. *miR-129-5p regulated HMGB1 expression in LPS stimulated rat spinal microglia cells.* ***A)*** *The expression of miR-129-5p in rat spinal microglia cells subjected to LPS stimulation for 6 h, 12 h and 24 h.* ***B)*** *The mRNA expression of HMGB1 in rat spinal microglia cells subjected to LPS stimulation for 6 h, 12 h and 24 h.* ***C)*** *The expression of miR-129-5p in rat spinal microglia cells subjected to miR-129-5p mimics or miR-129-5p inhibitors transfection for 24 h and then subjected to LPS stimulation for 24 h.* ***D)*** *The mRNA expression of HMGB1 in rat spinal microglia cells subjected to miR-129-5p mimics or miR-129-5p inhibitors transfection for 24 h and then subjected to LPS stimulation for 24 h.* ***E)*** *Western blotting was used to measure the protein expression of HMGB1 in rat spinal microglia cells subjected to miR-129-5p mimics or miR-129-5p inhibitors transfection for 24 h and then subjected to LPS stimulation for 24 h and relative expression was normalized to control group. Data are presented as mean ± SD. $^{*}p < 0.05$, $^{**}p < 0.01$ and $^{***}p < 0.001$ compared to control group. $^{\#}p < 0.05$, $^{\#\#}p < 0.01$ and $^{\#\#\#}p < 0.001$ compared to LPS stimulation group.*

129-5p mimics and significantly lower in cells treated with LPS + miR-129-5p inhibitor (Fig. 2C). On the contrary, cells subjected to LPS, LPS + miR control or LPS + miR-129-5p inhibitor treatment showed significantly higher mRNA and protein levels of HMGB1 compared with the control (Fig. 2 D-F). Compared with LPS treatment, LPS + miR-129-5p mimics significantly reduced, while LPS + miR-129-5p inhibitor significantly increased the mRNA and protein levels of HMGB1 (Fig. 2 D-F).

Effect of miR-129-5p on viability of LPS-stimulated rat spinal microglia cells

After treatment, the microglial morphology was observed using a high-resolution digital camera. The microglia in the control group showed bipolar or unipolar shape and elongated cell bodies, while LPS-stimulated microglia exhibited amoeboid cell bodies with retraction of extensions (data not shown). The LPS-induced morphological changes were attenuated by miR-129-5p mimics while exaggerated by miR-129-5p inhibitor (data not shown).

Compared with the control group, all cells subjected to LPS treatment showed significantly decreased PR and significantly increased LDH release (Fig. 3A and 3B). Compared with LPS treatment, LPS + miR-129-5p mimics significantly reduced LDH release and increased cell viability, while LPS + miR-129-5p inhibitor significantly increased LDH release and reduced cell viability (Fig. 3 A, B).

MiR-129-5p reduced LPS-induced production of NO and PGE2 in rat spinal microglia cells

Compared with control, all LPS-treated groups showed significantly increased NO production and PGE2 levels (Fig. 3 C, D). Compared with LPS treatment, LPS + miR-129-5p mimics significantly decreased NO production and PGE2 level, while LPS + miR-129-5p inhibitor significantly increased NO production and PGE2 level (Fig. 3 C, D).

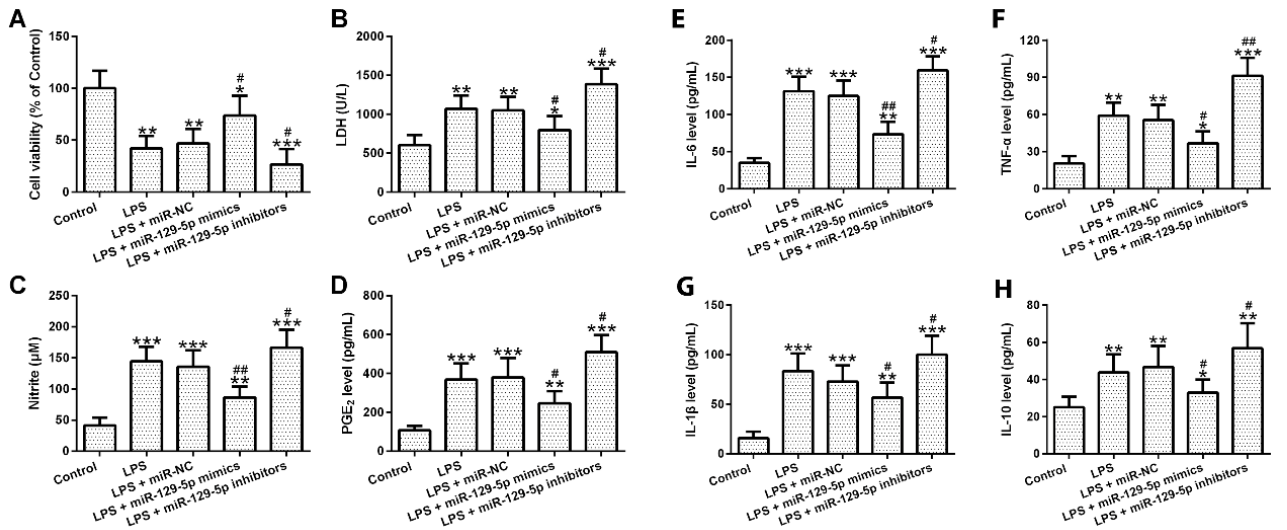

Fig. 3. *miR-129-5p regulated the apoptosis and cell injury of LPS stimulated rat spinal microglia cells, and the expression levels of IL-6, TNF-α, IL-1β and IL-10 in LPS stimulated rat spinal microglia cell supernatant. Rat spinal microglia cells were subjected to miR-129-5p mimics or miR-129-5p inhibitors transfection for 24 h and then subjected to LPS stimulation for 24 h.* ***A****) Cell viability was measured by the CCK-8 assay.* ***B****) Cell injury was examined with the LDH assay.* ***C****) Griess reaction was used to measure the NO concentration.* ***D****) PGE_2 level was accessed by ELISA. Rat spinal microglia cells were subjected to miR-129-5p mimics or miR-129-5p inhibitors transfection for 24 h and then subjected to LPS stimulation for 24 h. IL-6 (****E****), TNF-α (****F****), IL-1β (G) and IL-10 (****H****) levels were measured by ELISA. Data are presented as mean ± SD. $^{*}p < 0.05$, $^{**}p < 0.01$ and $^{***}p < 0.001$compared to control group. $^{\#}p < 0.05$, $^{\#\#}p < 0.01$ compared to LPS group.*

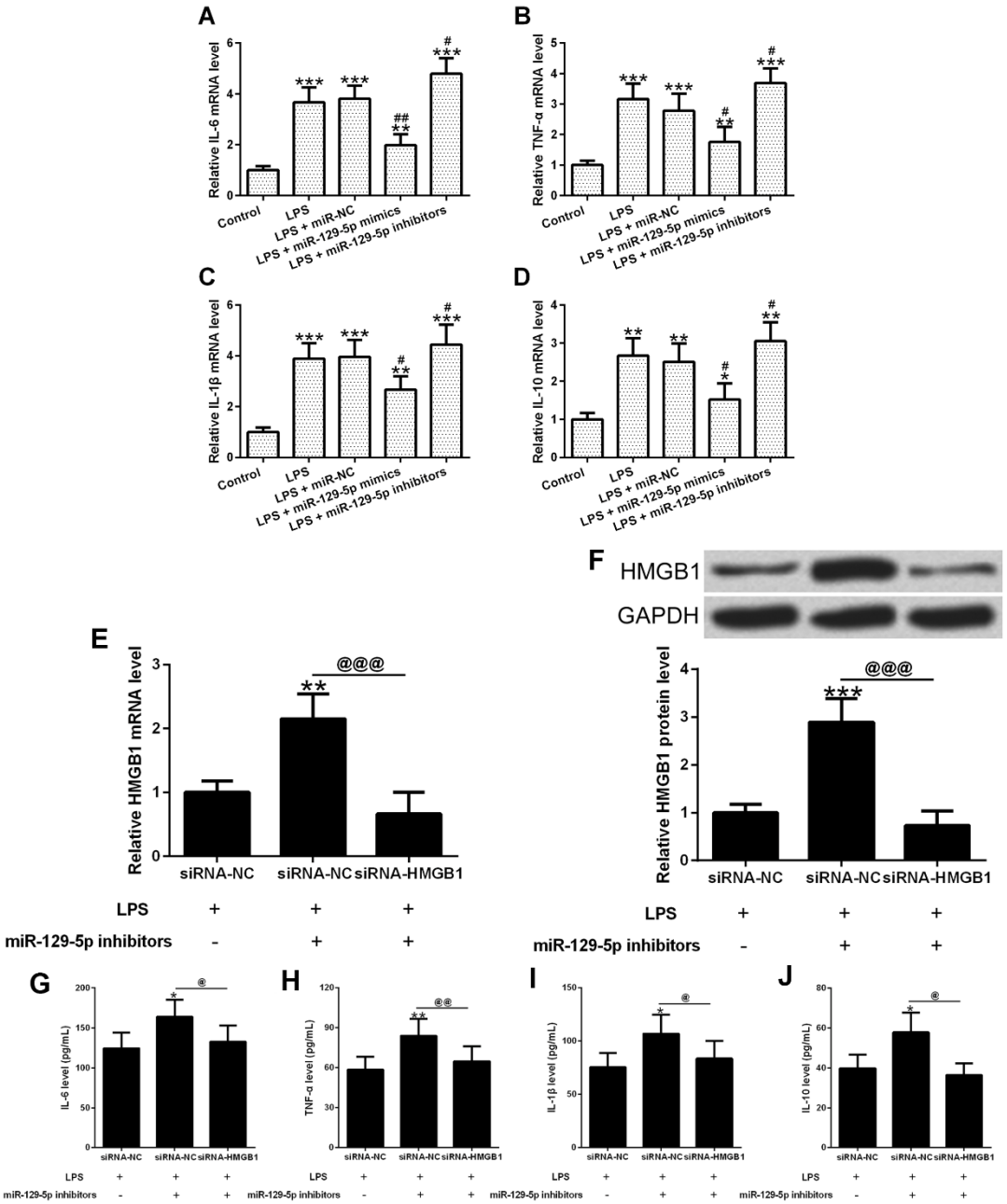

Fig. 4. *miR-129-5p regulated the mRNA expressions of IL-6, TNF-α, IL-1β and IL-10 in LPS stimulated rat spinal microglia cell supernatant, and targeted HMGB1 regulated inflammation in LPS stimulated rat spinal microglia cells. Rat spinal microglia cells were subjected to miR-129-5p mimics or miR-129-5p inhibitors transfection for 24 h and then subjected to LPS stimulation for 24 h. RT-PCR was used to measure the mRNA levels of IL-6 (**A**), TNF-α (**B**), IL-1β (**C**) and IL-10 (**D**). Data are presented as mean ± SD. $^{*}p < 0.05$, $^{**}p < 0.01$ and $^{***}p < 0.001$compared to control group. $^{\#}p < 0.05$ compared to LPS group. Rat spinal microglia cells were subjected to miR-129-5p inhibitors or shRNA HMGB1 transfection for 24 h and then subjected to LPS stimulation for 24 h. **E**) RT-PCR was used to measure the mRNA expression of HMGB1 among indicated groups. **F**) Western blotting was used to measure the protein expression of HMGB1 among indicated groups and the relative expression. **G-J**) ELISA was used the measure the levels of IL-6, TNF-α, IL-1β and IL-10 among indicated groups. Data are presented as mean ± SD. $^{*}p < 0.05$, $^{**}p < 0.01$ and $^{***}p < 0.001$compared to LPS + shRNA-NC group. $^{@}p < 0.05$, $^{@@}p < 0.01$ and $^{@@@}p < 0.001$ between the two groups.*

Effect of miR-129-5p on cytokine production after LPS-treatment

To detect cytokine production, we measured the concentration of cytokines in the cell culture media. The supernatants of cells subjected to LPS treatment contained significantly higher concentrations of IL-1β, IL-6, TNF-α and IL-10 than that of the control (Fig. 3 E-H). Compared with the supernatants of LPS treated cells, the supernatants of LPS + miR-129-5p mimics-treated cells contained significantly lower concentrations of these four cytokines, while the supernatants of LPS + miR-129-5p inhibitor-treated cells contained significantly higher concentrations of these four cytokines (Fig. 3 E-H).

Similar results were yielded when we measured the mRNA levels of these cytokines. Compared with the control group, cells subjected to LPS treatment showed significantly increased mRNA expressions of these four cytokines (Fig. 4 A-D). Compared with LPS treatment, LPS + miR-129-5p mimics significantly decreased mRNA expressions of these four cytokines, while LPS + miR-129-5p inhibitor significantly increased the mRNA expressions (Fig. 4 A-D).

MiR-129-5p regulates inflammation in LPS stimulated rat spinal microglia cells through targeting HMGB1

Mir-129-5p inhibitors significantly enhanced LPS-induced increase of HMGB1 mRNA expression and protein level in primary rat spinal microglia cells (Fig. 4 E, F). This effect was inhibited by HMGB1 shRNA. Compared with shRNA control, shRNA-HMGB1 significantly reduced the HMGB1 mRNA expression and protein level in cells treated with LPS and miR-129-5p inhibitors (Fig. 4 E, F), which confirmed the effectiveness of HMGB1 shRNA. Meanwhile, we also found that miR-129-5p inhibitors-enhanced productions of IL-1β, IL-6, TNF-α and IL-10 after LPS stimulation were inhibited by HMGB1 shRNA. Compared with shRNA control, shRNA-HMGB1 significantly reduced the production of these four cytokines in cells treated with LPS and miR-129-5p inhibitors (Fig. 4 G-J).

DISCUSSION

HMGB1 is an important target of many miRNAs. It was well studied and confirmed that several miRNAs, such as miR-505, miR-325, miR-21, could target HMGB1 and inhibit cell proliferation and invasion (7). Some miRNAs, including miR-142-3p and miR-205-5p, were also found to suppress inflammation via reducing the expression of HMGB1 and inhibiting NF-κB signaling (8).

It is worth noting that besides HMGB1, miR-129-5p could regulate other targets that might also be involved in the inflammatory process. For example, miR-129-5p could target and suppress Wnt5a, and inhibit the proliferation, invasion, migration and TMZ resistance of glioblastoma multiforme (9). Another study found that miR-129-5p alleviated myocardial injury induced by ischemia/reperfusion via targeting SOCS2 (10) Wnt5a could act as a proinflammatory factor and trigger pro-inflammatory signaling cascades, increasing secretion of pro-inflammatory cytokines and chemokines (11). SOCS2 protein has been shown to modulate the innate and adaptive immune response in animal models of infection (12). However, whether miR-129-5p target these factors to attenuate inflammation in microglia remains unclear. Although our data supported that miR-129-5p attenuate LPS-induced inflammation via targeting HMGB1, we could not exclude the possibility that other targets of miR-129-5p might be also involved in the inflammatory process. Therefore, further comprehensive studies should be carried out to investigate the mechanisms.

Together, this study demonstrated that miR-129-5p directly targets and down-regulates HMGB1. Through this anti-HMGB1 effect, miR-129-5p alleviates LPS-induced inflammation in spinal microglia cells. Further *in vivo* studies are warranted to demonstrate the possible effect of miR-129-5p in neuropathic pain models.

ACKNOWLEDGEMENTS

The study was supported the Project of Hebei Natural Science Foundation (H2017106022).

REFERENCES

1. Sayo A, Konishi H, Kobayashi M, et al. GPR34 in spinal microglia exacerbates neuropathic pain in mice. J Neuroinflamm 2019; 16:82.

2. Shen WS, Xu XQ, Zhai NN, Zhou ZS, Shao J, Yu YH. Potential mechanisms of microRNA-141-3p to alleviate chronic inflammatory pain by downregulation of downstream target gene HMGB1: in vitro and in vivo studies. Gene Ther 2017; 24:353-60.
3. Yang H, Tracey KJ. Targeting HMGB1 in inflammation. Biochim Biophys Acta. 2010; 1799:149-56.
4. Wan W, Cao L, Khanabdali R, Kalionis B, Tai X, Xia S. The emerging role of HMGB1 in neuropathic pain: a potential therapeutic target for neuroinflammation. J Immunol Res 2016; 2016:6430423.
5. Maeda T, Ozaki M, Kobayashi Y, Kiguchi N, Kishioka S. HMGB1 as a potential therapeutic target for neuropathic pain. J Pharmacol Sci 2013; 123:301-305.
6. Bronstein R, Torres L, Nissen JC, Tsirka SE. Culturing microglia from the neonatal and adult central nervous system. J Vis Exp 2013; 50647.
7. Yan J, Ying S, Cai X. MicroRNA-mediated regulation of HMGB1 in human hepatocellular carcinoma. BioMed Res Int 2018; 2018:10.
8. Yu X, Chen X, Sun T. MicroRNA-205-5p targets HMGB1 to suppress inflammatory responses during lung injury after hip fracture. BioMed Res Int 2019; 2019:7304895.
9. Zeng A, Yin J, Li Y, et al. miR-129-5p targets Wnt5a to block PKC/ERK/NF-κB and JNK pathways in glioblastoma. Cell Death Dis 2018; 9:394.
10. Ma R, Chen X, Ma Y, Bai G, Li D-S. MiR-129-5p alleviates myocardial injury by targeting suppressor of cytokine signaling 2 after ischemia/reperfusion. Kaohsiung J Med Sci 2020; doi: 10.1002/kjm2.12211. Online ahead of print
11. Pashirzad M, Shafiee M, Rahmani F, et al. Role of Wnt5a in the pathogenesis of inflammatory diseases. J Cell Physiol 2017; 232:1611-16.
12. Cramer A, de Lima Oliveira BC, Leite PG, et al. Role of SOCS2 in the regulation of immune response and development of the experimental autoimmune encephalomyelitis. Mediators Inflamm 2019; 2019:1872593.

LETTER TO THE EDITOR

Serum miRNA-27b-3p is a biomarker of diabetic retinopathy

X. Yang[1], X. Yu[2], R.-H. Zhou[3] and C. Liu[2]

[1]Department of Endocrine, General Hospital of Northern Theater Command, Shenyang, China;
[2]Department of Special Diagnosis, General Hospital of Northern Theater Command, Shenyang, China;
[3]Department of Ophthalmology, General Hospital of Northern Theater Command, Shenyang, China

Received March 30, 2020 – Accepted June 25, 2020

To the Editor,

Diabetic retinopathy (DR) is one of the most severe microvascular complications of diabetes mellitus (DM) that mainly affects people aged 20-65 years, leading to vision loss and blindness (1). DM affects the retinal microcirculation, resulting in microvascular structural abnormalities, including endothelial cell disorders, pericyte loss. Eventually, retinal endothelial cells experience proliferative change, edema and abnormal neovascularization. DR is classified into non-proliferative diabetic retinopathy (NPDR) and proliferative diabetic retinopathy (PDR),and involves multiple pathological factors, including hyperglycemia-induced retinal oxidative stress, inflammatory response and neuronal dysfunction (2).

MicroRNAs (miRNAs) are endogenous non-coding RNAs, 20-24 nucleotides long, which are highly conserved and incapable of encoding proteins. MiRNAs exert a tissue-specificity in retinal tissues, and regulate phenotypes of retinal cells. Kovacs et al. (3) discovered 80 upregulated miRNAs in the retina of DM rats and 6 downregulated ones through microarray analysis. Gong et al. (4) identified that the expression levels of miR-124-3p, miR-125b-5p, miR-135b-5p and miR-199a-5p gradually decrease with the prolongation of high glucose treatment in human retinal vascular endothelial cells and retinal pigment epithelial cells, while miR-145-5p and miR-146a-5p show the opposite trends.

Akhtar et al. (5) pointed out that miR-27b-3p is a vital regulator in the development of fibrosis. In addition, miR-27b-3p participates in kidney fibrosis progression of diabetic nephropathy (6). In the present study, the potential of serum miR-27b-3p as a biomarker of DR was explored.

MATERIALS AND METHODS

A total of 90 T2DM patients, including 30 non-diabetic retinopathy (NDR) cases, 30 NPDR cases and 30 PDR cases, admitted to our hospital from July 2016 to December 2018 were enrolled. Meanwhile, 90 healthy subjects in the same period were enrolled as controls. All subjects had no history of infectious diseases within the previous 6 months. The inclusion criteria were: T2DM was diagnosed based on the guidelines proposed by America Diabetes Association, 2011; subjects who cooperated with the study protocol; and clear imaging results of Optical Coherence Tomography (OCT), color fundus photography and fundus fluorescence angiography were obtained. The exclusion criteria were: other systematic diseases apart from T2DM; history of intraocular surgery and retinal laser photocoagulation; combined glaucoma, iridocyclitis and other serious eye diseases; combined eye diseases that could affect macular

Key words: diabetic retinopathy (DR); MiRNA-27b-3p; biomarker

Mailing address:
Cong Liu, MD
Department of Special Diagnosis,
General Hospital of Northern Theater Command,
83 Wenhua Road, Shenhe District,
Shenyang, Liaoning 110016, China
Tel.: +86 015309871622
e-mail: congla19900613@163.com

0393-974X (2020)
Copyright © by BIOLIFE, s.a.s.
This publication and/or article is for individual use only and may not be further reproduced without written permission from the copyright holder.
Unauthorized reproduction may result in financial and other penalties
DISCLOSURE: ALL AUTHORS REPORT NO CONFLICTS OF INTEREST RELEVANT TO THIS ARTICLE.

thickness; or clinical data were inadequate or subjects who would not cooperate. This study was performed after approval of the Ethic Committee of General Hospital of Northern Theater Command, and informed consent was obtained from all participants.

Blood sample collection

A 5-mL sample of venous blood was taken from each subject under fasting state in the morning. 3 mL of blood was used for determining biochemical indicators, including fasting plasma glucose (FPG), HbA1c, total cholesterol (TC), triglyceride (TG), low-density lipoprotein (LDL) and high-density lipoprotein (HDL). The remaining blood was centrifuged at 3,000 r/min for 10 min, and the serum was collected and stored at -80°C.

Quantitative real-time polymerase chain reaction (qRT-PCR)

TRIzol method (Invitrogen, Carlsbad, CA, USA) was applied for isolating RNAs from serum samples. Through reverse transcription of RNA, the extracted complementary deoxyribose nucleic acid (cDNA) was used for PCR detection by SYBR Green method (TaKaRa, Tokyo, Japan) at 95°C for 5 min, and 40 cycles at 95°C for 10 s and 60°C for 30 s, followed by 72°C for 5 min. U6 was used as the internal reference. The primer

Table I. *Baseline characteristics of subjects*

Variable	Control group	DNR group	NPDR group	PDR group	*P*
age	43.48±5.75	44.23±5.35	43.98±4.98	45.21±5.17	0.109
Sex (male/female)	45/45	15/15	15/15	15/15	NA
BMI (kg/m^2)	27.15 ± 3.28	26.73 ± 3.41	27.01±3.67	27.83 ± 3.94	0.298
SBP (mmHg)	131.21±19.27	133.73±22.09	135.11±22.76	133.17±21.23	0.423
DBP (mmHg)	82.35±9.07	84.32±9.89	84.87±8.91	85.17±9.66	0.160
FPG (mmol/L)	4.13±1.04	8.82±2.78*	9.36±3.55*	9.67±3.96*	<0.001
TC (mmol/L)	4.14±1.16	4.89±1.07	4.08±1.33	4.36±1.54	0.117
HDL-C (mmol/L)	1.31±0.45	1.44±0.62	1.38±0.56	1.43±0.71	0.472
LDL-C (mmol/L)	2.37±1.22	2.56±1.72	2.65±1.48	2.71±1.82	0.116
TG (mmol/L)	1.47±0.42	1.68±0.74	1.67±0.71	1.71±0.79	0.053
Scr (μmol/L)	54.31±15.72	55.12±15.91	56.32±16.98	56.87±16.75	0.068
BUN (mmol/L)	5.25 ± 1.45	5.33 ± 1.01	5.23 ± 1.10	5.31± 1.12	0.915
HbA1c (%)	5.17 ± 0.83	7.41 ± 1.16*	7.92 ±1.24*	7.89 ±1.31*	<0.001
Diabetes duration (years)	NA	6.78 ± 2.78*	7.98 ± 3.14*	8.23± 4.75*	<0.001

*BMI: body mass index; SBP: systolic blood pressure; DBP: diastolic blood pressure; FBG: fasting blood glucose; TC: total cholesterol; HDL-C: high-density lipoprotein cholesterol; LDL-C: low-density lipoprotein cholesterol; TG: triglyceride; Scr: serum creatinine; BUN: blood urea nitrogen; HbA1c: glycated hemoglobin; NA: no available. * P<0.001 vs Control group*

sequences were listed as follows: miRNA-27b-3p-F: 5′-GAACAGGTGCATCTCGTAGC-3′, and miRNA-27b-3p-R: 5′-CAGGAGACAGTGCATCCTTG-3′. U6-F: 5′-CTCGCTTCGGCAGCACA-3′, and U6-R: 5′-AACGCTTCACGAATTTGCGT-3′.

Statistical analysis

Statistical Product and Service Solutions (SPSS) 20.0 (IBM, Armonk, NY, USA) was used for all statistical analysis. Data were expressed as mean ± SD (standard deviation). The *t*-test was performed for analyzing differences between two groups, and multi-group comparison was conducted by one-way analysis of variance (ANOVA). Pearson's correlation test was applied for assessing the relationship between serum level of miRNA-27b-3p and clinical data of DR. Sensitivity and specificity of miRNA-27b-3p in diagnosing NDR and DR were assessed by depicting receiver operating characteristic (ROC) curves. $P<0.05$ indicated significant difference.

RESULTS

Baseline characteristics of subjects

Through analyzing clinical data of enrolled subjects, no significant differences in age, sex, BMI, SBP, DBP, TC, HDL-C, LDL-C, TG and BUN were found among the four groups ($P>0.05$). FPG, HbA1c and disease course of T2DM were significantly increased in NDR, NPDR and PDR groups in turn compared with those in the control group (Table I), suggesting that FPG, HbA1c and disease course of T2DM may affect the pathogenesis of DR.

Compared with controls, the serum level of miRNA-27b-3p was higher in NDR, NPDR and PDR patients. Moreover, its level was higher in NPDR and PDR patients than that in NDR patients (Fig. 1).

It has already been proven that FPG, HbA1c and disease course of T2DM may affect the pathogenesis of DR. Subsequently, Pearson correlation test revealed that miRNA-27b-3p level was positively correlated with FPG (r=0.437, P=0.041), HbA1c (r=0.613, P=0.033) and disease course of T2DM (r=0.814, P=0.007) (Table II).

Diagnostic potentials of miRNA-27b-3p in NDR and DR were assessed by depicting ROC curves. It was shown that AUC was 0.8750 (95%CI=0.8029-0.9471, $P<0.001$) when miRNA-27b-3p was used for diagnosing NDR. The sensitivity and specificity of miRNA-27b-3p in diagnosing NDR were 76.67% and 73.33%, respectively when the cut-off value was 2.485. AUC was 0.8994 as miRNA-27b-3p was used for diagnosing DR (95%CI=0.8382-0.9607,

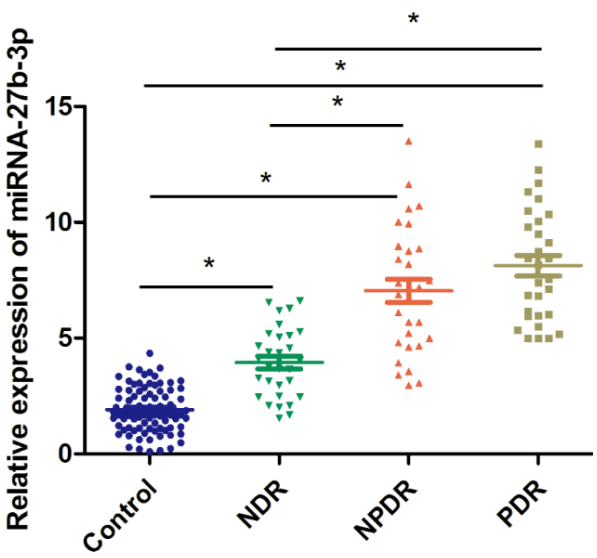

Fig. 1. *Serum level of miRNA-27b-3p. Serum level of miRNA-27b-3p was significantly elevated in NDR, NPDR and PDR group in turn compared with controls.*

Table II. *Pearson's correlation test on correlation between miRNA-27b-3p level and clinical data of DR patients*

Variable	r value	*P*
FPG	0.437	0.041
HbA1c	0.613	0.033
Diabetes duration	0.814	0.007

FBG: fasting blood glucose; HbA1c: glycated hemoglobin

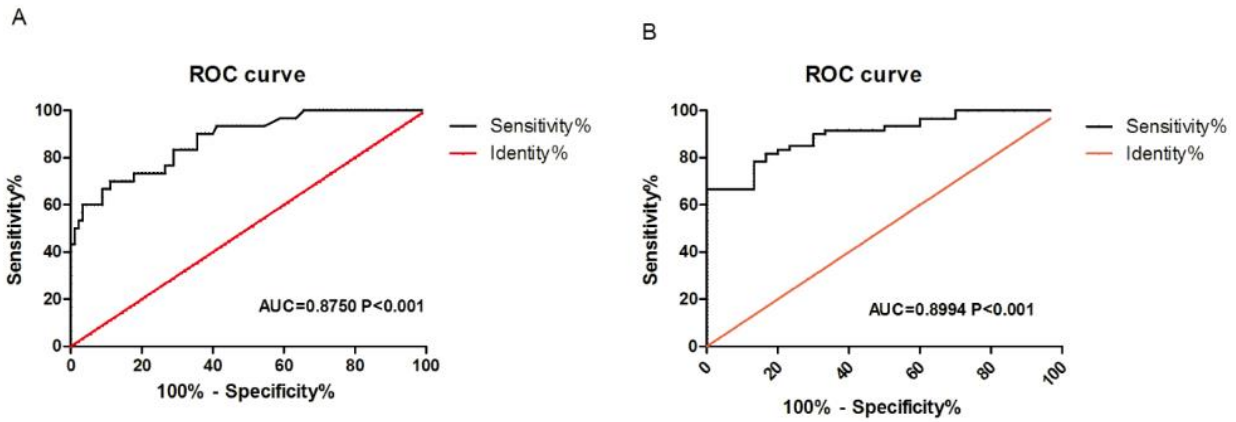

Fig. 2. *Diagnostic potentials of miRNA-27b-3p in NDR and DR. Diagnostic potential of miRNA-27b-3p in NDR (AUC=0.8750, P<0.001, cut-off value=2.485, sensitivity=76.67%, specificity=73.33%). Diagnostic potential of miRNA-27b-3p in DR (AUC=0.8994, P<0.001, cut-off value=5.2, sensitivity=83.33%, specificity=80%).*

P<0.001). Its sensitivity and specificity in diagnosing DR were 83.33% and 80%, respectively when the cut-off value was 5.2 (Fig. 2).

DISCUSSION

It is reported that 10% of DM patients develop DR after 5-9 years of disease course, which rises to 50% after 15 years. Seriously, about 80-90% DM patients with over 25 year of disease course suffer DR, and irreversible vision loss and blindness. Early screening and diagnosis of DR are able to reduce the blindness risk by 50% (7).

Feng et al. (8) suggested that the intraocular expression of miR-146 is downregulated in DM rats. NF-κB induces apoptosis of perivascular cells of retina and increases the number of acellular capillaries, thus leading to local microcirculation disturbance of retina (9). MiR-146 is able to inactivate the NF-κB pathway and is considered as a therapeutic target of DR (3). Silva et al. (10) showed that in the early phase of Streptozotocin-induced DM rats, miR-29b is upregulated in retinal ganglion cells and retinal inner layer cells; it inhibits apoptosis of diabetic retinal neurons through binding RAX, the vital regulator in the PKR pathway. Zhu et al. (11) found several upregulated miRNAs in mice with acute light-induced retinal injury.

Our findings showed higher serum levels of miRNA-27b-3p in NPDR and PDR patients than in controls, suggesting the involvement of miRNA-27b-3p in the development of DR by impairing retinal ganglion cells. However, with the deterioration of DR, no significant difference in serum levels of miRNA-27b-3p were found between NPDR and PDR patients. Further analysis demonstrated that serum level of miRNA-27b-3p was positively correlated with FPG, HbA1c and disease course of T2DM in DR patients. Moreover, diagnostic potentials of miRNA-27b-3p in NDR and DR were verified. Serum level of miRNA-27b-3p was increased in DR, which was related to FPG, HbA1c and disease course of T2DM. Serum miRNA-27b-3p may be a potential biomarker of DR.

REFERENCES

1. Antonetti DA, Klein R, Gardner TW. Diabetic retinopathy. N Engl J Med 2012; 366:1227-39.
2. Shin ES, Sorenson CM, Sheibani N. Diabetes and retinal vascular dysfunction. J Ophthalmic Vis Res 2014; 9:362-73.
3. Kovacs B, Lumayag S, Cowan C, Xu S. MicroRNAs in early diabetic retinopathy in streptozotocin-induced diabetic rats. Invest Ophthalmol Vis Sci 2011; 52:4402-9.
4. Gong Q, Xie J, Liu Y, Li Y, Su G. Differentially Expressed MicroRNAs in the Development of Early Diabetic Retinopathy. J Diabetes Res 2017; 2017:4727942.

5. Akhtar N, Rasheed Z, Ramamurthy S, Anbazhagan AN, Voss FR, Haqqi TM. MicroRNA-27b regulates the expression of matrix metalloproteinase 13 in human osteoarthritis chondrocytes. Arthritis Rheum 2010; 62:1361-71.
6. Conserva F, Barozzino M, Pesce F, et al. Urinary miRNA-27b-3p and miRNA-1228-3p correlate with the progression of kidney fibrosis in diabetic nephropathy. Sci Rep 2019; 9:11357.
7. Raja DS, Vasuki S. Automatic detection of blood vessels in retinal images for diabetic retinopathy diagnosis. Comput Math Methods Med 2015; 2015:419279.
8. Feng B, Chen S, McArthur K, et al. miR-146a-Mediated extracellular matrix protein production in chronic diabetes complications. Diabetes 2011; 60:2975-84.
9. Behl Y, Krothapalli P, Desta T, DiPiazza A, Roy S, Graves DT. Diabetes-enhanced tumor necrosis factor-alpha production promotes apoptosis and the loss of retinal microvascular cells in type 1 and type 2 models of diabetic retinopathy. Am J Pathol 2008; 172:1411-18.
10. Silva VAO, Polesskaya A, Sousa TA, et al. Expression and cellular localization of microRNA-29b and RAX, an activator of the RNA-dependent protein kinase (PKR), in the retina of streptozotocin-induced diabetic rats. Mol Vis 2011; 17:2228-40.
11. Zhu Q, Sun W, Okano K, Chen Y, Zhang N, Maeda T, Palczewski K. Sponge transgenic mouse model reveals important roles for the microRNA-183 (miR-183)/96/182 cluster in postmitotic photoreceptors of the retina. J Biol Chem 2011; 286:31749-60.

JOURNAL OF BIOLOGICAL REGULATORS & HOMEOSTATIC AGENTS Vol. 34, no. 4, 1437-1443 (2020)

LETTER TO THE EDITOR

Therapeutic effect and underlying mechanism of Gonadotropin-releasing hormone in uterine fibroids

YF. Gong[1*], W. Han[1*], Y. Cui[2], LY. Li[3], LY. Lu[4] and CN. Ren[5]

[1]Department of Obstetrics and Gynecology, The Second Affiliated Hospital of Mudanjiang Medical University, Mudanjiang City, Heilongjiang Province, China; [2]Department of Gynaecology, Affiliated Hongqi Hospital to Mudanjiang Medical University, Mudanjiang City, Heilongjiang Province, China; [3]The Second Affiliated Hospital of Harbin Medical University, Harbin City, Heilongjiang Province, China; [4]Personnel Section, The Second Affiliated Hospital of Mudanjiang Medical University, Mudanjiang, Mudanjiang City, Heilongjiang Province, China; [5]Clinical Laboratory, The Second Affiliated Hospital of Mudanjiang Medical University, Mudanjiang City, Heilongjiang Province, China

Received March 25, 2020 – Accepted June 29, 2020

[*]These authors contributed equally to this work

To the Editor,

Gonadotropin-releasing hormone (GnRH) is a decapeptide compound synthesized by hypothalamic neurons and secreted directly into the pituitary portal system (1). GnRH selectively stimulates gonadotropins to release luteinizing hormone (LH) and follicle-stimulating hormone (FSH) (1). The synthetic antagonists of GnRH (GnRHa) have two main characteristics: the high affinity for the GnRH receptor and resistance to endopeptidase degradation that leads to half-life increase (2). Uterine fibroids (UF) or myomas are benign tumors that develop in the uterus and can affect almost 70-80% of women during their lifetime. The fibroids do not have the potential to develop in cancer, and they are asymptomatic in the majority of cases. In some instances, fibroids can be complicated with anaemia, determined by heavy blood loss, and need treatment (2, 3). Studies have shown that the use of GnRHa in the treatment of UF could significantly reduce the volume of uterus and fibroids and alleviate the related symptoms, such as abnormal uterine bleeding (4). The imbalance between cell proliferation and cell apoptosis rate determines the rate and degree of UF (5).

Regarding the therapeutic effect and the underlying mechanism of GnRHa in UF, in most previous studies, gene detection was used to determine apoptosis. However, this method is one-sided and limited, because it cannot accurately reflect the typical biochemical and morphological characteristics of apoptosis, nor can it evaluate the apoptosis status at the individual level. The current study aimed to analyze the expression of apoptosis-related proteins in uterine myoma cells, the proliferation activity of uterine myoma cells and cell migration, and the influence of GnRHa treatment.

Key words: GnRHa; uterine fibroids; apoptosis; mechanism of action

Corresponding Author:
Dr Chunna Ren,
Clinical Laboratory, The Second Affiliated Hospital of Mudanjiang Medical University,
No.15 Dongxiaoyun Street, Aimin district, Mudanjiang City 157009, Heilongjiang Province, China
e-mail: renchunnawork@163.com

0393-974X (2020)
Copyright © by BIOLIFE, s.a.s.
This publication and/or article is for individual use only and may not be further reproduced without written permission from the copyright holder.
Unauthorized reproduction may result in financial and other penalties
DISCLOSURE: ALL AUTHORS REPORT NO CONFLICTS OF INTEREST RELEVANT TO THIS ARTICLE.

MATERIALS AND METHODS

Cases

The study included 30 women diagnosed with UF who were hospitalized in the Department of Gynecology of the Second Affiliated Hospital of Mudanjiang Medical University, China, between October 2017 and March 2019 and who underwent hysteromyomectomy. The women were diagnosed with hysteromyoma and suffered from abnormal symptoms of uterine bleeding. The surgery was performed one week after menstruation. The tumor nucleus was chosen as the experimental group. The normal uterine smooth muscle tissue around the uterine leiomyoma (paracancerous tissue) was chosen as the control group. The symptoms of abnormal uterine bleeding caused by hysteromyoma included menorrhagia, frequent menstruation and irregular bleeding, and secondary anaemia of different degrees. In the three months prior to surgery, the patients had not used hormones and did not suffer from other endocrine or immune system diseases. Signed informed consent was obtained from all patients. This study was approved by the Ethics Committee of The Second Affiliated Hospital of Mudanjiang Medical University.

Tissue samples and cell culture

Several samples of myoma nuclear tissue and surrounding normal smooth muscle tissue were collected from each patient during surgery. Each sample was about 1cm × 1cm × 1cm and was put into a sterile cold D-Hank's solution containing 100U/mL penicillin (Hangzhou Lianke Meixun Biomedical Technology Co., Ltd, China) and 100μg/mL streptomycin, and was taken to the laboratory within 20 min. In addition, the normal smooth muscle tissue and the nuclear tissue of uterine leiomyoma were removed for the paraffin section and hematoxylin and eosin (H&E) staining.

The blood from the samples was removed by washing with serum-free medium (Shanghai Huaying Biomedical Technology Co., Ltd., China) for three consecutive times. Then the culture medium was dried with filter paper and the tissue samples were placed on a watch glass with a small amount of calf serum (Gibco, USA). The tissues were cut into 1 mm^3 slices and inoculated onto 0.6cm × 0.6cm cover glass. On each piece, 20 small pieces of tissue were inoculated. A small amount of calf serum was used to keep the cover to one side of the flask. 4 mL DMEM / F12 (Dulbecco's Modified Eagle Medium; Gibco, USA) medium containing 10% fetal bovine serum (Gibco, USA) was added on the opposite side and placed in a 37°C incubator for 2 h, and then the bottle was turned and placed in a standing culture. After 24 hours, the culture medium was changed and then changed every two days.

When the cells gradually spread over the bottom of the bottle, they were subcultured. The culture medium was absorbed and discarded, and 2 mL of 0.25% trypsin (Shanghai Junrui Biotechnology Co., Ltd., China) was added and observed under a microscope (Beijing Prociss Instrument Co., Ltd., China). When the protuberance of cells shrank and the gap increased, the digestive fluid was sucked away and 2 mL DMEM/F12 medium containing 10% fetal bovine serum was added to finalize the digestion. The cells were inoculated into bottles according to the ratio of 1:2, and cultured in a 5% CO_2 incubator at 37°C. Later generations were the same. The passage period was 7-8 days.

For the cell culture with tissue block adherent, in the first passage, fibroblasts were removed using the poor time attachment method. Briefly, 60mg/L poly-l-lysine (Nanjing Dulai Biotechnology Co., Ltd., China) was added in the 24-hour culture bottle A and incubated at 37°C for 20-30 min. Then the culture medium was poured into bottle B, cultured for another 20-30 min, and then poured into bottle C. In this way, in bottle A remains fibroblasts, in bottle B remains mixed cell, and in bottle C remains pure myoma cell or smooth muscle cell.

Hematoxylin and eosin (HE) staining

A 10% neutral formaldehyde solution was used to fix specimens for more than 24 hours. Gradient alcohol was used for dehydration and then the slices were placed in an oven at 80°C for 1 h. Conventional alcohol was used to dehydrate and rinse. Then, the slices were stained with H&E. After sealing with neutral gum, histopathological changes were observed under an optical microscope (Beijing Prociss Instrument Co., Ltd., China).

Experimental groups

Four groups were used in this study, a control group (normal smooth muscle layer of uterus cells) and 3 experimental groups: 0 μmol/L GnRHa (Astra Zeneca UK Limited., UK) (UF cells untreated), 0.1 μmol/L GnRHa (UF cells treated with 0.1 μmol/L GnRHa) and 10 μmol/L

GnRHa (UF cells treated with 10 μmol/L GnRHa). Cells from each group were collected after 24 h, 48 h and 72 h hours of culture, respectively. After 72 hours, Western blot was used to detect matrix metalloprotein-2 (MMP-2) (Shanghai Yanjin Biotechnology Co., Ltd., China), extracellular regulated protein kinases ½ (ERK1/2) (Shanghai Yanjin Biotechnology Co., Ltd., China), p-ERK1/2 (Shanghai Yanjin Biotechnology Co., Ltd., China), B cell lymphoma/leukemia-2 (Bcl-2) (Shanghai Yanjin Biotechnology Co., Ltd., China), Bcl-2 Associated X Protein (Bax) (Shanghai Yanjin Biotechnology Co., Ltd., China) and Caspase-3 protein expression (Shanghai Yanjin Biotechnology Co., Ltd., China). Cell Counting Kit-8 (CCK-8) (Shanghai Yanjin Biotechnology Co., Ltd., China) was used to detect the proliferative activity of uterine leiomyoma cells after 24, 48, and 72 h, respectively. The apoptosis rate of UF cells under different concentrations of GnRHa was measured by Annexin V-FITC/PI (Fluorescein Isothiocyanate/ Propidium iodide) method and cell migration was measured by scratch test.

Western blot analysis

Lysates containing protease and phosphatase inhibitors were added to cells or tissues that needed to extract proteins. The cells were fully lysed at 4°C and heated for 10 min over 95°C. After centrifugation at 12000r/min for 10 min, the supernatant was collected, and after protein quantification, was stored at -80°C. Bicinchoninic acid (BCA) protein concentration kit (Shanghai Yaoyun Biotechnology Co., Ltd., China) was used to quantify protein concentration.

The protein separation was carried out by electrophoresis using 5% dodecyl sulfate, sodium salt (SDS)-Polyacrylamide gel electrophoresis stacking glue (SDS-PAGE) and 10% separating gel (Shanghai Kanglang Biotechnology Co., Ltd., China). A 20 μL protein sample was chosen for sampling. After electrophoresis, the protein was transferred to the polyvinylidene fluoride (PVDF) membrane (Hangzhou Henglv Membrane Technology Engineering Co., Ltd., China). The membrane transfer was successfully detected by fuchsin staining. After sealing with 10% skimmed milk powder solution (Qingdao Jieshikang Biotechnology Co., Ltd., China) for 2 h, diluted rabbit anti-human antibody MMP-2 (1:500), Bcl-2 (1:1000), Bax (1:1000), Caspase-3 (1:1000), p-ERK1/2 (1:1000), ERK1/2 (1:1000), HRP (Horseradish Peroxidase; Shanghai Yanjing Biotechnology Co., Ltd., China) labelled Glyceraldehyde-3-phosphate dehydrogenase (GAPDH) (Genemart Bioscience Inc., China) (1:2000) were added. The membrane incubated with the first antibody was washed with TBST (Tris-Buffered Saline +Tween) (Beijing Solabo Technology Co., Ltd., China) for 3 successive times, 15 min each time. The membrane was incubated at 37°C for 2 h with the Goat anti-rabbit second antibody (Abcam, USA) labelled with HRP (1:1000). The samples were washed with TBST for 3 successive times, 5 min each time. Chemiluminescence was used for protein colouring. The expression of each protein was semi-quantitatively expressed by the ratio of A value of protein to A value of GAPDH.

Cell counting kit-8 (CCK-8) test

The myoma cells in the logarithmic growth stage were digested by trypsin. After counting under a microscope, 3×10^4 cells/mL suspension was prepared and 100 μL was transferred into 96-well culture plates. In the cell plate of each group, three identical pores were inoculated, 3×10^3 cells/pores. 100 μL culture medium was used as blank control and cultured overnight at 37°C. The experimental groups were as follows: UF cells were cultured in 100 μL complete medium, UF cells + 0.1 μmol/L GnRHa and UF cells + 10 μmol/L GnRHa. After 24, 48, and 72 h of co-culture, CCK-8 and serum-free essential medium were mixed at a volume ratio of 1:10 and 400 μL was added in each pore for incubation in a 5% CO_2 incubator at 37°C for 1 h. After incubation for 1 h, the enzyme labelling instrument was used to determine the absorbance value at 450 nm wavelength.

Scratch test

In the experimental group, the logarithmic growth cells were collected. In the 6-well plate, 1×10^6 cells were inoculated into each well and cultured at 37°C, with 5% CO_2 atmosphere until 95% fusion. A 20 μL micropipette was used to make a vertical linear scratch in the 6-hole plate. D-Hank's solution was used to wash and remove the floating cells. The samples were collected at 24, 48 and 72 h after scratch. Five 100 × visual fields were randomly selected to take photos under the phase-contrast microscope. The difference in scratch healing between groups was compared. In the photo, five different positions

were selected to measure the scratch width, calculate the average value and count the number of migrating cells.

Annexin V-FITC/PI method of flow cytometry

The medium in the 6-well plate was removed. After washing the cells with 5 mL PBS, 2 mL trypsin was added and cultured at 37°C for 5 min. Then the cell solution was dropped in 8 mL medium containing serum till a cell suspension was obtained. Deionized water was used to dilute the binding buffer at 1:4. 4°C precooled PBS was used to wash cells once. The cells were resuspended in dilute buffer and the concentration was adjusted to 1×10^6/mL. 100 µL cell suspension was removed and placed in 5 mL flow tube. 5 µL Annexin V / FITC and 10 µL 10 µg/mL PI (Propidium Iodide) solution were added and mixed. After incubating at room temperature in the dark for 15 min, 400 µL of binding buffer was added into the reaction tube. Flow cytometry was used to detect apoptosis at 488 nm. The percentage of apoptotic cells was read directly. Normal living cells Annexin V and low staining PI AnnexinV$^-$PI$^-$ were distributed in the lower-left area of flow cytometry. The early apoptotic cells, Annexin V highly stained and PI low stained (AnnexinV$^+$PI$^-$), were distributed in the lower right area of flow cytometry. Late apoptosis or died Annexin V cells were distributed in the upper right region of flow cytometry. The sum of the percentage of early apoptotic cells and the percentage of late apoptotic cells is called the total apoptotic rate.

Statistical analysis

The results were processed by SPSS1 19.0 statistical software (IBM, USA), and one-way Analysis of Variance (ANOVA) was used for group comparison. Least-Significant Difference *t*-test (LSD-t) was used for those

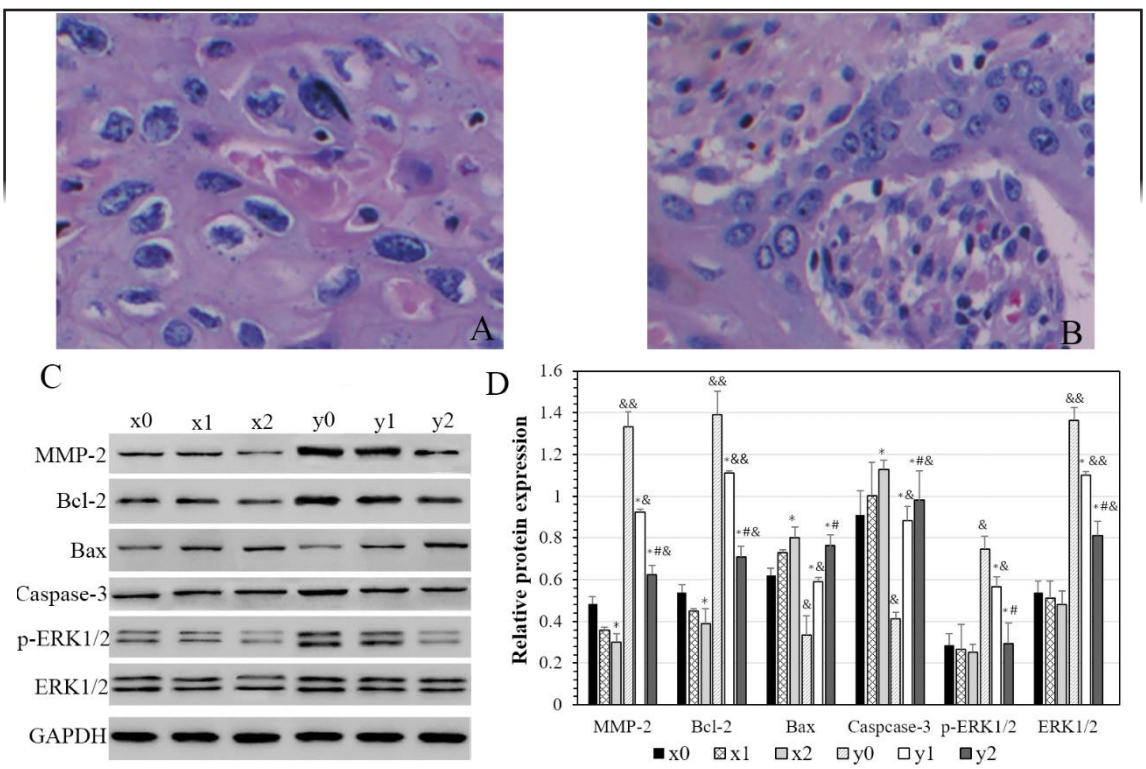

Fig. 1. *HE staining and Western blot results.* ***A)*** *normal smooth muscle cells HE staining results, × 200;* ***B)*** *myoma cells HE staining results, × 200;* ***C)*** *Western blot analysis results;* ***D)*** *Statistical chart of relative grey value. *P<0.05 compared with 0 µmmoL/L; #P<0.05 compared with 0.1 µmmoL/L; &P<0.05, &&P<0.01 compare with the same concentration groups. (x0:control group treated with 0 µmmoL/L GnRHa; x1: control group treated with 0.1 µmmoL/L GnRHa; x2: control group treated with 10 µmmoL/L GnRHa; y0:experimental group treated with 0 µmmoL/L GnRHa; y1: experimental group treated with 0.1 µmmoL/L GnRHa; y2: experimental group treated with 10 µmmoL/L GnRHa).*

with the same variance, and Dunnett *t*-test was used for those with different variance. The difference was statistically significant when $P < 0.05$.

RESULTS

Cell morphology

H&E staining results (Fig. 1 A, B) showed that there was no obvious hyperplasia in the smooth muscle layer of the uterus in the control group, the cell outline was clear, the nucleolus and cytoplasm were clearly visible, the myocytes were arranged orderly, the cytoplasmic red staining was polygonal, the chromatin was dense and condensed, the cells were closely connected, and there was no or very little inflammatory cell infiltration. In uterine leiomyoma tissue, the smooth muscle layer of the uterus was significantly thickened, myocytes proliferate and inflammatory cell infiltration was visible and cells were round or oval with visible nucleolus. Cell size

Table I. *CCK-8 detection of proliferation activity of UF cells*

GnRHa	24h	48h	72h
0 μmmoL/L	0.481±0.047	0.817±0.032a	1.282±0.041ab
0.1 μmmoL/L	0.411±0.031	0.574±0.041*a	0.694±0.031*ab
10 μmmoL/L	0.293±0.021*#	0.344±0.027*#	0.393±0.031*#a

*Note: *P<0.5, compared with 0 μmmoL/L; #P<0.5, compared with 0.1 μmmoL/L; aP<0.5 compared with 24 h; bP<0.5 compared with 48 h.*

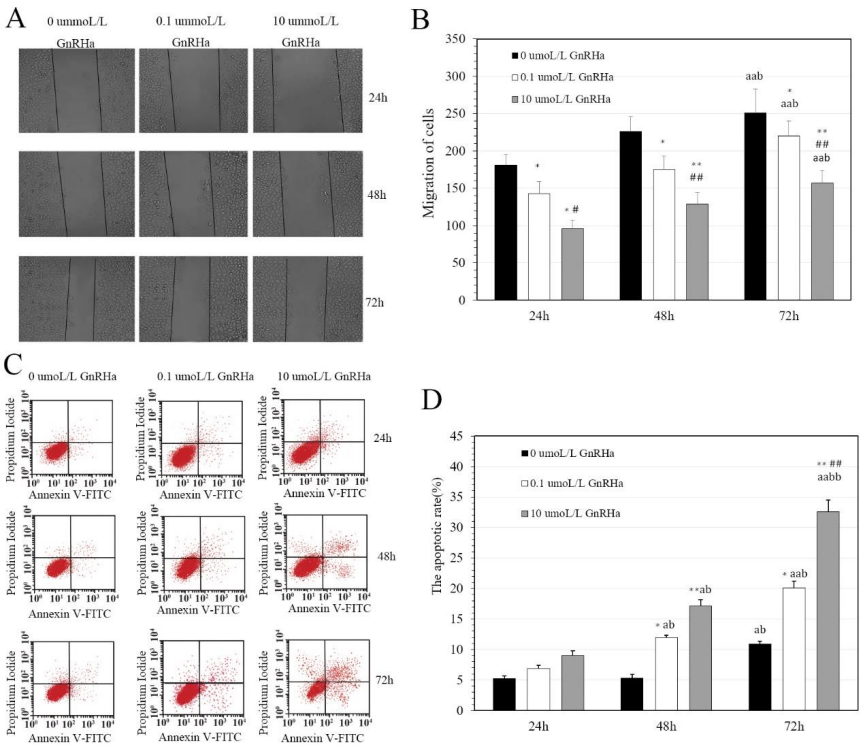

Fig. 2. *Changes in migration capacity of each group. **A**) The results of cell migration in different concentrations of GnRHa after 24, 48 and 72 h of exposure; **B**) Statistical chart of cell migration in the experimental groups after 24, 48 and 72 h of exposure; **C**) The apoptotic effect of GnRHa at different concentrations after 24, 48 and 72 h of exposure; **D**) Apoptosis rate in the experimental groups after 24, 48 and 72 h of exposure. *P<0.05; **P<0.01; compared with 0 μmmoL/L; #P<0.05, ##P<0.01 compared with 0.1 μmmoL/L; aP<0.05, aaP<0.01 compared with 24 h; bP<0.05, bbP<0.01 compared with 48h.*

was different, and some tumor tissues were divided into cancer nests of various sizes by fibrous tissue.

Western blot

In uterine leiomyoma tissue, a significant increase was observed in the expression of MMP-2, Bcl-2, ERK1/2 and p-ERK1/2 and a significant decrease in the expression of Bax and Caspase-3 compared with the normal cells from the smooth muscle layer of the uterus ($P<0.05$). After the treatment with different concentrations of GnRHa for 72 h, in both the control and experimental groups, the MMP-2, ERK1/2, p-ERK1/2 and Bcl-2 expression were down-regulated and Bax and Caspase-3 expression were up-regulated, with more significant changes in the experimental group in a dose-dependent manner ($P < 0.05$) (Fig. 1 C, D). The changes in protein expressions in the control group were not significant, which indicated that different concentrations of GnRHa had little effect on normal smooth muscle cells.

Proliferative activity

As it was shown that different concentrations of GnRHa had no significant effect on the normal smooth muscle cells (Fig. 1 C, D), the following experiments were focused on the uterine myoma cells. CCK-8 assay showed that cell proliferation in the 0.1 μmmoL/L and 10 μmmoL/L groups was significantly inhibited after 48 and 72 h of culture compared with the 0 μmmoL/L group ($P < 0.05$) (Table I). Moreover, the proliferation inhibition effect of 10 μmmoL/L group was more significant.

Cell migration

The treatment with 0.1 μmmoL/L and 10 μmmoL/L GnRHa significantly inhibited the cell migration of uterine leiomyoma cells and the effect was increased with the time of culture compared with 0 μmmoL/L group ($P < 0.05$) (Fig. 2 A and B).

Apoptosis rate of each group measured by AnnexinV-FITC/PI method of flow cytometry

The treatment with 0.1 μmmoL/L and 10 μmmoL/L GnRHa significantly increased the apoptosis rate of uterine leiomyoma cells and the effect was increased with the time of culture compared with 0 μmmoL/L group ($P < 0.05$) (Fig. 2 C and D).

DISCUSSION

Currently, the cause of UF is not clear. Studies have been shown that the occurrence and development of UF are related to a variety of growth factors, including TGF - β, IGF-1 and PCNA, which can promote the mitosis and growth of myoma cells (6, 7). MMPs are enzymes that depend on Zn^{2+} and Ca^{2+} as auxiliary factors and are important extracellular matrix-degrading enzymes that play an important role in tumour invasion, migration and wound healing (8), MMP-2 being the most important. Extracellular signal-regulated kinase (ERK) is a member of the mitogen-activated protein kinase (MAPK) family (9). It is an essential component of the Ras/Raf / MEK/ERK signaling pathway. After activation, the enzyme becomes phosphorylated ERK (p-ERK) that plays an important role in cell transformation and tumour development (10).

Bcl-2 is an anti-apoptotic gene and Bax protein is an apoptotic gene, usually in a state of mutual balance (11). Caspase-3 is the most important apoptotic executive protease in the process of apoptosis. Overexpression of Bcl-2 and Bax can control the activation of Caspase-3 protease and mediate cell survival or death (12).

The results of our study showed that the apoptosis rate of uterine leiomyoma cells increased after GnRHa treatment, providing robust evidence for the ability of GnRH to regulate autocrine/paracrine function. GnRHa significantly increased the apoptosis rate of uterine leiomyoma cells in a dose-dependent manner, while increasing the expression of MMP-2, p-ERK1/2 and Bcl-2 and decreasing the expression of Caspase-3 and Bax.

In conclusion, GnRHa can promote apoptosis of UF cells in a time- and dose-dependent manner.

ACKNOWLEDGEMENT

This work was supported by Scientific research project of Heilongjiang Health Committee (Project No. 2019-395).

REFERENCES

1. Chia CC, Huang SC, Chen SS, et al. Ultrasonographic evaluation of the change in uterine fibroids induced by treatment with a GnRH analog. Taiwan J Obstet Gynecol 2006; 45(2):124-28.
2. Sankaran S, Manyonda IT. Medical management of fibroids. Best Pract Res Clin Obstet Gynaecol 2008; 22(4):655-76.
3. Ples L, Carp D, Sima RM, Mirica A, Stanescu AD, Balalau DO, Balalau C. Endometrial safety of ulipristal acetate treatment for symptomatic uterine fibroids in premenopausal women - a systematic review. Farmacia 2018; 66(5):763-69.
4. Zhang Y, Sun L, Guo Y, Cheng J, Wang Y, Fan S, Duan H. The impact of preoperative gonadotropin-releasing hormone agonist treatment on women with uterine fibroids: a meta-analysis. Obstet Gynecol Surv 2014; 69(2):100-108.
5. Okuda S, Oshio K, Asada H, et al. Reduction in the vascular bed volume of uterine fibroids after hormonal treatment: evaluation with dynamic double-echo R_2* imaging. Magn Reson Med Sci 2012; 11(4):283-89.
6. Gkioka E, Msaouel P, Philippou A, Vlaghogiannis NI, Vogkou CT, Margiolis A, Koutsilieris M. Review: The Role of Insulin-like Growth Factor-1 Signaling Pathways in Uterine Leiomyoma. In Vivo 2015; 29(6):637-49.
7. Boda D, Docea AO, Calina D, et al. Human papilloma virus: Apprehending the link with carcinogenesis and unveiling new research avenues (Review). Int J Oncol 2018; 52(3):637-55.
8. Zou S, Yang J, Guo J, et al. RAD18 promotes the migration and invasion of esophageal squamous cell cancer via the JNK-MMPs pathway. Cancer Lett 2018; 417:65-74.
9. Tsai YR, Wang YJ, Lee MR, Hsu MF, Wang JP. p38 Mitogen-activated protein kinase and extracellular signal-regulated kinase signaling pathways are not essential regulators of formyl peptide-stimulated p47(phox) activation in neutrophils. Eur J Pharmacol 2013; 701(1-3):96-105.
10. Li P, Zhou X, Sun W, et al. Elemene Induces Apoptosis of Human Gastric Cancer Cell Line BGC-823 via Extracellular Signal-Regulated Kinase (ERK) 1/2 Signaling Pathway. Med Sci Monit 2017; 23:809-17.
11. Liman N, Alan E, Bayram GK, Gürbulak K. Expression of survivin, Bcl-2 and Bax proteins in the domestic cat (Felis catus) endometrium during the oestrus cycle. Reprod Domest Anim 2013; 48(1):33-45.
12. Scorrano L, Korsmeyer SJ. Mechanisms of cytochrome c release by proapoptotic BCL-2 family members. Biochem Biophys Res Commun 2003; 304(3):437-44.

LETTER TO THE EDITOR

Serum level of IL-10 and IL-10-1082G/A polymorphism are associated with the risk of ischemic stroke: A meta-analysis

XD. Rui[1*], YQ. Sha[2*], S. Wen[2*], QY. Sun[2], JM. Hu[2], FF. Yan[2], LP. He[3] and GH. Xie[4]

[1]Department of Rehabilitation, Liyang People's Hospital, Liyang, Jiangsu, China; [2]Department of Immunology, Nanjing Medical University, Nanjing, Jiangsu, China; [3]School of Medicine, Taizhou University, Taizhou, Zhejiang, China; [4]Department of Radiology, Nanjing First Hospital, Nanjing Medical University, Nanjing, Jiangsu, China

Received March 23, 2020 – Accepted June 29, 2020

[*]These Authors contributed equally to this work

To the Editor,

Stroke is one of the leading causes of disability and mortality among adults worldwide; about 85% of stroke cases are ischemic, whereas 15% are hemorrhagic. Ischemic stroke (IS) is a focal neurologic deficit syndrome because of sudden occlusion of a cerebral artery by thrombus, causing ischemia cerebral hypoxia. Stroke mortality rate is high in developing countries, which accounts for two-thirds of stroke mortality worldwide (1). It is estimated that the burden of IS will increase in the next 20 years with the increasing number of older adults in developing countries.

IS can be attributed to both genetic and environmental factors. Hypertension might be one of the most common risk factors leading to IS (2, 3). Genetic susceptibility may be closely related to the development of IS. Interleukin (IL)-10 as a key immunoregulatory cytokine plays a vital role in various pathophysiological processes (4), and previous studies have reported that IL-10 could exert anti-inflammatory effects and prevent the synthesis of inflammatory cytokines during IS (5). There are many studies on the relationship between the serum level of IL-10 or IL-10 gene polymorphism and the risk of ischemic stroke. Some studies showed that there is no relationship between IL-10 polymorphism and increased risk of IS, while others found that IL-10-1082G/A was associated with the risk of IS in an Asian population (6, 7). Due to difference of sample size and region, the conclusion of research is controversial.

The objective of this meta-analysis was to investigate the association of serum level of IL-10 and several IL-10 gene polymorphism with the risk of IS.

MATERIALS AND METHODS

This meta-analysis was carried out according to the 2016 Preferred Reporting Items for Systematic Review and Meta-analysis (PRISMA) statement (8). Eligible articles were searched by electronic database of PubMed, China Wanfang, Cochrane Library, the Web of Science, Embase and Springer up to September 2, 2019. The terms searched were Interleukin-10 and ischemic stroke. Both English and Chinese were used in the search process and articles in both English and Chinese were included in this meta-analysis.

Key words: IL-10; polymorphism; ischemic stroke

Corresponding Author:
Dr Guanghui Xie,
Department of Radiology, Nanjing First Hospital,
Nanjing Medical University. No.68 Road Changle,
Qinhuai district, Nanjing, Jiangsu,
210006, China
e-mail: skywaves@163.com

0393-974X (2020)
Copyright © by BIOLIFE, s.a.s.
This publication and/or article is for individual use only and may not be further reproduced without written permission from the copyright holder.
Unauthorized reproduction may result in financial and other penalties
DISCLOSURE: ALL AUTHORS REPORT NO CONFLICTS OF INTEREST RELEVANT TO THIS ARTICLE.

Eligibility criteria

Eligible studies had to meet the following criteria: i) all studies evaluating the relationship between serum level of IL-10, IL-10-1082A/G, IL-10-819C/T or IL-10-592C/A gene polymorphism and IS risk; ii) all studies were case-control design; iii) all study cases were diagnosed as ischemic stroke; iv) genotype distributions in both cases and controls were available to calculate an odds ratio (OR) with 95% confidence interval (CI); v) blood samples of ischemic stroke patients were collected on admission. Exclusion criteria: i) reviews, abstracts or animal studies; ii) studies not relevant to IL-10 serum level, gene polymorphism or IS; iii) studies with no target outcomes. No grey literature was included in this meta-analysis. Two investigators independently screened the articles. Eligible articles were included through reading the full text in detail.

Quality assessment

Newcastle-Ottawa Scale (9) (NOS) was used to evaluate the quality of articles included. All seventeen studies were evaluated strictly and scored at least 6 points.

Statistical analysis

Review Manager 5.3 (Cochrane IMS) was used for this meta-analysis. Random-effects model was conducted when heterogeneity is existing. Q-squared test and the I^2 index was calculated to assess the heterogeneity, I^2□50% defined as significant heterogeneity. Hardy-Weinberg equilibrium (HWE) in the control group of articles included was examined by using *Chi*-squared test. The dichotomous data of meta-analysis were reported as odds ratio (OR) and corresponding 95% confidence intervals (CIs). The mean difference (MD) and the associated 95% CI were calculated for continuous variables. In order to combine results, the sample mean and standard deviation were estimated if the study reported median and interquartile range using the methods reported by Wan (10) and Luo (11).

RESULTS

Based on our search strategy, 387 eligible studies were screened. The titles and abstracts of these studies were filtrated according to inclusion criteria. Finally, seventeen full text articles were eligible for this meta-analysis (Fig. 1).

Study characteristics

Three studies were included on the relationship between serum IL-10 level and ischemic stroke, including 274 patients. A total of fourteen studies which involved 3,480 patients with IS were included to explore the relationship between IL-10-1082G/A polymorphism and the risk of IS. Seven studies involved 1,604 patients on the relationship between IL-10-819C/T polymorphism and the risk of IS. In addition, four studies involving 1,040 patients were included to explore the association of IL-10-592C/A polymorphism with the risk of IS.

A comprehensive design was used in the study to minimize the publication bias. Two researchers performed an intact search strategy and selected studies strictly according to the eligibility criteria and exclusion criteria. Finally, a heterogeneity test was used to assess possible publication bias. In this system evaluation no evidence of publication bias was found.

The results of this meta-analysis and heterogeneity test are shown in Table I. We estimated the relationship between serum level of IL-10 or gene polymorphism and the risk of ischemic stroke with the dominant model and the recessive model. Combined analysis indicated that patients with ischemic stroke had significantly lower serum levels of IL-10 (Mean difference [MD]: -4.00; 95% confidence interval [CI]: -4.73 to -3.27, I^2=31%, Fig. 2).

The association between IL-10-1082G/A gene polymorphism and the risk of IS was then explored and significant heterogeneity was found among different ethnicities, therefore sub-group analysis was used. We conducted two subgroups, namely a Chinese population and other ethnic groups. Significant association was found between IL-10-1082G/A polymorphism and the risk of IS among the Chinese population (for AA *vs* AG+GG: OR=1.58, 95%CI:1.15-2.17, P=0.005, I^2=49%, Fig. 3) but not for other ethnic groups (for AA *vs* GA+GG: OR=1.08, 95% CI: 0.72-1.60, P=0.72, I^2=68%, Fig. 3). Therefore, individuals with AA-genotype might have increased

risk of IS among Chinese Han population. However, no association was found between polymorphism of IL-10-819C/T and IL-10- 592C/A (TT *vs* TC+CC for IL-10-819C/T: OR=0.95, 95% CI: 0.82-1.10, P=0.51, I^2=0%, Table I; AA *vs* AC+CC for IL-10-592C/A: OR=1.15, 95% CI: 0.83-1.61, P=0.40, I^2=54%, Table I) and the risk of IS among this population.

DISCUSSION

This meta-analysis is the first study to show that lower serum level of IL-10 was closely associated with the risk of IS although the association of IL-10 gene polymorphism and the risk of IS had been explored previously. We also confirmed that IL-10-1082G/A

Table I. *Association between IL-10 gene polymorphisms and ischemic stroke*

		Association		*Heterogeneity*	
Genetic model	*Subgroup*	*OR (95% CI)*	*P*	I^2 *(%)*	P_{het}
IL-10-1082G/A					
AA vs AG+GG	**Overall**	**1.32 (1.02-1.70)**	**0.04**	63	0.001
	Chinese	**1.58 (1.15-2.17)**	**0.005**	49	0.07
	Other	1.08 (0.72-1.60)	0.72	68	0.005
IL-10-819C/T					
TT vs TC+CC	Overall	0.95 (0.82-1.10)	0.51	0	0.57
IL-10- 592C/A					
AA vs AC+CC	Overall	1.15 (0.83-1.61)	0.40	54	0.09

Bold indicates significant differences between cases and controls.
OR: odds ratio; CI: confidence interval.

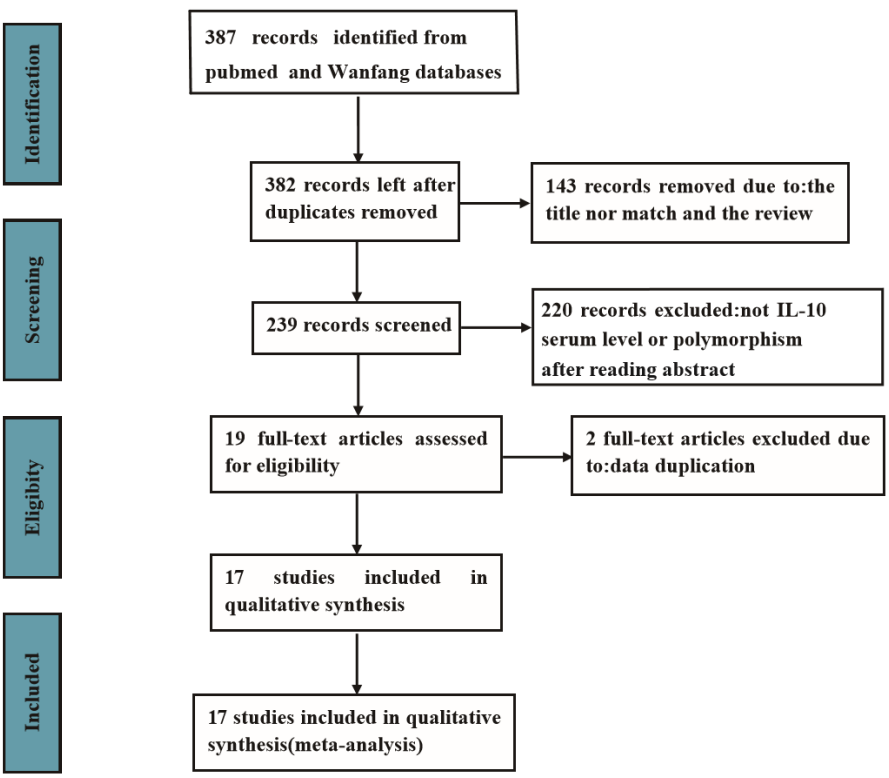

Fig. 1. *Flow chart of identifying candidate studies.*

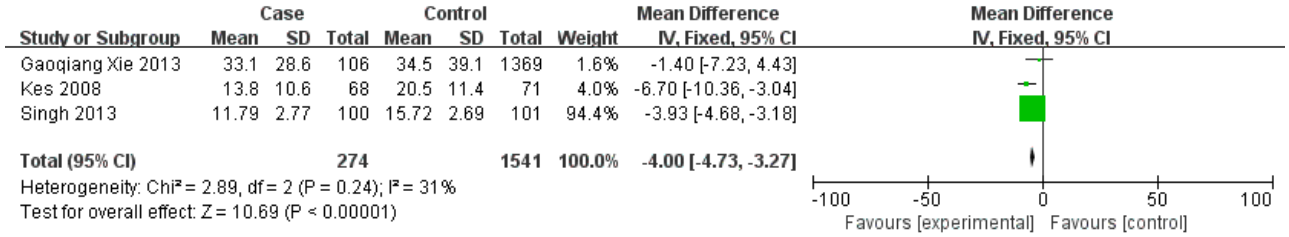

Fig. 2. *Forest plot of serum IL-10 level and ischemic stroke.*

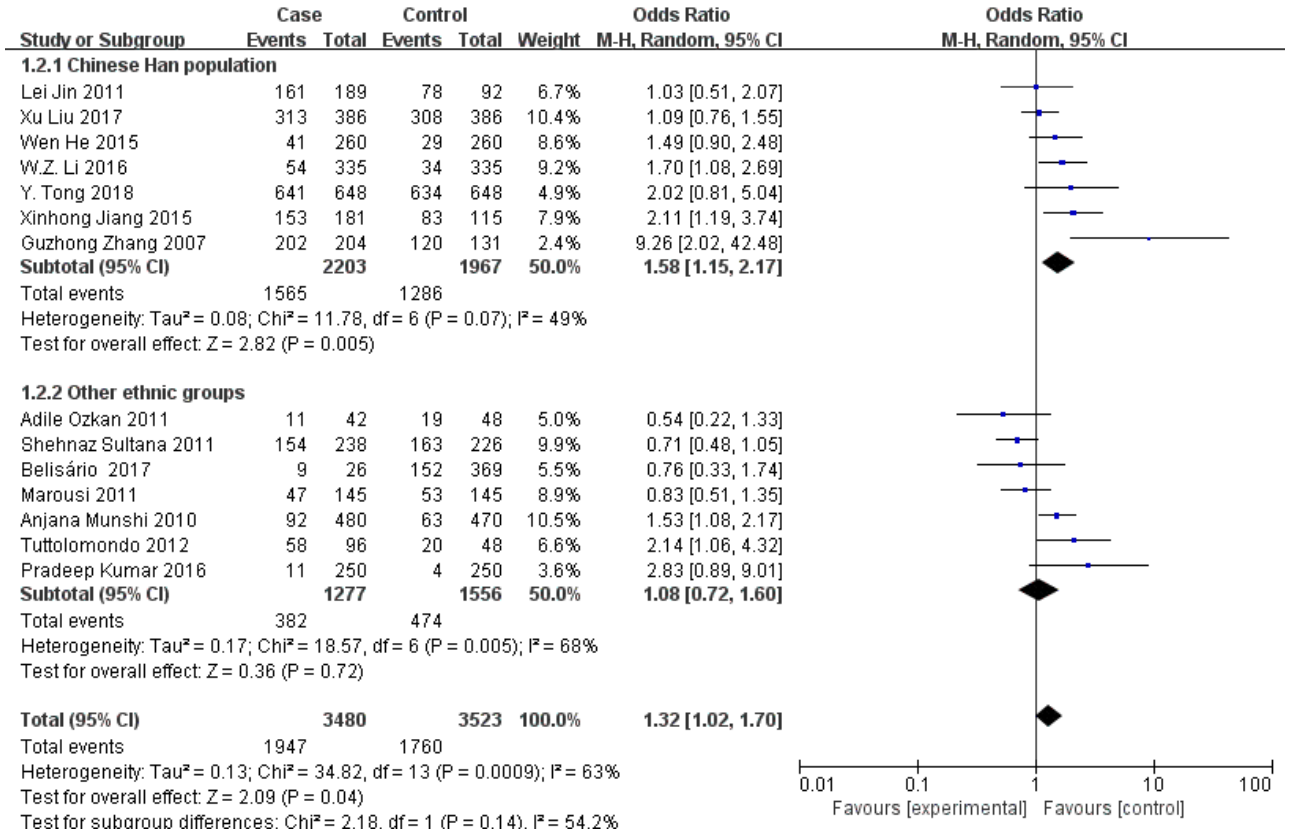

Fig. 3. *Forest plot of IL-10-1082G/A polymorphism and ischemic stroke: AA vs AG+GG.*

polymorphism had significant correlation with the risk of IS in a Chinese Han population. Other ethnicities did not show such association. Such correlation might be attributed to the possible mechanism that IL-10-1082G/A polymorphism might affect IL-10 synthesis, leading to the low serum level of IL-10. Low serum IL-10 level results in the synthesis of more inflammatory cytokines including IL-6, IL-1β, IL-1α and TNF-α, thus increasing the risk of IS.

In a previous study, it was indicated that IL-10-1082G/A was associated with the risk of IS in an Asian population, however, between-study heterogeneity was remarkable in their study (6). Due to its high heterogeneity, the results were not convincing enough, and more studies should be carried out to explore the sources of heterogeneity. Our study successfully solved the high heterogeneity by subgroup analysis, finding significant correlation between IL-10-

1082G/A polymorphism and the risk of IS among a Chinese population. However, the heterogeneity in a subgroup of other ethnic groups was still high, due to the small sample size, different regions and limited number of case-control studies.

Furthermore, our meta-analysis examined other common gene polymorphisms of IL-10 promoter region such as IL-10-819C/T and IL-10-592C/A and showed no correlation with the risk of IS. Considering the limited number of case-control studies exploring the correlation between IL-10-819C/T and IL-10-592C/A polymorphism and the risk of IS, more studies are needed to clarify its association. Our results suggested that IL-10-1082G/A may be the only one which is associated with IS susceptibility.

Despite the strict retrieval, statistical quality control, and publication bias test mentioned above, the current study still has some limitations that should be addressed. First of all, the sample size of serum IL-10 level between ischemic patients and healthy controls is limited. Secondly, comprehensive gene polymorphisms of IL-10 should be investigated to disclose its association with the risk of IS. Last but not the least, the mechanism of how IL-10 gene polymorphism is related to serum IL-10 level should be further investigated. In the future, we need high-quality studies which involve different ethnic and regional populations so that more comprehensive evaluation of the relationship between serum level of IL-10 or IL-10 gene polymorphism and the risk of IS can be carried out.

This meta-analysis suggested that the lower serum level of IL-10 was closely related to high risk of IS. IL-10-1082G/A polymorphism may be associated with the risk of IS in the Chinese population. More clinical studies should be conducted to confirm the relationship between the serum level of IL-10 and the risk of IS, and the relationship between lower serum level of IL-10 and IL-10 promotor gene polymorphism should be explored further.

REFERENCES

1. Brainin M, Teuschl Y, Kalra L. Acute treatment and long-term management of stroke in developing countries. Lancet Neurol 2007; 6:553-61.
2. He L, Lang L, Li Y, Liu Q, Yao Y. Comparison of serum zinc, calcium, and magnesium concentrations in women with pregnancy-induced hypertension and healthy pregnant women: A meta-analysis. Hypertens Pregnancy 2016; 35:202-9.
3. Yao Y, He L, Jin Y, et al. The relationship between serum calcium level, blood lipids, and blood pressure in hypertensive and normotensive subjects who come from a normal university in east of China. Biol Trace Elem Res 2013; 153:35-40.
4. Arponen O, Muuronen A, Taina M, et al. Acute phase IL-10 plasma concentration associates with the high risk sources of cardiogenic stroke. PLoS One 2015; 10:e0120910.
5. D'Andrea A, Aste-Amezaga M, Valiante NM, Ma X, Kubin M, Trinchieri G. Interleukin 10 (IL-10) inhibits human lymphocyte interferon gamma-production by suppressing natural killer cell stimulatory factor/IL-12 synthesis in accessory cells. J Exp Med 1993; 178:1041-48.
6. Jin J, Li W, Peng L, Chen J, Li R, Wu P, Tan S. Relationship between interleukin-10 -1082A/G polymorphism and risk of ischemic stroke: a meta-analysis. PLoS One 2014; 9:e94631.
7. Kumar P, Yadav AK, Misra S, Kumar A, Chakravarty K, Prasad K. Role of Interleukin-10 (-1082A/G) gene polymorphism with the risk of ischemic stroke: a meta-analysis. Neurol Res 2016; 38:823-30.
8. Preferred reporting items for systematic review and meta-analysis protocols (PRISMA-P) 2015: elaboration and explanation. BMJ 2016; 354:i4086.
9. Stang A. Critical evaluation of the Newcastle-Ottawa scale for the assessment of the quality of nonrandomized studies in meta-analyses. Eur J Epidemiol 2010; 25:603-5.
10. Wan X, Wang W, Liu J, Tong T. Estimating the sample mean and standard deviation from the sample size, median, range and/or interquartile range. BMC Med Res Methodol 2014; 14:135.
11. Luo D, Wan X, Liu J, Tong T. Optimally estimating the sample mean from the sample size, median, mid-range, and/or mid-quartile range. Stat Methods Med Res 2018; 27:1785-805.

LETTER TO THE EDITOR

Effect of sarcopenia combined with platelet-rich plasma on transverse tibial bone transport in diabetic foot

YX. He[1*], K. Kang[2*] and GX. Jia[2]

[1]*Department of Orthopaedics Trauma, The Third Hospital of Shijiazhuang, Shijiazhuang, China;*
[2]*Department of Orthopaedics, The First Hospital of Hebei Medical University, Shijiazhuang, China*

Received April 6, 2020 – Accepted June 29, 2020

[*]These Authors contributed equally to this work

To the Editor,

Diabetic foot is the damage of peripheral nerves and blood vessels caused by diabetes-related disease (1). Due to peripheral vascular disease, the blood supplied to the lower limbs is insufficient, which causes the ulcer to take a long time to heal (2). The incidence of diabetic foot is about 10% worldwide, and most patients present with symptoms such as foot ulcers or gangrene. In recent years, interventional therapy, hyperbaric oxygen therapy, and liver cell transplantation have improved the foot microcirculation, but there are still difficulties in the limb salvage treatment of diabetic foot patients (3). In this study, 76 diabetic foot patients received treatment of transverse tibial bone transport combined with platelet-rich plasma. By giving the bones an appropriate pulling force, the natural repairing ability of the tissue was mobilized, and the bones, fascia, muscles, blood vessels, and nerves were promoted to synchronously grow and restore function (4). Combined with autologous platelet-rich plasma treatment, the wound of diabetic foot patients was healed through multiple proteins and growth factors (5). In recent years, an increasing number of scholars have recognized that diabetic patients are often accompanied with sarcopenia, which is a common complication of diabetes. Sarcopenia is characterized by weakened muscle strength, decreased muscle mass and decreased activity. Skeletal muscle degeneration, lack of exercise, malnutrition, endocrine disorders, tumors and other diseases have been found to induce sarcopenia. Therefore, we hypothesised that sarcopenia also affected the postoperative efficacy of diabetic foot patients. In this study, the effect of sarcopenia under the treatment of transverse tibial bone transport combined with platelet-rich plasma in diabetic foot was investigated.

MATERIALS AND METHODS

The clinical data of 76 diabetic foot patients admitted to the Third Hospital of Shijiazhuang from January 2018 to January 2020 were retrospectively analyzed. There were 41 males and 35 females aged 42-77 (average 60.61±5.92) years. The duration of diabetes was 42-182 months, with an average of 95.38±6.13 months. There were 39 cases of diabetic foot in left foot, 34 cases in right foot and 3 biped cases. The course of disease was 3-18 months, with an average 5.98±0.71 months, and the average ulcer area was 8.89±3.24 cm^2. All patients signed the informed consent in this study.

Eligible trials had to fulfill the following criteria: i) clinically diagnosed diabetic foot; ii) individuals aged ≥18

Key words: diabetic foot; sarcopenia; transverse tibial bone transport; platelet-rich plasma

Corresponding Author:
Dr Guoxing Jia,
Department of Orthopaedics,
The First Hospital of Hebei Medical University,
Shijiazhuang, 050000, China
e-mail: yinirma2525@163.com

0393-974X (2020)
Copyright © by BIOLIFE, s.a.s.
This publication and/or article is for individual use only and may not be further reproduced without written permission from the copyright holder.
Unauthorized reproduction may result in financial and other penalties
DISCLOSURE: ALL AUTHORS REPORT NO CONFLICTS OF INTEREST RELEVANT TO THIS ARTICLE.

years; iii) successful completion of transverse tibial bone transport combined with platelet-rich plasma therapy; iv) complete clinical data and follow-up data. The exclusion criteria were: v) severe heart or lung diseases or tumors; i) severe immune system diseases; ii) women during pregnancy or lactation; iii) foot ulcers erosion due to other reasons; iv) missing clinical data or loss of follow up data.

Diagnostic criteria

The diagnosis criteria for sarcopenia: PACS 3.6 software (Philipe) was used to measure the images. Skeletal muscle index (SMI) was calculated by dividing the horizontal muscle cross-sectional area of the T12 by the height squared. Sarcopenia was defined as SMI<42.6cm^2/m^2 in male or SMI<30.6cm^2/m^2 in females. According to the SMI, 76 patients were divided into two groups: sarcopenia group (n=33) and non-sarcopenia group (n=43).

After treatment, the two groups were evaluated by Wagner grade and Michigan Neuropathy Screening Instrument (MNSI). In addition, the operative time, blood glucose with stably controlled, hospital stay, wound healing time, 1-year limb salvage rate, and wound healing rate between two groups were comparative analyzed.

Statistical analysis

Statistical analysis was performed by using SPSS 20.0 software. All data expressed as mean ± standard deviation (SD). Pearson's *Chi*-squared test or *t*-test were used for group comparisons. The rank sum test was used to compare Wagner grade. $p<0.05$was considered statistically significant.

Table I. *Comparison of Wagner grade after treatment.*

Group	No. of Cases	0 N (%)	I N (%)	II N (%)	III N (%)	IV N (%)
Sarcopenia group	33	0(0.00)	3(9.09)	8(24.24)	14(42.42)	6(18.18)
Non-sarcopenia group	43	0(0.00)	7(16.27)	15(34.88)	17(39.54)	3(6.98)
Z value				17.354		
p value				0.017		

Table II. *Comparison of MNSI score after treatment.*

Group	No. of Cases	Foot ulcer (point)	Ankle reflex (point)	Foot appearance (point)	Foot thumb vibration (point)	Nylon monofilament touch (point)	Total point
Sarcopenia group	33	0.95± 0.03	1.02± 0.23	1.08± 0.07	1.16± 0.17	1.38±0.22	5.54± 1.48
Non-sarcopenia group	43	0.48± 0.08	0.97± 0.09	0.64± 0.11	1.03± 0.15	1.28±0.10	4.06± 1.38
t value		2.084	2.580	1.975	2.823	2.435	2.559
p value		0.042	0.011	0.049	0.005	0.029	0.014

RESULTS

Comparisons between the two groups

After treatment with transverse tibial bone transport combined with platelet-rich plasma, the proportion of Wagner grade I and II in the non-sarcopenia group were less than the sarcopenia group (Table I, $p<0.05$). Moreover, the overall Wagner grade in the non-sarcopenia group was better than sarcopenia group ($p<0.05$).

The MNSI score of the sarcopenia group after treatment was higher than the non-sarcopenia group in terms of foot ulcer, ankle reflex, foot appearance, foot thumb vibration, nylon monofilament touch, and total score (Table II, $p<0.05$).

The operative time, blood glucose with stably controlled, hospital stay and wound healing time in the sarcopenia group were longer than those in the non-sarcopenia group (Table I, $p<0.05$). The wound healing rate and 1-year limb salvage rate in the non-sarcopenia group were 93.02% and 95.35%, respectively, which were higher than the 81.82% and 84.85% of the sarcopenia group (Table II, $p<0.05$).

DISCUSSION

In recent years, the treatment of transverse tibial bone transport combined with platelet-rich plasma for diabetic foot have been increasingly used in clinical practice (6, 7). During the rehabilitation process, sarcopenia affected the treatment and rehabilitation

Table III. *Comparison of operative time, blood glucose with stably controlled time, hospital stay and wound healing time.*

Group	No. of Cases	Operative time（min）	Blood glucose control（day）	Hospital stay（day）	Would healing time（month）
Sarcopenia g roup	33	60.21±2.45	5.27±1.34	15.27±2.22	2.45±0.19
Non-sarcope nia group	43	50.25±2.12	3.21±1.09	10.21±1.23	1.25±0.21
t value		2.317	2.517	3.098	2.186
p value		0.035	0.019	0.002	0.039

Table IV. *Comparison of wound healing rate and 1-year limb salvage rate after treatment in sarcopenia group and non- sarcopenia group*

Group	No. of Cases	Wound healing rate [N (%)]	1-year limb salvage ra within [N (%)]
Sarcopenia group	33	27（81.82）	28（84.85）
Non-sarcopenia group	43	40（93.02）	41（95.35）
x^2 *value*		4.385	6.536
p value		0.046	0.025

of diabetic foot patients. Hyperglycemia in diabetic patients increased the level of advanced glycation end products in cartilage and muscle, which caused muscle stiffness, decreased muscle function and induced sarcopenia (8). Han et al. found that muscle strength and muscle mass of elderly diabetic patients were significantly reduced compared with the normal population (9). Moreover, Fukuda et al. discovered that the muscle functions of patients with retinopathy were decreased, and the incidence of sarcopenia was increased significantly with the development of retinopathy (10). In this study, the MNSI score of the sarcopenia group was higher in foot ulcers, ankle reflexes, foot appearance, metatarso-toe vibration, nylon monofilament touch, and total scores than in the non-sarcopenia group. These results demonstrated that sarcopenia slowed down the wound healing of diabetic foot patients, affected the growth and regeneration of surrounding tissues and nerves, and thus delayed wound recovery after treatment (11). Our results showed that the proportion of Wagner grade I and II in the non-sarcopenia group was less than that in the sarcopenia group. In addition, sarcopenia delayed the wound healing and affected recovery in postoperative patients.

In summary, we suggest that clinically active treatment of sarcopenia should be performed to improve the prognosis of diabetic foot.

ACKNOWLEDGEMENT

This work was supported by the subject of Health and Family Planning Commission of Hebei (NO:20181050).

REFERENCES

1. Naqvi IH, Talib A, Naqvi SH, Yasin L, Rizvi NZ. The neuro-vascular consequence of diabetes: foot amputation and evaluation of its risk factors and health-related economic impact. Curr Vasc Pharmacol 2020; doi: 10.2174/1570161118666200320112401
2. Ahn J, Del Core MA, Wukich DK, et al. Scoring mental health quality of life with the SF-36 in patients with and without diabetes foot complications. Int J Low Extrem Wounds 2018; 17:30-35.
3. Samsell B, McLean J, Cazzell S, Dorsch K, Moyer PM, Moore M. Health economics for treatment of diabetic foot ulcers: a cost-effectiveness analysis of eight skin substitutes. J Wound Care 2019; 28:S14-S26.
4. Demirtas D, Kucukosmanoglu M. In patients with diabetic foot, improved left ventricular functions are detected by strain echocardiography after the diabetic foot treatment: A cross-sectional study. Medicine (Baltimore) 2019; 98:e17217.
5. Yakoot M, Abdelatif M, Helmy S. Efficacy of a new local limb salvage treatment for limb-threatening diabetic foot wounds - a randomized controlled study. Diabetes Metab Syndr Obes 2019; 12:1659-65.
6. Li H, You J, Liu C, Ma Y. Effectiveness of transverse tibial bone transport in treatment of diabetic foot ulcer. Zhongguo Xiu Fu Chong Jian Wai Ke Za Zhi 2019; 33:23-27.
7. Yin S, Yang X, Bi H, Zhao Z. Combined use of autologous stromal vascular fraction cells and platelet-rich plasma for chronic ulceration of the diabetic lower limb improves wound healing. Int J Low Extrem Wounds 2020; 1534734620907978.
8. Abidin Ozturk ZA, Turkbeyler IH, Demir Z, Bilici M, Kepekci Y. The effect of blood glucose regulation on sarcopenia parameters in obese and diabetic patients. Turk J Phys Med Rehabil 2018; 64:72-79.
9. Han P, Yu H, Ma Y, et al. The increased risk of sarcopenia in patients with cardiovascular risk factors in Suburb-Dwelling older Chinese using the AWGS definition. Sci Rep 2017; 7:9592.
10. Fukuda T, Bouchi R, Takeuchi T, et al. Association of diabetic retinopathy with both sarcopenia and muscle quality in patients with type 2 diabetes: a cross-sectional study. BMJ Open Diabetes Res Care 2017; 5:e000404.
11. Cheng Q, Hu J, Yang P, et al. Sarcopenia is independently associated with diabetic foot disease. Sci Rep 2017; 7:8372.

LETTER TO THE EDITOR

Clock genes may drive seasonal variation in SARS-CoV-2 infectivity: Are we due for a second wave of COVID-19 in the fall?

A. Goren[1], C.G. Wambier[2], J. McCoy[1], J. Shapiro[3], S. Vaño-Galván[4], S. Herrera[5] and L.M. Glode[6]

[1]Applied Biology, Inc. Irvine, CA, United States; [2]Department of Dermatology, Alpert Medical School of Brown University, Providence, RI, United States; [3]Ronald O. Perelman Department of Dermatology at the New York University School of Medicine, NY, USA; [4]Dermatology Department, Ramón y Cajal Hospital, Madrid, Spain; [5]Infectious Diseases Unit, Ramón y Cajal Hospital, Madrid, Spain; [6]University of Colorado Cancer Center, Golden, CO., USA

Received June 9, 2020 – Accepted July 3, 2020

To the Editor,

Over the course of late spring Coronavirus Disease 2019 (COVID-19) diagnosis and hospitalizations have declined in the subtropical northern hemisphere, while in the subtropical southern hemisphere, they have increased. An important question for healthcare preparedness and public policy makers is 'to what extent is COVID-19 seasonal?' Viral respiratory infections such as influenza follow a seasonal outbreak cycle; however, it is not known whether severe acute respiratory syndrome coronavirus (SARS-CoV)-2 infection follows a seasonal pattern.

SARS-CoV-2 infectivity is dependent on proteolysis of its spike protein by the TMPRSS2 enzyme expressed on the surface of type II pneumocytes in human lung tissue (1). In humans, the only known promoter of the TMPRSS2 gene is an androgen response element (2). In our recent publications, we have presented evidence that males with androgen sensitivity are more likely to exhibit severe symptoms following COVID-19 infection (3). It is important to note that androgen sensitivity denotes a genetic predisposition for genes under the control of the androgen receptor (AR) to be susceptible to the presence of androgens; this is distinct from the level of androgens present. For example, in androgenetic alopecia both the presence of the androgen sensitivity genotype and high levels of testosterone are required to produce the male pattern baldness phenotype.

A genetic predisposition for androgen sensitivity in males leads to androgenetic alopecia (male pattern hair loss) and increased risk of prostate cancer (4, 5). We have recently reported that among hospitalized men with COVID-19, 79% were diagnosed with androgenetic alopecia compared to the expected prevalence of 31-53% in aged matched controls of similar ethnicity (3). Further, Montopoli et al. (6) observed that COVID-19 infection rates were lower in prostate cancer patients receiving androgen deprivation therapy (ADT) *versus* prostate cancer patients not receiving ADTs (OR 4.05; 95% CI 1.55-10.59). Taken together, it appears that SARS-CoV-2 infectivity is likely to be mediated by androgen sensitivity and may respond to ADT. We are currently exploring this in several studies.

SARS-CoV-2 infection is likely to follow a similar chronobiological pattern. Since a strong dependence on androgen sensitivity has been

Key words: COVID-19; SARS-CoV-2; androgen receptor; androgenetic alopecia; daylight; sunlight

Corresponding Author:
Carlos Gustavo Wambier, MD, PhD
Department of Dermatology,
Rhode Island Hospital,
593 Eddy Street, APC building, 10th Floor,
Providence, RI, USA. 02903
e-mail: carlos_wambier@brown.edu

0393-974X (2020)
Copyright © by BIOLIFE, s.a.s.
This publication and/or article is for individual use only and may not be further reproduced without written permission from the copyright holder.
Unauthorized reproduction may result in financial and other penalties
DISCLOSURE: ALL AUTHORS REPORT NO CONFLICTS OF INTEREST RELEVANT TO THIS ARTICLE.

implied by the epidemiology of severe COVID-19 infections, we hypothesized that seasonal expression of proteins that affect androgen receptor function may provide an explanation. One such gene is the period circadian protein homolog 1 (Per1). Per1 is primarily expressed in the superchaismatic nucleus (SCN) located in the hypothalamus; the SCN acts as the primary circadian clock and produces signals that keep the body on an approximate 24-h schedule (7). Environmental cues, most importantly light, are required to reset the circadian clock; the SCN is synchronized via specialized photosensitive ganglion cells (photosensitive retinal ganglion cells) present in the retina. Per1 expression follows the circadian cycle of the SCN and is mediated by the seasonality of available light. Sumova et al. (8) demonstrated that rats exposed to a longer photoperiod (16 hours light and 8 hours darkness) exhibited at least 4 additional hours of Per1 expression compared to rats exposed to a shorter photoperiod (8 hours light and 16 hours darkness).

Per1 expression has been demonstrated to mediate androgen receptor function. Cao et al. demonstrated that Per1 inhibited transactivation of the AR. Moreover, they showed that overexpression of Per1 diminished the expression of androgen-sensitive genes following the addition of dihydrotestosterone. Finally, the overexpression of Per1 in prostate cancer cells inhibited their growth and led to apoptosis (7).

Other seasonally expressed genes have also been demonstrated to affect the androgen receptor. Dopico et al. (9) demonstrated large seasonal immune and endocrine variation in the expression of clock genes; they reported increased expression of estradiol receptor genes during summer and increased expression of IL-6 receptor genes in the winter. IL-6 regulates androgen receptor activity by causing ligand and synergistic activation of the AR. Such effect is down-regulated by nonsteroidal antagonists of the AR (10). Additionally, prostate specific antigen (PSA) levels have been shown to vary seasonally (11).

Taken together, longer day light associated with spring and summer months are likely to reduce androgen sensitivity. Reduced androgen sensitivity would lead to lower expression of TMPRSS2 and subsequently may reduce SARS-CoV-2 infectivity. Conversely, the lower available daylight associated with fall and winter months is likely to increase SARS-CoV-2 infectivity. While it is postulated that influenza's seasonal infectiveness rate is mediated by changes in immune response, it is important to note that influenza entry into lung cells is also dependent on the TMPRSS2 enzyme (12) and, as such, may be influenced by variation in the length of the daylight. It would be interesting to study the degree of variation in influenza's seasonal infectivity as a function of geographic latitude, i.e., would smaller annual variations in length of day (e.g., at the equator) lead to a broader distribution of annual influenza infection rates. In conclusion, because both SARS-CoV-2 and influenza are dependent on TMPRSS2 for infectivity, it is likely that SARS-CoV-2 will have a similar seasonal cycle; thus, the fall and winter are likely to see an increase in COVID-19 cases.

REFERENCES

1. Hoffmann M, Kleine-Weber H, Schroeder S, et al. SARS-CoV-2 Cell entry depends on ACE2 and TMPRSS2 and is blocked by a clinically proven protease inhibitor. Cell 2020; 181(2):271-80. doi:10.1016/j.cell.2020.02.052
2. Lucas JM, Heinlein C, Kim T, et al. The androgen-regulated protease TMPRSS2 activates a proteolytic cascade involving components of the tumor microenvironment and promotes prostate cancer metastasis. Cancer Discov 2014; 4(11):1310-25. doi:10.1158/2159-8290.CD-13-1010
3. Goren A, Vaño-Galván S, Wambier CG, et al. A preliminary observation: Male pattern hair loss among hospitalized COVID-19 patients in Spain - A potential clue to the role of androgens in COVID-19 severity [published online ahead of print, 2020 Apr 16]. J Cosmet Dermatol 2020. doi:10.1111/jocd.13443
4. Kim HS, Moreira DM, Jayachandran J, et al. Prostate biopsies from black men express higher levels of aggressive disease biomarkers than prostate biopsies from white men. Prostate Cancer Prostatic Dis 2011; 14(3):262-65. doi:10.1038/pcan.2011.18
5. Ellis JA, Stebbing M, Harrap SB. Polymorphism of the androgen receptor gene is associated with male pattern baldness. J Invest Dermatol 2001; 116(3):452-

55. doi:10.1046/j.1523-1747.2001.01261.x

6. Montopoli M, Zumerle S, Vettor R, et al. Androgen-deprivation therapies for prostate cancer and risk of infection by SARS-CoV-2: a population-based study (n=4532) [published online ahead of print, 2020 May 4]. Ann Oncol 2020; S0923-7534(20)39797-0. doi:10.1016/j.annonc.2020.04.479
7. Cao Q, Gery S, Dashti A, Yin D, Zhou Y, Gu J, Koeffler HP. A role for the clock gene per1 in prostate cancer. Cancer Res 2009; 69(19):7619-25. doi:10.1158/0008-5472.CAN-08-4199
8. Sumová A, Sládek M, Jác M, Illnerová H. The circadian rhythm of Per1 gene product in the rat suprachiasmatic nucleus and its modulation by seasonal changes in daylength. Brain Res 2002; 947(2):260-70. doi:10.1016/s0006-8993(02)02933-5
9. Dopico, X., Evangelou, M., Ferreira, R. et al. Widespread seasonal gene expression reveals annual differences in human immunity and physiology. Nat Commun 2015; 6,7000. https://doi.org/10.1038/ncomms8000
10. Culig Z, Bartsch G, Hobisch A. Interleukin-6 regulates androgen receptor activity and prostate cancer cell growth. Mol Cell Endocrinol 2002; 197(1-2):231-38. doi:10.1016/s0303-7207(02)00263-0
11. Salama G, Noirot O, Bataille V, Malavaud S, Rebillard X, Villers A, Malavaud B. Seasonality of serum prostate-specific antigen levels: a population-based study. Eur Urol 2007; 52(3):708-14. doi:10.1016/j.eururo.2006.11.042
12. Sakai K, Ami Y, Tahara M, et al. The host protease TMPRSS2 plays a major role in in vivo replication of emerging H7N9 and seasonal influenza viruses. J Virol 2014; 88(10):5608-16. doi:10.1128/JVI.03677-13

LETTER TO THE EDITOR

Correlation between peripheral blood level of miRNA-29a and diabetic peripheral neuropathy

Y. Zhang[1], R.-Q. Du[2], L. Li[2], X.-Q. Hu[2] and Q.-M. Li[2]

[1]Postgraduate Training Base of Jinzhou Medical University, The PLA Rocket Force Characteristic Medical Center, Beijing, China; [2]Department of Endocrinology, The PLA Rocket Forced Characteristic Medical Center, Beijing, China

Received March 2, 2020 – Accepted April 30, 2020

To the Editor,

Type 2 diabetes mellitus (T2DM) is a metabolic disease manifesting as insulin resistance and hyperglycemia (1). Notably, T2DM could result in severe complications, including cardiac diseases, stroke, kidney failure, blindness and nerve damage, if effective treatment is not administered, (2). Diabetic neuropathy (DN) seriously affects T2DM patients. In developed countries, its incidence is about 60%. Diabetic peripheral neuropathy (DPN) is the most common pathological symptom. DPN mainly affects lower limbs, posing high susceptibilities to lower extremity ulcer, amputation and disability (3, 4). DPN remarkably decreases the quality of life and self-control management in T2DM patients, leading to a poor prognosis (5).

The vital regulatory effects of miRNAs on T2DM have been highlighted in recent years. They are involved in metabolic disorder, immune response, β cell apoptosis and inflammatory response (6). MiRNA-29 participates in cell differentiation, nerve maturation, hematopoiesis, replicative senescence and tumorigenesis (7). MiRNA-29 is upregulated in different insulin-sensitive tissues, as well as serum of T1DM children and T2DM adults because inflammatory microvesicles containing miRNA-29 could be isolated in multiple organs and blood (8). MiRNA-29a is the precursor of miRNA-29. It is transcribed from chromosome 7q32.3, and exerts its biological functions through RNA-induced silencing complexes in the cytoplasm (9). In this paper, we detected peripheral blood level of miRNA-29a in DPN patients, providing new evidence for clinical diagnosis, treatment and research of diabetes.

MATERIALS AND METHODS

A case control study was designed including a total of 100 cases of T2DM and 60 cases of T2DM combined DPN treated in our hospital from June 2016 to December 2018. This study was approved by the Ethics Committee of The PLA Rocket Forced Characteristic Medical Center and was conducted in accordance with the Declaration of Helsinki. Signed written informed consents were obtained from all participants.

The inclusion criteria were T2DM diagnosed based on the standard proposed by WHO (10), complete clinical data, and DPN diagnosed as two or more of the following manifestations occurred at or after the diagnosis of T2DM: (a) foot sensory abnormalities, decreased sensation and loss of reflexes; (b) thermal paraesthesia; (c) vibrational sensory abnormality; (d) two or more abnormalities in

Key words: T2DM; DPN; MiRNA-29a

Corresponding Author:
Quanmin Li, MD
Department of Endocrinology,
The PLA Rocket Forced Characteristic Medical Center,
Beijing, China, 16 Xinjiekouwai Street,
Xicheng District, 100000.Beijing, China
Tel.: +86 018910883326
e-mail: quanlei19650518@163.com

0393-974X (2020)
Copyright © by BIOLIFE, s.a.s.
This publication and/or article is for individual use only and may not be further reproduced without written permission from the copyright holder.
Unauthorized reproduction may result in financial and other penalties
DISCLOSURE: ALL AUTHORS REPORT NO CONFLICTS OF INTEREST RELEVANT TO THIS ARTICLE.

nerve conduction velocity; (e) ankle reflex disappeared.

Exclusion criteria were: subjects with hematological diseases; abnormal bone metabolism; serious heart, liver, kidney and lung diseases; autoimmune diseases; malignant tumors, acute and chronic inflammatory diseases; diabetic acute complications and other causes of neuropathy; lack of clinical data.

Fasting venous blood of each subject was taken on the day after admission. BUN, Scr, FPG, TC and TG were detected by an automatic analyzer. HbA1c was tested by HPLC. Morning specimens were collected for measuring UAlb/Cr. SBP and DBP were measured. MCV and SCV in the right peroneal nerve of subjects were recorded by the Nicolet Viking Quest.

Real-time polymerase chain reaction (PCR)

TRIzol method (Invitrogen, Carlsbad, CA, USA) was applied for isolating RNAs from blood samples. Through reverse transcription of RNA, the extracted complementary deoxyribose nucleic acid (cDNA) was used for PCR detection by SYBR Green method (TaKaRa, Tokyo, Japan). U6 was used as the internal reference. The primer sequences were listed as follows: MiRNA-29a, F: 5'-CTAGCACCATCTGAAATCGGTTA-3', R: 5'-TGATTGGCTAAAGTCTACCAC-3'; U6, F: 5'-CTCGCTTCGGCAGCACATA-3', R: 5'-AACGAGACGACGACAGACTTT-3'. The relative expression of miRNA was measured using the method of $2^{-\Delta\Delta CT}$.

Table I. *Baseline characteristics of enrolled T2DM patients and those combined* DPN

Variable	T2DM+DPN	T2DM	t	P
age	62.98±9.75	61.23±8.39	1.201	0.232
BMI(Kg/m^2)	22.92±1.43	23.13±1.51	0.869	0.386
SBP(mmHg)	141.23±18.27	136.73±16.29	1.616	0.108
DBP(mmHg)	90.15±15.07	87.32±12.10	1.304	0.194
FPG(mmol/L)	10.08±3.01	9.82±2.78	0.555	0.58
HbAlc(%)	10.89±3.34	7.91±2.99	5.839	<0.001
TC(mmol/L)	5.34±1.56	5.09±1.47	1.018	0.31
TG(mmol/L)	2.08±1.15	1.87±0.98	1.229	0.221
BUN(mmol/L)	6.98±2.10	5.86±1.87	3.501	0.001
Scr(μmol/L)	81.21±19.72	78.12±15.91	1.086	0.279
UAlb/Cr(mg/g)	19.78±5.88	17.76±3.76	2.651	0.009
SCV(m/s)	35.23±11.12	45.87±19.21	3.912	<0.001
MCV(m/s)	36.09±12.98	60.12±20.11	8.274	<0.001
MNSI Score	1.29±0.55	4.77±1.92	13.691	<0.001

($\overline{x} \pm s$)

T2DM: Type 2 diabetes mellitus; DPN: Diabetic peripheral neuropathy; BMI: Body mass index: SBP: Systolic pressure; DBP: Diastolic pressure; FPG: Fasting plasma glucose; HbA1c: Glycated hemoglobin; TC: Total cholesterol; TG: Triglyceride; BUN: Blood urea nitrogen; Scr: Serum creatinine; UAlb/Cr: Urinary albumin/creatinine; SCV: Sensory nerve conduction velocity; MCV: Motor nerve conduction velocity; MNSI Score: Michigan neuropathy screening instrument score.

Statistical analysis

Statistical Product and Service Solutions (SPSS) 20.0 (IBM, Armonk, NY, USA) was used for all statistical analysis. Data were expressed as mean ± SD (standard deviation). The *t*-test was used for analyzing differences between two groups. Logistic regression analysis was conducted to assess potential factors that could affect miRNA-29a level. Potential correlations between miRNA-29a level and relevant data in patients with T2DM combined DPN were assessed by Pearson correlation analysis. Receiver operating characteristic (ROC) curves were depicted for evaluating the prognostic potential of miRNA-29a in DPN. P<0.05 indicated the significant difference.

RESULTS

HbA1c, BUN and UAlb/Cr were markedly higher in patients with T2DM combined DPN than those without diabetic complications; while SCV, MCV, MNSI score and miRNA-29a levels were lower. No significant differences in age, BMI, SBP, DBP, FPG, TC, TG and Scr were identified between two groups (Table I).

Compared with T2DM patients, those combined with DPN expressed lower peripheral blood level of miRNA-29a (Fig. 1). It is suggested that miRNA-29a was involved in the development of DPN.

Logistic regression analysis showed that HbA1c, SCV, MCV and MNSI score were the independent factors influencing miRNA-29a level in DPN patients (Table II).

Pearson correlation analysis was conducted to verify the correlation between miRNA-29a level and clinical data of T2DM patients combined DPN (Table III). It was shown that miRNA-29a level was negatively correlated to HbA1c (r=-0.442, P=0.039) and MNSI (r=-0.854, P<0.001), but it was positively

Table II. *Multivariate logistic regression analysis on potential factors influencing miRNA-29a expression*

Variable	OR	95%*CI*	P
HbAlc	1.773	1.214-5.332	0.042
SCV	2.681	1.781-4.872	0.035
MCV	1.564	1.032-2.651	0.011
MNSI Score	0.583	0.238-0.779	0.023

HbA1c: Glycated hemoglobin; SCV: Sensory nerve conduction velocity; MCV: Motor nerve conduction velocity; MNSI Score: Michigan neuropathy screening instrument score.

Table III. *Pearson correlation analysis on the correlation between miRNA-29a level and clinical data of T2DM patients combined DPN*

Variable	r value	P
HbAlc	-0.442	0.039
SVC	0.713	0.015
MCV	0.578	0.009
MNSI Score	-0.854	<0.001

HbA1c: Glycated hemoglobin; SCV: Sensory nerve conduction velocity; MCV: Motor nerve conduction velocity; MNSI Score: Michigan neuropathy screening instrument score.

correlated to SCV (r=0.713, P=0.015) and MCV (r=0.578, P=0.009) in DPN patients.

Prognostic potential of miRNA-29a in DPN

ROC curves were depicted for assessing the prognostic potential of miRNA-29a in DPN; AUC=0.9551, 95%CI=0.9257-0.9845 and P<0.005. Sensitivity=83.33%, specificity=95% and Youden index=0.7833 were calculated under the cut-off =1.365 (Fig. 2). The data demonstrated that the risk of DPN increased when miRNA-29a level was lower than 1.365.

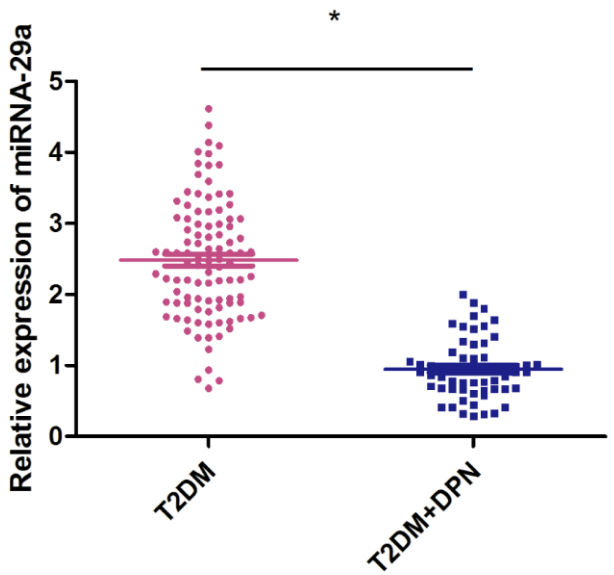

Fig. 1. *MiRNA-29a level in T2DM patients either combined either DPN or not Serum level of miR-29a in 60 cases of T2DM combined DPN and 100 cases of T2DM.*

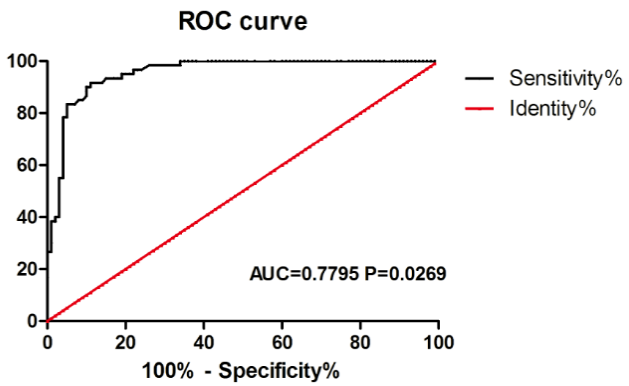

Fig. 2. *Prognostic value of miRNA-29a in DPN of T2DM patients*

DISCUSSION

Multiple miRNAs have been identified to be involved in T2DM-induced complications. Chen et al. (11) reported that abundant pro-inflammatory factors and ECM proteins are expressed in focal lesioned tissues (retina and kidney) of *in vivo* DR and DN models. They suggested that overexpression of miRNA-146a markedly downregulates these pro-inflammatory factors and ECM proteins, and alleviates relevant symptoms. Han et al. (12) demonstrated that Triptolide can reduce the secretion of ECM in kidney tissues during DN, and slow down DN-induced renal inflammation and fibrosis. Therefore, clinical application of miRNAs in prevention and treatment of T2DM is promising.

In the present study, peripheral blood level of miRNA-29a was markedly lower in DPN patients than T2DM patients without complications. MiRNA-29a level was negatively correlated to HbA1c and MNSI, but it was positively correlated to SCV and MCV, indicating that miRNA-29a may be an effective indicator for DPN. Moreover, its predictive potential in DPN was verified through ROC curves. We believe that miRNA-29a may be a novel target in DPN diagnosis. Peripheral blood level of miRNA-29a decreases in patients with T2DM-combined DPN. SCV and MCV are independent factors influencing miRNA-29a level in DPN patients. MiRNA-29a has a high predictive value for the occurrence of DPN in T2DM patients.

REFERENCES

1. Yang Z, Chen H, Si H, et al. Serum miR-23a, a potential biomarker for diagnosis of pre-diabetes and type 2 diabetes. Acta Diabetol 2014; 51:823-31.
2. Honardoost M, Sarookhani MR, Arefian E, Soleimani M. Insulin resistance associated genes and miRNAs. Appl Biochem Biotechnol 2014; 174:63-80.
3. Timar B, Timar R, Gaita L, Oancea C, Levai C, Lungeanu D. The impact of diabetic neuropathy on balance and on the risk of falls in patients with Type 2 diabetes mellitus: a cross-sectional study. Plos One 2016; 11:e154654.
4. Look AHEAD Research Group. Effects of a long-

term lifestyle modification programme on peripheral neuropathy in overweight or obese adults with type 2 diabetes: the Look AHEAD study. Diabetologia 2017; 60:980-88.
5. Smith AG, Russell J, Feldman EL, et al. Lifestyle intervention for pre-diabetic neuropathy. Diabetes Care 2006; 29:1294-99.
6. Calderari S, Diawara MR, Garaud A, Gauguier D. Biological roles of microRNAs in the control of insulin secretion and action. Physiol Genomics 2017; 49:1-10.
7. Slusarz A, Pulakat L. The two faces of miR-29. J Cardiovasc Med (Hagerstown) 2015; 16:480-90.
8. Peng H, Zhong M, Zhao W, et al. Urinary miR-29 correlates with albuminuria and carotid intima-media thickness in type 2 diabetes patients. Plos One 2013; 8:e82607.
9. Kriegel AJ, Liu Y, Fang Y, Ding X, Liang M. The miR-29 family: genomics, cell biology, and relevance to renal and cardiovascular injury. Physiol Genomics 2012; 44:237-44.
10. Silber HE, Nyberg J, Hooker AC, Karlsson MO. Optimization of the intravenous glucose tolerance test in T2DM patients using optimal experimental design. J Pharmacokinet Pharmacodyn 2009; 36:281-95.
11. Chen S, Feng B, Thomas AA, Chakrabarti S. miR-146a regulates glucose induced upregulation of inflammatory cytokines extracellular matrix proteins in the retina and kidney in diabetes. Plos One 2017; 12:e173918.
12. Han F, Wang S, Chang Y, et al. Triptolide prevents extracellular matrix accumulation in experimental diabetic kidney disease by targeting microRNA-137/Notch1 pathway. J Cell Physiol 2018; 233:2225-37.

LETTER TO THE EDITOR

Establishment and potential mechanism of recurrent cystitis-induced overactive bladder-like model in female rats

F. Gao[1], N. Zhang[2], J.M. Wen[2], S.J. Li[3], S.G. Zhang[2], B.Y. Zhang[4], Y.L. Dai[5], R.N. He[1], Y.S. Huang[1] and Q.Q. Yu[1]

[1]Department of Urology, Hangzhou Hospital of Traditional Chinese Medicine, China; [2]Department of Urology, Second Affiliated Hospital, School of Medicine, Zhejiang University, Zhejiang, China; [3]Department of Urology, Zhejiang Provincial People's Hospital, Zhejiang, China; [4]Department of Pathology, Second Affiliated Hospital, School of Medicine, Zhejiang University, Zhejiang, China; [5]Department of Clinical Laboratory, Zhejiang Provincial Hospital of Traditional Chinese Medicine, Zhejiang, China

Received January 8, 2020 – Accepted July 3, 2020

To the Editor,

Overactive bladder (OAB) is one of the common chronic diseases of the urinary system with an overall incidence rate of at least 10.7%, and up to 24.8% in women aged over 40 years (1). Primary symptoms of OAB include sudden urge to urinate and frequent micturition, with or without urge incontinence, which seriously affects the quality of life (1). Detrusor overactivity (DO) is responsible cause for the occurrence of OAB (2). Studies demonstrated that the number and overactivity of interstitial cells of Cajal (ICCs) in the bladder with DO increase significantly (3, 4). While studies have shown that ICCs serve as primary pacemaker cells that play a fundamental role in signal transmission from bladder nerves to smooth muscle cells (3), the pathogenesis of OAB remains to be defined. Currently, animal models of OAB are mainly established in rabbits, pigs, and rats, which are mostly induced by bladder outlet obstruction (BOO) or cyclophosphamide (5, 6). However, clinically, women with recurrent cystitis are more likely to suffer from OAB. Thus, the BOO model has limitations and is inconsistent with some clinical patients caused by cystitis.

Therefore, in this study, a recurrent cystitis-induced OAB-like rat model by four cycles of bladder infection with *Escherichia coli* (*E.coli*) followed by levofloxacin treatment was established. Moreover, the potential role of ICCs and associated protein stem cell factor (SCF) and its ligand c-kit, a tyrosine kinase receptor, were also explored.

MATERIALS AND METHODS

Thirty female Sprague Dawley (SD) rats, 40 ~ 45 days of age, weighing 150 ~ 180 g, were purchased from a commercial source (Shanghai Xipuer-Beikai Experimental Animal Co., Ltd., Shanghai, China) and housed in the Animal Experimental Center, Zhejiang University of Traditional Chinese Medicine. Animals were handled following the instruction of the Institutional Animal Care and Use Committee (IACUC), Zhejiang University of Traditional Chinese Medicine (License No. SCXK, Zhejiang, 2018-0012).

E.coli (ATCC35218) strain was purchased from a commercial source (Hangzhou BAISI Biotechnology Co.,

Key words: overactive bladder (OAB); cystitis; interstitial cell of cajal (ICCs); stem cell factor (SCF); c-kit

Corresponding Author:
Y.S. Huang, M.D, Ph.D.
Department of Urology,
Hangzhou Hospital of Traditional Chinese Medicine,
453# Tiyuchang Road,
Hangzhou, Zhejiang, China. 310007
e-mail: KK2158@qq.com

0393-974X (2020)
Copyright © by BIOLIFE, s.a.s.
This publication and/or article is for individual use only and may not be further reproduced without written permission from the copyright holder.
Unauthorized reproduction may result in financial and other penalties
DISCLOSURE: ALL AUTHORS REPORT NO CONFLICTS OF INTEREST RELEVANT TO THIS ARTICLE.

Ltd) and stored at -70°C. After incubation at 37°C for 24 h, the *E.coli* colony was suspended with a saline solution at a concentration of 1.0 ~ 1.2 × 10^8 CFU/mL, which was determined by spectrophotometer (Hitachi U-10080D). For the intravesical installation, a total 100 μL *E.coli* solution was instilled into the bladder through a 0.5mm diameter urinary catheter.

The rats were randomly assigned into the following two groups: an experimental group and a control group. As illustrated in Fig. 1, for the experimental group, Intravesical installation was carried out by 100 μL of *E.coli* followed by urine analysis and urine culture for 3 days to confirm cystitis. The rats were then treated with intragastric administration of levofloxacin (50mg/kg, Shanghai Yinshi Biotechnology Co., Ltd.) once a day for 7 days. Therapeutic outcomes of the cystitis were determined by urine analysis and urine culture. If the results of urine analysis and culture were normal, additional 3 cycles of intravesical instillation of 100 μL of *E.coli* followed by treatment with levofloxacin were performed (total 4 cycles) to mimic recurrent cystitis in patients. For the control group, the same volume of saline solution, instead of *E.coli*, was used for bladder irrigation with aseptic technique for a total of 4 cycles of the same procedure as the experimental group.

For the urine sample collection, the rats were given drinking water only and individually placed in an aseptic metabolic cage after the irrigation. Urine leukocyte count, and colony-forming unit (CFU) formation in the urine samples were performed. If the urine sample was contaminated with stool in the metabolic cage, the animal was transferred to a clean metabolic cage, and the whole procedure of sample collection was conducted again.

The urodynamic examination was performed as described previously (7). The rats were weighed, then anesthetized with an intraperitoneal injection of pentobarbital (35 mg/kg bodyweight, Shanghai Aiyan Biotechnology Co., Ltd.). The bladder was exposed through a midline incision of the lower abdomen. A 22-G catheter, which was connected to a pressure transducer, was inserted into the bladder through the urethra to measure the bladder pressure through Urodynamic Examiner (MMS Solar) with a speed of 0.5 mL/min injection for 15 min. The voiding pressure (VP), maximal bladder volume (MBV), and bladder compliance (BC) were measured. The occurrence of detrusor unstable contraction (DUC) was determined following the International Continence Society (ICS) definition. Specifically, when the bladder was full, detrusor instability and contraction led to unstable pressure on the bladder. When the curve of the pressure waved up and down periodically, DUC was confirmed even if the pressure was under 15 cmH_2O.

The rats were sacrificed by CO_2 inhalation immediately after completion of the urodynamic examination. The parietal part of the bladder was collected for histologic examination by HE and immunofluorescence staining as well as immunoblotting. Briefly, part of the parietal bladder tissue was fixed with a 10% formaldehyde solution, 4-μm sections were prepared for HE staining following the protocol, and part of the bladder tissue was snap-frozen with liquid nitrogen followed by storing at -80°C. For the immunofluorescence staining, the tissue was fixed by 4% polyformaldehyde, followed by washing with phosphate-buffered saline containing 0.1% Tween® 20 (PBST) and blocking with 5% normal donkey serum. The tissue was then incubated with a rabbit anti-rat c-kit antibody (1:100, EBIO SCIENCE Company) at 4°C for 48 h. The donkey anti-rabbit IgG (1:40, DAKO Company) was labeled with fluorescein isothiocyanate for immunofluorescence staining.

Immunoblotting

Total proteins were extracted from the frozen parietal bladder tissue and separated on the 10% SDS-PAGE (Image Quant LAS 4000, 50 μg/lane). Proteins were then transferred to cellulose nitrate membrane followed by blocking with 5% skimmed milk in PBS at room temperature for 2 h. Primary antibodies, including rabbit-anti-rat CF (1:200, Shanghai Rebiosci Biotech Co. Ltd), c-kit (1:100, EBIO SCIENCE Company), and GAPDH (1:500, Cell Signaling, Shanghai CST Biological Reagents Company, Shanghai, China), were allowed to react with proteins at room temperature for 30 min followed by overnight at 4°C. After washing with PBST three times, the horseradish peroxidase-labeled donkey anti-rabbit antibody (1:500, Abcam-China, Shanghai, China) was added and incubated at 37°C for 1 h. Protein bands were visualized with enhanced chemiluminescence (ECL) solution. The density of the proteins was analyzed using Quantity One software.

Statistical analysis

Immunofluorescence images were quantified by

Image-Pro Plus 7.0 software. All data were expressed as mean±standard error of the mean (SEM), and SPSS22.0 software was used for Student's *t*-test between two groups. $P < 0.05$ was considered statistically significant.

RESULTS

Induction of urinary infection by intravesical instillation of E.coli

Average CFU (Cycle 1: 519±137; Cycle 2: 483±122; Cycle 3: 416±135; Cycle 4: 503±102 10^5/ml) and white blood cell count (Cycle 1: 311±57; Cycle 2: 324±54; Cycle 3: 291±47; Cycle 4: 329±38 /HP) were significantly increased following each cycle of intravesical instillation of *E.coli*. In contrast, control group rats were negative in CFU, and white blood cell counts in the urine. These results indicated that recurrent cystitis was established in these rats by the recurrent installation of *E.coli* into the rat bladder. Data were expressed as means±SEM (n= 15).

Urodynamic examination in the OAB-like animal models

The urodynamic examination was conducted to evaluate whether the animal models with recurrent cystitis displayed OAB-like clinical features. As illustrated in Fig. 2, VP, MBV and BC were significantly decreased in the animals of OAB-like rat model compared to the control rats (VP: 33.4±3.9 *vs* 26.7±4.7 cmH_2O, Panel A, $P < 0.05$; MBV: 1.31±0.09 *vs* 1.10±0.07 mL, Panel B, $P < 0.05$; BC: 0.086±0.006 *vs* 0.055±0.007 mL/cmH_2O, Panel C, $P < 0.05$). In contrast, DUC was dramatically increased in the bladder filling period in the animals of OAB-like rat model compared to the control animals (Panel D and E, 2.9±0.3 *vs* 0.4±0.1 times/period).

H&E staining of the bladder tissue was employed to determine the histological changes of the bladder from the animals of the OAB-like model and control animals. Slight degeneration was found in the mucous membrane of the bladders from the animals of the OAB-like model while they were not seen in the normal bladders of control animals. However, infiltration of the inflammatory cells (monocytes/macrophages) into the bladder tissues was barely found in the animals either of the OAB-like model or the control animals (Fig. 3 A and B).

Studies have demonstrated that ICCs serve as primary pacemaker cells, which play a fundamental role in signal transmission from bladder nerves to smooth muscle cells, and the number and activity of ICCs were significantly increased in the bladder with DO (3). Thus, c-kit, a specific marker of ICCs, was examined by immunofluorescence staining in the current study. As illustrated in Fig. 4, The number of c-kit positive cells was significantly increased in the animals of the OAB-like model compared to that in the control group (7.8±0.3 *vs* 3.3±0.2, $P < 0.05$).

Protein levels of SCF and c-kit in the bladder tissues were further examined by immunoblotting. As illustrated in Fig. 5, both SCF and its ligand c-kit proteins were significantly increased in the bladder tissues of the animals of OAB-like model than those of control rats (SCF: 1.21±0.21 *vs* 1.00±0.15, Panel B, $P < 0.05$; c-kit: 2.20±0.19 *vs* 1.00±0.18, Panel C, $P < 0.05$).

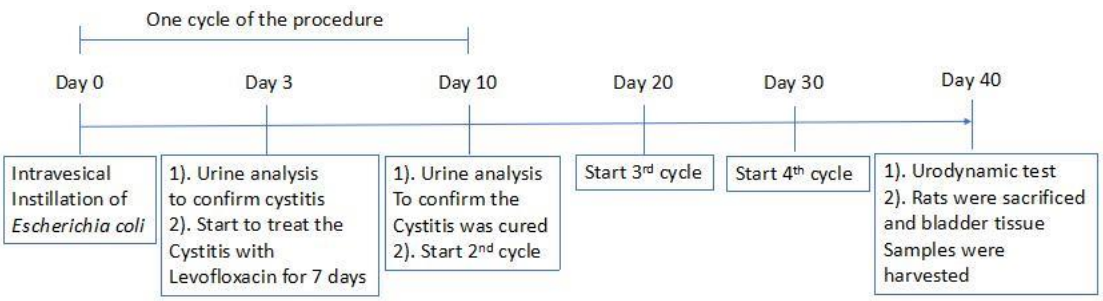

Fig. 1. *Schematic illustration of preparing cystitis-induced OAB-like rat model.*

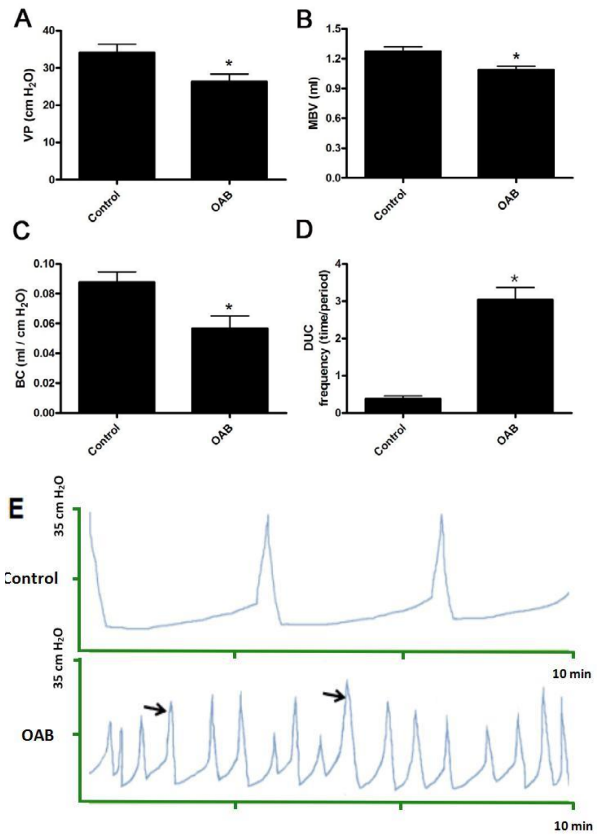

Fig. 2. *Comparison of the urodynamic test in the two groups.* ***A****) Voiding pressure (VP);* ***B****) Maximum bladder volume (BMV);* ***C****) Bladder compliance (BC);* ***D****) Detrusor unstable contraction (DUC);* ***E****) Urinary dynamic curve. Arrows indicate DUC. Data were expressed as mean±SEM (n= 15). *P <0.05 vs the control group.*

DISCUSSION

OAB in female patients is often caused by recurrent cystitis. Furthermore, nearly 85% of cystitis is caused by *E.coli* (8). The current study was, therefore, designed to establish an OAB-like rat model by *E.coli* in female rats. In addition to confirming that inflammation has been cured, H&E staining is more important for showing that DUC is not caused by inflammation. The urodynamic examination confirmed that a model was successfully established. After 4 cycles, 12 rats were successfully modeled. However, three rats (20%) in the experimental group had slight or even no significant alteration in DUC, which could be associated with the following: i) anesthesia may inhibit spontaneous contraction of the detrusor muscle and voiding reflex; ii) cystitis lasted a relatively short time, which might be insufficient to cause pathophysiological changes and subsequent DO.

Previous studies have reported that the number of ICCs in different parts of the bladder varied; that is, the parietal bladder had the highest number of ICCs (9, 10). Therefore, the parietal bladder tissue was harvested. It was found that the expression of ICCs and related proteins (SCF/c-kit) were significantly increased in the bladder tissue from the OAB-like rat model compared to that of the control group. However, the causal relationship between the result and OAB (DO/DUC) is still unclear in this study.

Overall, ICCs and SCF/c-kit may be involved in the development of the OAB-like animal model in female rats in response to *E.coli* bladder infection and antibiotic treatment. This animal model could be used

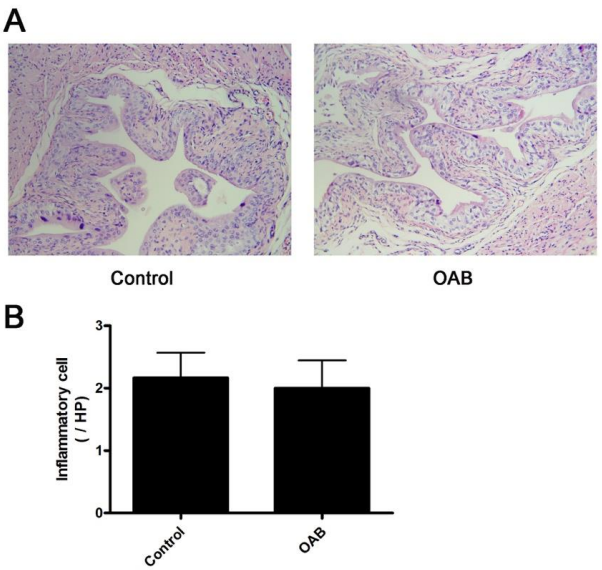

Fig. 3. *Comparison of histology and inflammatory cell infiltration into the bladder tissues.* ***A****) Histological comparison after 4 cycles of intravesical instillation of E.coli. Histological examination was performed by HE staining, as described in the methods. Magnification: × 200.* ***B****) Comparison of inflammatory cells in the animals of the OAB-like rat model and the control rats. Vertical axis: number of inflammation cells infiltrated into the bladder tissue; horizontal axis: groups of animals with or without OAB-like disease. Data were expressed as mean±SEM (n= 15).*

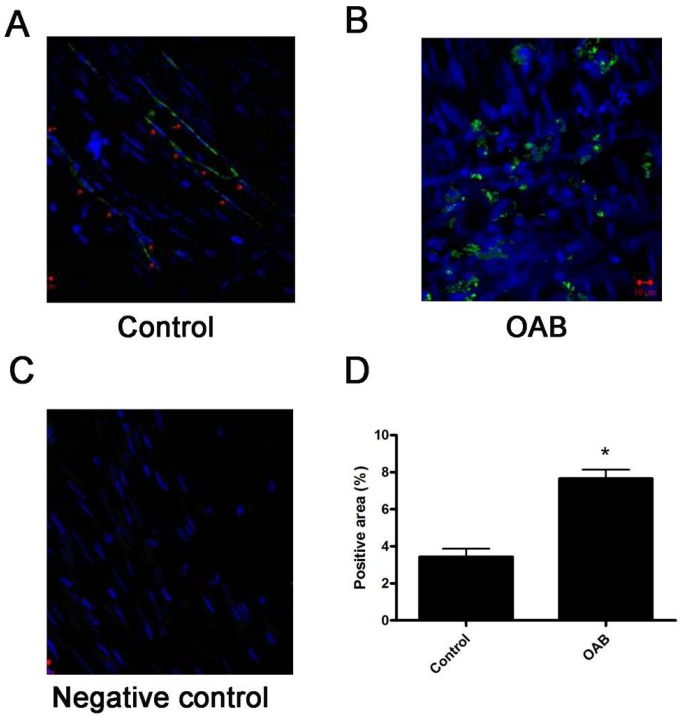

Fig. 4. *Immunofluorescence staining of c-kit in the ICCs from the two groups. **A**) Bladder from control animals; **B**) bladder from the animals of OAB-like model; **C**) negative control of immunofluorescence staining procedure, which was lack of primary antibody and only secondary antibody was applied. Magnification: x 400. Green represented positive c-kit staining; red arrows indicated ICCs with positive c-kit expression; blue indicated cell nuclei. **D**) quantitative comparison of the ICCs with positive c-kit expression. Vertical axis: percent of the positive area (%): the percentage of c-kit positive ICCs in the area of detrusor muscles; horizontal axis: animals with or without OAB-like disease. Data were expressed as mean±SEM (n= 15). *P < 0.05 vs control group.*

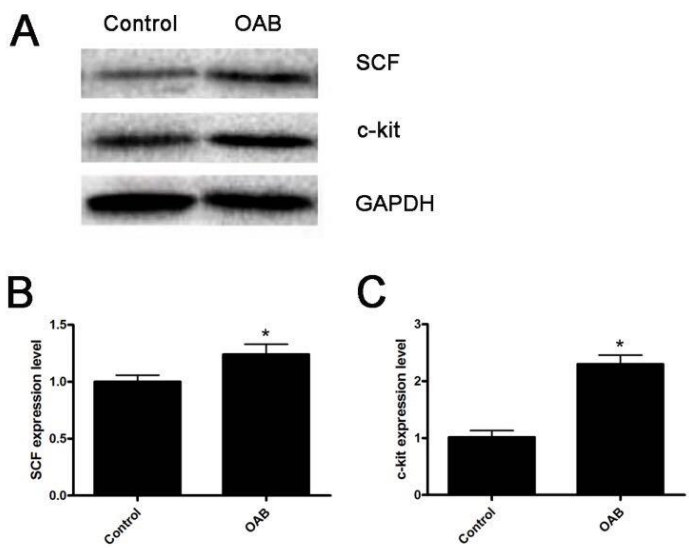

Fig. 5. *Immunoblotting of SCF and c-proteins. **A**) Representative image of immunoblotting. **B**) Comparison of SCF protein in the bladder tissues from the two groups. **C**) Comparison of c-kit protein in the bladder tissues from the two groups. Vertical axes: relative level of SCF (B) and c-kit (C); horizontal axes: animals with or without OAB-like disease. Data were expressed as mean±SEM (n= 15). *P < 0.05 vs control group.*

to investigate the pathogenesis of OAB further and to develop new treatments of cystitis-related OAB.

ACKNOWLEDGEMENT

This work was supported by grants from Hangzhou Science and Technology Development Plan Project (No. 20191203B138 to Yasheng Huang)

REFERENCES

1. Irwin DE, Kopp ZS, Agatep B, Milsom I, Abrams P. Worldwide prevalence estimates of lower urinary tract symptoms, overactive bladder, urinary incontinence and bladder outlet obstruction. BJU Int 2011; 108:1132-38.
2. Al Mousa RT, Al Dossary N, Hashim H. The role of urodynamics in females with lower urinary tract symptoms. Arab J Urol 2019; 17:2-9.
3. Feng J, Gao J, Zhou S, et al. Role of stem cell factor in the regulation of ICC proliferation and detrusor contraction in rats with an underactive bladder. Mol Med Rep 2017; 16:1516-22.
4. Pingyu Z, Binglei J, Qilong J, Tao W, Wei T. Cyclic stretch promotes proliferation and contraction of human bladder smooth muscle cells by cajal-mediated c-kit expression in interstitial cells. Med Sci Monit 2019; 25:4784-92.
5. Hughes FM, Jr., Hill HM, Wood CM, Yang YF. The NLRP3 Inflammasome mediates inflammation produced by bladder outlet obstruction. J Urol 2016; 195:1598-605.
6. Kim HS, Park WJ, Park EY, Koh JS, Hwang TK, Kim JC. Role of nicotinic acetylcholine receptor alpha3 and alpha7 subunits in detrusor overactivity induced by partial bladder outlet obstruction in rats. Int Neurourol J 2015; 19:12-8.
7. Cayan S,Canpolat B, Cayan F, Yilmaz N, Kartal A, Oguz I, Akabay E. The effect of chronic inflammatory condition of the bladder and estrogen replacement therapy on bladder functions and histology in surgically menopause and chronic cystitis induced rats. Neurourol. Urodyn 2006; 25:194-201.
8. Bao ZM. Introduction to urinary tract infection. In Wu Jieping urology. Wu JP, ed. Shandong science and technology Publishing Corp. Jinan, 2012; p.554.
9. McCloskey KD. Interstitial cells in the urinary bladder--localization and function. Neurourol Urodyn 2010; 29:82-87.
10. Kubota Y, Hamakawa T,Osaga S, et al. A kit ligand, stem cell factor as a possible mediator inducing overactive bladder. Neurourol Urodyn 2018; 37:1258-65.

LETTER TO THE EDITOR

Expression level of FGFR2 protein in patients with esophageal cancer and those with Barrett's esophagus-associated dysplasia

Y. Bai[1], LL. Lang[2], WT. Zhao[1], Q. Cao[1] and R. Niu[1]

[1]Chest Surgery, Gansu Cancer Hospital, Qilihe District, Lanzhou City, China; [2]Department of Radiology, Gansu Cancer Hospital, Qilihe District, Lanzhou City, China

Received February 2, 2020 – Accepted July 9, 2020

To the Editor,

Esophageal cancer is the eighth most common cancer, and the sixth most common cause of cancer-related deaths worldwide (1). In 2009-2015, the overall 5-year survival rate for esophageal cancer was 19.9%, while early detection and diagnosis have shown a positive influence on the treatment and prognosis of patients (2). Tumor neovascularization is significant for rapid tumor growth, infiltration, and metastasis. It has been found that bFGF (Basic Fibroblast Growth Factor) together with VEGF (Vascular Endothelial Growth Factor) plays a synergetic role in the process of tumor angiogenesis (3). bFGF is one of the main pro-angiogenic factors that promote tumor angiogenesis (4). bFGF exerts all these biological effects dependent on the receptor on the tissue cell membrane, that is, Fibroblast Growth Factor Receptors (FGFRs) (5). FGFR2 is a member of the FGFR family, and bFGF plays a biological role mainly through FGFR2 which is the product of the Bek oncogene expression and a transmembrane tyrosine kinase receptor with a high affinity for a variety of FGFs, highly expressed in malignant tumor tissues (6). In the present study, the expression levels of FGFR2 in esophageal cancer and esophageal dysplasia were analyzed, and the correlation between FGFR2 and clinicopathological features of patients with esophageal cancer was further investigated.

MATERIALS AND METHODS

Patients

Ninety-eight patients (group A) with esophageal cancer who underwent surgery between October 2017 and June 2019 in Gansu Cancer Hospital and 73 patients with Barrett's esophagus–associated dysplasia (group B) were enrolled in the study. None of the patients had undergone other anticancer treatments preoperatively, such as chemotherapy, radiotherapy, and immunotherapy. All patients signed informed consent forms prior to the study ,and the study was approved by the Ethics Committee of Gansu Cancer Hospital.

The patients in the esophageal cancer group were independently diagnosed as esophageal squamous cell carcinoma (ESCC) by two experienced pathologists. Esophageal cancer staging was defined by the American Joint Committee on Cancer (AJCC) Staging System that established tumor-node-metastasis (TNM) sub-classifications based on the depth of invasion of the primary tumor (T), lymph node involvement (N), and extent of metastatic disease (M).

Sectioning of paraffin-embedded tissues

Fresh esophageal cancer tissues and esophageal dysplasia tissues were removed, fixed in 10% formalin overnight, and then rinsed with clear water for 30 min. After that, 85% ethanol was used to soak the tissues for

Key words: esophageal cancer; esophageal dysplasia; FGFR2; tumor markers

Corresponding Author:
Dr Rong Niu
Chest Surgery,
Gansu Cancer Hospital,
No. 2 Little West Lake East Street, Qilihe District,
Lanzhou City, 730050, China
e-mail: niurongyishenggs@163.com

0393-974X (2020)
Copyright © by BIOLIFE, s.a.s.
This publication and/or article is for individual use only and may not be further reproduced without written permission from the copyright holder.
Unauthorized reproduction may result in financial and other penalties
DISCLOSURE: ALL AUTHORS REPORT NO CONFLICTS OF INTEREST RELEVANT TO THIS ARTICLE.

2-3 h. Next, they were immersed in 95% ethanol overnight. After soaking in anhydrous ethanol and xylene, the sections were embedded into paraffin. The wax blocks of groups A and B were stored at -20°C for more than 30 min. Immunohistochemical staining was performed on serial sections (thickness, 4 μm) of esophageal cancer.

EnVision system (a new immunohistochemical method for diagnosis and research)

The slides were placed in an incubator at 60°C for more than 30 min. The slices were routinely dewaxed, and then washed with phosphate buffered saline (PBS) three times. The diluted primary antibody (FGFR2; dilution ratio 1:1000) was dripped and maintained overnight at 4°C. PBS was then used to rinse three times. The MaxvisionTM2/HRP reagent was dripped onto the slice, kept at room temperature for 15 min, and then washed 3 times with PBS. Diaminobenzidine (DAB) substrate kit was used for immunohistochemistry (IHC) staining using horseradish peroxidase (HRP). Hematoxylin was used to re-dye for 1 min, and 0.1% hydrochloric acid alcohol was utilized for differentiation. After that, gradient alcohol precipitation was undertaken for dehydration and drying. Anhydrous sodium carbonate was added into xylene gum, and stirred at a low-temperature, and observed under a microscope.

Tonsil tissues were used as positive control tissues. PBS solution was used as negative control. The staining results were negative.

FGFR2 was stained with brown granules in the cytoplasm. According to the depth of staining, the scores of 0, 1, 2, and 3 corresponded to negative (colorless), weak-positive (light yellow), moderate-positive, and strong-positive, respectively. It was of great importance to observe the strongest colored area under a low power mirror. Then, under a microscope, five representative regions were randomly selected. The score of each field of vision was indicated by the proportion of positive cells, in which the scores of 1, 2, 3, and 4 corresponded to less than 10%, 10%-25%, 26%-50%, and more than 50%, respectively.

Detecting the expression level of FGFR2 by quantitative reverse transcription polymerase chain reaction (RT-qPCR)

Primer 5.0 was herein used to design FGFR2 and β-actin primers. The upstream primer of FGFR2 was 5'-AGCCAGAAATGTTTTGGTAA-3', and the downstream primer of FGFR2 was 5'-TCAGCAGCTTAAAAAGTTCC-3'. The length of products was also found to be 266-bp. The upstream primer of β-actin was 5'-GGACCTGACTGACTGACTACCT-3', and the downstream primer of β-actin was 5'-CATACTCCTGCTTGCTG-3' (length of products, 539-bp).

Additionally, 50 mg of the samples were weighed and chopped in an ice box. After blowing and mixing, they were kept at room temperature for 5 min. Then, 0.2 ml of chloroform was added. After shaking and mixing, they were maintained for 3 min. After centrifugation at 4°C for 15 min at 12000 rpm, RNA in the upper aqueous phase was absorbed into a new RNase-Free centrifuge tube. After centrifugation at 4°C for 15 min at 12000 rpm, the supernatant was discarded. Afterwards, 1 ml of 75% diethyl pyrocarbonate (DEPC) alcohol was added. After centrifugation at 4°C for 3 min at 12000 rpm, the supernatant was discarded. After keeping for 3 min at room temperature, 40 μL DEPC water was added to dissolve the precipitate. An ultra-violet (UV) spectrophotometer was used to detect RNA concentrations. The range of optical density (OD) value was 1.8-2.0. RNA was obtained and stored in a refrigerator at -80°C.

A reverse transcription kit manufactured by Takara (Dalian, China) was used for reverse transcription. On ice, 5 μgRNA, oligo(dT)18 primer 1 μL, and DEPC water 6 μL were subsequently added. After mixing, it was placed into the PCR instrument (at 65°C for 5 min). After the reaction, it was placed on ice. On ice, 5×Reaction Buffer 4 μL, RiboLock RNase Inhibitor (20u/ul) 1 μL, 10 Mm dNTP Mix 2 μL, RevertAid M-MuLV Reverse Transcriptase (200μ/μL) 1 μL were added in order to make the total reaction system reach 20 μL. The reaction was stopped at 42°C for 60 min and at 70°C for 5 min. The reaction products were stored at -20°C.

The PCR Amplification kit (Takara, Dalian, China) was used with a total reaction system of 50 μL. 2×Taq MasterMix 25 μL, upstream primer 1μL, downstream primer 1 μL, cDNA 3 μL, RNase-Free water 20 μL were subsequently added. After that, the reaction conditions were set as follows: at 95°C for 5 min → (at 9°C for 30 s → at 50°C for 30 s → at 72°C for 1 min) 35 cycles → at 72°C for 10 min.

The RT-qPCR products were separated by 1% agarose gel electrophoresis. The experimental conditions were at

75 V and 30 min. Results of RT-qPCR were processed by Image-Pro Plus 6.0 image analysis software. The gray value of FGFR2 bands in each group was compared with that of β-actin protein bands, in which the relative expression level of FGFR2 could be achieved.

Detecting the expression level of FGFR2 by Western blotting

The total protein was extracted from radio immunoprecipitation assay (RIPA) lysate. Concentrated glue and separated glue were prepared. After connecting the electrophoresis equipment and adding the electrophoresis buffer, the first pore was added with 5 μL Maker, and the sample size of each pore was adjusted to 50 μg. For concentrated gel electrophoresis, it was 90V constant pressure. When the protein sample reached the boundary between concentrated gel and separated gel, the voltage was adjusted to 150 V. After 1 h, the protein samples were fully separated, and then the electrophoresis was ended. Polyvinylidene fluoride (PVDF) membrane was then activated with methanol for 15 s. According to the maker strip, the glue was cut at the proper protein molecular weight. After about 20 min, membrane transfer was ended. Ponceau dye was also used to stain PVDF membranes. After successfully transferring PVDF membranes, they were rinsed with Tris-Buffered Saline +Tween (TBST) buffer for 3 times, 3 min each time. Skimmed milk powder and TBST buffer were utilized to prepare 5% blocking solution. PVDF membranes were then sealed for 1 h. FGFR2 mouse anti-human antibody and TBST buffer were prepared at a dilution of 1:1000. β-actin antibody was prepared at a dilution of 1:2000. A plate was used to make a wet box. The side of PVDF membranes was fully contacted with the antibody, and then maintained at 4°C overnight. PVDF membranes were taken out, and TBST buffer was added and rinsed in a shaker for 3 times. The secondary antibody and TBST buffer were prepared in dilution of 1:5000, and the wet box was made. One side of the electro protein of PVDF membranes was in full contact with the antibody, and it was left at room temperature for 1 h. PVDF membrane was taken out, and TBST buffer was added, and rinsed in a shaker three times. Western chromogenic solution was then prepared. PVDF membranes were further visualized and analyzed.

Statistical analysis

The data were statistically analyzed by SPSS 19.0 software (IBM, Armonk, NY, USA). The results obeyed normal distribution and homogeneity of variance after analysis of variance, and paired *t*-test was adopted for quantitative data. The bivariate correlation coefficient analysis and linear multiple regression analysis were used for correlation analysis. $P < 0.05$ was considered statistically significant.

RESULTS

Immunohistochemical results

It was revealed that the positive signals of FGFR2 protein were mainly located in the cytoplasm or/and

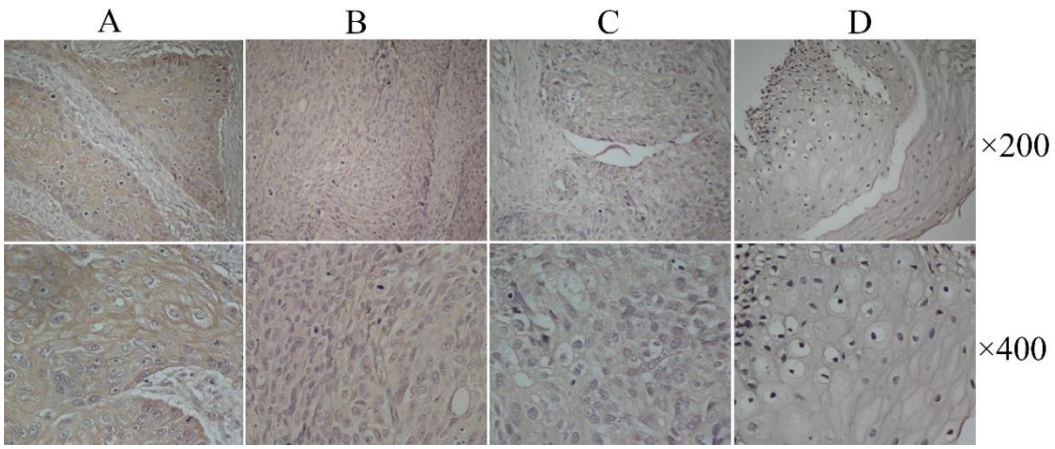

Fig. 1. *Immunohistochemical results. **A**) High expression levels of FGFR2 protein in esophageal cancer; **B**) Low expression levels of FGFR2 protein in esophageal cancer; **D**) Low expression levels of FGFR2 protein in esophageal dysplasia cells)*

Table I. *Differences in expression levels of FGFR2 in esophageal cancer group and Barrett's esophagus–associated dysplasia group*

Groups	FGFR2(-)	FGFR2(+)	FGFR2(++)	FGFR2(+++)	Total
Group A	51	25	12	10	98
Group B	64	9	0	0	73

Table II. R*elative expression levels of FGFR2 in esophageal cancer group and Barrett's esophagus–associated dysplasia group*

Group	Esophageal cancer group	Barrett's esophagus–associated dysplasia group	P
Relative expression levels of FGFR2	0.78±0.31	0.36±0.22	0.007

cell membrane of each tissue, and yellow-granules were visualized. After staining, brownish yellow granules were microscopically disclosed. As shown in Fig. 1, FGFR2 was expressed in different degrees in esophageal cancer, while was poorly expressed in esophageal dysplasia cells.

Differences in expression levels of FGFR2 protein in esophageal carcinoma and esophageal dysplasia cells

The expression levels of FGFR2 in esophageal tissues in group A and group B were analyzed. The expression level of FGFR2 in esophageal cancer (47.96%, 47/98) was significantly higher than that in esophageal dysplasia cells (12.33%, 9/73) ($P < 0.05$).

As shown in Table I, the expression levels of FGFR2 were higher in the esophageal cancer group. Among them, there were 22 samples of FGFR2 (+ +) and FGFR2 (+ + +).

Results of RT-qPCR

The results of RT-qPCR revealed that the relative expression level of FGFR2 in the esophageal cancer group was notably higher than that in Barrett's esophagus–associated dysplasia group ($P = 0.007$), as shown in Table II.

Detecting the expression levels of FGFR2 by Western blot analysis

Western blot analysis showed that the expression level of FGFR2 in the esophageal cancer group was markedly higher than that in Barrett's esophagus–associated dysplasia group. It was also indicated that differences in expression levels of FGFR2 protein were statistically significant ($P < 0.05$), as shown in Fig. 2.

Expression level of FGFR2 in esophageal cancer tissues and its relationship with clinical parameters

The expression level of FGFR2 protein in esophageal cancer tissues had no significant relationship with gender, age, and lymph node metastasis ($P > 0.05$), while there was a significant relationship with depth of tumor invasion, tumor grade, TNM stage, and tumor size ($P < 0.05$). The expression level of FGFR2 protein decreased in low-grade esophageal cancer, as presented in Table III.

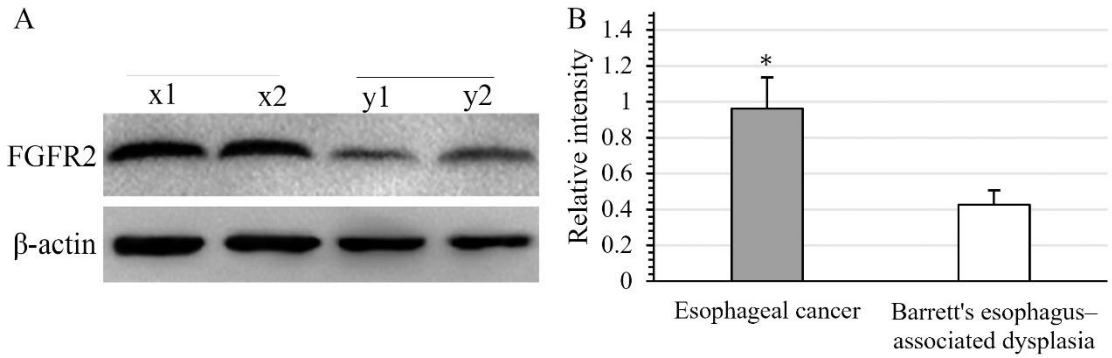

Fig. 2. *Expression levels of FGFR2 protein in tissues detected by Western blotting. **A**) Western blot analysis; **B**) Statistical chart of gray scales; Compared with dysplasia, P < 0.05)*

Table III. *Expression level of FGFR2 protein and its relationship with clinicopathological parameters*

Parameters		Number of Cases	FGFR2		P
			Positive	Negative	
Gender	Male	56	23(41.07%)	33(58.93%)	0.765
	Female	42	24(57.14%)	18(42.86%)	
Age	≥60 years old	67	34(50.75%)	33(49.25%)	0.961
	<60 years old	31	13(41.94%)	18(58.06%)	
Infiltration degree	T1~T2	48	19(39.58%)	29(60.42%)	0.032
	T3~T4	50	28(56.00%)	22(44.00%)	
Degree of differentiation	High and medium differentiation	33	5(15.15%)	28(84.85%)	0.006
	Poorly differentiated	65	42(64.62%)	33(35.38%)	
TNM staging	I and II periods	33	8(24.24%)	25(75.76%)	0.026
	III and IV periods	65	39(60.00%)	26(40.00%)	
Lymph node metastasis	Yes	39	23(58.97%)	16(41.03%)	0.596
	No	59	24(40.68%)	35(59.32%)	
Tumor size	≥3cm	68	43(63.24%)	25(36.76%)	0.005
	<3cm	30	4(13.33%)	26(86.67%)	

Correlation analysis

The results of correlation analysis are presented in Table IV. It can be seen that the expression level of FGFR2 in esophageal cancer tissues was negatively correlated with degree of differentiation (P < 0.05). Moreover, a significant positive correlation was noted between the expression level of FGFR2 and the degree of invasion (P < 0.05). The expression level of FGFR2 was higher in esophageal cancer tissues of patients with serosa immersion than that of patients without serosa immersion.

DISCUSSION

FGFR2 is a specific marker for tumor fibroblasts, and is highly expressed in several solid tumors (7). Fibroblast growth factor and its receptor play significant roles in a variety of biological activities,

Table IV. *Correlation coefficient analysis of FGFR2 expressions and clinicopathological parameters*

	Correlation coefficient	P
Gender	0.028	0.853
Age	0.037	0.780
Infiltration degree	0.275	0.034
Degree of differentiation	-0.417	0.004
TNM staging	0.384	0.017
Lymph node metastasis	0.200	0.126
Tumor size	0.402	0.008

such as cell proliferation, differentiation and migration (8, 9). Recently, FGFR2 has been found to play a substantial role in the transformation of mesenchymal epithelium. This transformation is highly significant for the secondary tumor growth of the deformed organ (10). The results of the present study showed that the expression level of FGFR2 protein in esophageal carcinoma group was notably higher than that in Barrett's esophagus–associated dysplasia group. Additionally, the Pearson's correlation analysis revealed that the expression level of FGFR2 in esophageal cancer was significantly correlated with the tumor size, TNM stage, degree of differentiation, and degree of infiltration ($P < 0.05$). In addition, the expression level of FGFR2 in esophageal cancer was negatively correlated with degree of differentiation ($P < 0.05$). The degree of differentiation was lower and the expression level of FGFR2 was higher ($P < 0.05$). Therefore, it can be hypothesized that FGFR2-positive fibroblasts are recruited by tumor cells in the early stage of tumor development, and may promote the occurrence and development of tumor cells. Other research confirmed that once FGFR2-positive fibroblasts settled in tumor tissues, they interacted with surrounding tumor cells (11). Also, by providing these tumor cells with various proteins that promote occurrence and development of tumors, a suitable environment for tumors was created (12).

In conclusion, FGFR2 is widely expressed in esophageal cancer cells, and is associated with the occurrence, development, and prognosis of esophageal cancer cells. Therefore, it can be used as a marker and a new target for the diagnosis and treatment of esophageal cancer cells.

REFERENCES

1. Huang FL, Yu SJ. Esophageal cancer: Risk factors, genetic association, and treatment. Asian J Surg 2018; 41(3):210-15.
2. Domper Arnal MJ, Ferrández Arenas Á, Lanas Arbeloa Á. Esophageal cancer: Risk factors, screening and endoscopic treatment in Western and Eastern countries. World J Gastroenterol 2015; 21(26):7933-43.
3. Du H, Shi H, Chen D, Zhou Y, Che G. Cross-talk between endothelial and tumor cells via basic fibroblast growth factor and vascular endothelial growth factor signaling promotes lung cancer growth and angiogenesis. Oncol Lett 2015; 9(3):1089-94.
4. Li D, Xie K, Zhang L, et al. Dual blockade of vascular endothelial growth factor (VEGF) and basic fibroblast growth factor (FGF-2) exhibits potent anti-angiogenic effects. Cancer Lett 2016; 377(2):164-73.
5. Akl MR, Nagpal P, Ayoub NM, et al. Molecular and clinical significance of fibroblast growth factor 2 (FGF2 /bFGF) in malignancies of solid and hematological cancers for personalized therapies. Oncotarget 2016; 7(28):44735-62.
6. Li X, Nie C, Tian B, et al. miR-671-5p Blocks the progression of human esophageal squamous cell carcinoma by suppressing FGFR2. Int J Biol Sci 2019; 15(9):1892-904.

7. Zhang C, Fu L, Fu J, et al. Fibroblast growth factor receptor 2-positive fibroblasts provide a suitable microenvironment for tumor development and progression in esophageal carcinoma. Clin Cancer Res 2009; 15(12):4017-27.
8. Dickson C, Spencer-Dene B, Dillon C, Fantl V. Tyrosine kinase signalling in breast cancer: Fibroblast growth factors and their receptors. Breast Cancer Res 2000; 2(3):191-96.
9. Dai S, Zhou Z, Chen Z, Xu G, Chen Y. Fibroblast growth factor receptors (FGFRs): structures and small molecule inhibitors. Cells 2019; 8(6):614.
10. Chaffer CL, Brennan JP, Slavin JL, Blick T, Thompson EW, Williams ED. Mesenchymal-to-epithelial transition facilitates bladder cancer metastasis: role of fibroblast growth factor receptor-2. Cancer Res 2006; 66(23):11271-78.
11. Shi Y, Liu X, Fredimoses M, et al. FGFR2 regulation by picrasidine Q inhibits the cell growth and induces apoptosis in esophageal squamous cell carcinoma. J Cell Biochem 2018; 119(2):2231-39.
12. Ishiwata T. Role of fibroblast growth factor receptor-2 splicing in normal and cancer cells. Front Biosci (Landmark Ed) 2018; 23:626-39.

LETTER TO THE EDITOR

Protective effects and underlying mechanism of sevoflurane pretreatment on cerebral ischemia-reperfusion injury in mice

DB. Xu[1,2], F. Lin[1,2], HJ. He[1,2] and Y. Ying[1,2]

[1]Department of Anesthesiology, Taizhou Hospital of Zhejiang Province Affiliated to Wenzhou Medical University, Linhai, Taizhou, Zhejiang Province, China; [2]Department of Anesthesiology, Taizhou Enze Medical Center (Group) Enze Hospital, Taizhou, Zhejiang Province, China

Received April 30, 2020 – Accepted July 9, 2020

To the Editor,

The re-establishment of blood supply in the brain after acute cerebral ischemia can cause tissue damage. These effects are known as cerebral ischemic reperfusion injury (CIRI) (1, 2). Sevoflurane (SVF) (3) is used as a common inhaled general anaesthetic. A previous study pointed out that SVF pretreatment can effectively reduce the damage of CIRI on brain tissues (4). Hippocampal CA1 pyramidal neurons are closely associated with learning and memory abilities and are sensitive to ischemic brain injury (5). Cognitive impairment caused by cerebral ischemia is tightly linked to neuronal damage in the hippocampal CA1 region (5). Prolonged ischemia may influence cell metabolism, induce apoptosis, and impair patients' cognitive function. It has been shown that CIRI selectively affects pyramidal neurons from the hippocampal CA1 region and increases the release of glutamic acid (6). Long-term potentiation dependent by NMDA receptor (LTP) in the hippocampal CA1 region is a recognised substrate for learning and memory, manifested mainly by continuous enhancement of efficacy of synaptic transmission (7). In this study the protective mechanism of SVF was investigated on a mice model of CIRI, focussing on the SVF effects on the morphology and synaptic transmission function of hippocampal CA1 neurons. Moreover, we attempted to indicate whether SVF can influence p-Akt protein expression and to prevent ischemia-induced LTP.

MATERIALS AND METHODS

Animals and groups

Fifty-one healthy male Kunming mice of clean grade (8 weeks old; body weight, 22-28 g) were selected. Mice were housed in a ventilated and clean environment at 22-25°C, with constant humidity (50-60%). The animals were divided into three groups, a sham group (n=17), a model group (n=17), and an SVF group (n=17) by random table method. The Ethics Committee of Taizhou Enze Medical Center (Group) Enze Hospital approved the animal experiment.

CIRI mouse model and treatment

Mice were kept without feed for 12 h and then were placed in a semi-closed plexiglass box. Soda-lime (Jining Bafang Mining Machinery Co., Ltd., China) was spread on the bottom of the box to keep the pressure of PCO_2 in the box below 375 mmHg, and the temperature of 35-38°C. Each box had two ventilation holes on the sides. Pure oxygen was administered for 60 min in the model and sham groups through one hole. In contrast, in the SVF group, the box was connected to an anaesthetic

Key words: sevoflurane; cerebral ischemic reperfusion injury; neuronal injury; LTP induction

Corresponding Author:
Dr Ying Ying,
Department of Anesthesiology,
Taizhou Hospital of Zhejiang Province, Affiliated to Wenzhou Medical University, No.150 Ximen Road, Linhai,
Taizhou, 317000, Zhejiang Province, China
e-mail: yingyingdoctor1@163.com

0393-974X (2020)
Copyright © by BIOLIFE, s.a.s.
This publication and/or article is for individual use only and may not be further reproduced without written permission from the copyright holder.
Unauthorized reproduction may result in financial and other penalties
DISCLOSURE: ALL AUTHORS REPORT NO CONFLICTS OF INTEREST RELEVANT TO THIS ARTICLE.

gas dispenser that provided O_2 and 2.4% SVF (Shanghai Hengrui Pharmaceutical Co., Ltd., China) for 60 min, with pure oxygen elution for 10 min. Sixty minutes after oxygenation the box from each group was connected through the other hole to an anaesthetic gas analyser used to administer 10% chloral hydrate (Xi'an Tianzheng Kangyuan Biotechnology Co., Ltd., China) for abdominal anaesthesia (300 mg/kg bw). After anaesthesia, the mouse model of CIRI was produced as previously described (8). In the sham group, the external and common carotid artery was isolated and ligated through neck surgery. In the model group and SVF group, the distal carotid artery was clamped with a blood vessel clip, and a small cut was made at the branch of the common carotid artery. A 50 mm long nylon fishing line was placed in the internal carotid artery, and it was stopped when there was a slight resistance, with a depth of 1.8-2.0 cm. The suture was removed to restore blood perfusion after 20 min of ischemia.

Four mice from each group were sacrificed 24 h after CIRI modelling, the brains were collected and used for triphenyl tetrazolium chloride (TTC) staining. On the 5th day after CIRI modelling, 8 mice were sacrificed and the brains from 4 of them were used for Western blot determination and the other 4 were used for TUNEL (terminal deoxynucleotidyl transferase dUTP nick end labeling) and H&E (hematoxylin and eosin) staining. Another 5 mice from each group were used for the evaluation of extracellular field potential (EFP).

Triphenyl tetrazolium chloride) staining

Four mice were selected from each group and sacrificed by decapitation 24 h after the CIRI model was obtained. The brain was isolated, and the brainstem, cerebellum and olfactory bulb were carefully separated. The brain was cleaned of blood with iced normal saline solution, dried with filter paper and frozen at -20°C for 5-10 min. The brain was then cut into 1.5 mm slices with a blade along the coronal surface and placed in 2% TTC staining solution (Shanghai Yuanmu Biotechnology Co., Ltd., China). The slices were stained in a 37°C water bath (Shanghai Ruiwen Instrument Equipment Factory, China) for 30 min without light and were frequently spun for uniform staining. The normal brain tissues were bright red after staining, while the infarcted brain tissue were grey-white after staining. The colored brain sections were placed in 4% paraformaldehyde (Shanghai Xinyu Biotechnology Co., Ltd., China) and maintained at 4°C overnight. The proportion of cerebral infarct volume was calculated.

H&E staining

On the 5th day after CIRI modelling, 4 mice from each group were anaesthetised with chloral hydrate (10%) in doses of 300 mg/kg, and the limbs were fixed on the operating table. The mice were perfused with saline solution and the brains were collected. The paraffin-embedded sections were routinely dewaxed in water, and H&E staining was then performed. Morphological changes of nerve cells were observed using a microscope (Shanghai Putan Optical Instrument Co., Ltd., China). The clear boundary of pyramidal neurons was used as the standard, and Image-Pro Plus 6.0 software (Media Cybernetics, USA) was used to count the number of viable pyramidal cells. Five views were randomly selected for each section and the average was calculated.

In situ detection of apoptosis by the TUNEL assay

The 4 μm paraffin-embedded sections were routinely dewaxed. In Situ Cell Death Detection Kit (Sigma-Aldrich, St. Louis, MO, USA) was used for TUNNEL assay. A positive control (with 100 μl DNasel) and negative control (with 50 μl fluorescein-12-dUTP solution) were simultaneously prepared. A fluorescence microscope (Shanghai Putan Optical Instrument Co., Ltd., China) was used to analyse the samples. The BI-2000 Medical Image Analysis System (Chengdu Taimeng Software Co., Ltd., China) was used for interpretation of the results. The percentage of positive cells in the hippocampal pyramidal neurons was calculated.

Western blot analysis

On the 5th day after CIRI modelling, 4 mice from each group were decapitated and the brains were collected. Hippocampal tissues were collected for Western blot analysis. Frozen hippocampal brain tissues were transferred into Eppendorf (EP) tubes (Hamburg, Germany). The proteins were extracted with RIPA (radioimmunoprecipitation assay) lysis buffer (Cida Biotechnology Co., Ltd., China). The determination of proteins was carried out using SDS-PAGE (sodium dodecyl sulfate-polyacrylamide gel electrophoresis) method. The PVDF (polyvinylidene difluoride)

membranes were incubated with rabbit anti-Akt and p-Akt antibody (1:1000) (Shanghai Xuanke Biotechnology Co., Ltd., China) overnight at 4°C. Then the membranes were washed with TBST (TBS+Tween) (Beijing baileibo Technology Co., Ltd., China) and incubated at room temperature for 2 h with the secondary horseradish peroxidase (HRP)-labeled antibody (Shanghai Bosheng Biotechnology Co., Ltd., China). The protein bands were incubated for 1 min at room temperature with enhanced chemiluminescence (ECL) working solution (Biyuntian Biotechnology Co., Ltd., China). Then the films were wrapped with plastic cling film to protect from light and were exposed to X-ray film (Shanghai Suolaibao Biotechnology Co., Ltd., China) and fixed after 2-3 min of development. Finally, the slit-scanning densitometry was performed on the film using a gel imaging system (Bio-Rad, USA), and the integrated optical density (IOD) value of the corresponding band was recorded to reflect the protein content.

Preparation of hippocampal slice

On the 5th day after CIRI modelling, five mice were selected from each group. The mice were anaesthetised with chloral hydrate (10%) (300 mg/kg) and then sacrificed through decapitation. The brain was quickly collected. The ischemic brain tissue was frozen in artificial cerebrospinal fluid (ACSF) at 0-4°C for about 2 min. ACSF contained the following components (mmol/L): 128.0 NaCl, 1.7 KCl, 1.3 $MgSO_4$, 2.4 $CaCl_2$, 26.0 $NaHCO_3$, 1.24 KH_2PO_4, and 10.0 D-glucose (Beijing Youchengjiaye Biotechnology Co., Ltd., China). An oxygen mixture (95% O_2, 5% CO_2) was used to stabilise the pH of ACSF around 7.4. After the mouse brain was slightly modified, 6-8 coronal sections (thickness, 400 μm) of the hippocampus were cut on a microtome. The brain sections were moved into a beaker containing ACSF at room temperature, and the oxygen mixture was administered. Then, these sections were incubated at 22-25°C for at least 1 h. The incubated brain sections were placed in a thermostatic bath (TC-202A; Medical Systems Corp., Fort Lauderdale, FL, USA). The perfusion of ACSF saturated with oxygen mixture was continuously performed (1-2 h), and the perfusion speed was set to 3.0-3.5 ml/min, at (32.0±0.5)°C.

Extracellular field potentials

The electrode recording was carried out in a standard borosilicate glass tube. After being drawn by a P-97 drawing machine (Sutter Inc., Sacramento, CA, USA) and rinsed with 2 mol/L NaCl, the electrode impedance was set to 3-8 MΩ. The tungsten wire electrode with a diameter of 50 μm, a bare tip of 40-60 μm, and an electrode spacing of 100-150 μm, was used as the stimulation electrode. The stimulation electrode was placed in the Schaffer side branch of the hippocampal CA1 region. The detachable glass electrodes used for recording field potentials were inserted into the radiation layer of the hippocampal CA1 region by a microelectrode pusher for forwarding stimulation. Excitatory postsynaptic potential (EPSP) was recorded. An amplifier (Axonclamp-2B; Axon Enterprise Inc., Scottsdale, AZ, USA) was used to amplify the recorded signal. The amplified signal was then imported into the PowerLab data acquisition system (ADInstmments, Australia). The Master-8, a general-purpose stimulator for nerve and muscle stimulation with eight channels, was utilised with a stimulation wave width of 0.1 ms. The input-output (I/O) curve was plotted by changing the stimulus intensity (0.1-1.0 mA). Five responses were measured for each stimulus intensity, and the average value was calculated (average I/O curve). According to the I/O curve, 50% of the stimulus intensity producing the maximum response was selected as the stimulus intensity. This stimulus intensity was also used when LTP and double-pulse responses were measured. The double-pulse stimulation experiment was performed by adjusting the interpulse interval (IPI). Each IPI was recorded for 5 times, and the average value was calculated. The stimulation interval was 15 s, and superimposition was carried out every 4 stimulations. When LTP was induced, the conditional stimulus was utilised to record stability for about 20 min, and the average slope of EPSP was calculated. Next, the stimulus intensity was set to 80% of the stimulus intensity that could produce the maximum response. Hippocampal brain sections were subjected to high-frequency stimulation (HFS). The HFS was set to 100 Hz for 1 s. After the end of HFS, the same conditions were used for testing, and the recording process was at least 60 min. If the slope of EPSP is still more than 20% before HFS, it can be concluded that LTP induction is successful.

Statistical analysis

The data were analysed using SPSS 19.0 software (IBM, Armonk, NY, USA). The data were expressed as mean±standard deviation *($\bar{x}$±s)*. ANOVA test was used for

comparison between the groups. Student-Newman-Keuls test was used for pairwise comparison of multiple samples. The statistical significance was considered when P <0.05.

RESULTS

Cerebral infarct volume

The ischemic area of mouse brain tissues was stained off-white as a background 24 h after CIRI modelling. In the model group, the cerebral infarct volume significantly increased compared with the Sham group (P <0.01). Pretreatment with SVF 1 h before ischemia noticeably reduced the cerebral infarct volume (P <0.05) (Fig.1 A and B).

Neuronal damage

In the sham group, the neurons that survived in the hippocampal CA1 region were intact and arranged neatly (Fig. 1 C and D). The nucleus was round or oval, and located in the center of the cell, with less chromatin and visible nucleoli. The neurons in the hippocampal CA1 region in the model group had unclear structure, sparse arrangement, darker staining, and nucleus shrinkage, and a greater number of neurons had died. The number of pyramidal cells that survived in the hippocampal CA1 region was remarkably increased after pretreatment with SVF compared with the Model group. Pretreatment with SVF alleviated ischemic neuronal damage in the mice hippocampal CA1 region.

Neuronal damage and neuronal apoptosis

On the 5th day after CIRI modelling, apoptotic bodies appeared in the hippocampal CA1 region in the Model group. In the Sham group, apoptotic cells were almost invisible. Apoptotic cells were significantly increased in the model group compared with the Sham group (P <0.01). The pretreatment with SVR significantly decreased the number of apoptotic cells compared with the Model group (P <0.01) (Fig. 2 A and B).

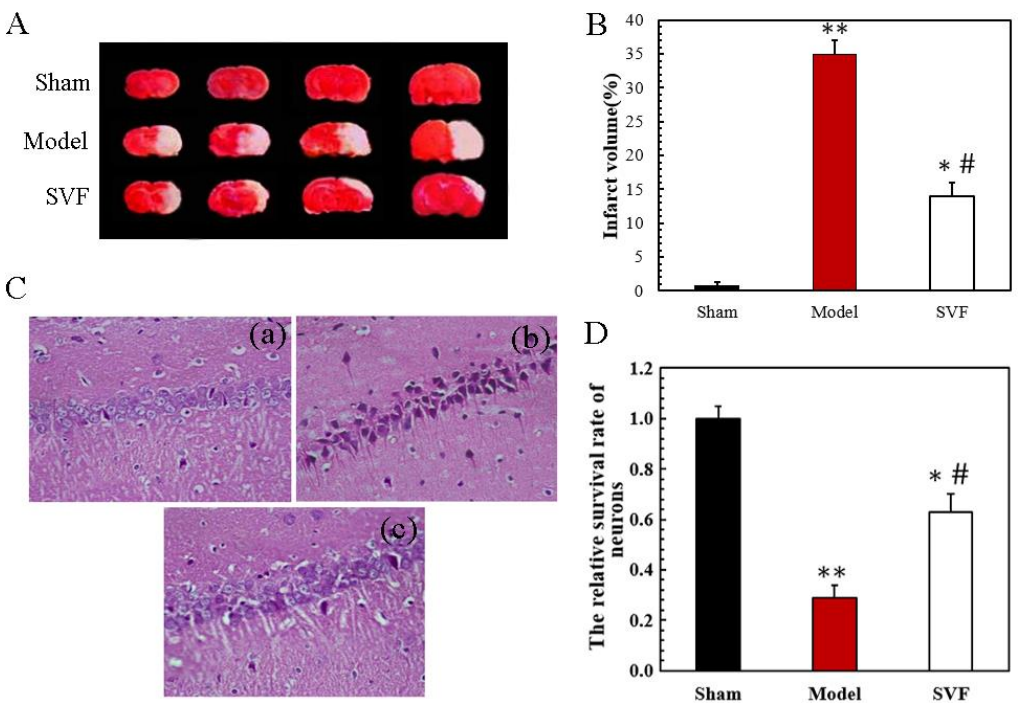

Fig. 1. *Changes in cerebral infarct volume and neuronal damage in the CA1 region of the hippocampus. **A**) Results of TTC staining; **B**) Comparison of cerebral infarct volume among the three groups; **C**) Results of H&E staining (×400) ((a). Sham group; (b). Model group; (c): SVF group)); **D**) The survival rate of pyramidal cells in CA1 region of the hippocampus of mice in each group. Compared with the Sham group, *P <0.05, **P <0.01; Compared with the Model group, #P < 0.05.*

CIRI-induced LTP damage

The NMDA receptor-dependent LTP induction was detected in the hippocampal CA1 region in order to assess the impact of SVF on the synaptic transmission function. HFS was performed on the mice hippocampal CA1 region in the Sham mice. The results revealed that the slope of EPSP markedly increased after HFS (183.2±6.4%) lasted for more than 60 min (163.6±4.8%). On the 5th day after CIRI modelling, although the slope of EPSP noticeably increased after

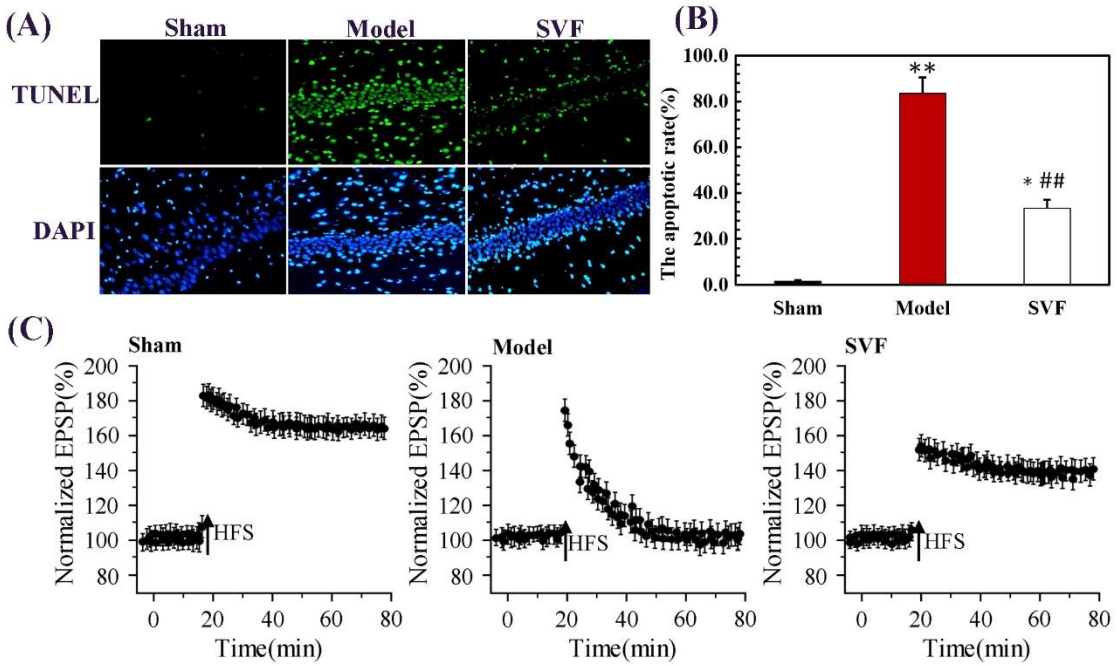

Fig. 2. *Detection of neuronal apoptosis in the CA1 region of the hippocampus and CIRI induced LTP damage. **A**) Detection of neuronal apoptosis in the CA1 region of the hippocampus by TUNEL assay; **B**) Statistical chart of apoptotic cells in CA1 region. Compared with the Sham group, **P <0.01; Compared with the Model group, ##P < 0.05; **C**) CIRI induced LTP damage in the CA1 region of the hippocampus of mice (↑: duration of HFS; horizontal axis represents recording time (min); vertical axis denotes the normalised slope of EPSP before and after HFS).*

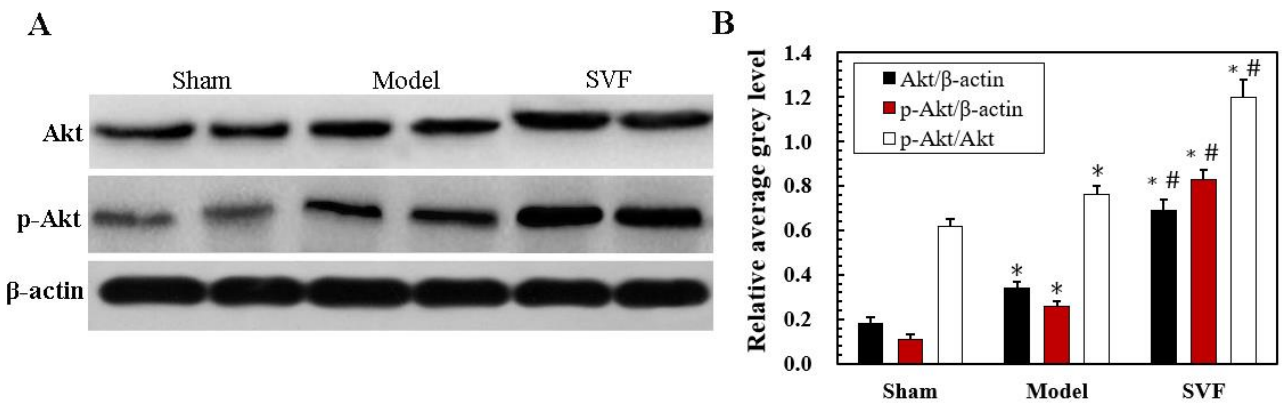

Fig. 3. *p-Akt and Akt in the CA1 region of the hippocampus of mice. **A**) Western blot results; **B**) Relative grey value statistics. *P <0.05 compared with the Sham group; #P <0.05 compared with the Model group.*

HFS in the Model group (173.8±11.8%), it promptly decreased. The slope of EPSP recorded at 60 min after HFS was 104.6±5.2% which showed that there was only a short-term potentiation (STP), indicating that CIRI induced LTP damage in the hippocampal CA1 region. The pretreatment with SVF successfully converted STP to LTP (slope of EPSP measured 1 min after HFS: 154.2±5.4%; the slope of EPSP measured 60 min after HFS was 140.8±5.6%). These findings indicated that pretreatment with SVF could improve the LTP-induced impairment of hippocampal CA1 region by CIRI, and enhance the learning and memory function (Fig. 2C).

Akt and p-Akt expressions in the hippocampal CA1 region

On the 5th day after CIRI modelling, the expressions of Akt and p-Akt in the Model group were significantly increased compared with the Sham group ($P < 0.05$). The expressions of Akt and p-Akt were remarkably increased in the SVF group compared with the Model group ($P < 0.05$) (Fig.3). These findings suggested that pretreatment with SVF may play a protective role against ischemic neuronal damage by promoting the expression of p-Akt.

DISCUSSION

CIRI is a common disease in the elderly with a high rate of increase nowadays. Moreover, CIRI can cause the death of pyramidal neurons in the hippocampal CA1 region (9). We showed that pretreatment with SVF had significant neuroprotective effects on a mouse model of CIRI, and can reduce the death of pyramidal neurons in the hippocampal CA1 region. The molecular biology of memory storage is associated with an interaction between genes and synapses. The development of the brain requires the participation of LTP (10). Paule et al. (11) found that NMDA participates in brain development and synaptic plasticity, and it also plays a vital role in the regulation of hippocampal LTP. The results of this study showed that LTP-induced disorder caused by CIRI might be related to the impairment of intracellular signal transduction pathways mediated by NMDA receptors. However, pretreatment with SVF improves CITP-induced LTP damage and dysfunction of synaptic transmission and can protect against LTP-induced disorders by increasing the number of survived neurons.

PI3K plays an essential role in the development of inflammation (12) and can regulate cell cycle and inhibit cell apoptosis by activating multiple downstream effector molecules. The current study showed that pretreatment with SVF could increase the p-Akt expression in a mouse model of CIRI.

In conclusion, pretreatment with SVF can alleviate the severity of CIRI in mice by activating the PI3K/Akt pathway.

ACKNOWLEDGEMENT

This work was supported by Science and Technology Project of Taizhou (Grant No.1801ky29).

REFERENCES

1. Ma X H, Gao Q, Jia Z, Zhang ZW. Neuroprotective capabilities of TSA against cerebral ischemia/reperfusion injury via PI3K/Akt signaling pathway in rats. Int J Neurosci 2015; 125(2):140-46.
2. Tsatsakis A, Docea AO, Calina D, et al. A mechanistic and pathophysiological approach for stroke associated with drugs of abuse. J Clin Med 2019; 8(9):1295.
3. Zhang Y, Zhang FG, Meng C, et al. Inhibition of sevoflurane postconditioning against cerebral ischemia reperfusion-induced oxidative injury in rats. Molecules 2011; 17(1):341-54.
4. Wang JK, Wu HF, Zhou H, Yang B, Liu XZ. Postconditioning with sevoflurane protects against focal cerebral ischemia and reperfusion injury involving mitochondrial ATP-dependent potassium channel and mitochondrial permeability transition pore. Neurol Res 2015; 37(1):77-83.
5. Li J, Yan D, Liu X, Wang Y, Zhao X, Zhang Y, Zhang C. U0126 protects hippocampal CA1 neurons against forebrain ischemia-induced apoptosis via the ERK1/2 signaling pathway and NMDA receptors. Neurol Res 2018; 40(4):318-23.
6. Pan J, Zhang QG, Zhang GY. The neuroprotective effects of K252a through inhibiting MLK3/MKK7/JNK3 signaling pathway on ischemic brain injury

in rat hippocampal CA1 region. Neuroscience 2005; 131(1):147-59.

7. Jiang M, Polepalli J, Chen LY, Zhang B, Sudhof TC, Malenka RC. Conditional ablation of neuroligin-1 in CA1 pyramidal neurons blocks LTP by a cell-autonomous NMDA receptor-independent mechanism. Mol Psychiatry 2017; 22(3):375-83.
8. Savchenko A S, Borissoff J I, Martinod K, et al. VWF-mediated leukocyte recruitment with chromatin decondensation by PAD4 increases myocardial ischemia/reperfusion injury in mice. Blood 2014; 123(1):141-48.
9. Sekeljic V, Bataveljic D, Stamenkovic S, et al. Cellular markers of neuroinflammation and neurogenesis after ischemic brain injury in the long-term survival rat model. Brain Struct Funct 2012; 217(2):411-20.
10. Schwarzbach E, Bonislawski DP, Xiong G, Cohen AS. Mechanisms underlying the inability to induce area ca1 ltp in the mouse after traumatic brain injury. Hippocampus 2006; 16(6):541-50.
11. Paule MG, Fogle CM, Allen RR, Pearson EC, Hammond TG, Popke EJ. Chronic exposure to NMDA receptor and sodium channel blockers during development in monkeys and rats: long-term effects on cognitive function. Ann N Y Acad Sci 2003; 993:116-22; discussion 123-24.
12. Ebner B, Lange S A, Hollenbach D, et al. In situ postconditioning with neuregulin-1β is mediated by a PI3K/Akt-dependent pathway. Can J Cardiol 2015; 31(1):76-83.

LETTER TO THE EDITOR

Predictive effect of strong ion gap on heart failure in patients with dilated cardiomyopathy

Q. Wang[1], F. Zhang[2], W. Cao[1], X-B. Wang[3], H-J. Wang[4] and Q-T. Han[5]

[1]Emergency Department, Zhangqiu District People's Hospital, Jinan, China; [2]No. 1 Department of Cardiology, Zhangqiu District People's Hospital, Jinan, China; [3]Department of Tumor Radiotherapy, Zhangqiu District People's Hospital, Jinan, China; [4]Department of Pediatrics, Zhangqiu District People's Hospital, Jinan, China; [5]Interventional Vascular Department, Zhangqiu District People's Hospital, Jinan, China

Received May 18, 2020 – Accepted July 9, 2020

To the Editor,

Dilated cardiomyopathy (DCM) is a common cardiac disease with more than 30% five-year fatality rate (1). The main clinical features of DCM patients are left ventricular (or biventricular) dysfunction, and myocardial hypertrophy, but patients sometimes appear with congestive heart failure, often accompanied by arrhythmia (2). The disease is a primary myocardial disease with highly heterogeneous pathogenic gene and complex pathogenesis, and there is no specific therapy (3). The treatment is still mainly drug therapy. Patients should receive treatment in time, otherwise the condition will deteriorate rapidly at any time, and even lead to death. Strong ion gap (SIG) is an indicator based on research models that can accurately reflect the acid-base balance disorder in patients. Compared with the traditional anion gap (AG), SIG, which is based on the Stewart-Figge model, can calculate the known charged components in the patient to obtain more accurate results (4). Relevant research has shown that the SIG significantly changes in the human body when a variety of organs are damaged, so SIG could be used to predict and judge the incidence of heart failure (5). There are many medical methods that can be used to predict heart failure in patients with dilated cardiomyopathy, such as left ventricular ejection branch, intracardiac physiological examination, and twelve-lead electrocardiogram, etc. However, research on the prediction of dilated cardiomyopathy by SIG remains unclear. Therefore, this article explored the predictive effect of SIG on diastolic heart failure (DHF) in patients with dilated cardiomyopathy.

MATERIALS AND METHODS

Study subjects

Patients with dilated cardiomyopathy diagnosed and treated in our hospital from January 2018 to December 2019 were selected as the study subjects. This study was conducted in accordance with the Declaration of Helsinki, and all patients provided written informed consent for participation.

The inclusion criteria were: enlarged heart - all heart chambers had the potential to expand, especially the left ventricle, and were often accompanied by mitral and tricuspid regurgitation, and pulmonary hypertension; the left ventricular wall was thinner, the exercise ability and contraction ability were weakened, and the right ventricular wall might also have this symptom; imaging examination results showed that the left ventricular ejection fraction (LVEF) was less than 0.45, and the left ventricular short axis shortening rate (LCFS) was less than 0.25; when

Key words: strong ion gap; dilated cardiomyopathy; heart failure

Corresponding Author:
Dr Qingtao Han,
Interventional Vascular Department,
Zhangqiu District People's Hospital,
1920 Huiquan Road, Zhangqiu District,
Jinan 250200, China
e-mail: uxj39z@163.com

0393-974X (2020)
Copyright © by BIOLIFE, s.a.s.
This publication and/or article is for individual use only and may not be further reproduced without written permission from the copyright holder.
Unauthorized reproduction may result in financial and other penalties
DISCLOSURE: ALL AUTHORS REPORT NO CONFLICTS OF INTEREST RELEVANT TO THIS ARTICLE.

accompanied by impaired right ventricular function, the tricuspid annular plane systolic excursion (TAPSE) was less than 1.7 cm, and the right ventricular fractional area change (RVFAC) was less than 0.35 cm (6).

Patients were excluded if they had: other blood diseases, such as anemia, coagulopathy; pulmonary hypertension and pulmonary heart disease; malignant tumors; severe internal organ loss or dysfunction; could not receive normal treatment because of mental retardation, or allergy to commonly used drugs; pregnant women, older people and young children.

Case classification criteria

The American NYHA classification method was used to classify the patients into four categories according to the level of cardiac function, three of which have different degrees of heart failure (7). Patients with grade I cardiac function have normal heart reserves, general activity is not restricted, there are no adverse reactions such as dyspnea, and no signs of heart failure. Patients with grade II have mildly reduced heart function, slightly restricted physical activity, no adverse reactions at rest, difficulty in engaging in moderate or high physical labor, and slight signs of heart failure, such as increased heart rate, slight hepatomegaly, etc. The heart function of patients with grade III is moderately reduced, the physical activity is obviously restricted, and they can only engage in slight physical work; there are signs of heart failure such as hepatomegaly and edema, which belong to II-degree heart failure. Patients with grade IV with severely reduced heart function are difficult to engage in physical activity, and still have symptoms such as fatigue, dyspnea, and heartache at rest. They have obvious signs of heart failure and belong to grade III heart failure. The patients with grade I heart function were regarded as the control group, and the patients with other three grade were regarded as the heart failure group.

Observation index

Basic clinical data of patients were collected, including age, gender, body mass index (BMI), length of hospitalization, whether they had diabetes, hypertension, smoking habit, etc. Various biochemical indicators including C-reactive protein (CRP), serum natriuretic peptide (BNP) level, anion gap (AG), strong ion gap (SIG), tumor necrosis factor (TNF-α) levels and plasma Ang II levels were detected. Among them, AG refers to the difference between the sum of cations and the sum of anions in serum. It was calculated according to the content of Cl^-, Na^+, K^+, and HCO_3^- plasma in the serum. The formula is: $AG = Na^+ + K^+ - Cl^- - HCO_3^-$. The calculation formula of SIG is: $SIG = AG + K^+ - ALB\ (g/dL) \times (1.2 \times pH^{-6.15}) - PO_4^{3-}(mg/dL) \times (0.097 \times pH^{-0.13})$; $PO_4^{3-}\ (mg/dL) = P\ (mmol/L)/0.323$. ALB means albumin, and PO_4^{3-} means phosphate, P means phosphorus (8).

Statistical analysis

SPSS 19.0 software was used for statistical analysis. The measurement data such as age, hospitalization time, body mass index, CRP, BNP, AG and other biochemical test results were expressed by $(\bar{x}\pm s)$, and *t*-test was performed. The gender, diabetes cases, hypertension cases, etc. were represented by n%, and the χ^2 test was adopted. $P < 0.05$ was considered statistically significant. Univariate analysis and multivariate logistic analysis were used to determine independent risk factors. ROC curve was used to analyze each prognostic diagnostic index, the value of cut-off point (Cut Off) was selected and the area under ROC curve compared for sensitivity and specificity.

RESULTS

Comparison of the two groups of patients

Table I shows that the average age and BMI of patients in the heart failure group were higher than those in control group ($P<0.05$), indicating that both aging and obesity were more likely to cause heart failure. Diabetes and hypertension accounted for a higher proportion of patients with heart failure ($P<0.05$). There was no significant difference between the male-to-female ratio and the proportion of smokers in the two groups ($P>0.05$).

The results showed that BNP, AG, and SIG were significantly different between the two groups of patients, and the three indicators of patients with heart failure were significantly higher than those of the control group ($P<0.05$) (Table II). There was no significant difference between CRP, TNF-α and Ang II ($P>0.05$) (Table II).

Taking whether the patient had heart failure as a variable, the three sets of data of BNP, AG, and SIG were used as independent variables for analysis. It could be seen that the SIG value was a risk factor for

Table I. *Comparison of basic clinical data between two groups of patients*

Indicator	Heart failure (52 cases)	Control group (55 cases)	χ^2/t	*P*
Age	55.68±18.23	48.36±15.36	2.226	0.039
Gender Male	33	34	0.017	0.832
Gender Female	19	21		
BMI	30.21±4.36	27.09±3.56	2.036	0.042
Diabetes	20	12	4.029	0.036
Hypertension	42	39	5.369	0.009
Smoke	39	40	2.801	0.103

Table II. *Univariate analysis of various indicators of the two groups of patients*

Indicator	Heart failure	Control group	t	*P*
CRP (mg/L)	11.56±5.22	5.36±2.36	0.603	0.623
BNP (pg/mL)	2089.56±400.32	1719.56±403.26	2.284	0.022
AG (mmol/L)	16.28±3.98	10.39±4.02	2.507	0.014
SIG (mmol/L)	7.03±3.21	3.49±2.22	3.298	0.001
TNF-α (μg/L)	36.78±7.96	29.49±5.46	0.644	0.521
AngII (ng/L)	152.47±21.06	105.36±19.56	1.802	0.086

Table III. *Multivariate logistic regression analysis of heart failure in patients*

Indicator	β	Std	Wald χ^2	*P*	OR (95% CI)
BNP	0.041	0.033	0.272	0.359	1.598 (1.013-1.017)
AG	2.349	2.254	3.326	0.047	1.612 (1.009-1.014)
SIG	4.112	0.649	36.229	<0.001	1.206 (1.061-1.272)

Table IV. *Comparison of the predicted values of the three indicators of BNP, AG and SIG*

Indicator	Cutoff value	AUC	*P*	Sensitivity %	specificity %
BNP	1826.5	0.802	0.359	75.6	83.6
AG	12.36	0.774	0.047	72.3	78.6
SIG	6.03	0.926	<0.001	83.7	96.3

Table V. *SIG levels of each cardiac function group*

Indicator	I	II	III	IV
SIG (mmol/L)	3.49±2.22	4.62±2.16	6.61±2.36	8.42±3.06

heart failure in patients with cardiomyopathy ($P<0.05$) (Table III).

The comparison results of the parameters of ROC curve of BNP, AG and SIG are shown in Table IV. The sensitivity and specificity of BNP were 75.6% and 83.6%, respectively. At this time, the corresponding cutoff value is 1826.5, indicating that when BNP was higher than this value, the patient might have heart failure. The sensitivity and specificity of AG were 72.3% and 78.6%, respectively, and the cutoff value was 12.36. The sensitivity and specificity of SIG were 83.7% and 96.3%, respectively, and the cutoff value was 6.03, indicating that when the patient's SIG value was higher than 6.03, there was a risk of heart failure.

Comparison of SIG levels in various cardiac function groups

As shown in Table V, SIG levels in patients with dilated cardiomyopathy were generally higher than normal, and as the patient's heart function declines, the degree of heart failure worsens, and the measured value of SIG gradually increased.

DISCUSSION

Heart failure in patients with dilated cardiomyopathy is a common idiopathic disease. With the increase of the aging population in China, the incidence of heart failure has increased yearly, and it often causes a series of other diseases. From the data in Table I, the average age of patients with heart failure was significantly higher than in the control group. Therefore, the prediction of heart failure in patients with dilated cardiomyopathy is very important.

The traditional AG is calculated according to the content of various ions in the patient's blood. This calculation method ignores the impact of other charged substances in the blood, therefore the measurement results are not sufficiently accurate. However, SIG has a greater advantage in predicting serious diseases and human body acid-base disorders caused by complex etiology (9). BNP has great value in the diagnosis of cardiac function. It can accurately and sensitively reflect the function of myocardium, and plays a key role in the diagnosis and prediction of heart failure (10). In the present study, the BNP level of the heart failure group was significantly higher than that of the control group, which was proportional to the severity of heart failure. The SIG test has little effect on patient protein levels and drugs in the body, and the test results are more accurate and sensitive. It can also be seen from the data in Table IV that the sensitivity of the SIG test results was higher than the results of the two traditional test methods AG and BNP.

In summary, the SIG test results of patients with dilated cardiomyopathy were significantly higher than normal levels, and as the severity of heart failure in patients increased, SIG levels were also increased (Table V). Thus, SIG could accurately and sensitively predict the occurrence of heart failure in patients. The test is convenient and fast, which is very helpful for clinical diagnosis and treatment, and prediction of the patient's condition.

REFERENCES

1. Song Y, Chen X. Application of predictive nursing in patients with dilated cardiomyopathy. Chin J Doctor 2019; 33:284-86.
2. Meng Y, Chen H, Chen Y, Xie S. The comparison of blood glucose and serum lipid level between the patients with dilated cardiomyopathy and ischemic cardiomyopathy and its relationship with cardiac function. J Guangzhou Med Uni 2017; 35:38-40.
3. Fu W, Wang X, Qiu C. Risk factors for dilated cardiomyopathy complicated with coronary microvascular disease. Henan Med Res 2019;

28:1768-71.

4. Zhang Z, Hu W, Xidi C, Ye G, Xu S, Zhang Y, Ye L. Application of strong ion gap and other indicators in ICU. Int J Lab Med 2014; 35:1683-85.
5. Pei Y, Chen J, Gong J. Change of strong ion gap in chronic heart failure patients and its clinical significance. Chin J Geriatr Heart Brain Vessel Dis 2014; 16:475-77.
6. Zhang J, Cao K. Diagnosis and treatment of hypertrophic cardiomyopathy-expert consensus guidance from the American College of Cardiology / European Society of Cardiology and the American College of Cardiology. Chin J Cardiol 2005; 33:491-94.
7. Zhang Z, Zhong Y, Rao Q, Kuang J, Dong X, Lv Y, Li Y. Correlation between incidence of perioperative cardiac events and SHFM score in patients with chronic heart failure during noncardiac surgery. Academ J Guangzhou Med Uni 2017; 045:P.32-35.
8. Zhang Z, Ye G, Hu W, Chi X, Zhang Y, Chen L, Chen J. An application of SIG and other diadynamic criteria of acid-base derangements intrauma. J Med Res 2009; 38:123-25.
9. Wang S, Luo Y, Dai L, Zhang Y. Clinical Significance of SIG in patients with acute myocardial infarction. J Med Clin Res 2014; 31:903-07.
10. Sun T, Zhou J, Chen X, Tang Z, Jin Y. Relationship between brain natriuretic peptide and left ventricular remodeling in patients with heart failure secondary to dilated cardiomyopathy. J Med Res 2012; 41:62-64.

JOURNAL OF BIOLOGICAL REGULATORS & HOMEOSTATIC AGENTS Vol. 34, no. 4, 1493-1500 (2020)

LETTER TO THE EDITOR

Hematotoxicity and testicular injury induced by Bisphenol A in *Rattus norvegicus*

N. Hameed[1*], M.H. Abbasi[1,2], T. Akhtar[1,3] and N. Sheikh[1]

[1]Department of Zoology, University of the Punjab Lahore, Pakistan; [2]Department of Zoology, University of the Okara, Pakistan; [3]Department of Pharmacology, University of Health Sciences Lahore, Pakistan

Received April 18, 2020 – Accepted July 10, 2020

*This is a part of Ph.D research work of 1st author under the supervision of last author

To the Editor,

Endocrine disrupters are the chemicals that inhibit or induce change in normal hormonal function of the body and occurrence of these chemicals in the environment is perilous for both the environment and living organism in many respects. Currently, it has been reported that some synthetic chemicals act as endocrine disruptors and affect the reproductive system (1).

Bisphenol A (BPA) is a potential endocrine disruptor that is extensively used in manufacturing polycarbonate plastics and epoxy resins (2). It is a major constituent of several industrial products such as pesticides, plasticizers, paints, dental sealants and thermal stabilizers. Manufacturing, treatment and recycling of plastic and epoxy resins contaminate the ecosystem and food web by releasing its monomers (3). Humans are at high risk of BPA exposure because of leaching of BPA from metal cans to sources of food and water (4). BPA exposure primarily occurs through ingestion, although dermal and inhalation routes may also be a source of exposure, especially in occupational population (5). BPA is metabolized in the liver to form bisphenol A glucuronide and most of the time is excreted with urine (6). BPA inhibits the action of androgen by binding to its receptors. It can also interfere with the synthesis and clearance of hormone (7). It has been reported that reactive oxygen species (ROS) formed by oxidative stress of BPA by attacking DNA and cell membrane caused tissue damage in kidney, liver, brain and other vital organs (8).

Even low dose exposure to BPA may also be of concern as it interferes with metabolic processes and causes cardiovascular problems as well as damage to body tissues. This may alter the efficiency of food, protein, fat and carbohydrate metabolism (9). Currently, this chemical has attained great attention for its association with many health issues. Therefore, the current study evaluated the possible effect of BPA oral administration on hematological and serological parameters along with histopathological alterations in testis of male albino rats.

MATERIALS AND METHODS

Animals

Male Wistar rats (*Rattus norvegicus*) weighing 125-130g were used in the study. The colony of rats was raised in the Department of Zoology, University of the Punjab, Lahore. Rats were kept in well-aerated stainless steel wire cages and were kept in a controlled 12 h light/dark photoperiod at 23±2°C. All rats were fed with commercially available standard rat chow and were given fresh water *ad libitum*. All procedures relating to the use

Key words: bisphenol A; endocrine disruptor; hematology; histopathology; testosterone; toxicosis

Corresponding Author:
Professor Dr. Nadeem Sheikh, Department of Zoology,
University of the Punjab, P.O. Box No. 54590
Quaid-i-Azam Campus, Lahore, Punjab, Pakistan
Tel. Office: +92 42 99231246/812
Mobile: +92 322 4222 036
e-mail: s_nadeem77@yahoo.com

0393-974X (2020)
Copyright © by BIOLIFE, s.a.s.
This publication and/or article is for individual use only and may not be further reproduced without written permission from the copyright holder.
Unauthorized reproduction may result in financial and other penalties
DISCLOSURE: ALL AUTHORS REPORT NO CONFLICTS OF INTEREST RELEVANT TO THIS ARTICLE.

of experimental animals were performed in accordance with the institutional guidelines for the use and care of animals for research purposes.

Dose preparation and administration

To scrutinize the toxicity of BPA, the animals were randomly divided into five groups (n=8). Different doses of BPA were prepared freshly by dissolving it in corn oil. To induce chronic inflammation, the experimental rats were orally administered specific doses of BPA via oral gavage.

Control Group: The rats were put on commercially available standard rat chow and drinking water.

Group I rats were given 10mg/Kg/body weight/day of BPA for six weeks.

Group II rats were given 25mg/Kg/body weight/day of BPA for six weeks.

Group III rats were given 10mg/Kg/body weight/day of BPA for twelve weeks.

Group IV rats were given 25mg/Kg/ body weight/day of BPA for twelve weeks.

The animals were sacrificed after BPA exposure of 6 and 12 weeks.

Blood sampling and hormonal assay

After 12 hours of receiving the last dose, the animals were weighed and anesthetized with intra-peritoneal injection of ketamine and pyrogen free H_2O. The blood samples were collected by puncturing the heart with the help of sterilized disposable syringes. Blood samples of 3 ml of blood were collected from each rat for serum separation in an anticoagulant vacutainer. Blood samples were incubated for 2-3 h at room temperature and centrifuged for 10 min at 4000 rpm. Then supernatant designated as serum was collected in new eppendorf cups and stored in aliquots at -20^{o}C for hormonal assay. Serum level of testosterone was determined by ELISA kit (MyBiosource, Inc. cat.# MBS775388) according to the manufacturer's instructions.

Hematological assay was performed on SYSME KX-21 Haematology Analyzer of control animals and BPA-treated animals.

Histopathological analysis

Immediately after the blood samples were collected, testes were excised and weighed. A small part was preserved in 10% formalin and then dehydrated in serial dilution of ethanol. Xylene was used to clear tissues. Embedding was carried out in paraffin wax and blocks of tissue were prepared. Tissue sectioning was carried out by microtome. Hematoxylin and eosin stain was used for histological investigation of testes.

Statistical analysis

All collected data were analyzed by Graph Pad Prism 5 software. Statistical significance was calculated by one-way ANOVA test followed by Tukey's post hoc analysis.

RESULTS

Body weight was decreased significantly in the BPA-treated animals of group I (13.97%), II (17.15%), III (28.29%) and IV (29.62%) in comparison to the control group when analyzed by one way ANOVA followed by Tukey's post-hoc test (Fig. 1A). Paired testes weight showed a decreasing trend in the BPA-treated groups I, II, III and IV (20.99%, 25.22%, 35.23% and 37.06%), respectively in comparison to the control group. However, relative tissue weight index of testes had no significant difference in comparison with the control group (Fig. 1 B and C) (Table I).

Testosterone level in serum

Significant decrease in serum testosterone was observed in the BPA-treated groups when compared to the control group (Table II). Testosterone level in serum was significantly decreased in groups II (69.09%), III (58.18%) and IV (80%); group I testosterone level was also reduced when compared to the control group, although this drop was not statistically significant when analyzed by Tukey's post hoc test. A significant decrease was also noticed in groups II, III and IV as compared to group I of low-dose for 6 weeks ($p=0.0003$) when compared by one-way ANOVA (Fig. 1D).

Hematological findings

The red blood cell indices and platelet count of chronically exposed rats is presented in Table III. Significant reduction was observed in Hb level of group III (11.419%) and IV (16.955%) as compared to controls (Fig. 2A). Significant decrease was noted in total RBCs in the BPA-treated groups III (11.42%) and

IV (16.96%) (Fig. 2B).The percentage of RDW-CV of rats was decreased significantly in groups III and IV (7.12% and 9.62%), respectively (Fig. 2C). Hematocrit level was decreased significantly in groups III and IV (13.06% and 17.57%), respectively, compared to the control group, while a nonsignificant decrease was also observed in groups I and II (Fig. 2D). MCV was decreased significantly in groups III (4.546%) and IV (8.64%) in comparison to control animals (Fig. 2E). Significant decrease in MCH percentage value of groups II (5.842%) and IV (9.426%) was noticed while MCHC level was increased insignificantly (Fig. 2F). Platelet count was increased to 39.02% in group IV as compared to controls, whereas MPV decrease was also significant in group IV (19.69%) in comparison to control animals (Fig. 2G).

Effect of chronic exposure of BPA on total and differential leukocyte count

The total and differential leukocyte count of chronically exposed rats is shown in Table III. The WBC count was significantly increase in groups II, III and IV (87.96%, 98.27% and 126.82%), respectively, compared to the control group. Group I also showed an increase in WBC count, however this difference was statistically nonsignificant after analysis of Tukey's post-hoc test (Fig. 2H). Neutrophils exhibited a significant increase in BPA-treated groups III (326.04%) and IV (417.55%) in comparison to control animals (Fig. 2I). A statistically significant decrease in percentage value of lymphocytes was noticed in groups III and IV (9.02% and 11.765%) (Fig. 2J). Percentage value of monocytes declined significantly by 55.57% and 60% in BPA-treated groups III and IV, respectively (Fig. 2K). Eosinophils showed a significant decrease (56.05% and 69.23%) in groups III and IV as compared to controls due to BPA oral administration when analyzed by one-way ANOVA followed by row stats (Fig. 2L).

Histological examination

Testis sections of the control group animals

Table I. *Mean ± S.E.M of body weight (g), paired testes weight (g) and relative tissue weight index (g%) in the control and BPA-treated rats.*

Groups/Parameter	Body weight (g)	Testes weight (g)	RTWI (g %)
Con	340.0±10.00	3.548 ±0.15	1.043±0.04
Group I	292.5±11.50	2.803 ±0.11	0.958±0.04
Group II	281.7±8.29	2.653 ±0.19	0.941±0.07
Group III	243.8 ±6.06	2.298 ±0.12	0.942±0.05
Group IV	239.3 ± 6.56	2.233 ±0.16	0.933±0.07

Table II. *Mean±S.E.M of Serum testosterone level of control and BPA-treated groups.*

Parameter/Groups	Con	Group I	Group II	Group III	Group IV
Testosterone level (ng/ml)	0.275±0.005	0.235±0.005	0.085±0.015	0.115±0.005	0.055±0.025

Table III. *Mean±S.E.M of hematological parameters of control and BPA-treated groups.*

Parameter/Groups	Con	Group I	Group II	Group III	Group IV
Hemoglobin (g/dl)	14.65±0.48	14.00±0.24	13.93±0.37	12.85±0.44	11.25±0.75
RBC (x10^6/uL)	7.22±0.09	7.160±0.19	7.050±0.25	6.400±0.12	6.00±0.20
RDW-CV (%)	13.20±0.27	12.54±0.24	12.40±0.10	12.26±0.15	11.93±0.22
HCT (%)	42.64±0.47	41.23±1.05	40.85±1.85	37.07±0.64	35.15±3.75
MCV (fL)	61.15±0.45	60.53±0.41	58.80 ±0.39	58.37±0.40	55.87±0.79
MCH (pg)	20.37±0.42	20.03±0.22	19.18±0.18	19.60±0.17	18.45±0.55
MCHC (g/dL)	32.70±0.70	33.33±0.35	33.45±0.45	33.82±0.66	34.60±1.30
Platelets (x10^3/uL)	400.3±38.4	456.5±24.2	488.4±19.7	481±8.65	556.5±30.5
MPV (fL)	6.60±0.28	6.075±0.09	5.767±0.32	5.900±0.23	5.300±0.30
WBC (x10^3/uL)	5.533±0.73	9.800±0.50	10.40±0.90	10.97±1.11	12.55±0.45
Neutrophil (%)	3.333±0.33	3.500±0.96	4.500±0.50	14.20±0.74	17.25±1.32
Lymphocytes (%)	89.25±0.63	88.33±1.02	87.80±0.58	81.20±0.49	78.75±2.10
Monocytes (%)	3.00±0.32	2.167±0.17	1.667±0.33	1.333±0.33	1.200±0.20
Eosinophil (%)	6.500±0.50	6.333±0.33	6.00±0.20	2.857±0.59	2.000±0.58

showed normal tissue architecture with normal and active pattern of spermatogenesis. Seminiferous tubules exhibited clear lumen and were lined with germinal epithelium. The intact basement membrane was also observed in the control group. Leydig cells were organized in the interlobular area of seminiferous tubules. Degenerative changes in the germinal layer of BPA-treated rat seminiferous tubules as well as in Leydig cell were observed when compared to the control group. Mild-to-severe atrophy of seminiferous tubules, vacuolization and decrease in Leydig cell was seen as the dose of BPA increased. Seminiferous lumen filled with cellular debris and an irregular ruptured basement membrane and separation within the spermatogenic cells was also found in all BPA-treated groups. The testes of group IV animals showed extensive histopathological variations including atrophy, sloughing, loss of spermatogenesis, reduction in spermatogenic cells and poorly developed Leydig cells. Immature sperms were found in seminiferous tubules lumen. Loose intercellular bridges between the germ cells and Sertoli cells were found in all BPA-treated groups.

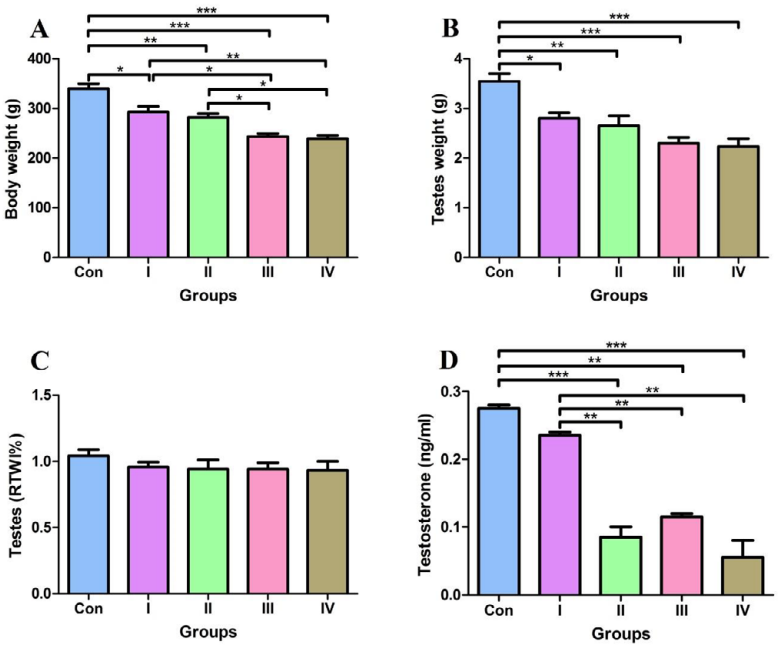

Fig. 1. *Alterations in body weight (**A**), testes weight (**B**), testes RTWI% (**C**) and serum testosterone level (**D**) of control group and BPA-treated groups; Group I and III (10mg/Kg/BW for six and twelve weeks, respectively) and Group II and IV (25mg/Kg/BW for six and twelve weeks, respectively). Values are mean ± S.E.M, standard error of mean represents by error bar. *P≤0.05, **P≤0.01, ***P≤0.001.*

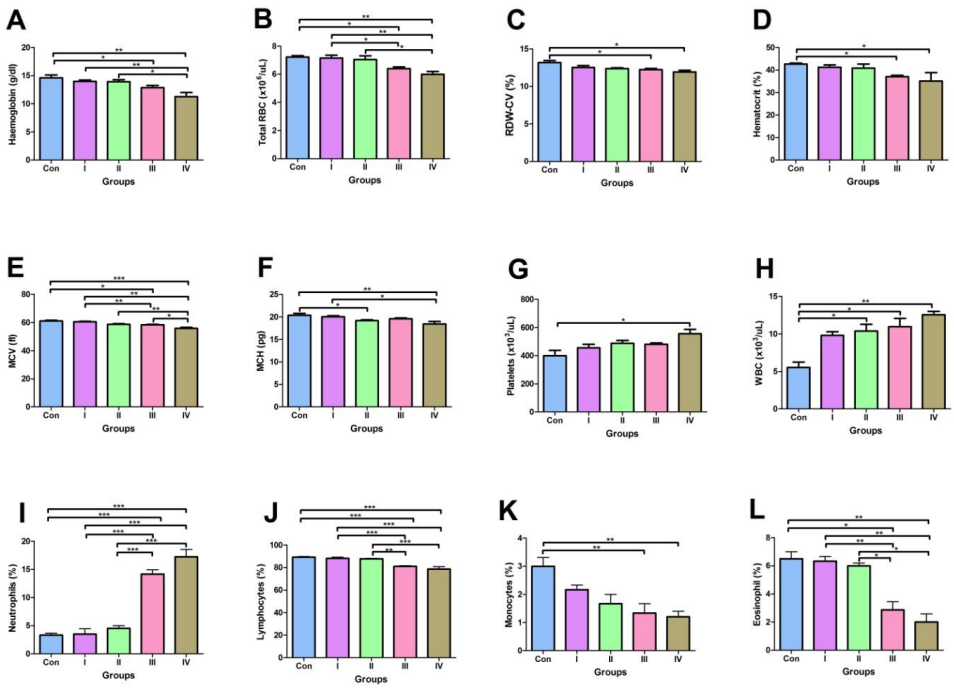

Fig. 2. *Chronic effect of BPA exposure on hematological parameters (**A**) Haemoglobin, (**B**) Total RBC, (**C**) RDW-CV, (**D**) Hematocrit, (**E**) MCV, (**F**) MCH, (**G**) Platelets, (**H**) WBC, (**I**) Neutrophils, (**J**) Lymphocytes, (**K**) Monocytes and (**L**) Eosinophils in adult male rats. Group I and II (10mg/Kg/BW for six and twelve weeks, respectively) and Group II and IV (25mg/Kg/BW for six and twelve weeks, respectively). Values are mean±S.E.M, standard error of mean represents by error bar.*P≤0.05, **P≤0.01, ***P≤0.001.*

DISCUSSION

The present study was outlined to evaluate BPA toxic effects on testes. Any disruption in spermatogenesis and steroidogenesis processes performed by testes will affect the reproductive system of males. BPA affected these processes and induced toxicity of the reproductive system. The body weight declined due to BPA oral administration showed changes in metabolic activity of rats. The present finding was supported by a previous study that showed rat body weight decreased after 1, 5 and 100mg/Kg/BW of BPA exposure (10). Paired and relative weight of testes declined significantly because of BPA chronic exposure and was associated with the decline in testosterone level and minute amount of germ cells. This suggests that maintenance and development of testes depends

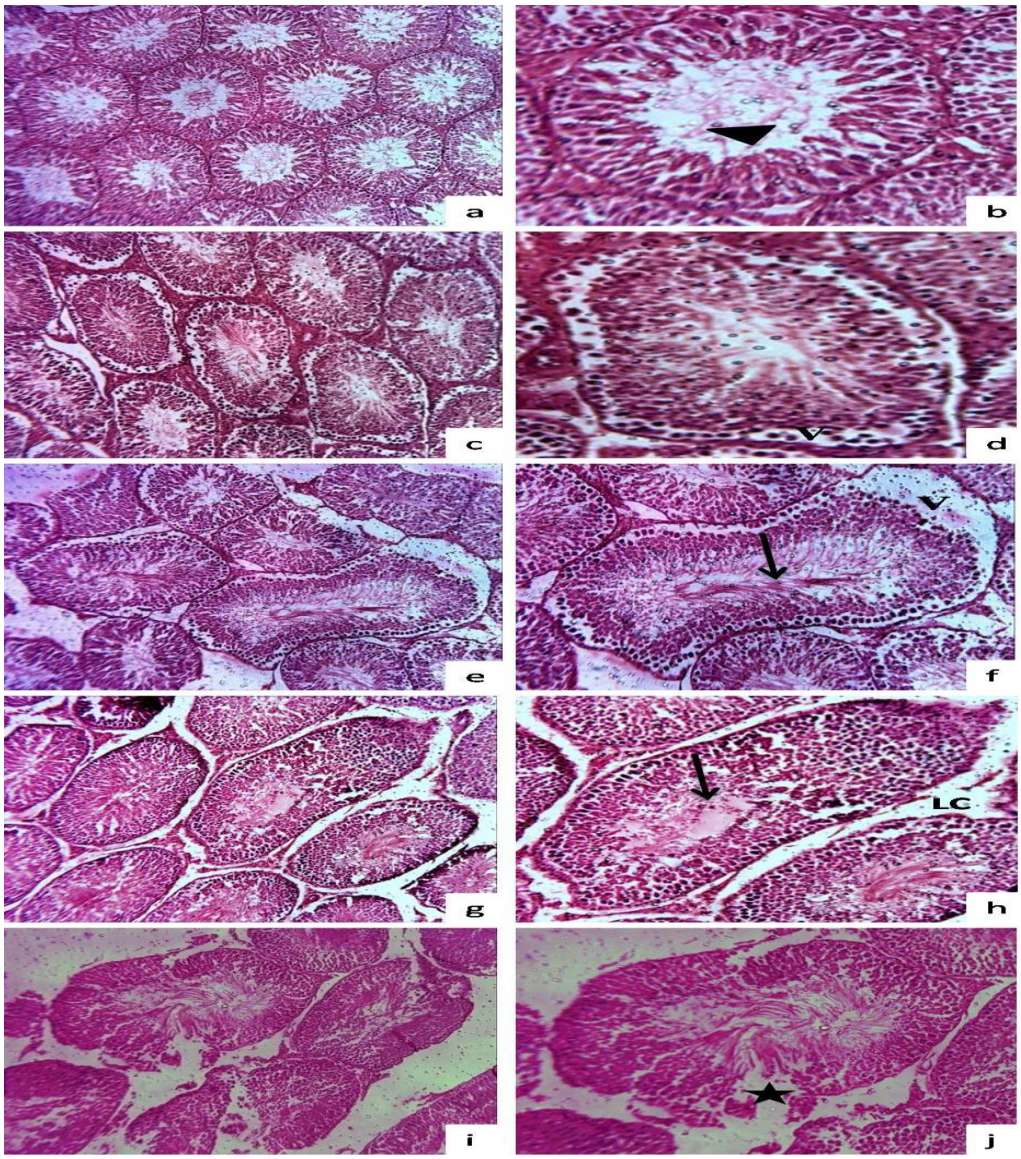

Fig. 3. *Hematoxylin and eosin staining of testes sections of BPA induced toxicity in Group I and III (10mg/Kg/BW for six and twelve weeks respectively) on 10X* ***(c, d, g, h)****. Group II and IV (25mg/Kg/BW for six and twelve weeks respectively) on 10X* ***(e, f, i, j)*** *and control sections* ***(a, b)*** *on 10X. Arrow head showing normal seminiferous tubules with active spermatogenesis, thin arrow showing lumen filled with cellular debris and immature germ cells, star showing sloughing of spermatogenic cells and ruptured basement membrane and LC showing poorly developed Leydig cells.*

on androgen. The same findings were found in the current investigation that testes absolute and relative weight declined significantly due to BPA low-dose exposure (11). The current findings agreed with another study in which testes weight decreased due to 20µg/Kg BW BPA exposure (12).

There was a significant decrease in the level of testosterone in all BPA-treated groups when compared to the control group. These results agree with findings of Gurmeet et al. (12) in which production of testosterone was dramatically suppressed. Testosterone plays an indispensable role to initiate the function of spermatogonia. There was a very low testosterone level in BPA-treated animals that caused the failure of spermatogenesis. This decrease might be linked with reduction in the number of Leydig cells because of oxidative damage and decreased activity of cytochrome P450 in the liver. Oxygen reactive species increased as a response to decline in the male specific cytochrome and destroyed the function of sperm (12). The decrease in hematological parameters of rats due to BPA chronic exposure may be due to hemolysis and shrinkage of RBCs by BPA, leading to a significant decrease in hematocrit value which causes anemia. The decrease rate of formation and increase destruction rate of RBCs might also be responsible for the decline in RBC count. The present findings are in agreement with previous studies (4). There was an increase in WBC count after chronic exposure of BPA that may be explained on the basis of the role of BPA in inflammation, or due to increased neutrophil percentage. This increase may be due to BPA-induced stress and activation of the immune system. This finding is in accordance with a previous study (13).

The decreased testosterone level and number of Leydig cells were also supported by histopathological study. The histopathological alterations in the current study indicated disruption in function and morphology of testes. It was noted that the process of spermatogenesis was affected in all the BPA-treated groups. Immature germ cells as well as degenerated germ cells were found in the lumen of seminiferous tubules. Vacuolization and ruptured epithelium were also observed. These results agree with the findings of Yousaf et al. (10). Significant decline in Leydig cell numbers might be the reason for these deformities. Testosterone is necessary for spermatogenesis and is also involved in further processing of spermatogenesis. As the spermatogenesis is suppressed due to decreased level of testosterone, the process of sperm formation is disrupted and causes infertility (14).

It can be concluded from the present investigations that BPA oral administration to adult male rats resulted in anemia and adverse effects on several hematological and hormonal parameters that indicates testicular injuries, which is confirmed by the histopathological changes.

ACKNOWLEDGEMENT

The authors acknowledge and are thankful to the Vice Chancellor, University of the Punjab, Lahore, Pakistan for providing funds for this study.

REFERENCES

1. Nah WH, Park MJ, Gye MC. Effects of early prepubertal exposure to bisphenol A on the onset of puberty, ovarian weights, and estrous cycle in female mice. Clin Exp Reprod Med 2011; 38:75-81.
2. Poormoosavi SM, Najafzadehvarzi H, Behmanesh MA, Amirgholami R. Protective effects of Asparagus officinalis extract against Bisphenol A-induced toxicity in Wistar rats. Toxicol Rep 2018; 5:427-33.
3. Ahmed WMS, Moselhy WA, Nabil TM. Bisphenol A toxicity in adult male rats: hematological, biochemical and histopathological approach. Glob Vet 2015; 14:228-38.
4. Vandenberg LN, Maffini MV, Sonnenschein C, Rubin BS, Soto AM. Bisphenol-A and the great divide: a review of controversies in the field of endocrine disruption. Endocr Rev 2009; 30:75-95.
5. Edres HA, Taha NM, Mandour AE-W, Lebda MA. Impact of L-Carnitine on Bisphenol A-induced kidney damage in rats. Alex J Vet Sci 2018; 56.
6. Pottenger LH, Domoradzki JY, Markham DA, Hansen SC, Cagen SZ, Waechter Jr JM. The relative bioavailability and metabolism of bisphenol A in rats is dependent upon the route of administration. Toxicol Sci 2000; 54:3-18.

7. Michalowicz J. Bisphenol A sources, toxicity and biotransformation. Environ Toxicol Pharmacol 2014; 37:738-58.
8. Mourad IM, Khadrawy YA. The sensetivity of liver, kidney andtestis of rats to oxidative stress induced by different doses of bisphenol A. Life Sci 2012; 2:19-28.
9. Hassan ZK, Elobeid MA, Virk P, Omer SA, ElAmin M, Daghestani MH, AlOlayan EM. Bisphenol A induces hepatotoxicity through oxidative stress in rat model. Oxid Med Cell Longev 2012: doi: 10.1155/2012/194829.
10. Yousaf B, Liu G, Wang R, et al. Bisphenol A exposure and healing effects of Adiantum capillus-veneris L. plant extract (APE) in bisphenol A-induced reproductive toxicity in albino rats. Environ Sci Pollut Res Int 2016; 23:11645-57.
11. Akingbemi BT, Sottas CM, Koulova AI, Klinefelter GR, Hardy MP. Inhibition of testicular steroidogenesis by the xenoestrogen bisphenol A is associated with reduced pituitary luteinizing hormone secretion and decreased steroidogenic enzyme gene expression in rat Leydig cells. Endocrinology 2004; 145:592-603.
12. Gurmeet KSS, Rosnah I, Normadiah MK, Das S, Mustafa AM. Detrimental effects of bisphenol A on development and functions of the male reproductive system in experimental rats. EXCLI J 2014; 13:151.
13. Abid QH, Hassan AH. Effect of Bisphenol-A-on some biochemical and hematological parameters of female rats (Rattus Norvegicus). Albahir J 2017; 6:33-40.
14. El Ghazzawy IF, Meleis AE, Farghaly EF, Solaiman A. Histological study of the possible protective effect of pomegranate juice on bisphenol-A induced changes of the caput epididymal epithelium and sperms of adult albino rats. Alex J Med 2011; 47:125-137.

LETTER TO THE EDITOR

Coronary thrombosis as an etiology of woven coronary artery

LL. Shi[1], WX. Peng[2], XZ. Hi[1], HL. Bi[1] and J. Li[1]

[1]Department of Cardiology, Zhuhai People's Hospital (Zhuhai hospital affiliated with Jinan University), Zhuhai, Guangdong Province, P.R. China; [2]Department of Nephrology, Zhuhai People's Hospital (Zhuhai hospital affiliated with Jinan University), Zhuhai, Guangdong Province, P.R. China

Received April 21, 2020 – Accepted July 10, 2020

To the Editor,

Woven coronary artery (WCA) is an extremely rare anomaly with unique properties on coronary angiograms. The coronary artery branches into twisted multiple thin channels which merge into a normal conduit in the distal segment. WCA was first described by Sane and colleagues (1) in 1988, and is typically classed as a congenital and benign abnormality (1, 2). Although it is reported that WCA may be associated with acute coronary syndromes, to date, WCA remains an angiographic diagnosis and its etiology remains unconfirmed. We report a case with a series of coronary angiograms, which demonstrates the evolution of a woven coronary artery.

Case presentation

A 60-year-old man was admitted to our hospital due to chest pain on the 25th July 2014. The pain had persisted for 23 hours. He was an ex-smoker that had quit 20 years previously. The following were measured upon examination: BP: 112/70mmHg, HR: 70bpm. TC: 3.94mmol/L, LDL-C: 2.56mmol/L, CTn-I: 5.45ug/L, FIB: 2.11g/L, D-dimer: 0.87mg/L, INR 1.02, BNP: 393.7pg/mL, Cr: 82umol/L. ECGs showed acute inferior myocardial infarction and CRBBB (Fig. 1A). UCG: post-inferior wall akinesia. EF 67%. CAG was performed. LCA was unremarkable. RCA was occlusive by the large levels of thrombus (Fig. 1B). The patient was left untreated until the symptoms relieved. After 23 hours, TIMI-III forward flow was achieved. He was discharged and prescribed warfarin and clopidogrel. Approximately 3 months later, the patient was re-admitted for angiogram follow-up and showed no symptoms. His examination parameters were as follows: TC: 3.06mmol/L, LDL-C: 1.76mmol/L, INR: 2.04, FIB: 2.47g/L. ECG: CRBBB (Fig. 1C). Angiography showed that the RCA was patent except for mild coronary ectasia (Fig. 2A). Following examination, warfarin was creased but the patient continued on aspirin medication. Approximately 4 months later, that patient was again admitted for syncope accompanied with incontinence. Angiography was re-performed. The LCA remained unremarkable, and a TIMI grade 1 collateral from the LCA to the distal RCA was observed (Fig. 2B). Thrombosis in the RCA was evident (Fig. 2C). Despite thrombus aspiration using a 6F EXPORT catheter and angioplasty with a 2.5x15 and 3.5x12 balloon, the flow recovered to TIMI-I. A large level of thrombus persisted in the vessel. (Fig. 3A). Warfarin plus aspirin were again prescribed and the patient began to feel better. Approximately 15 months later, angiography was performed during follow-up. Surprisingly, the RCA

Key words: woven coronary artery; coronary thrombosis; warfarin; aspirin

Corresponding Author:
Dr Jun Li,
Department of Cardiology, Zhuhai People's Hospital
(Zhuhai hospital affiliated with Jinan University),
79 Kangning Road, Zhuhai 519000,
Guangdong Province, P.R. China
e-mail: xuanchezhan35595@163.com

0393-974X (2020)
Copyright © by BIOLIFE, s.a.s.
This publication and/or article is for individual use only and may not be further reproduced without written permission from the copyright holder.
Unauthorized reproduction may result in financial and other penalties
DISCLOSURE: ALL AUTHORS REPORT NO CONFLICTS OF INTEREST RELEVANT TO THIS ARTICLE.

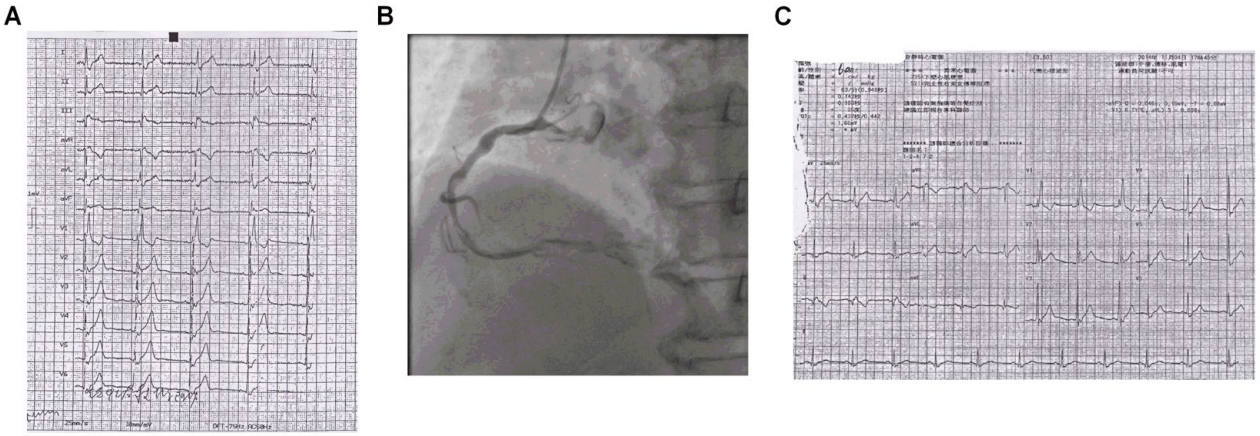

Fig. 1. ***A)*** *ECGs showed acute inferior myocardial infarction and CRBBB.* ***B)*** *RCA was occlusive by the large levels of thrombus.* ***C)*** *ECG: CRBBB.*

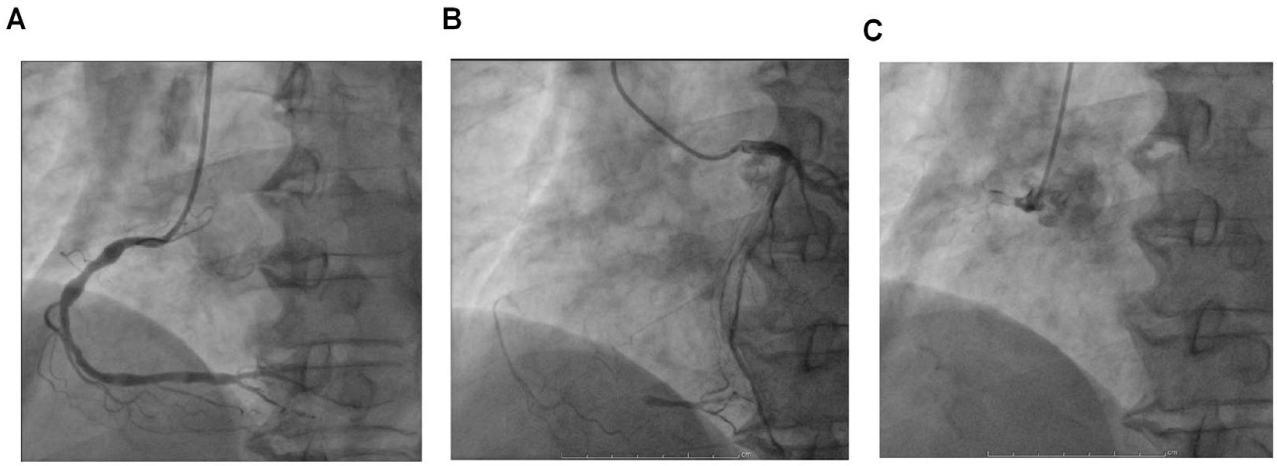

Fig. 2. ***A)*** *Left anterior oblique projection of right coronary artery was patent except for mild coronary ectasia.* ***B)*** *TIMI grade 1 collateral from the LCA to the distal RCA was observed.* ***C)*** *Thrombosis in the RCA was evident.*

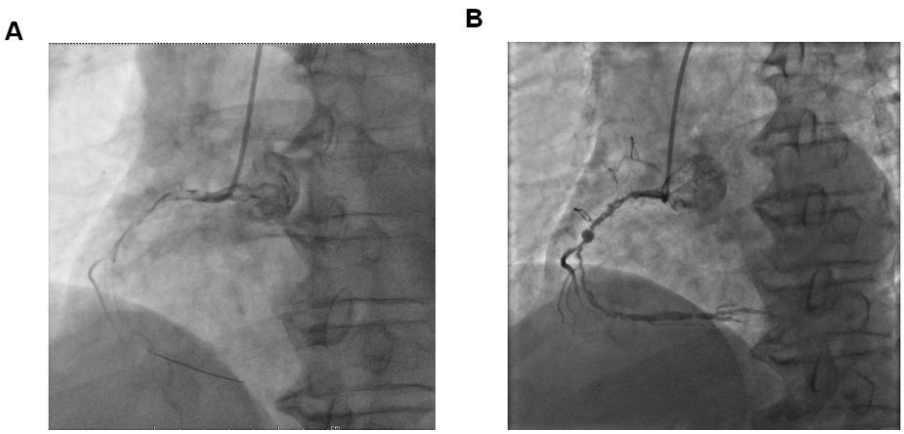

Fig. 3. ***A)*** *A large level of thrombus persisted in the vessel.* ***B)*** *Left anterior oblique projection of right coronary artery showing thin channels and distal reanastomosis.*

presented as a typical WCA (Fig. 3B) and the LCA remained unremarkable. Treatment with warfarin and aspirin was advised and no episodes of chest pain or syncope have been subsequently observed.
This study was approved by the Ethics Committee of Zhuhai People's Hospital. The patient signed the written informed consent.

DISCUSSION

As more cases of WCA are reported, its status as a rare abnormality is being challenged. Though it is classed as a congenital and benign abnormality, however, its relation to sudden death and acute coronary syndrome have been reported (3, 4). The case presented herein reveals the relationship between coronary thrombosis and WCA that is consistent with recent studies (5). Most importantly, abnormalities on OCT (6) and pathological examination have also been reported (7). No traces of thrombus or dissection flaps were observed. The woven channels were within the artery and had an endothelial lining as an innermost coat. There was a prominent thickening in the sub-endothelium which was composed of irregular fibrotic tissue. In this case, originally anticoagulation was effective as medical treatment until the patient stopped taking warfarin, and then the adverse event occurred. From these findings it is reasonable to speculate that WCA is not a congenital abnormality and coronary thrombosis may represent an etiology of WCA. This is most likely due to the characteristics of woven artery being due to recanalization of the thrombus.

The study was approved by the Ethics Committee of the Zhuhai People's Hospital. Signed written informed consents were obtained from the patients and/or guardians.

REFERENCES

1. Sane DC, Jr. HJV. "Woven" right coronary artery: A previously undescribed congenital anomaly. Am J Cardiol 1988; 61:1158-0.
2. Gregorini L, Perondi R, Pomidossi G, Saino A, Bossi IM, Zanchetti A. Woven left coronary artery disease. Am J Cardiol 1995; 75:311-12.
3. Val-Bernal JF, Malaxetxebarria S, González-Rodilla I, Salas-García M. Woven coronary artery anomaly presenting as sudden cardiac death. Cardiovasc Pathol 2016; 26:7-11.
4. Scharf RE. Woven coronary artery anomaly associated with acute coronary syndrome. Int J Angiol 2013; 22:055-58.
5. Soylu K, Meric M, Zengin H, Yüksel S, Kaya MG. Woven Right Coronary Artery. J Cardiac Surg 2012; 27:345-46.
6. Aitor U, Ricardo SR, Jaime E, Francisco FA. Pathological insights of a woven coronary artery with optical coherence tomography. Eur Heart J 2013; 38:3005
7. Abaci A, I.I G, Ozkan S, Cemri M, Yener A. Pathological examination of the woven coronary anomaly. Eur Heart J 2013; suppl_1. doi.org/10.1093/eurheartj/eht310.P5682

LETTER TO THE EDITOR

WTAP-mediated N6-methyladenosine modification on EGR3 in different types of epithelial ovarian cancer

Y. Fu[1] and XC. Jia[2]

[1]Department of Obstetrics and Gynecology, Jinshan Hospital, Fudan University, Shanghai, People's Republic of China; [2]Department of Ultrasonography, Jinshan Hospital, Fudan University, Shanghai, People's Republic of China

Received May 27, 2020 – Accepted July 13, 2020

To the Editor,

Ovarian cancer (OC) is the most lethal malignancy of the female genital tract, ranking the fifth leading cause of cancer deaths in women worldwide with more than 240,000 new cases in 2018 (1). Despite significant advances in surgery and chemotherapy, the curative trends and the 5-year survival rates are far from satisfactory. The poor clinical response and results are mainly due to the lack of early diagnosis as well as the frequent emergence of chemoresistance. Novel approaches and screening tools need to be developed for clinical diagnosis, and the molecular mechanisms underlying ovarian carcinogenesis also need to be deciphered to provide more therapeutic targets for OC treatment.

Epithelial OC (EOC) accounts for 85% of ovarian tumors and is generally in advanced stage at the time of diagnosis. EOC is typically classified into five histological subtypes (ranked by the frequency of morbidity): high-grade serous (HGSOC), endometrioid (EEC), clear cell (CCOC), low-grade serous (LGSOC) and mucinous (MOC). Although Wilms tumor 1-associated protein (WTAP) has been reported as a classical hallmark of the progression and metastasis of EOC and beneficial to EOC diagnosis and prognosis (2), the characteristics of WTAP expression in different subtypes of EOC are largely unknown. Moreover, WTAP has also been widely studied as a member of the nuclear multicomponent complex for N6-methyladenosine (m6A) methylation, which is the predominant internal chemical modification in eukaryotic mRNA and participates in various mRNA post-transcriptional regulations (3, 4). However, the role of m6A modification mediated by WTAP in EOC still remains unclear.

In the current study, the expression profile of WTAP in different subtypes of EOC cases was investigated and the relationship between WTAP and the tumor classification was analyzed *in vivo*. Furthermore, the biological functions of WTAP on m6A methylation in EOC tumorigenesis were also studied *in vitro*. The results provide illuminating insights into WTAP-mediated epigenetic regulation in EOC.

MATERIALS AND METHODS

Clinical specimen collection

A total of 122 EOC patients aged 59.74 ± 10.48 who received curative surgery between January 2015 and December 2019 at Jinshan Hospital were enrolled in this study. The clinical specimens included 49 HGSOC, 23 EEC, 20 CCOC, 15 LGSOC and 15 MOC. The tumor and

Key words: WTAP; m6A; epithelial ovarian cancer; EGR3

Corresponding Author:
Xiaochao Jia, MD,
No. 1508 Longhang Road,
Jinshan District, Shanghai,
201508, People's Republic of China
Tel.: +86 021 34189990.
e-mail: jiaxiaochao2020@163.com

0393-974X (2020)
Copyright © by BIOLIFE, s.a.s.
This publication and/or article is for individual use only and may not be further reproduced without written permission from the copyright holder.
Unauthorized reproduction may result in financial and other penalties
DISCLOSURE: ALL AUTHORS REPORT NO CONFLICTS OF INTEREST RELEVANT TO THIS ARTICLE.

adjacent tissues were subjected to protein detection. The clinic pathological information was harvested to analyze the correlation between WTAP and EGR3 expression. All the participants understood and signed the informed consent. The Ethics Committee of Fudan University approved of the study.

Immunohistochemistry (IHC) assay

Following fixation at 4°C overnight and paraffin embedding, the EOC tissues were sectioned at 2 to 4 μm thickness on a microtome. Immunohistochemistry was performed using WTAP and EGR3 primary antibodies working solution (1:1000, Abcam, Cambridge, MA, USA) and a REAL EnVision detection system (Dako; Agilent Technologies, Inc.) according to the manufacturer's instructions. Next, the sections were counterstained with hematoxylin and eosin (H&E) at room temperature for 10 min using an H&E staining kit (Solarbio, Beijing, China). Slides were independently examined using a microscope DM2000 (Leica Biosystems, Nussloch, Germany) with 400X magnification. The staining was scored semi-quantitatively and recorded based on both the cytoplasmic staining (0=negative, 1=1-25% immunoreactive cells, 2=26-50% immunoreactive cells, 3=51-75% immunoreactive cells, and 4=76-100% immunoreactive cells) and the staining intensity (0= negative, 1= weak, 2= moderate and 3= strong).

Cell culture

CRL-11731D (EEC), TOV-21G (CCOC) cell lines were obtained from American Type Culture Collection (ATCC, Manassas, VA, USA). CAOV3 (HGSOC), VOA5646 (LGSOC) and SKOV3 (MOC) were obtained from Type Culture Collection of the Chinese Academy of Sciences (Shanghai, China). Cells were cultured in DMEM medium with 10% FBS (Thermo Fisher Scientific, Waltham, MA, USA) at 37°C, 5% CO_2 and 100% humidity. The sequence of siRNA for WTAP (Genepharma, Shanghai, China) was 5'-GGUUCGAUUGAGUGAAACATT-3'. Human pcDNA3.1-EGR3 ectopic vector was purchased from Vigenebio (Jinan, Shandong, China). Plasmids and siRNA nucleotides were transfected into EOC cells using lipofectamine 3000 (Thermo Fisher Scientific) according to the manufacturer's instructions. Cells were harvested after 48 h transfection for the subsequent experiments. 20 mM cycloleucine (EMD Millipore, Billerica, MA, USA) were used to treat EOC cells for 6 h to reduce m6A methylation levels.

CCK-8 assay

EOC cells after 24-h transfection were cultured in 96-well plates with 80% density, then added with 10 μl CCK-8 solution (Solarbio) and incubated for additional 1 h. Absorption values of 450 nm were examined using Multiskan FC microplate reader (Thermo Fisher Scientific) to construct the regression equation and calculate IC50. The IC50 values were evaluated for the cell proliferation.

Transwell assay

1×10^5 cells were cultured within 200 μl suspension in upper and 800 μl fresh medium in lower Transwell chamber (Corning, New York City, NY, USA) on 24-well plates for 24 h. The cells in the lower chamber were cross-linked by 1% paraformaldehyde for 10 min and stained by 0.5% crystal violet (Sangon Biotech, Shanghai, China) for 5 min. The stained cells were counted under the fluorescence microscopy DM2000 (Leica Biosystems) to evaluate the cell invasion.

TUNEL assay

EOC cells were harvested by centrifugation, washed and resuspended into 1×10^7/mL in PBS, which was further transferred into 96-well plates (100 μl for each well) and fixed by 2% formaldehyde on ice for 15 min. After that, cells were washed by PBS and fixed with 70% ice-cold ethanol. 1×10^5 Cells were resuspended and gently mixed with 50 μl TdT equilibration buffer (Beyotime Biotechnology, Nantong, Jiangsu, China) at 37°C for 10 min. After washing twice with PBS, the cells were mixed with 100 μl TdT staining buffer at room temperature for 30 min in the dark, followed by the final PBS wash, then cells were attached to the coverslips using mounting medium (Beyotime Biotechnology) and examined under the fluorescence microscopy DM2000.

RNA immunoprecipitation (RIP) assay

Briefly, 1×10^7 EOC cells were harvested, resuspended in nuclear isolation buffer (1.28 M sucrose, 40 mM Tris pH 7.5, 20 mM MgCl2, 4% Triton X-100) and kept on ice for at least 30 min with frequent mixing. The pellet nuclei were centrifuged at 14000 rpm for 15 min, resuspended by wash buffer (150 mM KCl, 25 mM Tris pH 7.4, 5 mM EDTA, 0.5 mM DTT, 0.5% NP40, 100 U/ml RNAase inhibitor (Solarbo), 1×Protease inhibitors cocktail (Solarbo)). The chromatin was sheared through high-power sonication (5 s on, 30 s off) for 30 cycles. After that, 90% nuclei were

incubated with 1 μg m6A or WTAP antibodies (Abcam) overnight and 40 μl Protein A/G beads (Thermo Fisher Scientific) for 2 h by gentle rotation at 4°C while the rest of 10% were harvested as the input. The pellet beads were centrifuged at 3000 rpm for 3 min and washed three times. Both the input and pellet beads were purified by RNAiso plus (Takara, Kusatsu, Japan) and reverse transcription was conducted using QuantiTect Reverse Transcription Kit (Qiagen, Hilden, Germany).

Quantitative PCR (qPCR) assay

DNA templates obtained from RNA reverse transcription were used to detect the target gene transcription with the QuantStudio 3 system (Thermo Fisher Scientific). In accordance with the given instructions, 95°C for 30 s for initial denaturation, followed by 40 cycles at 95°C for 5 s, appropriate annealing temperatures of 10 s and 72°C, then 30 s were setup for PCR conditions. Ct values were harvested and calculated by the delta-delta method. The expression of GAPDH was used as the reference. The primers used in this study are listed in Table I.

Statistical analysis

The data are presented as the mean ± SEM. All statistical

Table I. *Primer sequences used in the study*

Symbol name	Primer sequences
WTAP	F:5'-AAGTCCAGCAGCCGAGCGTTGCCCAA-3'
	R:5'-CTTCTGTAAAGCCAACTCTGCTTCAA-3'
ABCD2	F:5'-TTGAAAGGATTATGTCTTCATACAAAGAG-3'
	R:5'-TTTTCCCACAACCATTGGGACCAGT-3'
ADAMTS5	F:5'-AAGAACGCTGCCACCACACTCAAGAACT-3'
	R:5'-ACAGTGAAGGCTGCGTGGAGGCCATCG-3'
CCL3	F:5'-CCCGGCAGATTCCACAGAATTTCAT-3'
	R:5'-GCACTCAGCTCCAGGTCGCTGACATAT-3'
EGR3	F:5'-CCCTATTACCCCTCTGGAGACCATC-3'
	R:5'-GGCCCGTGTGGATGCGCAGGTGCCGGGTC-3'
EMP1	F:5'-GGGGCCACCACACTGGTGTGCTGGCTGTGC-3'
	R:5'-CCAGATTCAACGGCTTCCTCCTCC-3'
FEZ1	F:5'-ACCGAGAACCTAGCTCCCGTGAAGAAC-3'
	R:5'-CCTGATCTGCTGTGAGCAGAGGCTCCTCG-3'
FREM1	F:5'-TAACTGTATTCTCCAGGCAGCACATGC-3'
	R:5'-TCCAAGCTTGGAGCGTTGAGAGGG-3'
PDGFRA	F:5'-GATCACCACTGATGTGGAAAAGATTCA-3'
	R:5'-GCACCTCACCGTCTGTCCCCCAGTTGA-3'
TP73	F:5'-GCCCTACGCACAACCCAGCTCCACCTT-3'
	R:5'-CTTGTAAACAGGCATGGCCCTTATGGC-3'
WNT2B	F:5'-TGTATATGCCATCTCATCAGCAGGGGT-3'
	R:5'-CTCCAGCTTCAGAAACCGCCGCACAG-3'
GAPDH	F:5'-GGTGAAGGTCGGAGTCAACG-3'
	R:5'-CAAAGTTGTCATGGATGACC-3'
ABCD2 for RIP assay	F:5'-ATATTGTGAAATTTTCAAAACCAAT-3'
	R:5'-AATTCATAAGGAATGATGAGTTCAAGTAAAT-3'
EGR3 for RIP assay	F:5'-TTTAAAAAAAAAAAGCAACAAAA-3'
	R:5'-TGGGGAATGAUATTTTTTGAAAGAC-3'
FREM1 for RIP assay	F:5'-TCTGTGAATATTGCTCCATAGAAAACAA-3'
	R:5'-ACAAAAATTGTATCTTATCTTGTAAAAA-3'

analyses were performed using SPSS 20.0 statistical software. Kaplan-Meier was used to analyze the relationship between WTAP expression and cancer patients' survival status. COX regression model was used to analyze the factors associated with clinical outcomes of EOC. The group comparisons were performed with One-way ANOVA. A *p*-value less than 0.05 was considered statistically significant.

RESULTS

Characterization of WTAP expression in EOC in vivo

To clarify the role of WTAP in different subtypes of EOC *in vivo*, the protein level of WTAP in 122 human EOC samples (including 49 HGSOC, 23 EEC, 20 CCOC, 15 LGSOC and 15 MOC) were investigated using IHC assay. The expression of WTAP was markedly higher in HGSOC, LGSOC and MOC, and slightly higher in CCOC and EEC compared to the corresponding adjacent tissues (Fig. 1 A, B). Moreover, the relationship between WTAP expression and clinical pathological features was investigated. Due to the relatively large sample size, we divided the tumor pathological grading of samples into two classes of low (stages I, II) and high (stages III, IV) and observed that WTAP expression was positively correlated with tumor

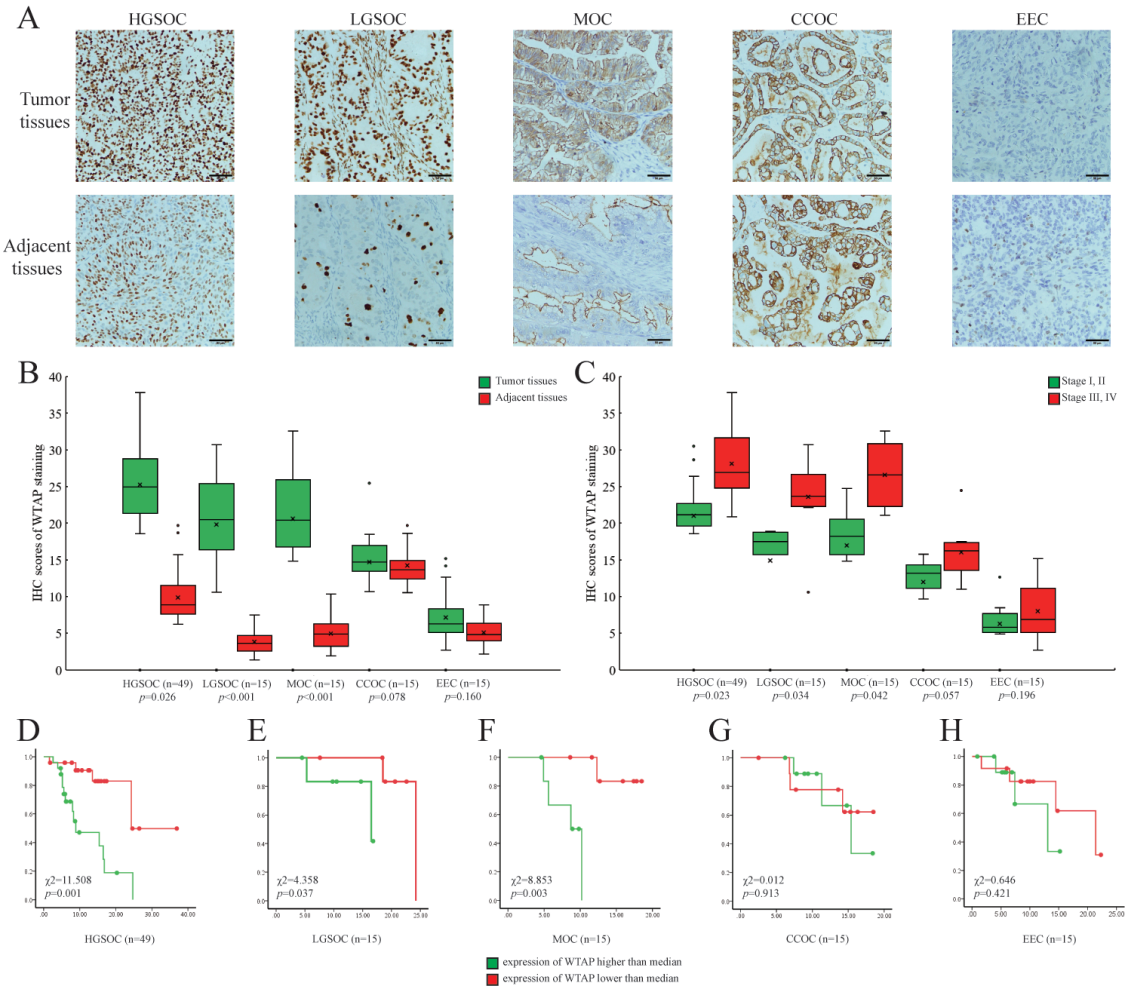

Fig. 1. *The relationship between WTAP expression and clinical outcomes of EOC.* ***A)*** *Representative IHC images of WTAP staining in different subtypes of EOC and adjacent tissues (scale bar 50 μm; magnification 400X).* ***B)*** *IHC scores of WTAP staining in 122 pairs of EOC tissues.* ***C)*** *IHC scores of WTAP staining in different stages of EOC.* ***D-H)*** *Kaplan-Meier analysis of overall survival of different subtypes of EOC with WTAP expression. HGSOC, LGSOC, MOC, CCOC and EEC are abbreviated as high-grade serous, low-grade serous, mucinous, clear cell and endometrioid ovarian cancer.*

malignancy in HGSOC, LGSOC and MOC (Fig. 1C). Furthermore, Kaplan-Meier analysis showed that WTAP expression was associated with poor overall survival of patients with HGSOC, LGSOC and MOC (Fig. 1D-F), but not with CCOC and EEC (Fig. 1 G, H). Furthermore, WTAP expression was

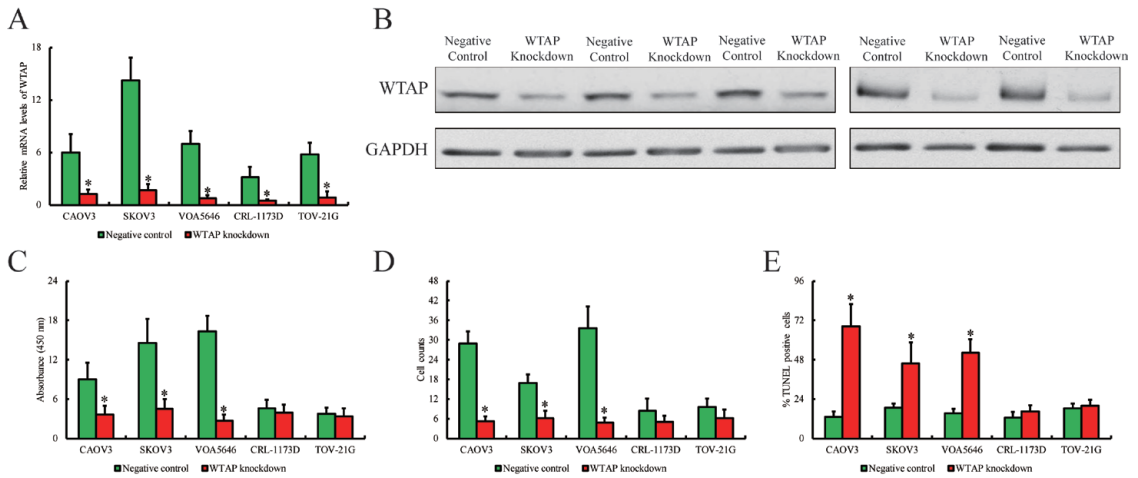

Fig. 2. *The oncogenic effects in EOC cells regulated by WTAP. The mRNA (**A**) and protein (**B**) levels of WTAP detected in different types of EOC cells treated with WTAP knockdown. CCK-8 (**C**), Transwell (**D**) and TUNEL (**E**) assays applied to investigate the cell proliferation, migration and apoptosis in different types of EOC cells treated with WTAP knockdown. Data are presented as the mean ± standard error of the mean of three individual experiments. *p<0.05 vs negative control group.*

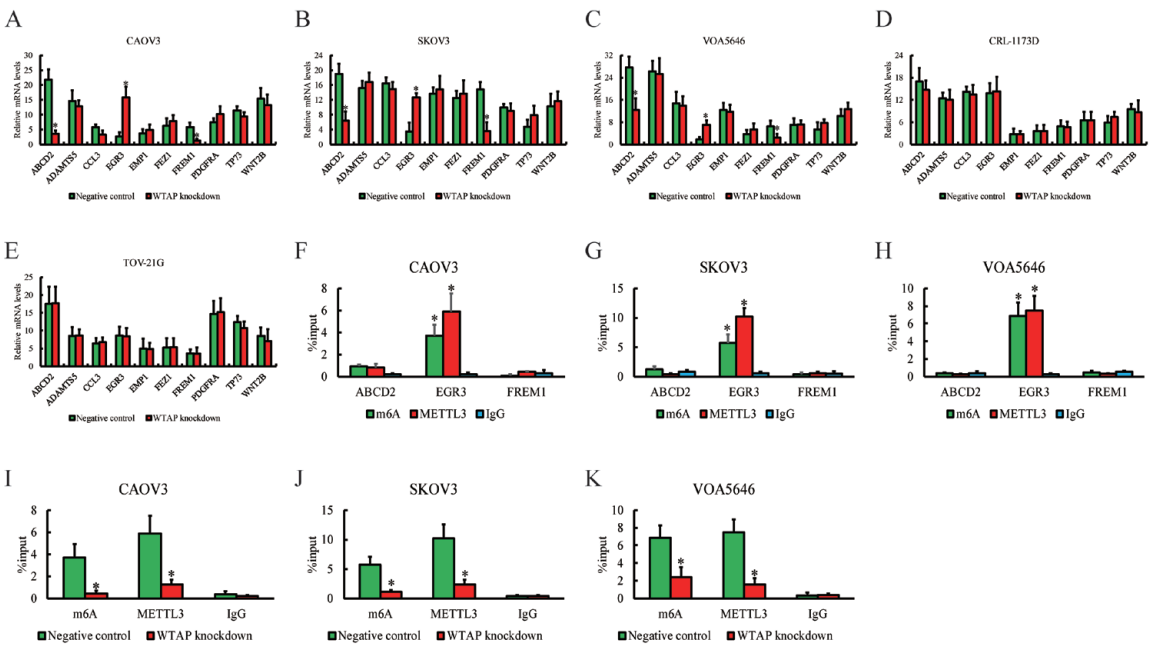

Fig. 3. *m6A methylation of EGR3 regulated by WTAP. **A-E**) The transcription of ABCD2, ADAMTS5, CCL3, EGR3, EMP1, FEZ1, FREM1, PDGFRA, TP73 and WNT2B in different types of EOC cells treated with WTAP knockdown. **F-H**) RIP assay applied to investigate the m6A enrichment and METTL3 binding on the mRNA of ABCD2, EGR3 and FREM1 in CAOV3, SKOV3 and VOA5646 cells. (I-K) RIP assay applied to investigate the m6A enrichment and METTL3 binding on EGR3 in in CAOV3, SKOV3 and VOA5646 cells with WTAP knockdown. Data are presented as the mean ± standard error of the mean of three individual experiments. *p<0.05 vs negative control group.*

observed to be an independent prognostic factor for tumor grading (HR=2.865, 95% CI=1.123-4.471, p=0.0014) and overall survival (HR=3.516, 95% CI=2.697-8.754, p=0.0036) in EOC patients. Taken together, we concluded that the expression of WTAP is significantly higher in HGSOC, LGSOC and MOC and its aberrant expression is closely related to the poor prognosis of EOC.

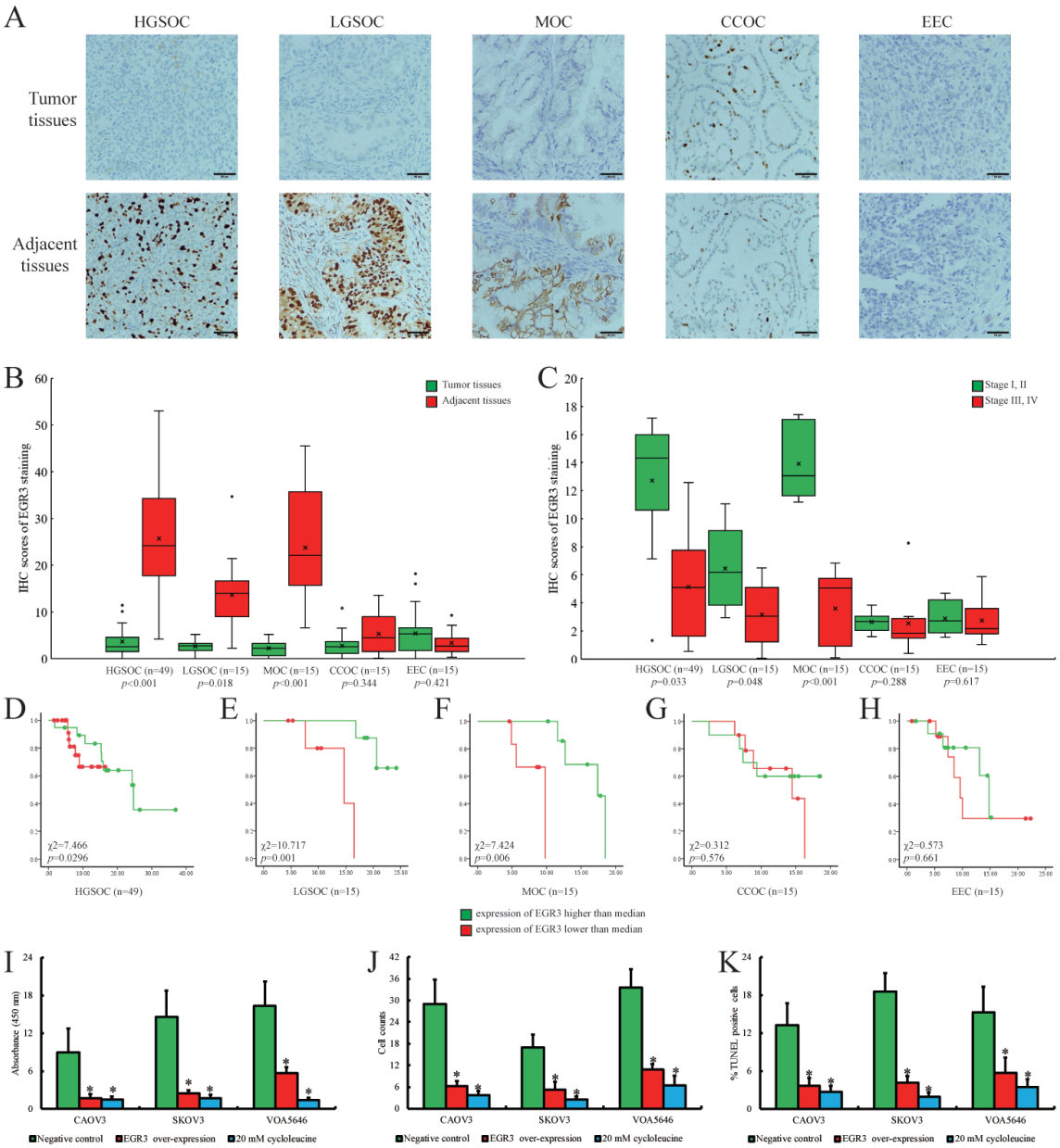

Fig. 4. *The tumor suppressive role of EGR3 in EOC in vivo and in vitro. **A**) Representative IHC images of EGR3 staining in different subtypes of EOC and adjacent tissues (scale bar 50 μm; magnification 400X). **B**) IHC scores of EGR3 staining in 122 pairs of EOC tissues. **C**) IHC scores of EGR3 staining in different stages of EOC. **D-H**) Kaplan-Meier analysis of overall survival of different subtypes of EOC with EGR3 expression. CCK-8 (**I**), Transwell (**J**) and TUNEL (**K**) assay applied to investigate the cell proliferation, migration and apoptosis in CAOV3, SKOV3 and VOA5646 cells treated with EGR3 over-expression or cycloleucine. Data are presented as the mean ± standard error of the mean of three individual experiments. *p<0.05 vs negative control group.*

Oncogenic role of WTAP in EOC cell lines in vitro

Next, the effects of WTAP on EOC tumorigenesis and development were investigated *in vitro*. Knockdown of WTAP was carried out in different subtypes of EOC cell lines including CAOV3 (HGSOC), CRL-11731D (EEC), VOA5646 (LGSOC), TOV-21G (CCOC), and SKOV3 (MOC) (Fig. 2 A, B). Compared to the corresponding negative controls, the capacities of cell proliferation and migration after WTAP deficiency were significantly reduced in CAOV3, SKOV3 and VOA5646, but stayed unchanged in CRL-11731D and TOV-21G cells (Fig. 2 C, D). Consistently, cell apoptosis was significantly enhanced by WTAP knockdown in CAOV3, SKOV3 and VOA5646, but did not change in CRL-11731D and TOV-21G cells (Fig. 2E). Taken together, WTAP performed an oncogenic function specifically in HGSOC, LGSOC and MOC of EOC.

Elevated m6A methylation of EGR3 regulated by WTAP in EOC

To investigate the mechanisms responsible for the distinct effects of WTAP on different subtypes of EOC, we searched the potential targets of WTAP from RNA-seq data of hepatocellular carcinoma cells with WTAP knockdown in a previous study (5) and picked out the top ten genes dysregulated by WTAP deficiency for further investigation in our systems. These 10 genes, reported to be associated with ovarian cancer, are listed as follows: ATP binding cassette subfamily D member 2 (ABCD2), A disintegrin and metallopeptidase with thrombospondin motif 5 (ADAMTS5), C-C motif chemokine ligand 3 (CCL3), early growth response 3 (EGR3), Epithelial membrane protein 1 (EMP1), Fasciculation and elongation protein zeta 1 (FEZ1), FRAS1-related extracellular matrix protein (FREM1), Platelet derived growth factor receptor alpha (PDGFRA), tumor protein p73 (TP73), Wnt family member 2B (WNT2B). We observed that the expressions of ABCD2, EGR3 and FREM1 were significantly impacted by WTAP knockdown in CAOV3, SKOV3 and VOA5646 cells (Fig. 3 A-C). None of these genes changed their expression in CRL-11731D and TOV-21G cells (Fig. 3 D, E). Given the essential role of WTAP in stabilizing m6A methyltransferase complex (METTL3, METTL14 and WTAP), we further studied m6A methylation and METTL3 binding of these target genes using RIP-assay. Only EGR3 was robustly bound by METTL3 and enriched in m6A methylation at the 3' UTR (Fig. 3 F-H) predicted by SRAMP tool (http://www.cuilab.cn/sramp), which was reversed after WTAP knockdown in CAOV3, SKOV3 and VOA5646 cells (Fig. 3I-K). Nevertheless, although we also observed the certain m6A methylation and slight METTL3 interaction on EGR3 in CRL-11731D and TOV-21G cells, we failed to find any changes after WTAP knockdown (data not shown). Taken together, the outcomes above suggested that WTAP partook in m6A methylation of EGR3 at least in several types of EOC.

Tumor suppressive role of EGR3 in EOC

Finally, the expression of EGR3 and the relationship with EOC was identified *in vivo*. Consistent with the *in-vitro* study, the repression of EGR3 expression was observed in HGSOC, LGSOC and MOC compared to the corresponding adjacent tissues (Fig. 4A). Moreover, EGR3 expression was negatively correlated with tumor malignancy (Fig. 4B) in HGSOC, LGSOC and MOC. Likewise, increased EGR3 expression was positively correlated with overall survival of patients with HGSOC, LGSOC and MOC (Fig. 4 E-G). Additionally, CAOV3, SKOV3 and VOA5646 cells with EGR3 ectopic expression or cycloleucine (m6A methylation inhibitor) treatment displayed a phenotype of compromised cell growth and migration as well as enhanced cell apoptosis (Fig. 4 H-J). Therefore, the expression of EGR3 exerted a suppressive role in the progression of EOC regulated by the WTAP/m6A-mediated manner.

DISCUSSION

Growing evidence suggests that the abnormal regulation of RNA m6A methylation profoundly contributes to carcinogenesis (6, 7). WTAP, one of the m6A methylases, has been found to be highly expressed in multiple cancers (8). In this study, we revealed that WTAP is indeed highly expressed in HGSOC, LGSOC and MOC but not in CCOC and EEC compared to the adjacent tissues, which is an interesting discovery. The methylation eraser METTL3

can play a role in translational control independent of METTL14 and WTAP (9), and our RIP-qPCR results also demonstrated that WTAP knockdown cannot change the interaction of METTL3 with EGR3 mRNA, indicating that WTAP may be dispensable for m6A modification in CCOC and EEC. Indeed, WTAP expression is a potential biomarker to partially discriminate subtypes of EOC. Furthermore, we demonstrated that WTAP plays an oncogenic role in HGSOC, LGSOC and MOC, which is consistent with previous studies on bladder cancer (10), HGSOC (11) and liver cancer (5). WTAP primarily functions as a scaffold to coordinate METTL3 and METTL14 in m6A methylase complex for RNA processing. Therefore, highly expressed WTAP may result in the excessive m6A methylation on whole transcriptome, leading to the dysregulated post-translational modification on the target oncogenes, such as EGR3. Overall, our study determines that the highly expressed WTAP indicates poor malignancy and survival of serous and mucinous EOC, and should be considered as a potential hallmark for EOC subtype diagnosis. WTAP promotes the aberrant mRNA methylation and suppresses the final transcription and translation of the target gene EGR3.

ACKNOWLEDGEMENTS

This project is supported by Jinshan Hospital (grant number. JYQN-LC-202009).

REFERENCES

1. Stewart C, Ralyea C, Lockwood S. Ovarian cancer: an integrated review. Semin Oncol Nurs 2019; 35:151-56.
2. Wu LS, Qian JY, Wang M, Yang H. Identifying the role of Wilms tumor 1 associated protein in cancer prediction using integrative genomic analyses. Mol Med Rep 2016; 14:2823-31.
3. Zhao BS, Roundtree IA, He C. Post-transcriptional gene regulation by mRNA modifications. Nature reviews. Mol Cel Biol 2017; 18:31-42.
4. Ma XX, Cao ZG, Zhao SL. m6A methyltransferase METTL3 promotes the progression of prostate cancer via m6A-modified LEF1. Eur Rev Med Pharmacol Sci 2020; 24:3565-71.
5. Chen Y, Peng C, Chen J, et al. WTAP facilitates progression of hepatocellular carcinoma via m6A-HuR-dependent epigenetic silencing of ETS1. Mol Cancer 2019; 18:127.
6. Pan Y, Ma P, Liu Y, Li W, Shu Y. Multiple functions of mA RNA methylation in cancer. J Hematol Oncol 2018; 11:48.
7. Sun T, Wu R, Ming L. The role of m6A RNA methylation in cancer. Biomed Pharmacother 2019; 112:108613.
8. Deng X, Su R, Weng H, Huang H, Li Z, Chen J. RNA N-methyladenosine modification in cancers: current status and perspectives. Cell Res 2018; 28:507-17.
9. Barbieri I, Tzelepis K, Pandolfini L, et al. Promoter-bound METTL3 maintains myeloid leukaemia by mA-dependent translation control. Nature 2017; 552:126-31.
10. Chen L, Wang X. Relationship between the genetic expression of WTAP and bladder cancer and patient prognosis. Oncol Lett 2018; 16:6966-70.
11. Yu HL, Ma XD, Tong JF, Li JQ, Guan XJ, Yang JH. WTAP is a prognostic marker of high-grade serous ovarian cancer and regulates the progression of ovarian cancer cells. Onco Targets Ther 2019; 12:6191-201.

LETTER TO THE EDITOR

LncRNA FBXL19-AS1 promotes the development of gastric cancer by regulating miR-876-5p/HMGB3 axis

R-X. Ji[1], F. Ren[1], X-Q. Liu[2] and X. Yuan[1]

[1]Department of Gastroenterology, Qingdao Hospital of Traditional Chinese Medicine, Qingdao Hiser Medical Group, Qingdao, Shandong Province, China; [2]Department of Ophthalmology, Qingdao Hospital of Traditional Chinese Medicine, Qingdao Hiser Medical Group, Qingdao, Shandong Province, China

Received April 29, 2020 – Accepted July, 2020

To the Editor,

Gastric cancer (GC) has a high morbidity and mortality rate in the world, especially in East Asia. Risk factors for GC include smoking, and atrophic gastritis, all of which are considered to be the cause of GC (1). Despite many achievements in diagnosis and treatment, the 5-year survival rate of GC patients is still poor. In addition, the pathogenesis of GC is complex, and the basic mechanism of GC initiation and progression remains largely unknown, therefore, it is essential to determine new effective targets for diagnosis and treatment.

Long noncoding RNA (lncRNA) is a RNA transcript that is more than 200 nucleotides in length and is associated with tumorigenesis in a variety of cancers, including GC. For example, knockdown of TPT1-AS1 inhibited cell proliferation, cell cycle G1/S transition, and epithelial–mesenchymal transition in GC (2). LncRNA FBXL19-AS1 has been found to promote cell proliferation and metastasis in non-small cell lung cancer via regulating epithelial-mesenchymal transition (3), and FBXL19-AS1 could promote breast cancer cell proliferation and inhibit apoptosis via miR-876-5p/FOXM1 axis (4). However, the relationship between lncRNA FBXL19-AS1 and miR-876-5p in GC remains unclear.

Here, high mobility group box 3 (HMGB3) is predicted as a potential target for miR-876-5p. To our knowledge, the relationship between HMGB3 and miR-876-5p or lncRNA FBXL19-AS1 in GC has not yet been reported. This study therefore aims to elucidate the regulatory mechanism of lncRNA FBXL19-AS1/miR-876-5p/HMGB3 in GC.

MATERIALS AND METHODS

From February 2017 to January 2019, tumor tissues and adjacent normal tissues were obtained from 64 GC patients in Qingdao Hospital of Traditional Chinese Medicine, and stored at −80°C. Patients who had received radiotherapy or chemotherapy were excluded from the study. All patients provided written informed consents. This study was approved by the Institutional Ethics Committee of Qingdao Hospital of Traditional Chinese Medicine.

Cell culture and transfection

Human gastric mucosal epithelial cells GES-1 and GC cells AGS were purchased from BeNa Culture Collection (BNCC, Beijing, China). All cells were maintained in DMEM medium with 10% FBS (Gibco, Grand Island, NY, USA) and cultured in an atmosphere with 5% CO_2 at 37°C.

FBXL19-AS1 siRNA and vector, miR-876-5p mimics

Key words: FBXL19-AS1; gastric cancer; miR-876-5p; HMGB3

Corresponding Author:
Dr Xue Yuan,
Qingdao Hospital of Traditional Chinese Medicine,
Qingdao Hiser Medical Group,
No. 4 Renmin Road, Shibei District, Qingdao,
266031, Shandong Province, China
Tel.: +86 0532-83777527
e-mail: xinliangu95778@163.com

0393-974X (2020)
Copyright © by BIOLIFE, s.a.s.
This publication and/or article is for individual use only and may not be further reproduced without written permission from the copyright holder.
Unauthorized reproduction may result in financial and other penalties
DISCLOSURE: ALL AUTHORS REPORT NO CONFLICTS OF INTEREST RELEVANT TO THIS ARTICLE.

or inhibitor, HMGB3 siRNA were obtained from Sangon Biotech Co., Ltd (Shanghai, China). Next, they were transfected into AGS cells using Lipofectamine 2000 (Invitrogen/Thermo Fisher Scientific), respectively. Cells without transfection were regarded as blank control (NC).

RT-qPCR

Total RNA was extracted from GC tissues and cells using TRIzol reagent (Invitrogen, USA). Reverse transcription was performed using a Reverse Transcription Kit (Takara, Otsu, Japan). SYBR® Premix DimerEraser Kit (TaKaRa) and primers were used for RT-qPCR. GAPDH and U6 were used as internal controls for lncRNA/mRNA and miRNA, respectively. Their expressions were quantified with the $2^{-\square\square cq}$ method. The primers sequences were the following: GAPDH forward, 5'-ACA ACT TTG GTA TCG TGG AAG G-3', and reverse, 5'-GCC ATC ACG CCA CAG TTT C-3'; FBXL19-AS1 forward,5'-TCC TCC AGC GTC TGT TAC-3', and reverse, 5'-TCC ATT TGC ATA GGC AGT-3'; miR-876-5p forward: 5'-ACU UAA UGA AAC AUU UGG UGG U-3', Reverse: 5'-TGU UTT UCT TTG TUU UCC UCC U-3'; HMGB3 forward: 5'-GAC CAG CTA AGG GAG GCA A-3', Reverse: 5'-ACA GGA AGA ATC CAG ACG GT-3'; U6 forward: 5'-GCT TCG GCA GCA CAT ATA CTA AAA T-3' and reverse, 5'-CGC TTC ACG AAT TTG CGT GTC AT-3'.

MTT assay

The transfected AGS cells were seeded into 96-well plates (5×10^3 cells/well) and cultured at 37°C for 0, 24, 48, and 72 h, respectively. Cells were incubated with MTT (5 mg/mL, Sigma, San Antonio, TX, USA) for 4 h. Then, the reaction was terminated using DMSO (150 μL/well). Cell viability was determined by measuring the optical density (OD) value at 490 nm with a microplate reader (Bio-Rad, Hercules, CA, USA).

Transwell assay

Transwell assay was used to detect cell migration and invasion. The only difference was that Matrigel (BD Biosciences, Franklin Lakes, NJ, USA) was required for cell invasion. Briefly, AGS cell suspension was added to the upper chamber. 600 μL of medium with 10% FBS was placed in the lower chamber. After 24 h, the migrated or invasive cells were fixed and stained with 0.1% crystal violet (Beyotime Biotechnology, Shanghai, China). Finally, the stained cells were photographed and counted under a microscope.

Dual luciferase reporter assay

The wt-FBXL19-AS1 and mut-FBXL19-AS1 or wt-HMGB3 and mut-HMGB3 were inserted into the pmiR-GLO vector (Promega, Madison, WI, USA). Next, AGS cells were transfected with the above reporter plasmid and miR-876-5p mimics and incubated for 24 h. Luciferase activity was detected using a luciferase reporter system (Promega).

Statistical analysis

The data were analyzed by SPSS 22.0 statistical software (SPSS Inc., Chicago, IL. USA) or Graphpad Prism 6. Data were shown as mean ± SD. Comparison between multiple groups was performed using Student's *t*-test or one-way ANOVA. The difference was considered statistically significant at $P < 0.05$.

RESULTS

LncRNA FBXL19-AS1 and miR-876-5p express abnormally in GC

First, the expression levels of lncRNA FBXL19-AS1 and miR-876-5p were detected in GC tissues and cells. Compared with normal tissues, lncRNA FBXL19-AS1 was upregulated in GC tissues (Fig. 1A). At the same time, upregulation of lncRNA FBXL19-AS1 was also found in AGS cells compared to gastric mucosal epithelial cells GES-1 (Fig. 1B). In addition, it was found that miR-876-5p expression in GC tissues was reduced compared to normal tissues (Fig. 1C). Compared with GES-1 cells, downregulation of miR-876-5p was also detected in AGS cells (Fig. 1D). These results indicate that lncRNA FBXL19-AS1 and miR-876-5p may be involved in the progression of GC.

LncRNA FBXL19-AS1 acts as a molecular sponge of miR-876-5p

The starBase database (http://starbase.sysu.edu.cn/) shows that lncRNA FBXL19-AS1 has a binding site to miR-876-5p (Fig. 2A). A dual luciferase reporter assay was performed to verify the above prediction. We found that miR-876-5p mimics reduced the luciferase activity of wt-FBXL19-AS1, but had little effect on the luciferase activity of mut-FBXL19-AS1 in AGS cells (Fig. 2B). In addition, lncRNA FBXL19-

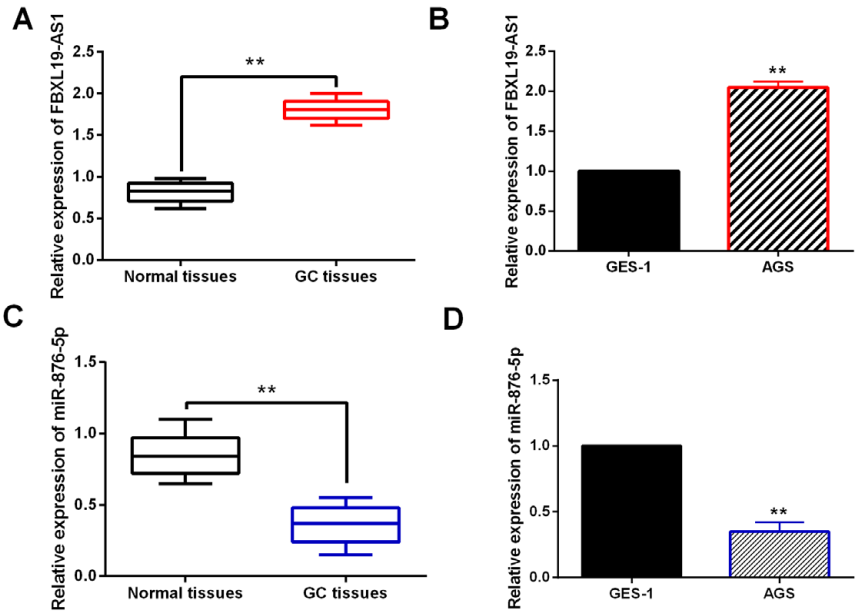

Fig. 1. *LncRNA FBXL19-AS1 and miR-876-5p express abnormally in GC. **A**) FBXL19-AS1 expression in GC tissues and normal tissues. **B**) FBXL19-AS1 expression in GES-1 and AGS cells. **C**) MiR-876-5p expression in GC tissues and normal tissues. **D**) MiR-876-5p expression in GES-1 and AGS cells *P < 0.01.*

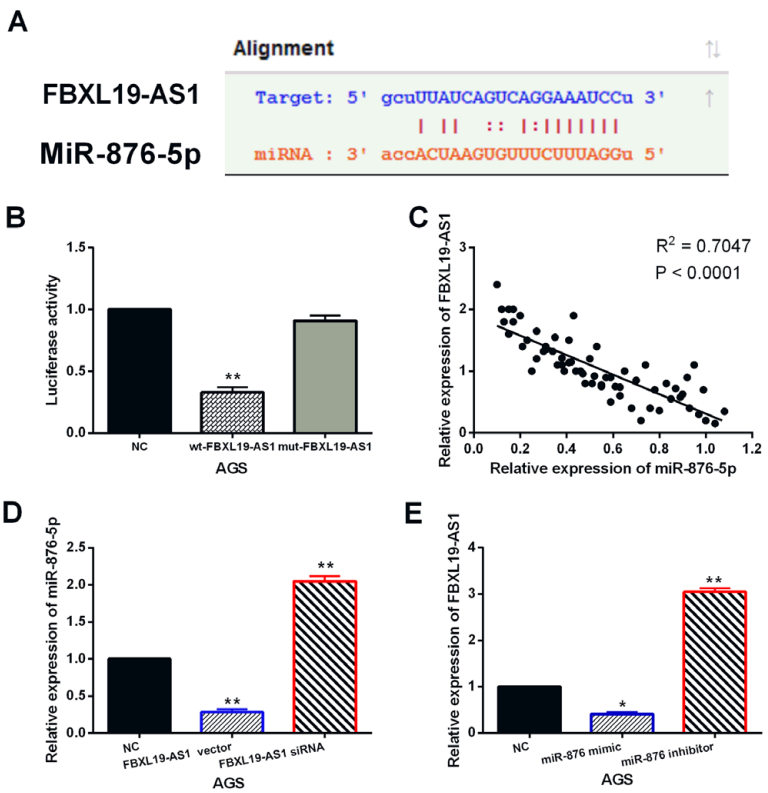

Fig. 2. *LncRNA FBXL19-AS1 acts as a molecular sponge of miR-876-5p. **A**) The binding sites between FBXL19-AS1 and miR-876-5p. **B**) Luciferase reporter assay. **C**) MiR-876-5p was negatively correlated with FBXL19-AS1 expression in GC tissues. **D**) MiR-876-5p expression in AGS cells with FBXL19-AS1 siRNA and vector. **E**) FBXL19-AS1 expression in AGS cells with miR-876-5p mimics or inhibitor *P <0.05, ** P <0.01.*

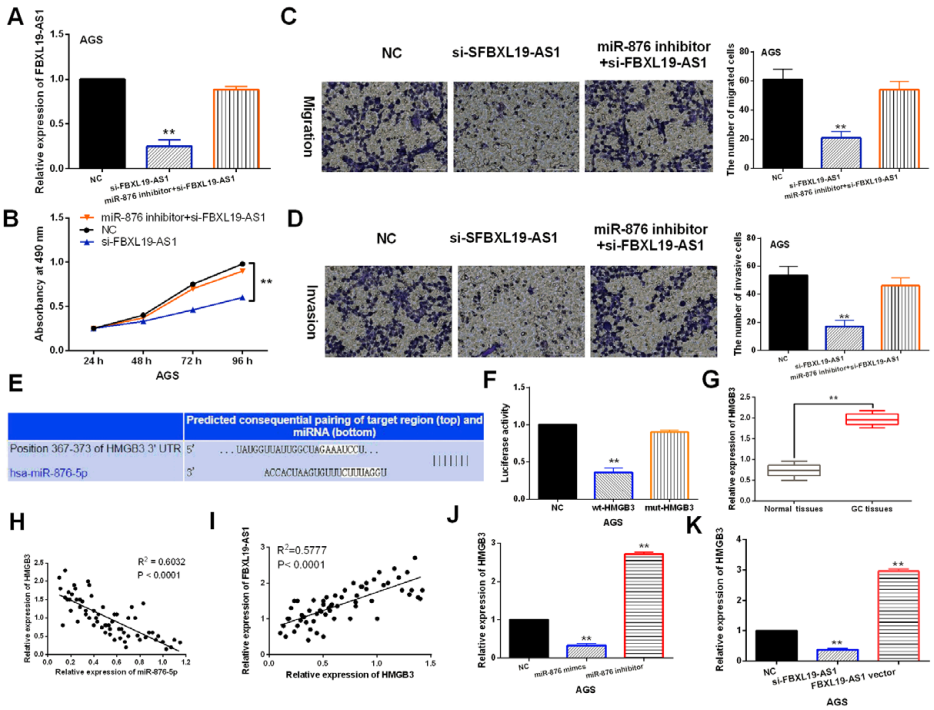

Fig. 3. *LncRNA FBXL19-AS1 promotes GC progression by regulating miR-876-5p/HMGB3. **A**) FBXL19-AS1 expression in AGS cells with si-FBXL19-AS1 or si-FBXL19-AS1+miR-876 inhibitor. **B-D**) Cell proliferation, migration and invasion in AGS cells with si-FBXL19-AS1 or si-FBXL19-AS1+miR-876 inhibitor. **E**) The binding site between HMGB3 and miR-876-5p. **F**) Luciferase reporter assay. **G**) HMGB3 expression in GC tissues and normal tissues. **H**) MiR-876-5p was negatively correlated with HMGB3 expression in GC tissues. **I**) LncRNA FBXL19-AS1 was positively correlated with HMGB3 expression in GC tissues. **J**) HMGB3 expression in AGS cells with miR-876-5p mimics or inhibitor. **K**) HMGB3 expression in AGS cells with FBXL19-AS1 siRNA or vector ** P <0.01.*

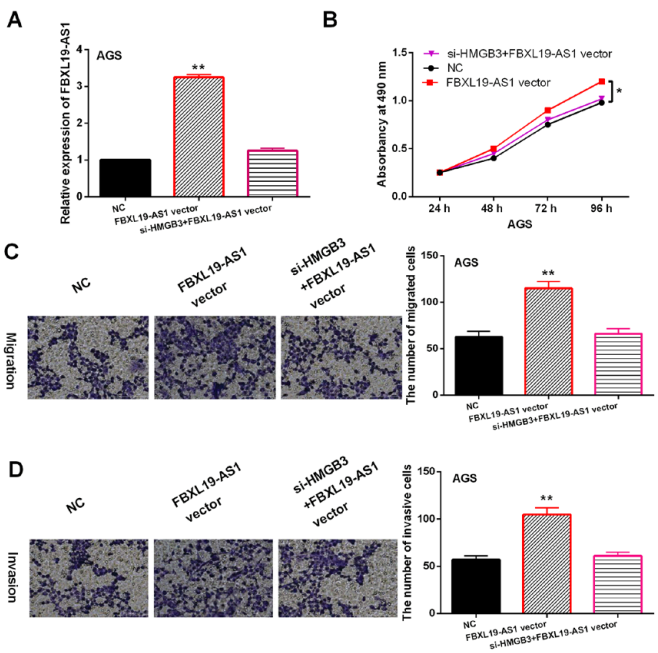

Fig. 4. *LncRNA FBXL19-AS1 induces GC tumorigenesis by upregulating HMGB3. **A**) FBXL19-AS1 expression in AGS cells with FBXL19-AS1 vector or si-HMGB3+ FBXL19-AS1 vector. **B-D**) Cell proliferation, migration and invasion in AGS cells with FBXL19-AS1 vector or si-HMGB3+ FBXL19-AS1 vector **P <0.01.*

AS1 was found to negatively regulate miR-876-5p expression in GC tissues (Fig. 2C). We also found that upregulation of FBXL19-AS1 reduced miR-876-5p expression, while downregulation of FBXL19-AS1 promoted miR-876-5p expression in AGS cells (Fig. 2D). At the same time, FBXL19-AS1 expression was also reduced by miR-876-5p overexpression and promoted by miR-876-5p downregulation in AGS cells (Fig. 2E). These findings indicate that lncRNA FBXL19-AS1 acts as a molecular sponge for miR-876-5p in GC.

LncRNA FBXL19-AS1 promotes GC progression by downregulating miR-876-5p

In order to explore the regulatory mechanism of lncRNA FBXL19-AS1/miR-876-5p in GC, miR-876-5p inhibitor was transfected into AGS cells containing FBXL19-AS1 siRNA. The reduced expression of FBXL19-AS1 induced by its siRNA has been restored in AGS cells by miR-876-5p inhibitor (Fig. 3A). MTT assay showed that downregulation of FBXL19-AS1 inhibited cell proliferation in AGS cells. After transfection with miR-876-5p inhibitor, the inhibitory effect of FBXL19-AS1 siRNA on AGS cell proliferation was abolished in AGS cells (Fig. 3B). In addition, Transwell assay showed that downregulation of FBXL19-AS1 suppressed cell migration and invasion in AGS cells. Moreover, downregulation of miR-876-5p also attenuated the inhibitory effect of FBXL19-AS1 siRNA on AGS cell migration and invasion (Fig. 3 C, D). These results suggest that lncRNA FBXL19-AS1 promotes GC progression by downregulating miR-876-5p.

LncRNA FBXL19-AS1 enhances the expression level of HMGB3 in GC

The TargetScan database (http://www.targetscan.org) predicts that HMGB3 is a potential target for miR-876-5p (Fig. 3E). Dual luciferase reporter assay showed that miR-876-5p mimics reduced the luciferase activity of wt-HMGB3, indicating that miR-876-5p directly targets HMGB3 (Fig. 3F). In order to explore whether HMGB3 is involved in GC progression, abnormal expression of HMGB3 was detected in GC tissues. Compared with normal tissues, HMGB3 was upregulated in GC tissues (Fig. 3G). Then, miR-876-5p was found to negatively regulate HMGB3 expression in GC tissues (Fig. 3H). At the same time, a positive correlation between lncRNA FBXL19-AS1 and HMGB3 expression was found in GC tissues (Fig. 3I). In addition, HMGB3 expression was reduced by miR-876-5p mimics and promoted by miR-876-5p inhibitor in AGS cells (Fig. 3J). Upregulation of FBXL19-AS1 promoted HMGB3 expression, while downregulation of FBXL19-AS1 inhibited HMGB3 expression in AGS cells (Fig. 3K). Collectively, lncRNA FBXL19-AS1 may enhance the expression level of HMGB3 in GC by downregulating miR-876-5p.

LncRNA FBXL19-AS1 induces GC tumorigenesis by upregulating HMGB3

To further investigate whether lncRNA FBXL19-AS1 promotes GC tumorigenesis by regulating HMGB3, HMGB3 siRNA was transfected into AGS cells containing FBXL19-AS1 vector. RT-qPCR showed that the increased expression of FBXL19-AS1 induced by its vector was reduced by HMGB3 siRNA in AGS cells (Fig. 4A). Functionally, upregulation of FBXL19-AS1 was found to promote the proliferation of AGS cells. HMGB3 siRNA attenuated the promoting effect of FBXL19-AS1 on the proliferation of AGS cells (Fig. 4B). In addition, upregulation of FBXL19-AS1 also promoted cell migration and invasion in AGS cells. The promoting effect of FBXL19-AS1 on AGS cell migration and invasion was abolished by HMGB3 siRNA (Fig. 4C, 4D). These results indicate that lncRNA FBXL19-AS1 induces GC tumorigenesis by upregulating HMGB3.

DISCUSSION

An increasing number of studies have shown that lncRNAs are abnormally expressed in GC. In our study, upregulation of lncRNA FBXL19-AS1 was found in GC tissues and cells. In addition, downregulation of lncRNA FBXL19-AS1 restrained cell proliferation, migration and invasion in GC. Consistent with our results, upregulation of lncRNA FBXL19-AS1 has also been found in other human cancers, such as lung adenocarcinoma (5). Functionally, lncRNA FBXl19-AS1 promoted osteosarcoma cell proliferation,

migration and invasion by sponging miR-346 (6). Furthermore, we found that lncRNA FBXL19-AS1 promotes GC progression by downregulating miR-876-5p. Similarly, it has been reported that lncRNA BXL19-AS1 promoted tumor growth in breast cancer by sponging miR-876-5p (4). Moreover, it was confirmed that HMGB3 is a direct target of miR-876-5p. Downregulation of HMGB3 was found to weaken the carcinogenesis of FBXL19-AS1 in GC, indicating that HMGB3 serves as an oncogene in GC. In addition, lncRNA SNHG5 was found to promote the progression of nasopharyngeal carcinoma by enhancing HMGB3 expression (7). In this study, we also found that lncRNA FBXL19-AS1 accelerated the progression of GC by upregulating HMGB3.

In conclusion, the FBXL19-AS1/miR-876-5p/HMGB3 axis can accelerate the GC tumorigenesis. Specifically, lncRNA FBXL19-AS1 promotes cell proliferation, migration and invasion in GC by downregulating miR-876-5p and upregulating HMGB3. This research may provide new insights into the potential therapeutic goals of GC therapy in the future.

REFERENCES

1. Waddell T, Verheij M, Allum W, Cunningham D, Cervantes A, Arnold D. Gastric cancer: ESMO-ESSO-ESTRO Clinical Practice Guidelines for diagnosis, treatment and follow-up. Radiother Oncol 2014; 110:189-94.
2. Tang J, Huang F, Wang H, Cheng F, Pi Y, Zhao J, Li Z. Knockdown of TPT1-AS1 inhibits cell proliferation, cell cycle G1/S transition, and epithelial-mesenchymal transition in gastric cancer. Bosn J Basic Med Sci 2020;
3. Yu DJ, Li YH, Zhong M. LncRNA FBXL19-AS1 promotes proliferation and metastasis via regulating epithelial-mesenchymal transition in non-small cell lung cancer. Eur Rev Med Pharmacol Sci 2019; 23:4800-06.
4. Dong G, Pan T, Zhou D, Li C, Liu J, Zhang J. FBXL19-AS1 promotes cell proliferation and inhibits cell apoptosis via miR-876-5p/FOXM1 axis in breast cancer. Acta Biochim Biophys Sin (Shanghai) 2019; 51:1106-13.
5. Wang L, Zhang X, Liu Y, Xu S. Long noncoding RNA FBXL19-AS1 induces tumor growth and metastasis by sponging miR-203a-3p in lung adenocarcinoma. J Cell Physiol 2020; 235:3612-25.
6. Pan R, He Z, Ruan W, et al. lncRNA FBXL19-AS1 regulates osteosarcoma cell proliferation, migration and invasion by sponging miR-346. Onco Targets Ther 2018; 11:8409-20.
7. Liu D, Wang Y, Zhao Y, Gu X. LncRNA SNHG5 promotes nasopharyngeal carcinoma progression by regulating miR-1179/HMGB3 axis. BMC Cancer 2020; 20:178.

LETTER TO THE EDITOR

Mechanism of MAPK/ERK1/2 signaling pathway and related proteins on receptor activity of rats with endometriosis

Y. Jiang[1], R. Li[1], Y. Zhao[2], J. Liu[2], X. Zhu[2] and L. Jin[2]

[1]Zhejiang Chinese Medical University, Hangzhou, Zhejiang Province, China; [2]Department of Obstetrics & Gynecology, The Second Affiliated Hospital of Zhejiang Chinese Medical University, Hangzhou, Zhejiang Province, China

Received April 29, 2020 – Accepted July 15, 2020

To the Editor,

Endometriosis (EM) refers to the endometrial tissues with growth function that appear outside the uterine cavity covering the mucosa, often found in the pelvic peritoneum and ovary (1). Current treatments for EM mainly include surgical removal of lesions and drug control of symptoms. However, surgical treatment is traumatic, and EM is prone to relapse after surgery. In addition, the shortcomings of drug treatment are that some drugs are ineffective, and some patients relapse after discontinuation (2). Therefore, exploring other better treatments has become the current research focus of EM. EM is a benign gynecological disease that depends on estrogen; it is generally recognized that no estrogen is no ectopia (3). Some studies have reported that the estrogen levels are the key factors and driving factors for the development of EM, but how estrogen promotes EM is still unclear.

In this study, rat models of endometriosis were established, then estrogen intervention was performed on the rat model. Next, peripheral blood estrogen levels and lesion size in each group of models were observed and recorded. As shown in Table I, the peripheral blood estrogen level of the rat model established with estrogen after ovariectomy was higher than that of other groups ($P<0.05$, Table I), and the peripheral blood estrogen level of the model increased with the increase dose of estrogen ($P<0.05$, Table I). At the same time, we also found that in rat models established with estrogen after ovariectomy, the lesion size was larger than that of the other groups ($P<0.05$, Table I), and the higher the estrogen dose, the larger the lesion area ($P<0.05$, Table I).

The effects of estrogen on the expression of proteins (ERK, CREB, MMP-9, VEGF) in the MAPK/ERK1/2 pathway were also investigated. On the 6th day of the rat models, we found that there were significant differences in the expressions of p-ERK, CREB, MMP-9, VEGF between different model groups, except ERK ($P<0.05$, Table II). On the 12th day, the expressions of ERK, p-ERK, CREB, MMP-9, and VEGF were found to be significantly different between the different model groups ($P<0.05$, Table III). Comparing the effects of estrogen on protein expression in the MAPK/ERK1/2 pathway on day 24, we found that all the above proteins were significantly different between the different model groups ($P<0.05$, Table IV). These results indicate that estrogen content can affect the MAPK/ERK1/2 pathway by regulating ERK, CREB, MMP-9 and VEGF protein expression.

MAPK is a mitogen/threonine protein kinase that is widely present in mammals and can be activated

Key words: MAPK/ERK1/2; related proteins on receptor activity; endometriosis

Corresponding Author:
Dr Yanjiao Jiang,
Zhejiang Chinese Medical University,
No.59-1-401, Hanggang Beiyuan, Banshan Street, Gongshu District,
Hangzhou, 310053, Zhejiang Province, China
Tel.: +86 13185719869
e-mail: zangytrdhe836@163.com

0393-974X (2020)
Copyright © by BIOLIFE, s.a.s.
This publication and/or article is for individual use only and may not be further reproduced without written permission from the copyright holder.
Unauthorized reproduction may result in financial and other penalties
DISCLOSURE: ALL AUTHORS REPORT NO CONFLICTS OF INTEREST RELEVANT TO THIS ARTICLE.

by a series of extracellular signals or stimuli. MAPK pathway is involved in the regulation of cell proliferation, differentiation, migration, and aging. It is also closely related to the occurrence of various diseases such as inflammation and tumor (4). MAPK mainly contains 4 classic pathways, among which ERKl/2 signaling pathway is related to cell proliferation, differentiation, migration and apoptosis. The ERK pathway includes two subclasses, ERK1 and ERK2, which can stimulate gene expression and cell proliferation through CREB, serum response factors and estrogen receptors (5). An increasing number of studies have shown that extracellular signals interact with the estrogen system in multiple pathways through the MAPK/ERK signaling pathway, thereby playing an important role in the occurrence and development of various estrogen-dependent diseases (6). At present, it has not been reported whether estrogen can participate in the occurrence and development of EM through the MAKP/ERK1/2 signaling pathway.

In the present study, EM rat models with different estrogen levels were established, and the differences in lesions between different groups were compared. The effects of different estrogen on the gene expression of MAKP/ERK1/2 signaling pathway in EM were analyzed. The results showed that the peripheral

Table I. *Peripheral blood estrogen levels and lesion size of each model ($\bar{x}\pm s$)*

Group	Peripheral blood estrogen levels（pg/ml）	Lesion size (mm*mm*mm)
Uncut ovary group	41.37±5.83	6.84*6.50*5.65±0.40*0.60*0.50
Ovariectomy group	45.00±3.74	6.39*3.55*5.93±0.5*0.50*0.50
Sham-operated group	46.00±3.67	5.97*9.16*7.15±0.51*0.62*0.43
1 dose group	1110.73±134.91	3.0*4.2*4.5±0.26*0.35*0.41
2 dose group	2583.24±137.41	5.34*4.0*0.3*±0.35*0.41*0.43
4 dose group	4759.07±145.67	6.77*4.68*4.02±0.35*0.62*0.57
t	100.645	29.388
P	0.000*	0.000*

**P<0.05, the difference was statistically significant*

Table II. *Effect of estrogen on protein expression in MAPK/ERK1/2 pathway [6 days, ($\bar{x}\pm s$)]*

Group	ERK	p-ERK	CREB	MMP-9	VEGF
Uncut ovary	2.35±0.39	1.11±0.13	0.39±0.03	1.04±0.10	0.79±0.05
Sham-operated	1.89±0.17	0.43±0.06	0.20±0.01	0.78±0.07	0.65±0.04
1 dose group	3.37±0.27	0.42±0.07	0.44±0.06	0.55±0.01	0.64±0.06
2 dose group	2.67±0.22	0.55±0.04	0.45±0.06	0.55±0.03	0.35±0.09
4 dose group	2.49±0.45	0.56±0.06	0.25±0.05	0.52±0.09	0.45±0.04
t	-0.878	18.333	8.325	15.401	21.867
P	0.231	0.005*	0.006*	0.004*	0.002*

**P<0.05, the difference was statistically significant*

blood estrogen level and lesion size in the rat model were closely related to the estrogen content. The higher the estrogen content, the higher the peripheral blood estrogen levels and lesions in the rat model. In addition, it was found that that estrogen affected the expressions of ERK, p-ERK, and CREB in the MAKP/ERK1/2 signaling pathway, which is consistent with previous studies (7). In this study, estrogen has been found to affect the expression of MMP-9 and VEGF. MMP-9 has been reported to promote the budding of vascular endothelial cells and leads to the formation of new blood vessels. Therefore, MMP-9 plays an important role in EM and various malignant tumors (8). The growth of ectopic endometrium depends on the formation of new blood vessels. VEGF is currently considered to be the most critical proangiogenic factor and plays an important role in regulating normal blood vessel growth and pathological neovascularization (9). Based on these results, we believe that estrogen may affect the adhesion, invasion and even angiogenesis of EM cells by regulating the MAKP/ERK1/2 signaling pathway and MMP-9 or VEGF expression.

In conclusion, the MAKP/ERK1/2 signaling pathway, MMP-9 and VEGF may play an important role in the occurrence and development of EM through the interaction with estrogen. Estrogen can effectively regulate the protein expression levels of molecular genes in the MAKP/ERK1/2 signaling pathway. In-depth study about the specific effects of MAKP/ERK1/2 signaling pathway, MMP-9 and VEGF on EM has a profound impact on clinical treatment, and needs to be performed in the future.

Table III. *Effect of estrogen on protein expression in MAPK/ERK1/2 pathway [12 days, ($\bar{x}$±s)] blood estrogen levels and lesion size of each model ($\bar{x}$±s)*

Group	ERK	p-ERK	CREB	MMP-9	VEGF
Uncut ovary	2.88±0.32	1.38±0.23	0.61±0.06	1.03±0.06	1.41±0.24
Sham-operated	2.36±0.26	0.72±0.07	0.27±0.09	0.74±0.08	0.47±0.07
1 dose group	3.02±0.38	1.02±0.10	0.71±0.07	0.82±011	0.95±0.12
2 dose group	2.58±0.67	1.06±0.12	0.53±0.05	0.65±0.04	0.76±0.16
4 dose group	2.41±0.17	1.02±0.13	0.37±0.04	0.49±0.07	0.63±0.09
t	5.981	6.183	14.433	21.823	15.172
P	0.012*	0.010*	0.008*	0.001*	0.003*

**P<0.05, the difference was statistically significant.*

Table IV. *Effect of estrogen on protein expression in MAPK/ERK1/2 pathway [24days ($\bar{x}$±s)]*

Group	ERK	p-ERK	CREB	MMP-9	VEGF
Uncut ovary	2.67±0.56	2.35±0.25	0.57±0.06	0.43±0.03	0.66±0.04
Sham-operated	1.92±0.25	1.16±0.14	0.45±0.05	0.41±0.10	0.44±0.06
1 dose group	2.46±0.12	1.65±0.15	0.46±0.03	0.28±0.01	0.83±0.09
2 dose group	1.91±0.09	0.85±0.09	0.50±0.05	0.37±0.05	0.60±0.04
4 dose group	1.27±0.16	0.29±0.07	0.38±0.03	0.48±0.04	0.52±0.07
t	12.518	41.430	13.262	-3.616	5.974
P	0.004*	0.000*	0.002*	0.009*	0.007*

**P<0.05, the difference was statistically significant*

ACKNOWLEDGEMENTS

This work was supported by the Application of welfare Technology in Zhejiang Province (animal experiment) (2017C37167) and basic public welfare research projects of Zhejiang Province (LQ18H040003).

REFERENCES

1. Matias-Guiu X, Stewart CJR. Endometriosis-associated ovarian neoplasia. Pathology 2018; 50:190-204.
2. Barra F, Romano A, Grandi G, Facchinetti F, Ferrero S. Future directions in endometriosis treatment: discovery and development of novel inhibitors of estrogen biosynthesis. Expert Opin Investig Drugs 2019; 28:501-04.
3. Jiang L, Tang C, Rao J, et al. Systematic identification of the druggable interactions between human protein kinases and naturally occurring compounds in endometriosis. Comput Biol Chem 2017; 71:136-43.
4. Yang F, Wen C, Zheng S, Yang S, Chen J, Feng X. Involvement of MAPK/ERK1/2 pathway in microcystin-induced microfilament reorganization in HL7702 hepatocytes. J Toxicol Environ Health A 2018; 81:1135-41.
5. Yeh HT, Tsai YS, Chen MS, et al. Flavopereirine induces cell cycle arrest and apoptosis via the AKT/p38 MAPK/ERK1/2 signaling pathway in human breast cancer cells. Eur J Pharmacol 2019; 863:172658.
6. Sadremomtaz A, Mansouri K, Alemzadeh G, Safa M, Rastaghi AE,Asghari SM. Dual blockade of VEGFR1 and VEGFR2 by a novel peptide abrogates VEGF-driven angiogenesis, tumor growth, and metastasis through PI3K/AKT and MAPK/ERK1/2 pathway. Biochim Biophys Acta Gen Subj 2018; 1862:2688-700.
7. Yu XY, Wang XT, Chu YL, Qu HM, Liu J, Zhang YH, Li MJ. Effect of FGF2 on the activity of SPRYs/DUSP6/ERK signaling pathway in endometrial glandular epithelial cells of endometriosis. Eur Rev Med Pharmacol Sci 2018; 22:1554-68.
8. Szymanowski K, Mikolajczyk M, Wirstlein P, Dera-Szymanowska A. Matrix metalloproteinase-2 (MMP-2), MMP-9, tissue inhibitor of matrix metalloproteinases (TIMP-1) and transforming growth factor-beta2 (TGF-beta2) expression in eutopic endometrium of women with peritoneal endometriosis. Ann Agric Environ Med 2016; 23:649-53.
9. Zhang F, Liu XL, Wang W, Dong HL, Xia YF, Ruan LP, Liu LP. Expression of MMIF, HIF-1alpha and VEGF in serum and endometrial tissues of patients with endometriosis. Curr Med Sci 2018; 38:499-504.

LETTER TO THE EDITOR

Crocin suppresses cell proliferation and migration by regulating miR-577/NFIB in renal cell carcinoma

L. Niu[1], X-F. Wang[2] and X-R. Wang[3]

[1]Department of Clinical Laboratory, Zouping People's Hospital, Binzhou, China; [2]Department of Clinical Laboratory, Zouping Hospital of Traditional Chinese Medicine, Binzhou, China; [3]Department of Clinical Laboratory, Wudi Hospital of Traditional Chinese Medicine, Binzhou, China

Received May 18, 2020 – Accepted July 20, 2020

To the Editor,

Renal cell carcinoma (RCC) is one of the most common malignancies of the urinary system, arising from the renal parenchyma. The treatment of RCC is mainly combined with radiotherapy and chemotherapy. However, patients are susceptible to develop radiosensitivity or drug resistance, which greatly influence the effect of later radiotherapy and chemotherapy (1). In recent years, the application of traditional Chinese medicine in the treatment of tumors has become a hot topic among scholars at home and abroad.

Studies have found that during the treatment with other anticancer drugs, crocin can reduce the adverse reactions of those drugs, such as cisplatin, and improve the efficacy (2). Crocin was confirmed to markedly inhibit cell proliferation of human lung adenocarcinoma cells and enhance the chemo sensitivity (3). Accumulating evidence has shown that crocin affected numerous disorders including hypertension, coronary artery diseases, ischemic retinopathy, various tumors, neuro-degeneration, behavioral disturbance as well as other inflammatory disorders (4).

MicroRNAs (miRNAs) are a group of non-coding single-stranded RNAs with the length of 20~24 nucleotides encoded by endogenous genes. Recently, emerging evidence verified that miRNAs were closely related to the occurrence, development and treatment of tumors. MiR-577 was proved to restrain cell proliferation, migration and invasion in papillary thyroid carcinoma (5). However, the role of miR-577 on the progression of RCC is still unreported. In this study, we aimed to make clear the effect of crocin on the progression of RCC. In addition, we also explored the link between crocin, miR-577 and Nuclear Factor I B (NFIB) in RCC.

MATERIALS AND METHODS

Human samples

Thirty-four RCC tissues and paracancer normal tissues were collected from Zouping People's Hospital. The samples were stored at -80°C. All RCC patients had not received any preoperative radiotherapy or chemotherapy. In our experiment, all patients signed the informed consents, and the study was approved by the ethics committee of Zouping People's Hospital.

Cell culture and crocin treatment

Human RCC cell lines (A498 and A704) were obtained from Shanghai JingKang Bioengineering CO., LTD (Shanghai, China). RCC cell line 786-O and human renal tubular epithelial cell (HK-2) were purchased from

Key words: crocin; renal cell carcinoma; miR-577; NFIB

Corresponding Author:
Dr L. Niu,
Department of Clinical Laboratory,
Zouping People's Hospital,
22 Huangshaner Road,
Binzhou 256600, China
e-mail: ij59z1@126.com

0393-974X (2020)
Copyright © by BIOLIFE, s.a.s.
This publication and/or article is for individual use only and may not be further reproduced without written permission from the copyright holder.
Unauthorized reproduction may result in financial and other penalties
DISCLOSURE: ALL AUTHORS REPORT NO CONFLICTS OF INTEREST RELEVANT TO THIS ARTICLE.

the Type Culture of the Chinese Academy of Sciences (Shanghai, China). Cells were cultured in DMSO (Dimethyl sulfoxide) medium containing penicillin (100 U/ml) and streptomycin (0.1mg/ml) at 37°C, 5% CO_2 and 95% humidity. Cells in the logarithmic growth stage were taken for the experiment.

Crocin was purchased from Sigma (St. Louis, MO, USA). To detect the role of crocin in RCC, A498 cells were cultured in designated cell plates and then treated with crocin at a concentration of 2.5, 5, 10 μM for 48 h.

Quantitative real-time PCR

Total RNA was extracted from RCC cells by TRIzol reagent (Invitrogen). Then, according to the manufacturer's protocol, 2 μg of total RNA has synthesized complementary DNA by AMV reverse transcriptase (Promega, Madison, WI, USA). The expression level of miR-577 was detected by mirVana™ qRT-PCR miRNA Detection kit (Invitrogen). Meanwhile, GAPDH was used as internal control.

Assays

Flow cytometry was used to test RCC cell apoptosis. Cells (3 x 10^5) were cultured in the 6-well plates with DMSO or crocin for 48 h. Cells were stained with 7-AAD and Annexin-V-FITC using an ANNEXIN V-FITC/7-AAD Kit (Beckman Coulter) for apoptosis analysis. Stained cells were immediately measured by fluorescence activated cell sorting (FACS; BD Immunocytometry Systems).

MTT assay was used to detect cell viability. Cells were cultured in 96-well plates (5 x 10^3 cells/well) with DMSO media supplemented with 10% FBS. Then, crocin (0, 2.5, 5 10 μM) was added to 96-well plates and cultured for another 48 hours at 37°C and 5% CO_2. Cells were incubated in MTT (0.5 mg/mL) solution for another 4 h. Finally, the medium with MTT solution was removed and 150 μL DMSO (Dimethyl sulfoxide) was added to each well. The absorbance of the cells were measured by the Microplate reader at 490 nm.

The cell migration was performed by Transwell assay performed in a 24-well chambers. Cells (3 x 10^4 cells/well) were plated in 200 μL medium without FBS (fetal bovine serum) and added into the upper chamber. Subsequently, 600 medium with 10% FBS was added to the lower chamber. After the incubation for 24 h, cells were fixed with ice methanol and stained with crystal violet. Finally, the number of migrated cells was counted under a microscope at the magnification of 200x.

The binding sequences of NFIB containing the miR-577 binding sites and mutant binding sites were inserted into pmirGLO luciferase plasmids to construct NFIB-wt and NFIB-mut reporter vectors. Then, all reporter vectors were co-transfected with miR-NC or miR-577 mimics into A498 cells. Cells were cultured in the incubator at 37°C, 5% CO_2, and 95% humidity. After 48 h, the luciferase activity was tested by the dual-luciferase reporter assay kit.

Statistical analysis

All data are presented as means±SD. Comparisons between two groups were analyzed by Student's *t*-tests. One-way ANOVA was performed to analyze the comparisons of multiple groups. All experiments were repeated at least three times, and representative experiments are shown. $P<0.05$ was deemed significant.

RESULTS

Crocin inhibited cell viability and promoted apoptosis in A498 cells

A498 cells were treated with different concentrations of crocin (0, 2.5, 5 and 10 μM). MTT assay and Transwell assay were used to measure A498 cell proliferation and invasion. We found that crocin dose-dependently inhibited cell proliferation and migration viability of crocin-treated A498 cells (Fig. 1A, C). Furthermore, flow cytometric analysis was adopted to measure the apoptosis rate of crocin-treated A498 cells. Our results indicated that crocin treatment significantly promoted A498 cell apoptosis in a dose-dependent manner (Fig. 1B). Combined with the above results, 5 μM crocin were selected to treat A498 cells for 48 h as the subsequent experimental conditions.

Crocin was involved in the effects of miR-577on cell proliferation and migration in A498 cells

The expression level of miR-577 in RCC by qRT-PCR assay were evaluated. The results displayed that miR-577 was lower expressed in RCC tissues than in normal RCC tissues (Fig. 2A). Also, there was a downtrend expression of miR-577 in RCC cell lines

(Fig. 2B). To explore whether crocin could regulate the expression of miR-577 in RCC, A498 cells were treated with 5 μM crocin for 48 h. As shown in Fig. 2C, crocin markedly increased the expression level of miR-577 compared to the control group.

To investigate how crocin affected the effects of miR-577 on cell proliferation and migration, miR-577 inhibitors were transfected into crocin-treated

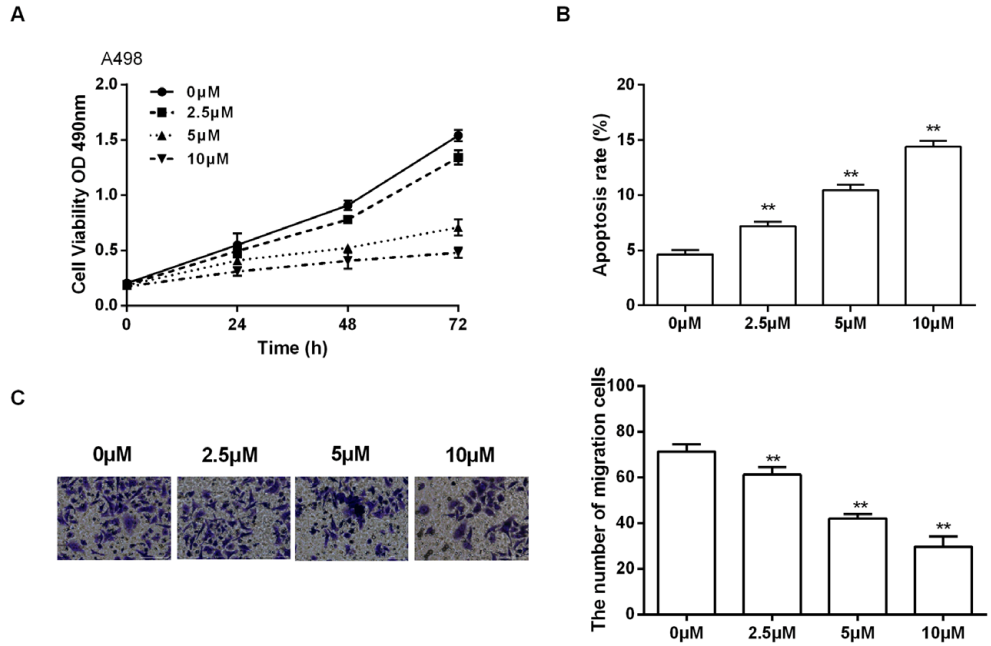

Fig. 1. *Crocin inhibited cell viability and promoted apoptosis in A498 cells. A) The cell proliferation of A498 cells treated with crocin (0, 2.5, 5, 10 μM).* ***B****) The cell apoptosis of A498 cells treated with crocin (0, 2.5, 5, 10 μM).* ***C****) The cell migration of A498 cells treated with crocin (0, 2.5, 5, 10 μM). **p<0.01*

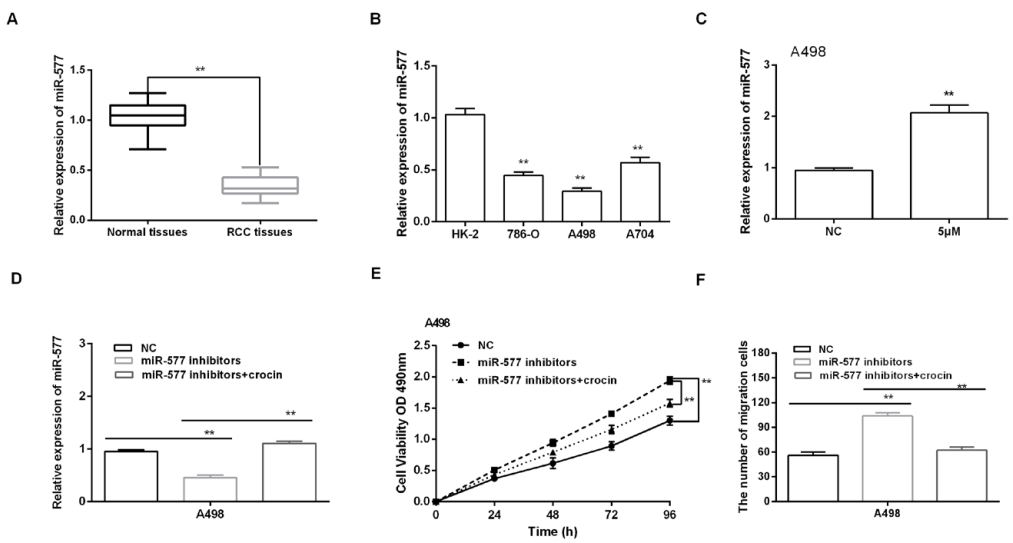

Fig. 2. *Crocin was involved in the effects of miR-577on cell proliferation and migration in A498 cells.* ***A****) There was a downtrend of miR-577 expression in RCC tissues.* ***B****) MiR-577 was downregulated in RCC cell lines.* ***C****) The expression of miR-577 was increased in A498 cells treated with crocin (5 μM) for 48 h.* ***D****) The expression of miR-577 in A498 cells transfected with miR-577 inhibitors or crocin.* ***E****) Cell proliferation was detected by MTT assay in A498 cells with miR-577 inhibitors or crocin.* ***F****) Cell migration was detected by Transwell assay in A498 cells with miR-577 inhibitors or crocin. **p<0.01*

A498 cells. As shown in Fig. 2D, miR-577 inhibitors reduced the expression level of miR-577 in A198 cells, while crocin alleviated the suppressive effect of miR-577 inhibitors. Functionally, we found that miR-577 inhibitors promoted cell proliferation and migration in A498 cells, while crocin notably attenuated the effect of miR-577 inhibitors on cell proliferation and migration (Fig. 2E, F). Our data indicated that crocin restrained cell proliferation and migration in RCC by elevating the expression of miR-577.

NFIB was a direct target gene of miR-577

The online TargetScan database was used to search the downstream targets of miR-577. As shown in Fig. 3A, there were special binding sites between miR-577 and NFIB. The luciferase reporter assay proved that miR-577 mimics significantly reduced the luciferase activity of NFIB-wt (Fig. 3B). To explore the relationship between miR-577 and NFIB in RCC, miR-577 mimics or miR-577 inhibitors were transfected into A498 cells. The results demonstrated that the mRNA expression of NFIB were reduced by miR-577 mimics, while increased by miR-577 inhibitors (Fig. 3C). Furthermore, it was revealed that the expression of NFIB was increased in RCC tissues and cell lines (Fig. 3D, E). In addition, there was a negative correlation between miR-577 and NFIB in RCC tissues (Fig. 3F). Taken together, NFIB was proved to be a direct target gene of miR-577 in RCC.

Crocin increased miR-577 expression to prevent NFIB expression

To evaluate the molecular mechanism of crocin/miR-577/NFIB on RCC cell progression, miR-577 inhibitors were transfected into A498 cells treated with crocin (5 μM). We discovered that miR-577 inhibitors increased the mRNA expression of NFIB, while crocin suppressed the effect of miR-577 inhibitors on NFIB mRNA expression (Fig. 3G).

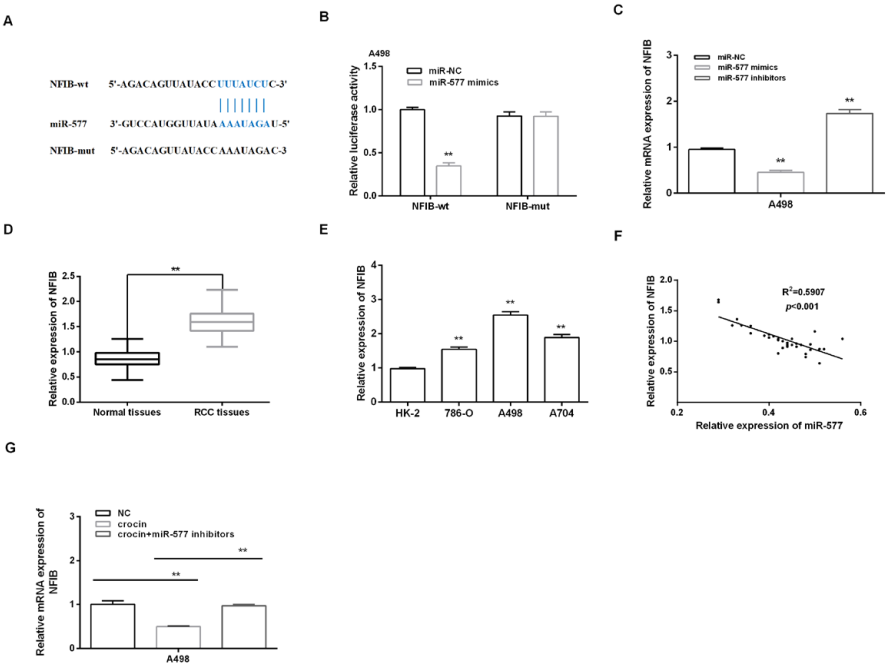

Fig. 3. *NFIB was a direct target gene of miR-577.* ***A)*** *There were special binding sites between miR-577 and NFIB in RCC.* ***B)*** *The luciferase activity of NFIB-wt and NFIB-mut in A498 cells with miR-577 mimics.* ***C)*** *The mRNA expression of NFIB in A498 cells.* ***D, E)*** *NFIB was upregulated in RCC tissues and cell lines.* ***F)*** *There was a negative correlation between miR-577 and NFIB in RCC. G) The mRNA expression of NFIB was detected by RT-qPCR analysis. **p<0.01*

According to the previous results, we confirmed that crocin retrained RCC cell progression by increasing miR-577 expression to reduce NFIB expression.

DISCUSSION

Crocin has been reported to significantly inhibit cell growth in a variety of human cancers (6). In this study, we discovered that crocin treatment significantly suppressed RCC cell proliferation and migration, and promoted cell apoptosis in a dose-dependent manner. Consistent with our findings, crocin inhibited gastric cancer cell migration, invasion and epithelial-mesenchymal transition by miR-320/KLF5/HIF-1 (7). Moreover, in retinoblastoma, crocin was confirmed to suppress cell proliferation and induce cell apoptosis by inhibiting MYCN expression (8).

MiR-577 has been discovered to act as a tumor suppressor in breast cancer (9). In this study, we found that miR-577 was down expressed in RCC tissues and cell lines. Moreover, miR-577 inhibitors promoted cell proliferation and cell migration in A498 cells. In line with our findings, miR-577 was downregulated in non-small cell lung cancer and suppressed cell proliferation, migration, invasion and epithelial mesenchymal transition (10). In addition, the expression of miR-577 was increased in A498 cells treated with crocin. Functional experiments discovered that crocin suppressed cell proliferation and migration by increasing miR-577 expression. In this article, NFIB was found to be up-expressed in RCC tissues and cell lines. Consistent with our results, NFIB was upregulated in non-small cell lung cancer (11) and colorectal cancer (12). Furthermore, miR-577 inhibitors increased the NFIB expression, while crocin suppressed the effect of miR-577 inhibitors on NFIB expression.

In conclusion, this study elucidated that crocin inhibited cell proliferation and migration by increasing miR-577 expression to reduce NFIB expression in RCC.

REFERENCES

1. Buti S, Bersanelli M, Sikokis A, et al. Chemotherapy in metastatic renal cell carcinoma today? A systematic review. Anticancer Drugs 2013; 24:535-54.
2. Luo Y, Cui S, Tang F, et al. The combination of crocin with cisplatin suppresses growth of gastric carcinoma cell line BGC-823 and promotes cell apoptosis. Pak J Pharm Sci 2017; 30:1629-34.
3. Chen S, Zhao S, Wang X, et al. Crocin inhibits cell proliferation and enhances cisplatin and pemetrexed chemosensitivity in lung cancer cells. Transl Lung Cancer Res 2015; 4:775-83.
4. Lin L, Liu G, Yang L. Crocin improves cognitive behavior in rats with Alzheimer's disease by regulating endoplasmic reticulum stress and apoptosis. Biomed Res Int 2019; doi:10.1155/2019/9454913.
5. Xue KC, Hu DD, Zhao L, Li N,Shen HY. MiR-577 inhibits papillary thyroid carcinoma cell proliferation, migration and invasion by targeting SphK2. Eur Rev Med Pharmacol Sci 2017; 21:3794-800.
6. Sun J, Xu XM, Ni CZ, et al. Crocin inhibits proliferation and nucleic acid synthesis and induces apoptosis in the human tongue squamous cell carcinoma cell line Tca8113. Asian Pac J Cancer Prev 2011; 12:2679-83.
7. Zhou Y, Xu Q, Shang J, Lu L,Chen G. Crocin inhibits the migration, invasion, and epithelial-mesenchymal transition of gastric cancer cells via miR-320/KLF5/HIF-1alpha signaling. J Cell Physiol 2019; 234:17876-85.
8. Deng L, Li J, Lu S, Su Y. Crocin inhibits proliferation and induces apoptosis through suppressing MYCN expression in retinoblastoma. J Biochem Mol Toxicol 2019; doi:10.1002/jbt.22292.
9. Yin C, Mou Q, Pan X, Zhang G, Li H, Sun Y. MiR-577 suppresses epithelial-mesenchymal transition and metastasis of breast cancer by targeting Rab25. Thorac Cancer 2018; 9:472-79.
10. Wang B, Sun L, Li J, Jiang R. miR-577 suppresses cell proliferation and epithelial-mesenchymal transition by regulating the WNT2B mediated Wnt/beta-catenin pathway in non-small cell lung cancer. Mol Med Rep 2018; 18:2753-61.
11. Wu Y, Zhang J, Hou S, Cheng Z, Yuan M. Non-small cell lung cancer: miR-30d suppresses tumor invasion and migration by directly targeting NFIB. Biotechnol Lett 2017; 39:1827-34.
12. Yu H, Ma J, Chen J, Yang Y, Liang J, Liang Y. LncRNA LINC00461 Promotes Colorectal Cancer Progression via miRNA-323b-3p/NFIB Axis. Onco Targets Ther 2019; 12:11119-29.

LETTER TO THE EDITOR

LncRNA SNHG17 acts as a ceRNA of miR-324-3p to contribute the progression of osteosarcoma

YT. Zhang[1] and GY. Yang[2]

[1]Department of Orthopedics and Traumatology, Zibo Integrated Traditional Chinese and Western Medicine Hospital, ZiBo, China; [2]Surgery of Osteoarthritis, ZiBo Central Hospital, ZiBo, China

Received March 22, 2020 – Accepted July 22, 2020

To the Editor,

Osteosarcoma (OS) is a common primary bone malignancy, which mainly occurs in adolescents aged 10 to 30 years. OS is the eighth most common malignancy tumor in children. At present, the main treatment option is surgery combined with chemotherapy (1). However, due to limited treatment options, the overall survival rate of OS patients with metastasis or recurrence is approximately 10-20% (2). Therefore, it is urgent to explore the mechanism of OS oncogenesis and development, to discover new and effective biomarkers for OS diagnosis, prognosis and treatment.

Recent studies have indicated that lncRNAs regulate various biological processes such as tumor initiation, growth, invasion, metastasis and chemoresistance (3). MATN1-AS1 was discovered to be down-expressed in glioblastoma, and suppressed cell viability by inhibiting the MAPK signaling pathway (4). SNHG17 has been found to be specifically expressed in several human tumors and enhanced tumor progression. In non-small cell lung cancer (NSCLC), SNHG17 was reported to accelerate cell proliferation and migration, and to be a potential biomarker of NSCLC (5). However, as far as we know, the function of SNHG17 on the progression of OS has not yet been reported.

This study is designed to verify the expression and role of SNHG17 in the tumorigenesis and progression of OS. Moreover, the expression of miR-324-3p in OS was also explored. In addition, we detected the function of SNHG17/miR-324-3p axis in the development of OS.

MATERIALS AND METHODS

OS patients and tissue samples

Forty-two OS tissues and noncancerous tissues were obtained from Zibo Integrated Traditional Chinese and Western Medicine Hospital. All patients were diagnosed pathologically and had not undergone radio-chemotherapy before surgery. After surgery, the specimens were immediately put into liquid nitrogen, and then stored at -80°C. Our experiments received informed consent from all patients, and were approved by the ethics committee of Zibo Integrated Traditional Chinese and Western Medicine Hospital.

Cells

Normal human OS cell line hFOB1.19 and HOS, U2OS and SaoS-2 were purchased from BeNa Culture Collection (Beijing, China). Cells were cultured in Dulbecco's Modified Eagle's Medium (DMEM) with 10% Fetal Bovine Serum (FBS), 100μg/ml streptomycin and 100 U/ml penicillin at 37°C and 5% CO2. Furthermore, 0.25% trypsin was used to cell passage every other day.

Key words: SNHG17; miR-324-3p; osteosarcoma

Corresponding Author:
Dr Guangyuan Yang,
Surgery of Osteoarthritis, ZiBo Central Hospital,
54 Gongqingtuan Road, ZiBo 255020, China
Tel.: +86 0533 2360360
e-mail: yangmsxunp843844@163.com

0393-974X (2020)
Copyright © by BIOLIFE, s.a.s.
This publication and/or article is for individual use only and may not be further reproduced without written permission from the copyright holder.
Unauthorized reproduction may result in financial and other penalties
DISCLOSURE: ALL AUTHORS REPORT NO CONFLICTS OF INTEREST RELEVANT TO THIS ARTICLE.

Si-SNHG17, miR-324-3p inhibitor, SNHG17 vector, miR-324-3p mimic and their corresponding negative control (NC) were synthesized by GenePharma (Shanghai, China), and were transfected into HOS cells by Lipofectamine 2000 (Thermo Fisher Scientific, USA).

RT-qPCR analysis

RNA samples were isolated from OS tissues and cells using TRIzol reagent. LightCycle 96 Thermocycle (Roche, Switzerland) was carried out to investigate the relative expression of SNHG17 and miR-324-3p. The expression of SNHG17 and miR-324-3p was normalized to GAPDH. Primer sequences were listed as followed: SNHG17, forward: 5'-TGGGAGTGTCACATGACTGC-3', reverse: 5'-GCAGCTCAGCCTCTTCTTGA-3'; miR-324-3p, forward: 5'-GACTATGCCTCCCCGCATC-3', reverse: 5'-GACTACAACCCCCAGCAGC-3'; GAPDH, forward: 5'-CCTGACCTGCGTGTGGACT-3', reverse: 5'-GCTGTGGATGGGGAGGTGTC-3'.

Assays

SNHG17-mut or SNHG17-wt, miR-NC or miR-324-3p mimic were co-transfected into HOS cells by Lipofectamine 2000 (Invitrogen, Waltham, USA). HOS cells were cultured at 37°C, 5% CO2 and 95% humidity. After 48 h of incubation, the luciferase activity of SNHG17 was estimated by dual luciferase reporter assay kit.

HOS cells were cultured in 96-well plates (2×10^3 cells/well) at 37°C and 5% CO_2. After incubation for 24, 48, 72 and 96 h, CCK-8 reagents were added into each well. At the value of 450 nm, the relative optical density (OD) was measured.

Transwell chambers (8 μm; Millipore) were performed to examine OS cell invasion abilities. Cell invasion was detected in the upper chamber with Matrigel. First, 1×10^5 cells were inoculated in the upper Transwell compartment. Then, 10% FBS was added into the lower compartment. After cultivated at 37°C for 24 h, cells were fixed and stained with 0.5% crystal violet. Finally, the invading cell numbers were counted under an optical microscope.

Statistical analysis

The experimental results were analyzed by SPSS 20.0 and Graphpad Prism 6.0. All data were expressed as mean ± standard deviation. One Way ANOVA was used for comparison between multiple groups. The pairwise comparison was performed by Student's *t*-test. The correlation between SNHG17 and miR-324-3p in OS tissues was measured by Pearson's correlation analysis. $p<0.05$ showed that the difference was statistically significant.

RESULTS

SNHG17 knockdown retarded OS cell proliferation and invasion

Primarily, to explore the role of SNHG17 in the progression of OS, the expression of SNHG17 in OS tissues and cell lines was detected by qRT-PCR analysis. The results demonstrated that SNHG17 was dramatically higher expressed in OS tissues than in normal OS tissues (Fig. 1A). Moreover, SNHG17 was found to be up-expressed in OS cell lines (HOS, U2OS and SaoS-2) compared with normal OS cell line hFOB1.19 (Fig. 1B). Based on the experimental results, HOS cells were chosen for the following experiments.

To investigate the specific role of SNHG17 in the progression of OS, si-SNHG17 was transfected into HOS cells. As shown in Fig 1C, the expression of SNHG17 in HOS cells was declined by si-SNHG17. Furthermore, the cell proliferation and invasion were detected by CCK-8 assay and Transwell assay. We found that the knockdown of SNHG17 inhibited the cell proliferation of HOS cells (Fig. 1D). Similarly, SNHG17 knockdown suppressed HOS cell invasion (Fig. 1E). These results displayed that SNHG17 was upregulated in OS tissues and cell line, and the knockdown of SNHG17 restrained cell proliferation and invasion of OS cells,

SNHG17 served as a molecular sponge in the expression of miR-324-3p

Then, the relationship between SNHG17 and miR-324-3p was analyzed by Starbase software. It predicted that there were putative target sequences between miR-324-3p and the 3'-UTR of SNHG17 (Fig. 2A). To verify the hypothesis, Dual luciferase reporter assay was performed to detect the relative luciferase activity when miR-324-3p mimic transfected into SNHG17-wt and SNHG17-mut,

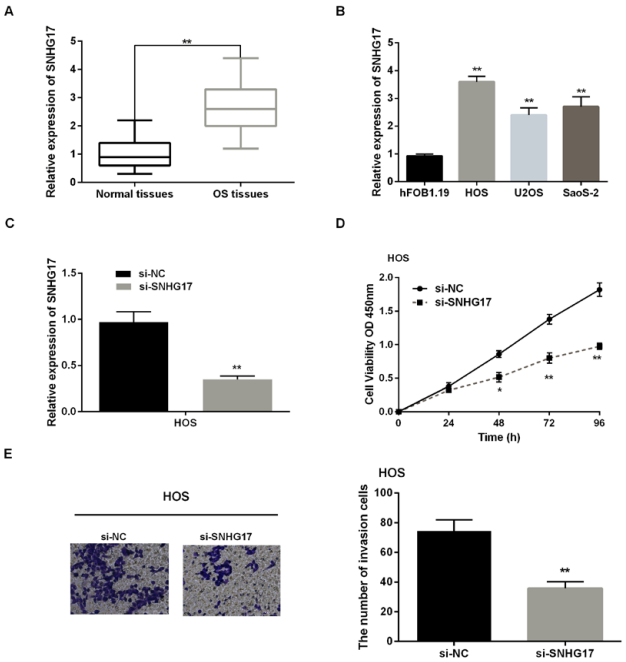

Fig. 1. *SNHG17 knockdown restrained OS cell proliferation and invasion. **A**) the expression of snhg17 was higher in OS tissues than normal tissues. **B**) SNHG17 was upregulated in OS cell lines. **C**) The expression of snhg17 in HOS cells. **D**) SNHG17 silencing repressed cell proliferation of HOS cells. **e**) SNHG17 silencing inhibited cell invasion of HOS cells (magnification: 20×). *p<0.05; **p<0.01*

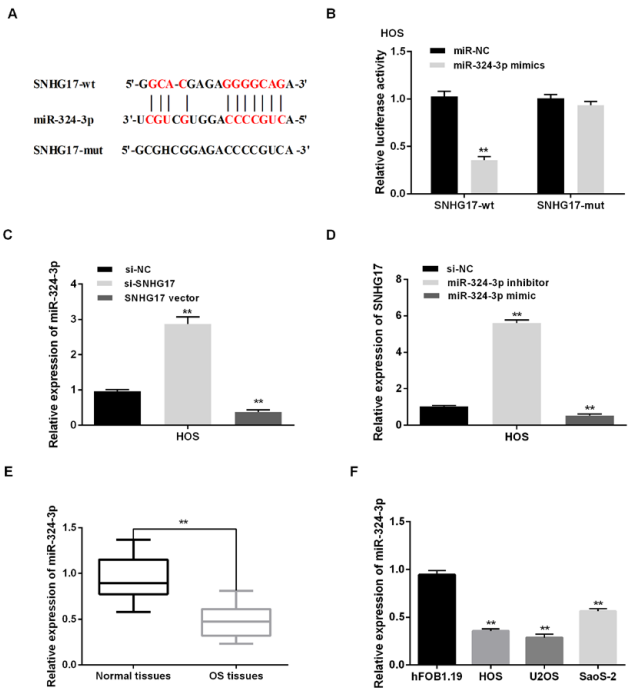

Fig. 2. *SNHG17 served as a molecular sponge in the expression of miR-324-3p. **A**) The binding sites between SNHG17 and miR-324-3p. **B**) The relative luciferase activity of SNHG17-wt and SNHG17-mut. **C**) The expression of miR-324-3p when HOS cells transfected with si-SNHG17 or SNHG17 vector. **D**) The expression of SNHG17 when HOS cells transfected with miR-324-3p mimic or miR-324-3p inhibitor. **E**) The expression of miR-324-3p was lower in OS tissues than normal tissues. **F**) MiR-324-3p was downregulated in OS cell lines. **p<0.01*

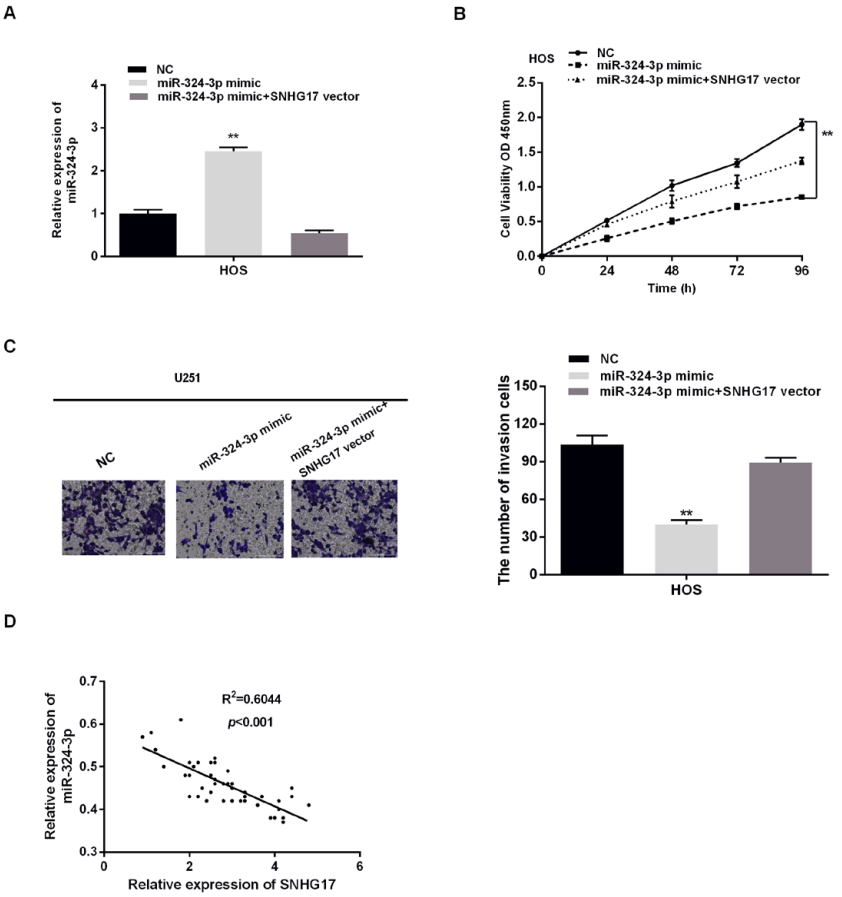

Fig. 3. *SNHG17 modulated the progression of OS via sponging miR-324-3p.* ***A****) The expression of miR-324-3p when SNHG17 vector transfected into HOS cells with miR-324-3p mimic.* ***B****) The cell proliferation of HOS cells with SNHG17 vector transfection.* ***C****) The invasion of HOS cells with SNHG17 vector transfection (magnification: 20×).* ***D****). The correlation between SNHG17 and miR-324-3p. **p<0.01*

which showed that miR-324-3p mimic declined the luciferase activity of SNHG17-wt, but had no effect on SNHG17-mut (Fig. 2B). Moreover, the relationship of SNHG17 and miR-324-3p was detected by qRT-PCR. The expression of miR-324-3p was reduced by si-SNHG17, but increased by SNHG17 vector (Fig. 2C). Furthermore, SNHG17 expression was down regulated by miR-324-3p mimic, but upregulated by miR-324-3p inhibitor (Fig. 2D). Next, the expression level of miR-324-3p in OS tissues and cell lines was studied. The data indicated that miR-324-3p was significantly lower expressed in OS tissues than normal tissues (Fig. 2E). In addition, miR-324-3p was downregulated in OS cell lines (HOS, U2OS and SaoS-2) (Fig. 2F). In consequence, we clarified that SNHG17 served as a sponge to modulate miR-324-3p expression in OS.

SNHG17 modulated the progression of OS via sponging miR-324-3p

To investigate whether SNHG17 regulating the progression of OS by targeting miR-324-3p, miR-324-3p mimic and SNHG17 vector were co-transfected into HOS cells. We found that the upregulation of miR-324-3p induced by miR-324-3p mimic was declined by SNHG17 vector in HOS cells (Fig. 3A). Moreover, CCK-8 assay and

Transwell assay were performed to verify their functional interaction in HOS cells. As shown in Fig. 3B, miR-324-3p mimic inhibited cell proliferation of HOS cells, while SNHG17 vector restored the effect. Transwell assay showed that the downtrend in cell invasion induced by miR-324-3p mimic was restored by SNHG17 vector (Fig. 3C). Furthermore, there was a negative correlation between SNHG17 and miR-324-3p in OS tissues (Fig. 3D). In conclusion, we considered that SNHG17 regulates cell proliferation and invasion in OS by competitively binding with miR-324-3p.

DISCUSSION

In recent studies, a large number of lncRNAs have been found to be involved in the tumorgenesis and development of OS. For instance, SERTAD2-3 suppressed OS progression and migration by sponging miR-29c (6). In our study, SNHG17 was highly expressed in OS tissues and cells, which was consistent with the expression of SNHG17 in gastric cancer in another study (7). Functionally, our results showed that SNHG17 silencing suppressed OS cell proliferation and invasion. Our findings were consistent with previous studies, and proved that SNHG17 functioned as a tumor promoter in OS.

LncRNAs acted as competitive endogenous RNAs (ceRNAs) of miRNAs in human tumors. In this study, SNHG17 was clarified to competitively bind with miR-324-3p. Furthermore, miR-324-3p was downexpressed in OS tissues and cell lines. MiR-324-3p was also found to be in a low expression level in nasopharyngeal carcinoma (8). Functionally, miR-324-3p inhibited cell proliferation and invasion of OS cells, while SNHG17 vector weakened the inhibition effect induced by miR-324-3p mimic. Our findings were in agreement with function of miR-324-3p in breast cancer (9) and prostate cancer (10). In addition, we discovered that there was a negative correlation between SNHG17 and miR-324-3p in 42 OS tissues.

In summary, SNHG17 was first elucidated to accelerate OS cell progression by downregulating miR-324-3p expression. Our findings might provide a novel potential biomarker for the diagnosis and therapy of OS.

REFERENCES

1. Hashimoto K, Nishimura S, Oka N, Akagi M. Outcomes of comprehensive treatment for primary osteosarcoma. SAGE Open Med 2020; doi: 10.1177/2050312120923177.
2. Tsuda Y, Tsoi K, Parry MC, Stevenson JD, Fujiwara T, Sumathi V, Jeys LM. Impact of chemotherapy-induced necrosis on event-free and overall survival after preoperative MAP chemotherapy in patients with primary high-grade localized osteosarcoma. Bone Joint J 2020; 102-B:795-803.
3. Lin W, Zhou Q, Wang CQ, et al. LncRNAs regulate metabolism in cancer. Int J Biol Sci 2020; 16:1194-206.
4. Han N, Yang L, Zhang X, et al. LncRNA MATN1-AS1 prevents glioblastoma cell from proliferation and invasion via RELA regulation and MAPK signaling pathway. Ann Transl Med 2019; 7:784.
5. Xu T, Yan S, Jiang L, et al. Gene amplification-driven long noncoding RNA SNHG17 regulates cell proliferation and migration in human non-small-cell lung cancer. Mol Ther Nucleic Acids 2019; 17:405-13.
6. Zhang Z, Liu J, Wu Y, et al. Long noncoding RNA SERTAD2-3 inhibits osteosarcoma proliferation and migration by competitively binding miR-29c. Genet Test Mol Biomarkers 2020; 24:67-72.
7. Zhang G, Xu Y, Wang S, et al. LncRNA SNHG17 promotes gastric cancer progression by epigenetically silencing of p15 and p57. J Cell Physiol 2019; 234:5163-74.
8. Liu C, Li G, Yang N, et al. miR-324-3p suppresses migration and invasion by targeting WNT2B in nasopharyngeal carcinoma. Cancer Cell Int 2017; 17:2.
9. Fang X, Zhang J, Li C, Liu J, Shi Z, Zhou P. Long non-coding RNA SNHG22 facilitates the malignant phenotypes in triple-negative breast cancer via sponging miR-324-3p and upregulating SUDS3. Cancer Cell Int 2020; 20:252.
10. Han Y, Hu H, Zhou J. Knockdown of LncRNA SNHG7 inhibited epithelial-mesenchymal transition in prostate cancer though miR-324-3p/WNT2B axis in vitro. Pathol Res Pract 2019; doi: 10.1016/j.prp.2019.152537.

LETTER TO THE EDITOR

SNHG16 regulated cerebral ischemia/reperfusion injury via sponging miR-183

Z-W. An[1], C. Chen[2], C-W. Wang[3], C. Zhu[4], F-Z. Chen[4], H-Z. Chen[4] and W. Zheng[4]

[1]Neurosurgery Department, Cangzhou Central Hospital, Cangzhou, Hebei Province, China; [2]Neurosurgery Department, Yanzhou Hospital, Affiliated Hospital of Jining Medical College, Jining, Shandong, China; [3]Neurosurgery Department, Jining NO.1 People's Hospital, Jining, Shandong, China; [4]Neurosurgery Department, The Second Affiliated Hospital of Shandong First Medical University, Taian, Shandong Province, China

Received May 18, 2020 – Accepted July 22, 2020

To the Editor,

Ischemic stroke accounts for more than 80% of strokes and is the third leading cause of death and disability worldwide (1). Although decades of research have focused on cerebral ischemia-reperfusion injury, therapeutic strategies for treating the disease are still limited.

Long non-coding RNAs (lncRNAs) is a subgroup of noncoding RNAs with a length larger than 200 bp (2). As an oncogene, SNHG16 can promote cell migration and cell invasion in multiple cancers (3), however, to the best of our knowledge, whether SNHG16 has a vital influence on the function of cerebral ischemia-reperfusion injury remains elusive.

MicroRNAs (miRNAs) are a type of non-coding RNA with a length of 19-25 nucleotides (4). MiRNAs are a key mediator of gene silencing at post-transcriptional level, which is achieved by binding to the 3'-untranslated region of its target mRNA (5). For example, miR-183 played a cancer-suppressing role in mediating cell migration, cell invasion, epithelial-mesenchymal transition (EMT) and microangiogenesis (6). MiR-183 regulated the maturation, survival and function of photoreceptor cells in the retin (7).

MATERIALS AND METHODS

Cell culture

The HCN-2 cell line (CVCL_3284) was purchased from the American Type Culture Collection (ATCC, Manassas, VA, USA). HCN-2 Cells were cultured in Dulbecco's modified eagle medium (DMEM) medium supplemented with 10% foetal bovine serum (FBS) and penicillin/streptomycin at 37°C in a humid atmosphere of 5% CO2.

Cell model of OGD/R

In order to simulate cerebral ischemia/reperfusion injury *in vivo*, HCN-2 cell oxygen and glucose deprivation reperfusion (OGD/R) model was established. During the process of hypoxia, cells were maintained in Dulbecco's phosphate buffered saline (DPBS) for 5 h. Then, the DPBS was replaced by DMEM medium supplemented with 10% FBS, and maintained in 95% air and 5% CO2 for 20 h to reoxygenate.

Transfection

GenePharma (Shanghai, China) synthesized pEX-SNHG16, shRNA-SNHG16, miR-183 mimic and the corresponding NC. Prior to OGD/R treatment, HCN-2 cells were seeded in six-well plates and transfected with pEX-SNHG16 or shRNA-SNHG16 at a final concentration of

Key words: SNHG16; miR-183; cerebral ischemia-reperfusion injury; apoptosis; proliferation

Corresponding Author:
Wei Zheng,
Neurosurgery Department,
The Second Affiliated Hospital of Shandong First Medical University,
No. 366, Taishan Street, Tai'an 271000, Shandong Province, China
Tel.: +86 13953373558
e-mail: ricaichao78871@163.com

0393-974X (2020)
Copyright © by BIOLIFE, s.a.s.
This publication and/or article is for individual use only and may not be further reproduced without written permission from the copyright holder.
Unauthorized reproduction may result in financial and other penalties
DISCLOSURE: ALL AUTHORS REPORT NO CONFLICTS OF INTEREST RELEVANT TO THIS ARTICLE.

30 nM to produce cells that overexpressed or knocked out SNHG16. In the rescue experiment, shRNA-SNHG16 was transfected into HCN-2 cells overexpressing miR-183. All cell transfections were performed using Lipofectamine 2000 (Invitrogen, Carlsbad, California, USA) according to the manufacturer's instructions.

Cell viability assay

Cell viability was measured by Cell Counting Kit-8 (CCK-8) assay. For CCK-8 analysis, HCN-2 cells were seeded in 96-well plates at a density of 3000 cells per well, and incubated with 100 µl of CCK-8 solution (Dojindo, Kumamoto, Japan) at 37°C for 1 h. The absorbance at 450 nm was measured with a microplate reader, and the cell survival rate was evaluated according to the following formula: (OD treatment-OD blank)/(OD control-OD blank) × 100%.

Cell apoptosis

Following the manufacturer's instructions apoptosis was analyzed on a flow cytometer using an Annexin V-FITC kit (Beyotime, China). Briefly, HCN-2 cells were collected to make a cell suspension (concentration of about 100 cells /ml). Then, FITC-conjugated Annexin V and propidium iodide were sequentially added to these cells, and incubated in the dark at room temperature for 15 min. After that, the cell apoptosis rate was analyzed by flow cytometry (BD FACSCalibur, USA) using CellQuest Pro software.

To determine the interaction between SNHG16 and miRNAs, Starbase was used to predict the miRNAs binding to SNHG16.

Luciferase reporter gene experiment

Luciferase activity experiments were performed to confirm the interaction between miR-183 and SNHG16. The luciferase reporter gene was constructed by cloning the SNHG16 3'UTR sequence including the seed region sequence into plasmid pGL6. To verify miR-183 and SNHG16, HCN-2 cells were co-transfected with wild-type SNHG16 or mutant SNHG16 and miR-183 mimic or miR-NC. All these transfections were performed using Lipofectamine 2000 (Invitrogen). After transfecting for 48 h, the luciferase activity was measured using the Dual Luciferase Reporter Assay System (Promega), and the relative luciferase activity was calculated as the ratio of firefly luciferase to seaweed luciferase. The primers used were: SNHG16 forward 5'-GCAGAATGCCATGGTTTCCC-3' and reverse 5'-GGACAGCTGGCAAGAGACTT-3'; GAPDH forward 5'-ACAACTTTGGTATCGTGGAAGG-3', and reverse 5'-GCCATCACGCCACAGTTTC-3'; miR-183 forward 5'-AGGAGCAGAGGAGGTCTTT-3' and reverse 5'-TATGGCACTGGTAGAATTCACT-3'; U6 forward 5'-GCTTCGGCAGCACATATACTAAAAT-3' and reverse 5'-CGCTTCACGAATTTGCGTGTCAT-3'.

Quantitative real-time PCR

The total RNA of each sample was extracted according to the method described in the Trizol kit (TakaRa Biotechnology Co., Ltd., Dalian, China). Spectrophotometric determination of the purity and concentration of extracted RNA. According to the method described in the commercial transcription kit (TaKaRa), 100 ng RNA in each sample was used for reverse transcription. Using the ABI 7300 Real-Time PCR system, the expression levels of SNHG16 and miR-183 were quantitatively determined by SYBR Premix Ex Taq (TaKaRa) using real-time PCR. Using ABI software, data analysis was performed using the comparative Ct method.

Statistical analysis

All statistical analyses were performed using SPSS 19.0 software (IBM Corp., Armonk, NY, USA), and quantitative data are expressed as the mean ± standard deviation (SD) from three independent experiments. Differences between two groups were analyzed using Student's *t*-test and among multiple groups were analyzed by one-way analysis of variance, followed by Tukey's post hoc test. Values of P less than 0.05 were considered to be statistically significant differences.

RESULTS

Increased expression of SNHG16 in the OGDR model

An OGD/R model was established to simulate the cerebral ischemia-reperfusion injury. The expression of SNHG16 was tested in the OGD/R model. The results showed that compared with the control group, the expression of SNHG16 was significantly up-regulated in OGD/R-treated HCN-2 cells, indicating that cerebral ischemia/reperfusion can enhance the expression level of SNHG16 ($P<0.05$) (Fig. 1A). Next, pEX-SNHG16 or shRNA-SNHG16 was transfected

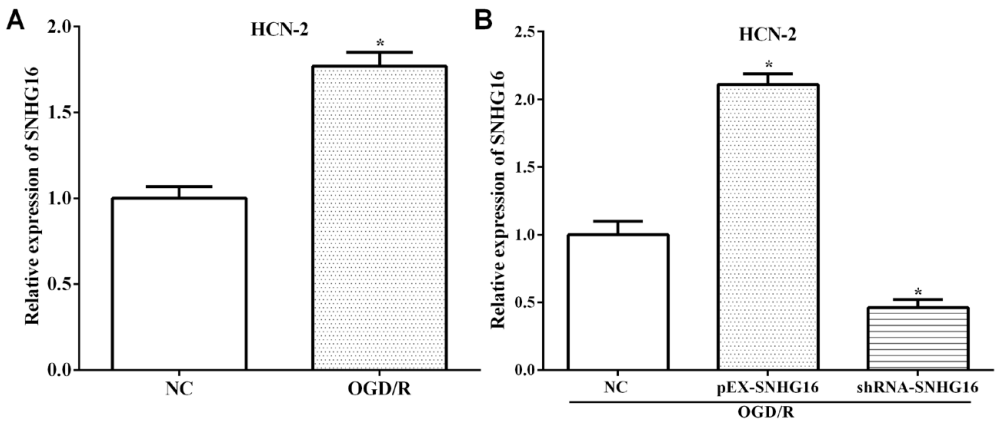

Fig. 1. *The expression of SNHG16 was increased in the OGDR model. OGD/R model was established to simulate the cerebral ischemia-reperfusion injury. The expression of SNHG16 was tested in the OGD/R model. The results showed that compared with the control group, the expression of SNHG16 was significantly up-regulated in OGDR-treated HCN-2 cells, indicating that cerebral ischemia/reperfusion can enhance the expression level of SNHG16. Next, pEX-SNHG16 or shRNA-SNHG16 was transfected into HCN-2 cells cultured under OGDR conditions. Compared with the OGDR group, pEX-SNHG16 can promote its expression, while shRNA-SNHG16 can reduce its expression in HCN-2 cells, indicating that the expression of SNHG16 has been successfully regulated manually.*

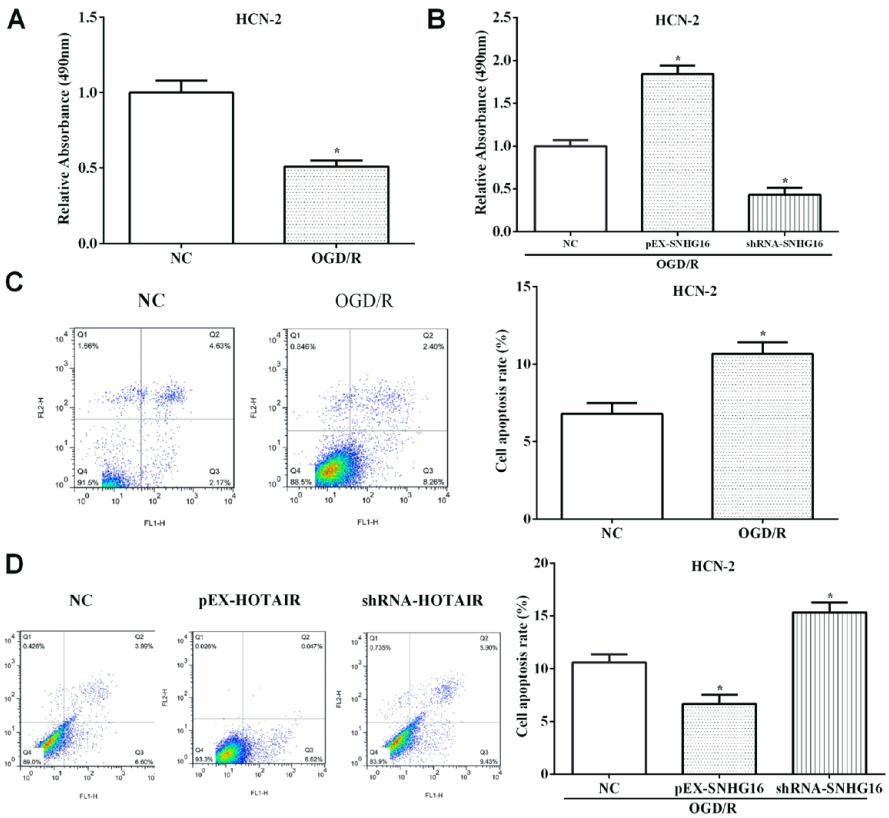

Fig. 2. *SNHG16 regulated cell viability and apoptosis in HCN-2 cells. **A**) OGDR significantly inhibited the viability of HCN-2 cells. **B**) Compared with the NC group, pEX-SNHG16 promoted the proliferation, and shRNA-SNHG16 can inhibit cell proliferation in HCN-2 cells under OGDR. **C**) OGDR treatment promoted cell apoptosis. **D**) Under OGD/R treatment, transfection of pEX-SNHG16 in HCN-2 cells can inhibit cell apoptosis, while shRNA-SNHG16 promotes cell apoptosis.*

into HCN-2 cells cultured under OGD/R conditions. Compared with the OGD/R group, pEX-SNHG16 could promote its expression, while shRNA-SNHG16 could reduce its expression in HCN-2 cells (P<0.05) (Fig. 1B), indicating that the expression of SNHG16 was successfully regulated manually.

SNHG16 regulated the viability and apoptosis in HCN-2 cells

MTT assay was used to detect the effect of SNHG16 on cell viability. The results showed that OGD/R significantly inhibited the viability of HCN-2 cells (P<0.05) (Fig. 2A). Moreover, compared with the NC group, pEX-SNHG16 promoted the proliferation of HCN-2 cells under OGD/R conditions (P <0.05). In contrast, shRNA-SNHG16 can inhibit the proliferation in HCN-2 cells under OGD/R (P <0.05) (Fig. 2B). Therefore, SNHG16 is believed to reverse the role of OGD/R. Next, flow cytometry was used to study the apoptosis of HCN-2 cells regulated by SNHG16 after cerebral ischemic injury. We found that OGD/R treatment promoted cell apoptosis (P <0.05) (Fig. 2C). Moreover, under OGD/R treatment, transfection of pEX-SNHG16 in HCN-2 cells inhibited cell apoptosis (P <0.05), while shRNA-SNHG16 promoted cell apoptosis (P <0.05) (Fig. 2D). These results indicated that overexpression of SNHG16 under OGDR promoted the viability of HCN-2 cells and inhibits apoptosis.

SNHG16 directly binds to miR-183

In addition, the molecular mechanism of SNHG16 inhibiting OGD/R was studied. Starbase database found that SNHG16 had a binding site to miR-183 (Fig. 3A). To confirm the interaction between SNHG16 and miR-183, dual luciferase reporter gene detection was performed in HCN-2 cells. The results showed that up-regulation

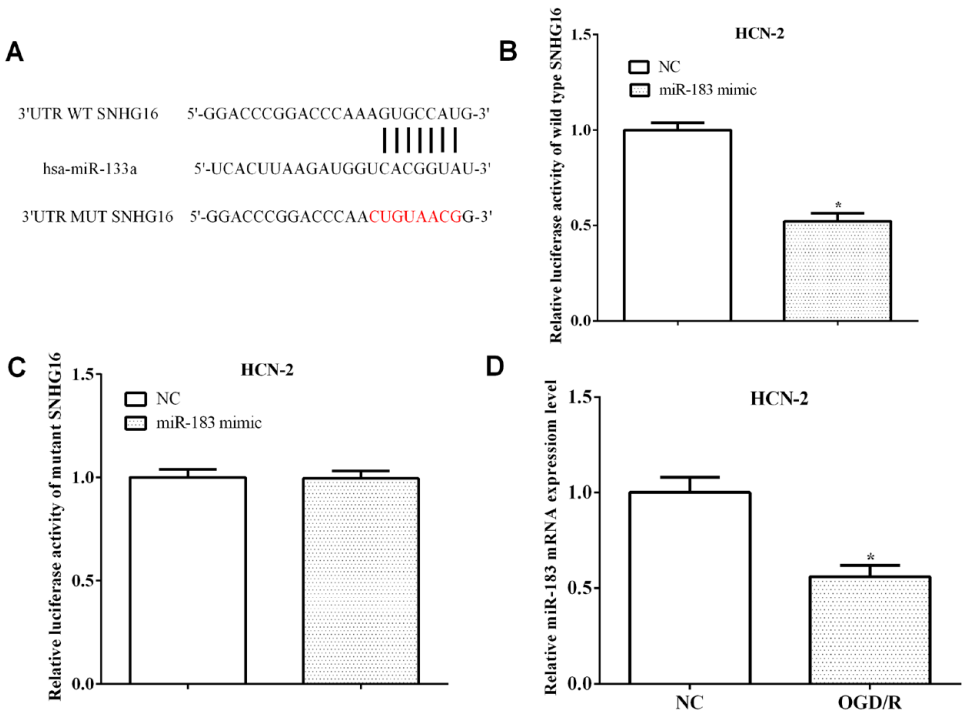

Fig. 3. *SNHG16 directly binding miR-183.* ***A****) Starbase predicted SNHG16 had a binding site of miR-183.* ***B****) Up-regulation of miR-183 significantly inhibited the luciferase activity of wild-type SNHG16.* ***C****) miR-183 mimic had no effect on mutant SNHG16.* ***D****) The expression of miR-183 was significantly reduced under OGDR.*

of miR-183 significantly inhibited the luciferase activity of wild-type SNHG16 (P <0.05) (Fig. 3B). However, miR-183 mimic had no effect on the mutant SNHG16 (P >0.05) (Fig. 3C). The results indicated that SNHG16 directly bind to miR-183. In addition, compared with the group without OGDR, the expression of miR-183 was significantly reduced under OGDR (P <0.05) (Fig. 3D). Therefore, we believe that SNHG16 can regulate cerebral ischemic injury by inhibiting the expression of miR-183.

miR-183 partially revered the effects of SNHG16 on cell viability

Interestingly, pEX-SNHG16 reduced the expression of miR-183 in HCN-2 cells treated with OGD/R (P <0.05) (Fig. 4A). However, shRNA-SNHG16 promoted the expression level of miR-183 (P <0.05) (Fig. 4B). Under OGDR conditions, shRNA-SNHG16 and miR-183 inhibitor were co-transfected into HCN-2 cells to further detect their interaction in cerebral ischemic injury. The results of RT-qPCR analysis showed that the increased expression of miR-183 induced by shRNA-SNHG16 was reversed by the miR-183 inhibitor (P <0.05) (Fig. 4C). More importantly, under OGDR conditions, miR-183 inhibitor partially reversed shRNA-SNHG16's promotion of HCN-2 cell proliferation (P <0.05) (Fig. 4D). Combining these results, we hypothesise that SNHG16 promotes the viability of HCN-2 cells and inhibits apoptosis by regulating miR-183 under OGDR conditions.

DISCUSSION

LncRNA plays an important role in many pathophysiological conditions through sponging miRNA (8). Previously, many studies eported

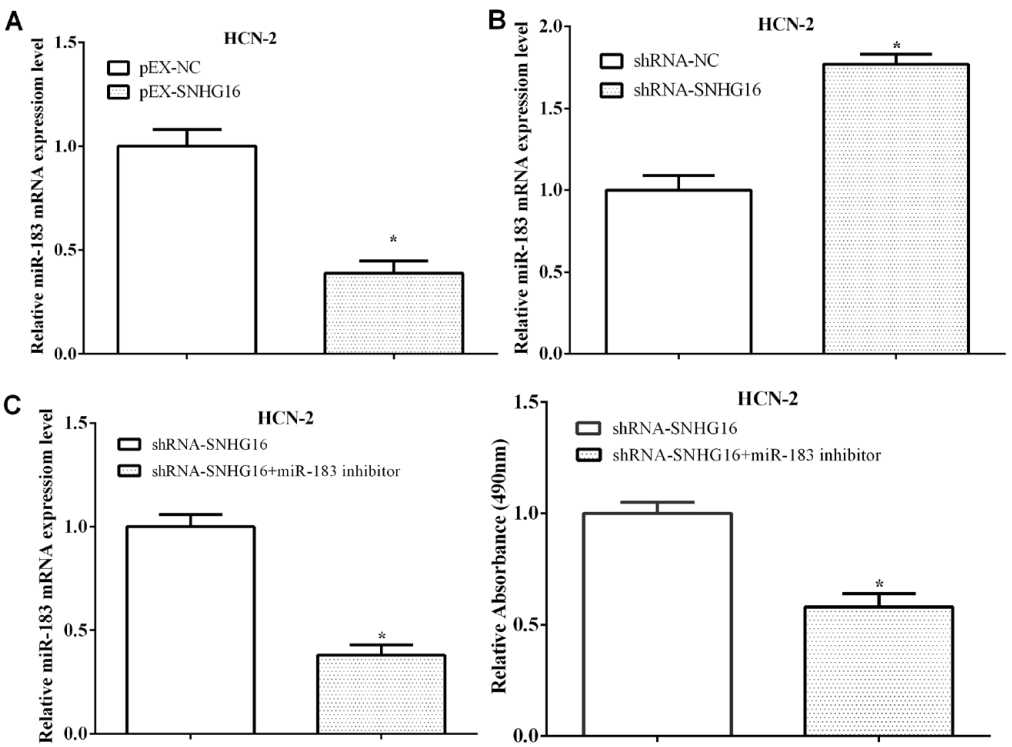

Fig. 4. *miR-183 partially revered the effects of SNHG16 on cell viability.* ***A)*** *pEX-SNHG16 reduced the expression of miR-183 in HCN-2 cells treated with OGDR.* ***B)*** *shRNA-SNHG16 can promote the expression level of miR-183.* ***C)*** *The increased expression of miR-183 induced by shRNA-SNHG16 has been reversed by the miR-183 inhibitor.* ***D)*** *Under OGDR conditions, miR-183 inhibitor reversed shRNA-SNHG16's promotion of HCN-2 cell proliferation.*

that lncRNA can mediate ischemic injury by inhibiting miRNA to regulate brain tissue injury in a model of ischemic stroke (9). In the present study, we found that SNHG16 was overexpressed in OGD/R treated cells compared to the normal HCN-2 cells. The cell proliferation was inhibited in HCN-2 cells treated with OGD/R. Moreover, overexpression of SNHG16 enhanced the proliferation of OGD/R-treated HCN-2 cells compared to normal cells. In contrast, silencing of SNHG16 inhibited the proliferation in OGD/R-treated HCN-2 cells. Treating with OGD/R promoted cell apoptosis by enhancing the expression of Bax but reducing the expression of Bcl-2. In addition, upregulation of SNHG16 suppressed cell apoptosis whereas downregulation of SNHG16 enhanced cell apoptosis. Therefore, these findings suggest a neuroprotective role of SNHG16 in the cerebral ischemia model.

SNHG16 acted as a ceRNA through competitively binding to miR-520a, thereby regulating cell proliferation, migration and invasion, but inducing apoptosis (10). In this study, we first explored that SNHG16 directly binds to miR-183 in OGDR-treated HCN-2 cells, and it was confirmed by using luciferase reporter gene assay. In addition, the expression of miR-183 was regulated by exogenous altering SNHG16. Through rescue experiments, we found that knockdown of miR-183 partially restored the suppressive roles of shRNA-SNHG16 in OGD/R-treated cells.

In conclusion, this study shows that SNHG16 can promote cell viability and inhibit cell apoptosis by sponging miR-183, thereby negatively regulating the brain I/R. This is the first study to explore the neuroprotective effect of SNHG16 /miR-183 axis in cerebral ischemia/reperfusion injury. Our findings will provide new insights into the treatment strategies of brain I/R injury.

REFERENCES

1. Mendis S, Davis S, Norrving B. Organizational update: the world health organization global status report on noncommunicable diseases 2014; one more landmark step in the combat against stroke and vascular disease. Stroke 2015; 46:e121-2.
2. Kondo Y, Shinjo K, Katsushima K. Long non-coding RNAs as an epigenetic regulator in human cancers. Cancer Sci 2017; 108:1927-33.
3. Wu W, Guo L, Liang Z, Liu Y, Yao Z. Lnc-SNHG16/miR-128 axis modulates malignant phenotype through WNT/beta-catenin pathway in cervical cancer cells. J Cancer 2020; 11:2201-12.
4. Armand-Labit V, Pradines A. Circulating cell-free microRNAs as clinical cancer biomarkers. Biomol Concepts 2017; 8:61-81.
5. Galardi A, Colletti M, Businaro P, Quintarelli C, Locatelli F, Di Giannatale A. MicroRNAs in neuroblastoma: biomarkers with therapeutic potential. Curr Med Chem 2018; 25:584-600.
6. Cao D, Di M, Liang J, Shi S, Tan Q, Wang Z. MicroRNA-183 in cancer progression. J Cancer 2020; 11:1315-24.
7. Amini-Farsani Z, Asgharzade S. The impact of miR-183/182/96 gene regulation on the maturation, survival, and function of photoreceptor cells in the retina. 2020; 528:1616-25.
8. Paraskevopoulou MD, Hatzigeorgiou AG. Analyzing MiRNA-LncRNA interactions. Methods Mol Biol 2016; 1402:271-86.
9. Xu X, Ma S, Liu Y. LncRNA SND1-IT1 is involved in rat myocardial ischemia/reperfusion injury via regulating miR-183-5p. Panminerva Med 2020; doi: 10.23736/S0031-0808.20.03905-1.
10. Yu L, Chen D, Song J. LncRNA SNHG16 promotes non-small cell lung cancer development through regulating EphA2 expression by sponging miR-520a-3p. 2020; 11:603-11.

JOURNAL OF BIOLOGICAL REGULATORS & HOMEOSTATIC AGENTS Vol. 34, no. 4, 1541-1543 (2020)

LETTER TO THE EDITOR

Reverse-view pharyngeal swab collection method

L. Zhang*, J-F. Guan* and L. Qu

The Second Affiliated Hospital of Dalian Medical University, Dalian, Lioning, China

Received June 8, 2020 – Accepted July 27, 2020

#These Authors contributed equally to this work

To the Editor,

Novel coronavirus pneumonia (COVID-19) is an infectious disease to which the population is generally susceptible and is mainly transmitted through respiratory droplets and close contact (1). At present, nucleic acid detection is the most important method for diagnosing COVID-19 and plays an important role in early detection, isolation, and treatment (2). Nucleic acid is detected mainly through pharyngeal swab collection. To collect specimens, the original pharyngeal swab method requires the sampled person to open their mouth wide and make an "ah" sound. The sampling person simultaneously wipes the bilateral pharyngeal tonsils and the posterior pharyngeal wall three times with a sampling cotton swab. During the sampling process, when the sampling cotton swab touches the pharyngeal tonsils and the posterior pharyngeal wall, it is easy to cause the sampled person to cough, vomit, or sneeze. The resulting droplets carry viruses that can lead to a risk of infection; even with protection, some sampling personnel will become concerned and try to make accommodations for the sampled person's discomfort. Sometimes this can lead to non-standard sampling operations, which will lead to false negatives. To address this, we tested the pharyngeal swab collection using the reverse view method.

Reverse-view pharyngeal swab collection method

The pharyngeal swab collection method for the reverse-view requires the pharyngeal swab collection item and a round mirror with a diameter of about 13 cm.

Collection method: i. when collecting pharyngeal swabs, the sampled person takes a sitting or a semi-sitting position; ii. the head and face of the sampling staff are located above or behind the head and face of the sampled person. The sampler's angle of view is the same as that of the sampled person (not face-to-face as in the traditional method). iii. take a circular mirror with a diameter of approsimately13 cm and align it with the sampled person's oropharynx to fully expose the oropharynx. The sampling staff then collects pharyngeal swabs using the reflection in the mirror. iv. the remaining steps are the same as the common method for pharyngeal swab collection (Fig. 1).

Advantages of the reverse-view pharyngeal swab collection method

Reduced risk of infection in sampling personnel. The traditional pharyngeal swab collection method requires the sampling staff to face the sampled

Key words: novel coronavirus pneumonia (COVID-19); pharyngeal swab; reverse- view method; specimen collection

Corresponding Author:
Dr Li Qu,
The Second Affiliated Hospital of Dalian Medical University,
No.467, Zhongshan Road, Shahekou District,
Dalian City, Liaoning Province, China
e-mail: qyequ6@163.com

0393-974X (2020)
Copyright © by BIOLIFE, s.a.s.
This publication and/or article is for individual use only and may not be further reproduced without written permission from the copyright holder.
Unauthorized reproduction may result in financial and other penalties
DISCLOSURE: ALL AUTHORS REPORT NO CONFLICTS OF INTEREST RELEVANT TO THIS ARTICLE.

person. Research has found that when people speak loudly, cough, sneeze, or have severe wheezing symptoms, they may produce and expel fine droplets. The trajectory of the majority of generated droplets is to the front of the person, and very few travel to the back, therefore, the sampling staff is much less likely be infected by a virus when standing behind the sampled person, when compared with standing face-to-face.

Alleviates the psychological fear of the sampling personnel in the operation. In early 2020, the novel coronavirus epidemic broke out in China. Sixty-one nurses helping during the pandemic in Wuhan were randomly sampled during my volunteer assistance in Wuhan. When we sampled the nucleic acid throat swabs of patients with the new coronary pneumonia, only 19.67% had no worries at all, 55.74% were a little worried, 11% were more worried, and 6.56% were extremely worried about being infected. These result show that even with a full set of personal protection, many nurses are concerned when sampling nucleic acid pharyngeal swabs for patients with the new coronavirus pneumonia. When the pharyngeal swab is collected using the reverse view method, the sampling staff does not need to directly face the open mouth of the sampled person, which adds additional protection for the sampling staff ‘s mental and physical health.

Makes the operation more standardized and ensures that the sampling results are more accurate. When the sampling personnel are afraid of being infected with such highly contagious and infectious diseases, sometimes the sampling operation feels inconvenient and is not standardized, which will lead to the appearance of false negatives. When using the reverse-view pharyngeal swab collection method, the sampling staff stands behind the sampled person, and is less likely to receive the virus than when standing face-to-face; such a position is safer, thus the psychological fear of the sampling staff is reduced, and the sampling operation is more standardized to ensure the accuracy of the sampling results

Social needs

At present, the diagnosis of the novel coronavirus pneumonia mainly depends on nucleic acid detection. Whether the nucleic acid test results are accurate depends largely on whether the pharyngeal swab specimen collection is standardized. At present, the epidemic situation in China is coming under control. The resumption of production has started, and students have started school. The demand for nucleic acid detection is extremely large, which also places stress on the sampling personnel. A problem that urgently needs to be resolved is how to better protect the sampling personnel to ensure that the collected specimens are more accurate and more standardized. The reverse-view pharyngeal swab collection method, compared with the traditional

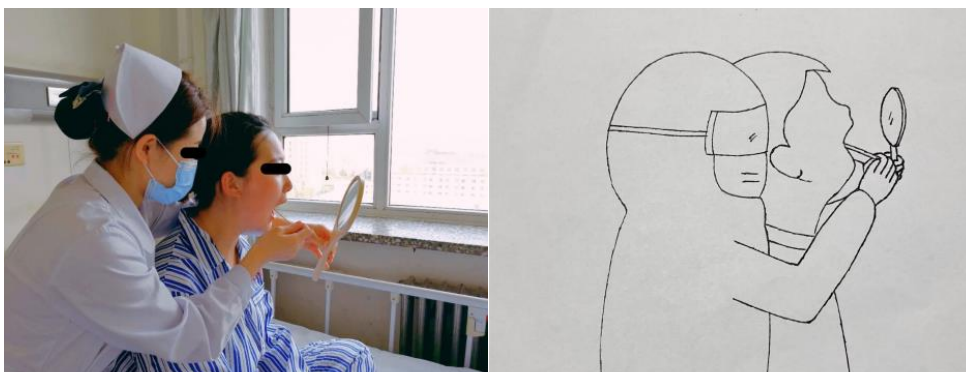

Fig. 1. *Reverse-view pharyngeal swab collection method*

sampling method, reduces both the risk of infection and the psychological pressure of the sampling personnel.

Contraindications of reverse-view pharyngeal swab collection method

When the pharyngeal swab specimens are collected using the reverse-view method, the sampled person needs to be seated, be conscious, and be able to cooperate. It is not suitable for patients in bed, children, or patients with neurological and mental disorders who cannot cooperate.

DISCUSSION

At this stage, COVID-19 has created a global pandemic, and pharyngeal swabs are collected using traditional methods all over the world. Sneezing, coughing, talking, breathing, and other behaviors can produce airborne droplets, which are a source of the infectious virus (3). Breathing, uttering "ah," talking, coughing, sneezing, etc. all cause droplet particles to be released from a person's mouth and nose, but the particle concentration, diameter, and spread range are different (4, 5). Many scientists at home and abroad have studied imaging of these particles. When the droplets are released, they are mainly distributed in front of the sampled person; therefore, if the sampling staff stands behind the patient and collects the pharyngeal swab using the reverse-view method, this can effectively reduce the risk of infection in sampling personnel. Of course, the reverse-view pharyngeal swab collection method is also suitable for the collection of pharyngeal swabs in clinical patients. Our medical staff were infected at the beginning of the novel coronavirus pneumonia pandemic because the arrival of respiratory infectious diseases are often unexpected by humans, not because we were not adequately prepared. In addition, this method is simple and easy to follow, and the cost is very low, which is conducive to promotion.

REFERENCES

1. The General Office of the National Health Commission. Novel coronavirus pneumonia Diagnosis and Treatment Program (Trial Version 7). http://www.nhc.gov.cn/yzygj/s7652m/ the sampled person's 202003/a31191442e29474b98bfed5579d5af95.shtml. 2020-03-04.
2. Han Y, Luan R. Analysis of the application of nucleic acid testing in the diagnosis for novel coronavirus pneumonia. China Meas Test 2020; 46(3):73-76.
3. Feng G, Cai Y, Zhang Y, et al. Research situation of characteristics of aerosol droplet pollution sources. J Heat Ventilat Aircondit 2018, 48(7):22-30.
4. Morawska L, Johnson GR, Ristovski ZD, et al. Size distribution and sites of origin of droplets expelled from the human respiratory tract during expiratory activities. J Aerosol Sci 2009; 40(3):256- 269.
5. Johnson GR, Morawska L, Ristovski ZD, et al, Modality of human expired aerosol size distributions. J Aerosol Sci 2011,42(12): 839-851.

LETTER TO THE EDITOR

Possible phenotyping of apnoea obstructive sleep of female patients

A. Spacone[1], T. Paolucci[2], P. Prosperi[1], N. Giannandrea[2], L. Pezzi[2], R.g. Bellomo[3] and R. Saggini[2]

[1]Respiratory Medicine Department, "Santo Spirito" Hospital, Pescara, Italy; [2]Physical Medicine and Rehabilitation Unit, Department of Medical and Oral Science and Biotechnology (DSMOB), G. D'Annunzio University of Chieti-Pescara, Chieti, Italy; [3]Physical Medicine and Rehabilitation, Carlo Bò University of Urbino, Urbino, Italy

Received December 17, 2019 – Accepted May 21, 2020

To the Editor,

Obstructive sleep apnoea (OSA) is one of the most common form of sleep disordered breathing (SDB) (1). It is characterized by repetitive nocturnal complete collapses (*apnoea*) or partial collapses (*hypopneas*) of the upper airway during sleep. These events are associated with oxygen desaturation and/or arousal from sleep. The severity of OSA is measured by the number of occurrences of airway collapse per hour according to the apnoea-hypopnea index (AHI) (2). Some studies, mostly conducted on men, emphasize how body mass index (BMI), and neck and waist circumference as major predictors of OSA (3). Women with OSA were usually older and more obese than men but had smaller neck circumference (NC) and less centrally distributed fat (3, 4). Several authors have explained the differences between men and women in the symptoms, characteristics, and severity of OSA. The focus of several studies has been on the upper airway: airway length, the tongue, the soft palate, and the total amount of soft tissue in the throat are all smaller in women than in men. Although, intuitively, a smaller airway might be expected to occlude more easily than a larger one, this does not seem to be the case. It appears that men have a longer, softer oropharynx and a larger, fatter, more posterior tongue, increasing the susceptibility of the large airway to collapse (5). Upper airway collapsibility, determined by the pharyngeal critical closing pressure, has been shown to be less in women compared to men when the severity of OSA is the same (6). Also, obesity is an important risk factor for OSA, and higher BMI is associated with greater severity of OSA for both sexes (7). A recent paper has documented important differences between gender (8). Females presented with less severe OSA, lower AHI and shorter apnoeic events. The distribution of fat in the upper airways and visceral abdominal, that is important in the pathogenesis of OSA, appears to be related to gender. Hypothesizing a gender gap compared to OSA, the purpose of this study was to observe the home respiratory sleep test data and correlate them to the anthropometric parameters regarding the two sexes in patients symptomatic for sleep apnoea.

MATERIALS AND METHODS

One hundred and fifty patients with suspected OSA, referred to the Sleep Clinic- Respiratory Medicine Department of "Santo Spirito" Hospital, Pescara (Italy), during six consecutive months, were observed with a home respiratory sleep test. This study was performed per the Helsinki Declaration on human experimentation and

Key words: obstructive sleep apnoea; gender; sleep disordered; rehabilitation; exercise

Corresponding author:
Dr Teresa Paolucci,
Physical Medicine and Rehabilitation Unit,
Department of Medical and Oral Science and Biotechnology (DSMOB),
G. D'Annunzio University of Chieti-Pescara,
Viale Abruzzo 322, 66100 Chieti, Italy
e-mail: teresapaolucci@hotmail.com

0393-974X (2020)
Copyright © by BIOLIFE, s.a.s.
This publication and/or article is for individual use only and may not be further reproduced without written permission from the copyright holder.
Unauthorized reproduction may result in financial and other penalties
DISCLOSURE: ALL AUTHORS REPORT NO CONFLICTS OF INTEREST RELEVANT TO THIS ARTICLE.

all patients gave written informed consent after receiving detailed information on the study aims and procedures. Apnoea was defined by absence of airflow lasting 10 seconds or longer, and hypopnea was defined as any airflow reduction ≥30 or ≥50% lasting 10" or longer, associated, respectively, with either oxygen desaturation ≥4% or arousal (2). AHI was defined as the number of apnoeas and hypopneas per hour/sleep. OSA was diagnosed if AHI was ≥5 events/h. The severity of OSA was determined from AHI and was classified as mild (5 to 15 events/h), moderate (16 to 30 events/h), and severe (> 30/events/h). Subjects with a BMI equal or greater than 30 kg/m^2 were considered obese. Subjective daytime sleepiness, evaluated by the Epworth Sleepiness Scale (ESS), was defined as a score ≥10 (9). A descriptive statistical analysis was carried out reporting the mean and standard deviation (SD) of each parameter and clinical scale used: the continuous and categorical variables were synthesized and the comparison between the groups was checked with the *t*-test, the *chi*-squared test and the analysis of variance. The Pearson's test was performed for correlation. A $p < 0.05$ was statistically significant.

RESULTS

Of the 150 patients with suggestive clinical symptoms of OSA observed in the study, 91 patients confirmed the diagnosis of OSA: 21 females and 70 males (female/male ratio 1:3.3). Characteristics of the study population are shown in Table I. Moreover, Table II shows anthropometrics and sleep data for both gender groups.

Compared with males, females showed higher BMI,

Table I. *Characteristics of study population*

Parameters	Age (yrs)	ESS	NC (mm)	WC (mm)	BMI (Kg/m^2)	AHI (n/h)	A/h (n/h)	H/h (n/h)	SpO2 (%)	T<90%
Patients (N=91)	59.9±13.2	12±3	41±5.3	90±10.2	31.6±5.1	28.7±21.4	87.7±7.8	99.2±4.9	91.3±3.2	20.5±13.2

T: time, SpO2: oxygen saturation; H/h: number of hypopneas in an hour; A/h: number of apneas in an hour; AHI: index of apneas and hypopneas; ESS: Epworth Sleepiness Scale; WC: waist circumference; NC: neck circumference; BMI: body mass index

Table II. *Anthropometrics and sleep data for both genders*

Clinical Parameters	Female (N=21)	Male (N=70)	*p* * (female/male)
Age (yrs)	62.8±11.8	59.1±13.7	-
ESS	13± 2	15± 3	-
NC (mm)	38±4.2	43±4.5	-
WC (mm)	102±4.5 *	88±6.5 *	p<0.05
BMI (Kg/m^2)	34.5±5.8 *	30.7±4.5 *	p<0.05
AHI (n/h)	24.9±24.9	29.9±20.3	-
A/h (n/h)	57.9±4.2	96.7±4.2	-
H/h (n/h)	121.2±4.2*	92.3±3.2*	p<0.05
SpO2 (%)	90.3±4.2	92.3±2.4	-
T<90%	30±12.4 *	18.7±9.4 *	p<0.05

T: time, SpO2: oxygen saturation; H/h: number of hypopneas in an hour; A/h: number of apneas in an hour; AHI: index of apneas and hypopneas; ESS: Epworth Sleepiness Scale; WC: waist circumference; NC: neck circumference; BMI: body mass index

and had lower neck and higher waist circumference. The females had a significantly greater proportion of hypopneas (121.2±4.2 *vs* 92.3±3.2 $p<0.05$). There were no statistical differences in terms of obstructive apnoea and central apnoea. Comparing the two sexes, there was no statistically significant difference in AHI and there was a homogeneous distribution of the gravity of the OSA. Correlation analyses showed significant correlations between anthropometric indexes in females compared to males.

DISCUSSION

Our results confirmed the ratio of 3:1 (M:F) as the community-based studies showed the range of 2:1 or 3:1 for OSA (2). Also, Guilleminault et al. (6) found among the females a relevant underlying psychological distress related to the obesity characterized by the presence of tension and depression, by a different hormonal or metabolic configuration between obese women and obese men. In our work, waist circumference and BMI suggested to be independent risk factors for females, and daytime sleepiness was similar in both sexes. Despite the same severity of OSA, the females presented sleep disturbances characterized from more nocturnal hypoventilation events than the men with similar age. These results were consistent with other previous studies that reported a difference of upper airway collapsibility, difference in terms of central and peripheral stimuli causing the end of apnoea events and hormonal difference in males in respect to females (4).

Better knowledge of gender differences in OSA could help to improve the awareness and diagnosis of OSA in females, and the development and availability of therapeutic options that consider differences in the physiology of OSA in females should have the potential to improve outcomes for patients. The results suggested that females showed a greater clustering of hypoventilation events during sleep than males with a precise gender gap: also, obesity and visceral adiposity index were good marker of phenotyping of obstructive sleep apnoea in respect to gender.

REFERENCES

1. Orjuela-Cañón AD, Cerquera A, Freund JA, Juliá-Serdá G, Ravelo-García AG. Sleep apnea: Tracking effects of a first session of CPAP therapy by means of Granger causality. Comput Methods Programs Biomed 2019; 187:105235. doi: 10.1016/j.cmpb.2019.105235.
2. Vishesh KK, Dennis H, et al. Clinical Practice Guideline for Diagnostic Testing for Adult Obstructive Sleep Apnea: An American Academy of Sleep Medicine Clinical Practice Guideline 2017.
3. Kapsimalis F, Kryger MH. Gender and obstructive sleep apnea syndrome, part 2: mechanisms. Sleep 2005; 25:499-506.
4. Quintana_Gallego E, Carmona-Beranl C, Capote F, et al. Gender differences in obstructive sleep apnea syndrome: a clinical study of 1166 patients. Respir Med 2004; 98(10): 984-989.
5. Millman RP, Carlisle CC, McGarvey ST, Chervin R, Black J, Clerk A. Body fat distribution and sleep apnea severity in women. Chest 1995; 107:362-66.
6. Guilleminault C, Stoohs R, Kim YD, et al. Upper airway sleep-disordered breathing in women. Ann Intern Med 1995; 122:493-501.
7. Strobel RJ, Rosen RC. Obesity and weight loss in obstructive sleep apnea: a critical review. Sleep 1996; 19:104-15.
8. Wimms A, Woehrle H, Ketheeswaran S, Ramanan D, Armitstead J. Obstructive sleep apnea in women: specific issues and interventions. Bio Med Res Int 2016; 27:1-27.
9. Johns MW. A new method for measuring daytime sleepiness: the Epworth sleepiness scale. Sleep 1991; 14(6):540-45.
10. Jordan AS, Wellman A, Edwards JK, et al., Respiratory control stability and upper airway collapsibility in men and women with obstructive sleep apnea. J App Physiol 2005; 5:20-27.

LETTER TO THE EDITOR

Antibiotic therapy in oral surgery: a cross sectional survey among Italian dentists

S. D'Agostino and M. Dolci

Department of Medical, Oral and Biotechnological Sciences, University of Chieti Pescara, Chieti, Italy

Received March 24, 2020 – Accepted June 4, 2020

To the Editor,

Antibiotic prescription for oral surgery procedures and infective disease represents a highly debated topic in dentistry. As is well known from the literature, oral microbiome is composed by 700 taxa, of which 170 are also isolated in the blood stream, and it is also well known that oral procedures, invasive or non, are involved in transient bacteremia (1). It is for that reason we decided to conduct a study to better understand what kind of antibiotic therapy or prophylaxis was mostly used in order to avoid local and systemic complications. This is a cross-sectional study describing Italian dentists' knowledge in Abruzzo (Italy) in 2012 regarding the use of antibiotic prophylaxis in certain oral surgery procedures, as well as the molecule choice, dosage, modality and the timing of administration. As a secondary aim, we decided to investigate the knowledge and use of the antibiotic scheme proposed by the American College of Cardiology/American Heart Association (ACC/AHA) in 2008 for the IE prophylaxis (2).

MATERIALS AND METHODS

One thousand questionnaires were sent by mail to dentists in private practices in Abruzzo, of which only 93 were filled in anonymously and returned for review. The questionnaire was made up of 8 questions based on essay questions and multiple choice. Only one question was related to the use of the scheme for Infective Endocarditis prophylaxis proposed by the ACC/AHA in 2007, whereas five questions concerned oral surgery, antibiotic administration, chosen drugs, administration via, amount and timing.

In 2007, the American Heart Association revised the guidelines for the prevention of Infective Endocarditis, establishing that a single oral administration of 2 grams of Amoxicillin 30 to 60 minutes before the dental procedure was sufficient to protect from an infective event. Other possibilities related to the impossibility of oral subministration, as in allergic patients, are described in Table I (2). Each dentist who participated in the anonymous study was required to report only their graduation year and the university they attended. The collected data were tested for statistical analysis.

RESULTS

The survey was conducted in an Italian region, Abruzzo, of about 1,300,000 people. As previously indicated, 1,000 anonymous questionnaires were sent by mail. Only 93 dentists participated in the study, and they all graduated between 1973 and 2009. The reason for which the remaining (907 dentists) did not cooperate is unknown, and only one of them justified their non-participation in the questionnaire due to an internship in England. With reference to their graduations, 64 of them achieved their degree in

Key words: antibiotic therapy; dentistry; infective endocarditis; oral surgery

Corresponding Author:
Prof. Marco Dolci,
c/o Dept. Of Medical, Oral and Biotechnological Sciences,
University of Chieti Pescara
Via dei Vestini, 31, 66100 Chieti, Italy
Tel.: +39 328 1665925
e-mail: marco.dolcimd64@gmail.com

0393-974X (2020)
Copyright © by BIOLIFE, s.a.s.
This publication and/or article is for individual use only and may not be further reproduced without written permission from the copyright holder.
Unauthorized reproduction may result in financial and other penalties
DISCLOSURE: ALL AUTHORS REPORT NO CONFLICTS OF INTEREST RELEVANT TO THIS ARTICLE.

the University "G. d'Annunzio" of Chieti and in the University of L'Aquila, both located in Abruzzo cities. The remaining 29 dentists completed their studies in other Italian universities.

The analyzed data showed that 53.06% of the dentists were used to prescribing antibiotic coverage for all oral surgeries, 25.51% only in case of infective complications, and 20.41% solely in interventions with flap preparation. The molecule choice was amoxicillin, of which 24.3% used it pure, 21.5% in association with clavulanic acid, whereas 7.48% used clarithromycin. The remaining 46.72% used a variety of molecules belonging to the group of penicillins, macrolide, cephalosporins and lincosamides, although in low doses. The first choice for administration was oral in 65.26%, followed by 2.11% through intramuscular administration. Surprisingly 30.53% declined answering this question. In regard to antibiotic posology, 42.71% did not answer, and 37.5% administer ed 1g/*bis in die*. Antibiotic administration was started in 34.38% of cases the day before the surgical operation, in 19.79% of cases the same day, and in 15.63% two or more days before. Administration lasted up to 5/6 days in 51.06% of cases, and also in this case 30.85% did not give an answer. The scheme proposed by the ACC/AHA in 2008 for the prophylaxis of infective endocarditis was used by 52.69% of dentists, with no response in 10.75%. Last, but not least, it emerged that the main reason that influenced the choice of the antibiotic molecule was in 30.25% a summoned "clinical efficacy" and only in 15.97% a review of the literature, or the application of guidelines, was considered.

DISCUSSION

The debate on antibiotics in dental procedures has always been controversial, especially in the field of oral surgery and in the need to prevent infections in surgical sites or infections of distant organs (involving principally the endocardium), and avoiding overtreatment and possible side effects,

Table I. *(From Wilson 2007, modified)*

Regimen for a Dental Procedure			
		Regimen: single dose 30 to 60 min before procedure	
Situation	Agent	Adults	Children
Oral	Amoxicillin	2 g	50 mg/kg
Unable to take oral medication	Ampicillin OR Cefazolin or Ceftriaxone	2 g IM or IV 1 g IM or IV	50 mg/kg IM or IV 50 mg/kg IM or IV
Allergic to penicillins or ampicillin-oral	Cephalexin OR Clindamicin OR Azithromycin or Claritromycin	2 g 600 mg 500 mg	50 mg/kg 20 mg/kg 15 mg/kg
Allergic to penicillins or ampicillin and unable to take oral medication	Cefazolin Or Ceftriaxone OR Clindamycin	1 g IM or IV 600 mg IM or IV	50 mg/kg IM or IV 20 mg/kg IM or IV

IM: intramuscular

IV: intravenous

high costs and antibiotic resistance related to their use. According to our data, practitioners are more likely to prescribe antibiotic therapy for any kind of oral surgical procedure, thereby disregarding the fact that patients could be high or low risk patients. According to Lodi et al., the of antibiotic prophylaxis led to a lower risk of infection, dry sockets and pain following third molar extraction and resulted in an increase in mild and transient adverse effects. In the same paper the authors highlighted the fact that, due to an increasing prevalence of bacteria which are resistant to treatment by current available antibiotics, clinicians should carefully consider whether treating 12 healthy patients with antibiotics to prevent one infection is likely to do more harm than good (3). Singh et al. shared the same opinion, and concluded that clinicians should decide on the actual need to use antibiotics after a careful evaluation of the risks in developing an allergic reaction or antibiotic resistance (4). Menon et al. examined data related to 1,615 tooth extractions over 5 years in clinical records of 992 patients. Antibiotics were prescribed postoperatively in 44% of the extractions. The overall infection rate was 2.05%. There was no significant difference in infection rates between the groups which underwent extractions with or without antibiotics (OR = 0.68; P = 0.289). We found a significantly higher risk for infections with increasing age (P = 0.002) (5).

According to one systematic review, literature reveals ambivalent results in antibiotic use for dentoalveolar procedures, such as third molar or implant surgery (6). In our study, amoxicillin was the antibiotic of choice for oral surgery, although it was preferably used by only 24.3% of the operators examined, and 1.87% used ampicillin which has the same spectrum of amoxicillin, but it is absorbed less and has more gastro-intestinal side effects.

The combination of amoxicillin and clavulanic acid was used by 21.5%, and should be considered a second choice antibiotic; this is probably due to the killing strategy of beta-lactamase-producing bacteria. Macrolides (erythromycin, spiramycin, clarithromycin, roxithromycin) were prescribed for a total of 13.08%, but clarithromycin is a second choice antibiotic for all, though it becomes the first choice for the treatment of penicillins-allergic patients. Other antibiotics were not considered as the first choice, such as Lincosamides and Cephalosporins, which are normally considered as reserve antibiotics for the treatment of bone infections or anaerobic infections refractory to common treatments. These data seem to concur with the literature. Thornhill et al. (2019) pointed out amoxicillin as molecule of choice, leaving other drugs as second-rate therapy (7). The preferred administration route was oral, as also emphasised by the literature. Crincoli (2014) noted that there is no difference between oral and intramuscular via, with the exception of reduced gastrointestinal disorders related to oral administration (8).

With regard to posology, 42.71% did not give an answer and 37.5% administered 1g every 12 hours, even though no one indicated the reason for that kind of timing. In accordance with the literature, there is no advantage in postoperative recovery following or not an antibiotic scheme of therapy in healthy patients (9). Only 15.97% answered that molecule choice was related to a review of scientific literature, while other responses indicated that the drug choice was based on pharmacokinetic characteristics (good absorption in bone tissue 1.68%, better absorption 0.84%, elimination path 0.84%). Finally, there is still someone who nowadays relies on the experience of others (4.2%) and on the greater knowledge of a given molecule (1.18%).

With reference to Taubert and Wilson (2017), it seems that there is no need for infectious endocarditis (IE) prophylaxis for dental treatments, except for surgery, such as tooth extraction, in patients with cardiac problems. It is due to this fact that normal dental procedures imply a transient bacteremia, and IE prophylaxis does not seem to avoid it. For that reason the UK has deleted IE prophylaxis entirely, while the USA and European societies have not (10).

According to our data, it emerges from this study that there is an irrational choice about the use of antibiotics, and prescribing it for all oral surgery procedures. As well stated in literature, these habits could lead to an antibiotic lack of efficacy due to inducted resistance. In light of this, patients who do not need antibiotic prophylaxis should receive a careful post-operative follow-up, and only when there is an actual onset of infection signs or symptoms, a

correct antibiotic therapy should be undertaken, which has been proved conclusive in literature, in controlling a confirmed infection.

REFERENCES

1. Kilian M, Chapple IL, Hannig M, et al. The oral microbiome - an update for oral healthcare professionals. Br Dent J 2016; 221:657-66
2. Wilson W, Taubert KA, Gewitz M, et al. Prevention of infective endocarditis: guidelines from the American Heart Association: a guideline from the American Heart Association Rheumatic Fever, Endocarditis, and Kawasaki Disease Committee, Council on Cardiovascular Disease in the Young, and the Council on Clinical Cardiology, Council on Cardiovascular Surgery and Anesthesia, and the Quality of Care and Outcomes Research Interdisciplinary Working Group. Circulation 2007; 116:1736-54.
3. Lodi G, Figini L, Sardella A, et al. Antibiotics to prevent complications following tooth extractions. Cochrane Database Syst Rev 2012; 11:CD003811.
4. Singh Gill A, Morrissey H, Rahman A. A systematic review and meta-analysis evaluating antibiotic prophylaxis in dental implants and extraction procedures. Medicina (Kaunas) 2018; 54:95
5. Menon RK, Kar Yan L, Gopinath D, Botelho MG. Is there a need for postoperative antibiotics after third molar surgery? A 5-year retrospective study. J Investig Clin Dent 2019; 10(4):e12460.
6. Blatt S, Al-Nawas B. A systematic review of latest evidence for antibiotic prophylaxis and therapy in oral and maxillofacial surgery. Infection 2019; 47:519-55.
7. Thornhill MH, Dayer MJ, Durkin MJ, et al. Oral antibiotic prescribing by NHS dentists in England 2010-2017. Br Dent J 2019; 227:1044-50.
8. Crincoli V, Di Comite M, Di Bisceglie MB, et al. Which route of antibiotic administration should be used for third molar surgery? A split-mouth study to compare intramuscular and oral intake. Clin Ter 2014; 165(1):e12-e16.
9. Milani BA, Bauer HC, Sampaio-Filho H, et al. Antibiotic therapy in fully impacted lower third molar surgery: randomized three-arm, double-blind, controlled trial. Oral Maxillofac Surg 2015; 19:341-46.
10. Taubert KA, Wilson W. Is endocarditis prophylaxis for dental procedures necessary? Heart Asia 2017; 9:63-67.

LETTER TO THE EDITOR

Evaluation of the effect of protective genetic variants on cART success in HIV-1-infected patients

E.M. Lori[1], A. Cozzi-Lepri[2], A. Tavelli[3], V. Mercurio[1], S.V. Ibba[1], S. Lo Caputo[4], F. Castelli[5], A. Castagna[6], A. Gori[7], G. Marchetti[8], C. Venditti[9], M. Clerici[10-11], A. D'Arminio Monforte[8] and M. Biasin[1]: for Icona Foundation Study Group

[1]Department of Biomedical and Clinical Sciences, University of Milan, Milan, Italy; [2]Institute for Global Health, University College London. London, United Kingdom; [3]Icona Foundation, Milan, Italy; [4]Clinic of Infectious Diseases, University of Bari, University Hospital Policlinico. Bari, Italy; [5]University Department of Infectious and Tropical Diseases, ASST degli Spedali Civili di Brescia, University of Brescia. Brescia, Italy; [6]Department of Infectious Diseases; San Raffaele Scientific Institute, University Vita-Salute San Raffaele. Milan, Italy; [7]Infectious Diseases Unit, Fondazione IRCCS Ca' Granda Ospedale Maggiore Policlinico, Department of Pathophysiology and Transplantation, School of Medicine and Surgery, University of Milan. Milan, Italy.; [8]Clinic of Infectious and Tropical Diseases, ASST Santi Paolo and Carlo, Department of Health Sciences, University of Milan. Milan, Italy; [9]UOC Microbiologia, Banca Biologica e Cell Factory, National Institute for Infectious Diseases 'Lazzaro Spallanzani' IRCCS. Rome, Italy; [10]Department of Physiopathology Medical-Surgery and Transplantation, University of Milan, Milan, Italy; [11]Don C. Gnocchi Foundation ONLUS, IRCCS, Milan, Italy

Received December 2, 2019 – Accepted June 10, 2020

To the Editor,

HIV-1 infection is not a genetic disease; nevertheless, genetic factors could influence its susceptibility and progression. First evidence of this assumption dates back to 1996, when a homozygous variant for CCR5 chemokine receptor, Δ32, was described showing a strong association with HIV-1 sexual transmission (1). Indeed, different phenotypes associated with non-classical outcomes to HIV-1 exposure and infection have been observed, leading to the development of the "immunological advantage" concept; a condition where the genetic background allows to control HIV-1 infection/replication in fortunate patients (2, 3). Some of the genes to date associated to this peculiar state include the ones briefly described hereafter. Endoplasmic Reticulum Associated Aminopeptidase type 2 (ERAP2) plays a key role in antigen presentation mechanisms. Trimming the N-terminal region of peptides ERAP2 adjusts the final peptide length for optimal binding to HLA class I molecules and modulates specific CTL responses (4). Haplotype-specific alternative splicing of ERAP2 gene results in either full-length (FL, hapA) or alternatively spliced (AS, haplotype B) mRNA; HapA is observed to be higher in HIV-Exposed Sero-Negative (HESN) individuals, suggesting its involvement in conferring natural resistance to HIV-infection (5, 6). APOBEC3H, part of the APOBEC3 family, controls HIV-1 resistance at different levels (7). HAPI APOBEC3H haplotype is associated with sexual protection in HIV-1 transmission (7). Myxovirus resistance 2 (MX2) interferes with the

Key words: HAART, polymorphisms, ICONA, ERAP2, HIV-1

Corresponding Author:
Prof. Mara Biasin, Associate Professor,
Chair of Immunology, Department of Biomedical and Clinical Sciences
"L. Sacco", University of Milan,
Via G.B. Grassi, 74, 20157, Milan, Italy
Tel.: +39 0250319679 - Fax: +39 02 50319677
e-mail: mara.biasin@unimi.it

0393-974X (2020)
Copyright © by BIOLIFE, s.a.s.
This publication and/or article is for individual use only and may not be further reproduced without written permission from the copyright holder.
Unauthorized reproduction may result in financial and other penalties
DISCLOSURE: ALL AUTHORS REPORT NO CONFLICTS OF INTEREST RELEVANT TO THIS ARTICLE.

viral replication, decreasing nuclear viral DNA accumulation and integration (8). The G allele of rs2074560 in MX2 gene reveals protection from HIV-1 infection regardless of the transmission route (9). Regarding Toll-like receptor 3 (TLR3), in two HESN cohorts, a higher frequency of rs3775291 SNP (Leu412Phe) was observed, suggesting protection against HIV-1 infection (10). Keeping in mind that none of the above-mentioned polymorphisms provides an absolute protection for HIV-1 infection, we decided to verify whether these genetic variants - individually or in combination - might modulate the initial immunological and virological responses to antiretroviral therapy (ART).

MATERIALS AND METHODS

Sample collection

Three hundred HIV-infected patients from the ICONA Foundation Study cohort undergoing a first ART regimen were enrolled in the study. These were a random sample of the cohort for which there were at least one year of virological follow-up and a full blood sample collected at some point in the study. Blood samples were collected from each patient in EDTA Vacutainer® tubes. Immediately after collection, peripheral blood mononuclear cells (PBMCs) were isolated and stored at -80°C. Subsequently, cells were transferred to the laboratories of the University of Milan for genotyping analyses. Periodically (6 months and 1 year) HIV-infected patients' clinical parameters (genotype, gender, $CD4^+$ cell count, viral load, therapies, year of infection, clinical evolution) were analyzed and inserted into a predisposed electronic database. The study was designed and conducted in accordance with the Declaration of Helsinki and approved by the Ethics Committee of the hospitals involved in the study. After thoroughly explaining the project and clarifying any doubt concerning the research, all subjects signed an informed consent and the biological material collected was anonymized to ensure the privacy of each individual.

Genotyping

DNA was extracted by the Maxwell® RSC Instrument automated following a nucleic acid purification method (Promega, Madison, Wisconsin, USA) associated with Maxwell® RSC Blood DNA Kit Technical Manual (Promega, Madison, Wisconsin, USA). Genomic DNA was used as template for PCR amplification using TaqMan probes specifically designed to perform an SNP genotyping assay (Applied Biosystems, Foster City, CA, USA). The amplification and fluorescence reading were carried out as previously described.

Statistical analyses

The allelic discrimination method was used to determine the frequency of each single nucleotide polymorphism (SNP). The main characteristics of the study population at the time of ART initiation are described and tabulated (Table I). Separate models were employed to evaluate the association between the detection of the genetic variants and HIV-RNA, $CD4^+$ cell count and $CD8^+$ cell count (as well as their ratio) responses to ART. For the HIV-RNA response, the time to achieving a value ≤50 copies/mL after ART initiation was evaluated by means of standard survival analysis and Kaplan-Meier curves. The date of the first HIV-RNA value ≤50 copies/mL after ART initiation (a single value) was used to define the time of achievement of viral suppression. Participants' follow-up was censored at the date of their last available viral load. For each gene and all four endpoints (HIV-RNA, $CD4^+$ cell count, $CD8^+$ cell count and CD4/CD8 ratio) a linear mixed model was used to compare intercept and slopes according to variant detection. Variability between patients was controlled using random intercepts and slopes. Viral load (VL) was fitted in the log10 scale to achieve distribution symmetry. Besides testing the associations with each gene variant, also a genotypic score was constructed by allocating 1-point every time a variant was detected and summing all points per participants (i.e. a patient in whom ERAP2 rs2549782 G/G was detected as well as rs3775291 C/T or T/T for TL3 and none of the others would have a value of 2 for the score, etc.). In detail, participants were stratified in 3 groups for the survival analysis (with score values >3; 2-3 and 0-1) and comparing those with extremes scores in the mixed linear regression by fitting a binary variable. The score is referred as 'supergenotype' throughout the results of this chapter. All models were fitted on the whole dataset of 300 participants, and after restricting to 255 participants of Caucasian origins.

RESULTS

Analysis of allelic variants in the ICONA cohort

Analysis of SNP prevalence in the selected genes did not show any difference compared with the European population distribution reported in the U.S. National Library of Medicine Database (Table II A-B). The presence of single and combined polymorphisms is reported in Table II C.

Correlation between single allelic variants and clinical parameters at baseline and 1 year after first ART administration

We did not observe any significant association between the analyzed allelic variants and clinical parameters of HIV$^+$ patients enrolled in the ICONA cohort at baseline. No correlation between APOBEC3H, TLR3 and MX2 SNPs and either HIV-1 viral load or CD4$^+$ or CD8$^+$ T cell count slopes was observed in our cohort 12 months post-cART administration (data not shown). Conversely, we observed an association between the rs2549782 GG variant of ERAP2 and the HIV viral load decay after first cART start (Fig. 1A). After adjusting for age, gender, CD4$^+$ T cell count and HIV-RNA at cART start, use of INSTI or >3 drugs, ART-naive and year of cART starting, a non-significant steeper decline in HIV VL was detected for GG genotype compared

(A)

	ERAP2 rs2549782			
	TT/GT	GG	Δ VL	p
Baseline VL	3.30 (3.16, 3.45)	3.70 (3.41, 3.98)	-0.39 (-0.71, -0.08)	0.015
VL change/year	-2.54 (-2.73, -2.35)	-3.07 (-3.44, -2.69)	0.53 (0.11, 0.94)	0.013
Adjusted* VL change/year	-2.59 (-2.79, -2.39)	-3.05 (-3.44, -2.65)	0.46 (0.02, 0.90)	0.042

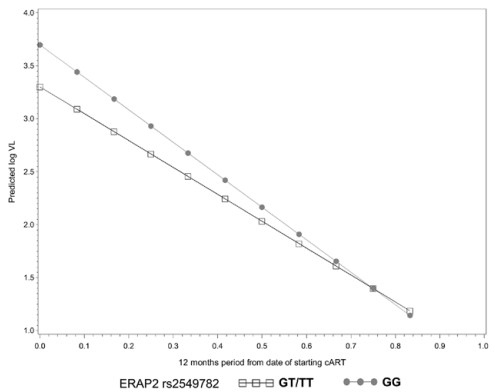

(B)

	ERAP2 rs2549782			
	TT/GT	GG	Δ CD4 count	p
Baseline CD4 count	457.6 (426.0, 489.2)	399.4 (336.9, 461.8)	58.2 (-11.4, 127.9)	0.101
CD4 count change/year	214.3 (182.0, 246.5)	257.9 (194.3, 321.5)	-43.6 (-115.0, 27.4)	0.228
Adjusted* CD4 count change/year	222.9 (189.3, 256.5)	272.2 (205.6, 338.9)	-49.3 (-124.0, 24.9)	0.193

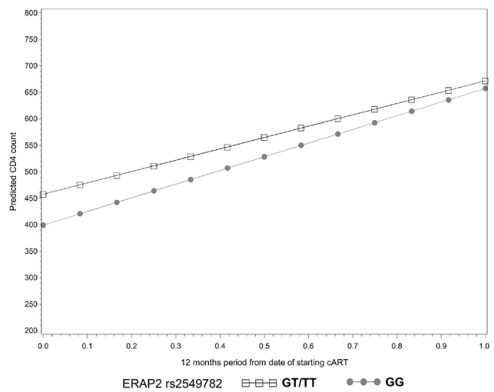

(C)

	ERAP2 rs2549782			
	TT/GT	GG	Δ CD8 count	p
Baseline CD8 count	1227 (1147, 1308)	1077 (917.3, 1236)	150.4 (-27.3, 328.2)	0.097
CD8 count change/year	-142 (-208, -75.9)	-0.10 (-132, 132.0)	-142 (-289.0, 5.1)	0.058
Adjusted* CD8 count change/year	-133 (-205, -62.4)	-12.2 (-160, 135.6)	-121 (-284.0, 41.8)	0.145

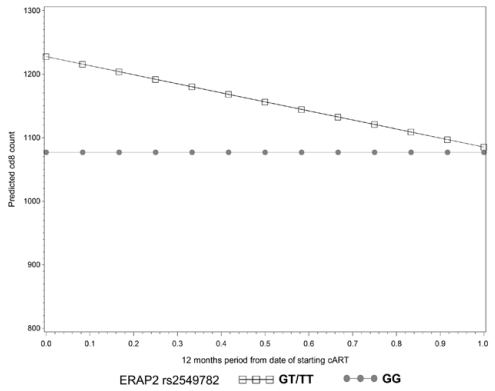

(D)

	ERAP2 rs2549782			
	TT/GT	GG	Δ ratio	p
Baseline ratio	0.43 (0.39, 0.47)	0.47 (0.39, 0.55)	-0.03 (-0.12, 0.06)	0.456
Ratio change/year	0.28 (0.24, 0.32)	0.30 (0.23, 0.38)	-0.02 (-0.11, 0.06)	0.604
Adjusted* ratio change/year	0.28 (0.24, 0.32)	0.33 (0.24, 0.41)	-0.04 (-0.13, 0.05)	0.341

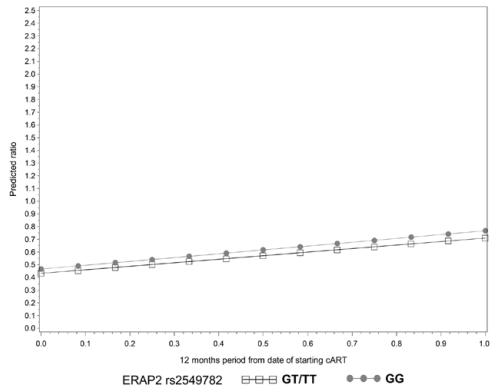

Fig. 1. *Mean intercept and slope of log10 Viral Load (**A**), CD4$^+$ T Cells (**B**), CD8$^+$ T Cells (**C**) and ratio of CD4/CD8$^+$ T cells (D) from fitting a mixed-linear model in Caucasian subjects of ICONA cohort according to ERAP2 genotype (data adjusted for age, gender, ratio and VL at cART, use of INSTI or >3 drugs, ART-naïve and year of cART starting.*

Table I. *Clinical parameters of HIV+ patients enrolled in the ICONA cohort.*

Characteristics	Total
	N = 300
Age, years Median (IQR)	38 (32-45)
Gender, n (%) Female	31 (10.3%)
Mode of HIV transmission n (%) IDU Homosexual contacts Heterosexual contacts Others/Unknown	 13 (4.4%) 198 (66.4%) 77 (25.7%) 10 (3.4%)
AIDS, diagnosis n (%) Yes	24 (8.0%)
HBsAb, n(%) Negative Positive Not tested	 228 (76.0%) 3 (1.0%) 69 (23.0%)
HCVAb, n(%) Negative Positive Not tested	 229 (76.3%) 21 (7.0%) 50 (16.7%)
Calendar year of starting ART Median (IQR)	2013 (2012-2014)
Time from HIV diagnosis, months Median (IQR)	12 (1 - 50)
CD4 count nadir, cells/mmc Median (IQR)	354 (242 - 450)
CD4 count at ART, cells/mmc Median (IQR)	385 (268 - 496)
CD8 count at ART, cells/mmc Median (IQR)	1047 (775 - 1396)
Viral load set point, log10 copies/ml Median (range)	4.5 (3.8 – 5.1)
Viral load at cART, log10 copies/ml Median (range)	4.6 (1.6 – 7.0)
Time to VL suppression, months Median (IQR)	4 (3-7)

AIDS: acquired immune deficiency syndrome; ART: antiretroviral therapy; IDU: injective drug users; HB: hepatitis; HCV: hepatitis C; HIV: human immunodeficiency virus; VL: viral load.

to GT and TT variants: difference in adjusted HIV-RNA mean change/year (GT/TT – GG): +0.36 log10 copies/mL; p=0.09. (26).

Caucasian patients carrying this genotype also showed a trend towards a steeper increase in $CD4^+$ T cell count (difference in adjusted $CD4^+$ mean change/year (GT/TT - GG)= -49 cells/mmc; p=0.19) (Fig. 1B). As for $CD8^+$ data in GG patients, TT/GT genotyped patients showed a significant decrease in $CD8^+$ T cell count over the year (adjusted $CD8^+$ mean change/year=-133 cells/mmc (95% CI: -205, -62.4), while the same marker in GG patients remained constant (as supported by the analysis showing a the significant difference in slope) (p=0.14) (Fig. 1C). Indeed, we observed no differences in CD8+ T cell count over 1-year-treatment (adjusted $CD8^+$ mean

Table II. ***A)*** *Genotyping results of prevalence and frequency of single SNPs for ERAP2 (endoplasmic reticulum associated aminopepetidase type 2), MX2 (myxovirus resistance 2), APOBEC3H, TLR3 (Toll-like receptor 3) in subjects of the ICONA cohort. Protective SNPs are underlined.* ***B)*** *References and distribution of of genetic variants reported in U.S. National Library of Medicine Database (1000Genome).* ***C)*** *Number/ Sum of protective alleles in subjects of ICONA cohort.*

A

	ERAP2		
	GG	GT	TT
Frequency	60	157	83
%	20	52.33	27.67

	APOBEC3H		
	CC	CG	GG
Frequency	63	140	97
%	21	46.67	32.33

	MX2		
	AA	AG	GG
Frequency	135	134	31
%	45	44.67	10.33

	TLR3		
	CC	CT	TT
Frequency	155	120	25
%	51.67	40	8.33

B

Gene	Variant	Alleles	Frequency
ERAP2	rs2549782	G>T	G=0.447284/2240
MX2	rs2074560	A>G	G=0.454872/2278
APOBEC3H	rs139299	G>C	G=0.470248
TLR3	rs3775291	C>T	T=0.231829/1161

C

No. of protecting variants in the super-genotype score*	No. HIV+ participants (N=300)
0-1	N= 131 (44%) No variants n=25 (19%) ERAP n=5 (5%) MX2 n=5 (5%) TL3 n=14 (13%) APOBECC3H n=82 (77%)
1.5-2.5	APOBECC3H+ERAP+MX2 n=1 (0.6%) N=157 (52%) MX2+ TL3 n=2 (1%) APOBECC3H+MX2+TL3 n=3 (2%) APOBECC3H+MX2 n=12 (8%) ERAP+ TL3 n=22 (14%) APOBECC3H+ERAP n=25 (15%) APOBECC3H+TL3 n=92 (58%)
3+	N=12 (4%) ERAP+ MX2+TL3 n=1 (8%) APOBECC3H+MX2+TL3 n=5 (42%) APOBECC3H+ERAP+TL3 n=4 (33%) All four variants n=2 (17%)

(A)

	ERAP2		
	GG	GT	TT
SNP score	1	0	0

	APOBEC3H		
	CC	CG	GG
SNP score	0	0.5	1

	MX2		
	AA	AG	GG
SNP score	0	0	1

	MX2		
	CC	CT	TT
SNP score	0	1	1

(B)

SNP score	Frequency	%	Cumulative frequency	Cumulative %
0	25	8.3	25	8.3
0.5	53	17.7	78	26.0
1	53	17.7	131	43.7
1.5	72	24.0	203	67.7
2	70	23.3	273	91.0
2.5	15	5.0	288	96.0
3	10	3.3	298	99.3
4	2	0.7	300	100.0

(C)

SNP score	Frequency	%	Cumulative frequency	Cumulative %
0	19	7.5	19	7.5
0.5	49	19.2	68	26.7
1	43	16.9	111	43.5
1.5	63	24.7	174	68.2
2	59	23.1	233	91.4
2.5	14	5.5	247	98.9
3	7	2.8	254	99.6
4	1	0.4	255	100.0

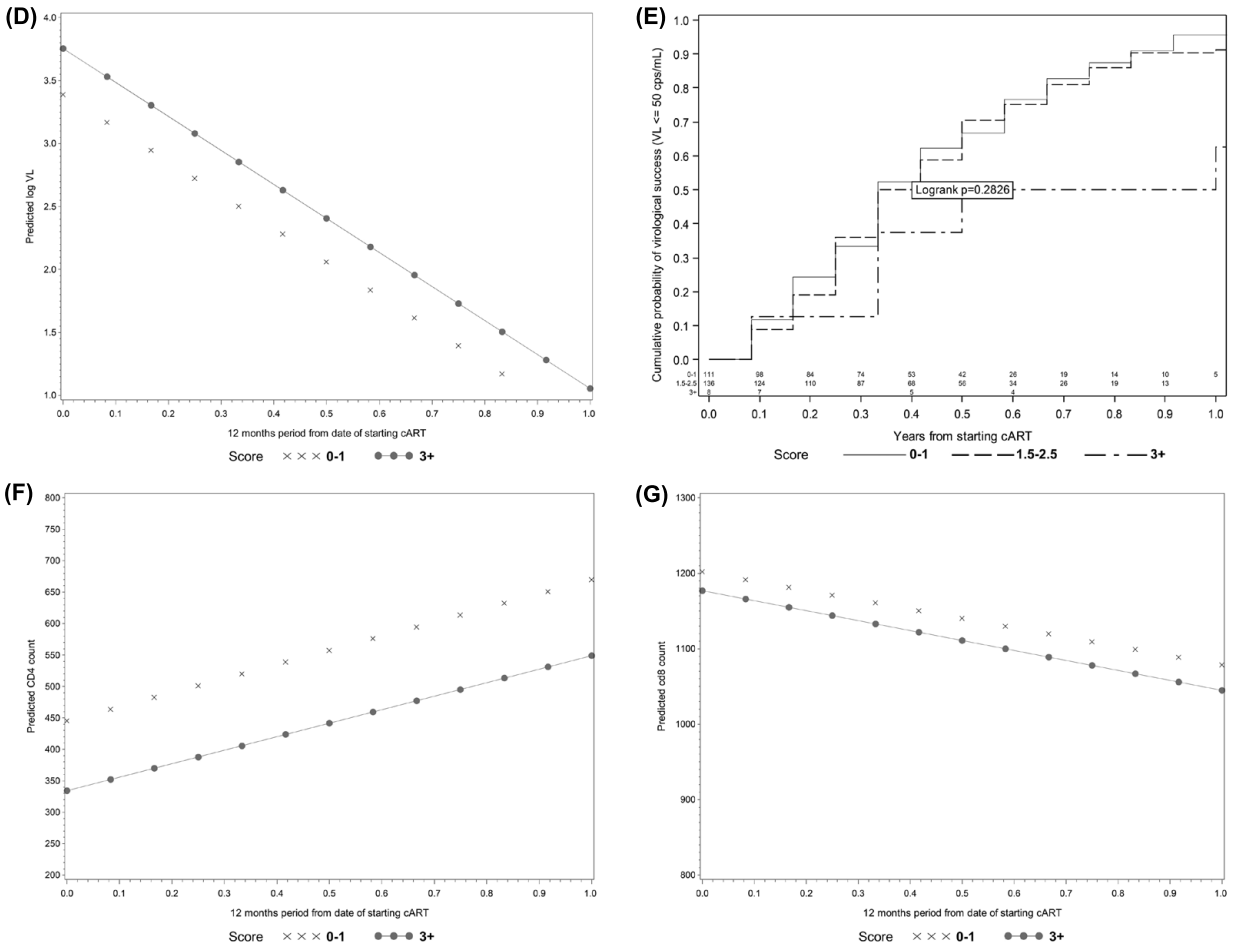

Fig. 2. *SNP score assigned to each variant (**A**) and frequency-percent of total cohort subjects (**B**) and Caucasian subjects (**C**) related to the score. Mean intercept and slope of log10 Viral Load (**D**), CD4$^+$ T Cells (**F**) and CD8$^+$ T cells (**G**) after cART start from fitting a mixed-linear model in Caucasian subjects according to SNPs score strata (data adjusted for age, gender, ratio and VL at cART, use of INSTI or >3 drugs, ART-naive and year of starting ART) and Kaplan-Meier curves estimating the cumulative probability of virological success (E) according to SNPs score strata.*

change/year=-12.2 cells/mmc) (95% CI: -160,135.6). Nevertheless, independently from the genotype, no significant differences in $CD4^+/CD8^+$ cell ratio were observed over time in our cohort (p=0.34) (Fig. 1D).

Correlation between combined allelic variants and clinical parameters

One of the aims of this study was also to identify polymorphism combinations (a "supergenotype") in genes that are considered to be protective in viral infection/replication control and response to ART by monitoring the clinical parameters of interest (VL and CD4 or CD8 cell count). Therefore, a score (SNP score) was assigned to each SNP (Fig. 2 A-C) in order to identify a combination of variants that could provide an immunological benefit in terms of infection progression and response to therapy. The analysis, however, did not show significant correlations between variant combinations and response to therapy either in terms of VL (Fig. 2 D-E) or of $CD4^+$ or $CD8^+$ T cell count (Fig. 2 F-G).

DISCUSSION

As per definition, the immune system of HIV-infected individuals is not characterized by the "immunological advantage" observed in HESN (2). However, one or more protective genetic variants could confer a better control over disease progression if compared with patients who do not express such haplotypes. The aim of this study was to investigate a possible correlation between response to ART and selected host genetic variants in HIV-infected patients, with the goal to optimize pharmacological intervention in HIV-1-infected subjects. Results showed that allelic variants in ERAP2 gene result in a more favorable virologic and immunologic response to therapy. Indeed, a significant reduction in viral load and a trend in $CD4^+$ cell recovery was observed at 12 months post-ART initiation in GG homozygous (Hap A), compared to TT homozygous (Hap B) or G/T heterozygous patients at ERAP2 SNP rs2549782. Considering the key role played by ERAP2 in the activation of antiviral (11) and HIV-specific immune response (5, 6, 12), it is possible to speculate that HapA ERAP2 generates more immunogenic peptides able to trigger a more efficient CTL HIV-specific response, even in ART-treated HIV patients.

As corollary of our results, a "super genotype" associated with a better response to ART response and characterized by the presence of several "protective" allele variants was still not observed. Nevertheless, the preliminary results obtained upon analyzing ERAP2 warrant the usefulness of investigating the role of Hap A in a case/control study, both in the progression of the infection and in response to treatment.

ACKNOWLEDGEMENTS

ICONA Foundation is supported by unrestricted grants from Gilead Science, Janssen, MSD and ViiV Healthcare. This project was realized with the support of Gilead Fellowship Program (Italy) who provided an unrestricted grant.

REFERENCES

1. Deng H, Liu R, Ellmeier W, et al. Identification of a major co-receptor for primary isolates of HIV-1. Nature 1996; 381(6584), 661.
2. Miyazawa M, Lopalco L, Mazzotta F, Lo Caputo S, Veas F, Clerici M, ESN Study Group. The 'immunologic advantage'of HIV-exposed seronegative individuals. AIDS 2009; 23(2):161-75.
3. Fenizia C, Rossignol JF, Clerici M, Biasin M. Genetic and immune determinants of immune activation in HIV-exposed seronegative individuals and their role in protection against HIV infection. Infect Genet Evol 2018; 66:325-34
4. Stratikos E, Stern LJ Antigenic peptide trimming by ER aminopeptidases—Insights from structural studies. Mol Immunol 2013; 55(3-4):212-19.
5. Cagliani R, Riva S, Biasin M, et al. Genetic diversity at endoplasmic reticulum aminopeptidases is maintained by balancing selection and is associated with natural resistance to HIV-1 infection. Hum Mo Genet 2010; 19(23):4705-14.
6. Biasin M, Sironi M, Saulle I, et al. Endoplasmic reticulum aminopeptidase 2 haplotypes play a role in modulating susceptibility to HIV infection. AIDS 2013; 27(11):1697-706.

7. Cagliani R, Riva S, Fumagalli M, et al. A positively selected APOBEC3H haplotype is associated with natural resistance to HIV-1 infection. Evolution 2011; 65(11):3311-22.
8. Kane M, Yadav SS, Bitzegeio J, et al. MX2 is an interferon-induced inhibitor of HIV-1 infection. Nature 2013; 502(7472):563.
9. Sironi M, Biasin M, Cagliani R, et al. Evolutionary analysis identifies an MX2 haplotype associated with natural resistance to HIV-1 infection. Mol Biol Evol 2014; 31(9):2402-14.
10. Sironi M, Biasin M, Cagliani R, et al. A common polymorphism in TLR3 confers natural resistance to HIV-1 infection. J Immunol 2012; 188(2):818-23.
11. Saulle I, Ibba SV, Torretta E, et al. Endoplasmic reticulum associated aminopeptidase 2 (ERAP2) is released in the secretome of activated MDMs and reduces in vitro HIV-1 Infection. Front Immunol 2019; 10:1648.
12. Saulle I, Vicentini C, Clerici M, Biasin M. An Overview on ERAP Roles in Infectious Diseases. Cells 2020; 9(3):720.

LETTER TO THE EDITOR

Microcurrents in the treatment of chronic pain: biological, symptomatological and life quality effects

G. Barassi[1*], A. Younes[1], P.A. Di Felice[1], A. Di Iulio[2], S. Guerri[1], L. Prosperi[1], A. Stamile[3] and A. Di Iorio[4]

[1]Physiotherapy Rehabilitation and Re-education Centre (Ce.Fi.R.R.) venue 'G. d'Annunzio University', Chieti-Pescara, Italy; [2]UOC Thoracic Surgery, 'Santo Spirito' Hospital Pescara – ASL Pescara, Italy; [3]University Hospital Polyclinic 'G. Martino', University of Messina, Messina, Italy; [4]Department of Aging Sciences, 'G. Annunzio' University Chieti-Pescara, Chieti, Italy

Received March 18, 2020 – Accepted June 11, 2020

To the Editor,

Chronic Pain (CP) is a condition, with or without a specific organic cause, that persists longer than a usual three to six months of organic recovery. A functional somatic syndrome (FSS) is characterized by a persistent pattern of bodily symptoms that cannot be sufficiently pathologically explained after adequate physical examination (1). CP and FSS include fibromyalgia (FM) and often involve psychological or social problems. Comorbid mental disorders have been found in 35% of patients with CP. In addition, economic costs of sick leave and early retirement exceed the total amount of medical expenditures associated with both CP and FM (2). Many different approaches have been proposed in the past for the management of CP and FM (3). Recognition of the role of bioelectricity in tissue healing provides a rationale for the therapeutic application of electrical stimulation. Microcurrent therapy (MCT) is one example (4, 5). HD2000+ (Luxxamed GmbH, Kassel, Germany) is a therapeutic machine based on the principle of cellular bioregulation (BCR). It is a type of MCT which is able to analyze the patient's cellular metabolism through an internal impedance meter, detects a measurement and modulate the micro-current in intensity, polarity, frequency and damping in a completely automatic way. During the treatment, the modulation of the current changes with the variation of the tissue resistance in response to the metabolic modification of the cells. The aim of this is to stimulate a homeostasis status in the treated tissue through the application of microcurrents characterized by low intensities (variable between 1μA and 999μA) and modulated frequencies (variable between 0.1Hz and 10kHz). The purpose of this study is to evaluate the effects on CP in patients with FM associated with FSS evaluated through Visual Analogue Scale (VAS), the European Quality of Life-5D (EQ-5D), Fibromyalgia Sympotms Severity Scale (FSSc) and Bioelectrical Impedance Analysis (BIA) (6).

MATERIALS AND METHODS

Patients were recruited at the Physiotherapy Rehabilitation and Re-education Center (CeFiRR) venue at Gabriele d'Annunzio University, Chieti-Pescara, to allow interested parties to assess their suitability. All patients selected from March to October 2019 with CP with a diagnosis of FM associated with FSS were chosen for this study. The exclusion criteria were: cancer, antihypertensives, antidepressants, anxiolytics drugs, pregnant women and pacemacker

Key words: chronic pain; fibromyalgia; electric stimulation therapy; myofascial pain syndromes

Corresponding Author:
Dr Giovanni Barassi,
Physiotherapy Rehabilitation
and Re-education Centre (Ce.Fi.R.R.) venue
"Gabriele d'Annunzio University" Chieti-Pescara,
Viale Abruzzo, 322 Chieti Scalo 66100, Italy
e-mail: coordftgb@unich.it

0393-974X (2020)
Copyright © by BIOLIFE, s.a.s.
This publication and/or article is for individual use only and may not be further reproduced without written permission from the copyright holder.
Unauthorized reproduction may result in financial and other penalties
DISCLOSURE: ALL AUTHORS REPORT NO CONFLICTS OF INTEREST RELEVANT TO THIS ARTICLE.

carriers. A total of 24 Caucasian subjects affected by CP were enrolled in the study (4 males and 20 females, aged 26 to 60 years with an average age of 41.9±8.2). Patients gave informed consent to the experimental procedure, which was in accordance with the latest revision of the Helsinki Declaration for human research and with the procedures relating to the protection of privacy of the subjects participating in biomedical research, as defined by ISO 9001- 2015 for research and experimentation (7).

Patients received a total of 10 MCT treatments, 2 times a week for 5 weeks. Each session consisted of the administration of microcurrents through the BCR system. The hypothesis is based on the principle that MCT are similar to the MCT produced by the body during tissue healing and can therefore be particularly useful where endogenous healing has failed. This means that tissue organs, such as skin, tendons and muscles, which are in a pathological metabolic state, are treated until an impedance shift in the desired direction occurs. In the therapeutic context, this can be observed through relaxation of the muscles (rebalancing of the tone), better elasticity of the fascia, and reduction of pain in the patient. All patients underwent a treatment of 24 minutes per session with the "Inflammation" program. The "Inflammation" program is divided into 6 steps (4 minutes each) shown in Table I.

The microcurrents provided by the device work in the range of 0.1Hz-10kHz (in 0.1Hz steps) and 1μA-999μA (in 1μA steps) and can be administered through 4 channels, each one able to transmit microcurrents through 2 electrodes. All the 4 channels were used, and the electrodes were placed as shown in Table II. Patients were evaluated at T0 (before treatment) and T1 (after five weeks of treatment) and the results were measured using VAS which is a well-known scale used for the evaluation of perceived subjective pain, indicated as values in a defined numerical scale normally between 0 and 10. The EQ-5D defines the health status and it is measured in terms of five dimensions (5D) such as mobility, self-care, usual activities, pain/discomfort, and anxiety/depression. FSSc is a diagnostic and evaluative instrument for FM. It is composed by 2 subscales: Widespread Pain Index (WPI) and the Symptoms Severity scale (SS). BIA measures body composition by sending a low and safe electric current through the body. The parameters considered for this study were the basal metabolic rate (BMR), the percentage of lean mass and fat mass (% LEAN and% FAT) and the total body water in liters (water). Each patient needed four hours fasting with no physical exercise for at least 12 hours.

Table I. *Steps of the "Inflammation" program*

- Step 1: current = 150 μA, frequency = 40 Hz, rising time = 0.8 seconds, polarity = + (plus)
- Step 2: current = 150 μA, frequency = 81 Hz, rising time = 0.8 seconds, polarity = + (plus) - Step 3: current = 150 μA, frequency = 284 Hz, rising time = 0.8 seconds, polarity = + (plus)
- Step 4: current = 150 μA, frequency = 396 Hz, rising time = 0.8 seconds, polarity = + (plus)
- Step 5: current = 150 μA, frequency = 91 Hz, rising time = 0.8 seconds, polarity = +/- (bi-polar)
- Step 6: current = 150 μA, frequency = 9 Hz, rising time = 0.8 seconds, polarity = +/- (bi-polar)

Table II. *Electrode positioning*

- Channel A: from right plantar fascia to the right lumbar area (approximately at the level of L1)
- Channel B: from left plantar fascia to the left lumbar area (approximately at the level of L1)
- Channel C: from the right to the left paravertebral area (approximately at the level of T5)
- Channel D: from the right to the left-hand palm

RESULTS

Statistical analysis was performed using the NCSS 11 software (Kaysville, Utah, United States of America), using the non-parametric Wilcoxon Signed-Rank Test. The level for significance was set at $p < 0.05$.

Statistical analysis of outcome measures showed that there was a statistically significant improvement on VAS scale. There was a decrement in the level of perceived pain of a better feeling that promotes the recovery and reduces the discomfort. A statistically significant improvement should be noted also in the EQ-5D measure of health-related quality of life (Table III). The results confirmed that this approach is not detrimental to the wellbeing of patients in terms of autonomy and perception of themselves. Moreover, BIA measures showed that there was an increment of lean mass and total body water and a decrement of fat mass, even if none of these variations resulted statistically significant (Table IV). Finally, a statistically significant reduction in the score of the FSSc was detected, indicating an improvement of the symptomatology in terms of number of painful areas and of severity of symptoms (Table V).

Table III. *Comparison of the significance of changes in health status and pain variables from T0 to T1*

Variables	Mean ± SD	*p**
(T0) EQ-5D index	0.47±0.27	
(T1) EQ-5D index	0.81±0.17	0.00003
(T0) VAS	6.9±2.4	
(T1) VAS	4.41±1.8	0.001

EQ-5D index: European Quality of Life-5D indexM; VAS: Visual Analogue Scale for pain; p value is referred to the difference between T0-T1 of variables (Wilcoxon matched-pairs signed rank test)

Table IV. *Comparison of the significance of changes in Body Impedence Analysis variables from T0 to T1*

Variables	Mean ± SD	*p**
(T0) BMR	1510.8±49.4	
(T1) BMR	1578.4±37.3	n.s.
(T0) %FAT	34.7±10.5	
(T1) %FAT	31.6±11.1	n.s.
(T0) %LEAN	63.7±13.78	
(T1) %LEAN	68.19±11.2	n.s.
(T0) Water	35.125 5.23	
(T1) Water	36.2±6.31	n.s.

BMR: Basal Metabolic Rate (Kcal); %FAT: Fat Mass Percentage; %LEAN: Lean Mass Percentage; Water: Total Body Water (Liters); p value is referred to the difference between T0-T1 of variables (Wilcoxon matched-pairs signed rank test)

Table V. *Comparison of the significance of changes in FSSc variables from T0 to T1*

Variables	Mean ± SD	*p**
(T0) FSSc	21.45±3.97	
(T1) FSSc	16.83±3.46	0.00002

FSSc: Fibromyalgia Symptom Severity Scale; p value is referred to the difference between T0-T1 of variables (Wilcoxon matched-pairs signed rank test)

DISCUSSION

MCT is an innovative treatment for different CP disorders and this can also be confirmed with positive results observed in patients with FM associated to FSS (8). Furthermore, precise frequencies seem to interact through resonance with biological tissues and biochemical regulators in such a way as to reduce inflammatory conditions, and address specific tissues, possibly by changing membrane configuration (9). Considering the mentioned positive effects of MCT, we can attribute the positive results obtained in this study on fibromyalgic patients to a multitude of possible explanations. MCT proved to be effective in the management of CP, with mechanisms involving the reduction of central pain sensitization mediated by the increase of inflammatory factors (10). Other possible explanations for the antalgic effects of MCT can depend on the ability of low frequency electrical impulses to influence nervous activity, especially at the level B and C fibers (11, 12). In this study, pain, disability and quality of life improved statistically significantly after therapeutic intervention of MCT, as demonstrated by changes in VAS, FSSc and EQ-5D. Although not statistically significant, MCT showed changes in patients' body composition, by increasing their lean body mass and general hydration status. Luxxamed BCR system would seem an effective therapy to reduce the pain and improve the quality of life of individuals affected by a complex FSS as in FM. In response to our hypothesis, the biochemical regulation of tissues, which come from MCT, can stimulate the body to change its altered state. This is relevant for those individuals who endure this chronic condition, and it is therefore important to make it public. It is hoped that this will provide impetus for further studies to provide more solid evidence of the influence of microcurrent therapy on the signs and symptoms of FM associated with FSS. Further randomized controlled trials with a larger sample should confirm these findings and include patient evaluation and follow-up to establish the large-scale efficacy of this therapeutic approach.

REFERENCES

1. Gatchel RJ, Peng YB, Peters ML, Fuchs PN, Turk DC. The biopsychosocial approach to chronic pain: Scientific advances and future directions. Psychol Bull 2007; 133(4):581-624.
2. Konnopka A, Kaufmann C, König HH, et al. Association of costs with somatic symptom severity in patients with medically unexplained symptoms. J Psychosom Res 2013; 75(4):370-75.
3. Evcik D, Ketenc, A, Sindel D. The Turkish Society of Physical Medicine and Rehabilitation (TSPMR) guideline recommendations for the management of fibromyalgia syndrome. Turkish J Physical Med & Rehab 2019; (2587-0823) 65(2).
4. Funk RH, Monsees TK. Effects of electromagnetic fields on cells: physiological and therapeutical approaches and molecular mechanisms of interaction: a review Cells Tissues Organs 2006; 182(2):59-78
5. Poltawski L, Watson T. Bioelectricity and microcurrent therapy for tissue healing–a narrative review. Physical Therapy 2009; 14.2:104-14.
6. Wolfe F, Clauw DJ, Fitzcharles, et al. The American College of Rheumatology preliminary diagnostic criteria for fibromyalgia and measurement of symptom severity. Arthritis Care Res 2010; 62(5):600-610.
7. World Medical Association. WMA Declaration of Helsinki–Ethical principles for medical research involving human subjects 2018; Internet: https://www.wma. net/policies-post/wma-declaration-of-helsinki-ethical-principles-for-medical-research-involving-human-subjects.
8. McMakin CR, Microcurrent therapy: a novel treatment method for chronic low back myofascial pain. J Bodywork Movement Ther 2004; 8(2):143-53.
9. Saranya B, Ahmed J, Shenoy N, Ongole R, Sujir N, Natarajan S. Comparison of transcutaneous electric nerve stimulation (TENS) and microcurrent nerve stimulation (MENS) in the management of masticatory muscle pain: a comparative study. Pain Res Manag 2019; 23(2019):8291624
10. McMakin CR, Gregory WM, Phillips TM. Cytokine changes with microcurrent treatment of fibromyalgia associated with cervical spine trauma. J Bodywork Movement Ther 2005; 9(3):169-76.

11. Allen JD, Mattacola CG, Perrin DH. Effect of microcurrent stimulation on delayed-onset muscle soreness: a double-blind comparison. J Athl Train1999; 34(4):334-37.

12. Koopman JS, Vrinten DH, van Wijck A. J. Efficacy of microcurrent therapy in the treatment of chronic nonspecific back pain: a pilot study. Clin J Pain 2009; 25(6):495-99.

LETTER TO THE EDITOR

Treatment of genitourinary syndrome of menopause with a new radiofrequency device

P. Amori[1], G. Vitiello[1], A. Cancelli[2], K. M. Lomonosov[3], L. Antognoli[1], R. Sadoughifar[1], M. Goldust[4], M. Tirant[5], N. Van Thuong[5] and T. Lotti[1,3]

[1]Department of Dermatology, University of Rome G. Marconi, Rome, Italy; [2]LET'S – ISTC- CNR, Rome Italy; [3]Department of Dermatology and Venereology, I.M. Sechenov First Moscow State Medical University, Russia; [4]Department of Dermatology, University Hospital Basel, Switzerland; [5]Hanoi Medical University, Department of Dermatology, Hanoi, Vietnam

Received May 13, 2020 – Accepted June 25, 2020

To the Editor,

The set of symptoms that can occur in women during and after menopause, and involving genital, sexual and urinary fields, is described as Genitourinary Syndrome of Menopause (GSM). (1) The GSM, previously named as Vulvovaginal Atrophy (VVA), affects about 70% of the postmenopausal women in Western countries (1-4). It is a direct consequence of the lowering of the sexual hormones that occurs during the menopause. Estrogens, indeed, regulate trophism of the vaginal epithelium, its secretions, and Ph. It is also responsible of the trophism of external genitalia (5). Vaginal dryness, irritation, burning and itching, bleeding, dyspareunia, urgency, dysuria and recurrent urinary tract infections are symptoms that make up the GSM (2, 6). The most reported complaint by patients affected by the GSM is vaginal dryness. This symptom, associated with mucosal pallor, rugae thinning, and vaginal Ph>5, is the most important one for diagnosing GSM (4, 7). This syndrome causes a worsening of women's quality of life (2, 3). A wide possibility of therapy exists; recently the treatment of GCM became very simple and is based on general or topical supply of estrogen. The treatments include selective estrogen receptor modulators, lubricants and local moisturizers, including hyaluronic acid for injective use, laser and radio-frequency devices. Hormone therapy has been regarded as the gold standard for decades, with general administration to patients suffering mainly from systemic menopausal symptoms, and local administration, instead, when vaginal disorders are predominant (8). The success of hormone therapy, however, is connected with adherence and compliance of the women. Furthermore, it is commonly believed that this therapy increases the risk of estrogen-dependent tumors. Vaginal lubricants and moisturizers are useful to treat vaginal dryness from mild to moderate. They can, however, cause inflammation of the mucosa, vulvar irritation, contact dermatitis and alterations in the microbiota, for the frequent use and the excipients present in the various formulations (4). The injective use of hyaluronic acid, which has entered clinical practice in recent years, is not always well accepted. There is no unanimous agreement on the use of laser devices, despite several studies showing an improvement of GSM symptoms after laser therapy (4, 7). Short follow-up, small cohorts and lack of a control group, are the most common limits affecting the medical trials on this topic. Radio-frequency devices are employed for their ability to induce internal thermogenesis. Increased internal temperature, in turn, determines vasodilation and increases microcirculation, and new collagen formation (9). Data exists on improvement of GSM

Key words: genitourinary syndrome of menopause; radiofrequency; vulvovaginal atrophy; aesthetic gynecology

Corresponding Author:
Dr Roxanna Sadoughifar
Department of Dermatology University of Rome,
Via Pilinio, 44, 00193 Roma RM, Italy
Tel.: +39 06 377251 - Fax: +39 0637725647
e-mail: bidarskincenter@gmail.com

0393-974X (2020)
Copyright © by BIOLIFE, s.a.s.
This publication and/or article is for individual use only and may not be further reproduced without written permission from the copyright holder.
Unauthorized reproduction may result in financial and other penalties
DISCLOSURE: ALL AUTHORS REPORT NO CONFLICTS OF INTEREST RELEVANT TO THIS ARTICLE.

vaginal symptoms by radio-frequency treatments (4, 5, 7). More recently a new radiofrequency device by GMV, Italy, has been introduced. To date, improvement of GSM vaginal symptoms by radio-frequency treatments has been reported. However, the current devices are monopolar or bipolar, and thus able to work only on a single depth. Furthermore, most of them do not include accurate temperature and contact controls, which are crucial for the efficacy and safety of the treatment. Recently, a new Italian radio-frequency device has been demonstrated to work both in monopolar and in bipolar mode, and supplies controlled concatenate double waves with the handpiece used to treat external genitalia. In

Table I. *Questionnaire to be completed by each patient*

Symptoms	**None**	**Very Mild**	**Mild**	**Moderate**	**Sever**	**Very Sever**
Vaginal itching						
Vaginal dryness						
Spontaneous vaginal pain						
Urinary incontinence						
Urine loss when evacuating						
Urine loss when coughing						
Pain during sexual intercourse						

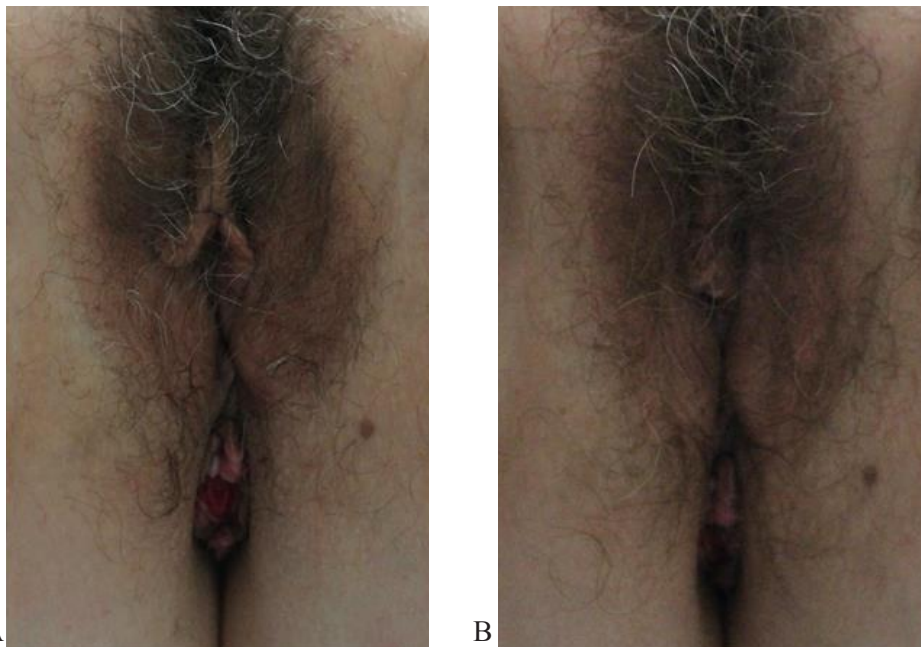

Fig. 1. ***A)*** *Before treatment;* ***B)*** *After treatment*

this cross-sectional study, 10 women aged between 45 and 62, all affected by GSM were treated with this radiofrequency device. The diagnosis of GSM was made by collecting personal history, clinical examination, and according to Vaginal Health Index (VHI). Photographs were taken of each patient before and after the treatment (Fig. 1 A, B), in a single projection showing the appearance of external genitalia. A questionnaire was also completed by each patient, before and after the treatment (Table I), to evaluate the perception of the symptoms constituting the GSM.

Each patient underwent 10 sessions of application of radiofrequency energy, by the radiofrequency device (GMV, Rome, Italy). Ten sessions formed a cycle. Each session was performed using two handpieces, one for the vaginal channel and another for the external genitalia. In the vaginal channel, the working time was 10 minutes for monopolar mode, and 10 minutes for bipolar mode; on the labia the time was 5 minutes per side.

All patients completed the treatment cycle. Photographs showed an improvement of appearance of the external genitalia. VHI also demonstrated improvement. All patients declared a high degree of satisfaction as well as improvement of symptoms, particularly vaginal dryness, as shown by a completed questionnaire. As a result, sexually active patients also reported an improvement in their relationship with their partner. Patients also reported the sensation of better protection of the vaginal entrance, due to the enlargement of the labia majora, as visible on the photographs (Fig. 1B). The patients also reported an improvement in the intensity and frequency of urinary symptoms

REFERENCES

1. Portman DJ, Gass ML. Vulvovaginal Atrophy Terminology Consensus Conference Panel. Genitourinary syndrome of menopause: new terminology for vulvovaginal atrophy from the International Society for the Study of Women's Sexual Health and the North American Menopause Society. J Sex Med 2014; 11:2865-72.
2. Nappi RE, Biglia N, Cagnacci A, Di Carlo C, Luisi S, Paoletti AM. Diagnosis and management of symptoms associated with vulvovaginal atrophy: expert opinion on behalf of the Italian VVA study group. Gynecol Endocrinol 2016; 32(8):602-6.
3. Nappi RE, Martini E, Cucinella L, et al. Addressing Vulvovaginal Atrophy (VVA)/Genitourinary Syndrome of Menopause (GSM) for healthy aging in women. Front Endocrinol (Lausanne) 2019; 10:561.
4. Szymański J, Zaręba K, Jakiel G, Słabuszewska-Jóźwiak A. Genitourinary syndrome of menopause - is the problem solved? State of the art 2018. Prz Menopauzalny 2018; 17(4):168-74.
5. Szymański JK, Siekierski BP, Kajdy A, Jakiel G. Post-menopausal vulvovaginal atrophy - an overview of the current treatment options. Ginekol Pol 2018; 89(1):40-47.
6. La Rosa VL, Ciebiera M, Lin LT, et al. Treatment of genitourinary syndrome of menopause: the potential effects of intravaginal ultralow-concentration oestriol and intravaginal dehydroepiandrosterone on quality of life and sexual function. Prz Menopauzalny 2019; 18(2):116-22.
7. Karcher C, Sadick N. Vaginal rejuvenation using energy-based devices. Int J Womens Dermatol 2016; 2(3):85-88.
8. Scavello I, Maseroli E, Di Stasi V, Vignozzi L. Sexual health in menopause. Medicina (Kaunas) 2019; 55(9).
9. Meyer PF, de Oliveira P, Silva FKBA, et al. Radiofrequency treatment induces fibroblast growth factor 2 expression and subsequently promotes neocollagenesis and neoangiogenesis in the skin tissue. Lasers Med Sci 2017; 32(8):1727-36.

LETTER TO THE EDITOR

Diagnosis and grading of laryngopharyngeal reflux disease with narrow band imaging: preliminary study

A. Pace, V. Rossetti, M. de Vincentiis, A. Greco, A. Colizza, G. Iannella, G. Gulotta, I.C. Visconti, P. Mastino and G. Magliulo

Department of Sense Organs, Sapienza University of Rome, Rome, Italy

Received May 25, 2020 – Accepted July 6, 2020

To the Editor,

Laryngopharyngeal reflux (LPR) disease is a common problem in ear, nose and throat practice and involves about 4-10% of the general population. Symptomatology is characterized by dysphonia, chronic cough, sore throat, throat mucus and pharyngeal globous (1). LPR signs include mucosal modification, mucus dryness, epithelium thickening and occasional evidence of granuloma, contact between the epiglottis and hypertrophied lingual tonsil and oropharyngeal posterior wall (2).

The gold standard in LPR diagnosis is pH-metry. This is an invasive and expensive method that presents a poor reproducibility and lacks a clear pH cut-off level. In order to avoid this exam, two questionnaires are used in clinical practice for LPR diagnosis: the reflux symptoms index (RSI) and reflux findings score (RFS). In particular, the RFS is based on endoscopic evaluation and catalogues the various reflux lesions that may be present.

In recent years, some studies have proposed narrow band imaging (NBI) laryngoscopy as a useful method for diagnosing LPR, to quantitatively evaluate the signs of LPR observed (3). The aim of this preliminary study was to evaluate the potential use of NBI for the diagnosis of LPR. It is based on the research for a lowly invasive method that can help to improve the visualization of LPR signs, currently conducted with white light. Moreover, the NBI score was introduced as a possible grading system of LPR disease.

MATERIALS AND METHODS

This study was performed at the Department of Sense Organs of "Sapienza" University of Rome. Fifty-two patients (47 males, 5 females; 24-76 years of age, average 57 years) were enrolled between November 2019 and January 2020. All patients gave their written consent for all the tests and for their enrolment in the study. This research was performed in accordance with the principle of the Declaration of Helsinki and approved by the local Ethics Committee of "Sapienza" University of Rome.

The exclusion criteria applied were age <18 years, presence of oral disease, presence of laryngeal cancer, use of pump inhibitors or other drugs for LPR treatment at the time of and three months prior to the study.

All patients completed the Reflux Symptom index (RSI) questionnaire and white light laryngoscope evaluation calculating Reflux Findings Score (RFS) (Table I) (4-5). RSI is a self- conducted questionnaire based on nine questions with a maximum of 5 points for each answer that give a total maximum score of 45 points. A high suspicion of LPR is considered with a score ≥ 13. RFS considers 8 findings with a scale that goes from 0 to 26, gives a diagnosis of LPR

Key words: laryngopharyngeal reflux disease; RSI; RFS; NBI; LPR grading

Corresponding Author:
Giuseppe Magliulo, M.D.
Via Gregorio VII n.80,
Rome, 00165, Italy
Tel.: +39 3388622344
Fax: +39 0649976817
e-mail: giuseppe.magliulo@uniroma1.it

0393-974X (2020)
Copyright © by BIOLIFE, s.a.s.
This publication and/or article is for individual use only and may not be further reproduced without written permission from the copyright holder.
Unauthorized reproduction may result in financial and other penalties
DISCLOSURE: ALL AUTHORS REPORT NO CONFLICTS OF INTEREST RELEVANT TO THIS ARTICLE.

presence/absence, and indicates a pathological situation when RFS ≥ 7, but it is not able to estimate the grade of LPR disease.

Two groups were identified: patients evaluated with white light laryngoscope with RFS ≥7 were enrolled in Group A, while patients with RFS <7 were enrolled in Group B. RSI score was performed to estimate the grade of symptomatology of the patients, but it was not considered so relevant for LPR diagnosis and grading, in consideration of the high subjectivity of the answers. Therefore, it was not

Table I. *Reflux Symptoms Index and Reflux Finding Score*

REFLUX SYMPTOMS INDEX	
Hoarseness or a problem with voice	0 1 2 3 4 5
Clearing your throat	0 1 2 3 4 5
Excess throat mucus or postnasal drip	0 1 2 3 4 5
Difficulty swallowing food, liquids, or pills	0 1 2 3 4 5
Coughing after eating or after lying down	0 1 2 3 4 5
Breathing difficulties or choking episodes	0 1 2 3 4 5
Troublesome or annoying cough	0 1 2 3 4 5
Sensations of something sticking in your throat or lump in your throat	0 1 2 3 4 5
Heartburn, chest pain, indigestion, or stomach acid coming up	0 1 2 3 4 5
REFLUX FINDING SCORE	
Subglottic edema	2=present 0= absent
Ventricular obliteration	2= partial 4= complete
Erythema/ hyperemia	2= arytenoids only 4=diffuse
Vocal fold edema	1= mild 2= moderate 3= severe 4= polypoid
Diffuse laryngeal edema	1= mild 2= moderate 3= severe 4= obstruction
Posterior commissure hypertrophy	1= mild 2= moderate 3= severe 4= obstruction
Granuloma/ granulation	2=present 0= absent
Thick endolaryngeal mucus	2=present 0= absent

taken into consideration for the division of the groups. The RFS score is also subjective, but this error was reduced by training the authors in RFS evaluation criteria. According to this, endoscopic evaluation of LPR with RFS was conducted by the same author using a white light flexible endoscope connected to a camera and a high-definition monitor (Full HD). Moreover, the exam was recorded and independently evaluated some days later, by other two authors in order to confirm the results.

Considering that with white light laryngoscopy the presence of LPR could be under-rated, the patients of both groups underwent RFS evaluation conducted with narrow band imaging (NBI) system endoscope (Olympus, Japan) which is an optical technology able to identify the micro vessel on the mucosa surface (6). Also in this case, endoscopic evaluation of LPR with RFS was conducted by the same author and the exam was recorded and independently evaluated by two other authors.

Comparison of both RFS scores, calculated with white light and NBI, was performed and patients affected by LPR visible only with NBI system were identified (Figs. 1-3).

As previously stated, the RFS score defines only the presence or the absence of LPR but is not able to grade it. Therefore, the NBI score was performed to improve the evaluation of LPR signs, including a grading score that could help to classify different types of LPR damage. Beginning from RFS score, the most important LPR signs were considered and the NBI score was calculated (Table II).

NBI maximum total score was 13. NBI grading score of LPR included:

- Grade 1 (0-2 points) = Absent or Mild LPR
- Grade 2 (3-7 points) = Moderate LPR
- Grade 3 (8-13 points) = Severe LPR

Statistical analysis was performed using Stat view statistical software version 8.0. The Student's t-test was employed to compare the data of the study. A value of $p<0.05$ was considered statistically significant.

RESULTS

As mentioned in the methods section, fifty-two patients were enrolled in the study. Thirty-four patients with RFS≥7, evaluated with white light laryngoscope, were classified as Group A (30 males, 4 females; average 57.53 years of age). Eighteen patients,

Table II. *NBI Score*

Erytema/ Hyperemia	0= absent 1= arytenoids only 2= diffuse erythema
Vocal Fold Edema	0= absent 1= mild 2= moderate 3= severe 4= contact ulcerus 5= polypoid
Posterior Commissure Hypertrophy	0= absence of green spots 1= presence of green spots that involves <25% of posterior commissure 2= presence of green spots that involves between 25 and 50% of posterior commissure 3= presence of green spots that involves between 50 and 75% of posterior commissure 4= presence of green spots that involves >75% of posterior commissure
Granuloma	0= absent 1= Initial 2= Present

evaluated with white light laryngoscope and with RFS <7 belonged to Group B (17 males, 1 female; average 56 years of age). No statistically significant difference emerged between two groups regarding age (p=0.34).

In Group A, analysis of the data showed an average value of RSI of 18.35 (range 13-27) while in Group B the average value of RSI was 13.78 (range 6-26). No statistically significant difference emerged between the two groups (p=0,03). These data confirmed that the RSI was too subjective and barely useful in LPR

Fig. 1. *Comparison between laryngoscope performed with white light and NBI. Patient is not affected by LPR.*

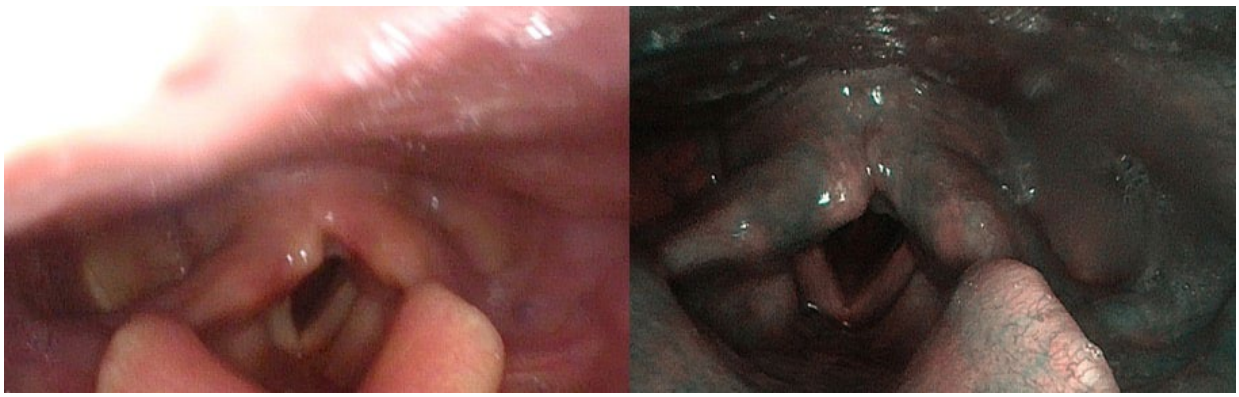

Fig. 2. *Comparison between laryngoscope performed with white light and NBI. The presence of green spots is evident in the posterior commissure that involves about 50% of the region with NBI technique.*

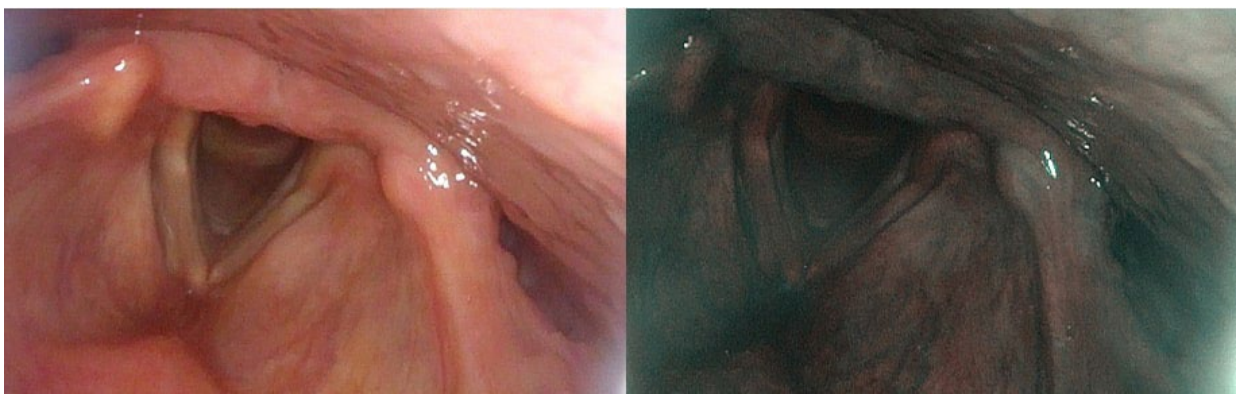

Fig. 3. *Comparison between laryngoscope performed with white light and NBI. A diffuse increasing of vascularization is presented with NBI technique.*

screening, so it was decided not to consider it for the creation of the groups. In Group A, the average RFS values, evaluated with white light, was 11.94 (range 8-15) while in Group B the average of RFS was 4.89 (range 3-6). A statistically significant difference was observed between the two groups ($p<0.00003$). In Group A, the average value of RFS, evaluated with NBI laryngoscopy, was 12.65 (range 9-21), while in group B, it was 7.89 (range 3-13). A statistically significant difference was observed between the two groups ($p<0.001$). In Group A, a comparison of RFS values calculated with white light and RFS values calculated with NBI resulted statistically different ($p< 0.005$).

In Group B, a comparison between RFS values calculated with white light and RFS values calculated with NBI resulted statistically different ($p<0.005$). Moreover, analysing the data of RFS estimated with white light, it was possible to diagnose LPR in 65% of patients enrolled in the study (34/52 patients). In contrast, the data regarding RFS evaluated with NBI showed that 88% of patients presented signs of LPR (46/52 patients).

A statistically significant difference emerged between the number of patients suffering from LPR diagnosed with white light compared to the NBI technique ($p<0.001$). According to the methods described, it is evident that the RFS is a score able to estimate the presence or the absence of LPR disease, but not able to grade LPR lesions. Therefore, use of the NBI score was proposed. The average NBI score in Group A was 7.6 (range 3-11). In group B, the average NBI score value was 4.4 (range 1-6). The NBI score in the two groups statistically differed ($p=0,00106$). In group A, 22 patients (64%) presented a Grade 3 NBI score, 12 patients (35%) Grade 2 and none of the patients Grade 1. In group B, 6 patients (33%) presented a Grade 1 NBI score, 10 patients (55%) Grade 2 and 2 patients (11%) Grade 3.

According to these results it is possible to point out that NBI increased the possibility of recognizing LPR disease in comparison to white light laryngoscopy. In fact, in group B, 12 patients (67%) affected by LPR, were considered healthy according to white light laryngoscope evaluation, despite a moderate/severe pathological grade employing NBI. These data confirmed that NBI increased the chance of a precise evaluation of the severity of LPR in respect to white light laryngoscopy.

DISCUSSION

Clinical diagnostic assessment of LPR is still not well-defined. The gold standard is Multichannel Intraluminal Impedence pH monitoring (MII pH). The latter presents some limitations as it could be associated with false positives since the number and type of reflux episodes may vary during the day; it is invasive and expensive with a poor reproducibility due to the position of the proximal sensor (in the case of suspected LPRD), and without a clear pH cut-off level (7-8).

Moreover, the proximal sensor could be inaccurate, resulting in pseudo-reflux because, during the exam, the superior and inferior esophageal sfincters are opened (9). Other diagnostic methods for LPR, used in clinical practice, include RSI and RFS that are easy to administer. However, RSI presents some limitations as it is a subjective score that evaluates LPR complaints with a visual analogue scale, and is related to socio-cultural factors without taking into consideration all LPR symptoms. Moreover, RSI does not consider the duration and frequency of symptoms during LPR disease. According to all these limitations, it was decided not to take RSI into consideration.

On the other hand, RFS is a more objective score. Thus, three authors, trained for the evaluation of LPR signs, independently analysed the signs to minimize potential errors of interpretation. In the event of disagreement between the three observers, the patient was excluded from the study group.

RFS performed with white light was used to identify two groups of patients, one affected by LPR (Group A) and the other non-LPR (Group B). The groups resulted statistically different, confirming that the score is able to distinguish LPR patients from healthy ones.

In recent years, the international literature has indicated that NBI laryngoscopy is useful for diagnosing not only laryngeal neoplastic disease but also inflammatory diseases (10-11). Galli et al. studied NBI for rhino-pharyngo-laryngeal reflux in paediatric patients and observed that NBI furnished evidence of LPR signs not observed by white light (12).

The aim of the present study was to evaluate the possible use of NBI in adult patients as an integrated endoscopic examination in LPR diagnosis, owing to its ability to highlight superficial microvessels and the vascularity of the mucosa. Our outcomes showed that RSF assessed by white light examination recognized LPR signs in 65% of the patients, while the same score calculated with NBI laryngoscopy recognized 88% of patients affected by LPR disease. This information testified to the greater sensitivity of NBI laryngoscopy in LPR diagnosis in comparison to the white light one.

As previously described, RFS is a score able to indicate the presence/absence of LPR disease but is unable to estimate its grade. This prompted us to devise an NBI classification system. The score was based on the ability of NBI to assess the micro-vessels of the larynx and to better visualize some initial lesions, such as granuloma. Therefore, the four points of the RFS were considered and adapted to define specific LPR grades based on characteristic signs.

Erythema/hyperaemia is better evidenced with green light, showing an increased presence and localization of micro-vessels. White light examination is less able to analyse contact ulcera in the vocal fold and initial granuloma than the NBI technique, so they were included in the score. Furthermore, the most important point in the NBI score regards the presence of green spots in the posterior commissure. Considering the percentage of surface taken up by green spots in this area, it is possible to quantify the damage caused by chronic insults.

This study showed that NBI laryngoscopy recognized 23% of patients with LPR signs more than the white light method, which indicates that white light is able to recognize LPR disease when there are severe signs of LPR, but is unable to recognize the less severe signs that only NBI showed. This is confirmed by the data regarding the severity of LPR observed with our system of classification. The patients of Group A showed mainly LPR grade 3 (65%), while in group B LPR Grade 2 was predominant (55%).

In conclusion, the results of this preliminary study suggest that NBI could improve the identification of LPR signs, thanks to its ability to identify green spots and vascularity. This study could be a starting point for further ones, based on larger populations, able to assess the also grade of the LPR disease.

REFERENCES

1. Magliulo G, Iannella G, Polimeni A et al. Laryngopharyngeal reflux in obstructive sleep apnoea patients: literature review and meta-analysis. Am J Otolaryngol 2018; 39:776-80.
2. Lechien J, Akst L, Hamdan A, et al. Evaluation and management of laryngopharyngeal reflux disease: state of the art review. Otolaryngol Head Neck Surg 2019; 160:762-82.
3. He C, Yu J, Huang F, Shao J. The utility of narrow band imaging in endoscopic diagnosis of laryngopharyngeal reflux. Am J Otolaryngol 2019; 40:715-19.
4. Belafsky P, Rees C. Laryngopharyngeal Reflux: The value of otolaryngology examination. Curr Gastroenterol Rep 2008; 10:278-82.
5. Wan Y, Yan Y, Ma F, Wang L, Lu P, Maytag A, Jiang JJ. LPR: How different diagnostic tools shape the outcomes of treatment. J Voice 2014; 28:362-8.
6. Wang WH, Tsai KH. Narrow-band imaging of laryngeal images and endoscopically proven reflux esophagitis. Otolaryngol Head Neck Surg 2015; 152:874-80.
7. Nennstiel S, Andrea M, Abdelhafez M, Haller B, Schmid RM, Bajbouj M, Becker V. pH/multichannel impedance monitoring in patients with laryngo-pharyngeal reflux symptoms prediction of therapy response in long-term follow-up. Arab J Gastroenterol 2016; 17:113-16.
8. Harrell SP, Koopman J, Woosley S, Wo JM. Exclusion of pH artifacts is essential for hypopharyngeal pH monitoring. Laryngoscope 2007; 117:470-474.
9. Maldonado A, Diederich L, Castell DO, Gideon RM, Katz PO. Laryngopharyngeal reflux identified using a new catheter design: defining normal values and excluding artifacts. Laryngoscope 2003; 113:349-55.
10. Wu D, Cui X, Guo Y, Geng B, Gao F, Liang H. Narrow band imaging might contribute to the diagnosis of laryngopharyngeal reflux. Am J

Otolaryngol 2020; 41:102403.

11. Lechien J R, Schindler A, Robotti C, Lejeune L, Finck C. laryngopharyngeal reflux disease in singers: pathophysiology, clinical findings and perspectives of a new patient-reported outcome instrument. Eur Ann Otorhinolaryngol Head Neck Dis 2019; 136:S39-S43.
12. Galli J, Meucci D, Salonna G, Anzivino R et al. Use OF NBI for the assessment of clinical signs of rhino-pharyngo-laryngeal reflux in pediatric age: preliminary results. Int J Pediatr Otorhinolaryngol 2020; 128:109733.

LETTER TO THE EDITOR

Clinical analysis on efficacy of root-surface conditioning by ethylenediaminetetraacetic acid on surgical treatment of gingival recessions with coronally advanced flap and enamel matrix derivative peptide: a retrospective study

C. Bertoldi[1], P. Cortellini[2], S. Spinato[3] and D. Zaffe[4]

[1]Department of Surgery, Medicine, Dentistry and Morphological Sciences with Transplant Surgery, Oncology and Regenerative Medicine Relevance, University of Modena and Reggio Emilia, Modena, Italy; [2]European Research Group on Periodontology (ERGOPERIO), Bern, Switzerland; [3]Private Practice, Sassuolo MO, Italy [2]Private Practice, Sassuolo MO, Italy; [4]Department of Biomedical, Metabolic and Neural Sciences, University of Modena and Reggio Emilia, Modena, Italy

Received May 5, 2020 – Accepted July 9, 2020

To the Editor,

The treatment of gingival recession defects is successfully achieved by different methodologies of mucogingival plastic surgery. Therapy depends on the type of gingival recession, specifically on its width, depth, oral situation and interproximal involvement of the periodontal ligament as well as on the depth of vestibular fornix, the Miller class of the recession, and site-, oral- and patient-depending variables (1-4). Enamel matrix derivative peptide (EMP) is often used for periodontal regeneration, with the complementary treatment of exposed dental roots by ethylenediaminetetraacetic acid (EDTA) (2, 3). All current plastic mucogingival surgical techniques, allowing a less invasive approach to the patients, are particularly suited to the use of EMP often in association with root conditioning by EDTA (1-4). To treat gingival recession, the coronally advanced flap (CAF) therapy is a benchmark technique and it has been widely analyzed in association with EMP (2, 3). However, the role of the use of EDTA, citric acid and other root surface modifiers is debatable in periodontal regeneration (5, 6). The aim of the present study is to compare the efficacy of EMP, with or without dental root conditioning by EDTA, in the treatment of gingival recessions by CAF surgical technique.

MATERIALS AND METHODS

This retrospective study was performed at the Periodontology Unit of Dentistry and Oral-Maxillofacial Surgery of Modena University Hospital. All the patients considered in this retrospective study signed the informed consent detailing all procedures of the treatment, as requested by Helsinki protocols. The considered patients had to be healthy and not suffering from periodontal disease (1, 5). Moreover, they had to satisfy the following systemic and local inclusion criteria: absence of relevant medical conditions (1, 5), to be of adult age, not pregnant or lactating, non-smokers, not undergoing antibiotic or anti-inflammatory therapy and not suffering recently from relevant affective symptoms (e.g. anxiety, depression, etc.) or psychotic disorders or personality disorders in lifetime medical history (4). The full-mouth plaque score (FMPS) and the full-mouth bleeding score (FMBS), had to be maintained ≤25% (measured at 4 aspects per tooth).

Selected patients had at least a gingival recession of

Key words: gingival recession; enamel matrix proteins; EDTA; periodontal plastic surgery

Corresponding Author:
Prof. Carlo Bertoldi,
Department of Surgery, Medicine, Dentistry,
Transplantation Morphology, Oncology, and Regenerative Medicine,
University of Modena and Reggio Emilia,
Via del Pozzo 71, 41124, Modena, Italy
Tel.: +39 0594224101 - Fax: +39 0594224795
e-mail: carlo.bertoldi@unimore.it

0393-974X (2020)
Copyright © by BIOLIFE, s.a.s.
This publication and/or article is for individual use only and may not be further reproduced without written permission from the copyright holder.
Unauthorized reproduction may result in financial and other penalties
DISCLOSURE: ALL AUTHORS REPORT NO CONFLICTS OF INTEREST RELEVANT TO THIS ARTICLE.

Miller class I or II, and needing surgical treatment by CAF. The teeth interested by recession defects had to be viable or endodontically treated correctly. Only defects with identifiable cemento-enamel junction (CEJ) were included in the study. Cases with conservative/prosthetic restoration involving the considered teeth and/or with presence of deep abrasion defects or caries that made CEJ undetectable were excluded. The considered defects did not include furcations. Patients suffering from parafunctions were excluded. Since the use of CAF technique is not expected to show advantages in patients with inadequate keratinized tissue, these patients were also excluded from the study. Additional exclusion criterion was the presence of detectable bleeding on probing (BoP) recorded at treated sites during the study.

Dental-periodontal procedures and clinical measurements

Subjects were included in the study after completion of cause-related therapy consisting of scaling and root-planing, motivation, and oral-hygiene instructions and ending with very high compliance and very low levels of plaque and BoP. When indicated, surgical periodontal therapy was performed on the remaining portions of the dentition of each patient. The CAF surgical procedure was always implemented (1-3).

Treatment of teeth was performed using the enamel matrix derivative peptide (EMP - Emdogain, Biora AB, Malmö, Sweden) close to dental roots in:

- Treatment group-1 (TG1) patients, having root surfaces not previously conditioned;
- Treatment group-2 (TG2) patients, having root surfaces conditioned by EDTA (PrepHgelA, Biora, AB, Malmö, Sweden) immediately before EMP application.

Probing depth (PD) and gingival recession depth (GR) were recorded at the experimental sites at baseline, immediately before surgical treatment (T0), and at the end of the follow-up period of 12 months (T1). In particular, mid-buccal PD, from the gingival margin to the base of the defect, and GR, from the cemento-enamel junctions (CEJ) to the free gingival margin, were evaluated by periodontal probe. The corresponding clinical attachment level (CAL) was calculated as the sum of PD and GR. Also, FMPS and FMBS were measured at the same time-points. BoP had never to be marked in relation to the treated sites during all the follow-up period.

Statistical analysis

The primary outcomes of this study were the PD, GR and CAL comparisons between TG1 and TG2. The secondary outcome was the evaluation of PD, GR and CAL changes during follow-up. The adjusted Fisher–Pearson standardized moment coefficient G was calculated, and skewness was refused if $-2 < G < +2$.

Statistical analysis was performed using the parametric *t*-test for the comparison of two groups of patients in the same phase (T0 or T1), and paired *t*-test for the clinical data taken before and after the surgical treatment. The χ^2 test (nominal data) was applied to compare the gender distribution between the two treated groups (5). For all measured variables, the null hypothesis (H_0) of no difference among groups was rejected for a critical significance level of $p < 0.05$ (1, 5).

RESULTS

Thirty patients, 17 women and 13 men, aged 20-60 years (mean±SD – median = 37.6±12.4 – 37 years) fulfilled the entry criteria of the retrospective study. Fifteen patients, 9 women and 6 men, aged 20-59 years (37.1±12.9 – 34 years) were enrolled in TG1 and fifteen patients, 8 women and 7 men, aged 22-60 years (mean±SD = 38.1±12.3 – 39 years) were enrolled in TG2 (Table I).

At baseline (T0), the adjusted Fisher–Pearson test, calculated from numerical data, resulted always $-2 < G < +2$, so skewness hypothesis was refused (14). At baseline (T0), the FMPS and FMBS were 12.8±2.5 - 16.7% and 7.7±2.8 – 7.1%, respectively, in TG1, and resulted 16.5±3.1 – 16.7% and 8.1±3 - 8.3%, respectively, in TG2. PD resulted 1.3±0.4 - 1 mm in TG1 and 1.3±0.5 – 1 mm in TG2. GR was 3±0.8 – 3 mm in TG1 and 2.7±0.7 – 3 mm in TG2. CAL resulted 4.2±1 – 4 mm in TG1 and 4±0.9 – 4mm in TG2 (Table I and Table II). The comparison between TG1 and TG2 at T0 (Tab. II) was not statistically significant for age, FMPS, FMBS, PD, GR, CAL and gender ($p > 0.05$, *t*-test analysis and χ^2 test for gender).

Twelve months afterward (T1), the adjusted Fisher–Pearson test resulted always $-2 < G < +2$, so the skewness hypothesis was again refused. FMPS and FMBS were 15.5±3 - 14.8% and 5.9±2.3 – 5.4% respectively in TG1 while resulted 15.4±3.1 -14.8%

and 6.7±2.1 – 7.7%, respectively, in TG2. PD resulted 1.4±0.5 – 1 mm in TG1 and 1.2±0.4 – 1 mm in TG2. GR resulted 3±0.8 – 3 mm in TG1 and 2.7±0.7 – 3 mm in TG2. CAL was 1.6±0.7 – 2 mm in TG1 and 1.2±0.4 – 1 mm in TG2 (Table I and Table II). The statistical comparison between TG1 and TG2 at T1 (Table II) was significant for PD and CAL ($p < 0.05$) and not significant for FMPS, FMBS and GR ($p \geq 0.05$, *t*-test analysis).

The index comparison between baseline (T0) and the end of follow-up period (T1) was statistically significant for FMPS, FMBS, GR, and CAL in

Table I. *Demographic and periodontal indices raw data of the patients completing the study*

TG1		AGE	20	23	26	34	56	24	29	49	23	59	40	48	49	34	42																	
		G	M	M	F	F	M	M	F	F	F	M	F	F	M	F	F																	
	T0	FMPS	16.1	19.2	20.8	16.7	15.2	14.4	19.2	14.6	12.0	19.4	18.3	19.4	16.7	16.1	14.3																	
		FMBS	7.1	5.8	10.4	5.6	7.1	4.8	3.8	6.3	7.0	4.6	10.6	11.1	13.9	8.9	8.0																	
		PD	1	1	2	1	2	1	1	1	2	1	1	2	1	1	1	1	2	1	1	2	1	1	1	2	1	1	1	1	1	1	2	
		GR	2	2	2	3	3	2	3	3	5	4	3	4	3	3	2	2	3	3	3	3	2	3	2	3	4	4	3	3	3	3	4	
		CAL	3	3	4	4	5	3	4	4	7	5	4	6	4	4	3	3	5	4	4	5	3	4	3	5	5	5	4	4	4	4	6	
	T1	FMPS	14.3	18.3	20.8	14.8	13.4	12.5	20.2	12.5	11.0	18.5	16.3	17.6	14.8	14.3	12.5																	
		FMBS	4.5	3.8	8.3	3.7	5.4	4.8	3.8	6.3	5.0	1.9	8.7	8.3	9.3	7.1	8.0																	
		PD	2	2	2	1	2	2	1	1	2	1	1	2	1	1	1	1	2	1	1	2	1	2	2	2	1	1	1	1	1	1	2	
		GR	1	0	0	0	0	1	1	0	0	0	0	0	0	1	0	0	0	1	0	0	0	0	1	0	0	0	0	0	0	0	0	
		CAL	3	2	2	1	2	3	2	1	2	1	1	2	1	2	1	1	2	2	1	2	1	2	3	2	1	1	1	1	1	1	2	
TG2		AGE	48	29	25	55	35	46	39	40	60	53	27	22	28	24	41																	
		G	M	F	F	M	F	M	F	M	F	F	F	M	F	M	M																	
	T0	FMPS	17.3	15.7	18.3	12.5	17.7	10.7	12.5	20.8	16.7	15.2	14.4	19.4	16.7	19.2	20.8																	
		FMBS	7.7	4.6	8.7	2.7	8.3	9.8	10.7	10.4	5.6	7.1	4.8	11.1	13.9	5.8	10.4																	
		PD	1	2	1	1	1	2	2	1	1	1	1	3	1	1	1	1	1	1	2	2	2	1	1	1	1	2	1	1				
		GR	3	2	4	2	2	2	2	3	3	3	2	4	3	3	3	2	3	2	3	3	3	2	2	3	4	3	3	2				
		CAL	4	4	5	3	3	4	4	4	4	4	3	7	4	4	4	3	4	3	5	5	5	3	3	4	5	5	4	3				
	T1	FMPS	17.3	13.9	13.5	12.5	16.7	10.7	13.4	20.8	14.8	13.4	12.5	17.6	14.8	18.3	20.8																	
		FMBS	7.7	4.6	6.7	3.6	8.3	8.9	8.9	8.3	3.7	5.4	4.8	8.3	9.3	3.8	8.3																	
		PD	1	2	1	1	1	1	2	1	1	1	1	2	1	1	1	1	2	1	1	2	1	1	1	1	1	1	1	1				
		GR	1	0	0	0	0	0	0	0	0	0	0	0	0	0	0	0	0	0	0	0	0	0	0	0	0	0	0	0				
		CAL	2	2	1	1	1	1	2	1	1	1	1	2	1	1	1	1	2	1	1	2	1	1	1	1	1	1	1	1				

T0: Baseline; T1: 12-month after surgery; TG1: treatment group-1 patients; TG2: treatment group-2 patients; AGE: patient' age at baseline time; G: patients' gender; FMPS: Full mouth plaque score; FMBS: Full mouth bleeding score; PD: Probing depth; GR: gingival recession; p: value of comparison between the baseline (T0) and the end of follow-up (T1) in the same treatment group (TG).*

Table II. *Average of all measurements (PD, GR, CAL, FMPS and FMBS) at T0 and T1 in TG1 and TG2*

	Treatment Group	PD	GR	CAL	FMPS	FMBS
T0	TG1	1.3±0.4mm	3±0.8mm	4.2±1mm	16.8±2.5%	7.7±2.8%
	TG2	1.3±0.5mm	2.7±0.7mm	4±0.9mm	16.5±3.1%	8.1±3%
P*		0.626	0.080	0.089	0.777	0.687
T1	TG1	1.4±0.5mm	0.2±0.4mm	1.6±0.7mm	15.5±3%	5.9±2.3%
	TG2	1.2±0.4mm	0.04±0.2mm	1.2±0.4mm	15.4±3.1%	6.7±2.1%
P**		0.046	0.063	0.009	0.959	0.687
TG1	T1	1.3±0.4mm	3±0.8mm	4.2±1mm	16.8±2.5%	7.7±2.8%
	T2	1.4±0.5mm	0.2±0.4mm	1.6±0.7mm	15.5±3%	5.9±2.3%
p§		0.023	<.001	<.001	<.001	<.001
TG2	T1	1.3±0.5mm	2.7±0.7mm	4±0.9mm	16.5±3.1%	8.1±3%
	T2	1.2±0.4mm	0.04±0.2mm	1.2±0.4mm	15.4±3.1%	6.7±2.1%
p°		0.103	<.001	<.001	0.007	0.002

T : Baseline; T1: 12-month after surgery; TG1: treatment group-1 patients; TG2: treatment group-2 patients; AGE: patient' age at baseline time; G: patients' gender; FMPS: Full mouth plaque score; FMBS: Full mouth bleeding score; PD: Probing depth; GR: gingival recession; p: value of comparison between TG1 and TG2 at baseline (T0); p**: value of comparison between TG1 and TG2 at the end of follow-up (T1); p§: value of comparison between T0 and T1 in TG1; p°: value of comparison between T0 and T1 in TG2.*

both TG1 and TG2 ($p < 0.05$ paired *t*-test). On the contrary, PD comparison between T0 and T1 was not significant in TG2 ($p \geq 0.05$) and significant in TG1 ($p < 0.05$ paired *t*-test). However, with the exception of PD in TG1, that resulted significantly greater at T1 compared with T0, all the recorded indices of TG1 decreased at T1 compared with T0.

DISCUSSION

Tissue regeneration depends on several variables, such as the materials used (7), and the devices used to apply them (8-10). Nevertheless, the defect properties and the surgical technique chosen to obtain the flap, as well as the stabilization of the clot beneath the flap, also play a fundamental role in periodontal regeneration (1-3). Furthermore, even the patients' lifestyles and psychological profile matter (4, 11). The study design required stringent criteria of inclusion in the retrospective study, to characterize as much as possible the periodontal defects and the patients to avoid disturbing variables. In particular, BoP is an inflammation index closely connected to periodontal disease and to periodontal CAL loss, so it had never to be recorded in the considered defects (5). The study was carried out on patients characterized by a good hygienic control and affected by gingival recession of Miller class I or II. The gingival recessions were treated only by CAF flap technique without subepithelial connective tissue graft (CTG). CAF + CTG might be considered the gold standard in root coverage procedures (12), however, it seems to be particularly established in cases of gingival recession with a relevant defect in gingival thickness and/or in those cases in which the increase in width of keratinized gingival tissue (wKT) is requested. Nevertheless, the combined use of CAF and EMP seems to guarantee a significant favorable clinical outcome for GR and CAL also at 10-year follow-up (3). Moreover, no differences in effectiveness were recorded among the use of CAF + EMP, CAF + CTG and CAF + CTG + EMP in root coverage in several studies (2, 3). Besides, McGuire et al. (3) even observed an increase of wKT using CAF + EMP in 10-year follow-up clinical results similar to those achieved with CAF + CTG. So, both GR, CAL and also PD could significantly decrease within a year from surgery using CAF + EMP (2, 3).

In this study a significant clinical improvement of the measured periodontal indices at T1 compared with the values at T0 was always observed in both the TGs, with the exception of PD that significantly increased in TG1, but (not significantly) decreased in TG2. However, PD was always comprised between 1 and 3, so remaining in a physiological range.

Using CAF+EMD, a not significant decreasing trend of PD was observed also in other studies (2, 3), and EMP seemed helpful in wound healing by its potential in the PD reduction (12), but all these studies applied the TG2 protocol, using EDTA. In this study, TG1 protocol did not include the EDTA application. The PD significantly increased from T0 to T1. At T1, the comparison between TG1 and TG2 of PD and of CAL (greater in TG1) was significant, but not GR. GR resulted lower in TG2, but without statistical significance. Therefore, the significant CAL decrease of TG2, compared with the value of TG1, could be mostly due to PD behavior.

In conclusion, the primary clinical outcomes resulted mostly favorable for TG2, while the analysis of the secondary clinical outcomes showed a clinical advantage of GR and CAL in both the TGs. In addition, in comparison with T0, a FMPS and FMBS reduction was observed in both treatments at T1. This study considered a clinical setting in which the stabilization of the flap and of the clot beneath the flap is not guaranteed by the morphology and the biological properties of the defect to the same extent to which it could be in 2-3-wall intrabony defects, that have the self-ability to maintain the regeneration space (5, 6). The use of a dental root surface modifier such as the EDTA (5), improving the flap stability, could make all the difference to obtain significant clinical results in defects not predisposed to shunt the strain forces from the regeneration space.

REFERENCES

1. Bertoldi C, Bencivenni D, Lucchi A, Consolo U.

Augmentation of keratinized gingiva through bilaminar connective tissue grafts: a comparison between two techniques. Minerva Stomatol 2007; 56:3-20.
2. Alexiou A, Vouros I, Menexes G, Konstantinidis A. Comparison of enamel matrix derivative (Emdogain) and subepithelial connective tissue graft for root coverage in patients with multiple gingival recession defects: A randomized controlled clinical study. Quintessence Int 2017; 48:381-9.
3. McGuire MK, Scheyer ET, Nunn M. Evaluation of human recession defects treated with coronally advanced flaps and either enamel matrix derivative or connective tissue: comparison of clinical parameters at 10 years. J Periodontol 2012; 83:353-62.
4. Bertoldi C, Venuta M, Guaraldi G, et al. Are periodontal outcomes affected by personality patterns? A 18-month follow-up study. Acta Odontol Scand 2018; 76:48-57.
5. Bertoldi C, Labriola A, Generali L. Dental root surface treatment with ethylenediaminetetraacetic acid does not improve enamel matrix derivative peptide treatment within intrabony defects: a retrospective study. J Biol Regul Homeost Agents 2019; 33:1945-7.
6. Liu X, Mao M, Ma T. The effect of EDTA root conditioning on periodontal surgery outcome: A meta-analysis. Quintessence Int 2016; 47:833-41.
7. Bertoldi C, Zaffe D. In vivo comparison of two bone substitutes in the distal femur of the rabbit. Int J Oral Maxillofac Implants 2012; 27:119-27.
8. Consolo U, Bertoldi C, Zaffe D. Intermittent loading improves results in mandibular alveolar distraction osteogenesis. Clin Oral Implants Res 2006; 17:179-87.
9. Bertoldi C, Pradelli JM, Consolo U, Zaffe D. Release of elements from retrieved maxillofacial plates and screws. J Mater Sci Mater Med 2005; 16:857-61.
10. Bertoldi C, Lusuardi D, Battarra F, Sassatelli P, Spinato S, Zaffe D. The maintenance of inserted titanium implants: in-vitro evaluation of exposed surfaces cleaned with three different instruments. Clin Oral Implants Res 2017; 28:57-63.
11. Monari E, Cuoghi A, Bellei E, et al. Analysis of protein expression in periodontal pocket tissue: a preliminary study. Proteome Sci 2015 30; 13:33. doi: 10.1186/s12953-015-0089-y
12. Buti J, Baccini M, Nieri M, La Marca M, Pini-Prato GP. Bayesian network meta-analysis of root coverage procedures: ranking efficacy and identification of best treatment. J Clin Periodontol 2013; 40:372-86.

JOURNAL OF BIOLOGICAL REGULATORS & HOMEOSTATIC AGENTS Vol. 34, no. 4, 1585-1588 (2020)

LETTER TO THE EDITOR

Management of an anterior mandibular fracture in a 13-year-old patient

P.M. Marra[1], A. Itro[1], R. Santoro[2] and A. Itro[1]

[1]Complex Operative Unit of Stomatological Surgery in Developmental age, University of Campania Luigi Vanvitelli, Naples, Italy; [2]Multidisciplinary Department of Medical-Surgical and Dental Specialties, University of Campania Luigi Vanvitelli, Naples, Italy

Received April 19, 2020 – Accepted July 13, 2020

To the Editor,

Paediatric mandible fractures are the most common paediatric facial injuries requiring hospitalization and are rarer than in adults. Proper and rapid treatment is required to restore the patient's oral function and aesthetics (1). In addition to road traffic accidents, both direct and indirect trauma can occur as a result of sports activities and falls (2). Furthermore, damage to the lower jaw may be caused by cystic lesions, neoplasms, and metabolic diseases (1-2). The mandible is one of the most frequently injured areas, accounting for 23-97% of all facial fractures. (3), with the mandible involved in 16–42% of cases (3). After analysing 700 maxillofacial injuries, Halazonetis (3) noticed that the most frequent fractures involved the lower and middle third of the facial skeleton, with single fractures frequently occurring in the angle region of the male dentulous jaw (38%) as a result of fights and sports. An association between condylar injuries and concomitant fractures of the mandibular body was addressed by Lindahl (4), demonstrating the impact of the occlusion. The prevalence of these injuries increases with age (1-2). Additionally, some regions of the mandible present with weakness, including the mental foramen, mandibular angle, and the condylar neck (3, 5). The aim of this case report is to show the management of an anterior mandibular fracture in a 13-year-old patient, also presenting with a unilateral right subcondylar fracture. The patient was treated with open reduction internal fixation with two titanium miniplates to fix and immobilize the bone segments, restore the occlusion, and stimulate bone healing in the labio-inferior position.

Case presentation

A 13-year-old Caucasian male presented to the Complex Operative Unit of Stomatological Surgery in Developmental Age in Naples complaining of pain in the lower right mandibular region two days following a fall from a bicycle. Intraorally, the patient presented with permanent dentition, and bone crepitation and pain without any bone exposure. There were no signs of dental trauma, enamel fractures, or teeth subluxation. The vitality test was positive.

Extraorally, the patient presented with monolateral submandibular oedema, as well as swelling and redness in the lower right mandibular region. No swelling or redness were present in the mandibular condyle region. Panoramic X-ray demonstrated a vertical fracture in the mandible as well as a right condylar fracture (Fig. 1A). Cone Beam Computed Tomography (CBCT) was performed to differentiate the fracture lines and for the final diagnosis (Fig. 1B). The 3D examination confirmed the diagnosis of a mandibular fracture in the anterior region between

Key words: growing patient; mandibular fractures; two miniplates

Corresponding Author:
Paola Martina Marra, DDS, MS, research fellow
Complex Operative Unit of Stomatological surgery in Developmental age
University of Campania Luigi Vanvitelli,
Piazza Miraglia 2, 80138 - Naples, Italy
Tel.: +39 3338626207 - Fax: +39 0818614680
e-mail: pablati3@hotmail.it

0393-974X (2020)
Copyright © by BIOLIFE, s.a.s.
This publication and/or article is for individual use only and may not be further reproduced without written permission from the copyright holder.
Unauthorized reproduction may result in financial and other penalties
DISCLOSURE: ALL AUTHORS REPORT NO CONFLICTS OF INTEREST RELEVANT TO THIS ARTICLE.

the lower right canine and the lower right first premolar, as well as a unilateral fracture in the right subcondylar region.

Written consent for surgery was obtained from the

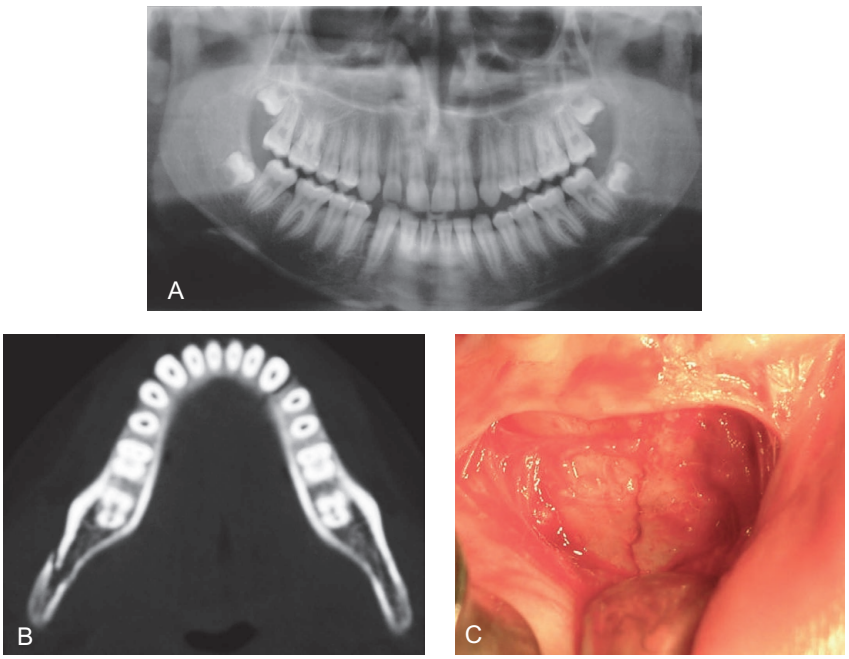

Fig. 1. ***A)*** *Initial panoramic X-ray highlighting the fracture line in the lower right mandible and the right subcondylar region;* ***B)*** *Initial CBCT showing the two fractures; C: Mandibular fracture exposure during open surgery.*

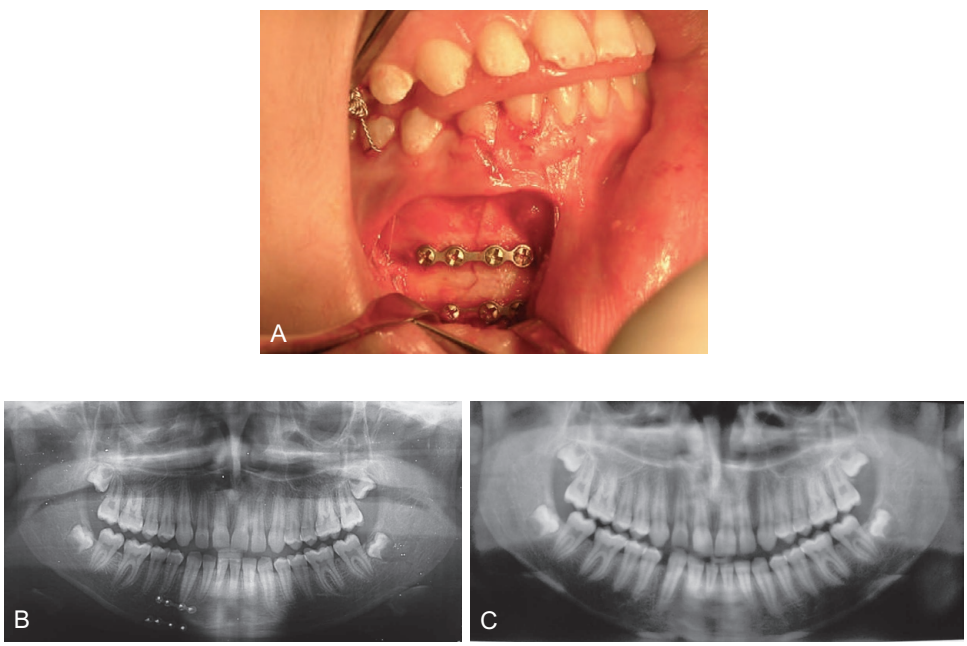

Fig. 2. ***A)*** *Titanium miniplates were used with 2 mm × 6 mm screws in the upper and lower borders****; B)*** *Panoramic X-ray 1 month postoperatively;* ***C)*** *Panoramic X-ray 3 months postoperatively after removal of the titanium miniplates.*

patient's parents. The treatment plan was based on an open reduction and internal fixation of the fracture segments, since it was necessary to immobilize the bone segments as well as to recover the contour of the mandibular fracture. As the patient was a teenager and the lower jaw is habitually well-developed at this age, the risk of facial asymmetry caused by plating was highly unlikely.

Before surgery, laboratory diagnostic tests, as well as cardiological and anesthetic examinations, were performed. The patient was administered antibiotic prophylaxis before and after surgery to reduce the risk of infection (6). Under general anaesthesia, an intraoral approach with vestibular incision was performed. The injured area (Fig. 1C) was exhibited, with segments of the mandibular body reduced and fixed with two miniplates (Fig. 2A) in the labio-inferior position. Titanium miniplates were used with 2 mm × 6 mm screws in the upper and lower borders. Closure was performed with 4-0 non-absorbable sutures, which were removed 10 days post-surgery. The procedure was performed by a single surgeon. Fracture healing was evaluated radiographically after 1 month (Fig. 2B). The plates were observed to be firmly stable, with progression of segment reduction. The patient did not complain of pain or discomfort. Considering the management of the current paediatric lateral condyle fracture with an acceptable occlusion, no other intervention measures were indicated.

Postoperative surgical complications, including infection, pain, paraesthesia, or implant failure, were not observed. Titanium plates were removed 3 months postoperatively under local anaesthesia through a vestibular incision. A renewed panoramic X-ray showed good wound healing and proper fracture reduction, with no signs of condylar ankylosis (Fig. 2C).

DISCUSSION

Although paediatric mandible fractures are rare (1-2), they primarily affect the maxillofacial skeleton with the mandible usually compromised, since it moves anteriorly and inferiorly and is more susceptible to trauma (7). The paediatric skeleton is more resilient to traumatic forces, presenting a higher elasticity, higher proportion of cancellous and cortical bone and a thicker overlying soft tissue (1, 2, 7). If recognized and treated immediately, recovery usually occurs after 2.5 to 8 weeks (7). If left untreated, they can cause severe functional and aesthetic consequences. Paediatric mandible fractures can be corrected using different techniques (1, 4), with conservative approaches based on observation and a soft diet or maxillomandibular fixation favoured in the literature (4). Another technique is open reduction internal fixation with miniplates (4), which is less commonly indicated in children due to the risk of long-term facial deformity. Other fixation options reported for the anterior mandible include transosseous wiring, miniplates, lag screws, and dynamic compression plates (1-5). Two miniplates are indicated for anterior mandibular fractures to obtain adequate stability and proper osteosynthesis, with positioning of the plates on the labial cortex (7). For this reason, rigid and proper surgical fixation is required to avoid several complications, such as malunion, non-union, delayed fracture healing, plate fracture, infection, and implant failure (8-12). This case report describes an uncommon and unusual method to treat a vertical mandibular fracture in a paediatric patient and demonstrates the stable outcome of the conservative approach in an isolated condylar fracture.

Further studies are required to compare surgical approaches on a larger patient cohort, also using 3D miniplates to ensure minimal stress of the fracture fragments.

REFERENCES

1. Ferreira PC, Amarante JM, Silva PN, et al. Retrospective study of 1251 maxillofacial fractures in children and adolescents. Plast Reconstr Surg 2005; 115:1500-508.
2. Edwards TJ, David DJ, Simpson DA, Abbott AA. Patterns of mandibular fractures in Adelaide, South Australia. Aust and N Z Surg 1994; 64:307-11.
3. Halazonetis JA. The 'weak' regions of the mandible. Br J Oral Surg 1968; 6:37-48.
4. Lindahl L. Condylar fractures of the mandible. I. Classification and relation to age, occlusion, and concomitant injuries of teeth and teeth-supporting

structures, and fractures of the mandibular body. Int J Oral Surg 1977; 6:12-21.
5. Pickrell BB, Hollier LH Jr. Evidence-Based Medicine: Mandible Fractures. Plast Reconstr Surg 2017; 140:192e-200e.
6. Staderini E, Patini R, Guglielmi F, Camodeca A, Gallenzi P. How to Manage Impacted Third Molars: Germectomy or Delayed Removal? A Systematic Literature Review. Medicina (Kaunas) 2019; 26:55(3).
7. Kao R1, Rabbani CC1, Patel JM2, Parkhurst SM1, Mantravadi AV1, Ting JY1, Sim MW1, Koehler K1, Shipchandler TZ1. management of mandible fracture in 150 children across 7 years in a US tertiary care hospital. JAMA Facial Plast Surg. 2019; 21:414-18.
8. McGoldrick DM, Parmar P, Williams R, Monaghan A, McMillan K. Management of pediatric condyle fractures. J Craniofac Surg 2019; 30:2045-47.
9. Patini R, Staderini E, Camodeca A, Guglielmi F, Gallenzi P. Case reports in pediatric dentistry journals: a systematic review about their effect on impact factor and future investigations. Dent J (Basel). 2019; 24:7(4).
10. Pelo S, Saponaro G, Patini R, et al. Risks in surgery-first orthognathic approach: complications of segmental osteotomies of the jaws. A systematic review. Eur Rev Med Pharmacol Sci 2017; 21:4-12.
11. Marra PM, Nucci L, Abdolreza J, Perillo L, Itro A, Grassia V. Odontoma in a young and anxious patient associated with unerupted permanent mandibular cuspid: a case report. J Int Oral Health 2020; 12:182-6.
12. Marra PM, Lupo G, Itro A. Surgical management of compound Odontomas: piezoelectric surgery or rotary instruments? A clinical study. Minerva Stomatol 2020; 16.

JOURNAL OF BIOLOGICAL REGULATORS & HOMEOSTATIC AGENTS Vol. 34, no. 4, 1589-1592 (2020)

LETTER TO THE EDITOR

Biological approach to minimally invasive, flapless, bone augmentation using innovative manual expanders

F.M. Filannino[1*], A. Pacifici[2*], D. Carbone[2,3] and L. Pacifici[2]

[1]Private practice, Milan, Italy; [2]Department of Oral and Maxillofacial Science, Sapienza University, Rome, Italy; [3]Department of Urgency and Surgery, Operative Unit of Odontostomatology, Military Policlinic of Rome, Rome, Italy

Received June 5, 2020 – Accepted July 15, 2020

**These Authors contributed equally to this article*

To the Editor,

Pre-implant oral reconstructive surgery aims to obtain the biological and functional restoration of bone morphology related to maxillary ridge, in order to allow dental implantology with a predictable success rate (1). Following various conditions, including tooth loss, significant volumetric defects may arise in the alveolar bone, making rehabilitation with dental implants impossible. The main goal of pre-implant reconstructive surgery consists in restoring an adequate morphology of the alveolar ridge in terms of height and thickness, in order to allow the correct implant placement even in cases in which the maxillary or mandibular hard tissues are affected by severe bone atrophy (2). Over the years, various techniques have been developed to treat bone defects of the jaws including guided bone regeneration (GBR), sinus lifting, Le Fort I osteotomy with inter-positional grafting, osteogenetic distraction, onlay grafts. Some of these involve the use of autologous, homologous, or heterologous grafting materials, often together with resorbable or non-resorbable membranes (3). These techniques showed comparable long-term results (4). The expansion of the alveolar ridge is one of the procedures described in the literature for increasing bone volume in cases of horizontal atrophy. The surgical procedure on the bone can be performed utilizing rotary instruments, ultrasound tools, and chisel osteotomes, which require the use of mallets or tapered screw expanders (5). The insertion of dental implants can be contextual to bone expansion or delayed. Bone augmentation techniques are usually applied on the upper jaw as it presents more frequently a suitable elasticity, due to a lower density and thinner bony cortical plates when compared to the mandible. As previously reported in the topical literature, dental implants inserted in bones expanded after a split crest technique showed comparable results to those positioned in non-expanded bones, with success rates ranging between 86% and 97% (6). In our article, we describe a new surgical technique first reported in the literature, based on a system of manual screw-tapered expanders with simultaneous insertion of a bone implant.

MATERIALS AND METHODS

To describe our technique, we report the clinical case of a 69-year-old female patient, non-smoker and in good health, requiring a prosthetic rehabilitation of the missing first left upper premolar. Our patient gave informed, signed

Key words: bone loss; bone augmentation; maxillary atrophy; guided bone regeneration

Corresponding Author:
Dr. Andrea Pacifici,
Department of Oral and Maxillofacial Sciences,
Sapienza University of Rome,
Via Caserta, 6, 00161 Rome, Italy
Tel./Fax: +39 0649976620
e-mail: dott.andreapacifici@libero.it

0393-974X (2020)
Copyright © by BIOLIFE, s.a.s.
This publication and/or article is for individual use only and may not be further reproduced without written permission from the copyright holder.
Unauthorized reproduction may result in financial and other penalties
DISCLOSURE: ALL AUTHORS REPORT NO CONFLICTS OF INTEREST RELEVANT TO THIS ARTICLE.

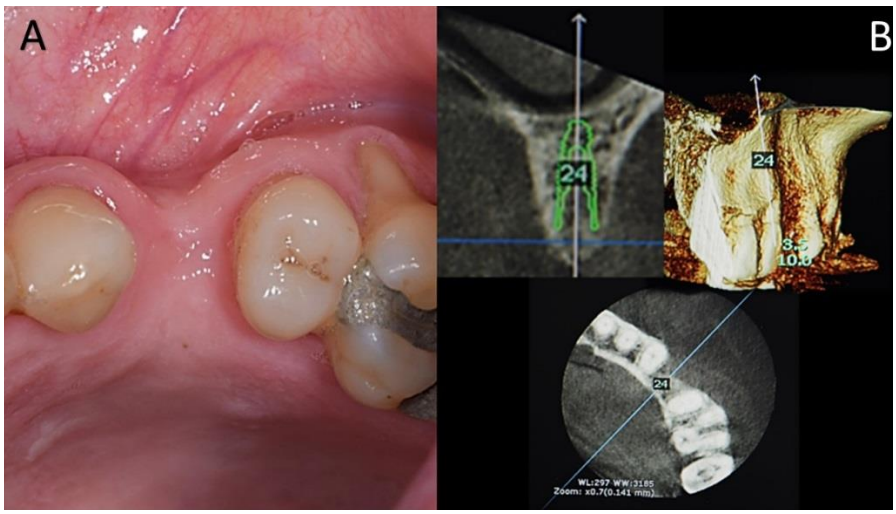

Fig. 1. A*) Composite Fig. showing the pre-operative intra-oral view of the edentulous ridge.* ***B****) Pre-operative Tomography Computerized Cone-Beam in different views.*

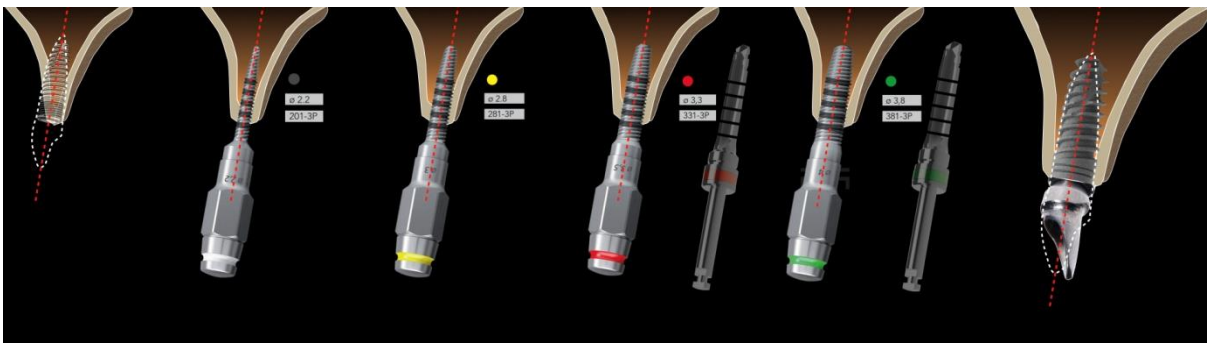

Fig. 2. *Innovative surgical and sinus lift kit with manual expanders.*

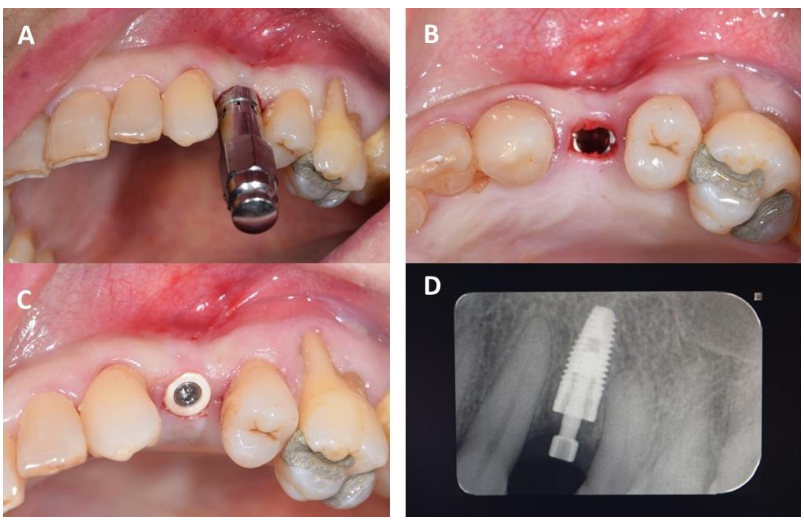

Fig. 3. ***A)*** *Flapless bone expansion with innovative surgical and sinus lift kits manual screw-tapered expanders.* ***B)*** *Occlusal view of the surgical site after implant positioning.* ***C)*** *Positioning the healing screw. D) Post-operative intraoral radiography of the implant.*

consent to participate in the study. The analysis of the pre-operative cone-beam computed tomography reported a 3.5 mm thickness on the edentulous crest (Fig. 1).

To restore the case with insufficient bone volume and make it suitable for dental implant insertion, a ridge expansion was planned. Local anesthesia was performed with infiltration of 3 vials of 1.7 ml of Articaine with adrenaline 40 mg/ml + 10 mg/ml. A circular incision was made in the soft tissue overlying the edentulous area with a mucotome. With a pilot drill, a first hole was made in the cortical bone for a depth of about 1-2mm, under abundant irrigation. B&B Dental surgical and sinus lift kits (Fig. 2) were used for the alveolar ridge expansion; it includes a series of screw-tapered expanders with increasing diameters (2.2 mm, 2.8 mm, 3.3 mm, 3.8 mm), which are activated using a manual wrench tool. The expanders were used in sequence from the one with a smaller diameter to the one with the larger diameter (Fig. 3A). After expanding the ridge, a 4 mm diameter and 10 mm long implant was placed in the expanded bone and a healing screw was applied (Fig. 3 B-D). As post-surgery profilaxis, the patient was prescribed an antibiotic treatment with Amoxicillin + Clavulanic acid (875 mg + 125 mg), two tablets per day for 5 days. The patient was asked to rinse with chlorhexidine 0.12%-based mouthwash twice per day for 7 days, until the sutures were removed. The post-operative period was uneventful and the patient reported that pain and swelling were negligible.

The implant was loaded about 4 months after surgery with the placement of a temporary crown. After a further month the final prosthetic crown was placed. Clinical and radiographic control at six months showed excellent conditions of both hard and soft tissues surrounding the implant-prosthetic rehabilitation.

DISCUSSION

Bone defects in the jaws can result from various inflammatory, traumatic or oncological conditions (7, 8). After tooth loss, a progressive bone reabsorption, first horizontally and then vertically happens (9). The bone augmentation technique presented in this article is meant to be less traumatic and simplified. The newly formed space in the center fills with blood, forming a clot that will be replaced by newly formed bone: this is not comparable to a simple bone substitute use with other biologically active membranes (10). The split crest technique allows bone expansion without the use of graft material or membranes. Furthermore, the immediate insertion of the implants causes a reduction in surgical sessions and treatment times compared to other regeneration techniques in which the recipient site requires a healing time lasting months (11).

This technique takes into consideration the traditional split crest technique in which the separation between the bone cortical plates was carried out by chisels osteotomes, air-driven rotary handpieces, or oscillating saws , to which were later added tapered screw expanders and piezo-electric tools (8-10). The use of a manual tapered screw expander allows to avoid such trauma with consequent improvement of patient comfort as well as a constant and precise control of the axis of action and the pressure exerted during the expansion of the bone crest (6, 12). The present case report illustrates a minimally invasive procedure which, in cases of moderate insufficiency of horizontal bone volume, allows the expansion of the alveolar ridge and the simultaneous insertion of the dental implant with reduction of the operative time, good acceptability of the procedures by the patient and reduction of the risks of post-operative complications. Such novel expanders can be also used in maxillary orthopedics and related implantology. The authors proposed a surgical procedure which, although promising in view of an increasingly widespread minimally invasive dentistry, requires further studies on more extensive clinical cases.

REFERENCES

1. Buser D, Mericske-Stern D, Beranrd PJ, et al. Long-term evaluation of nonsubmerged ITI implants. Part I: 8-year life table analysis of a prospective multicenter study with 2359 implants. Clin Oral Implants Res 1997; 8:161-72.
2. Tatullo M, Codispoti B, Pacifici A, Palmieri F, Marrelli M, Pacifici L, Paduano F. Potential use of human periapical cyst-mesenchymal stem cells (hpcy-mscs) as a novel stem cell source for regenerative medicine applications. Front Cell Dev Biol 2017; 5:103.
3. Chiapasco M, Zaniboni M, Boisco M. Augmentation procedures for the rehabilitation of deficient edentulous ridges with oral implants. Clin Oral Implants Res

2007; 17:136-59.
4. Marrelli M, Maletta C, Inchingolo F, Alfano M, Tatullo M. Three-point bending tests of zirconia core/veneer ceramics for dental restorations. Int J Dent 2013; 2013: 831976.
5. Spagnuolo G, De Vito D, Rengo S, Tatullo M.COVID-19 outbreak: an overview on dentistry. Int J Environ Res Public Health 2020; 17(6):2094.
6. Simion M, Baldoni M, Zaffe D. Jawbone enlargement using immediate implant placement associated with a split-crest technique and guided tissue regeneration. Int J Periodontics Restorative Dent 1992; 12: 462-73.
7. Marrazzo P, Paduano F, Palmieri F, Marrelli M, Tatullo M. Highly Efficient In Vitro Reparative Behaviour of Dental Pulp Stem Cells Cultured With Standardised Platelet Lysate Supplementation. Stem Cells Int 2016; 2016 7230987.
8. Cantore S, Ballini A, Mori G, et al.Anti-plaque and antimicrobial efficiency of different oral rinses in a 3-day plaque accumulation model. J Biol Regul Homeost Agents 2016; 30(4):1173-78.
9. Apicella D, Aversa R, Tatullo M, et al. Direct restoration modalities of fractured central maxillary incisors: A multi-levels validated finite elements analysis with in vivo strain measurements. Dent Mater 2015; 31(12):e289-e305.
10. Ballini A, Cantore S, Scacco S, Coletti D, Tatullo M. Mesenchymal Stem Cells as Promoters, Enhancers, and Playmakers of the Translational Regenerative Medicine. Stem Cells Int 2018; 6927401.
11. Vercellotti T. Piezoelectric surgery in implantology: a case report–a new piezoelectric ridge expansion technique. Int J Periodont Rest 2000; 20:358-65.
12. Anitua E, Begona L, Orive G. Clinical evaluation of split-crest technique with ultrasonic bone surgery for narrow ridge expansion: status of soft and hard tissues and implant success. Clin Implant Dent R 2013; 15:176-87.

LETTER TO THE EDITOR

Oral quail egg homogenate in the treatment of allergic rhinitis: a first experience in clinical practice

D. Passali[1], G. Motta[2], F.M. Passali[3], M. Nunziata[2] and G. Ciprandi[4]

[1]IFOS, Rome, Italy; [2]ENT Clinic, University of Campania L. Vanvitelli, Naples, Italy; [3]ENT Clinic, University Tor Vergata ENT, Rome, Italy; [4]Allergy Clinic, Casa di Cura Villa Montallegro, Genoa, Italy

Received April 23, 2020 – Accepted July 22, 2020

To the Editor,

Allergic rhinitis (AR) is a very common disease as it may affect up to 30% of the general population, including children, worldwide (1, 2). Type 2 inflammation, characterized by T helper 2 polarization, allergen-specific production, and eosinophilic mucosal infiltration, leads to AR. Inflammatory events cause the typical symptoms, including those nasal and ocular, as well as itching, sneezing, watery rhinorrhoea, lacrimation, and congestion.

Allergen-specific IgE production by B-lymphocytes is orchestrated by type-2 cytokines, including IL-4 and IL-13. After exposure to specific allergen, IgE activates mast cells to degranulate, triggering the release of the preformed mediators, including histamine, cytokines, pro-inflammatory agents, trypsin homolog proteases, that start the allergic inflammatory cascade (1). Moreover, also basophils are involved in type 2 inflammation, as they are a major source for IL-4 production (3). Tryptase, a trypsin homolog protease, is a signaling molecule that binds to the protease-activated receptor (PAR)-2 located on inflammatory cells (eosinophils, neutrophils, and macrophages) as well as neurons. Binding of tryptase to these receptors amplifies the inflammation, resulting in symptom worsening (4). Ovomucoids, derived from quail egg, are competitive inhibitors of trypsin. These specific glycoproteins bind to the trypsin-like serine proteases of the allergen and decrease their activity by blocking the enzyme active site so that the IgE are not able to enter the effector cells. By forming a physical barrier around the proteases, allergens will be less able to bring about an IgE-mediated response. Ovomucoids block the serine proteases from allergens, before the allergy chain reaction starts, and act as a protective barrier against exogenous allergens absorbed in the body (5). They also prevent tryptase binding with PAR-2, so it blocks the superoxide anion production by NADPH oxidase, associated with intra-cytoplasmic degranulation (major basic protein, eosinophil peroxidase, cytokines), resulting in less inflammation and local tissue degradation.

The history of quail eggs began in the early 1970s. A French general practitioner noticed that farmers who raised quails (*Coturnix coturnix*) presented fewer allergic symptoms than the general population in the same area. He prescribed raw quail eggs to his allergic patients, including both adults and children, and observed a reduction in their symptoms (6). This finding was subsequently investigated in several human clinical trials carried out by a larger group of physicians. In these studies, subjects suffering from outdoor and indoor allergens were given quail egg powder tablets or placebo. The results of these studies

Key words: Allergic rhinitis; quail egg; SNOT score; nasal mucociliary transport time

Corresponding Author:
Prof. Giorgio Ciprandi,
Casa di Cura Villa Montallegro,
Via Monte Zovetto 27, 16145,
Genova 010-35111
e-mail: gio.cip@libero.it

0393-974X (2020)
Copyright © by BIOLIFE, s.a.s.
This publication and/or article is for individual use only and may not be further reproduced without written permission from the copyright holder.
Unauthorized reproduction may result in financial and other penalties
DISCLOSURE: ALL AUTHORS REPORT NO CONFLICTS OF INTEREST RELEVANT TO THIS ARTICLE.

indicated that consumption of quail egg powder led to relief of subjects' symptoms with good tolerability of the administered product (7). A further randomized, double-blind, placebo-controlled study demonstrated that quail egg reduced symptoms and nasal inspiratory flow after allergen challenge (8). Based on this background, the current study investigated the effect of a quail egg treatment on patients with allergic rhinitis examined in real-world setting.

MATERIALS AND METHODS

Forty-five patients (21 males and 24 females, mean age 32.48 years, age range 18-60) suffering from allergic rhinitis and with moderate-severe nasal obstruction were enrolled in this study. The patients were examined at 3 otorhinolaryngological clinics located in Rome, Naples, and Bari. The inclusion criteria were: adult age, either gender, diagnosis of allergic rhinitis performed according to validated criteria (12), and nasal obstruction assessed by endoscopic evaluation. Exclusion criteria were: mechanical nasal obstruction, relevant septal deviation, non-allergic rhinitis, chronic diseases and concomitant treatments that could interfere with interpretations of results. All patients gave written informed consent to participate.

The patients were examined at baseline (T0) and at the end of the treatment (T1). Patients took 2 tablets twice a day. The tablet was a proprietary blend made of *C. coturnix* quail egg (Narivent compresse, DMG, Pomezia, Rome, Italy). Patients were instructed to slowly chew two tablets in the morning and in the evening for 30 consecutive days.

The parameters were sino-nasal outcome test (SNOT) score and nasal mucociliary transport time, both assessed at T0 and T1. SNOT-20 is a questionnaire containing 20 items with a 6-point scale. The sum of each item-score was calculated and expressed the SNOT score. At present, SNOT is the most commonly utilized and highest quality sinus-specific quality-of-life method available, as documented also by a meta-analysis (9). Nasal mucociliary transport time is calculated by placing attracting powder (vegetal charcoal powder) to the head of the inferior turbinate (10, 11); through direct pharyngoscopy it is then possible to detect the transit of the tracer from the posterior pharyngeal wall. The test requires quite some collaboration by the patient, who must keep a seated position without either blowing or sniffing. The charcoal powder is used as a tracer, as it is insoluble and clearly visible in a pink environment such as that of the nasopharyngeal area, and behaves as an inert material, adhering to the mucosa and is transported passively by the movement of mucus and cilia. Normally, the tracer is found in the pharynx after about 10–15 min. Adverse events were recorded in a diary card.

RESULTS

All patients completed the study. The mean SNOT score was 38.14 (min value 12 – max value 72) at T0. The most bothersome complaints were nasal obstruction in 40 patients, post-nasal drip in 22, discharge in 10, sneezing in 9, and hyposmia in 9. At T1, the mean SNOT score significantly ($p<0.05$) diminished to 26.14 (8-44) as shown in Fig. 1; 90% of patients reported a relevant symptom improvement, namely 43 patients perceived a relevant improvement of nasal obstruction, 32 of the need to blow the nose, 25 of rhinorrhea, 23 of sneezing, and 15 of hyposmia. The mean mucociliary transport time was 24 (19-40) min at T0 which significantly ($p<0.05$) decreased to 12 at T1 (Fig. 2). No clinically-relevant adverse events were reported.

DISCUSSION

Allergic rhinitis is a very common disorder, characterized by bothersome symptoms, mainly concerning nasal obstruction, that negatively affect the quality of life of patients (1). The present study showed that quail egg significantly improved nasal symptoms and quality of life of these patients. Moreover, quail egg also significantly improved the mucociliary transport time. This parameter provides information about the clearance capacity of nasal mucosa to remove pathological secretions, mediators, allergen, and pollutants from the nasal surface. It is affected by inflammatory and infectious diseases, and a reduced mucus clearance worsens symptoms.

The current study is the first demonstration that a one-month course of quail egg was able to significantly improve nasal complaints, quality of life, and nasal mucociliary transport time in patients with allergic rhinitis. These outcomes were consistent with a previous study that used the allergen nasal

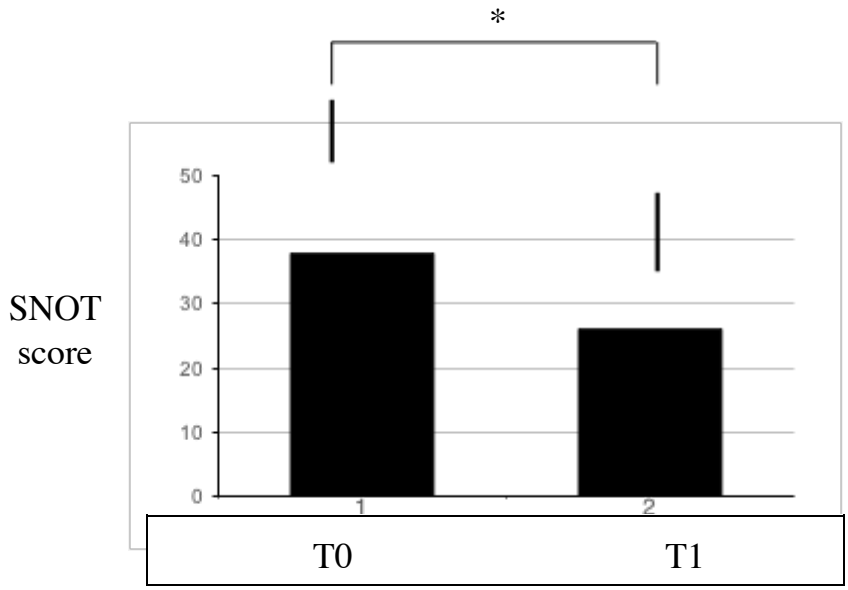

Fig. 1. *SNOT score in patients with allergic rhinitis evaluated at baseline (T0) and after one-month course (T1) with quail egg. * = p<.05.*

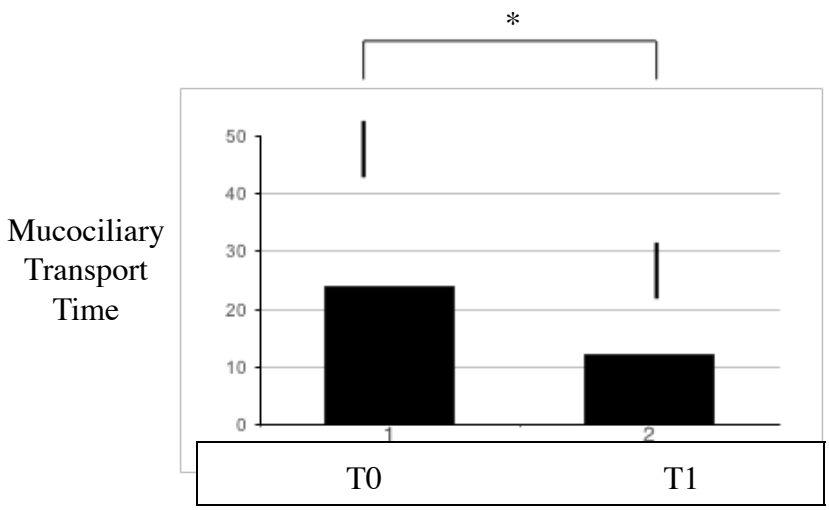

Fig. 2. *Nasal mucociliary transport time (minutes) in patients with allergic rhinitis evaluated at baseline (T0) and after one-month course (T1) with quail egg. * = p<.05*

challenge model (12). Of course, nasal challenge is an experimental method to investigate the allergic reaction, but does not completely mirror the natural exposure to allergens. Therefore, the present study has a greater clinical relevance. Moreover, it was conducted in a real-world setting, such as an out-patients clinic. As a result, the present findings could be reproduced in clinical practice.

On the other hand, this study has some limitations, including the open design, the lack of a control group and the calculation of the sample size, no biomarker was assessed, and nasal airflow was not measured. To respond to these unmet needs, further studies should be conducted using more rigorous methodology. On the other hand, the study was conducted in a real-life setting, so the outcomes could mirror what happens in clinical practice.

In conclusion, the current study demonstrated for the first time that a one-month course with quail egg could improve symptoms, quality of life, and nasal mucociliary transport time in patients with allergic rhinitis.

REFERENCES

1. Wise SK, Lin SY, Toskala E. International consensus statement on allergy and rhinology: allergic rhinitis. Int Forum Allergy Rhinol 2018; 8(2):85-107.
2. Licari A, Marseglia A, Caimmi S, et al. Emerging and future therapies for allergic rhinitis. J Biol Regul Homeost Agents 2015; 29(S1):38-46.
3. Poddighe D, Mathias CB, Freyschmidt EJ, Kombe D, Caplan B, Marseglia GL, Oettgen HC. Basophils are rapidly mobilized following initial aeroallergen encounter in naïve mice and provide a priming source of IL-4 in adaptive immune responses J Biol Regul Homeost Agents 2014; 28(1):91-103.
4. Minai-Fleminger MY, Schaffer FL. Mast cells and eosinophils: the two key effector cells in allergic inflammation. Inflamm Res 2009; 58:631-38.
5. Lianto P, Ogutu FO, Zhang Y, He F, Che H. Inhibitory effects of quail egg on mast cells degranulation by suppressing PAR2-mediated MAPK and NF-kB activation. Food Nutrit Res 2018; 62:1084.
6. Truffier JC. Approchetherapeutic de la maladieallergique par ingestion d'oeufs de caille. La Clinque 1978; 22:3-4.
7. Bruttman G. "Ovix" Quail egg homogenate: a clinical evaluation. Med Biologic 1995; 2:25-29.
8. Benichou AC, Armanet M, Bussiere A, Chevreau N. A proprietary blend of quail egg for the attenuation of nasal provocation with a standardized allergenic challenge: a randomized, double-blind, placebo-controlled study. Food Sci Nutrit 2014; 2:655-63.
9. Soler ZM, Jones R, Le P,Rudmik L, Mattos JL, Nguyen SA, Schlosser RJ. SNOT-22 outcomes after sinus surgery: a systematic review and meta-analysis. Laryngoscope 2018; 128:581-92.
10. Passàli D, Bellussi L, Bianchini Ciampoli M, De Seta E. Experiences in the determination of nasal mucociliary transport time. Acta Otolaryngol. 1984; 97:319-23.
11. Passàli D, Bianchini Ciampoli Bellussi L Normal values of mucociliary transport time in young subjects. Int J Pediatr Otorhinolaryngol. 1985; 9:151-6.
12. Ciprandi G, Cirillo I, Klersy C, Marseglia GL, Caimmi D, Vizzaccaro A Nasal obstruction is the key symptom in hay fever patients. Otolaryngol Head Neck Surg. 2005; 133:429-35.

LETTER TO THE EDITOR

Pidotimod in children with infectious mononucleosis: a preliminary randomized controlled study

I. La Mantia[1], A. Varricchio[2], C. Andaloro[1] and G. Ciprandi[3]

[1]Unit of Otolaryngology, Department of General Surgery and Medical-Surgical Specialties, University of Catania, Catania, Italy; [2]Uosd Video-Endoscopia Delle Vas, P.O. San Gennaro – ASL Napoli 1-Centro, Naples, Italy; [3]Allergy Clinic, Casa di Cura Villa Montallegro, Genoa, Italy

Received April 23, 2020 – Accepted July 22, 2020

To the Editor,

Epstein-Barr virus (EBV) infection in adolescence and early adulthood may lead to infectious mononucleosis (IM) in 35-50% of the cases (1). The symptoms of IM typically subside in 1 to 2 months, even though a chronic disease may persist.

In many IM patients, the initial infection weakens the immune system by promoting subsequent secondary bacterial and viral infections (2). Therefore, secondary infections are possible during the acute phase of IM and include severe conditions, such as pneumonia and pericarditis.

From an immunopathological point of view, it has been reported that EBV infection interferes with transcription factors involved in immune response, promoting EBNA2 production that may allow secondary infections. Moreover, reactivation of the EBV is also possible: once IM (first infection) has been cured, it is never really eliminated from the body and may remain confined within the B lymphocytes in a state of quiescence. However, various pathogenic mechanisms, including stress, immunosuppressive treatment, and intercurrent viral diseases, may lower the immune function that induces a second IM infection (reactivation). Therefore, to increase immune response could be an intriguing new perspective in IM management. In this regard, pidotimod is a systemic thymic dipeptide that exerts an immunomodulatory activity (2). There is evidence that pidotimod causes maturation of dendritic cells, increases antigen presentation and toll-like receptors (TLR) 2 and 4, and induces cytokines of the innate and adaptive immunity affecting metabolomics (3). Based on this background, a recent study explored the clinical effect of pidotimod as adjuvant therapy in children suffering from IM (4). Children treated with pidotimod experienced shorter fever clearance time and hospitalization duration than controls. Moreover, pidotimod induced a significant reduction in the percentages of $CD3^+$ and $CD8^+$ T cells and an increase in the $CD4^+$ T cells and $CD4^+/CD8^+$ ratio. The current study was performed to investigate the effects of pidotimod concerning the resolution time and possible secondary infections in children and adolescents with IM.

MATERIALS AND METHODS

Forty patients, aged between 7 and 16, with symptomatic IM, were enrolled. The IM diagnosis was performed considering the clinical features and positive immunological tests. The 40 patients were randomly subdivided into two groups: group A

Key words: pidotimod; Epstein-Barr virus; children; ENT Infection

Corresponding Author:
Giorgio Ciprandi,
Casa di Cura Villa Montallegro
Via Montezovetto 27, 16145, Genova, Italy
Tel.: +39 010 35311
e-mail: gio.cip@libero.it

0393-974X (2020)
Copyright © by BIOLIFE, s.a.s.
This publication and/or article is for individual use only and may not be further reproduced without written permission from the copyright holder.
Unauthorized reproduction may result in financial and other penalties
DISCLOSURE: ALL AUTHORS REPORT NO CONFLICTS OF INTEREST RELEVANT TO THIS ARTICLE.

included 25 patients (15 males and 10 females - aged between 7 and 16 years); group B included 15 patients (7 males and 8 females) between 9 and 15 years. The random list was based on blocks of 5 consecutive patients with a 5:3 ratio. The parents of the patients signed informed consent for participation in the study, and the Ethics Committee approved the procedure.

Group A was treated with pidotimod, administered on an empty stomach once a day, from the day of diagnosis and 30 consecutive days. The daily dose was 400 mg in patients between 7 and 12 years (10 patients) and 800 mg in patients between 12 and 16 years (15 patients). At the end of the first course, there was a 15-day suspension. Successively, a 10-day/monthly course was performed for six months. Group B (15 patients) was considered as a control arm and treated only with as-needed medications.

All patients underwent clinical monitoring at the end of the first month (T0), after four months (T1) and seven months (T2). The patients' parents had a clinical diary to record symptoms and medications. The primary outcome was the resolution time of IM, categorized if it occurred before the 14th day after the diagnosis or after. Secondary outcomes were the number of secondary infections.

The statistical analysis was performed using the χ^2 test.

RESULTS

Recovery time

At T0, at the end of the first Pidotimod course, 22 (88%) subjects of Group A and 3 of Group B recovered before the 14th day; 3 (20%) of Group A and 12 of Group B recovered after the 14th day ($p<0.0001$) (Table I). Stratifying for age, 10 children (< 12 years) were in Group A and 12 in Group B; there were 15 adolescents in Group A and 3 in Group B. In Group A, 7 (70%) children recovered before the 14th day as well as all the 15 (100%) adolescents. In Group B, 2 (16.7%) children recovered before the 14th day, and only one (33.3%) adolescent. The intergroup difference was significant in both groups: $p=0.0113$ in children and $p=0.0008$ in adolescents.

Reinfections

In Group A, only two (8%) subjects had reinfections, whereas 12 (80%) subjects of Group B had reinfections ($p<0.0001$), as reported in Table II. At T1, there were 16 infectious episodes in Group B:

Table I. *Recovery time in subjects with infectious mononucleosis and treated with pidotimod (Group A) and controls (Group B).*

	Group A (n.25)		Group B (n.15)	
	children ≤ 12 years	adolescents > 12 years	children ≤ 12 years	adolescents > 12 years
Resolution time ≤ 14 days	7 **(70.0%)**	15 **(100.0%)**	2 **(16.7%)**	1 **(33.3%)**
Resolution time > 14 days	3 **(30.0%)**	--	10 **(83.3%)**	2 **(66.7%)**
	n. 10	n. 15	n. 12	n.3

Table II. *Reinfections in subjects with infectious mononucleosis and treated with pidotimod (Group A) and controls (Group B).*

	Patients with ≥ 1 reinfection	Patients without reinfection
Group A (n.25)	2 **(8.0 %)**	23 **(92.0%)**
Group B (n.15)	12 **(80.0%)**	3 **(20.0%)**
χ^2 Test	P<0.0001	

10 infections were treated with acetaminophen and 6 with antibiotics. At T2, there were two infections in Group A treated with antibiotics, and four infections in Group B: 2 treated with acetaminophen and 2 with antibiotics. In Group A, the recovery time of reinfections was within the third day in one subject and the fifth day in the second subject. In Group B, the recovery time was within the third day in 2 subjects, Within the fourth day in six subjects, within the fifth day in 7; within the sixth day in 2; and within the seventh day in 3.

All subjects in Group A tolerated pidotimod, and no clinically relevant adverse event was reported.

DISCUSSION

The current preliminary study showed a shortening of IM resolution time: about 90% of pidotimod-treated achieved the complete recovery by two weeks, whereas about only 20% of controls recovered within that time. The other relevant outcome was the significant prevention of secondary infections: more than 90% of pidotimod-treated subjects did not experience any infection during the study, whereas 80% of controls had at least one infectious episode. Also, the resolution time of the secondary infections was remarkably shorter in the active group.

These results are consistent with the findings obtained in previous studies and confirm the immunomodulatory activity of pidotimod (5). In particular, pidotimod potentiated the beneficial effect of immunization of the influenza vaccine, possibly resulting in a more substantial activity of innate and adaptive immunity (6). *In vivo* studies showed a beneficial pidotimod effect on children, reducing the number of RI, the number of fever days, and the severity of signs and symptoms of acute infections (7, 8). A further clinical study reported that pidotimod improved the respiratory ciliary epithelium in children with RRI (9).

The current preliminary study had some limitations, including the open design, the limited number of participants, and the lack of objective parameters, even though it was designed as randomized and controlled. However, other studies should be conducted to confirm these preliminary findings.

In conclusion, the present study evidenced that pidotimod was able to shorten the recovery time, prevent secondary infections, and abbreviate their duration in children and adolescents with infectious mononucleosis.

REFERENCES

1. Rostgaard K, Balfour HH, Jarrett R, et al. Primary Epstein-Barr virus infection with and without infection mononucleosis. PlosOne 2019; 14:e0226436.
2. D'Amato M, Paris D, Molino A, et al. The immune-modulator pidotimod affects the metabolic profile of exhaled breath condensate in bronchiectasis patients: a metabolomics pilot study. Frontiers Pharmacol 2019; 10:1115.
3. Mahashur A, Thomas PK, Mehta P, Nivangune K, Muchhala S, Jain R. Pidotimod: an in-depth review of current evidence. Lung India 2019; 36:422-33.
4. Lyu HT, Zheng TT, Xu HQ. Clinical effects of pidotimod oral liquid as adjuvant therapy for infectious mononucleosis. Chin J Contemp Pediatr 2018; 20:563-6.
5. Zuccotti GV, Mameli C. Pidotimod: the past and the present. It J Ped 2013; 39:75.
6. Zuccotti GV, Mameli C, Trabattoni D, Beretta S, Biasin M, Guazzarotti L, Clerici M. Immunomodulating activity of pidotimod in children with Down syndrome. J Biol Regul 2013; 27:253-8.
7. Burgio GR, Marseglia GL, Severi F, et al. Immunoactivation by pidotimod in children with recurrent respiratory infections. Arzneimittelforschung 1994; 44:1525-9.
8. Careddu P, Mei V, Venturoli V, Corsini A. Pidotimod in the treatment of recurrent respiratory infections in paediatric patients. Arzneimittelforschung 1994; 44:1485-9.
9. Passali D, Calearo C, Conticello S. Pidotimod in the management of recurrent pharyngotonsillar infections in childhood. Arzneimittelforschung 1994; 44:1511-6.

LETTER TO THE EDITOR

Probiotics may modulate the impact of aging on adults

L. Signorini[1*], F. De Leonardis[2*], L. Santacroce[3,4], K. Haxhirexha[5], S. Topi[4], L. Fumarola[6], G. Dipalma[7], M. F. Coscia[6§] and F. Inchingolo[7§]

[1]Private Practice, Rome, Italy; [2]Department of Biosciences, Biotechnologies and Biopharmaceutics, Campus Universitario "Ernesto Quagliariello", University of Bari "Aldo Moro", Bari, Italy; [3]School of Technical Medical Sciences, "A. Xhuvani" University, Elbasan, Albania; [4]Ionian Department, University of Bari "Aldo Moro", Bari, Italy; [5]Medical Faculty University of Tetova, Macedonia; [6]Department of Basic Medical Sciences, Neurosciences and Sense Organs, University of Bari Aldo Moro, Bari, Italy; [7]Department of Interdisciplinary Medicine, University of Bari "Aldo Moro", Bari, Italy

To the Editor,

The ability to modulate the intestinal microbiota, exploiting the immunomodulatory properties of the "beneficial" bacteria, has led to the hypothesis of the use of probiotics in some pathological conditions that develop in the elderly, such as irritable bowel syndrome (modulating intestinal sensitivity), chronic inflammatory bowel diseases (through an anti-inflammatory action), but also in some secondary conditions that develop following inflammation such as cognitive deficits (1). Some probiotic bacteria of the genus *Lactobacillus* (*plantarum, rhamnosus GG* and *acidophilus*) are capable of exerting an anti-inflammatory action even *in vitro* and compare their action with that of a pathogenic strain (*Salmonella typhimurium*). In the elderly, the intestinal flora changes in relation to numerous phenomena including reduced gastric secretion, motility disorders and alterations in the diet, consequently these changes cause alteration of the intestinal barrier and therefore encourage the onset of inflammatory phenomena (2). Studies in the literature would seem to show that, in the elderly intestine, the production of pro-inflammatory cytokines, such as IL-6, corresponds to changes in the composition of the intestinal microbiota, which would encourage the onset of numerous inflammations and/or infections. By studying the effects of a mix of probiotic strains, frequently used in Great Britain, VSL # 3, a mixture of eight different bacterial strains, *B. longum DSM 24736*, *B. short DSM 24732, B. infantis DSM 24737, L. acidophilus DSM 24735, L. plantarum DSM 24730, L. paracasei DSM 24733, L. debrueckii subsp. Bulgaricus DSM 24734*, showed the anti-inflammatory effects on the intestines of elderly mice (Balb/c) with induced colitis that were given 4 mg of probiotic compound. Histological and metabolomic analyses showed that the treated mice started a healing process of colitis, with reduction of all inflammatory markers (5). This pilot study sheds light on the ability of specific probiotics stains (PRO-Bifido, Hyperbiotics, USA) on biochemical markers that affect adulthood.

MATERIALS AND METHODS

Participants

The present project was conducted at the American Stem Cell Hospital (AMEJSC), Health Centre (Vietnam), in collaboration with the University of Bari Aldo Moro, Italy and the School of Technical Medical Sciences, "A. Xhuvani" University, Elbasan, Albania. The Institutional Ethics Committee of the Faculty of Technical Medical

Key words: probiotics; gut microbiota; aging; adulthood

Corresponding Author:
Prof. L. Santacroce,
Ionian Department,
Microbiology and Virology Laboratory,
Policlinico University Hospital,
University of Bari "Aldo Moro", 70124 Bari, Italy
e-mail: luigi.santacroce@uniba.it

0393-974X (2020)
Copyright © by BIOLIFE, s.a.s.
This publication and/or article is for individual use only and may not be further reproduced without written permission from the copyright holder.
Unauthorized reproduction may result in financial and other penalties
DISCLOSURE: ALL AUTHORS REPORT NO CONFLICTS OF INTEREST RELEVANT TO THIS ARTICLE.

Sciences of Elbasan "Aleksandër Xhuvani" approved the application to conduct the clinical trial in the Faculty. Title of the Protocol: Probiotics efficacy and safety in humans. Protocol Identification: INTL_ALITCOOP/Probiotics/INRES2019_w/a/c. The study was carried out according to the Helsinki Declaration and informed written consent was obtained from all the subjects.

Twenty male and female adults (aged 50 years and over) were enrolled in the present study. The participants had not taken antibiotics for ≥3 months prior to study participation. Nor had they taken medications or supplements (e.g. fibre supplements) that could influence the dependent variables of this study. All participants followed a standardized diet. Participants were allowed to consume 450 g/day (~16 fl. oz./day) caffeinated black coffee or unsweetened black tea if used to consuming them regularly. Furthermore, on the first visit, the participants were instructed on the objectives and methods of the clinical trials. Subjects who agreed to participate in the study, after having signed the informed consent, were randomly included and divided into two groups: a test group using probiotics, and a group without probiotics.

Experimental design

A randomized double-blind, placebo-controlled, parallel group design was used for this study. After completing baseline measures, participants were stratified by sex and randomized into one of two groups: Test Group, supplementation with PRO-Bifido, Hyperbiotics, USA (1 tablet daily), containing *Bifidobacterium infantis, Bifidobacterium bifidum, Bifidobacterium breve, Bifidobacterium lactis, Bifidobacterium longum, Lactobacillus plantarum* and *Lactobacillus acidophilus* or Placebo Group with a placebo for 7 weeks. The 20 enrolled subjects were divided as follows: A) Placebo Group: 4 women and 6 men; B) Test group: 6 women and 4 men.

Blood collection, glycaemic control, immunological and inflammatory markers

All measurements were registered between the hours of 7:00 and 11:00 a.m. Blood was collected at baseline (T0) and after 7 weeks (T1), for monitoring the glycaemic status and specific serum immunological (immunoglobulin A - IgA) as well as inflammatory markers (IL-6 and TNF-alpha). In addition, clinical signs were recorded.

Table I. *Glycemic state and concentration of serum IgA, IL-6 and TNF-alpha in Placebo group at T0 and T1.*

BLOOD TESTS (T0) PLACEBO GROUP						**BLOOD TESTS (T1) PLACEBO GROUP**			
ID	***M / F***	***GLYCEMIA (mg/dl)***	***IL-6 (pg/ml)***	***TNF- α (pg/ml)***	***IgA (mg/dl)***	***GLYCEMIA (mg/dl)***	***IL-6 (pg/ml)***	***TNF- α (pg/ml)***	***IgA (mg/dl)***
DC	M	96	7.5	8.1	200	97	7.6	8	200
PS	F	90	6.7	7.7	205	90	6.7	7.8	204
CS	F	83.8	7	8	199	83.8	7.1	8	200
TG	F	95	6	7.1	158	94	6	7	158
MTP	M	92	5.9	6.4	169	92	5.9	6.4	170
LP	M	103.8	7.1	7.9	210	103	7	8	210
RD	F	80.9	6.8	6.9	207	81	6.5	6.8	206
MI	M	99.7	6.8	6	299	99.7	6.9	6	301
FA	M	102	7	7.8	256	102.9	6.7	7.7	255
SB	M	95.5	7.3	8.3	211	95	7.5	8.4	211

Statistical analyses

Outcome measures of the exploratory study were analysed with a *t*-test for paired samples for pre–post differences with time as the factor using Statistical Package for Social Sciences (SPSS for Windows, Version 11.5, Chicago, Ill) software, to detect significant differences between pre-test and post-test scores.

RESULTS

The data regarding the glycaemic status and concentration of serum IgA, IL-6 and TNF-alpha in the Placebo Test group at T0 and T1 obtained in the study, including the average values are shown in Tables I-III.

As seen in Fig. 1, the blood sugar levels changed in control *vs* placebo subjects. On the one hand from T0 to T1 there were no variations and glycemic levels were standard in group A. On the other hand, the same figure shows how blood sugar levels changed in the Test group B, that is after taking the probiotic. It is noted that the introduction of the probiotic in the normal diet improved the parameters by 2%.

Fig. 2 shows IL-6 and TNF-α levels in the Placebo *vs* Test group at T0 and T1. For IL-6 and TNF-α in the Placebo Group there was a similar trend variation of 0.2%, even if at T0 the values were almost high due to the age of the subjects. In the Test Group, who introduced the probiotic into their diet, IL-6 decreased by 10%, allowing us to underline how the use of probiotics can help reduce inflammatory processes. Moreover, in the TNF-α levels of the Test group, there was a 7% reduction from T0 to T1, in favor of the fact that taking probiotics in the diet for 7 weeks encourages an improvement in inflammation, thanks to an improvement in the immune system.

Finally, Fig. 3 shows the changes in IgA levels in

Table II. *Glycaemic state and concentration of serum IgA, IL-6 and TNF-alpha in Test group at T0 and T1*

BLOOD TESTS (T0) TEST GROUP						**BLOOD TESTS (T1) TEST GROUP**			
ID	***M / F***	***GLYCEMIA (mg/dl)***	***IL-6 (pg/ml)***	***TNF- α (pg/ml)***	***IgA (mg/dl)***	***GLYCEMIA (mg/dl)***	***IL-6 (pg/ml)***	***TNF-α (pg/ml)***	***IgA (mg/dl)***
ADS	M	97	5.9	8	278	95	5	7.5	280
SP	F	81	7	8.2	215	79.5	6	7.8	218
LR	F	99.5	6.8	7	199	98	5.8	6.2	201
MP	F	80	7.3	8	230	79	6.5	7.5	232
GS	M	92	7.1	7.6	256	90.1	6.5	7	255
RP	M	100	7	7.9	197	97.3	5.7	7.1	199
DA	F	84	6.5	6.7	188	83	5.5	6	190
FC	F	79.7	6.4	6.5	206	78.5	5.9	6	208
YM	M	102	7.2	7.6	233	101.2	6.4	7	235
RM	F	83.3	6.8	6	238	81	5.8	5.8	240

Table III. *Average values of the markers in Placebo and Test groups.*

Marker	**Placebo**	**Test**
Glycemia (Average)	**±0.03**	**±1.60**
IL-6 (Average)	**±0.02**	**±0.90**
TNF- α (Average)	**±0.01**	**±0.60**
IgA (Average)	**±0.1**	**±1.80**

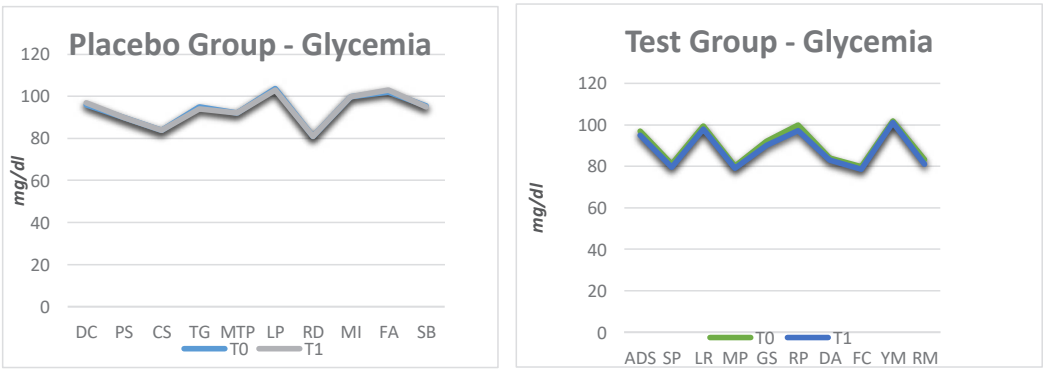

Fig. 1. *Glycemic values in Placebo vs Test group*

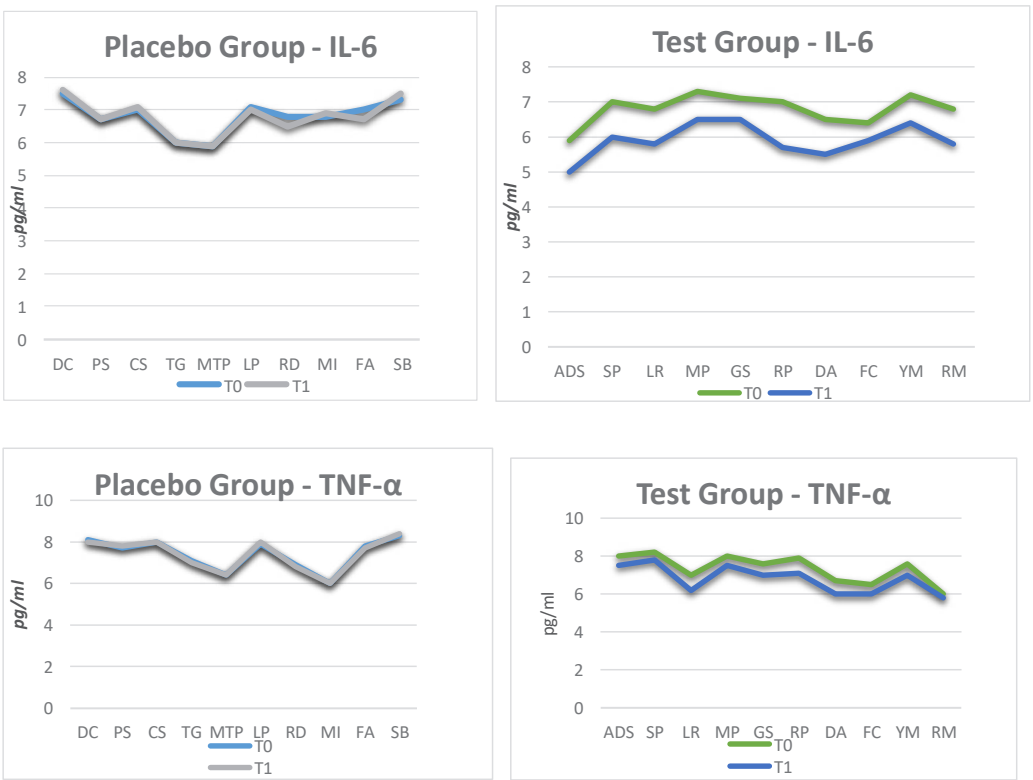

Fig. 2. *Inflammatory markers (IL-6 and TNF-α) in Placebo vs Test group*

the Placebo group *vs* Test Group. It is noted that at T0 the IgA levels are more or less low, demonstrating the fact that due to age, the subjects show a weakened immune system. The changes to T1 are irrelevant. In the Test Group, there was a 2% increase in Ig-A levels, given in favor of the fact that probiotics stimulate the production of immunoglobulins, improving the functionality of the immune system and reducing the inflammatory process.

DISCUSSION

Maintaining health in old age depends on the correct function of the homeostatic systems i.e. nervous,

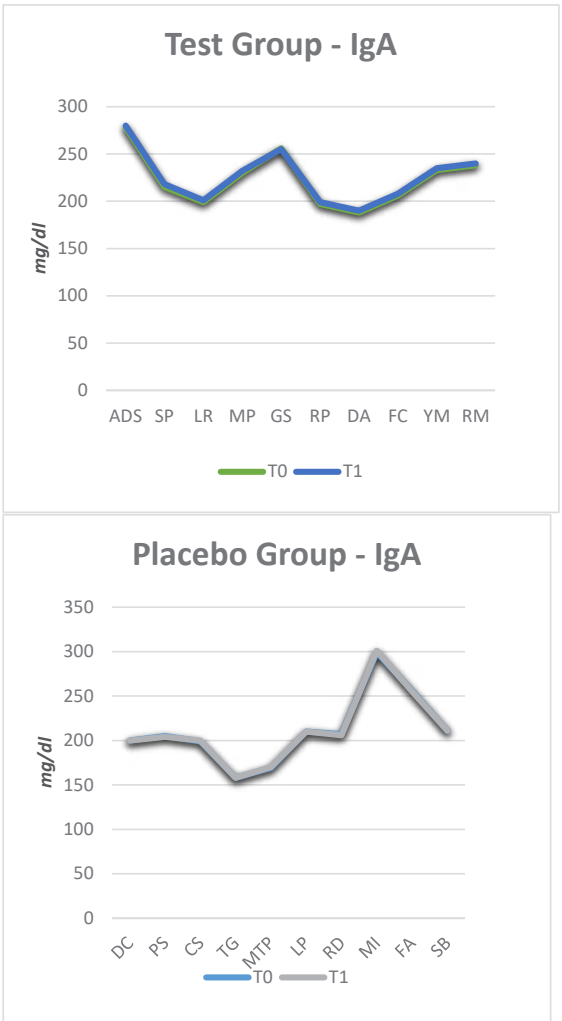

Fig. 3. *Immunomodulatory markers (IgA) in Placebo vs Test group*

endocrine and immune systems, with sequentially correct interactions between these systems and the intestinal microbiota (6). However, in the elderly, there is a reduction in the body's functional capacity, which, in turn, can evolve towards "inflammation". Probiotics can have a particular application in elderly populations, especially in terms of protection against infections and perhaps also in the prevention of various age-related diseases (7). Current evidence shows a correlation between the composition of the gut microbiota and cognitive performance, frailty and comorbidity in the elderly. Studies conducted over the years on animals have shown a benefit of guided therapy with probiotic supplement on the microbiota in reducing chronic low-grade inflammation in the elderly; however, this remains controversial in clinical trials. A correct diet with the addition of probiotics reduces reactive protein C and tumour necrosis factor, modulating the release of cytokines (8, 9). However, some studies say otherwise, therefore suggesting that the use of probiotics in the elderly does not affect the inflammatory state and therefore does not improve life expectancy (10-12). In our study, we demonstrated a close correlation with the trend of inflammatory markers and the use of PRO-Bifido Hyperbiotics, USA. The role of probiotics in maintaining well-being and health is confirmed, as mentioned, on the control of low-grade systemic inflammation in the elderly, a common risk factor for the development of chronic, cardiometabolic diseases (type 2 diabetes, obesity, metabolic syndrome, cardiovascular disease) and liver disease, developing during aging. The use of PRO-Bifido Hyperbiotics, USA, may also have preventive effects on the onset of age-related obesity. In fact, blood sugar values were decreased by 2%. In our study, the additional use of PRO-Bifido Hyperbiotics, USA, improved the serum concentration of IgA, thereby promoting better immune defense in the elderly. However, further clarification is needed to better understand the correlation between the gut microbiota, the aging process and the degenerative diseases typical of the elderly.

REFERENCES

1. Inchingolo F, Dipalma G, Cirulli N, et al. Microbiological results of improvement in periodontal condition by administration of oral probiotics. J Biol Regul Homeost Agents 2018; 32:1323-28.
2. Cantore S, Ballini A, Mori G, et al. Anti-plaque and antimicrobial efficiency of different oral rinses in a 3-day plaque accumulation model. J Biol Regul Homeost Agents 2016; 30:1173-78.
3. Cantore S, Ballini A, Farronato D, et al. Evaluation of an oral appliance in patients with mild to moderate obstructive sleep apnea syndrome intolerant to continuous positive airway pressure use: Preliminary results. Int J Immunopathol Pharmacol 2016; 29:267-73.
4. Ballini A, Scacco S, Coletti D, Pluchino S, Tatullo

M. Mesenchymal stem cells as promoters, enhancers, and playmakers of the translational regenerative medicine. Stem Cells Int 2017; 2017:3292810.
5. Ballini A, Cantore S, Farronato D, et al. Periodontal disease and bone pathogenesis: the crosstalk between cytokines and porphyromonas gingivalis. J Biol Regul Homeost Agents 2015; 29:273-81.
6. Ballini A, Gnoni A, De Vito D, et al. Effect of probiotics on the occurrence of nutrition absorption capacities in healthy children: a randomized double-blinded placebo-controlled pilot study. Eur Rev Med Pharmacol Sci 2019; 23:8645-57.
7. Foti C, Romita P, Rigano L, et al. Isobornyl acrylate: an impurity in alkyl glucosides. Cutan Ocul Toxicol 2016; 35:115-19.
8. Grassi FR, Pappalettere C, Di Comite M, et al. Effect of different irrigating solutions and endodontic sealers on bond strength of the dentin-post interface with and without defects. Int J Med Sci 2012; 9:642-54.
9. Cicinelli E, Ballini A, Marinaccio M, Poliseno A, Coscia MF, Monno R, De Vito D. Microbiological findings in endometrial specimen: our experience. Arch Gynecol Obstet 2012; 285:1325-29.
10. Ballini A, Santacroce L, Cantore S, et al. Probiotics Efficacy on oxidative stress values in inflammatory bowel disease: a randomized double-blinded placebo-controlled pilot study. Endocr Metab Immune Disord Drug Targets 2019; 19:373-81.
11. Ballini A, Santacroce L, Cantore S, et al. Probiotics improve urogenital health in women. Open Access Maced J Med Sci 2018; 6:1845-50.
12. Cantore S, Mirgaldi R, Ballini A, et al. Cytokine gene polymorphisms associate with microbiogical agents in periodontal disease: our experience. Int J Med Sci 2014; 11:674-79.

LETTER TO THE EDITOR

Management of patients suffering from xerostomia with a combined mouthrinse containing sea salt, xylitol and lysozyme

S. Cantore[1,2,3*], A.D. Inchingolo[1*], E. Xhajanka[3], V. Altini[2], I.R. Bordea[4], G. Dipalma[1§] and F. Inchingolo[1§]

[1]Department of Interdisciplinary Medicine , School of Medicine, University "Aldo Moro", Bari, Italy; [2]Sorriso & Benessere Ricerca e Clinica S.r.l., Bari, Italy; [3]University of Medicine, Tirana, Faculty of Dentistry (Fakulteti i Mjekësisë Dentare-FMD), Tirana, Albania; [4]University of Medicine and Pharmacy "Iuliu Hatieganu", Department of Oral Health, Cluj-Napoca, Romania

Received July 8, 2020 - Accepted August 6, 2020

[*]Contributed equally to this work as co-first authors

[§]Contributed equally to this work as co-last authors

To the Editor,

Dry mouth, including xerostomia, is a common symptom especially in older adults. The causes of dry mouth include medication, autoimmune disease (Sjögren's Syndrome), radiotherapy or chemotherapy for cancer, hormone disorders and infections (1-3). There is a huge variety of therapeutic approaches for relieving dry mouth symptoms such as chewing-gum, sugar-free lozenges, moisturizers and toothpastes, but most of them are are frequently restricted to palliative treatment. A Cochrane review concluded that there is no strong evidence that any topical therapy is effective in relieving the symptom of dry mouth, and more studies are required to provide evidence to guide clinical care (4-7).

The inclusion of antimicrobial agents, such as lysozyme, lactoferrin, lacoperoxidase, or xylitol in xerostomia healthcare products, was proposed as early as the 1990s, and appears to be a promising approach for the prevention of microbial-related diseases in xerostomic patients (8, 9). Despite the significant prevalence of xerostomia in the general population, however, no standard treatment guidelines exist. Successful treatments are typically individualized for the specific patient and should be targeted at the underlying pathophysiology of the disease (10-12).

The aim of the present study was to evaluate the efficiency of a combined mouthrinse containing purified water, sea salt, xylitol, lysozyme, and menthol (H2Ocean Sea Salt Mouthwash) in the management of patients suffering from xerostomia and hyposalivation.

MATERIALS AND METHODS

Study subjects

The present study was conducted at a dental community cabinet in collaboration with the University of Bari Aldo Moro, Italy. A total of 30 patients between the ages of 40 and 70 years (mean age 57±1) were enrolled and divided into two categories. In order to have the unbiased and accurate clinical data, a double-blind protocol was followed for enrolment of the patients in terms of treatment plan and further categorization into a study group. All eligible

Key words: sea salt; mouthwash; xylitol; lysozyme; oral health-related quality of life; xerostomia

Corresponding Author:
Prof. F. Inchingolo,
Department of Interdisciplinary Medicine,
University of Bari "Aldo Moro", P.zza G. Cesare, 11,
70124 Bari, Italy
Tel./Fax: +39 0805478889
e-mail: francesco.inchingolo@uniba.it

0393-974X (2020)
Copyright © by BIOLIFE, s.a.s.
This publication and/or article is for individual use only and may not be further reproduced without written permission from the copyright holder.
Unauthorized reproduction may result in financial and other penalties
DISCLOSURE: ALL AUTHORS REPORT NO CONFLICTS OF INTEREST RELEVANT TO THIS ARTICLE.

subjects were given oral information about the products and the purpose of the study and signed an informed consent, in accordance with the ethical principles originating in the Declaration of Helsinki and consistent with good clinical practices.

Participants with dry mouth symptoms, regardless of their salivary flow, were included in the study, while patients having major systemic diseases, patients who had taken pilocarpine or cevimeline in the 7 days preceding the study and who refused to participate during the follow-up were excluded from the study group. The two groups of patients were called for follow-up after treatment on the 90th day to check the overall response on the mouthwash or placebo treatment.

A randomized double-blind, placebo-controlled, parallel group design was used for this study. A computer-generated double randomization sequence was carried out by an investigator who was not directly involved in the treatment and the assessment of the subjects. After completing baseline measures, participants were stratified by gender and randomized into one of two groups. The subjects were then categorized into two treatment regimes in groups I and II (15 in each group). Both the mouthrinses were made to look identical:

Group I (n = 15): H2Ocean Sea Salt Mouth rinse (H2Ocean, Inc. FL. USA);

Group II (n = 15): Placebo mouth rinse (physiologic saline solution with no mouthwash dilution added).

Participants were asked to rinse twice a day after brushing - once in the morning and once at night before going to bed - for 12 weeks. Patients were instructed to rinse with 15 mL of the solution for at least 1 min followed by expectoration of the residual mouthrinse and to avoid eating and drinking for 30 min afterwards. To avoid the effect of new variables, subjects were asked to continue their usual daily brushing method during the study period using a toothbrush with extra soft bristles and non-medicated fluoride free dentifrice. Written instructions were provided explaining how to use the mouthwash. Rinsing was performed at home without supervision. To check for

Table I. *Variations reported between baseline (T_0) and after a cycle of treatments (T_1) with the 2 proposed protocols in the 2 different groups.*

Unstimulated whole salivary flow	**T_0**	**T_1**
Group 1(Test)	0.21	0.56
Group 2(CTRL)	0.34	0.62
Stimulated whole salivary flow		
Group 1 (Test)	0.99	1.20
Group 2(CTRL)	1.12	1.31
Salivary pH		
Group 1(Test)	6.82	7.06
Group 2(CTRL)	6.44	6.60

compliance, subjects were asked to note the times of day when they rinsed.

Signs of oral dryness were registered clinically by clinical observation of lip and oral mucosa dryness. Oral mucosa dryness was recorded when the investigator noticed the absence of a saliva coating over most of the dorsum of the tongue, buccal and labial mucosa as well as the absence of pooled saliva in the floor of the mouth.

Clinical parameters

Plaque Index (PI) was taken from all participants by the same blinded trained examiner at baseline and at the end of the sudy. The PI was recorded by assigning a score to each surface (5 for great amount of plaque present, 0 for totally absent) and calculating the percentage of total tooth surfaces that revealed the presence of plaque.

Salivary flow rate and pH

In order to measure salivary flow rate, unstimulated saliva was collected by direct emission into a sterile plastic glass. Measurements were performed between 8 and 10 a.m. using the expectoration method. Saliva was weighed with high precision scales. Patients did not drink, perform oral hygiene, or smoke for at least 60 min beforehand. Salivary flow above 0.25 ml/min was considered normal.

The pH value of the saliva is lower in unstimulated than in stimulated saliva. The pH value of saliva cited in literature is in the range of 6-7, making it slightly acidic, but when stimulated it may increase to about 7.8. Evaluations were made before and after 12 weeks of product/placebo application.

Statistical analysis

Outcome measures of the exploratory study were analyzed with a *t*-test for paired samples for pre/post differences with time as the factor using Statistical Package for Social Sciences (SPSS for Windows, Version 11.5, Chicago, Ill) software, to detect significant differences between pre-test and post-test scores.

RESULTS

All subjects (N = 30) completed the trial, and there were no missing values. No adverse events or

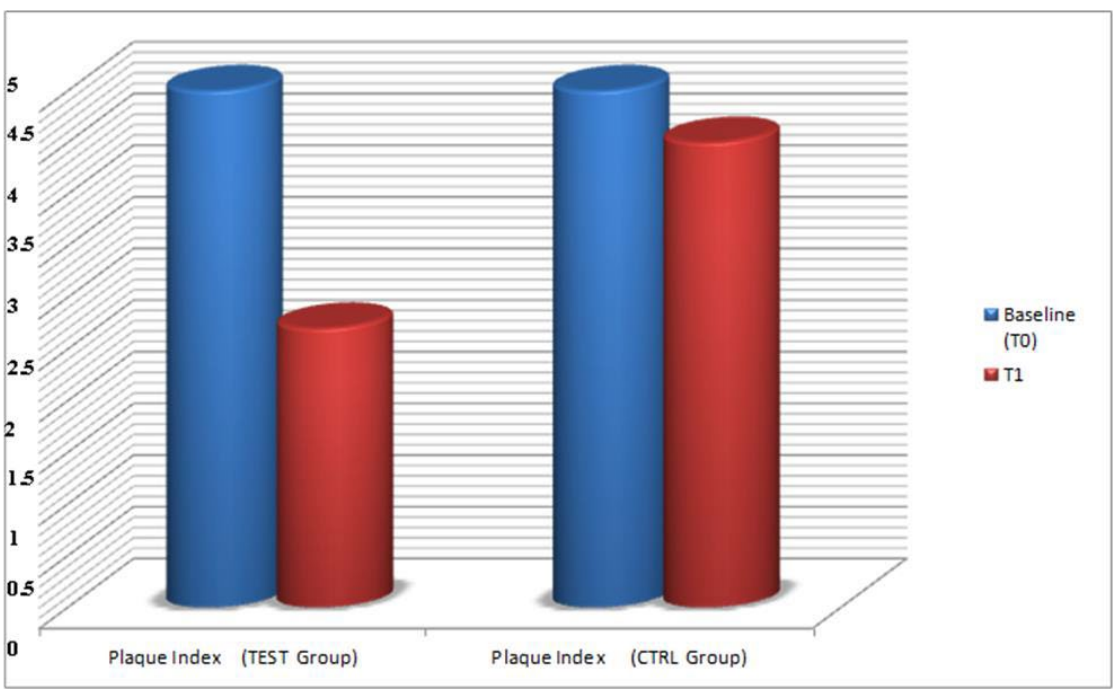

Fig. 1. *Clinical Index results before and after the study period.*

side effects were reported or observed. All the clinical parameters were recorded for both groups during the study at baseline (TO) and at the end of study, i.e. at 90 days (T1). The amounts of mouthwash used indicated good compliance with the instructions. No adverse events or side effects were reported or observed. A sample of 18 women and 12 men with xerostomia underwent treatment with H2Ocean Sea Salt Mouthrinse or a similar placebo-mouthrinse.

Salivary flow rate and pH analysis, at 12 weeks of treatment application in the test group, showed an improvement of approximately 19.9% and 9.52%, respectively, for unstimulated vs stimulated whole salivary flow, and 33.33% of pH parameters compared to the control group (Table I). The clinical scores for the test and control groups at baseline and at the end of the experimental study period are shown in Fig. 1, showing a reduction of 50% from baseline in the test group compared to the control group (16% from baseline). These results support that H2Ocean Sea Salt Mouthwash worked significantly to improve all the clinical parameters and to promote salivary flow activity in patients affected by Xerostomia.

DISCUSSION

Xerostomia, the main causes of which are the use of drugs and hormonal disorders, is a condition that affects 1-29% of the population, especially adults and the elderly (4-8). This condition is on the rise and negatively affects the quality of life of patients, causing problems with swallowing, chewing and speech, therefore leading to social and psychological problems. There are no products or drugs that can cure all the symptoms of this condition, however various topical products such as gels, sprays, mouthwashes and toothpastes which can improve the patient's quality of life have been tested (2, 6). This is, of course, also possible through timely diagnosis and appropriate treatment for each patient.

There is a lack studies in the literature that have tested the effectiveness and effects of a sea salt and xylitol rinse on dry mouth and xerostomia patients. The results reported in this pilot study after H2Ocean Sea Salt Mouthwash treatment are significantly positive in all aspects and symptoms of xerostomia. Obviously, further clinical studies should be carried involving a larger cohort of subjects, and perhaps a longer trial period.

This approach may provide a valuable addition or alternative to the armamentarium of treatment options for oral hygiene procedures in xerostomia and dry mouth syndrome, preventing dental plaque formation, with the additional benefit of no alcohol presence in the solution. It could be concluded that H2Ocean Sea Salt Mouthrinse contains excellent daily oral hygiene agents, and its use should be promoted based on the present and previous scientific knowledge of its benefits and proper use.

REFERENCES

1. Inchingolo F, Dipalma G, Cirulli N, et al. Microbiological results of improvement in periodontal condition by administration of oral probiotics. J Biol Regul Homeost Agents 2018; 32:1323-28.
2. Cantore S, Ballini A, Mori G, et al. Anti-plaque and antimicrobial efficiency of different oral rinses in a 3-day plaque accumulation model. J Biol Regul Homeost Agents 2016; 30:1173-78.
3. Ballini A, Scacco S, Coletti D, Pluchino S, Tatullo M. Mesenchymal stem cells as promoters, enhancers, and playmakers of the translational regenerative medicine. Stem Cells Int 2017; 2017:3292810.
4. Ballini A, Cantore S, Farronato D, et al. Periodontal disease and bone pathogenesis: the crosstalk between cytokines and porphyromonas gingivalis. J Biol Regul Homeost Agents 2015; 29:273-81.
5. Ballini A, Gnoni A, De Vito D, et al. Effect of probiotics on the occurrence of nutrition absorption capacities in healthy children: a randomized double-blinded placebo-controlled pilot study. Eur Rev Med Pharmacol Sci 2019; 23:8645-57.
6. Foti C, Romita P, Rigano L, et al. Isobornyl acrylate: an impurity in alkyl glucosides. Cutan Ocul Toxicol 2016; 35:115-9
7. Grassi FR, Pappalettere C, Di Comite M, et al. Effect of different irrigating solutions and endodontic sealers on bond strength of the dentin-post interface with and without defects. Int J Med Sci 2012; 9:642-54.

8. Cicinelli E, Ballini A, Marinaccio M, Poliseno A, Coscia MF, Monno R, De Vito D. Microbiological findings in endometrial specimen: our experience. Arch Gynecol Obstet 2012; 285:1325-29.
9. Ballini A, Santacroce L, Cantore S, et al. Probiotics efficacy on oxidative stress values in inflammatory bowel disease: a randomized double-blinded placebo-controlled pilot study. Endocr Metab Immune Disord Drug Targets 2019; 19:373-381.
10. Ballini A, Santacroce L, Cantore S, et al. Probiotics improve urogenital health in women. Open Access Maced J Med Sci 2018; 6:1845-50.
11. Cantore S, Mirgaldi R, Ballini A, et al. Cytokine gene polymorphisms associate with microbiogical agents in periodontal disease: our experience. Int J Med Sci 2014; 11:674-79.
12. Cantore S, Ballini A, Farronato D, et al. Evaluation of an oral appliance in patients with mild to moderate obstructive sleep apnea syndrome intolerant to continuous positive airway pressure use: Preliminary results. Int J Immunopathol Pharmacol. 2016 Jun;29(2):267-73.

Efficacy evaluation of commercial vaccines against circulating filed isolates of avian influenza H9N2 and infectious bronchitis viruses in broiler chickens

G. Mustafa[1], A. Aslam[1], M.Y. Tipu[1], S. Masood[2], U. Iqbal[1], A. Mahmood[1], M. Tayyab[3] and I. Irshad[4]

[1]Department of Pathology, University of Veterinary and Animal Sciences, Lahore, Pakistan; [2]Department of Anatomy and Histology, University of Veterinary and Animal Sciences, Lahore, Pakistan; [3]Department of Parasitology, University of Veterinary and Animal Sciences, Lahore, Pakistan; [4]Institute of Continuing Education and Extension, University of Veterinary and Animal Sciences, Lahore, Pakistan

Received November 18, 2019 - Accepted March,11 2020

To the Editor,

One of the primary measures used for prevention of infectious diseases is vaccination. Avian influenza (AI) is a viral disease that is contagious in nature and is caused by avian influenza virus (AIV) (1). Infectious bronchitis (IB) is caused by infectious bronchitis virus (IBV) belonging to genus gammacoronavirus of the *Coronaviridae* family (2). An optimum approach to control a disease and obtain maximum protection is to use the vaccines based on the strain prevalent in the area. Despite continuous vaccination against H9N2 and IBV, outbreaks of H9N2 and IBV are often reported in the vaccinated poultry flocks. This situation has challenged the efficacy of control strategies of poultry diseases. A new debate has started whether the vaccinal strains are different from field strains or whether new strains have emerged as a result of immune pressure (3).

Continuous surveillance is needed as IBV and H9N2 are both RNA viruses and undergo a high rate of mutations; which often render the subsequent viral mutants less antigenic, or non-antigenic compared with previous viral strains, thus undermining any vaccine cross reactivity. In the areas where a local strain is not available for vaccination, heterologous vaccines are more likely to be useful. In this case, using different serotypes of vaccines increases the likelihood that at least one of the strains will prove to be antigenic, and capable of eliciting an effective host immune response (4). The aim of this study was to survey protective effects of most frequently used vaccines against H9N2 and IBV.

MATERIALS AND METHODS

Sixty day-old broiler chicks were obtained from a commercial hatchery and were divided into four different groups (A, B, C and D) with 15 birds per group. Standard rearing and management conditions were followed. *Ad libitum* feed and water were offered to these birds. At the age of 7 days, 0.25 mL H9N2 vaccine (Otto Fluvac) was administered subcutaneously to all birds of group A while group B was kept as positive control for H9; this group

Key words: IBV, H9N2, ELISA, vaccination, broiler chicken, Pakistan

Corresponding Author:
Dr Ghulam Mustafa,
Department of Pathology,
University of Veterinary and Animal Sciences,
Lahore, 54000, Pakistan
e-mail: gmustafa@uvas.edu.pk

0393-974X (2020)
Copyright © by BIOLIFE, s.a.s.
This publication and/or article is for individual use only and may not be further reproduced without written permission from the copyright holder.
Unauthorized reproduction may result in financial and other penalties
DISCLOSURE: ALL AUTHORS REPORT NO CONFLICTS OF INTEREST RELEVANT TO THIS ARTICLE.

received only H9 challenge but no H9 vaccine. Similarly, again at 0-day of host age, 0.2 mL IBV vaccine (Gallivac IB 88 and Bioral H120, Merial) and at day 14 the second dose (0.2 mL) of IBV (Bioral H120 and Merial) was administered intranasally to all birds of group C while group D was kept as positive control for IBV as this group received only IBV challenge without vaccine.

Serum antibody titer

At 21 days of age, serum was collected from all birds. Antibody titer against H9N2 of group A and B and titers against IBV of group C and D weere checked by ELISA (IDEXX, USA) according to the guidelines of the manufacturer. S/P ratio was calculated, and a ratio greater or equal to 0.5 was considered positive for H9N2 while ratios greater or equal to 0.2 were considered positive for IBV antibodies, suggesting that the birds were vaccinated.

Challenge experiment

The birds in groups A and B were challenged with H9N2 field isolate according to the recommended EID50 (106.5/0.1 mL/dose) and birds in group C and D were challenged with IBV field isolate according to the recommended EID50 (106/0.1 mL/dose). After challenge, the birds were monitored under close observation for clinical signs/ mortality over a two-week period.

Histopathological examination

On days seven and fourteen post-challenge, five birds from each group (A, B, C and D) were randomly sacrificed, and the trachea, lungs and intestine from birds of groups A and B while trachea, lungs and kidney from the birds of group C and D were collected and preserved in 10 % neutral buffered formalin for processing in the Pathology section of QOL, UVAS, Lahore, Pakistan.

RESULTS

The results of this study showed that effective antibody response was generated when the hosts were vaccinated with Otto Fluvac, Gallivac IB 88 and Bioral H120 vaccines. No mortality or morbidity was observed in groups A and C (vaccinated groups) while the mortality rate observed in group B (H9 challenged group) was 10%, and 60% in group D (IBV challenged group). H9N2 ELISA S/P ratio in H9 vaccinated group A ranged between 0.518-1.618 and IBV ELISA S/P ratio in IBV vaccinated group C ranged between 0.167-0.413. At day 28, the groups of the birds treated with the vaccines showed no gross or microscopic lesions. The tissues collected on day 35 (one-week post infection) showed histological changes. Kidneys of group D hosts that were challenged with filed isolate of IBV showed severe peritubular congestion and renal tubular degeneration (Fig. 1A), while the tracheas of the same group showed sloughing and degeneration of tracheal epithelium and rounding of tracheal epithelial cells (Fig. B). Similarly, the lungs of the birds of group B that were challenged with H9N2 filed strain showed congestion and hemorrhaging in the pulmonary syncytia (Fig. C) and infiltration of inflammatory cells (Fig. 1D).

DISCUSSION

In this study, efficacy of commercially available vaccines against the field isolates of IBV and H9N2 were evaluated. Fluvac, an inactivated vaccine, was used against H9N2; Gallivac IB 88, a live attenuated vaccine of 793B IBV variant and Bioral H120, a live attenuated vaccine of H120 strain, were used against IB. These vaccines are the most commonly used in Pakistan and have been shown to provide more than 80% immunization against IBV and H9N2. Our finding is in agreement with the study of Terregino et al. 2008 (5). They demonstrated that a single serotype does not provide complete protection against heterologous strains. The use of different types of live IBV vaccines can however provide protection against a wide variety of different heterologous viral strains of IBV. However, many outbreaks of H9 (6) and IBV (7) have been reported in Pakistan in vaccinated flocks. Disease outbreaks among vaccinated host populations may be due to different efficacies of vaccine under field and experimental conditions (8). Apart from these, there are many other factors to be considered regarding

Table I. *ELISA results of Group A, B (H9N2) and C, D (IBV)*

Sample ID	H9N2 ELISA titer results (S/P ratio)		IBV ELISA titer results (S/P ratio)	
	Vaccinated group (Group A)	Control group (Group B)	Vaccinated group (Group C)	Control group (Group D)
1	0.531	0.238	0.236	0.011
2	0.612	0.169	0.301	0.004
3	0.579	0.018	0.214	0.018
4	0.644	0.171	0.205	0.019
5	0.518	0.250	0.273	0.009
6	0.599	0.301	0.367	0.019
7	1.235	0.246	0.413	0.003
8	0.768	0.118	0.189	0.129
9	1.029	0.289	0.255	0.008
10	0.581	0.098	0.167	0.001
11	1.618	0.173	0.311	0.005
12	0.671	0.013	0.257	0.013
13	0.817	0.145	0.289	0.013
14	0.649	0.212	0.311	0.014
15	0.538	0.311	0.291	0.011
Mean	**0.759**	**0.183**	**0.272**	**0.017**

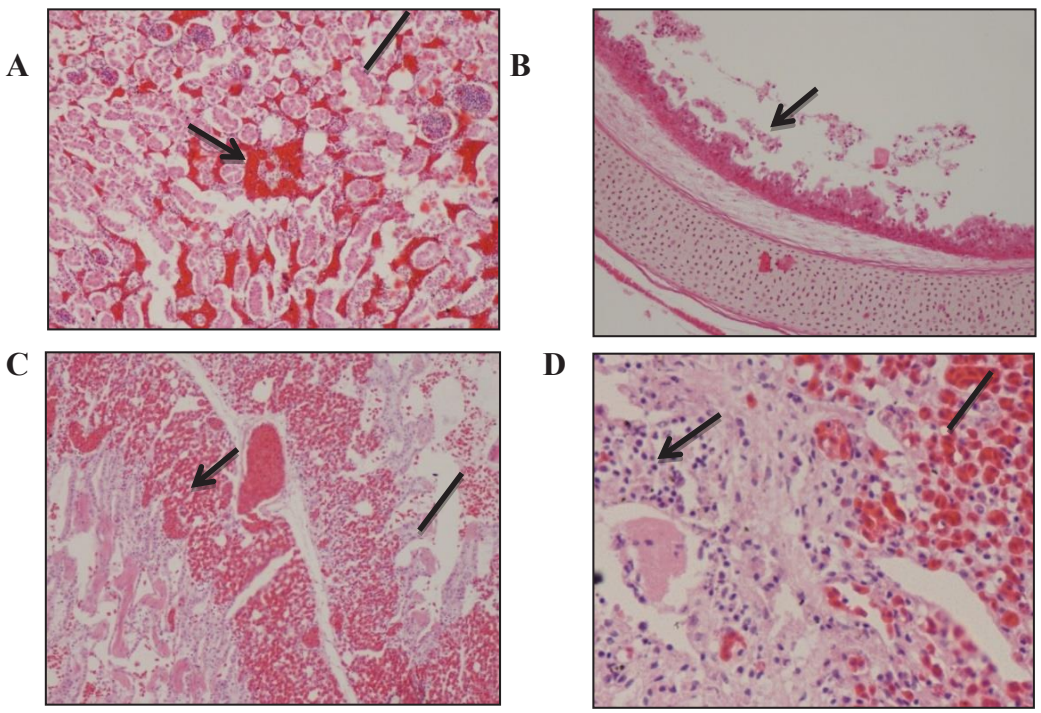

Fig. 1. *Various micrographs depicting pathological lesions.* ***A)*** *Kidney from a group D bird showing severe peritubular congestion, renal tubular degeneration at one week (35th day) post-infection (H and E staining, 10X).* ***B)*** *Trachea from a group D bird showing sloughing and degeneration of tracheal epithelium and rounding of tracheal epithelial cells at one week (35th day) post-infection (H and E staining, 10X).* ***C)*** *Lungs from a group B bird showing congestion and hemorrhages in the pulmonary syncitia at one week (35th day) post-infection (H and E staining, 10X).* ***D)*** *Lungs from a group B bird showing hemorrhage and infiltration of inflammatory cells at one week (35th day) post-infection (H and E staining, 10X).*

lack of vaccine efficacy. These may be infectious, non-infectious or both. Among non-infectious factors are high ammonia levels, high levels of mycotoxins in the feed, poor feed intake. Many infectious factors are immunosuppressive diseases like IBD, Marek's disease and chicken infectious anemia which can affect both types of immunities (innate and acquired) (9). This study is in complete agreement with the results of Shaukal et al. 2016 (10) who reported high efficacy of avian influenza vaccine against prevalent isolates of H9N2 in Pakistan. Macroscopic as well as microscopic changes, such as congestion, hemorrhage and infiltration of inflammatory cells, were observed in kidney, trachea and lungs, and these changes are reported by Zhao et al. 2014 (11).

It is concluded that, despite the reports of genetic mutations and emergence of some new isolates of H9N2 and IBV, the current commercially available vaccines are still effective in providing protective antibody titers under controlled experimental conditions. Poor vaccine protection may be attributed to other environmental or infection-related factors. Furthermore, farm biosecurity needs to be strengthened along with effective vaccination program. Focusing on these will improve the control and prevention of avian diseases including influenza and infectious bronchitis at commercial farms.

ACKNOWLEDGEMENTS

The Authors would like to thank Avian Respiratory System Infectious diseases Laboratory, HVRI, CAAS, China, Molecular Pathology Laboratory and Quality Operations Laboratory, University of Veterinary and Animal Sciences, Lahore for providing necessary facilities for the research.

REFERENCES

1. Fouchier RA, Munster V, Wallensten A, et al. Characterization of a novel influenza A virus hemagglutinin subtype (H16) obtained from black-headed gulls. J Virol 2005; 79:2814-22.
2. Masters PS. The molecular biology of coronaviruses. Adv Virus Res 2006; 66:193-292.
3. Ali M, Yaqub T, Mukhtar N, et al. Prevalence and phylogenetics of H9N2 in backyard and commercial poultry in Pakistan. Avian Dis 2018; 62:416-24.
4. De Wit J, Nieuwenhuisen-van Wilgen J, Hoogkamer A, van de Sande H, Zuidam GJ, Fabri TH. Induction of cystic oviducts and protection against early challenge with infectious bronchitis virus serotype D388 (genotype QX) by maternally derived antibodies and by early vaccination. Avian Pathol 2011; 40:463-71.
5. Terregino C, Toffan A, Serena Beato M, et al. Pathogenicity of a QX strain of infectious bronchitis virus in specific pathogen free and commercial broiler chickens, and evaluation of protection induced by a vaccination programme based on the Ma5 and 4/91 serotypes. Avian Pathol 2008; 37:487-93.
6. Abid M, Yaqub T, Mehboob A, Shabbir MZ. Characterization and phylogenetic analysis of avian influenza virus subtype H9N2 in Pakistan. Hosts Viruses 2017; 4:62-69.
7. Ahmed Z, Naeem K, Hameed A. Detection and seroprevalence of infectious bronchitis virus strains in commercial poultry in Pakistan. Poult Sci 2007; 86:1329-35.
8. Perozo F, Marcano R, Afonso CL. Biological and phylogenetic characterization of a genotype VII Newcastle disease virus from Venezuela: efficacy of field vaccination. J Clin Microbiol 2012; 50:1204-08.
9. Hoerr FJ. Clinical aspects of immunosuppression in poultry. Avian Dis 2010; 54:2-15.
10. Shaukat TM, Muneer MA, Ahmad MUD, Maqbool A, Shaukat TM.. Efficacy of avian influenza virus locally manufactured and imported vaccines. J Anim Plant Sci 2016; 26:653-57.
11. 11. Zhao K, Zhang Y, Zhang X, et al. Preparation and efficacy of Newcastle disease virus DNA vaccine encapsulated in chitosan nanoparticles. Int J Nanomed 2014; 9:389-402.

Efficacy of combined sea salt based oral rinse with xylitol in improving healing process and oral hygiene among diabetic population after oral surgery

L. Signorini[1*], A.D. Inchingolo[2*], L. Santacroce[3], E. Xhajanka[4], V. Altini[5], I.R. Bordea[6], G. Dipalma[2§], S. Cantore[2,6 §] and F. Inchingolo[2§]

[1]Unicamillus University, Rome, Italy; [2]Department of Interdisciplinary Medicine, University of Bari "Aldo Moro", Bari, Italy; [3]Ionian Department, University of Bari "Aldo Moro", Bari, Italy; [4]University of Medicine, Tirana, Faculty of Dentistry (Fakulteti I Mjekësisë Dentare-FMD), Tirana, Albania; [5]Sorriso & Benessere Ricerca e Clinica S.r.l., Bari, Italy; [6]Department of Oral Health, University of Medicine and Pharmacy "Iuliu Hatieganu", Cluj-Napoca, Romania

Received July 2, 2020 – Accepted September 1, 2020

[*]Contributed equally to this work as co-first authors
§Contributed equally to this work as co-last authors

To the Editor,

Diabetes may be considered a disease characterized by dysmetabolic and increased levels of blood glucose. The impaired metabolism of glucose, lipids, and proteins produces alterations in macro- and micro-vascular circulation, giving rise to the risk of several complications in patients with diabetes, including retinopathy, neuropathy, nephropathy, cardiovascular complications (1), and delayed wound healing (2). Periodontal disease is a chronic inflammatory disease of tissues that supports and affects the teeth and the jaws. Substantial evidence suggests a relationship between diabetes and periodontal disease (3). Many studies in several populations have demonstrated that diabetic patients tend to have a higher prevalence of and more severe periodontitis than non-diabetics (4). Hyperglycaemia, a key abnormality in diabetes, plays an important role in the development of inflammation in diabetic complications. It has been demonstrated that high blood sugar promotes inflammation and inhibits wound healing by altering angiogenesis (5). Periodontal lesions are observed in the presence of plaque and tartar and are more serious in diabetics. Therefore, it seems that proper hygiene and adequate plaque control can play a therapeutic role not only in bacterial control, but also in the resolution of oral surgery procedures (6). *In-vitro* studies have demonstrated the use of stem cells of oral origin to restore the integrity of tissues damaged by periodontitis, a difficult but certainly very innovative clinical practice (7). Recent researches have focused on Xylitol, that inhibits bacterial growth, reduces their number and the amount of plaque (8). Moreover, the presence of sea salt in the mouth increases its pH balance. The environment that results is very alkaline, and bacteria cannot survive in an alkaline environment. In fact, bacteria are only able to thrive in a very acidic atmosphere. The aim of this study was to evaluate

Key words: xylitol; sea salt; oral rinse; healing index; oral hygiene; diabetic patients, wound healing

Corresponding Author:
Prof. F. Inchingolo,
Department of Interdisciplinary Medicine,
University of Bari "Aldo Moro",
P.zza G. Cesare, 11, 70124 Bari, Italy
Tel./Fax: +39 0805478889
e-mail: francesco.inchingolo@uniba.it

0393-974X (2020)
Copyright © by BIOLIFE, s.a.s.
This publication and/or article is for individual use only and may not be further reproduced without written permission from the copyright holder.
Unauthorized reproduction may result in financial and other penalties
DISCLOSURE: ALL AUTHORS REPORT NO CONFLICTS OF INTEREST RELEVANT TO THIS ARTICLE.

a combined mouth rinse containing purified water, sea salt, xylitol, lysozyme, and menthol [H2Ocean Sea Salt Mouthwash (H2Ocean, Inc. FL. USA)] in improving the healing process and oral hygiene in a diabetic population after oral surgery procedures.

MATERIALS AND METHODS

Study design

The present study was conducted at the Faculty of Dentistry (FMD), University of Medicine (Tirana, Albania), in collaboration with the University of Bari Aldo Moro, Italy, and according to the Helsinki declaration. Twenty diabetic patients aged 55–65 years, with blood sugar levels ranging from 150 to 200 (mg/dl), were enrolled in the present study. Participants were selected as under clinical diabetic condition (according to American Diabetes Association risk assessment). Participants did not take any medications except for the oral anti-diabetic treatment, so as not to affect the blood chemistry and tissue reply. Patients who had undergone simple (not complicated) dental extraction were selected for the evaluation of the results. Simple "x"-stitch design was used for the haemostasis. Written and verbal informed consent was obtained from each participant.

Experimental design

A randomized double-blind, placebo-controlled design was used for this study. Participants were stratified by gender and randomized into one of two groups: supplementation with H2Ocean Sea Salt Mouth rinse (2 rinses daily) or 2 rinses of a placebo (mint flavoured and coloured water) for 4 weeks, as per standard protocol. Twenty diabetic patients were enrolled as follows:

A) Placebo Group: 4 men and 6 women; B) Test group: 6 men and 4 women.

Patients undergoing tooth extraction were evaluated for wound healing at baseline and at 10, 20, 30 days after surgery.

Statistical analyses

Outcome measures of the exploratory study were analysed with a *t*-test for paired samples for pre–post differences with time as the factor using Statistical Package for Social Sciences (SPSS for Windows, Version 11.5, Chicago, Ill, USA) software, to detect significant differences between pre-test and post-test scores.

RESULTS

For the evaluation of the healing, in Placebo *vs* Test Group, we used modified Landry, Turnbull and Howley index to describe the extent of clinical healing (Tables I-III). Fig. 1 shows how the healing index changed in the Placebo group from time T0 to T3, then from baseline to 30 days after surgery. The Placebo group rinsed with a placebo substance (mint flavoured and coloured water) in the 4 weeks. At T0 all patients showed an index equal to 2, synonymous with the fact that they had recently undergone surgery, in fact the healing index increased to values equal to 3 and in a few patients even to 4.

The healing index values changed in the test group from baseline to 30 days after surgery (Fig. 2). The figures show that in the test group, there was a greater improvement. Also in this situation, all subjects at baseline had values of 2 which changed to values of 4 at T3. These data allow us to understand how in diabetic subjects a mouthwash combined formula with sea salt, lysozyme and xylitol can be a valid help. Unlike commonly used sucrose, xylitol is not fermented by bacteria in the oral cavity. As a result, the acid that damages the enamel of the teeth is not produced and the development of bacterial plaque seems to be limited, consequently, caries is less likely to form. As can be seen in the literature, the regular consumption of xylitol, present in some chewing-gums but above all in mouthwashes, is related to many effects including the regeneration of tooth enamel, the lower incidence of halitosis as well as to an improvement in gingivitis and related inflammation.

Some cases belonging to the Test Group have been documented, therefore they have undergone post-extraction rehabilitation with a mouthwash based on sea salt and xylitol. The figures show how proper oral hygiene can increase the success of wound healing. Fig. 3 shows a rehabilitation of a simple extraction. The site of surgical interest, after suturing with resorbable stitches, at 30 days, shows a complete scarring without signs of inflammation, redness and suppuration. The surrounding tissue shows no signs of injury, therefore a complete recovery.

It could be concluded that this new oral rinse contains important elements for adequate oral hygiene

Table I. *Healing index*

HEALING INDEX	CRITERIA
Very poor 1	Tissue colour: more than 50% of gingivae red Response to palpation: bleeding Granulation tissue: present Incision margin: not epithelialized, with loss of epithelium beyond margins Suppuration: present
Poor 2	Tissue colour: more than 50%of red gingivae Response to palpation: bleeding Granulation tissue: present Incision margin: not epithelized with connective tissue exposed
Good 3	Tissue colour: less than 50% of red gingivae Response to palpation: no bleeding Granulation tissue: none Incision margin: no connective tissue exposed
Very good 4	Tissue colour: less than 25% of red gingivae Response to palpation: no bleeding Granulation tissue: none Incision margin: no connective tissue exposed
Excellent 5	Tissue colour: all pink gingivae Response to palpation: no bleeding Granulation tissue: none Incision margin: no connective tissue exposed.

not only daily, but also in particular and complex conditions, such as those following tooth extraction.

DISCUSSION

In this study, we have shown that a mouthwash based on sea salt and xylitol helps in the healing of wounds and, above all, contributes to keeping the buccal environment clean in subjects who tend to have difficulty healing wounds after oral surgery, in order to avoid bacterial and especially viral infections (9). The current literature considers the use sweeteners and/or chewing-gum with xylitol as a safe and effective method in the prevention of dental caries and periodontitis. (1, 10).

The novelty of sea salt in oral clinical practice also in homecare has brought numerous benefits. Several studies have been conducted *in vivo* on both animals and human models. Studies conducted on humans, however, show that the use of xylitol, in the normal diet, can reduce caries by 30-85% and keep the oral cavity healthier (11). Xylitol is an anticariogenic agent because of its ability to be transported in oral pathogenic bacteria, inhibiting their fermentation process and bio-film adhesion. The use of sea salt has recently gained popularity in the homecare of oral wounds and more generally of mouth hygiene

Table II. *Healing index in the Placebo group at different times*

Placebo Group					
Healing Index					
ID	***M/F***	***T0 Baseline***	***T1 10days after surgery***	***T2 20days after surgery***	***T3 30days after surgery***
AS	F	2	2	3	3
CLP	M	2	3	3	3
LE	F	2	3	3	3
BM	F	2	2	3	3
EU	M	2	2	3	3
PV	F	2	2	3	3
CE	F	2	3	3	4
MS	F	2	3	3	3
AC	M	2	3	3	4
CN	M	2	2	3	3

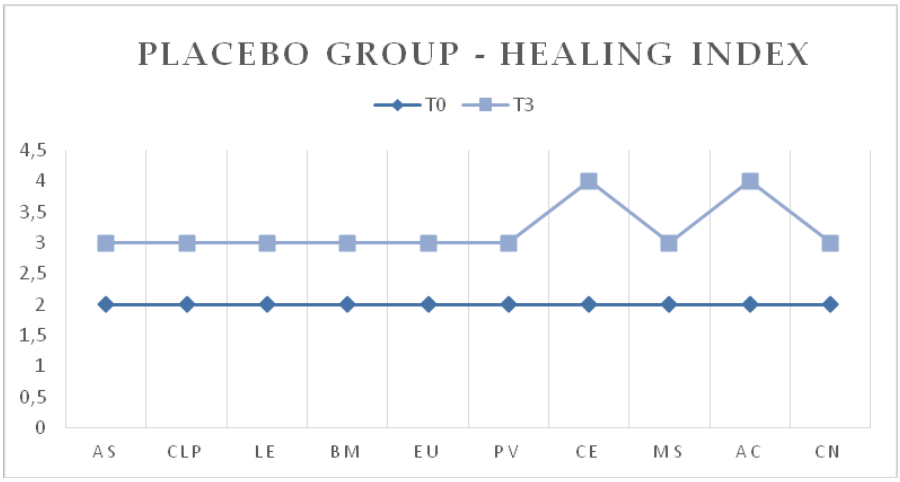

Fig. 1. *Healing Index Placebo Group*

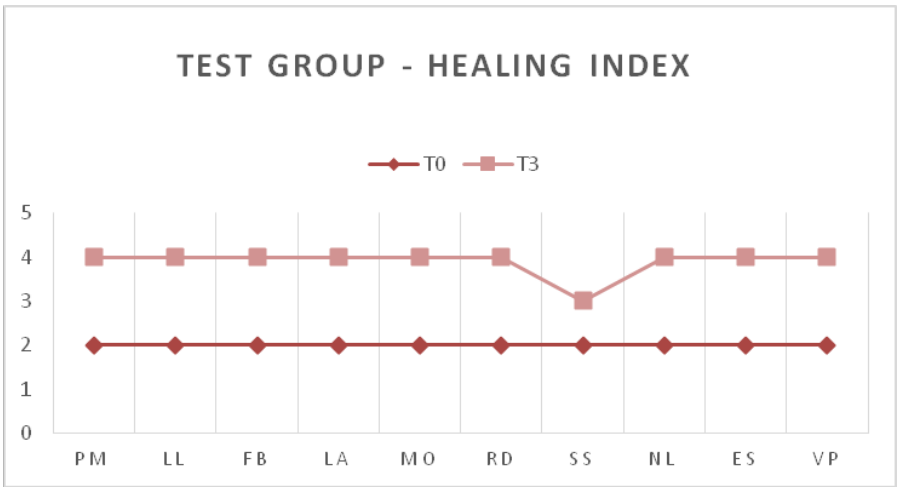

Fig. 2. *Healing Index Test Group*

Fig. 3. *Radiographic image and clinical pictures before and after extraction; test group*

Table III. *Healing index in the Test group at different times*

Test Group Healing Index					
ID	***M/F***	***T0 Baseline***	***T1 10days after surgery***	***T2 20days after surgery***	***T3 30days after surgery***
PM	M	2	2	3	4
LL	F	2	3	4	4
FB	F	2	3	4	4
LA	M	2	3	4	4
MO	M	2	3	3	4
RD	M	2	3	4	4
SS	F	2	2	3	3
NL	F	2	2	3	4
ES	M	2	3	3	4
VP	M	2	3	4	4

(12). Numerous benefits have been observed; in fact, the use of salt water promotes simple healing by inducing vasodilation and encouraging phagocytes at the site of the injury. It also lowers the bacterial load from saliva and acts as an astringent agent. In conclusion, many studies have been carried out in the dental field for the treatment of post-operative wounds, and without doubt the use of drugs is more effective, but certainly the use of substances such as H2Ocean Sea Salt Mouth rinse seems to be highly recommended in the practice of oral hygiene immediately after oral surgery.

REFERENCES

1. Inchingolo F, Dipalma G, Cirulli N, et al. Microbiological results of improvement in periodontal condition by administration of oral probiotics. J Biol Regul Homeost Agents 2018; 32:1323-28.
2. Cantore S, Ballini A, Mori G, et al. Anti-plaque and antimicrobial efficiency of different oral rinses in a 3-day plaque accumulation model. J Biol Regul Homeost Agents 2016; 30:1173-78.
3. Dohan Ehrenfest DM, Del Corso M, Inchingolo F, Charrier JB. Selecting a relevant in vitro cell model for testing and comparing the effects of a Choukroun's platelet-rich fibrin (PRF) membrane and a platelet-rich plasma (PRP) gel: tricks and traps. Oral Surg Oral Med Oral Pathol Oral Radiol Endod 2010; 110:409-11; author reply 411-34.
4. Ballini A, Scacco S, Coletti D, Pluchino S, Tatullo M. Mesenchymal stem cells as promoters, enhancers, and playmakers of the translational regenerative medicine. Stem Cells Int 2017; 2017:3292810.
5. Ballini A, Cantore S, Farronato D, et al. Periodontal disease and bone pathogenesis: the crosstalk between cytokines and porphyromonas gingivalis. J Biol Regul Homeost Agents 2015; 29:273-81.
6. Crincoli V, Ballini A, Di Comite M, Tettamanti L, Coscia MF, Mastrangelo F, De Vito D. Microbiological investigation of medication-related osteonecrosis of the jaw: preliminary results. J Biol Regul Homeost Agents 2015; 29:977-83.
7. Dohan Ehrenfest DM, Del Corso M, Inchingolo F, Sammartino G, Charrier JB. Platelet-rich plasma (PRP) and platelet-rich fibrin (PRF) in human cell cultures: growth factor release and contradictory results. Oral Surg Oral Med Oral Pathol Oral Radiol Endod 2010; 110:418-21; author reply 421-2.
8. Grassi FR, Pappalettere C, Di Comite M, et al. Effect of different irrigating solutions and endodontic sealers on bond strength of the dentin-post interface with and without defects. Int J Med Sci 2012; 9:642-54.
9. Cicinelli E, Ballini A, Marinaccio M, Poliseno A, Coscia MF, Monno R, De Vito D. Microbiological findings in endometrial specimen: our experience. Arch Gynecol Obstet 2012; 285:1325-29.
10. Ballini A, Santacroce L, Cantore S, et al. Probiotics Efficacy on oxidative stress values in inflammatory bowel disease: a randomized double-blinded placebo-controlled pilot study. Endocr Metab Immune Disord Drug Targets 2019; 19:373-81.
11. Ballini A, Santacroce L, Cantore S, et al. Probiotics

improve urogenital health in women. Open Access Maced J Med Sci 2018; 6:1845-50.
12. Cantore S, Mirgaldi R, Ballini A, et al. Cytokine gene polymorphisms associate with microbiogical agents in periodontal disease: our experience. Int J Med Sci 2014; 11:674-79.